NEUROENDOCRINE RESEARCH IN HEALTH AND DISEASE

EDITED BY: Yu-Feng Wang, Xue Qun Chen, Lei Sha, Leo T. O. Lee, Keith Maurice Kendrick and Christopher H. K. Cheng

PUBLISHED IN: Frontiers in Neuroscience and Frontiers in Endocrinology

frontiers Research Topics

ISSN 1664-8714
ISBN 978-2-88963-714-0
DOI 10.3389/978-2-88963-714-0

About Frontiers

Frontiers is more than just an open-access publisher of scholarly articles: it is a pioneering approach to the world of academia, radically improving the way scholarly research is managed. The grand vision of Frontiers is a world where all people have an equal opportunity to seek, share and generate knowledge. Frontiers provides immediate and permanent online open access to all its publications, but this alone is not enough to realize our grand goals.

Frontiers Journal Series

The Frontiers Journal Series is a multi-tier and interdisciplinary set of open-access, online journals, promising a paradigm shift from the current review, selection and dissemination processes in academic publishing. All Frontiers journals are driven by researchers for researchers; therefore, they constitute a service to the scholarly community. At the same time, the Frontiers Journal Series operates on a revolutionary invention, the tiered publishing system, initially addressing specific communities of scholars, and gradually climbing up to broader public understanding, thus serving the interests of the lay society, too.

Dedication to Quality

Each Frontiers article is a landmark of the highest quality, thanks to genuinely collaborative interactions between authors and review editors, who include some of the world's best academicians. Research must be certified by peers before entering a stream of knowledge that may eventually reach the public - and shape society; therefore, Frontiers only applies the most rigorous and unbiased reviews.
Frontiers revolutionizes research publishing by freely delivering the most outstanding research, evaluated with no bias from both the academic and social point of view. By applying the most advanced information technologies, Frontiers is catapulting scholarly publishing into a new generation.

What are Frontiers Research Topics?

Frontiers Research Topics are very popular trademarks of the Frontiers Journals Series: they are collections of at least ten articles, all centered on a particular subject. With their unique mix of varied contributions from Original Research to Review Articles, Frontiers Research Topics unify the most influential researchers, the latest key findings and historical advances in a hot research area! Find out more on how to host your own Frontiers Research Topic or contribute to one as an author by contacting the Frontiers Editorial Office: researchtopics@frontiersin.org

NEUROENDOCRINE RESEARCH IN HEALTH AND DISEASE

Topic Editors:
Yu-Feng Wang, Harbin Medical University, China
Xue Qun Chen, Zhejiang University, China
Lei Sha, China Medical University, China
Leo T. O. Lee, University of Macau, China
Keith Maurice Kendrick, University of Electronic Science and Technology of China, China
Christopher H. K. Cheng, The Chinese University of Hong Kong, China

Citation: Wang, Y.-F., Chen, X. Q., Sha, L., Lee, L. T. O., Kendrick, K. M., Cheng, C. H. K., eds. (2020). Neuroendocrine Research in Health and Disease. Lausanne: Frontiers Media SA. doi: 10.3389/978-2-88963-714-0

Table of Contents

frontiers in Neuroscience

EDITORIAL
published: 24 March 2020
doi: 10.3389/fnins.2020.00176

Editorial: Neuroendocrine Research in Health and Disease

Yu-Feng Wang[1], Xuequn Chen[2]*, Lei Sha[3]*, Keith M. Kendrick[4]*, Leo T. O. Lee[5]* and Christopher H. K. Cheng[6]**

[1] Department of Physiology, Harbin Medical University, Harbin, China, [2] Division of Neurobiology and Physiology, Department of Basic Medical Sciences, School of Medicine, Zhejiang University, Hangzhou, China, [3] Department of Neuroendocrine Pharmacology, School of Pharmacy, China Medical University, Shenyang, China, [4] Key Laboratory for Neuroinformation, The Clinical Hospital of Chengdu Brain Science Institute, University of Electronic Science and Technology of China, Chengdu, China, [5] Faculty of Health Sciences, University of Macau, Shanghai, China, [6] School of Biomedical Sciences, The Chinese University of Hong Kong, Hong Kong, China

Keywords: hormone, hypothalamus, innervation, neuropeptide, receptor

OPEN ACCESS

Edited and reviewed by:
Hubert Vaudry,
Université de Rouen, France

****Correspondence:***
Yu-Feng Wang
yufengwang@ems.hrbmu.edu.cn
Xuequn Chen
chewyg@zju.edu.cn
Lei Sha
lsha@cmu.edu.cn
Keith M. Kendrick
k.kendrick.uestc@gmail.com
Leo T. O. Lee
ltolee@umac.mo
Christopher H. K. Cheng
chkcheng@cuhk.edu.hk

Specialty section:
This article was submitted to Neuroendocrine Science, a section of the journal Frontiers in Neuroscience

Received: *25 December 2019*
Accepted: *17 February 2020*
Published: *24 March 2020*

Citation:
Wang Y-F, Chen X, Sha L, Kendrick KM, Lee LTO and Cheng CHK (2020) Editorial: Neuroendocrine Research in Health and Disease. Front. Neurosci. 14:176. doi: 10.3389/fnins.2020.00176

Editorial on the Research Topic

Neuroendocrine Research in Health and Disease

To facilitate interactions between Chinese neuroendocrine researchers and the international neuroendocrine community, promote the growth of neuroendocrine research, and explore optimal treatment strategies for neuroendocrine diseases, we opened this topic on February 10, 2018. At the end of this topic, we had reviewed 31 manuscripts and accepted 22 for publication in the Neuroendocrine Science Section of the Journals of Frontiers in Neuroscience and Frontiers in Endocrinology. Among these papers, there were 19 original research contributions and three reviews. The research reported in these papers covered neuroendocrine regulation of mental activity, novel neuroendocrine pathways, peripheral effects of neuropeptides, receptor signaling, neuroendocrine diseases and treatments, and other associated areas.

NEUROENDOCRINE REGULATION OF MENTAL ACTIVITY

Kendrick and colleagues initiated the publications by presenting findings that stated "oxytocin (OT) facilitates empathic- and self-embarrassment ratings through attenuating amygdala and anterior insula responses" (Geng et al.). OT, a hypothalamic neuropeptide, can enhance emotional empathy in association with reduced amygdala activation. By using a randomized, double-blind placebo controlled functional MRI experiment on 70 male and female subjects, the authors investigated the effects of intranasal OT (40 IU) on behavioral and neural responses to embarrassment experienced by the self or others. The results demonstrated that OT increases ratings of self- and other embarrassment and that this is associated with reduced physiological arousal and activity in neural circuitry involved in emotional arousal. Interestingly, the neural effects of OT are stronger in individuals with high trait anxiety, suggesting that they may particularly reduce their anxiety in embarrassing situations.

Next, Lin et al. reported that high plasma levels of irisin, a humoral factor important for metabolism and homeostasis of energy balance, are associated with early cognitive deficits in Chinese patients with Type 2 diabetes mellitus (T2DM). In this study on 133 Chinese

patients with T2DM, the authors found that a higher level of irisin in the plasma is associated with impaired overall cognition, specifically in executive function. It is likely that irisin functions both as "a sports pill" and as a signal of impaired cognition.

In a morphometric MRI study, Yang H. et al. reported alterations in cortical thickness in young male patients with childhood-onset adult growth hormone deficiency. They revealed a close correlation between serum growth hormone (GH)/insulin-like growth factor-1 (IGF-1) levels and age-related cognitive function. This correlation is based on alterations in cortical thickness in different brain lobes/regions.

In another study, Liu X. Y. et al. reported that intranasal OT alleviated maternal postpartum depression while improving milk production. Findings demonstrated that pup deprivation can evoke aberrant maternal behavior and hypogalactia in rat dams and that OT significantly improves these symptoms. In the supraoptic nucleus (SON), a major source of brain OT, intranasal administration can reverse pup deprivation -evoked reduction of c-Fos and increases glial fibrillary acidic protein (GFAP) filaments. Notably, OT also increases plasma levels of adrenocorticotropic hormone and corticosterone in pup-deprived dams. These Liu X. Y. et al. findings highlight the therapeutic potential of OT in pup-deprived dams by restoring the activity of the hypothalamic OT-secreting system involving modulation of astrocytic plasticity. However, OT's activation of the hypothalamic pituitary adrenal (HPA) axis likely compromises the facilitatory effects of intranasal administration.

Involvement of the HPA axis in mental activity has been well-known for decades. In the report by Zhou et al., the causal association between cortisol levels and depression is verified through a Mendelian randomization approach in a CORNET consortium of 12,597 participants (Zhou and Qiao). The result confirmed that a genetic predisposition to higher serum morning cortisol levels is associated with an increased depression score. Moreover, Wu R. et al. reported that prenatal dexamethasone exposure causes depression-like behavior in adult rats due to mitochondrial dysfunction. Intervention with treadmill exercise in early life can reverse this depression through improving mitochondrial function in the hippocampus (Wu T. et al.). Consistent with these latter findings, Qin et al. show that in rhesus macaques, a non-human primate, chronic glucocorticoid exposure leads to depression-like behavior and reduces dopamine (DA) levels in cerebrospinal fluid (CSF). Paradoxically, this treatment decreases cortisol concentration in the blood but increases them in hair. Thus, chronic glucocorticoid exposure may disturb both acute and chronic HPA axis reactivity, which eventually disturbs neurotransmitter systems and leads to a depression-like phenotype.

In addition to OT and corticosteroid hormones, sex steroid hormones are also involved in the regulation of mental activity. A paper by Cheng et al. demonstrated that androgens and androgenic signaling are involved in the occurrence of depression and anxiety. Following exposure to androgen during pregnancy, rats manifest depressive, anxious, and stereotypical behaviors in the adolescent period. These phenotypes are possibly associated with changes in neurogenesis in the dentate gyrus of the hippocampus.

NOVEL NEUROENDOCRINE PATHWAYS

Neuroendocrine regulation of bodily activity can be influenced by direct neural innervation along with the actions of circulating neurohormones. In studying the mechanism underlying gastroparesis in patients with Parkinson's disease (PD), Yang Y.-L. et al. demonstrated that DA neurons in the substantia nigra (SN) project to and activate the lateral hypothalamic nucleus (LH) via the D1 receptor. LH neurons expressing orexin A also innervate the dorsal motor nucleus of the vagus (DMV). By activating the orexin receptor 1 of DMV, orexin A from the LH can alter gastric motility. Reduction of DA in the SN of PD patients decreases the activity of this SN-LH-DMV pathway, which ultimately leads to gastric dysfunction via the vagal nerve (Yang Y.-L. et al.).

Zhou et al. also reported that dopaminergic neurons in the SN are involved in the regulation of glucose metabolism through corticotropin-releasing hormone (CRH) neurons that express DA receptor 2 (D2) in the hypothalamic paraventricular nucleus (PVN). Bilateral SN lesions decrease glucose tolerance in rats by down-regulating the D2 receptor and up-regulating CRH in the PVN (Zhou et al.). These findings highlight that high prevalence of glucose metabolism abnormalities in PD patients associates with down-regulation of D2 and up-regulation of CRH in the PVN.

The review by Li et al. systematically demonstrated how pancreatic endocrine secretion is under the regulation of extrapancreatic nerves projecting to the islet directly, or converging on intrapancreatic ganglia, innervated by sympathetic, parasympathetic, enteric, sensory nerve fibers, and other intrapancreatic ganglia. It also highlighted the necessity of clarifying the roles and the mechanisms of intrapancreatic ganglia in physiological and disease states of the pancreas (Li et al.).

PERIPHERAL EFFECTS OF NEUROPEPTIDES

Neuropeptides have extensive influences on bodily functions and this view is illustrated further in the current topic. Zhang J. et al. or demonstrated that the neuropeptide substance P released from primary sensory fibers promotes proliferation of adult pancreatic ductal cells—one of the important sources of pancreatic islet β-cell neogenesis—but not their differentiation into β-cells. The observed effect of substance P involves the NK-1 receptor and Wnt signaling pathway. This finding indicates that lack of substance P may be a possible risk factor for diabetes development (Zhang N. et al.).

The review by Wang et al., comprehensively demonstrated the therapeutic potential of OT in atherosclerotic cardiovascular disease and the underlying mechanisms and signaling pathways. This review first linked atherosclerosis with varieties of immunometabolic disorders that can suppress OT receptor

(OTR) signaling in the cardiovascular system (CVS). Next, the authors discussed evidence for this and the cellular and molecular mechanisms underlying CVS protective effects of OT. Finally, the authors also presented evidence for OT-evoked cardiovascular disturbance and the strategy for applying OT safely in clinical practice.

RECEPTOR SIGNALING

Different hormones can have multiple receptors and the effects of activating a specific receptor rely on specific signaling events. The report by Ding et al. showed that activation of the G protein-coupled estrogen receptor (GPER) elicits the release from calcium stores and phosphorylation of the mu-opioid receptor by regulating reproduction and metabolism in human neuroblastoma cells. Activation of GPER is followed by rapid calcium mobilization, translocation, and activation of protein kinase C-α and -ε at the plasma membrane leading to mu-opioid receptor phosphorylation. The GPER-mediated rapid calcium signal may also transmit to the nucleus to impact on gene transcription (Ding et al.). Such a signaling cascade may play an important role in the regulation of opioid signaling in the brain.

The review by Wang et al., discussed cellular and molecular mechanisms underlying cardiovascular protective effects of OT. The OT receptor signals mainly belong to the reperfusion injury salvage kinase pathway composed of PI3K-Akt-endothelial nitric oxide synthase cascades and extracellular signal-regulated protein kinase 1/2 (ERK 1/2). Additionally, AMP-activated protein kinase, Ca^{2+}/calmodulin-dependent protein kinase signaling, and many others can influence OTR signaling related to cardiovascular protection. These signaling events coordinate at many levels to suppress metabolic disorders, reduce the production of inflammatory cytokines, and inhibit the activation of apoptotic pathways, particularly endoplasmic reticulum stress and mitochondrial oxidative stress. This comprehensive review expands our understanding of the immunoregulatory functions of OT.

DISEASE AND TREATMENT

Neuroendocrine studies have established the involvement and treatment effects of neuropeptides in a variety of diseases. In their study, Ma et al. found for the first time that the expression of OT and OTR declines in human colorectal tissues as malignancy of colorectal cancer (CRC) increases. They reported that OT can suppress the expression of tumor-associated immunosuppressive proteins fibroblast activation protein-α (FAPα) and chemokine (C-C motif) ligand 2 (CCL-2). The reduction in OT-OTR expression can unleash the expression of FAPα and CCL-2 and, thus, facilitates CRC metastasis. Importantly, OT can reduce the invasion ability of human CRC cells. Although the authors limited their findings to colorectal adenocarcinoma, the therapeutic potential of directly applying OT to inhibit CRC migration is worthy of further exploration.

The report by Zhu et al., studied the spatial distribution patterns of primary age-related tauopathy (PART) in subcortical nuclei, including the neuroendocrine hypothalamus of post-mortem human brains. They found that the prevalence and severity of tau pathology in subcortical nuclei of PART and AD positively correlate with the stage of NFT Braak neurofibrillary tangles, suggesting that these nuclei are increasingly involved as PART and AD progress. Thus, these subcortical nuclei are probably the sites initially affected by aging associated tau pathology, especially brainstem nuclei.

Zou et al., reviewed the role of leptin in mood disorders and neurodegenerative diseases and summarized findings that leptin can improve learning and memory, affect hippocampal synaptic plasticity, exert neuroprotective efficacy, and reduce the risk of several neuropsychiatric diseases, including depression. These effects are associated with leptin regulation of the release of neurotransmitters and neurotrophic factors and can reverse dysfunction in the HPA axis.

Sheng et al. demonstrated an involvement of mitogenic signaling in the regulation of thyroid proliferation by insulin glargine and human insulin. Their results show that therapeutic doses of glargine do not stimulate thyroid cell proliferation, despite longer-lasting hypoglycemic control than human insulin. However, high doses of these insulin products can stimulate thyroid cell proliferation, which should therefore be a consideration in the clinical use of insulin glargine.

OTHERS

The topic also includes neuroendocrine studies in other associated research areas. Liu L. L. et al. reported CSF metabolite profiles in neurosyphilis patients following an untargeted metabolomics analysis. These differential metabolites may potentially improve neurosyphilis diagnostics in the future and deserve further exploration. Xiao et al. demonstrated that prenatal ethanol exposure produces age-dependent changes in glucose metabolism, pancreatic morphology, and function in male offspring rats. This intrauterine programming alteration in the GC-IGF1 axis may contribute to prenatal and postnatal pancreatic dysplasia and impaired insulin biosynthesis in male offspring.

In addition, Wu R. et al. presented research suggesting that brief mindfulness meditation can significantly improve emotion processing. The beneficial effect correlates with reduced activity of the HPA-axis and stress responses (Wu R. et al.). The report by Zhang J. et al. revealed that voluntary wheel running reverses deficits in social behavior following chronic social defeat stress in mice due to the reversal of reduced levels of tyrosine hydroxylase in the ventral tegmental area and the D2 receptor in the nucleus accumbens shell.

Taken together, our topic submissions demonstrate that Chinese neuroendocrine researchers are contributing significantly to the field of neuroendocrinology. While many challenges remain, the growth of a new generation of Chinese neuroendocrine researchers will, we hope, result in even stronger contributions to novel approaches, concepts, and principles in both fundamental and clinical neuroendocrine research.

AUTHOR CONTRIBUTIONS

All six authors contributed to organizing the Research Topic, in which XC has taken the most editorial assignments. Y-FW wrote the first draft, all participated in the correction of this editorial and KK made the final revision.

ACKNOWLEDGMENTS

We thank Drs. Pierrette Gaudreau, Sebastien G. Bouret, Lee E. Eiden, and James A. Carr for participation in the editorial process and Dr. Benjamin C. Nephew and the many other reviewers for their valuable contributions to the quality of our accepted papers.

Conflict of Interest: The authors declare that the research was conducted in the absence of any commercial or financial relationships that could be construed as a potential conflict of interest.

frontiers in Endocrinology

ORIGINAL RESEARCH
published: 25 September 2018
doi: 10.3389/fendo.2018.00572

Oxytocin Facilitates Empathic- and Self-embarrassment Ratings by Attenuating Amygdala and Anterior Insula Responses

YaYuan Geng, Weihua Zhao, Feng Zhou, Xiaole Ma, Shuxia Yao, Benjamin Becker and Keith M. Kendrick**

MOE Key Laboratory for Neuroinformation, Clinical Hospital of Chengdu Brain Science Institute, University of Electronic Science and Technology of China, Chengdu, China

The hypothalamic neuropeptide oxytocin has been reported to enhance emotional empathy in association with reduced amygdala activation, although to date studies have not investigated empathy for individuals expressing self-conscious, moral emotions which engage mentalizing as well as emotion processing networks. In the current randomized, double-blind placebo controlled functional MRI experiment in 70 male and female subjects we have therefore investigated the effects of intranasal oxytocin (40 IU) on behavioral and neural responses to embarrassment experienced by others or by self. Results showed that oxytocin significantly increased ratings of both empathic and self-embarrassment and concomitantly decreased skin conductance response, activation in the right amygdala and insula but not in the medial prefrontal cortex. The amygdala effects of oxytocin were associated with the magnitude of the skin conductance response and trait anxiety scores. Overall our results demonstrate that oxytocin increases ratings of self- and other embarrassment and that this is associated with reduced physiological arousal and activity in neural circuits involved in emotional arousal. The neural effects of oxytocin were more pronounced stronger in individuals with high trait anxiety suggesting that it may particularly reduce their anxiety in embarrassing situations.

Keywords: oxytocin, empathy, embarrassment, anxiety, insula, amygdala, prefrontal cortex, sex differences

OPEN ACCESS

Edited by:
James A. Carr,
Texas Tech University, United States

Reviewed by:
Ben Nephew,
Worcester Polytechnic Institute, United States
Aldo Lucion,
Universidade Federal do Rio Grande do Sul (UFRGS), Brazil

****Correspondence:***
Benjamin Becker
ben_becker@gmx.de
Keith M. Kendrick
k.kendrick.uestc@gmail.com

Specialty section:
This article was submitted to Neuroendocrine Science, a section of the journal Frontiers in Endocrinology

Received: *12 June 2018*
Accepted: *06 September 2018*
Published: *25 September 2018*

Citation:
Geng Y, Zhao W, Zhou F, Ma X, Yao S, Becker B and Kendrick KM (2018) Oxytocin Facilitates Empathic- and Self-embarrassment Ratings by Attenuating Amygdala and Anterior Insula Responses. Front. Endocrinol. 9:572. doi: 10.3389/fendo.2018.00572

INTRODUCTION

Our ability to empathize with others is a core feature influencing our social behavior through allowing us to understand both what others are thinking and feeling and thereby promoting our social interactions with them. As such, impaired ability to empathize with others is often a core feature of disorders where social communication and interactions are dysfunctional, such as autism spectrum disorders (1), depression (2) and psychopathy (3).

Even though empathy has been extensively investigated, its sub-components and associated neural mechanisms are still not fully established (4). The most prevalent view considers empathy as a multidimensional construct including both cognitive (identifying emotions expressed by another person) and emotional components (being aroused by or feeling the same emotion expressed by another person) (5). Meta-analytic data has suggested that a network including left orbital frontal cortex, left anterior mid-cingulate cortex, left anterior insula and left dorsal medial thalamus is

involved in cognitive-evaluative empathy, whereas another network including the dorsal anterior cingulate cortex, bilateral anterior insula, right dorsal medial thalamus and midbrain is involved in affective-perceptual empathy (6). Studies that directly compared the two empathy components additionally proposed that the inferior frontal gyrus is essential for emotional empathy, whereas the superior and middle frontal gyrus and the orbital gyrus are specifically engaged in cognitive empathy (7). However, the derived empathy network can differ dependent upon the paradigm used (4) thus making it important to establish a core network that is maintained across different paradigms.

The hypothalamic neuropeptide oxytocin (OXT) has been implicated in a number of crucial aspects of social cognition and emotional bonds (8, 9) and importantly studies have reported that it can enhance components of empathy (10–12). The most consistent findings have been in studies using paradigms that distinguish cognitive from emotional empathy components. For example, in male Caucasian subjects OXT was found to enhance both direct and indirect aspects of emotional empathy, but not cognitive empathy *per se*, in the Multifaceted Empathy Task (MET) (12). Urbach-Wiethe disorder patients with selective and complete bilateral amygdala-lesions also exhibited deficits in emotional but not cognitive empathy in the MET suggesting that the emotional empathy enhancing effects of OXT might be mediated by the amygdala (12). We recently confirmed these behavioral findings in Chinese male, as well as female subjects using a Chinese version of the MET and demonstrated that OXT effects on emotional empathy were associated with decreased amygdala activity and increased physiological arousal (10). Finally, another study using dynamic, empathy-inducing video clips in which protagonists expressed sadness, happiness, pain or fear demonstrated that OXT exerted no effects on cognitive empathy but selectively enhanced emotional empathy for fear (11). Thus, OXT may particularly enhance emotional empathy, although in the context of the strong modulatory influence of personal and social contextual factors on the specific effects of OXT (8, 13) it is important to extend these observations using other paradigms and contexts where empathic responses are evoked.

Some initial support for OXT also influencing aspects of cognitive empathy has been reported using the reading the mind in the eyes test (RMET) where participants identify from visual cues restricted to the eye regions which of four different complex emotions is being experienced by subjects. Thus, in one study OXT was reported to increase accuracy, particularly for more difficult items (14). However, subsequent studies found that OXT either only increased RMET accuracy for difficult items in individuals with low empathy scores (15) or generally only in individuals with lower socially proficiency associated with higher levels of maternal love withdrawal (16). Furthermore, a final comprehensive study failed to observe any effects of OXT on RMET performance even taking into account item difficulty, gender and valence and subject traits (17). Thus, evidence for OXT enhancing cognitive empathy using the RMET paradigm remains equivocal.

In the current double-blind, placebo-controlled study we therefore investigated whether OXT would enhance empathy in social situations involving more complex moral, "self-conscious," emotions such as embarrassment. Embarrassment is primarily a self-reflection and self-evaluative process which serves as a way to help humans adapt their behavior to social norms by punishing non-compliance to such norms with a negative emotional state (18). The neural pathways involved in embarrassment include both those controlling mentalizing and emotional arousal (19). Oxytocin has previously been shown to modulate activity in both of these networks in the context of processing self-referential information (mPFC–(20, 21)) and emotional stimuli [amygdala and anterior insula–(22–27)].

We can experience empathic-embarrassment (EE) toward others we see in embarrassing situations irrespective of whether they are familiar or not (28), and so in the current paradigm we investigated OXT effects on behavioral and neural responses to pictures depicting others in embarrassing situations. Additionally, we also asked subjects to imagine their own feelings if they experienced a similar situation themselves (i.e., self-embarrassment–SE). We reasoned that the latter self-related context would involve a stronger mentalizing component, although both contexts should have strong arousal components. On the behavioral level, we hypothesized that, in line with its enhancement of emotional empathy (10, 12), OXT would increase both EE and SE ratings. At the neural level we hypothesized that in line with previous findings, both in the context of emotional empathy (10) and responses to fear and other arousing stimuli (8, 24), OXT would decrease amygdala activity and also change that of the insula (22, 25–27). We additionally hypothesized that given the mentalizing component associated with embarrassment there would be involvement of the mPFC which could also be modulated by OXT given previous findings (20, 21), but in view of the greater self-orientation and mentalizing component in SE we additionally hypothesized that the effects of OXT on mPFC activation would be greater in this condition. We have previously shown that some behavioral and neural effects of OXT on empathy and other behaviors are associated with increased physiological arousal and modulated by autistic traits (10, 29). The neural effects of embarrassment are also modulated by anxiety (30) and autism (19). Thus, in the current study we also investigated the effects of OXT on physiological arousal as assessed by electrodermal activity and associations of its effects with autism and anxiety traits.

MATERIALS AND METHODS

Participants

A total of $n = 70$ participants were enrolled in the present randomized double-blind, placebo-controlled between-subject experiment. Participants were randomly assigned to receive OXT (40 International Units, IU) or placebo (PLC) intranasal treatment resulting in 35 participants (female $n = 17$) in the OXT treatment group and 35 (female $n = 15$) in the PLC treatment group. Both groups were of comparable age [mean ± STD, OXT: 22.03 ± 2.15; PLC: 21.86 ± 1.97; $p = 0.73$,$t_{(70)} = -0.35$], education [OXT: 16.09 ± 1.65; PLC: 15.89 ± 1.64; $p = 0.61$, $t_{(70)} = -0.51$], and gender distribution [$\chi^2(1) = 0.23$, $p = 0.63$]. All participants reported having no past / current physical,

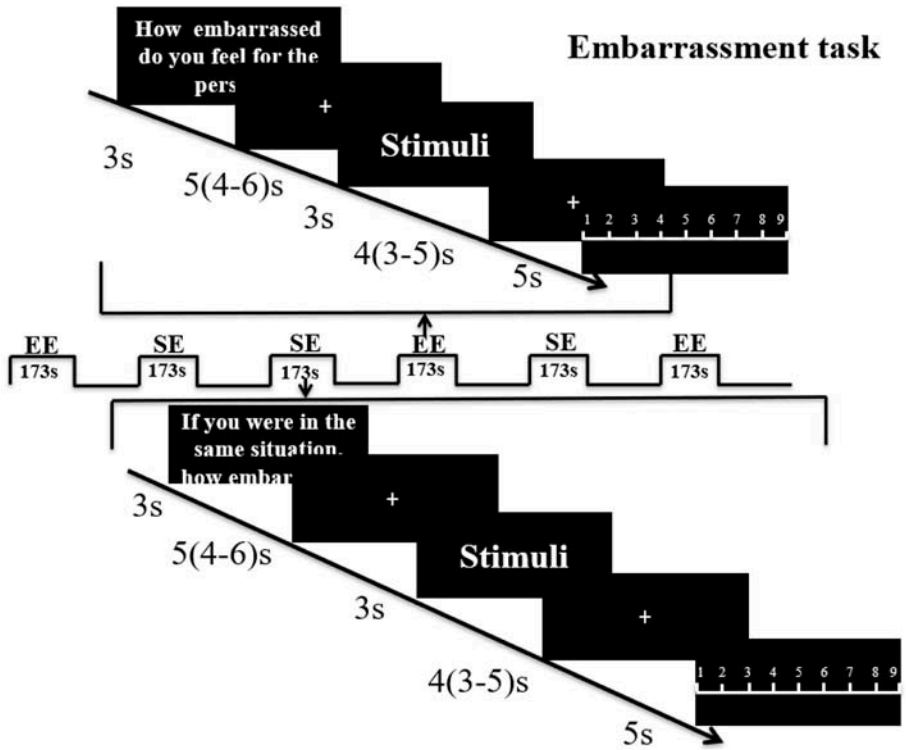

FIGURE 1 | Paradigm for the embarrassment task. Subjects were first shown an instruction for 3 s to indicate whether it was an empathic embarrassment (EE) or self-embarrassment (SE) trial followed by a jittered fixation cross (5 s mean duration with 4–6 s range. The picture stimulus was then presented for 3 s, followed by another fixation jittered mean duration of 4 s (range 3–5 s). A rating slide (1–9) was then shown for 5 s. Each run included one EE block and one SE block of 10 stimuli and the run order was counterbalanced using an ABBA design.

psychiatric or neurological disorders or regular/current use of medication or tobacco. Subjects were required to refrain from nicotine, alcohol or caffeine intake for at least 12 h before the experiment. None of the female participants were taking oral contraceptives or were in their menstrual period. The distribution of females estimated to be in their follicular or luteal phases did not differ significantly between the groups ($\chi^2 = 0.06$, $p = 1.00$). Written informed consent was obtained from each participant before the experiment. The study was approved by the ethical committee of the University of Electronic Science and Technology of China, and all procedures were in accordance with the latest revision of the declaration of Helsinki.

Experimental Paradigm

40 pictures depicting male or female protagonists (Chinese protagonists; 20 male, 20 female) in everyday embarrassing situations were evaluated by an independent sample ($n = 29$, 14 females) prior to the experiment to balance mean ratings for empathic embarrassment (EE–how embarrassed do you feel for the person in the picture?) and self-embarrassment (SE–if you were in the same situation, how embarrassed would you feel?) in response to the pictures and the gender of the protagonist (EE: females, 6.54 ± 1.14, males, 6.65 ± 0.89; SE: females, 7.91 ± 0.55, males, 7.58 ± 0.67). No significant differences were found with regard to both EE and SE ratings between male and female participants (EE, $p = 0.77$, $t = -0.30$; SE, $p = 0.17$, $t = 1.41$). For the fMRI experiment stimuli were presented in a mixed block/event related design during four subsequent runs. Each run containing one block of EE and one block of SE trials, with 10 trials of stimuli presented during each block. Each block started with a 3 s cue presentation indicating whether the subject was required to rate EE or SE. Within each block stimuli were presented for 3 s, followed by a jittered low-level baseline during which a fixation cross was presented for 4 s (3–5 s). After each stimulus, subjects were given 5 s to rate EE or SE using a 1–9 Likert rating scale (1 = not at all, 9 = very strong) followed by another 5 s (4–6 s) jittered inter-trial interval. An ABBA block-design was used to counterbalance the order of conditions (see **Figure 1** for paradigm details).

Procedure

To control for potential confounders, all participants completed a test battery of Chinese versions of mood and trait questionnaires before intranasal administration: Beck's Depression Inventory (BDI) (31), Emotional Intelligence Scale (Wleis-C) (32), Empathy Quotient (EQ) (33), Liebowitz Social Anxiety Scale (LSAS) (34) and Positive and Negative Affect Scale (PANAS) (35). Based on previous research reporting that individual variations in autism and anxiety influence (1) embarrassment-associated neural

activity (30), as well as (2) effects of OXT on embarrassment-related functional domains (e.g., emotional arousal, empathy and self-appraisal) and neural activity in embarrassment-related regions, including the insula (10, 29, 36–38), levels of anxiety and autism were assessed in the present sample. To this end, participants additionally completed the State Trait Anxiety Inventory (STAI) (39) and Autism Spectrum Quotient (ASQ) (40). Next, subjects self-administered intranasal spray (either 40IU of OXT or PLC lacking the neuropeptide, both supplied by the Sichuan Meike Pharmaceutical Co., Ltd, Sichuan, China). The PLC spray had identical packing and ingredients as the OXT spray (sodium chloride and glycerine, minus the peptide). In accordance with previous recommendations for the intranasal administration of OXT in humans (8, 41), the experimental paradigm started 45 min after treatment. In post-experiment interviews participants were unable to guess better than chance which treatment they had received (34 subjects guessed correctly; $\chi^2 = 0.22$, $p = 0.64$), confirming successful blinding.

During the experiment electrodermal activity was also measured to assess skin conductance responses (SCR) to the stimuli as an index of autonomic sympathetic activity (42) using the same approach as previously described (10). For the SCR data an event-related analysis approach was employed focusing on SCR responses associated with the presentation of SE and EE stimuli (procedures for preprocessing and event-related analysis of the SCR data were identical to our previous study, details provided in Geng et al. (10).

fMRI Acquisition

MRI data was acquired using a GE (General Electric Medical System, Milwaukee, WI, USA) 3T Discovery 750 MRI system with a standard head coil. fMRI time series were acquired using a T2*-weighted echo planar imaging pulse sequence (repetition time, 2,000 ms; echo time, 30 ms; slices, 39; thickness, 3.4 mm; gap, 0.6 mm; field of view, 240 × 240 mm^2; resolution, 64 × 64; flip angle, 90°). Additionally, a high resolution T1-weighted structural image was acquired using a 3D spoiled gradient recalled (SPGR) sequence (repetition time, 6 ms; echo time, 2 ms; flip angle 9°; field of view, 256 × 256 mm^2; acquisition matrix, 256 × 256; thickness, 1 mm without gap) to exclude subjects with apparent brain pathologies and to improve normalization of the fMRI data.

fMRI Data Processing

fMRI data were analyzed using SPM12 (Wellcome Trust Center of Neuroimaging, University College London, London, United Kingdom). The first five volumes were discarded from further analyses and images were realigned to the first image to correct for head motion using a six-parameter rigid body algorithm and unwarping. Tissue segmentation, bias-correction and skull-stripping were performed for the high-resolution structural images. Functional images were further corrected for slice-acquisition time differences, co-registered to the anatomical scan and subsequently spatially normalized to the standard Montreal Neurological Institute (MNI) template. The normalized functional volumes were written out at a 3 × 3 × 3 mm voxel size and were finally smoothed with an 8 mm full-width-at-half-maximum (FWHM) isotropic Gaussian kernel.

On the first level, separate event-related regressors for the EE and SE conditions were included as main regressors of interest. Additionally, separate regressors for the rating phases, the cue phase and the six head motion parameters were included. The regressors were convolved with the standard hemodynamic response function (HRF). To evaluate the sex-dependent effects of OXT on embarrassment an ANOVA including treatment (OXT, PLC), sex (male, female) as between-subject factors and embarrassment type (EE, SE) as a within-subject factor was conducted on the second level.

Based on previous studies indicating that regions involved in arousal (amygdala, anterior insula, AI) and mentalizing (mPFC) neurally underpin embarrassment processing a region-of-interest (ROI) analysis specifically focused on these regions. The amygdala was structurally defined based on masks from the Automated Anatomical Labeling (AAL) atlas (43). Given the size and functional heterogeneity of these regions, the ROIs for the mPFC and anterior insula (specifically dorsal AI, dAI) were defined using 6 mm spheres centered at peak coordinates of these regions reported in a previous study examining the neural basis of embarrassment (30). For the five a priori defined ROIs the first eigenvariate was extracted using Marsbar (44). The individual activity estimates were subsequently subjected to mixed ANOVAs with the between-subject factors treatment (OXT, PLC) and sex (male, female) and the within-subject factor embarrassment type (EE and SE) in SPSS (Statistical Package for the Social Sciences, Version 22). Multiple comparisons for the ROI analysis were controlled for by applying False Discovery Rate (FDR) correction. To explore effects in regions beyond the predefined ROIs an exploratory whole brain analysis was conducted in SPM using cluster-level Family-Wise Error (FWE) correction for multiple comparisons. In line with recent recommendations (45) for the control of false positives using cluster based methods (46) an initial cluster defining threshold of $p < .001$ (uncorrected) was applied to the data resampled at 3 mm voxel resolution. This voxel-wise analysis employed a flexible factorial design to model the mixed ANOVA computed on the extracted regional estimates and included the within-subject factor embarrassment type (EE and SE) and the between subject factors sex (male, female) and treatment (OXT, PLC). Due to limitations of the flexible factorial design to estimate between-subject main effects, the corresponding main effects of the between-subject factors were additionally examined using separate independent sample *t*-tests and appropriate first level contrasts. Significance level for the corrected *p*-values was $p < 0.05$.

RESULTS

No significant trait and mood differences were observed between participants in the OXT and PLC group (see **Supplementary Table S1**).

Behavioral and SCR Results

An ANOVA analysis with treatment and sex as between-subject factors, embarrassment context as a within-subject factor and embarrassment rating as dependent variable, revealed a significant treatment main effect [PLC: 6.45 ± 0.11, OXT: 6.77 ± 0.11, $F_{(1,66)} = 4.30$, $p = 0.04$, $\eta_p^2 = 0.06$] with OXT

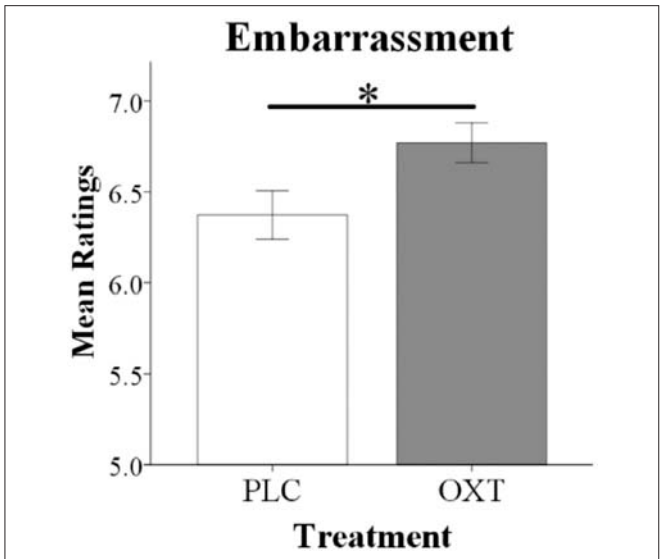

FIGURE 2 | Oxytocin significantly increased overall embarrassment ratings in behavioral tests. Histograms show mean ratings for EE and SE trials combined (*$p < 0.05$).

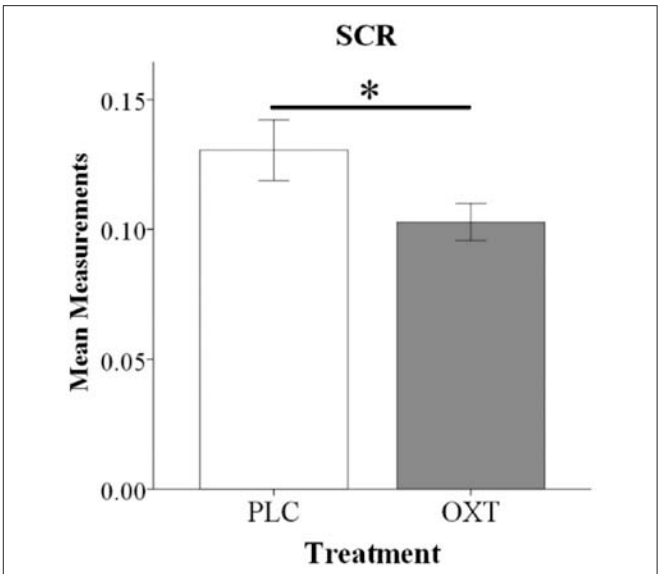

FIGURE 3 | Oxytocin reduced SCR magnitude during the embarrassment task. Histograms show mean SCR magnitude for EE and SE trials combined (*$P < 0.05$).

enhancing embarrassment ratings in both contexts (**Figure 2**). No significant interaction effects involving treatment were found [Sex * Treatment, $F_{(1,66)} = 2.20$, $p = 0.14$, $\eta_p^2 = 0.03$; Sex * Treatment * embarrassment context, $F_{(1,66)} = 0.09$, $p = 0.76$, $\eta_p^2 = 0.001$].

As a result of scanner-induced noise SCR data from $n = 12$ subjects had to be excluded (baseline readings could not be reliably obtained in >50% of trials) leading to a final sample size of $n = 58$ subjects for the SCR analysis ($n = 33$, OXT; $n = 25$, PLC). An ANOVA analysis including the same factors as for the behavioral analysis and SCR response as dependent variable revealed a significant main effect of treatment [$F_{(1,54)} = 7.35$, $p = 0.009$, $\eta_p^2 = 0.12$] with OXT decreasing the SCR magnitude in both EE and SE conditions (see **Figure 3**).

fMRI Results

For the ROI-based analysis we initially explored whether there were either effects of embarrassment type or gender in the PLC group. This revealed a main effect of embarrassment type in the mPFC [$F_{(1,33)} = 5.54$, $P_{FDR} = 0.04$, $\eta_p^2 = 0.14$] and in the amygdala [$F_{(1,33)} = 7.21$, $P_{FDR} = 0.01$, $\eta_p^2 = 0.18$] but not in the dAI. This confirmed our expectation that there would be a difference in activation in mentalizing in the SE compared to the EE condition and additionally that there was greater activation in the amygdala during EE compared to SE trials. Examination of OXT by comparing the OXT and the PLC treated groups revealed significant main effect of treatment on right amygdala [$F_{(1,66)} = 9.97$, $P_{FDR} = 0.01$, $\eta_p^2 = 0.10$] and right dAI [$F_{(1,66)} = 5.82$, $P_{FDR} = 0.03$, $\eta_p^2 = 0.08$] responses, with OXT reducing activity in both EE and SE contexts (see **Figure 4**). No interactions between treatment and gender and embarrassment type were found in these regions. The exploratory whole-brain analysis did not reveal significant main or interaction effects of treatment on the neural level ($P_{FWE} < 0.05$).

Correlation Between Behavioral, Physiological, and Neural Data and Trait Questionnaires

There was a negative association between overall embarrassment ratings (average of EE and SE) and STAI Trait scores in the OXT but not the PLC group (STAI Trait: PLC, $r = 0.06$, $p = 0.75$, OXT, $r = -0.34$, $p = 0.05$), suggesting that ratings were particularly increased under OXT in more anxious individuals. However, the correlation difference did not achieve significance (Fisher's Z-Test, $z = 1.66$, $p = 0.098$). For the neural data there was a similar negative association between right amygdala activation and STAI trait scores in the OXT group but not the PLC group (STAI Trait: PLC, $r = 0.13$, $p = 0.44$, OXT, $r = -0.35$, $p = 0.04$) and in this case the correlation difference was significant (Fisher's Z-Test, $z = 1.99$, $p = 0.05$) (see **Figure 5**). There was also a negative association between right amygdala activation and the magnitude of the SCR in the OXT group whereas in the PLC group there was a positive association (PLC, $r = 0.32$, $p = 0.12$, OXT, $r = -0.33$, $p = 0.06$; Fisher's Z-Test, $z = 2.40$, $p = 0.016$) (see **Figure 5**). In contrast, no significant associations between levels of autism (ASQ scores) and behavioral, SCR or neural effects were observed (all $ps > 0.15$).

DISCUSSION

The current experiment demonstrated for the first time that OXT increases both empathic- and self-embarrassment ratings in male and female subjects and that its behavioral effects are associated with decreased responses in the right amygdala and

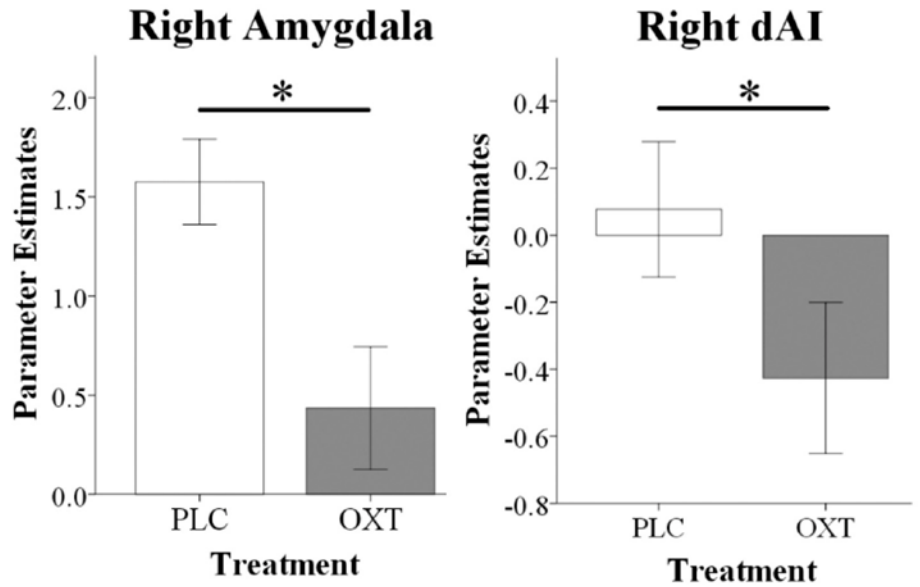

FIGURE 4 | fMRI analysis showing that oxytocin significantly reduced right amygdala and right dAI responses during EE and SE trials. Histograms show parameter estimates for EE and SE trials combined ($^{*}P < 0.05$).

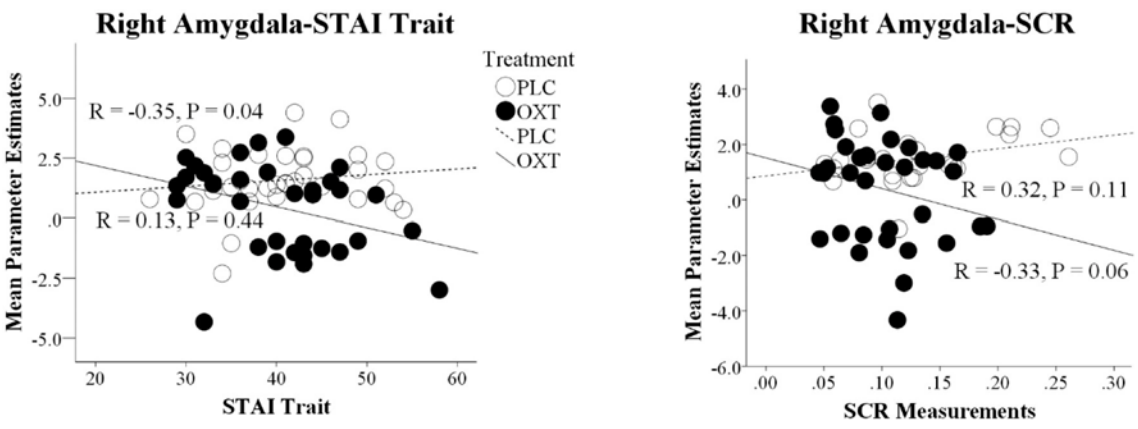

FIGURE 5 | Correlation differences between parameter estimates of right amygdala and trait anxiety scores (STAI Trait) and the magnitude of the skin conductance responses (SCR) in the placebo (PLC) and oxytocin (OXT) groups. Data from EE and SE trials are combined. In both cases the correlation difference between the OXT and PLC groups is significant (Fisher's Z-test $p < 0.05$).

in the right dAI and the magnitude of physiological arousal (SCR). On the other hand, OXT appeared to have no effects on responses in the mentalizing network (mPFC) during either of the embarrassment rating contexts. Furthermore, in contrast with the PLC group the effects of OXT in reducing amygdala responses were negatively correlated with both STAI trait scores and SCR magnitude, implying that it had an anxiolytic effect and particularly in individuals with higher trait anxiety.

Our ROI-based findings in the PLC group that empathic embarrassment primarily increases activation in both mentalizing (mPFC) and emotion processing (amygdala and insula) brain regions is consistent with previous studies (18, 19, 30). Our expectation that the mentalizing component in self- compared to empathic embarrassment would be different was also supported in terms of differential mPFC activation in the PLC group. The effects of OXT in both embarrassment contexts were however restricted to emotion processing regions with reduced amygdala activation, similar to our previous findings for emotional empathy (10) and additionally decreased insula activation. Thus, although a number of studies have reported effects of OXT on both dorsal and ventral mPFC activation in the context of self-vs. other referential and ownership contexts (20, 21) it would appear that this does not occur in self-vs. other-embarrassment. However, these previous studies demonstrating OXT effects on the mPFC in self-vs. other processing have shown that in both behavioral and neural term's it reduced the

normal self-bias. Thus, it is possible that OXT had no effects on the mPFC since EE and SE ratings were similar and there was therefore no indication of self-bias for embarrassment experience in the present paradigm.

In contrast to the lack of effects of OXT on self-vs. other processing in the mPFC it increased embarrassment across both, EE and SE in the context of attenuated amygdala and insula reactivity. Although EE trials produced stronger amygdala responses than SE ones following PLC, OXT suppressed them equivalently in both conditions. In line with the social salience hypothesis of OXT (47) the general enhancement of embarrassment may reflect an increased awareness and impact of the social context. However, previous studies reporting OXT-enhanced salience of external social stimuli commonly report decreased amygdala and concomitantly increased insula activity (9, 25, 48) which would be difficult to reconcile with the observed OXT-induced attenuation in both regions in the present study. Decreased insula activity following OXT has been previously observed in response to pain empathy (22), negative social feedback (49) and approach behavior (48). Moreover, in concert with concomitantly decreased amygdala activity attenuated stress in response to negative interactions (50) and reduced anxiety during social sharing (in women) have been reported (51). In line with these previous findings the suppression of both regions may thus rather reflect the stress-buffering or anxiolytic effects of OXT. Together with the hippocampus, the amygdala and insula are considered core nodes of the threat and anxiety circuitry (52, 53) and are hyperactive across anxiety disorders (52)–particularly social anxiety disorder (54). Moreover, successful non-pharmacological therapy for exaggerated anxiety has been accompanied by decreased hyperactivity in these regions (55, 56). The amygdala is also critically involvemed in emotional modulation of the SCR (57) and during OXT-enhanced empathy and protective responses suppression of amygdala reactivity was accompanied by increased SCR (10) and acoustic startle response (26). On the other hand, OXT decreased the SCR in response toward conditioned threat stimuli (58) and decreased autonomic stress reactivity (59). Moreover, increased activity in the dAI has been specifically associated with increased arousal during embarrassing social situations (30), however not embarrassment-related schadenfreude (60). Together, the pattern of decreased reactivity in the two threat nodes as well as the autonomic arousal measures during exposure to embarrassing, social-stressful situations may thus reflect anxiolytic effects of OXT. This interpretation is further supported by a negative association between amygdala activation and trait anxiety scores and the magnitude of the SCR in the OXT group suggesting that it reduced anxiety and particularly in more anxious individuals.

It seems paradoxical therefore that in the context or empathic and self-embarrassment OXT-reduced amygdala responses were associated with a decreased SCR and yet ratings were still increased. This demonstrates that OXT-induced reduction of amygdala activity per se is not sufficient to infer anxiolytic effects of OXT, and indeed another study has also reported that OXT can promote an anxiogenic response in the context of concomitantly reduced amygdala activation (25). It thus may be hypothesized that the insula plays an important role in shaping the specific behavioral effects of an unspecific OXT-attenuation of the amygdala. Whereas concomitantly increased insula activity may promote the salience-enhancing effects of OXT (25, 26, 48), a concomitant reduction may reflect anxiogenic or arousal reducing effects of OXT (22, 48, 49) which is in line with the contribution of the anterior insula to several functional domains including salience, and arousal (61, 62). The observed pattern of neural effects of OXT in the present study may thus favor an anxiolytic interpretation of its action during embarrassment processing. This may also reflect a reduction of the aversive and threatening affect evoked by the embarrassment stimuli and facilitate a more cognitive appraisal of the social contexts and their implications thus enhancing embarrassment levels across situations experienced both by others or by self.

Thus, OXT may have reduced the feelings of both pain and anxiety experienced during embarrassment, leading to a more cognitive assessment such that subjects rated the level of embarrassment experienced as higher. In this respect it should be noted that subjects in our task were asked to rate the level of embarrassment being experienced in a particular situation and not specifically to rate the intensity of their feelings for others in embarrassing situations, or of their own personal feelings in the self-condition. It is possible therefore that in the context of moral self-conscious emotions such as embarrassment, OXT may actually reduce emotional empathy toward others in order to promote a more accurate cognitive assessment of what someone is feeling. This might in turn promote more efficient avoidance of potential embarrassing situations in the future. Further experiments are required to disentangle these cognitive and emotional factors.

In our previous experiment using the MET task we observed that the OXT enhancement of emotional empathy ratings and reduced amygdala activity showed some associations with trait autism, however in the current study we did not find this. Previous studies have reported decreased responses in the anterior insula to social pain in adults with autism spectrum disorder (19), although not for empathic neural responses toward physical pain (63). However, we found no associations between neural responses to embarrassment and autistic traits in healthy subjects. On the other hand, we did find a negative association between trait anxiety and the effect of OXT on the amygdala and SCR, which contrasted with no such association in the PLC group. This suggested that OXT was particularly attenuating neural and behavioral indices of anxious arousal in subjects with high trait anxiety, and resonates with previous findings suggesting that OXT particularly reduced negative appraisal following social stress induction in high trait anxiety subjects (36). These observations conflict with a recent report on OXT-induced increased startle responsivity in high anxious subjects (38). However, in this previous study OXT specifically increased startle responsivity toward non-social stimuli, further emphasizing how complex interactions between personal and social contextual factors may moderate the specific effects of OXT.

No sex-differential effects were observed in the behavioral effects of OXT on embarrassment ratings or on right amygdala or right insula responses, which is consistent with our previous

observations that OXT enhanced emotional empathy in the MET in both sexes (10). These findings contrast with other studies reporting sex-dependent responses in amygdala and insula (23, 64) in the context of the impact of positive and negative personal characteristics on face attraction and sub-liminal processing of emotional faces. However, this may reflect the fact that exhibiting empathic-embarrassment and self-embarrassment are of equal adaptive importance in males and females and that OXT only tends to promote or amplify sex-differences in behavioral and neural responses associated with sex-specific priorities in social salience and social preference processing (see 22).

It is still unclear how intranasal administration of OXT exerts its neural and behavioral effects. While it has been questioned whether OXT administered via an intranasal spray does actually enter the cerebrospinal fluid (CSF) and influence brain OXT receptors (65) it is now established from work using labeled peptides in monkeys that it does enter into the CSF as well as the blood (66). In humans intranasal OXT does also increase CSF as well as blood OXT concentrations although with different time courses (67). It has still to be demonstrated however whether it can both enter the brain across the blood brain barrier from increased concentrations in the peripheral vasculature (66) and directly via the established lymphatic or other transport mechanisms at the back of the nasal cavity [see (8)]. Importantly however, despite some early studies in autistic subjects reporting behavioral effects of intravenous oxytocin (68, 69) recent studies have failed to find any behavioral or neural effects of intravenous compared with intranasal routes of administration (70, 71). Intranasal administration of OXT in humans also results in extensive increases in regional cerebral blood flow in the majority of brain regions containing OXT receptors at the same time course as routinely used in the current as well as most previous intranasal treatment studies (i.e., around 45 min)(72). Thus, in the context of the findings in the current experiment it is likely that functional effects of OXT on embarrassment and reduced physiological arousal, as well as those on the amygdala and insula, are caused primarily by its actions following entry into the brain, although we cannot rule out some contributions from indirect actions via receptors in peripheral organs.

Findings of the present study need to be interpreted in the context of limitations. Firstly, compared to previous studies that determined sex-differential neural effects of OXT during evaluation social-emotional stimuli the present sample was smaller [$n = 70$, previous studies enrolled slightly higher samples between around $n = 80$–90 subjects, (23, 64)]. The lack of sex-differential effects of OXT on embarrassment therefore needs to be replicated in larger samples. Secondly, our task did not adequately separate cognitive from emotional components of embarrassment in order to provide a better understanding of how OXT attenuation of both amygdala and insula responses resulted in increased ratings of embarrassment.

Overall therefore we have demonstrated for the first time that OXT can enhance ratings of both empathic and self-embarrassment in males and females, showing that it also influences moral, self-conscious emotional responses. These behavioral effects of OXT are associated with decreased physiological arousal and decreased responses in both the right amygdala and anterior insula, but not in mentalizing networks (mPFC). Furthermore, OXT effects on the amygdala are strongest in individuals with high trait anxiety. Thus, OXT in this context may be promoting an anxiolytic effect resulting in a more cognitive rather than emotional appraisal of embarrassment levels.

AUTHOR CONTRIBUTIONS

YG and KK designed this experiment, YG collected the data, YG, WZ, FZ, KK, and BB analyzed the data, YG, WZ, XM, SY, BB, and KK interpreted the results. YG, BB, and KK wrote the paper.

ACKNOWLEDGMENTS

This study was supported by the National Natural Science Foundation of China (NSFC) grant 563 (grants 31530032; 91632117), the Fundamental Research Funds for the Central Universities of China (ZYGX2015Z002) and the Sichuan Science and Technology Department (2018JY0001).

SUPPLEMENTARY MATERIAL

The Supplementary Material for this article can be found online at: https://www.frontiersin.org/articles/10.3389/fendo.2018.00572/full#supplementary-material

REFERENCES

1. Lombardo MV, Barnes JL, Wheelwright SJ, Baron-Cohen S. Self-referential cognition and empathy in autism. *PLoS ONE* (2007) 2:e883. doi: 10.1371/journal.pone.0000883
2. Tully EC, Ames AM, Garcia SE, Donohue MR. Quadratic associations between empathy and depression as moderated by emotion dysregulation. *J Psychol.* (2016) 150:15–35. doi: 10.1080/00223980.2014.992382
3. Ali F, Amorim IS, Chamorro-Premuzic T. Empathy deficits and trait emotional intelligence in psychopathy and Machiavellianism. *Pers Individ Dif.* (2009) 47:758–62. doi: 10.1016/j.paid.2009.06.016
4. Moya-Albiol L, Herrero N, Bernal MC. The neural bases of empathy. *Rev Neurol.* (2010) 50:89–100. doi: 10.1146/annurev.neuro.27.070203.144230
5. Shamay-Tsoory SG. The neural bases for empathy. *Neuroscientist* (2011) 17:18–24. doi: 10.1177/1073858410379268
6. Fan Y, Duncan NW, de Greck M, Northoff G. Is there a core neural network in empathy? An fMRI based quantitative meta-analysis. *Neurosci Biobehav Rev.* (2011) 35:903–11. doi: 10.1016/j.neubiorev.2010.10.009
7. Preston SD, Bechara A, Damasio H, Grabowski TJ, Stansfield RB, Mehta S, et al. The neural substrates of cognitive empathy. *Soc Neurosci.* (2007) 2:254–75. doi: 10.1080/17470910701376902
8. Kendrick KM, Guastella AJ, Becker B. Overview of human oxytocin research. *Curr Top Behav Neurosci.* (2017) 35:321–48. doi: 10.1007/7854_2017_19

9. Striepens N, Kendrick KM, Maier W, Hurlemann R. Prosocial effects of oxytocin and clinical evidence for its therapeutic potential. *Front Neuroendocrinol*. (2011) 32:426–50. doi: 10.1016/j.yfrne.2011.07.001
10. Geng Y, Zhao W, Zhou F, Ma X, Yao S, Hurlemann R, et al. Oxytocin enhancement of emotional empathy: generalization across cultures and effects on amygdala activity. *Front Neurosci*. (2018) 12:512. doi: 10.3389/fnins.2018.00512
11. Hubble K, Daughters K, Manstead A, Rees A, Thapar A, Van SG. Oxytocin increases attention to the eyes and selectively enhances self-reported affective empathy for fear. *Neuropsychologia* 106:350–57. doi: 10.1016/j.neuropsychologia.2017.10.019
12. Hurlemann R, Patin A, Onur OA, Cohen MX, Baumgartner T, Metzler S, et al. Oxytocin enhances amygdala-dependent, socially reinforced learning and emotional empathy in humans. *J Neurosci*. (2010) 30:4999–5007. doi: 10.1523/JNEUROSCI.5538-09.2010
13. Olff M, Frijling JL, Kubzansky LD, Bradley B, Ellenbogen MA, Cardoso C, et al. The role of oxytocin in social bonding, stress regulation and mental health: an update on moderating effects of context and interindividual differences. *Psychoneuroendocrinology* (2013) 38:1883–94. doi: 10.1016/j.psyneuen.2013.06.019
14. Domes G, Heinrichs M, Michel A, Berger C, Herpertz SC. Oxytocin improves "mind-reading" in humans. *Biol Psychiatry* (2007) 61:731–3. doi: 10.1016/j.biopsych.2006.07.015
15. Feeser M, Fan Y, Weigand A, Hahn A, Gärtner M, Böker H, et al. Oxytocin improves mentalizing–pronounced effects for individuals with attenuated ability to empathize. *Psychoneuroendocrinology* (2015) 53:223–32. doi: 10.1016/j.psyneuen.2014.12.015
16. Riem MME, Bakermans-Kranenburg MJ, Voorthuis A, van IJzendoorn MH. Oxytocin effects on mind-reading are moderated by experiences of maternal love withdrawal: an fMRI study. *Prog Neuropsychopharmacol Biol Psychiatry* (2014) 51:105–12. doi: 10.1016/j.pnpbp.2014.01.014
17. Radke S, de Bruijn ERA. Does oxytocin affect mind-reading? A replication study. *Psychoneuroendocrinology* (2015) 60:75–81. doi: 10.1016/j.psyneuen.2015.06.006
18. Melchers M, Markett S, Montag C, Trautner P, Weber B, Lachmann B, et al. Reality TV and vicarious embarrassment: an fMRI study. *Neuroimage* (2015) 109:109–17. doi: 10.1016/j.neuroimage.2015.01.022
19. Krach S, Müller-Pinzler L, Rademacher L, Sören Stolz D, Paulus FM. Neuronal pathways of embarrassment. *e-Neuroforum* (2016) 7:37–42. doi: 10.1007/s13295-016-0024-4
20. Zhao W, Yao S, Li Q, Geng Y, Ma X, Luo L, et al. Oxytocin blurs the self-other distinction during trait judgments and reduces medial prefrontal cortex responses. *Hum Brain Mapp*. (2016) 37:2512–27. doi: 10.1002/hbm.23190
21. Zhao W, Geng Y, Luo L, Zhao Z, Ma X, Xu L, et al. Oxytocin increases the perceived value of both self- and other-owned items and alters medial prefrontal cortex activity in an endowment task. *Front Hum Neurosci*. (2017) 11:272. doi: 10.3389/fnhum.2017.00272
22. Bos PA, Montoya ER, Hermans EJ, Keysers C, van Honk J. Oxytocin reduces neural activity in the pain circuitry when seeing pain in others. *Neuroimage* (2015) 113:217–24. doi: 10.1016/j.neuroimage.2015.03.049
23. Gao S, Becker B, Luo L, Geng Y, Zhao W, Yin Y, et al. Oxytocin, the peptide that bonds the sexes also divides them. *Proc Natl Acad Sci USA*. (2016) 113:7650–4. doi: 10.1073/pnas.1602620113
24. Kirsch P. Oxytocin modulates neural circuitry for social cognition and fear in humans. *J Neurosci*. (2005) 25:11489–93. doi: 10.1523/JNEUROSCI.3984-05.2005
25. Riem MME, Bakermans-Kranenburg MJ, Pieper S, Tops M, Boksem MAS, Vermeiren RRJM, et al. Oxytocin modulates amygdala, insula, and inferior frontal gyrus responses to infant crying: a randomized controlled trial. *Biol Psychiatry* (2011) 70:291–7. doi: 10.1016/j.biopsych.2011.02.006
26. Striepens N, Scheele D, Kendrick KM, Becker B, Schafer L, Schwalba K, et al. Oxytocin facilitates protective responses to aversive social stimuli in males. *Proc Natl Acad Sci USA*. (2012) 109:18144–9. doi: 10.1073/pnas.1208852109
27. Yao S, Becker B, Zhao W, Zhao Z, Kou J, Ma X, et al. Oxytocin modulates attention switching between interoceptive signals and external social cues. *Neuropsychopharmacology* (2017) 43:294–301. doi: 10.1038/npp.2017.189
28. Miller RS. Empathic embarrassment: situational and personal determinants of reactions to the embarrassment of another. *J Pers Soc Psychol*. (1987) 53:1061–9. doi: 10.1037/0022-3514.53.6.1061
29. Scheele D, Kendrick KM, Khouri C, Kretzer E, Schlapfer TE, Stoffel-Wagner B, et al. An oxytocin-induced facilitation of neural and emotional responses to social touch correlates inversely with autism traits. *Neuropsychopharmacology* (2014) 39:2078–85. doi: 10.1038/npp.2014.78
30. Müller-Pinzler L, Gazzola V, Keysers C, Sommer J, Jansen A, Frässle S, et al. Neural pathways of embarrassment and their modulation by social anxiety. *Neuroimage* (2015) 119:252–61. doi: 10.1016/j.neuroimage.2015.06.036
31. Beck AT. Beck Depression Inventory. *Depression* (1961) 2006:2–4. doi: 10.1093/ndt/gfr086
32. Wong C-S, Law KS. The effects of leader and follower emotional intelligence on performance and attitude: an exploratory study. *Leadersh Q*. (2002) 13:243–74. doi: 10.1016/S1048-9843(02)00099-1
33. Baron-Cohen S, Wheelwright S. The empathy quotient (EQ): an investigation of adults with asperger syndrome or high functioning autism and normal sex differences. *J Autism Dev Disord*. (2004) 34:163–75. doi: 10.1023/B:JADD.0000022607.19833.00
34. Liebowitz MR. Liebowitz social anxiety scale. *Mod Probl Pharmapsychiatry* (1987) 22:141–73.
35. Watson D, Clark LA, Tellegen A. Development and validation of brief measures of positive and negative affect: the PANAS scales. *J Pers Soc Psychol*. (1988) 54:1063–70.
36. Alvares GA, Chen NT, Balleine BW, Hickie IB, Guastella AJ. Oxytocin selectively moderates negative appraisals in high trait anxious males. *Psychoneuroendocrinology* (2012). 37:2022–31. doi: 10.1016/j.psyneuen.2012.04.018
37. Bartz JA, Zaki J, Bolger N, Hollander E, Lduwing NN, Kolevzon A, et al. Oxytocin selectively improves empathic accuracy. *Psychol Sci*. (2010) 21:426–8. doi: 10.1177/0956797610383439
38. Schumacher S, Oe M, Wilhelm FH, Rufer M, Heinrichs M, Weidt S, et al. Does trait anxiety influence effects of oxytocin on eye-blink startle reactivity? A randomized, double-blind, placebo-controlled crossover study. *PLoS ONE* (2018) 13:e0190809. doi: 10.1371/journal.pone.0190809
39. Spielberger CD, Gorsuch RL, Lushene RE. *Manual for the State-Trait Anxiety Inventory*. Pao Alto, CA (1970).
40. Baron-Cohen S, Wheelwright S, Skinner R, Martin J, Clubley E. The autism-spectrum quotient (AQ): evidence from Asperger syndrome/high-functioning autism, males and females, scientists and mathematicians. *J Autism Dev Disord*. (2001) 31:5–17. doi: 10.1023/A:1005653411471
41. Guastella AJ, Hickie IB, McGuinness MM, Otis M, Woods EA, Disinger HM, et al. Recommendations for the standardisation of oxytocin nasal administration and guidelines for its reporting in human research. *Psychoneuroendocrinology* (2013) 38:612–25. doi: 10.1016/j.psyneuen.2012.11.019
42. Stern RM, Ray WJ, Quigley KS. *Psychophysiological Recording*. Oxford: Oxford University Press (2001).
43. Tzourio-Mazoyer N, Landeau B, Papathanassiou D, Crivello F, Etard O, Delcroix N, et al. Automated anatomical labeling of activations in SPM using a macroscopic anatomical parcellation of the MNI MRI single-subject brain. *Neuroimage* (2002) 15:273–89. doi: 10.1006/nimg.2001.0978
44. Brett M, Anton J-L, Valabregue R, Poline J-B. Region of interest analysis using the MarsBar toolbox for SPM 99. *Neuroimage* (2002) 16:S497.
45. Slotnick SD. Cluster success: fMRI inferences for spatial extent have acceptable false-positive rates. *Cogn Neurosci.* (2017) 8:150–5. doi: 10.1080/17588928.2017.1319350
46. Eklund A, Nichols TE, Knutsson H. Cluster failure: why fMRI inferences for spatial extent have inflated false-positive rates. *Proc Natl Acad Sci USA*. (2016) 113:7900–05. doi: 10.1073/pnas.1602413113
47. Shamay-Tsoory SG, Abu-Akel A. The social salience hypothesis of oxytocin. *Biol Psychiatry* (2016) 79:194–202. doi: 10.1016/j.biopsych.2015.07.020
48. Yao S, Zhao W, Geng Y, Chen Y, Zhao Z, Ma X, et al. Oxytocin facilitates approach behavior to positive social stimuli via decreasing anterior insula activity. *Int J Neuropsychopharmacol*. (2018). doi: 10.1093/ijnp/pyy068. [Epub ahead of print].

49. Gozzi M, Dashow EM, Thurm A, Swedo SE, Zink CF. Effects of oxytocin and vasopressin on preferential brain responses to negative social feedback. *Neuropsychopharmacology* (2017) 42:1409–19. doi: 10.1038/npp.2016.248
50. Chen X, Hackett PD, DeMarco AC, Feng C, Stair S, Haroon E, et al. Effects of oxytocin and vasopressin on the neural response to unreciprocated cooperation within brain regions involved in stress and anxiety in men and women. *Brain Imaging Behav.* (2016) 10:581–93. doi: 10.1007/s11682-015-9411-7
51. Ma X, Zhao W, Luo R, Zhou F, Geng Y, Xu L, et al. Sex- and context-dependent effects of oxytocin on social sharing. *Neuroimage* (2018) 183:62–72. doi: 10.1016/j.neuroimage.2018.08.004
52. Etkin A, Wager TD. Functional neuroimaging of anxiety: a meta-analysis of emotional processing in PTSD, social anxiety disorder, and specific phobia. *Am J Psychiatry* (2007) 164:1476–88. doi: 10.1176/appi.ajp.2007.07030504
53. Williams LM. Defining biotypes for depression and anxiety based on large-scale circuit dysfunction: a theoretical review of the evidence and future directions for clinical translation. *Depress Anxiety* (2017) 34:9–24. doi: 10.1002/da.22556
54. Brühl AB, Delsignore A, Komossa K, Weidt S. Neuroimaging in social anxiety disorder—a meta-analytic review resulting in a new neurofunctional model. *Neurosci Biobehav Rev*. (2014) 47:260–80. doi: 10.1016/j.neubiorev,.2014.08.003
55. Li Y, MengY, Yuan M, Zhang Y, Ren Z, Zhang Yet al. Therapy for adult social anxiety disorder: A meta-analysis of functional neuroimaging studies. *J Clin Psychiatry* (2016) 77:e1429–38. doi: 10.4088/JCP.15r10226
56. Goossens L, Sunaert S, Peeters R, Griez EJ, Schruers KR. Amygdala hyperfunction in phobic fear normalizes after exposure. *Biol Psychiatry* (2007) 62:1119–25. doi: 10.1016/j.biopsych.2007.04.024
57. Becker B, Mihov Y, Scheele D, Kendrick KM, Feinstein JS, Matusch A, et al. Fear processing and social networking in the sbsence of a functional amygdala. *Biol Psychiatry* (2012) 72:70–7. doi: 10.1016/j.biopsych.2011.11.024
58. Eckstein M, Scheele D, Patin A, Preckel K, Becker B, Walter A, et al. Oxytocin facilitates Pavlovian fear learning in males. *Neuropsychopharmacology* (2015) 41:932–9. doi: 10.1038/npp.2015.245
59. Heinrichs M, Baumgartner T, Kirschbaum C, Ehlert U. Social support and oxytocin interact to suppress cortisol and subjective responses to psychosocial stress. *Biol Psychiatry* (2003) 54:1389–98. doi: 10.1016/S0006-3223(03)00465-7
60. Paulus FM, Müller-Pinzler L, Stolz DS, Mayer AV, Rademacher L, Krach S. Laugh or cringe? Common and distinct processes of reward-based schadenfreude and empathy-based fremdscham. *Neuropsychologia* (2018) 116:52–60. doi: 10.1016/j.neuropsychologia.2017.05.030
61. Cauda F, Costa T, Torta DME, Sacco K, Duca S, D'Agata F, et al. Meta-analytic clustering of the insular cortex: characterizing the meta-analytic connectivity of the insula when involved in active tasks. *Neuroimage* (2012) 62:343–55. doi: 10.1016/j.neuroimage.2012.04.012
62. Berntson GG, Norman GJ, Bechara A, Bruss J, Tranel D, Cacioppo JT. The insula and evaluative processes. *Psych Sci*. (2011) 22:80–6. doi: 10.1177/0956797610397
63. Hadjikhani N, Zürcher NR, Rogier O, Hippolyte L, Lemonnier E, Ruest T, et al. Emotional contagion for pain is intact in autism spectrum disorders. *Transl Psychiatry* (2014) 4:e343. doi: 10.1038/tp.2013.113
64. Luo L, Becker B, Geng Y, Gao S, Zhao W, Yao S, et al. Sex-dependent neural effect of oxytocin during subliminal processing of negative emotional faces. *Neuroimage*. (2017) 162:127–37. doi: 10.1016/j.neuroimage.2017.08.079
65. Leng G, Ludwig M. Intransasal oxytocin: myths and delusions. *Biol Psychiatry* (2016) 79:243–50. doi: 10.1016/j.biopsych.2015.05.003
66. Lee MR, Scheidweiler KB, Dioao XX, Akhlaghi F, Cummins A, Huestis MA, et al. Oxytocin by intranasal and intravenous routes reaches the cerebrospinal fluid in rhesus macaques: determination using a novel oxytocin assay. *Mol Psychiatry* (2018) 23:115–22. doi: 10.1038/mp.2017.27
67. Striepens N, Kendrick KM, Hanking V, Landgraf R, Wüllner V, Maier W, et al. Elevated cerebrospinal fluid and blood concentrations of oxytocin following its intranasal administration in humans. *Sci Rep*. (2013) 3:3440. doi: 10.1038/srep03440
68. Hollander E, Novotny S, Hanratty M, Yaffe R, DeCaria CM, Aronowitz BR, et al. Oxytocin infusion reduces repetitive behaviors in adults with autistic and Asperger's disorders. *Neuropsychopharmacology* (2003) 28:193–8. doi: 10.1038/sj.npp.1300021
69. Hollander E, Bartz J, Chaplin W. Phillips A, Sumner J, Soorya L, et al. Oxytocin increases retention of social cognition in autism. *Biol Psychiatry* (2007) 61:498–503. doi: 10.1016/j.biopsych.2006.05.030
70. Quintana DS, Alvares GA, Hickie IB, Guastella AJ. Do delivery routes of intranasally administered oxytocin account for observed effects on social cognition and behavior? A two-level model. *Neurosci Biobehav Rev*. (2015) 49:182–92. doi: 10.1016/j.neubiorev.2014.12.011
71. Quintana DS, Westlye LT, Alnæs D, Rustan ØG, Kaufmann T, Smerud KT, et al. Low dose intranasal oxytocin delivered with Breath Powered device dampens amygdala response to emotional stimuli: a peripheral effect-controlled within-subjects randomized dose-response fMRI trial. (2016) *Psychoneuroendocrinology* 69:180–8. doi: 10.1016/j.psyneuen.2016.04.010
72. Paloyelis Y, Doyle OM, Zelaya FO, Maltezos S, Williams SC, Fotopoulou A, et al. A spatiotemporal profile of *in vivo* cerebral blood flow changes following intranasal oxytocin in humans. *Biol Psychiatry* (2016) 79:693–705. doi: 10.1016/j.biopsych.2014.10.005

Conflict of Interest Statement: The authors declare that the research was conducted in the absence of any commercial or financial relationships that could be construed as a potential conflict of interest.

frontiers in Neuroscience

ORIGINAL RESEARCH
published: 05 November 2018
doi: 10.3389/fnins.2018.00806

Effects of Neuropeptide Substance P on Proliferation and β-Cell Differentiation of Adult Pancreatic Ductal Cells

*Nan Zhang, Di Gao, Yudan Liu, Sihan Ji and Lei Sha**

Department of Neuroendocrine Pharmacology, School of Pharmacy, China Medical University, Shenyang, China

Purpose: The pancreas is innervated by sensory nerves, parasympathetic and sympathetic nerves. The classical neurotransmitters, acetylcholine and noradrenaline, and some kind of neuropeptides are contained in the terminals of these nerves. Neuropeptides substance P (SP) and calcitonin gene-related peptide (CGRP) co-released from the primary sensory fibers have been identified as the key neurotransmitters in pancreas. Pancreatic ductal epithelium cells are one of the important sources of the pancreatic islet β-cell neogenesis. We hypothesized that SP and CGRP might play a role on proliferation of ductal cells and differentiation of ductal cells toward the β-cell neogenesis.

Methods: Primary ductal cells of rat pancreas at the third passage (P3) were used. The identification of P3 cells were confirmed with flow cytometry analysis and immunostaining by CK19 (the ductal cell marker). Proliferation of ductal cells was verified by CCK-8 assay and Ki67 immunostaining. Differentiation of ductal cells was determined with immunostaining and flow cytometry. Possible mechanism was explored by testing the key proteins of Wnt signaling using Western blot analysis.

Results: Our data showed that SP but not CGRP promoted proliferation of ductal cells. Moreover, NK-1 receptor antagonist L-703,606 blocked the SP-induced stimulation of proliferation. The results of Western blot analysis showed that L-703,606 attenuated the effects of substance P on NK1R, GSK-3β, and β-catenin expression. However, SP did not directly induce the differentiation of ductal cells into β-cells, and did not promote the progression of ductal cells to differentiate into more insulin-produced cells in induction medium.

Conclusions: These findings suggested that SP but not CGRP promoted proliferation of adult pancreatic ductal cells. SP promoted proliferation of ductal cells but not differentiation into β-cells. NK1R and Wnt signaling pathway might be involved in the mechanism of promoting the proliferation of ductal cells by SP. Findings in this study indicated the lack of SP might be a possible indicator for the initial of diabetes. SP could also be used as a drug candidate for the treatment of diabetes.

Keywords: Substance P, calcitonin gene-related peptide, pancreatic ductal cells, proliferation, β-cell differentiation, NK-1 receptor

OPEN ACCESS

Edited by:
Lee E. Eiden,
National Institutes of Health (NIH), United States

Reviewed by:
Eberhard Weihe,
Philipps-Universität Marburg, Germany
Terry Moody,
National Cancer Institute (NCI), United States

****Correspondence:***
Lei Sha
lsha@cmu.edu.cn

Specialty section:
This article was submitted to Neuroendocrine Science, a section of the journal Frontiers in Neuroscience

Received: *30 June 2018*
Accepted: *16 October 2018*
Published: *05 November 2018*

Citation:
Zhang N, Gao D, Liu Y, Ji S and Sha L (2018) Effects of Neuropeptide Substance P on Proliferation and β-Cell Differentiation of Adult Pancreatic Ductal Cells. Front. Neurosci. 12:806. doi: 10.3389/fnins.2018.00806

INTRODUCTION

The β-cell mass is dynamic and is regulated to maintain glucose homeostasis in response to the changes in physiological and pathological demands (Bonner-Weir, 2000; Halban et al., 2010; Juhl et al., 2010). When the demand for insulin is increased, the β-cell mass is expanded by replication and/or hypertrophy of pre-existing β-cells (Dor, 2006), and β-cell neogenesis from pancreatic progenitor cells located in duct epithelial cells or surrounding centroacinar cells/terminal ductules (Bonner-Weir et al., 2010). Therefore, strategies targeted to improve proliferation or differentiation of ductal cells may lead to improvements in the alleviation of β-cell loss pathology.

Pancreatic ductal cells are a part of exocrine component of pancreas and can act as pancreatic stem cells and the progenitor cells of islet β cells. In injured adult mouse pancreas, β-cell progenitors located in the ductal lining were activated (Xu et al., 2008). Several *in vitro* studies have shown that adult pancreatic ductal cells can differentiate into insulin-producing cells (Fukazawa et al., 2006; Seeberger et al., 2006; Li et al., 2011). Proliferating pancreatic ductal epithelium cells were induced to differentiate into β-cells with TNF-like weak inducer of apoptosis (Wu et al., 2013). Expanded pancreatic ductal cells also differentiated into insulin-producing β-cells in an appropriate environment (Rovira et al., 2010). Capacity of self-renewal and pluripotency is an important feature of stem cells. Despite the differentiation capability of ductal cells has been demonstrated, the proliferation potential and the possible factors controlling of growth in these cells is not well-understood.

The importance of the nervous system in maintaining body homeostasis has previously been described, and it is suggested that organogenesis and tissue repair are under neural control (Besedovsky and del Rey, 1996). There is increasing evidence that neuroendocrine-remodeling does take place in the pancreatic islets of diabetic disease models (Persson-Sjögren et al., 2005; Razavi et al., 2006). Two neuropeptide substance P (SP) and calcitonin gene-related peptide (CGRP) have been found to tightly link to the development of diabetes. SP mediates insulin secretion and plays an important role in the development of type I diabetes (Razavi et al., 2006). CGRP is also involved in the activity of insulin secretion and contributes to the development of type II diabetes (Gram et al., 2007; Tanaka et al., 2011). SP and CGRP fibers not only innervate islets, but also innervate pancreatic ducts (Razavi et al., 2006; Gram et al., 2007), suggesting that SP and CGRP might modulate the activity of pancreatic ducts. We hypothesized that the innervations of the primary sensory fibers to the pancreatic ducts play a role on ductal epithelium cells proliferation and differentiation toward the β-cell neogenesis.

In the present study we investigated the effects of SP and CGRP on primary cultured ductal cells of rat pancreas. We examined the effects of SP and CGRP on proliferation of pancreatic ductal cells, and further the effect of SP on differentiation of ductal cells toward β-cells. Moreover, we investigated the possible mechanism of the proliferative promotion effects of SP.

MATERIALS AND METHODS

Animals

Sprague Dawley rats (male, 2 months old) were purchased from the Animal Center of China Medical University. All animal protocols were approved by the Animal Care Commitee in China Medical University (Shenyang, China) and performed according to institutional guidelines.

Preparation of Substance P (SP) and Calcitonin Gene Related Peptide (CGRP)

SP was purchased from Millipore Co. (Catalog number: 05-23-0600-1MGCN, Billerica, MA, USA), CGRP was gained from Bioss Co. (Catalog number: bs-0791P, Beijing, China), and both kept protected from light during the experiments. Stock solution of SP (1 mg/ml) and CGRP (1 mg/ml) were dissolved in distilled water and stored at −20°C.

Primary Culture and Identification of Pancreatic Ductal Cells

Adult Sprague Dawley rats were sacrificed and the pancreases were rapidly removed. Pancreases were then dissociated with V collagenase (1.5 g/L). The digested tissues were triturated through 600 μm cell strainer to obtain primary ductal cells. The cultures were grown in the complete medium containing DMEM/F12 supplemented with 10% fetal bovine serum (FBS), 100 U/ml Penicillin and 100 μg/ml Streptomycin (all from Gibco) at 37°C in a humidified atmosphere with 5% CO_2. The medium was changed 24 h after, and the non-adherent cells were discarded. The attached cells were labeled P0, and the medium was changed again every 3 days. When cells became 90% confluent, cultures were dissociated with trypsin (1 ml 0.25% trypsin) at 37°C 2–3 min, and serum was used to inactivate the enzyme. Cells were then expanded at the third passage (P3) for purification. Cells were characterized for the ductal cell marker cytokeratin19 (CK19) by immunocytochemistry and flow cytometry.

Cells were plated at a density of 1.0×10^5 cells/ml and cultured. At day 1, 3, 5, 7, and 9. Cells in each well were collected and counted by hemocytometer. At least 6 wells were assessed at each time point. Growth curve was designed to reveal the self-renewal capacity of the cells.

Assay for Proliferation of Ductal Cells

Disassociated ductal cells at 3rd passage (P3) were plated in 96 well-plates at a density of around 1.0×10^5 cells per well. The cells were divided into groups randomly and treated with saline (1 mM) or serial concentrations of SP (10^{-6}, 10^{-5}, 10^{-4}, 10^{-3}, 10^{-2}, 10^{-1}, 1, and 10 μM; $n = 6$ wells for each) or CGRP (10^{-6}, 10^{-5}, 10^{-4}, 10^{-3}, 10^{-2}, 10^{-1}, 1, and 10 μM; $n = 6$ wells for each) for 3 days. In the other experiment, cells were treated with SP or SP plus L-703,606 (1, 2, 4, 6, 8, 10 μM) for 3 days. The medium containing SP or CGRP was changed every 24 h to ensure the concentration of neuropeptides in the medium. After treatments, cell viability was determined by CCK-8 test. Briefly, the cells were incubated with 10 μl CCK-8 (Invitrogen) at 37°C for 4 h. Absorbance at 490 nm was determined with a microplate reader

(Thermo Fisher Scientific Inc., USA). The results were presented as percentages of the value of normal control cells.

The proliferation potential of ductal cells was tested by Ki67 immunostaining after treated with serial doses of SP (10^{-3}, 10^{-2}, 10^{-1}, and 1 μM $n = 6$ wells for each) with or without L-703,606 (2 μM) for 3 days. The medium containing SP was changed every 24 h. Cells were fixed with 4% paraformaldehyde and then incubated with primary antibody at 4°C overnight. The primary antibodies used were as follows: mouse anti CK19 (1:100; Proteintech, Wuhan, China) and rabbit anti Ki67 (1:50, Abcam, Cambridge, UK), rabbit anti NK1R (1:100) and mouse anti Ki67 (1:100, All from Bioss, Beijing, China). After rinsing with PBS, cells were incubated with Cy3 or FITC-conjugated secondary antibodies (1:200; all from Jackson ImmunoResearch Lab, West GroveCity, PA, USA) at room temperature for 1 h. Immunofluorescence controls were performed without primary antibodies. The cells were covered with mounting medium (Vector Laboratories, Burlingame, CA, USA) containing DAPI (0.5 μg/mL; Sigma, St. Louis, MO, USA). Results were visualized with fluorescence microscopy (Nikon Eclipse E600; Nikon Corporation, Tokyo, Japan). Cells were counted in triplicate cultures in ten randomly chosen areas under the microscope. NIH ImageJ was used to count $Ki67^+/CK19^+$ cells, and the mean numbers were used for analysis.

Detection of Differentiation and Immunocytochemistry

P3 ductal cells were directly treated with SP (10^{-2}, 10^{-1}, and 1 μM) or treated with SP and insulin-produced cell induction medium (DMEM/F12 plus 2% FBS, 10 mmol/L Niacinamide, 20 ng/ml HGF, 20 μg/L bFGF, and 10 nmol/L exendin-4) for 28 days and immunostained with CK19 and Pdx-1, or Pdx-1 and insulin antibodies to detect differentiation. The medium containing SP was changed every 24 h. Cells were fixed with 4% paraformaldehyde and then were permeabilized with 0.5 ml of 0.1% Triton X-100. After blocking with 3% BSA, cells were incubated with primary antibody at 4°C overnight. The following primary antibodies were used: mouse anti-CK19 (1:100; Proteintech, Wuhan, China), rabbit anti-Pdx-1(1:100; Proteintech, Wuhan, China) and mouse anti-insulin (1:100; NovusBio, Littleton CO, USA). Cells were then stained with FITC- or Cy3-labeled secondary antibodies (Jackson ImmunoResearch Lab, West Grove, PA at 1:200 dilution). Nuclei were stained with DAPI. Results were visualized with fluorescence microscopy (Nikon Eclipse E600; Nikon Corporation, Tokyo, Japan). The proportion of cells labeling with specific marker in total number of DAPI+ cells was accessed and expressed as the mean percentage of specific differentiation.

Flow Cytometry Analysis

To determine the percentage of CK19+ cells in total ductal cells, ductal cells at 3rd passage were stained with CK19. Cells were fixed and permeabilized using Cytofix/Cytoperm system (BD Bioscience, San Diego, CA, USA). After permeabilization, cells were stained with mouse anti Cytokeratin 19 (CK19) antibody for 30 min at 4°C. Then cells were incubated with FITC-labeled secondary antibody for 30 min at room temperature. To detect the differeciation of ductal cells, intracellular staining was performed for insulin production and CK19 expression. After cell permeabilization, cells were stained with mouse anti CK19 and PE-labeled insulin antibodies, following incubation of FITC-labeled secondary antibody. Mouse anti CK19 and PE-labeled anti-insulin antibodies were purchased from Novus Biologicals(Littleton, CO, USA). FITC-labeled anti-mouse secondary antibody was purchased from Santa Cruz Biotechnology (Santa Cruz, CA, USA). Data were analyzed by FACScan flow cytometer (BD Biosciences) using the CellQuest software (BD Biosciences).

Western Blot Analysis

Cells were lysed by pre-cooling cell lysis buffer for Western and IP (Beyotime biotechnology, Shanghai, China) supplemented with 1 mM PMSF (Beyotime biotechnology, Shanghai, China) on ice for 15 min and centrifuged at 12,000 × g for 15 min at 4°C. Protein qualification was measured by using a BCA kit (Beyotime biotechnology, Shanghai, China). Forty micrograms total proteins in each lane were electrophoretically separated by 10% SDS-PAGE (Beyotime biotechnology, Shanghai, China) and transferred onto polyvinylidene difluoride (PVDF) membranes (Millipore, Billerica, MA). Membranes were blocked with 3% BSA in TBST buffer (50 mM Tris•HCl, pH 7.4, 150 mM NaCl, 0.1% Tween-20) for 1 h at room temperature. After rinsing with TBST buffer three times, membranes were incubated with primary antibodies overnight at 4°C. The following primary antibodies were used: rabbit anti NK1R (1:1,000; AbSci, Baltimore, MD), rabbit anti GSK-3β (1:1,000; AbSci, Baltimore, MD), rabbit anti β-catenin (1:1,000; Cell Signaling Technology, Boston, MA) and mouse anti β-actin (1:10,000; Sigma, St. Louis, MO). After washing with TBST, membranes were incubated by horseradish peroxidase (HRP)-conjugated anti-rabbit or anti-mouse secondary antibodies for 1 h at room temperature. ECL chemiluminescence solution (Bio-Rad Laboratories, Hercules, CA) was added after rinsing with TBST. Signal intensity of immunoreactive bands was analyzed using Image Lab software (Bio-Rad Laboratories, Hercules, CA) and ImageJ software (Version 1.48v, National Institutes of Health, Bethesda, MD). For the Western blot assay, the optical density of the protein bands was normalized to the density of β-actin band to yield the densitometric ratio value.

Statistical Analysis

Statistical analysis was performed with SPSS version 16.0 (2007; Chicago, IL, USA). Most data are expressed as the mean ± SD, data of Western blot are expressed as the mean ± SEM, and one-way ANOVA with Bonferroni correction for multiple comparisons was used to analyze the differences between the groups. $p < 0.05$ was determined as significance.

RESULTS

Generation and Identification of Rat Pancreatic Ductal Cells

The ductal cells obtained from rat pancreas were expanded at 3rd passage (P3) for purification and characterized phenotypically

and molecularly. Cells at P3 were adherent in serum containing medium, and were long, spindle shaped cells in morphology. Majority of the P3 cells were positive for CK19 (**Figure 1A**), a ductal cell marker. Flow cytometry results showed that more than 80% of single P3 cells were positive for CK19 (**Figure 1B**), indicating that the isolated cells were ductal cells and qualified for subsequent experiments.

Cell growth was measured at day 1, 3, 5, 7, and 9 to assess the self-renewal capacity of ductal cells. The result showed that the cells expanded rapidly between day 1 and day 5 and plateaued after day 5 (**Figure 1C**).

Substance P but Not CGRP Enhanced Self-Renewal Capacity of Ductal Cells

Proliferation is tightly linked to self-renewal capabilities of ductal cells. To determine the effects of SP or CGRP on proliferation, P3 ductal cells were treated with series concentrations of SP (10^{-6}, 10^{-5}, 10^{-4}, 10^{-3}, 10^{-2}, 10^{-1}, 1, and 10 μM) or CGRP (10^{-6}, 10^{-5}, 10^{-4}, 10^{-3}, 10^{-2}, 10^{-1}, 1, and 10 μM) in growth medium for 3 days. Cell viability was assessed by CCK-8 test. Compared with control cells, SP (10^{-6}, 10^{-5}, 10^{-3}, 10^{-2}, 10^{-1}, and 1 μM) treated cells exhibited a stronger proliferation capacity (**Figure 2A**). However, there was not a significant effect of CGRP on cell viability (**Figure 2B**), indicating that SP but not CGRP promoted cell proliferation of pancreatic ductal cells.

To further confirm the effect of SP on ductal cell proliferation, the proliferation of ductal cells was tested with Ki67 (a marker for cell proliferation) immunostaining. After incubation with SP (10^{-6}, 10^{-3}, 10^{-2}, 10^{-1}, and 1 μM) for 3 days, ductal cells were immunostained with Ki67 followed by image analysis. As shown in **Figures 3A,B**, significantly higher levels of Ki67-positive cells were found in SP treated groups compared with control ($P < 0.05$, $P < 0.05$, $P < 0.05$, $P < 0.01$, $P < 0.05$, respectively). Moreover, growth curves of day 1, 3, 5, 7, and 9 were plotted to assay the self-renewal capacity of ductal cells

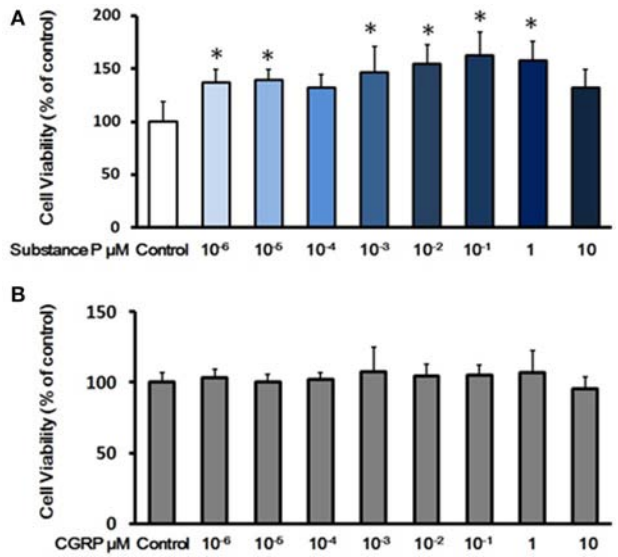

FIGURE 2 | Effects of substance P or CGRP on self-renewal capacity of adult pancreatic ductal cells. **(A)** Cell viability assay with treatment of substance P. Cells were treated with a serial of concentrations of substance P (10^{-6}, 10^{-5}, 10^{-4}, 10^{-3}, 10^{-2}, 10^{-1}, 1, and 10 μM; $n = 6$ wells for each) for 72 h, and the cell viability was measured by CCK-8 assay. **(B)** Cell viability assay with treatment of CGRP. Cells were treated with different concentrations of CGRP (10^{-6}, 10^{-5}, 10^{-4}, 10^{-3}, 10^{-2}, 10^{-1}, 1, and 10 μM; $n = 6$ wells for each) for 72 h, following assayed by CCK-8 test. *$P < 0.05$, compared with control groups.

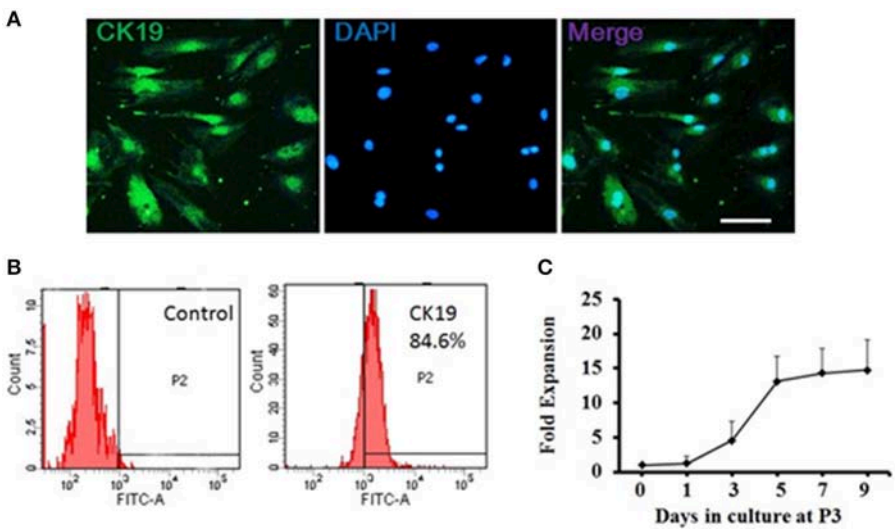

FIGURE 1 | Generation and characterization of adult pancreatic ductal cells *in vitro*. **(A)** Pancreatic ductal cells were cultured and expanded at the third passage (P3) for purification. The P3 cells were immunostained by CK19 (green) antibody and visualized by fluorescent microscopy. Scale bar: 100 μm. **(B)** Flow cytometric analysis of CK19 expression on pancreatic ductal cells. One representative experiment of three is shown. **(C)** Growth curve. Dissociated ductal cells were plated at a density of 1.0×10^5 cells/ml and cultured. At day 1, 3, 5, 7, and 9, the cells were collected and counted by hemocytometer. At least 6 wells were assessed at each time point.

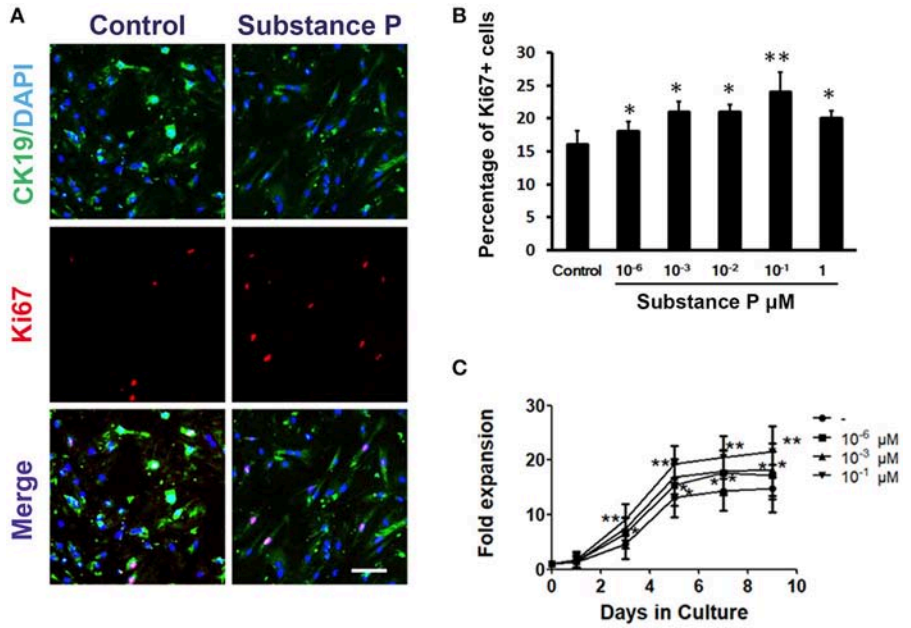

FIGURE 3 | Promotion effects of substance P on proliferation of adult pancreatic ductal cells. **(A)** Ki67 labeling. Cells were treated with substance P (10^{-6}, 10^{-3}, 10^{-2}, 10^{-1}, 1, and 10 μM; $n = 3$ wells for each) for 72 h and immunostained by CK19 (green) and Ki67 (red) antibodies. Scale bar: 100 μm. **(B)** Quantitative analysis of Ki67 positive cells. **(C)** Growth curves. Dissociated ductal cells were plated at a density of 1.0×10^5 cells/ml and cultured. Cells were treated without or with substance P (10^{-6}, 10^{-3}, 10^{-1} μM). At day 1, 3, 5, 7, and 9, the cells were collected and counted by hemocytometer. At least 6 wells were assessed at each time point. $^*P < 0.05$, $^{**}P < 0.01$, compared with control groups.

treated with different concentrations of SP (10^{-6}, 10^{-3}, and 10^{-1} μM). The results indicated that cells incubated with SP expanded more rapidly on day 3, 5, 7, and day 9 (**Figure 3C**). These findings indicated that SP promoted proliferation of ductal cells.

Substance P Did Not Induce Differentiation of Ductal Cells Into β-Cells

Above results showed ductal cells were sensitive to SP, and cell proliferation was promoted at a concentration of 10^{-6} μM. Next, we tested whether SP further promotes differentiation on ductal cells. To determine the effects of SP on differentiation of ductal cells, cells were treated with serial doses of SP (10^{-6}, 10^{-}1, and 1 μM) for 28 days. In substance P treated groups, cells positive for CK19 and Pdx-1 were negative for insulin (**Figures 4A,B**), as verified by triple immunostaining, indicating that SP dose not directly induce differentiation of adult pancreatic ductal cells into β-cells.

Further, cell culture medium was replaced by insulin-produced induction medium with or without SP (10^{-6}, 10^{-1}, and 1 μM). After 28 days, ductal cells developed into insulin-produced cells (insulin+) (**Figure 4C**). Flow cytometric analysis showed that SP did not promote ductal cells differentiated into greater numbers of insulin-produced cells ($P > 0.05$, $P > 0.05$, respectively, **Figure 4D**) as compared with induction medium control group. All these results indicated that SP did not affect the differentiation potential of ductal cells into β-cells.

Blockade of SP-Induced Stimulation of Proliferation With NK-1 Receptor Antagonist L-703,606

To evaluate the influence of NK-1 receptor (NK1R) antagonist L-703,606 on the effects of SP on duct cells, cells were incubated with SP (10^{-1} μM) plus L-703,606 (1, 2, 4, 6, 8, 10 μM) for 72 h. After 72 h incubation, cell viability was measured by CCK8 assay. Exposure of SP-treated cells to L-703,606 (2, 4, 6, 8, 10 μM) significantly inhibited the cell proliferation induced by SP ($P < 0.01$, $P < 0.01$, $P < 0.01$, $P < 0.01$, $P < 0.01$, respectively, **Figure 5A**). The dose of 2 μM of L-703,606 was used to block the stimulatory effects of SP on duct cells in further experiments.

To investigate whether SP could mediate ductal cell proliferation via NK-1 receptor, we added NK1R antagonist L-703,606 (2 μM) into the culture medium containing different doses of SP (10^{-2}, 10^{-1}, and 1 μM). In L-703,606 plus SP-treated groups, L-703,606 treatment decreased cell viability of ductal cells compared with SP-treated groups (percentage of control without SP or L-703,606, 108.02 ± 19.65 vs. 136.10 ± 20.59 in 10^{-2} μM, $P < 0.05$; 128.50 ± 16.33 vs. 172.81 ± 24.15 in 10^{-1} μM, $P < 0.01$; 110.95 ± 10.78 vs. 137.14 ± 17.06 in 1 μM, $P < 0.01$; **Figure 5B**).

Ki67 immunostaining was performed to verify the inhibition of L-703,606 on proliferation effects of SP on ductal cells. Compared with control groups, the SP-treated cells showed a significantly higher number of cells positive for Ki67 (21.34 ± 1.89% vs. 16.17 ± 1.04%, $P < 0.05$, **Figures 5C,D**). Compared with SP-treated groups (10^{-1} μM), L-703,606 treatment decreased the number of Ki67 positive cells (16.17±1.04% vs.

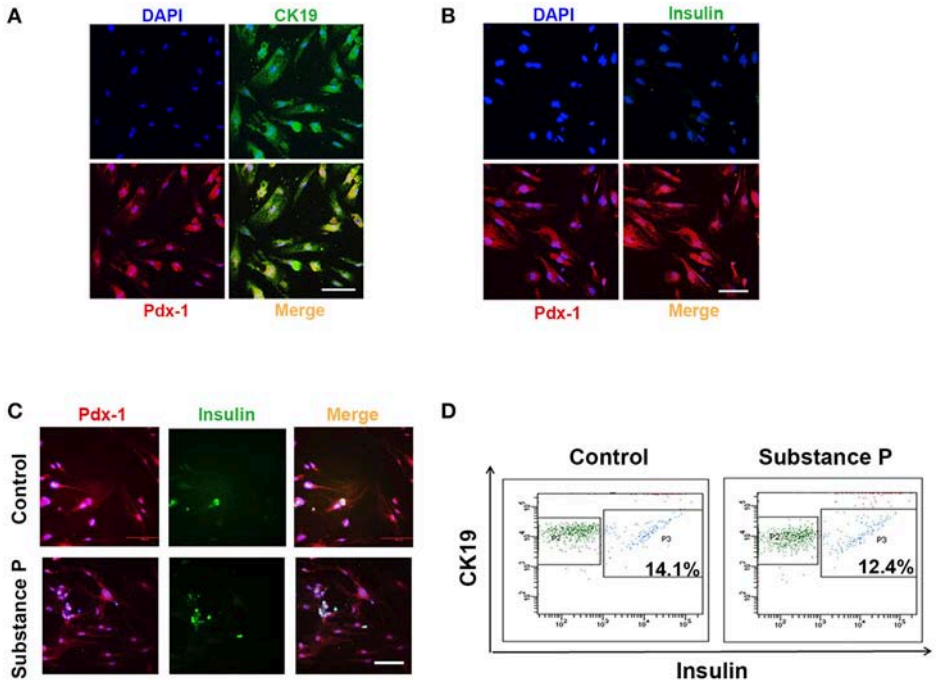

FIGURE 4 | Substance P did not promote differentiation of adult pancreatic ductal cells into Beta-Cells. P3 ductal cells were treated with substance P (10^{-6}, 10^{-2}, and 10^{-1} μM) for 28 days. Immunostaining was performed to identified the differentiation of ductal cells. **(A)** Cells were Pdx-1 (red) and CK19 (green) positive. Scale bar: 100 μm. **(B)** Cells were Pdx-1 (red) positive but insulin (green) negative. Scale bar: 100 μm. **(C)** After 28 incubation of induction medium (DMEM/F12 plus 2% FBS, 10 mmol/L Niacinamide, 20 ng/ml HGF, 20 μg/L bFGF, and 10 nmol/L exendin-4) with or without substance P (10^{-6}, 10^{-2} and 10^{-1} μM) for 28 days, ductal cells were immunostained by Pdx-1 (red) and insulin (green) antibodies. A portion of Pdx-1 positive cells expressed insulin. Scale bar: 100 μm. **(D)** Flow cytometric analysis of CK19 and insulin expression on pancreatic ductal cells. Data was compared with isotype-matched controls. One representative experiment of three is shown.

21.34 ± 1.89%, $P < 0.05$, **Figures 5C, D**). These results mean that SP plays its role in proliferation of ductal cell via NK-1 receptor.

Substance P Promotes NK1R Expression, Decreases GSK-3β and Increased β-Catenin in Ductal Cells

We performed double immunostaining of NK1R and ki67 expression on ductal cells. Similar to Garland's finding (Garland et al., 1994), we found that NK1R was expressed in cytoplasm after SP treatment (**Figure 6A**). To investigate whether SP affect NK1R, and GSK-3β/β-catenin pathway, cells were treated with SP (10^{-1} μM), SP (10^{-1} μM)+L-703,606 (2 μM) and L-703,606 (2 μM) alone for 72 h, total protein was harvested and Western blot analysis was performed to test expression of NK1R, GSK-3β and β-catenin (**Figures 6B,D**). Quantitative analysis revealed that NK1R protein levels were significantly increased in SP treated cells as compared with control groups (**Figure 6C**, $P < 0.01$), but L-703,606 treatment significantly decreased NK1R levels (**Figure 6C**, $P < 0.05$). Quantitative analysis of GSK-3β and β-catenin protein showed that SP treatment significantly decreased GSK-3β levels (**Figure 6E**, $P < 0.01$) and significantly increased β-catenin levels (**Figure 6E**, $P < 0.01$) compared with control group, whereas L-703,606 treatment decreased these effects of SP on ductal cells (SP+L-703,606 group vs. SP group, $P < 0.05$, $P < 0.05$, respectively).

DISCCUSION

In the present study, we demonstrated that SP but not CGRP promoted cell viability and proliferation of ductal cells derived from rat pancreas, which is inhibited by the NK1 receptor antagonist. SP did not exert the effects of differentiation toward β-cell of these cells. Our experiments also revealed that SP treatment enhanced NK1R expression, reduced GSK-3β levels and increased β-catenin levels. However, treatment with NK1R inhibitor L-703,606 attenuated the effects of SP on NK1R, GSK-3β and β-catenin levels. Collectively, these findings suggest that SP promotes pancreatic duct cell proliferation via NK1R, and the Wnt/β-catenin pathway is involved in the mechanisms of SP-induced proliferation of ductal cells.

SP and CGRP have been showed to be capable to promote proliferation in some other tissues. SP has been reported to promote proliferation of adult neural progenitor cells (NPCs) (Park et al., 2007), cord blood CD34+ hematopoietic stem cells (Shahrokhi et al., 2010), and fibroblast-like cells derived from bile duct (Tian et al., 2014). CGRP stimulates cell proliferation and inhibits cell apoptosis of bone-marrow MSCs in short term culture, and promotes osteogenetic differentiation in long term culture (Xu and Jiang, 2014; Liang et al., 2015). It has been reported that CGRP overexpressed rat adipose-derived stem cells (ADSCs) exerted more potency of proliferation, neurosphere

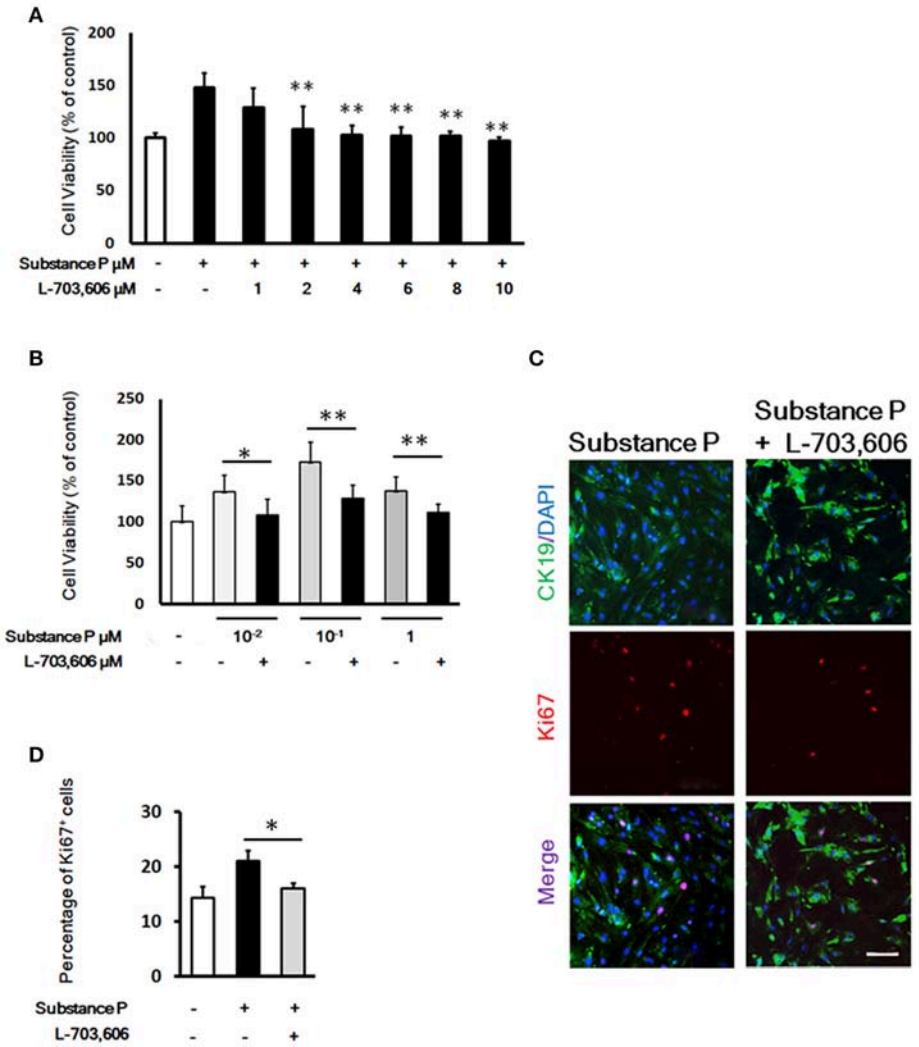

FIGURE 5 | L-703,606 blocked the promotion effects of substance P on proliferation of pancreatic ductal cells. **(A)**. Effect of L-703,606 on proliferative effects of substance P in pancreatic ductal cells. Cells were treated with SP (10^{-1} μM) plus different concentrations of L-703,606 (1, 2, 4, 6, 8, 10 μM) for 72 h, and the cell viability was measured by CCK-8 assay. **(B)** Cell viability assay. Cells were treated with different concentrations of substance P (10^{-2}, 10^{-1}, and 1 μM) with or without L-703,606 (2 μM) for 72 h, and the cell viability was measured by CCK-8 assay. **(C)** Ki67 labeling. Cells were treated with substance P (10^{-1} μM) with or without L-703,606 (2 μM) for 72 h. Cells were immunostained by CK19 (green) and Ki67 (red) antibodies. Scale bar: 100 μm. **(D)** Quantitative analysis of Ki67 positive cells. $^{*}P < 0.05$, $^{**}P < 0.01$, as compared with substance P treated groups.

formation (Yang et al., 2014), and osteoblastic differentiation (Fang et al., 2013). Moreover, CGRP and SP treatment promoted human skin keratinocyte proliferation (Shi et al., 2013). Besides promoting proliferation, SP has also been shown to stimulate differentiation of mesenchymal stem cells (MSCs) into osteoblastic cells through neurokinin (NK)-1 receptor (Sun et al., 2010).

Our results showed that SP stimulated proliferation of pancreatic ductal cells and pancreatic ductal cells were very sensitive to SP on proliferation. Opolka et al. (2012) reported that SP at the concentration of 10^{-4} μM promoted proliferation of murine chondrocytes. SP at 10^{-3} μM induces pro-proliferation effects on fibroblast-like cells from bile duct and hematopoietic stem cells (Shahrokhi et al., 2010; Tian et al., 2014). In bone marrow-derived mesenchymal stem cell-like cells and bone marrow stromal stem cells, 10^{-2} μM SP is needed to promote cell proliferation (Mei et al., 2013; Dubon and Park, 2015; Liu et al., 2016). SP concentration as high as 10^{-1} μM is needed in ARPE-19 cells, a human retinal pigmented epithelial (RPE) cell line (Baek et al., 2016), and neural stem/progenitor cells derived from spinal cord to show its effect (Kim et al., 2015). In bone marrow mesenchymal stem cells (MSCs), SP at as low as 10^{-6} μM enhances osteoblast differentiation of MSCs (Wang et al., 2009) and protects against apoptosis induced by serum deprivation (Fu et al., 2015). Our results indicated that SP at as low as 10^{-6} μM had pro-proliferation effect on ductal cells. Thus, pancreatic ductal cells are among the most sensitive cells to SP, similar to MSCs.

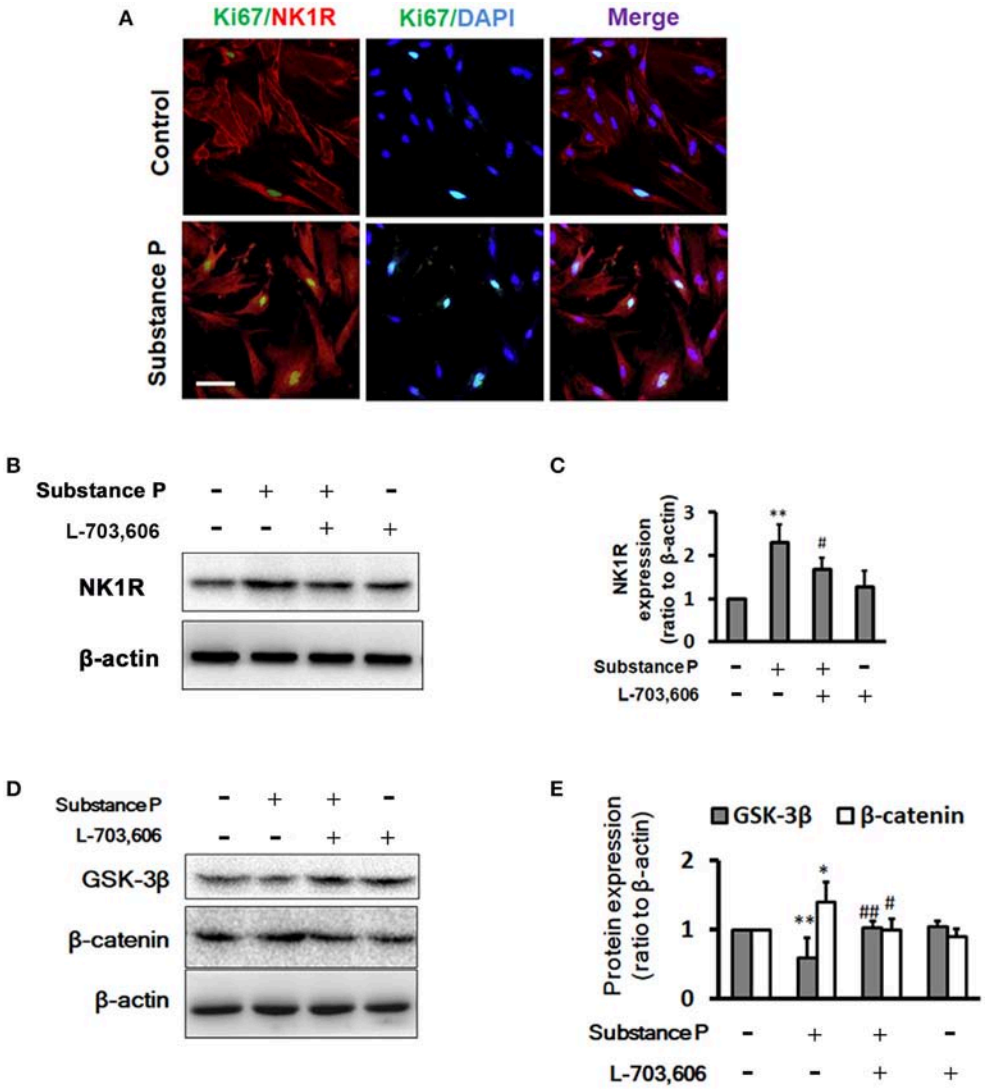

FIGURE 6 | L-703,606 attenuated the effects of substance P on NK1R, GSK-3β, and β-catenin expression. **(A)** Cells were NK1R (red) and Ki67 (green) positive in cells treated without (control cells) or with substance P (10^{-1} μM). Scale bar: 100 μm. **(B)** Western Blot images of NK1R. Cells were incubated with or without substance P (10^{-1} μM) and/or L-703,606 (2 μM) for 72 h. Cell extracts were analyzed for the expression of NK1R. **(C)**. Quantitative analysis of NK1R. Substance P increased NK1R expression, whereas L-703,606 blocked the effects of substance P on NK1R. **(D)** Western Blot images of GSK-3β and β-catenin. Cells were incubated with or without substance P (10^{-1} μM) and/or L-703,606 (2 μM) for 72 h. GSK-3β and β-catenin expression were measured in cell extracts by Western blot. **(E)** Quantitative analysis of GSK-3β and β-catenin. Substance P reduced GSK-3β levels and increased β-catenin levels, whereas L-703,606 blocked the effects of substance P on GSK-3β and β-catenin. Densitometric ratios are the mean ± SEM of three experiments. $^{**}P < 0.01$, $^{*}P < 0.05$ as compared with control groups. $^{\#\#}P < 0.01$, $^{\#}P < 0.05$ as compared with substance P treated groups.

The actions of SP are mediated by three G protein–coupled receptors, NK-1, NK-2, and NK-3 receptors; among these, the NK-1 receptor (NK1R) has the highest affinity for SP (Takeda et al., 1991). In Kim's (Kim et al., 2015) and Park's (Park et al., 2007) reports, NK1R inhibitor L-703,606 (1–10 μM) decreased SP-induced proliferation of spinal cord-derived neural stem/progenitor cells (SC-NSPCs). We examined the inhibitory effect of L-703,606 (1–10 μM) on SP-stimulated cell proliferation. Our results indicated that L-703,606 at dose of 2–10 μM effectively blocked the proliferative effect of SP. Our results showed that L-703,606 inhibited the proliferation effects of SP on pancreatic ductal cells, indicating the proliferation stimulating effect of SP on ductal cells through NK1R. Notably, several studies are consistent with our results. Glaser et al. (2011) reported that knockout of the NK1R reduced cholangiocyte proliferation in bile duct-ligated mice, indicating a specific mitotic effect of SP on bile ductal cells. In Liu's study (Liu et al., 2016), they demonstrated that SP enhanced proliferation of bone marrow mesenchymal stem cell derived osteoblasts (BMSC-OB), and this effect would be inhibited by adding NK1R antagonist.

In has been shown that pretreatment with the NK1R antagonist reduced the effect of SP on proliferation of ARPE-19 cells (Baek et al., 2016).

It has been reported that SP at concentration of 1 μM increased NK1R mRNA expression in pancreatic acinar cells (Koh et al., 2012). In our study, we performed double immunostaining of NK1R and ki67 expression on ductal cells. The images showed that the ductal cells had stronger NK1R immune staining in SP-treated cells by compared with control cells. Garland et al. (1994) reported that NK1R was located in intracellular vesicles, rather than aggregated in the plasma membrane in epithelial cells after incubation with SP. Similar to Garland's finding, we found that NK1R was expressed in cytoplasm after SP treatment. Consistent with the results of staining, our results of Western blotting showed that the level of NK1R was significantly higher in SP treated group, compared with control group.

It is interesting that CGRP did not show any effect on proliferation of ductal cells. SP and CGRP are two important neurotransmitters released from primary sensory fibers of dorsal root ganglia. CGRP and SP are colocalized and co-released from these fibers (Gibbins et al., 1985). Besides primary sensory fibers of dorsal root ganglia, SP was also from another important source which is intrapancreatic ganglia. Neurons in pancreatic ganglia innervate islets as well as pancreatic ducts (Sha et al., 2001; Love et al., 2007). Our study (Shen et al., 2016) revealed that intrapancreatic ganglia contain SP neurons and contribute around 50% of SP in pancreas. Our results suggested that SP released from primary sensory fiber and fibers of pancreatic ganglia stimulate proliferation of pancreatic ducts. Pancreatic ganglia don't contain any CGRP neurons (our unpublished data) and all CGRP fibers appear coming from primary sensory neurons (Russell et al., 2014). Thus, via release of CGRP, primary sensory fibers might uniquely modulate activity other than proliferation of pancreatic duct.

Pancreatic ductal cells play as pancreatic stem cells that exhibit stem cell properties, including proliferation and differentiation potential. Even though SP showed pro-proliferation activity, we did not find SP exert any promoting effect on the ductal cells differentiating toward β-cells. Our results showed that SP did not induce pancreatic ductal cells differentiate into insulin-positive cells directly, although the ductal cells all expressed Pdx-1, a pancreatic progenitor cell marker (Murtaugh, 2007). Further, in insulin-produced cell induction medium, SP did not promote pancreatic ductal cells differentiating into greater numbers of insulin-produced cells either.

Activation of Wnt signaling has been shown to be essential for proliferation of multiple cells (Mah et al., 2016; Arrigoni et al., 2018; Majidinia et al., 2018). Glycogen synthase kinase-3β (GSK-3β), a key molecule of the Wnt pathway, induces phosphorylation of β-catenin, causing the degradation of β-catenin. GSK-3β activity is inhibited following activation of the Wnt pathway, stimulating the accumulation of β-catenin in the cytoplasm, and β-catenin transferred into the nucleus, serving as a transcription factor to induce the activation of downstream target genes (Wang et al., 2018). We propose that SP regulates ductal cell proliferation via activation of Wnt pathway. Our results of western blot showed that SP treatment enhanced NK1R expression, decreased GSK-3β levels and increased β-catenin levels. Moreover, L-703,606, a NK1R antagonist, decreased NK1R expression and attenuated the effects of SP on GSK-3β and β-catenin levels, indicating that SP may promote proliferation of ductal cells via augmenting NK1R and GSK-3β/β-catenin signaling.

Our study was designed to understand the possible effects of neuropeptides released by primary sensory nerve fibers on pancreatic ductal cells. However, we found that only SP promoted the proliferation of pancreatic ductal cells. Moreover, SP did not induce or promote the differentiation of ductal cells into β-cells. The onset of diabetes is related to the lack of SP. Razavi et al. (2006) reported that reduced release of substance P initiates immune stress response of islet β-cells, leading to inflammation of islet cells and invasion of lymphocytes. On top of that, the ductal cells in the pancreas have stem cell properties and are one of the sources of β-cell neogenesis (Xu et al., 2008; Bonner-Weir et al., 2010). The proliferative effect of SP on ductal cells may explain another possible pathological course in the developmental stage of diabetes. The stabilization of SP levels might indicate that the pancreatic endogenous β-cell pool is abundant and is one of the conditions for maintaining β-cell homeostasis. Therefore, the lack of SP might be an indicator of the initial of diabetes. In addition, SP can also be used as a drug candidate for the treatment of diabetes.

In summary, SP but not CGRP stimulates the proliferation of pancreatic ductal cells. SP does not induce or promote the differentiation of ductal cells toward β-cells. Moreover, SP may promote proliferation of pancreatic ductal cells through enhancing NK1R expression, decreasing GSK-3β and increasing β-catenin levels.

INFORMED CONSENT

Informed consent was obtained from all individual participants included in the study.

AUTHOR CONTRIBUTIONS

NZ, DG, YL, and SJ participated as investigators and reviewed, edited, and approved of the final version of the manuscript. LS initiated the study of neuropeptides substance P and CGRP in diabetes, is the guarantor of this work, had full access to all the data in the study and takes responsibility for the integrity of the data and the accuracy of the data analysis. NZ and LS wrote the manuscript.

ACKNOWLEDGMENTS

This work was supported by the National Natural Science Foundation of China (grant NO. 81270900; 81503273; 81670492).

REFERENCES

Arrigoni, E., Del Re, M., Galimberti, S., Restante, G., Rofi, E., and Crucitta, S., et al. (2018). Concise review: chronic myeloid leukemia: stem cell niche and response to pharmacologic treatment. *Stem Cells Transl. Med.* 7, 305–314. doi: 10.1002/sctm.17-0175

Baek, S. M., Yu, S. Y., Son, Y., and Hong, H. S. (2016). Substance P promotes the recovery of oxidative stress-damaged retinal pigmented epithelial cells by modulating Akt/GSK-3beta signaling. *Mol. Vis.* 22, 1015–1023.

Besedovsky, H. O., and del Rey, A. (1996). Immune-neuro-endocrine interactions: facts and hypotheses. *Endocr. Rev.*, 17, 64–102. doi: 10.1210/edrv-17-1-64

Bonner-Weir, S. (2000). Life and death of the pancreatic beta cells. *Trends Endocrinol. Metab.* 11, 375–378. doi: 10.1016/S1043-2760(00)00305-2

Bonner-Weir, S., Li, W. C., Ouziel-Yahalom, L., Guo, L., Weir, G. C., and Sharma, A. (2010). Beta-cell growth and regeneration: replication is only part of the story. *Diabetes* 59, 2340–2348. doi: 10.2337/db10-0084

Dor, Y. (2006). beta-Cell proliferation is the major source of new pancreatic beta cells. *Nat. Clin. Pract. Endocrinol. Metab.* 2, 242–243. doi: 10.1038/ncpendmet0187

Dubon, M. J., and Park, K. S. (2015). Substance P enhances the proliferation and migration potential of murine bone marrow-derived mesenchymal stem cell-like cell lines. *Exp. Ther. Med.* 9, 1185–1191. doi: 10.3892/etm.2015.2291

Fang, Z., Yang, Q., Xiong, W., Li, G. H., Liao, H., Xiao, J., et al. (2013). Effect of CGRP-adenoviral vector transduction on the osteoblastic differentiation of rat adipose-derived stem cells. *PLoS ONE* 8:e72738. doi: 10.1371/journal.pone.0072738

Fu, S., Jin, D., Liu, S., Wang, L., Wang, Z., Mei, G., et al. (2015). Protective effect of neuropeptide substance P on bone marrow mesenchymal stem cells against apoptosis induced by serum deprivation. *Stem Cells Int.* 2015:270328. doi: 10.1155/2015/270328

Fukazawa, T., Matsuoka, J., Naomoto, Y., Nakai, T., Durbin, M. L., Kojima, I., et al. (2006). Development of a novel beta-cell specific promoter system for the identification of insulin-producing cells in *in vitro* cell cultures. *Exp. Cell Res.* 312, 3404–3412. doi: 10.1016/j.yexcr.2006.07.015

Garland, A. M., Grady, E. F., Payan, D. G., Vigna, S. R., and Bunnett, N. W. (1994). Agonist-induced internalization of the substance P (NK1) receptor expressed in epithelial cells. *Biochem. J.* 303 (Pt 1), 177–186.

Gibbins, I. L., Furness, J. B., Costa, M., MacIntyre, I., Hillyard, C. J., and Girgis, S. (1985). Co-localization of calcitonin gene-related peptide-like immunoreactivity with substance P in cutaneous, vascular and visceral sensory neurons of guinea pigs. *Neurosci. Lett.* 57, 125–130. doi: 10.1016/0304-3940(85)90050-3

Glaser, S., Gaudio, E., Renzi, A., Mancinelli, R., Ueno, Y., and Venter, J., et al. (2011). Knockout of the neurokinin-1 receptor reduces cholangiocyte proliferation in bile duct-ligated mice. *Am. J. Physiol. Gastrointest. Liver Physiol.* 301, G297–G305. doi: 10.1152/ajpgi.00418.2010

Gram, D. X., Ahrén, B., Nagy, I., Olsen, U. B., Brand, C. L., Sundler, F., et al. (2007). Capsaicin-sensitive sensory fibers in the islets of Langerhans contribute to defective insulin secretion in Zucker diabetic rat, an animal model for some aspects of human type 2 diabetes. *Eur. J. Neurosci.* 25, 213–223. doi: 10.1111/j.1460-9568.2006.05261.x

Halban, P. A., German, M. S., Kahn, S. E., and Weir, G. C. (2010). Current status of islet cell replacement and regeneration therapy. *J. Clin. Endocrinol. Metab.* 95, 1034–1043. doi: 10.1210/jc.2009-1819

Juhl, K., Bonner-Weir, S., and Sharma, A. (2010). Regenerating pancreatic beta-cells: plasticity of adult pancreatic cells and the feasibility of *in-vivo* neogenesis. *Curr. Opin. Organ Transplant.* 15, 79–85. doi: 10.1097/MOT.0b013e3283344932

Kim, K. T., Kim, H. J., Cho, D. C., Bae, J. S., and Park, S. W. (2015). Substance P stimulates proliferation of spinal neural stem cells in spinal cord injury via the mitogen-activated protein kinase signaling pathway. *Spine J.* 15, 2055–2065. doi: 10.1016/j.spinee.2015.04.032

Koh, Y. H., Moochhala, S., and Bhatia, M. (2012). Activation of neurokinin-1 receptors up-regulates substance P and neurokinin-1 receptor expression in murine pancreatic acinar cells. *J. Cell. Mol. Med.* 16, 1582–1592. doi: 10.1111/j.1582-4934.2011.01475.x

Li, X. Y., Zhan, X. R., Liu, X. M., and Wang, X. C. (2011). CREB is a regulatory target for the protein kinase Akt/PKB in the differentiation of pancreatic ductal cells into islet beta-cells mediated by hepatocyte growth factor. *Biochem. Biophys. Res. Commun.* 404, 711–716. doi: 10.1016/j.bbrc.2010.12.048

Liang, W., Zhuo, X., Tang, Z., Wei, X., and Li, B. (2015). Calcitonin gene-related peptide stimulates proliferation and osteogenic differentiation of osteoporotic rat-derived bone mesenchymal stem cells. *Mol. Cell. Biochem.* 402, 101–110. doi: 10.1007/s11010-014-2318-6

Liu, H. J., Yan, H., Yan, J., Li, H., Chen, L., Han, L. R., et al. (2016). Substance P promotes the proliferation, but inhibits differentiation and mineralization of osteoblasts from rats with spinal cord injury via RANKL/OPG system. *PLoS ONE* 11:e0165063. doi: 10.1371/journal.pone.0165063

Love, J. A., Yi, E., and Smith, T. G. (2007). Autonomic pathways regulating pancreatic exocrine secretion. *Auton. Neurosci.* 133, 19–34. doi: 10.1016/j.autneu.2006.10.001

Mah, A. T., Yan, K. S., and Kuo, C. J. (2016). Wnt pathway regulation of intestinal stem cells. *J. Physiol.* 594, 4837–4847. doi: 10.1113/JP271754

Majidinia, M., Aghazadeh, J., Jahanban-Esfahlani, R., and Yousefi, B. (2018). The roles of Wnt/beta-catenin pathway in tissue development and regenerative medicine. *J. Cell Physiol.* 233, 5598–5612. doi: 10.1002/jcp.26265

Mei, G., Xia, L., Zhou, J., Zhang, Y., Tuo, Y., Fu, S., et al. (2013). Neuropeptide SP activates the WNT signal transduction pathway and enhances the proliferation of bone marrow stromal stem cells. *Cell Biol. Int.* 37, 1225–1232. doi: 10.1002/cbin.10158

Murtaugh, L. C. (2007). Pancreas and beta-cell development: from the actual to the possible. *Development* 134, 427–438. doi: 10.1242/dev.02770

Opolka, A., Straub, R. H., Pasoldt, A., Grifka, J., and Grässel, S. (2012). Substance P and norepinephrine modulate murine chondrocyte proliferation and apoptosis. *Arthritis Rheum.* 64, 729–739. doi: 10.1002/art.33449

Park, S. W., Yan, Y. P., Satriotomo, I., Vemuganti, R., and Dempsey, R. J. (2007). Substance P is a promoter of adult neural progenitor cell proliferation under normal and ischemic conditions. *J. Neurosurg.* 107, 593–599. doi: 10.3171/JNS-07/09/0593

Persson-Sjögren, S., Holmberg, D., and Forsgren, S. (2005). Remodeling of the innervation of pancreatic islets accompanies insulitis preceding onset of diabetes in the NOD mouse. *J. Neuroimmunol.* 158, 128–137. doi: 10.1016/j.jneuroim.2004.08.019

Razavi, R., Chan, Y., Afifiyan, F. N., Liu, X. J., Wan, X., Yantha, J., et al. (2006). TRPV1+ sensory neurons control beta cell stress and islet inflammation in autoimmune diabetes. *Cell* 127, 1123–1135. doi: 10.1016/j.cell.2006.10.038

Rovira, M., Scott, S. G., Liss, A. S., Jensen, J., Thayer, S. P., and Leach, S. D. (2010). Isolation and characterization of centroacinar/terminal ductal progenitor cells in adult mouse pancreas. *Proc. Natl. Acad. Sci. USA.* 107, 75–80. doi: 10.1073/pnas.0912589107

Russell, F. A., King, R., Smillie, S. J., Kodji, X., and Brain, S. D. (2014). Calcitonin gene-related peptide: physiology and pathophysiology. *Physiol. Rev.* 94, 1099–1142. doi: 10.1152/physrev.00034.2013

Seeberger, K. L., Dufour, J. M., Shapiro, A. M., Lakey, J. R., Rajotte, R. V., and Korbutt, G. S. (2006). Expansion of mesenchymal stem cells from human pancreatic ductal epithelium. *Lab. Invest.* 86, 141–153. doi: 10.1038/labinvest.3700377

Sha, L., Westerlund, J., Szurszewski, J. H., and Bergsten, P. (2001). Amplitude modulation of pulsatile insulin secretion by intrapancreatic ganglion neurons. *Diabetes* 50, 51–55. doi: 10.2337/diabetes.50.1.51

Shahrokhi, S., Ebtekar, M., Alimoghaddam, K., Pourfathollah, A. A., Kheirandish, M., Ardjmand, A., et al. (2010). Substance P and calcitonin gene-related neuropeptides as novel growth factors for ex vivo expansion of cord blood CD34(+) hematopoietic stem cells. *Growth Factors* 28, 66–73. doi: 10.3109/08977190903369404

Shen, Q., Wang, Y., Zhang, N., Gao, D., Liu, Y., and Sha, L. (2016). Substance P expresses in intrapancreatic ganglia of the rats. *Neuropeptides* 59, 33–38. doi: 10.1016/j.npep.2016.06.004

Shi, X., Wang, L., Clark, J. D., and Kingery, W. S. (2013). Keratinocytes express cytokines and nerve growth factor in response to neuropeptide activation of the ERK1/2 and JNK MAPK transcription pathways. *Regul. Pept.* 186, 92–103. doi: 10.1016/j.regpep.2013.08.001

Sun, H. B., Chen, J. C., Liu, Q., Guo, M. F., and Zhang, H. P. (2010). Substance P stimulates differentiation of mice osteoblast through up-regulating Osterix expression. *Chin. J. Traumatol.* 13, 46–50. doi: 10.3760/cma.j.issn.1008-1275.2010.01.009

Takeda, Y., Chou, K. B., Takeda, J., Sachais, B. S., and Krause, J. E. (1991). Molecular cloning, structural characterization and functional expression of the human substance P receptor. *Biochem. Biophys. Res. Commun.* 179, 1232–1240. doi: 10.1016/0006-291X(91)91704-G

Tanaka, H., Shimaya, A., Kiso, T., Kuramochi, T., Shimokawa, T., and Shibasaki, M. (2011). Enhanced insulin secretion and sensitization in diabetic mice on chronic treatment with a transient receptor potential vanilloid 1 antagonist. *Life Sci.* 88, 559–563. doi: 10.1016/j.lfs.2011.01.016

Tian, Y., Yang, G., Zhang, X., Shen, W., Dong, J., and Xu, Z. (2014). Effects of substance P on growth of fibroblast-like cells derived from bile duct: an *in vitro* cell culture study. *Chin. Med. J.* 127, 3121–3126. doi: 10.3760/cma.j.issn.0366-6999.20140765

Wang, L., Zhao, R., Shi, X., Wei, T., Halloran, B. P., Clark, D. J., et al. (2009). Substance P stimulates bone marrow stromal cell osteogenic activity, osteoclast differentiation, and resorption activity *in vitro*. *Bone* 45, 309–320. doi: 10.1016/j.bone.2009.04.203

Wang, Y., Yin, S., Xue, H., Yang, Y., Zhang, N., and Zhao, P. (2018). Mid-gestational sevoflurane exposure inhibits fetal neural stem cell proliferation and impairs postnatal learning and memory function in a dose-dependent manner. *Dev. Biol.* 435, 185–197 doi: 10.1016/j.ydbio.2018.01.022

Wu, F., Guo, L., Jakubowski, A., Su, L., Li, W. C., Bonner-Weir, S., et al. (2013). TNF-like weak inducer of apoptosis (TWEAK) promotes beta cell neogenesis from pancreatic ductal epithelium in adult mice. *PLoS ONE* 8:e72132. doi: 10.1371/journal.pone.0072132

Xu, G., and Jiang, D. (2014). The role and mechanism of exogenous calcitonin gene-related peptide on mesenchymal stem cell proliferation and osteogenetic formation. *Cell Biochem. Biophys.* 69, 369–378. doi: 10.1007/s12013-013-9809-z

Xu, X., D'Hoker, J., Stangé, G., Bonn,é, S., De Leu, N., Xiao, X., et al. (2008). Beta cells can be generated from endogenous progenitors in injured adult mouse pancreas. *Cell* 132, 197–207. doi: 10.1016/j.cell.2007.12.015

Yang, Q., Du, X., Fang, Z., Xiong, W., Li, G., Liao, H., et al. (2014). Effect of calcitonin gene-related peptide on the neurogenesis of rat adipose-derived stem cells *in vitro*. *PLoS ONE* 9:e86334. doi: 10.1371/journal.pone.0086334

Conflict of Interest Statement: The authors declare that the research was conducted in the absence of any commercial or financial relationships that could be construed as a potential conflict of interest.

frontiers in Endocrinology

ORIGINAL RESEARCH
published: 04 February 2019
doi: 10.3389/fendo.2019.00034

Age-Characteristic Changes of Glucose Metabolism, Pancreatic Morphology and Function in Male Offspring Rats Induced by Prenatal Ethanol Exposure

Di Xiao[1†], Hao Kou[2,3†], Shuxia Gui[1], Zhenyu Ji[1], Yu Guo[1,3], Yin Wu[1,3] and Hui Wang[1,3]*

[1] Department of Pharmacology, School of Basic Medical Sciences of Wuhan University, Wuhan, China, [2] Department of Pharmacy, Zhongnan Hospital, Wuhan University, Wuhan, China, [3] Hubei Provincial Key Laboratory of Developmentally Originated Diseases, Wuhan, China

OPEN ACCESS

Edited by:
Yu-Feng Wang,
Harbin Medical University, China

Reviewed by:
Wen Xie,
University of Pittsburgh, United States
Yuping Wang,
Louisiana State University Health Sciences Center Shreveport, United States

***Correspondence:**
Hui Wang
wanghui19@whu.edu.cn

[†] These authors have contributed equally to this work

Specialty section:
This article was submitted to Neuroendocrine Science, a section of the journal Frontiers in Endocrinology

Received: *09 August 2018*
Accepted: *16 January 2019*
Published: *04 February 2019*

Citation:
Xiao D, Kou H, Gui S, Ji Z, Guo Y, Wu Y and Wang H (2019) Age-Characteristic Changes of Glucose Metabolism, Pancreatic Morphology and Function in Male Offspring Rats Induced by Prenatal Ethanol Exposure. Front. Endocrinol. 10:34. doi: 10.3389/fendo.2019.00034

Intrauterine growth restricted offspring suffer from abnormal glucose homeostasis and β cell dysfunction. In this study, we observed the dynamic changes of glucose metabolic phenotype, pancreatic morphology, and insulin synthesis in prenatal ethanol exposure (PEE) male offspring rats, and to explore the potential intrauterine programming mechanism of the glucocorticoid-insulin-like growth factor 1 (GC-IGF1) axis. Ethanol (4 g/kg·d) was administered through oral gavage during gestational day (GD) 9–20. Serum glucose and insulin levels, pancreatic β cell mass, and expression of glucocorticoid receptor (GR), IGF1 and insulin were determined on GD20, postnatal week (PW) 6, PW12 with/without chronic stress (CS), and PW24, respectively. Both intraperitoneal glucose and insulin tolerance tests were conducted at PW12 and PW24. Results showed that the serum glucose and insulin levels as well as pancreatic β cell mass were reduced on GD20 in PEE males compared with the controls, while pancreatic GR expression was enhanced but IGF1 and INS1/2 expression were suppressed. After birth, compared with the controls, β cell mass in the PEE males was initially decreased at PW6 and gradually recovered from PW12 to PW24, which was accompanied by increased serum glucose/insulin levels and insulin resistance index (IRI) at PW6 and decreased serum glucose contents at PW12, as well as unchanged serum glucose/insulin concentrations at PW24. In addition, both improved glucose tolerance and impaired insulin sensitivity of the PEE males at PW12 were inversed at PW24. Moreover, at PW6 and PW12, pancreatic GR expression in the PEE group was decreased, while IGF1 expression was reversely increased, resulting in a compensatory increase of insulin expression. Moreover, CS induced pancreatic GR activation and inhibited IGF1 expression, resulting in impaired insulin biosynthesis. Conclusively, the above changes were associated with age and the intrauterine programming alteration of GC-IGF1 axis may be involved in prenatal and postnatal pancreatic dysplasia and impaired insulin biosynthesis in PEE male offspring.

Keywords: prenatal ethanol exposure, intrauterine growth restriction, pancreatic β cell development, insulin expression, glucocorticoids-insulin-like growth factor 1 axis

INTRODUCTION

Alcohol consumption is common in both developing and developed countries. Epidemiological studies have shown that the alcoholism rate in young women has increased in recent years (1), and some of female alcoholics could not quit drinking during pregnancy (2). Prenatal alcohol exposure can lead to a range of adverse developmental outcomes in offspring, which are collectively termed fetal alcohol spectrum disorder (FASD) (3). In European countries, the morbidity of FASD is 0.97 per 1,000 births, whereas the morbidity of FASD in U.S. is 1.95 per 1,000 births (4). As one of the primary symptoms of FASD, intrauterine growth restriction (IUGR) is usually diagnosed with a birth weight and/or length below the 10th percentile for gestational age and an abdominal circumference that is less than the 2.5th percentile, with pathologic restriction of fetal growth (5). Human surveys and animal studies indicate that IUGR offspring induced by prenatal ethanol exposure (PEE) are characterized by altered glucose homeostasis and an increased risk of type 2 diabetes (T2DM) in adulthood (6, 7). It has been suggested that PEE induces glucose intolerance and hyperinsulinemia in IUGR male rats on postnatal day (PD) 91 (6, 8) and that the abnormality of glucose metabolism is more substantial in PEE male offspring (9, 10).

Intrauterine environmental challenges can "program" pancreatic β-cell structure and function (11, 12), which lead to glucose-insulin metabolic dysfunction and increased T2DM risk in adult offspring (13). The postnatal dysfunction of metabolic phenotype and abnormal pancreatic morphology induced by PEE have been reported in some studies (6–8, 14). However, these studies have some contradictory results, which might be attributed to a single selected time point for the investigations (15). Therefore, the dynamic changes of pancreatic development and glucose metabolism in PEE offspring, as well as the intrauterine programming mechanism, remains to be clarified.

It has been documented that glucocorticoids (GC) could affect pancreatic differentiation *in utero* (16, 17). High levels of glucocorticoids might induce an imbalance of pancreatic differentiation, reduction of β cell mass, and deceleration of insulin expression and secretion (16, 18). Insulin-like growth factor 1 (IGF1) is one of the key factors regulating pancreatic development (19). IGF1 not only promotes rapid division and proliferation of pancreatic β cells (20, 21) but also suppresses their apoptosis (20, 22). Furthermore, the IGF1 signaling pathway could regulate the proliferation of pancreatic precursor cells to affect the directional differentiation of β cells (23). It has been documented that glucocorticoids could reduce IGF1 expression in various cells via glucocorticoid receptor (GR) activation (24, 25). The evidence mentioned above suggests that the effect of glucocorticoids on IGF1 expression may play an important role in pancreatic development and β cell mass.

Previously, we have demonstrated that ethanol administered though oral gavage on gestational day (GD) 9–20 caused IUGR in rats (26). Furthermore, PEE can induce fetal rat over-exposure to maternal GC, which program IUGR offspring to be susceptible to multiple adult diseases (26–28). It is still unknown whether high levels of glucocorticoids in fetal blood can change the expression of IGF1 in the pancreas and further affect pre- and postnatal pancreatic development and insulin synthesis. In previous studies, we found a negative relationship between serum corticosterone (CORT) levels and IGF1 contents in PEE offspring before and after birth; this negative relationship also correlates to the increased susceptibility to metabolic diseases. Based on these findings, we proposed a programming alteration mechanism of the glucocorticoid-insulin-like growth factor 1 (GC-IGF1) axis to explain multi-organ development toxicity and disease susceptibility in PEE offspring (26, 28).

Researches reveal that IUGR is associated with glucose intolerance in both men and women during adulthood (29), while the female offspring of undernourished rats do not develop glucose intolerance (30) or develop insulin resistance only in old age (31), suggesting gender-specific programming of glucose metabolism in these animals. Evidence also reveals that males are more sensitive to early life programming of insulin action than females (32). In this study, we observed dynamic changes in the glucose metabolic phenotype, pancreatic morphology and insulin synthesis in the PEE male offspring. The selected time points include GD20, postnatal week (PW) 6, 12, and 24, which are approximately equivalent to the fetus, childhood, early, and late stages of adulthood in humans (33). Moreover, a previously described chronic stress (CS) test, induced by a 2-week ice-water swimming test from PW10 (33, 34), was used to confirm the involvement of the GC-IGF1 axis in the alteration of pancreatic development and insulin synthesis induced by PEE. This study is significant for clarifying the developmental toxicity of ethanol and seeking early prevention and treatment strategies for fetal-originated adult diabetes.

MATERIALS AND METHODS

Chemicals and Reagents

Ethanol (analytical pure grade) was purchased from Zhen Xin Co., Ltd. (Shanghai, China). Isoflurane was obtained from Sinopharm Chemical Reagent Co., Ltd. (Shanghai, China). Ultrasensitive Rat insulin ELISA kits, Rat insulin ELISA kits and Rat/Mouse Proinsulin ELISA kits were provided by Mercodia (Uppsala, Sweden). Glucose oxidase assay kits were purchased from Mind Bioengineering Co. Ltd. (Shanghai, China). TRIzol reagent was purchased from Invitrogen Co. (Carlsbad, CA, USA). Reverse transcription and real-time quantitative polymerase chain reaction (RT-qPCR) kits were offered by TaKaRa Biotechnology Co., Ltd. (Dalian, China). Oligonucleotide primers for rat RT-qPCR genes (PAGE purification) were custom synthesized by Sangon Biotech Co., Ltd. (Shanghai, China). RNAlater was provided by Qiagen (Düsseldorf, North Rhine-Westphalia, Germany). Glucocorticoid receptor (GR), IGF1, and insulin gene enhancer protein isl1 (ISL1) antibodies were obtained from Abcam (San Francisco, California, USA). Insulin antibody was provided by Sigma-Aldrich (St. Louis, Missouri, USA). Immunohistochemical staining agents were purchased from Zhongshan Golden Bridge Biotechnology Co. Ltd. (Beijing, China).

Animals and Treatment

This project was performed at the Center for Animal Experiment of Wuhan University (Wuhan, China), which is recognized and designated by the Association for Assessment and Accreditation of International Laboratory Animal Care. This study was carried out in accordance with the Guidelines for the Care and Use of Laboratory Animals of the Chinese Animal Welfare Committee (AAALAC International). The protocol was approved by the Committee on the Ethics of Animal Experiments of the Wuhan University School of Medicine (permit number: 14016). Specific pathogen free Wistar rats (12∼13-week-old, with weights of 197–221 g for females and 241–275 g for males) were purchased from the Experimental Center of Hubei Medical Scientific Academy (No. 2012–2014, certification number: 42000600002258, license number: SCXK [Hubei]).

Animals were fed in metal wire cages in temperature-controlled conditions and allowed *ad libitum* access to tap water and standard chow at all times (room temperature: 18–22°C; humidity: 40–60%, light cycle: 12 h light-dark cycle; 10–15 air changes per hour). After 7 days of acclimation, each two female rats and one male rat were mated from 7:00 p.m. to 7:00 a.m. The appearance of a vaginal plug or vaginal smear with sperm cells was confirmed as successful mating. We designated that day as GD0. Pregnant rats were then transferred to individual cages. From GD9 to GD20, the pregnant rats were given ethanol (4 g/kg·d, 40%) or distilled water through oral gavage at 8:00 a.m. every day as described in previous studies (26, 35). The animal processing schedule was shown in **Figure 1**.

For fetal rat experiment, a portion of pregnant rats were anesthetized with isoflurane and decapitated, and fetal rats were obtained through cesarean section on GD20. To eliminate the interferences induced by litter size, only pregnant rats with 8∼14 pups were included and each group finally contained 14 pregnant rats. The fetal rats were quickly picked and weighed. Fetal rats were decapitated, and the pancreases were weighed. The fetal blood or pancreases (per litter) were collected and pooled into one independent sample, respectively. Fetal blood was centrifuged at 2263 × g for 15 min, and the serum was stored at −80°C. Some intact fetal pancreases (including the head, body and tail) were weighed and put into RNAlater (1 mg: 100 μl) overnight at 4°C, and then transferred to the −80°C refrigerator for gene expression analysis. Other intact fetal pancreases (head, body, and tail) were selected and fixed per litter ($n = 5$) for histology observation or fixed for electron microscope observation.

For postnatal rat experiment, the remaining pregnant rats (including the control and PEE groups) were subjected to delivery. The pups remained with their original mothers after birth and throughout lactation. To ensure adequate and relatively equal intake of nutrients during the suckling period, only litters with 8∼14 pups were chosen for the following experiment and normalized to 8 pups per litter (male: female = 1:1) (36). Finally, a total of 16 litters (8 controls & 8 PEEs) were included and all pups were weaned until postnatal week (PW) 4. Four male offspring rats from each litter were selected and assigned to the four studies at different postnatal time points or condition (i.e., PW6, PW12, PW12 with CS and PW24), respectively. The CS test was achieved by forced 5-min ice-water swimming per day (5–7°C) from PW10 to PW12 (33, 34). Intraperitoneal glucose tolerance tests (IPGTT) and insulin tolerance tests (ITT) were performed at PW12 and PW24. Pups were anesthetized with isoflurane and then decapitated. Blood and pancreases were collected. Intact pancreases (including head, body, and tail) were weighed. Blood was centrifuged at 2263 × g for 15 min, and the serum was stored in an −80°C refrigerator for gene expression analysis. Some pancreases were weighed and put into RNAlater (1 mg: 100 μl) overnight at 4°C, and then they were restored at −80°C. Other pancreases ($n = 5$) were fixed in a 10% neutral formalin solution for histology observation.

IPGTT, ITT, and Area Under the Curve (AUC)

Based on the reference (37), rats were pre-fasted for 12 h before the IPGTTs, which started at 8:00 a.m. Each rat was intraperitoneally administered glucose (2 g/kg). The interval time of administration to each animal was 2 min, and the total operating time was limited to within 30 min. Blood glucose levels which measured 0, 15, 30, 60, and 120 min after the glucose challenge were determined using a glucometer (ACCU-CHEK Performa, Roche). The AUCs were calculated using the trapezoidal rule (38). ITTs were administered after a 5 h fast (8:00 a.m.−1:00 p.m.) (39), and insulin (1 unit/kg) was intraperitoneally injected. The measurement of blood glucose levels which measured 0, 15, 30, 60, and 120 min after the insulin challenge and calculation of the corresponding AUCs was the same as that described for the IPGTTs. Con. N min represented serum glucose at each time point. Time N min-N min represented the time gap between two time points.

$$\text{Con. } N_{min}\ (\%) = \text{Con. } N_{min} \,/\, \text{Con. } 0_{min}$$

$$\text{AUC} = (\text{Con. } 0_{min} + \text{Con. } 15_{min})/2 \times \text{Time } 0_{min}\text{-}15_{min} + (\text{Con. } 15_{min} + \text{Con. } 30_{min})/2 \times \text{Time } 15_{min}\text{-}3_{min} + (\text{Con. } 30_{min} + \text{Con. } 60_{min})/2 \times \text{Time } 30_{min}\text{-}60_{min} + (\text{Con. } 60_{min} + \text{Con. } 120_{min})/2 \times \text{Time } 60_{min}\text{-}120_{min}$$

Serum Glucose/Insulin Concentrations and Pancreatic Insulin/Proinsulin Contents Determination

The serum insulin and glucose levels were measured through ELISA and biochemical assay kits, respectively, following the manufacturer's protocol. The fasting glucose (FG), fasting insulin (FI) and insulin resistance index (IRI) was acronymized as b. Pancreatic insulin and proinsulin were extracted with acidic ethanol (1.5% [vol/vol] HCl in 75% [vol/vol] ethanol) and assayed using ELISA kits.

$$\text{IRI} = \text{FG (mmol/L)} \times \text{FI (mIU/L)}/22.5$$

Pancreatic Morphometric Analysis

Pancreases at GD20, PW6, PW12, and PW24 were weighed and fixed in 10% neutral buffered formalin overnight, dehydrated, and embedded in paraffin. Each analytical result of the pathological indices was obtained from a total of five animals per group, with five complete longitudinal sections (5 μm) per embedded pancreas (i.e., at their maximum widths) in (at minimum) 200 μm intervals. The hematoxylin-eosin (HE) and insulin immunohistochemical staining were subjected to the

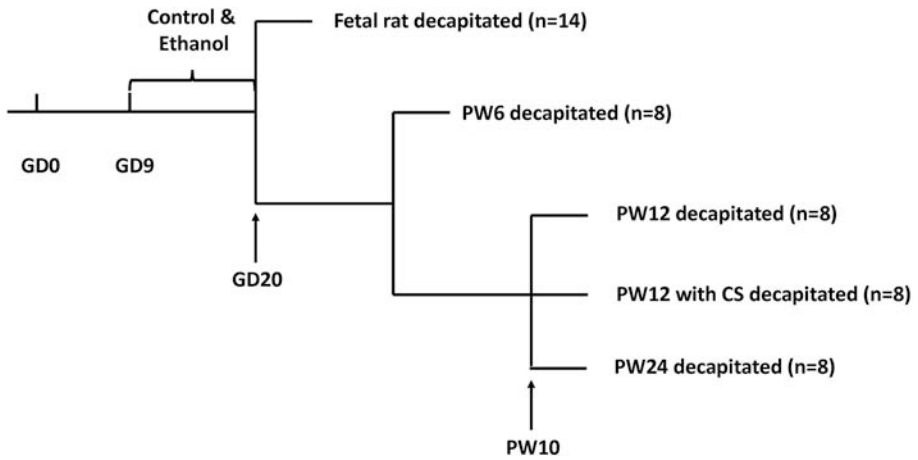

FIGURE 1 | Animal processing schedule. Intrauterine growth restriction modeling was performed using prenatal ethanol exposure (4 g/kg.d) from gestational day (GD) 9 to GD20. Beginning at postnatal week (PW) 10, some pups were subjected to a 5 min ice-water swim (5–7°C) to induce chronic stress. Pups were decapitated at GD20, PW6, PW12, PW12 with chronic stress, and PW24.

TABLE 1 | Oligonucleotide primers and PCR conditions of rat in quantitative real-time PCR.

Genes	Forward primer	Reverse primer	Accession number	Product (bp)	Annealing (°C)
ISL1	ACTGAGTGACTTCGCCTTGC	ATCTGGGAGCTGAGAGGACA	NM_017339.3	133	60
INS1	TCAGCAAGCAGGTCATTGTT	AGGTACAGAGCCTCCACCAG	NM_019129.3	147	57
INS2	TCTTCTACACACCCATGTCCC	GGTGCAGCACTGATCCAC	NM_019130.2	149	55
IGF1	GACCAAGGGGCTTTTACTTCAAC	TTTGTAGGCTTCAGCGGAGCAC	NM_178866.4	148	60
GR	CACCCATGACCCTGTCAGTG	AAAGCCTCCCTCTGCTAACC	NM_012576.2	156	54
GAPDH	GCAAGTTCAACGGCACAG	GCCAGTAGACTCCACGACA	NM_017008.4	140	60

ISL1, insulin gene enhancer protein isl1; INS1, insulin 1; INS2, insulin2; IGF1, insulin-like growth factor 1; GR, glucocorticoid receptor; GAPDH, glyceraldehyde-3-phosphate dehydrogenase.

pancreases of GD20 to PW24. As a negative control, pancreatic sections underwent similar treatment, and no positive reactions to the antibody against insulin were observed (data not shown). Sections were viewed at a magnification of ×40. Approximately 3–4 fields per fetal pancreas section and 30–40 fields per postnatal pancreas section were acquired, and we used NIS-Elements Br 4.20 (Nikon, USA) to analyze the total pancreas areas and β-cell areas (insulin-positive cells). The size of the insulin-positive cell area and the pancreatic tissue area were measured (average value, five sections per animal). The β cell fraction and mass were calculated according to the formula provided below (40). The unit of β cell mass/body weight was μg/g (39). Fetal pancreases were cut and fixed with 2.5% glutaraldehyde in 0.1 M phosphate buffer (pH 7.4) for 2 h at 4 °C and post fixed with 1% osmium tetroxide. We dehydrated these tissues with a graded series of ethanol and then embedded them in Epon 812. Ultrathin sections (∼50 nm) were cut with LKB-V ultramicrotome (Bromma, Sweden), dual stained with uranyl acetate and lead citrate and observed with a Hitachi H600 transmission electron microscope (EM) (Hitachi, Tokyo, Japan).

β cell fraction (%) = β cell area/total pancreas area × 100

β cell mass (mg) = β cell fraction × pancreas weight.

Pancreatic mRNA and Protein Expression Analysis

GD20 and PW6 pancreases (including the head, body, and tail) were grinded and mixed in liquid nitrogen. We used 25 mg of pancreatic tissue to extract total RNA, based on the manufacturer's protocol (RNA-Solv Reagent). The concentrations and purity of total RNA were measured in A_{260nm} and A_{280nm}, and the rates of A_{260nm} /A_{280nm} were kept between 1.8 and 2.0. The total RNA concentrations were adjusted to 1 μg/μL. cDNA synthesis and RT-qPCR amplification were performed using the manufacturer's protocol. Relative standard curves were constructed for the following target genes: GR, IGF1, ISL1, insulin 1 (INS1), and INS2. The oligonucleotide primers and annealing temperatures in RT-qPCR are listed in **Table 1**. To precisely quantify the gene transcripts, the mRNA level of the housekeeping gene glyceraldehyde phosphate dehydrogenase (GAPDH) was measured and used as the quantitative control (26, 35).

The relative protein expressions of GR, IGF1, ISL1, and insulin in PW12 and PW24 were semi-quantified by immunohistochemistry (IHC) and the area of these protein expression in the pancreatic tissues also could be observed. PW12 and PW24 pancreases were embedded and sliced as

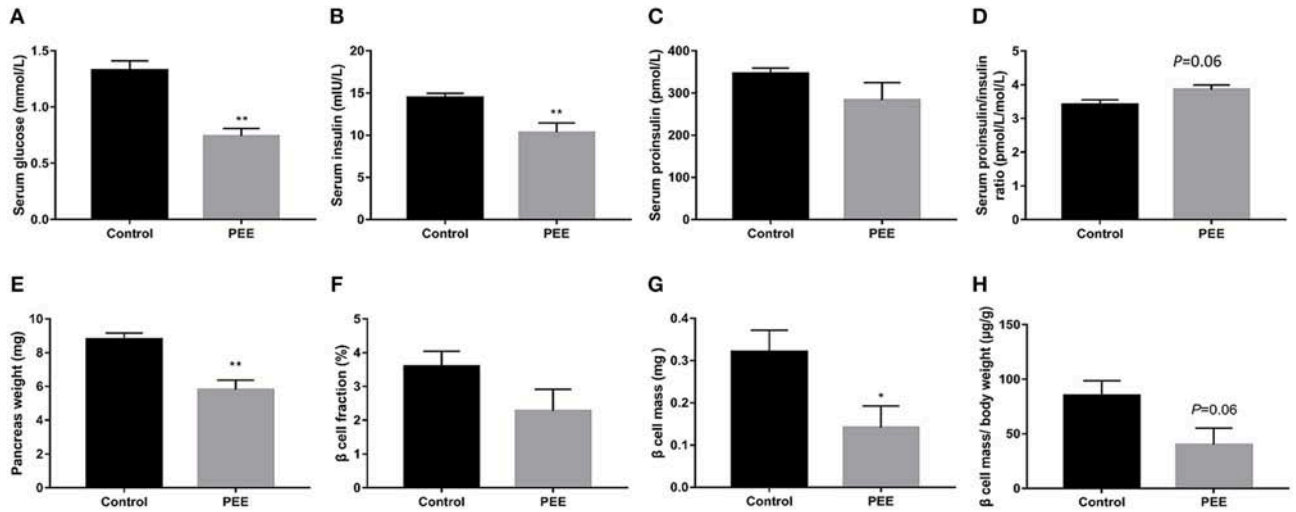

FIGURE 2 | Effects of prenatal ethanol exposure (PEE) on islet function and pancreatic morphology in male fetal rats. **(A)** Serum glucose, **(B)** serum insulin, **(C)** serum proinsulin, **(D)** ratios of serum proinsulin/insulin, **(E)** pancreas weight, **(F)** pancreatic β cell fraction, **(G)** pancreatic β cell mass, **(H)** pancreatic β cell mass/ body weight ratio, Mean ± S.E.M., $n = 14$ for fasting glucose serum and insulin. $^{*}P < 0.05$, $^{**}P < 0.01$ vs. control. The representative images of pancreatic insulin immunohistochemical staining (×40 and ×400) were shown in **Supplementary Figures 1A–D**.

mentioned above. As negative controls, pancreatic sections underwent similar treatment, and no positive reactions to the antibody against GR, IGF1, ISL1, and insulin were observed (data not shown). The mean density for pancreases in the same group was taken as the expression level for the protein of interest. Sections were viewed at a magnification of ×400. Approximately 200 fields per postnatal pancreas section were acquired, and we used NIS-Elements Br 4.20 (Nikon, USA) to analyze the mean density of GR, IGF1, ISL1, and insulin staining.

Statistical Analysis

All data presented were expressed as the mean ± S.E.M., and the statistical analysis was performed with SPSS for Windows version 19 (SPSS Science Inc., Chicago, IL, USA). The normality and homogeneity of the variances were analyzed using the one-sample Kolmogorov–Smirnov test and Levene's test, respectively. Differences between the control and PEE groups were compared using a repeated measures ANOVA (IPGTT and ITT) or two-tail Student's test. Groups which were assumed to have normal distribution, and equal variances were compared through repeated measures ANOVA and Student's two-tailed *t*-test. When data failed tests for normal distribution and homogeneity of variance, we chose the Mann–Whitney U test (equivalent to Wilcoxon W). Statistical significance was designated at $P < 0.05$ and $P < 0.01$.

RESULTS

In Male Fetal Rats

Islet Function and Pancreatic Morphological Changes

In our previous study, a decrease bodyweight and a high IUGR rate were observed in PEE male fetal rats (26). Based on this batch of animals, we further observed changes in islet function and pancreatic morphology of fetal rats. Compared with the controls, serum glucose and insulin levels of the PEE fetal rats were decreased ($P < 0.01$, **Figures 2A,B**), while serum proinsulin level was unchanged (**Figure 2C**), as a result, the ratio of serum proinsulin and insulin presented increasing trend in the PEE offspring ($P = 0.06$, **Figure 2D**). Pancreas weight ($P < 0.01$, **Figure 2E**), β cell mass ($P < 0.05$, **Figure 2G**), and β cells mass/body weight ($P = 0.06$, **Figure 2H**) were all decreased or showed a decreasing trend in the PEE fetal rats, whereas the β cell fraction (**Figure 2F**) did not change. The typical β cell ultrastructure could be observed in the fetal pancreases from the control group (**Supplementary Figures 1E,F**): the mature dense-core β-granules were highly populated, and there were halo spaces between the core and β-granule membrane. However, there was lower electron density and a lack of the characteristic halos of mature β-granules in the PEE group. The above data suggest that islet function was reduced, and pancreatic morphology was impaired in the PEE male fetal rats.

Pancreatic Insulin Biosynthesis, GR and IGF1 Expression Changes

The results indicated that the contents of pancreatic insulin and proinsulin in the PEE group were lower than those in the controls ($P < 0.05$, $P < 0.01$, **Figures 3A,B**), whereas the ratio of proinsulin/insulin was unchanged (**Figure 3C**). Furthermore, compared with the controls, the expression levels of ISL1, INS1, and INS2 mRNA were decreased in the PEE fetal pancreases ($P < 0.01$, **Figure 3D**). Meanwhile, the GR mRNA expression level was increased, while the expression level of the IGF1 gene was decreased ($P < 0.01$, **Figure 3E**). These results suggest that pancreatic insulin biosynthesis was inhibited and that this inhibition was accompanied by increased Gr expression and decreased IGF1 expression.

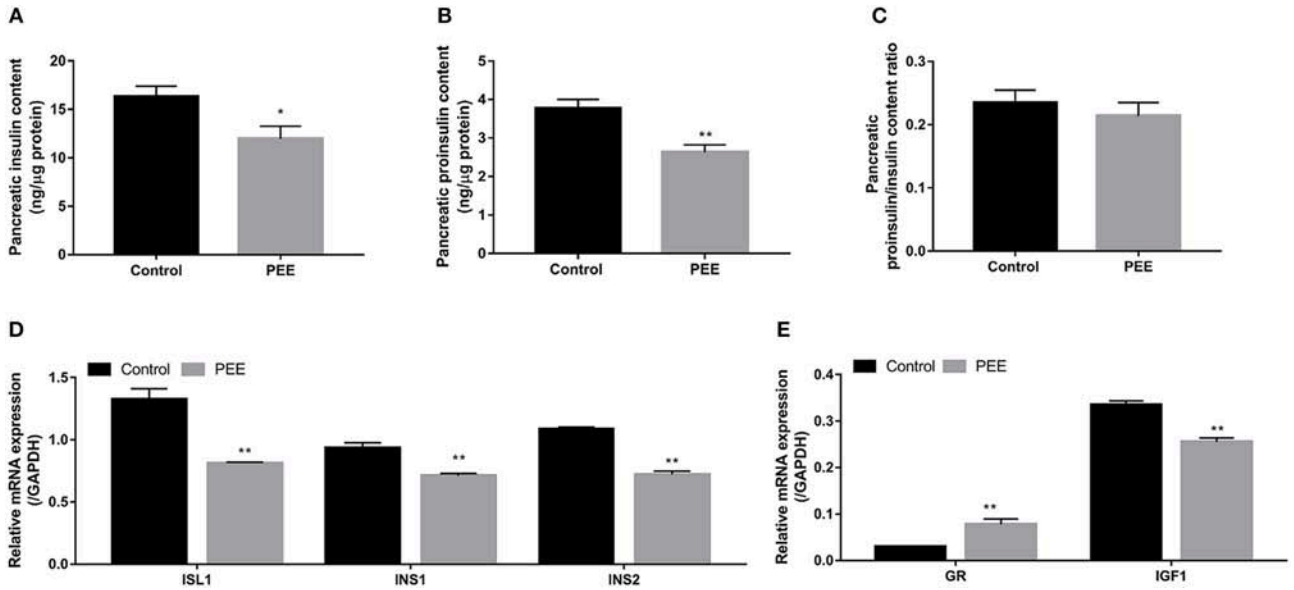

FIGURE 3 | Effects of prenatal ethanol exposure (PEE) on pancreatic insulin synthesis, mRNA expression of glucocorticoid receptor (GR), and insulin-like growth factor 1 (IGF1) in male fetal rats. **(A)** Insulin contents, **(B)** proinsulin contents, **(C)** ratios of proinsulin/insulin, **(D)** mRNA expression of insulin gene enhancer protein isl1 (ISL1), insulin 1 (INS1) and INS2, and **(E)** gene expression of GR and IGF1. Mean ± S.E.M., $n = 14$. $^{*}P < 0.05$, $^{**}P < 0.01$ vs. control.

In Male Offspring Rats at Different Time Points After Birth

Glucose Metabolic Phenotype Changes at Different Time Points

At PW6, serum glucose, insulin levels and IRI were increased in the PEE group compared with the controls ($P < 0.05$, $P < 0.01$, **Figures 4A–C**). However, at PW12, the basal level of serum glucose was significantly decreased ($P < 0.01$, **Figure 4D**), while the serum insulin concentration and IRI did not change in the PEE group (**Figures 4E,F**). In the IPGTT of the PEE group, when compared with the controls, the serum glucose concentration at 30 min was lower in the PEE male pups ($P < 0.05$, **Figure 4G**), while the corresponding AUC was not obviously changed. In the ITT of the PEE group, the 15 min serum glucose concentration was higher than that of the control ($P < 0.01$), whereas the corresponding AUC in the PEE group was 1.13-fold higher than that of the controls ($P = 0.08$, **Figure 4H**). These results suggest that the glucose tolerance was increased, while the insulin sensitivity was decreased in the PEE male pups of PW12. At PW24, the basal serum glucose and insulin levels, as well as the IRI of the PEE male rats, were not altered (**Figures 4I–K**). However, the glucose tolerance of the PEE offspring was remarkably weakened compared with the control, as evidenced by the conspicuous increase in the concentration of blood glucose at 30 min and the increased corresponding AUC after adding the glycemic load ($P < 0.01$, **Figure 4L**). Furthermore, in the ITT, the serum glucose levels of the PEE males at 30 and 120 min, as well as the corresponding AUC, were decreased ($P < 0.01$, $P < 0.05$, **Figure 4M**). These data suggest that a weakened glucose intolerance and enhanced insulin sensitivity existed, although there was no significant change in the glucose metabolic phenotype in the PEE male offspring rats for PW24.

Pancreatic Morphological Changes at Different Time Points

At PW6, compared with the controls, the pancreas weight ($P < 0.01$, **Figure 5A**), β cell fraction ($P = 0.088$, **Figure 5B**), β cell mass ($P < 0.05$, **Figure 5C**), and β cell mass/body weight rate ($P < 0.05$, **Figure 5D**) were all decreased or showed a decreasing trend in the PEE offspring. However, at PW12, the β cell fraction (**Figure 5F**), β cell mass and β cell mass/body weight rate (**Figures 5G,H**) showed no obvious changes, except for the lower pancreas weight ($P < 0.01$, **Figure 5E**). At PW24, the pancreas weight ($P < 0.05$, **Figure 5I**) was still decreased, while the β cell mass ($P = 0.055$, **Figure 5K**) and β cell mass/body weight rate ($P = 0.058$, **Figure 5L**) only showed a decreasing tendency in the PEE group, and the β cell fraction did not show any obvious changes (**Figure 5J**). The above data suggest that β cells demonstrate a "catch-up" growth pattern in the PEE male offspring.

Pancreatic Insulin Biosynthesis, GR and IGF1 Expression Changes at Different Time Points

At PW6, when compared with the respective controls, the GR mRNA expression was unchanged while the IGF1 mRNA expression was increased ($P<0.05$, **Figure 6A**), meanwhile, the expression levels of ISL1, INS1 and INS2 mRNA were significantly increased ($P < 0.01$, **Figure 6B**). At PW12 (**Figures 6C,D**), the GR protein expression level was decreased, however, the IGF1 protein expression level was increased in the PEE offspring rats ($P < 0.01$, $P < 0.05$), and the

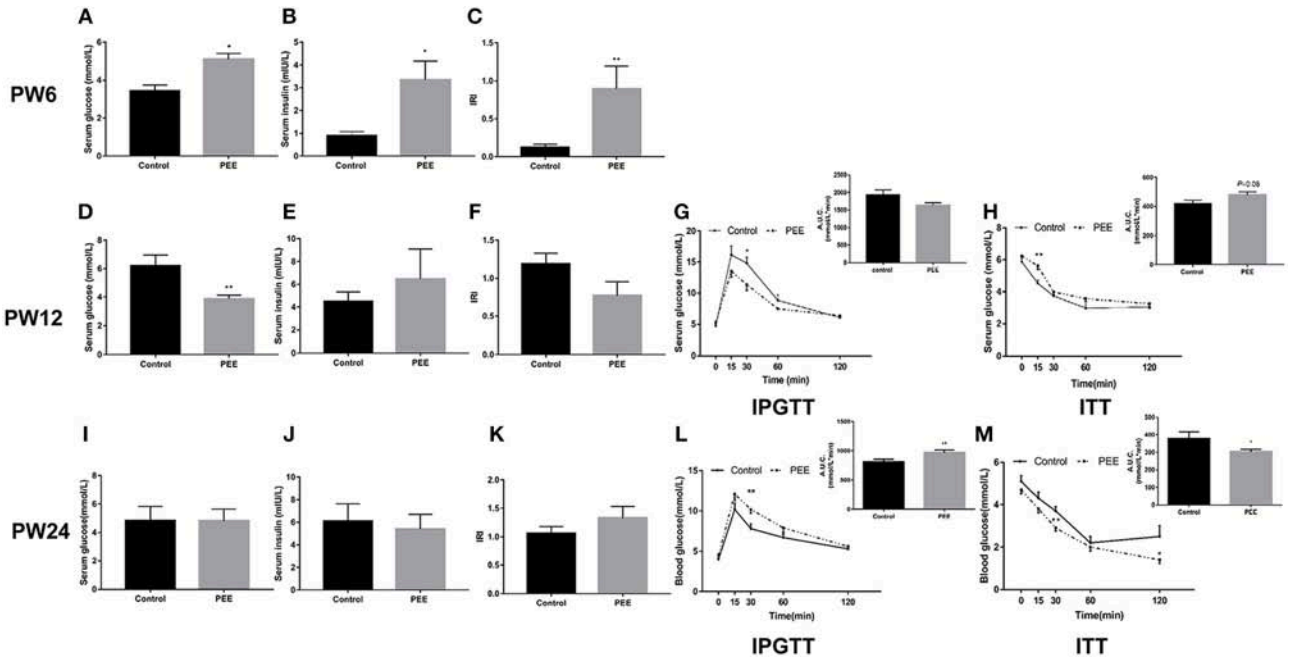

FIGURE 4 | Effects of prenatal ethanol exposure (PEE) on the glucose metabolism phenotype at postnatal week (PW) 6, PW12, and PW24 male offspring rats. **(A–C)** Serum glucose and insulin levels, as well as insulin resistance index (IRI) at PW6, **(D–F)** serum glucose and insulin levels, as well as IRI at PW12, **(G)** blood glucose concentrations during intraperitoneal glucose tolerance test (IPGTT) and area under the curve (AUC) at PW12, **(H)** blood glucose concentrations during insulin tolerance test (ITT) and the AUC at PW12, **(I–K)** serum glucose and insulin levels as well as IRI at PW24, **(L)** blood glucose concentrations during IPGTT and AUC at PW12, and **(M)** blood glucose concentrations during ITT and AUC at PW24. Mean ± S.E.M., $n = 8$. $^{*}P < 0.05$, $^{**}P < 0.01$ vs. control.

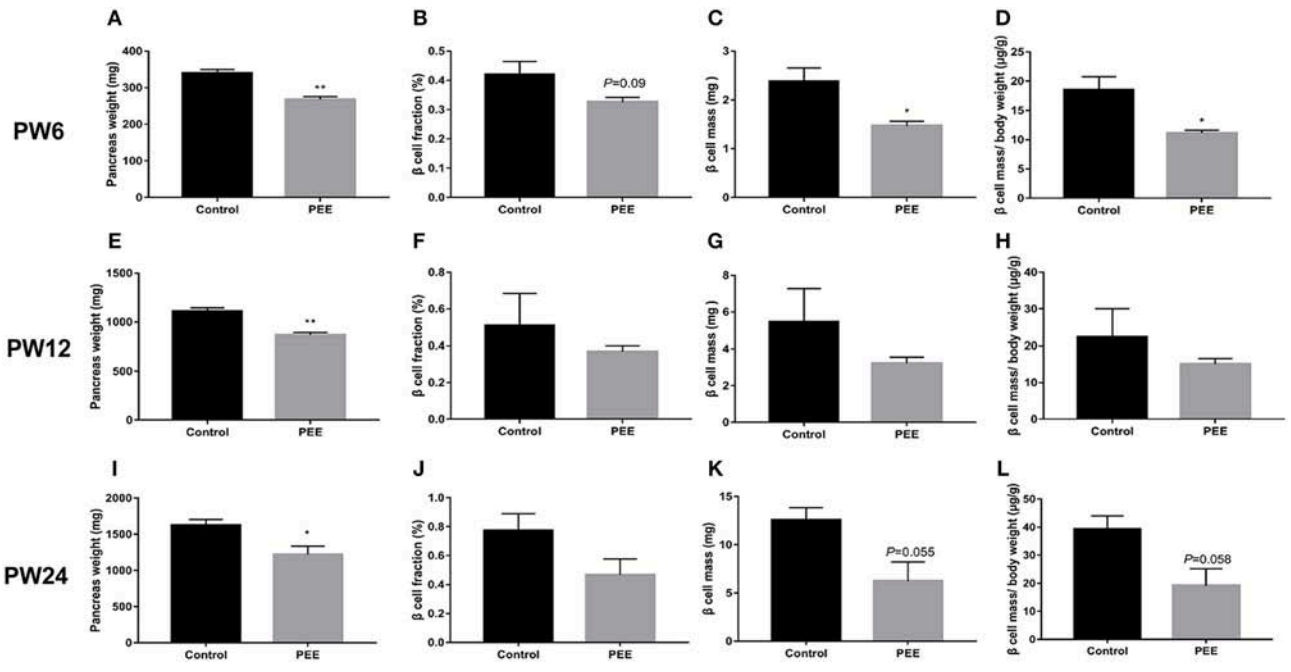

FIGURE 5 | Effects of prenatal ethanol exposure (PEE) on the pancreatic morphology of offspring male rats at postnatal week (PW) 6, PW12 and PW24. **(A)** pancreas weight at PW6, **(B)** β cell fraction at PW6, **(C)** β cell mass at PW6, **(D)** β cell mass/body weight rates at PW6, **(E)** pancreas weight at PW12, **(F)** β cell fraction at PW12, **(G)** β cell mass at PW12, **(H)** β cell mass/body weight rates at PW12, **(I)** pancreas weight at PW24; **(J)** β cell fraction at PW 24, **(K)** β cell mass at PW 24, and **(L)** β cell mass/body weight rates at PW24. Mean ± S.E.M., $n = 5$. $^{*}P < 0.05$ $^{**}P < 0.01$ vs. control. The representative images of pancreatic insulin immunohistochemical staining (×40) were shown in **Supplementary Figures 2A,B,E,F,I,J**.

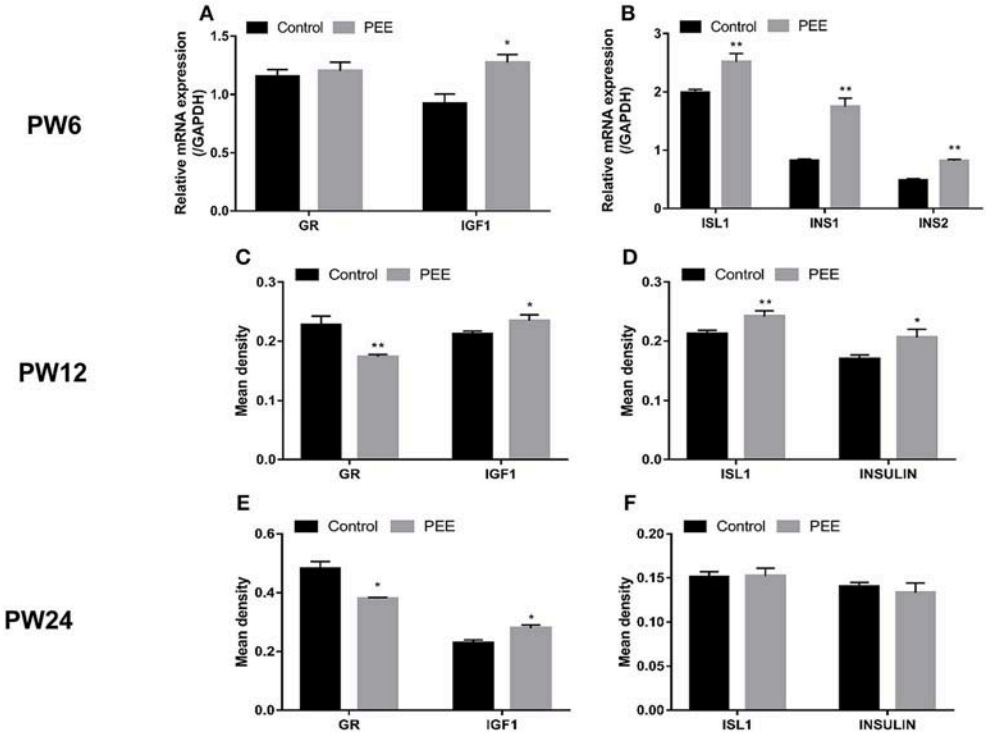

FIGURE 6 | Effects of prenatal ethanol exposure (PEE) on the expression of pancreatic insulin, glucocorticoid receptor (GR) and insulin-like growth factor 1 (IGF1) at postnatal week (PW) 6, PW12, and PW24 male offspring rats. **(A,B)** mRNA expression levels of GR, IGF1, insulin gene enhancer protein isl1 (ISL1), insulin1 (INS1) and INS2 at PW6, **(C,D)** the mean density of the immunohistochemistry of GR, IGF1, ISL1 and insulin at PW12, **(E,F)** the mean density of immunohistochemistry of GR, IGF1, ISL1 and insulin at PW24. Mean ± S.E.M., $n = 5$. $^{*}P < 0.05$, $^{**}P < 0.01$ vs. control. The representative images of pancreatic GR, IGF1, and ISL1 immunohistochemical staining (×400) were shown in **Supplementary Figure 3** and the representative images of pancreatic INSULIN immunohistochemical staining (×400) were shown in **Supplementary Figures 2C,D,G,H,K,L**.

expression levels of ISL1 and insulin protein were increased ($P < 0.01$, $P < 0.05$). At PW24 (**Figures 6E,F**), the GR protein expression level was decreased, while that of the IGF1 protein was still increased ($P < 0.05$, $P < 0.05$), however, the protein expression levels of ISL1 and insulin were not significantly changed. These results suggest that the insulin synthesis was enhanced after birth in the PEE male offspring and that this enhancement was accompanied by the down-regulated expression of GR and the up-regulated expression of IGF1 and ISL1. Finally, the expression levels of ISL1 and insulin decreased to the control levels during the late stage of adulthood.

Glucose Metabolic Phenotype, Pancreatic GR/IGF1 Expression, and Insulin Biosynthesis Changes at PW12 After a Chronic Stress Test

Furthermore, we aimed to confirm the involvement of the GC-IGF1 axis in pancreatic development and insulin synthesis in the PEE offspring. The results showed that, in the PEE group subjected to the CS, the serum glucose level was higher, while the serum insulin level was lower ($P < 0.01$, $P < 0.05$, **Figures 7A,B**), and the IRI was unchanged (**Figure 7C**). Meanwhile, the protein expression level of GR was higher, and those of IGF1, ISL1 and insulin were all decreased, compared with the controls ($P < 0.05$, $P < 0.01$, **Figures 7D,E**).

DISCUSSIONS

Age-Characteristic Changes of Glucose Metabolic Abnormalities in Male PEE Offspring Rats

We have previously demonstrated that PEE causes a reduced birth weight and a high IUGR rate (26). Based on this batch of animals, in the present study, we found that the basal serum glucose and insulin levels of the PEE male offspring rats were decreased at GD20, however, transient insulin resistance appeared at PW6, manifesting as increased basal serum glucose and insulin levels and IRI, which is similar to the finding of age-dependent insulin resistance in a childhood cohort study (41). At PW12, the basal level of serum glucose was remarkably diminished, however, the basal level of serum insulin showed no significant change, and the glucose tolerance was increased, while the insulin sensitivity was decreased in the PEE male offspring. At PW24, the basal levels of serum glucose and insulin were not changed, however, weakened glucose intolerance and enhanced insulin sensitivity were found in the PEE male offspring. The evidences described above confirmed the abnormalities of glucose metabolic phenotype before and after birth, glucose tolerance and insulin sensitivity after birth in the PEE male offspring rats, which were age-characteristic changes and at least partially resulted from pancreatic dysplasia.

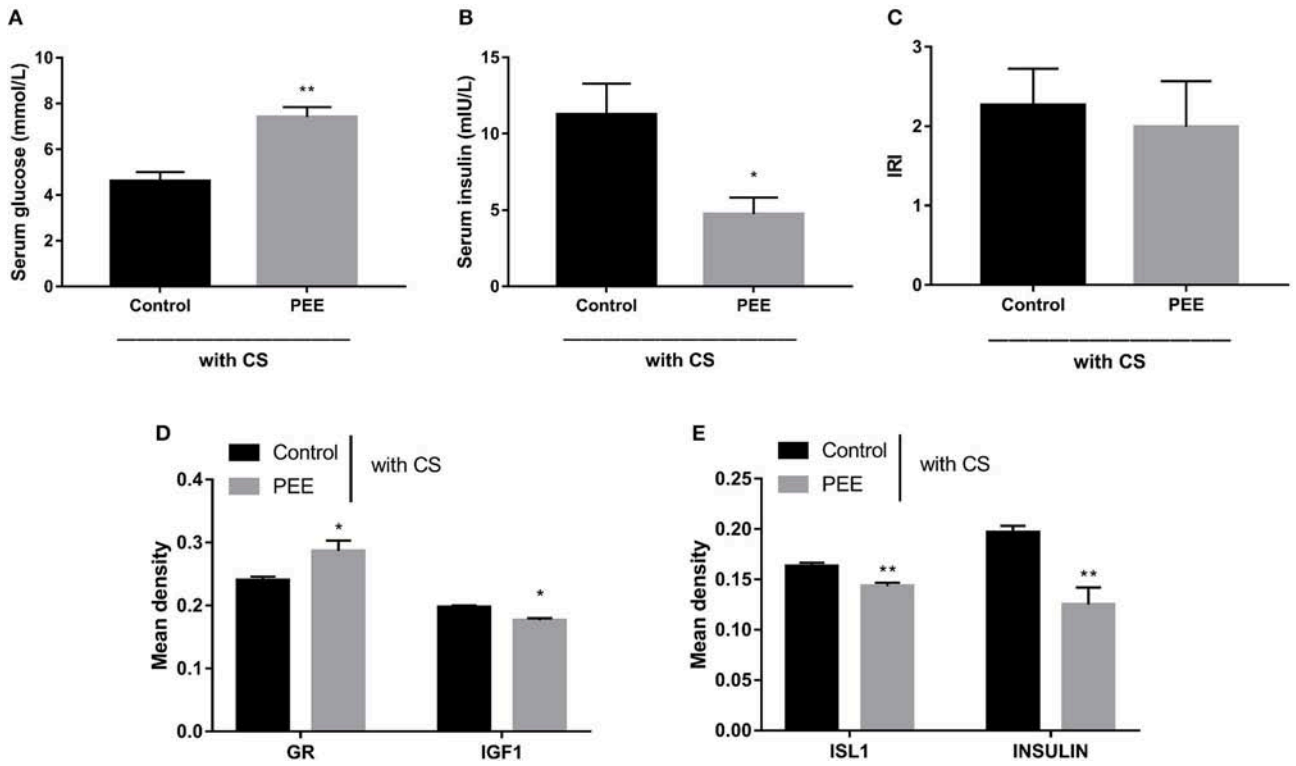

FIGURE 7 | Effects of prenatal ethanol exposure (PEE) on the glucose metabolic phenotype and the expression levels of pancreatic insulin, glucocorticoid receptor (GR), and insulin-like growth factor 1 (IGF1) at postnatal week (PW) 12 in male offspring rats undergoing chronic stress (CS). **(A,B)** Fast serum glucose and insulin, **(C)** insulin resistance index (IRI), **(D,E)** the mean density of immunohistochemistry of glucocorticoid receptor (GR), IGF1, insulin gene enhancer protein isl1 (ISL1) and insulin, Mean ± S.E.M., $n = 5$. $^{*}P < 0.05$, $^{**}P < 0.01$ vs. control. The representative images of pancreatic GR, IGF1, ISL1 and INSULIN immunohistochemical staining (×400) were shown in **Supplementary Figure 4**.

The Abnormalities of Pancreatic β Cell Morphology and Function in Male PEE Fetal Rats

As the sole source organ of insulin, pancreas plays an important role in the regulation of glucose metabolism. Multiple adverse intrauterine environments can induce developmental programming alterations of offspring's pancreas, further affecting its insulin synthesis (40, 42–44). In clinical studies (45–47) and IUGR animal model of food restriction (11, 48), low-protein diet and placenta-uterine deficiency (49–51), a reduction in β cell mass could often be observed. In the present study, the fetal serum glucose and insulin levels were decreased in the male fetal rats of PEE. Meanwhile, the damages in islet morphology and the EM images also suggested that PEE resulted in pancreatic morphological and insulin synthetic function abnormalities in the male fetal rats.

It has been suggested that "fetal over-exposure to maternal glucocorticoids" is one of the important factors contributing to the permanent changes in fetal structure, physiology and metabolism (52). *In vivo* and *in vitro* experiments have shown that dexamethasone can induce pancreatic dysplasia, reduce cell number, and decrease insulin expression and secretion (16). Glucocorticoids could repress IGF1 expression in multiple types of organs and cells via GR activation (24, 25), and decreased IGF1 expression could further inhibit the expression of ISL1 (53), which is one of the most important transcription factors involved in the regulation of pancreatic development and insulin expression (54). In our previous researches, we have demonstrated that PEE could induce fetal over-exposure to maternal glucocorticoids *in utero* (26, 55, 56), which further increased the GR expression [e.g., hippocampus (56) and adrenals (26)] and decreased IGF1 expression [e.g., adrenals (26), and liver (28)] of multiple fetal organs, and thus resulted in their developmental programming alterations. In addition, in other IUGR models induced by prenatal exposure to xenobiotics [such caffeine (57), nicotine (58)], we have also found the fetal over-exposure to maternal glucocorticoids, and the alterations of GR expression in multiple fetal organs, accompanied with related developmental programming changes. In the present study, we found that the contents of pancreatic insulin and proinsulin were lower, and the expression levels of INS1, INS2 and ISL1 mRNA were decreased in the PEE group, furthermore, the GR mRNA expression level was increased but the expression level of IGF1 mRNA was decreased. These results suggested that the lower insulin biosynthesis was likely associated with the pancreatic increased GR expression and decreased IGF1 expression by PEE-induced fetal over-exposure to maternal glucocorticoids.

The Postnatal Changes of Glucose Homeostasis, Pancreatic β Cell Morphology and Function in Male PEE Offspring Rats

The changes of pancreatic β cell morphology and function induced by adverse intrauterine environments not only appeared *in utero* but also emerged after birth (40, 59, 60). In the present study, the β cell mass of PEE fetal rats were significantly decreased, however, this reduction of β cell population became progressively less obvious after birth. In addition, both serum insulin levels and the insulin gene expression of the PEE offspring were not lower than those of the controls at all selected postnatal time points, which was accompanied by persistent enhanced pancreatic IGF1 expression. As we know, IGF1 is important in regulating β cell growth (61) and usually mediates the postnatal catch-up growth pattern in IUGR offspring (62). Therefore, we presumed that this persistent enhanced pancreatic IGF1 expression might contribute to the postnatal dynamic changes of pancreatic β cell morphology and function in the PEE offspring.

Glucose tolerance relies on several important aspects, including β cell mass and function-associated insulin secretion, as well as insulin availability of the targeted organs (63). At PW12, for the PEE male offspring, although the basal serum insulin level showed no significant changes, the basal serum glucose level was remarkably diminished, while the glucose tolerance was increased but the insulin sensitivity was decreased, suggesting that the sensitivity of peripheral tissues to endogenous insulin might be higher than the sensitivity to exogenous insulin. However, at PW24 in the PEE male offspring, the glucose tolerance was impaired while the insulin sensitivity seems to be improved, suggesting that the sensitivity of peripheral tissues to endogenous insulin might be lower than that to exogenous insulin in the late stage of adulthood. A previous study showed that total insulin and IGF1 resistance in pancreatic β cells causes overt diabetes (64). Therefore, we speculated that the progressive glucose intolerance of PEE offspring from PW12 to 24 might be due to the loss of sensitivity to endogenous insulin and IGF1.

GC-IGF1 Axis Programming Mechanism Might May be Involved in Age-Characteristic Changes of Pancreatic β Cell Morphology and Function Induced by PEE

Glucocorticoids are a class of key metabolic hormones regulating fetal growth and development as well as the organ maturity *in utero*, while IGF1 plays an insulin-like growth promoting role and is the main factor contributes to IUGR and postnatal catch-up growth (65, 66). In a series of our previous studies, we have demonstrated that PEE induces fetal overexposure to maternal glucocorticoids. The excessive circulatory glucocorticoids in fetus not only inhibits the functional development of HPA axis (67), but also alters the structure and function of multiple fetal multi-organs [i.e., liver (28) and adrenal (26)] via local GR activation and the downstream IGF1 signaling suppression. Furthermore, these changes, particularly the negative regulatory relationship between circulatory glucocorticoids (accompany

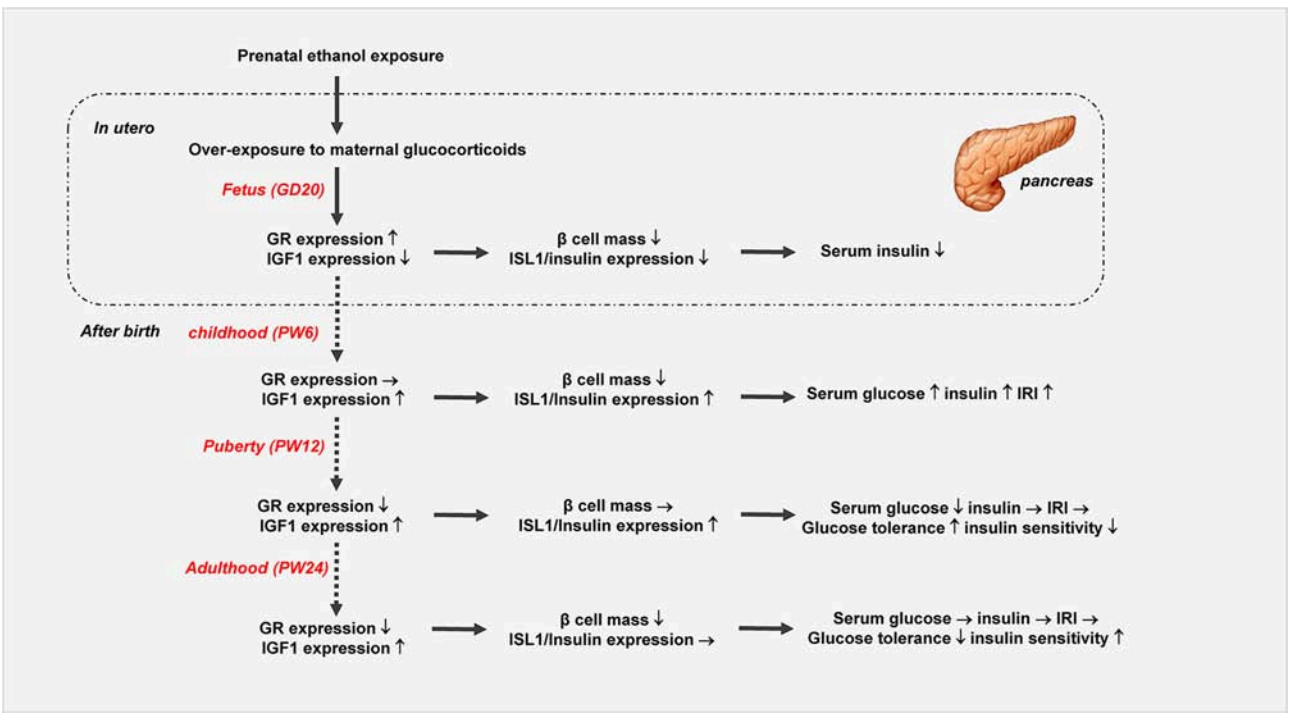

FIGURE 8 | Prenatal ethanol exposure (PEE) induced dynamic changes of pancreatic development and glycometabolism in male offspring rats. GR, glucocorticoid receptor; ISL1, insulin gene enhancer protein isl1; IGF1, insulin-like growth factor 1.

with GR expression) and IGF1 signaling in various tissues, could be maintained after birth and may contribute to organ dysfunction and lead to enhanced susceptibility to adult diseases. Basing on the above, we proposed the "GC-IGF1 axis programming" mechanism might be involved in the PEE-induced multi-organ dysfunction and predisposition to adult diseases. In the present study, we also observed that the alterations of local pancreatic glucocorticoid action mediated by GR expression presented a negative relationship with changes of pancreatic IGF1, ISL1, and insulin expressions as well as insulin secretion in PEE offspring rats before (GD20) and after birth (PW12 and 24).

Recently, we have demonstrated that PEE programs the hypersensitivity of hypothalamic-pituitary-adrenal (HPA) axis of PW12 male offspring rats, presenting by the increased levels of circulatory CORT after the CS (67). Basing on this, the previously well-described CS model was employed to further verify the negative regulatory relationship between circulatory glucocorticoid (accompany with GR expression) and IGF1 signaling in pancreas and its influence on insulin biosynthesis function in PEE males. Here we found the pancreatic IGF1, ISL1, and insulin expressions of PEE males at PW12 were increased as well as the insulin secretion (**Figure 6**) which might be attributed to the weaken local glucocorticoid action evidenced by both unchanged CORT levels (67) and decreased pancreatic GR expression. Furthermore, for these PEE male offspring characterized by programmed hypersensitivity of HPA axis, the CS-induced elevation of circulatory CORT activated pancreatic GR, which further inhibits the downstream pancreatic IGF1 and ISL1 expressions thereby causing dysfunction of insulin biosynthesis in PEE males (**Figure 7**). To sum up, these results observed in PW12 animals without/with CS just collectively revealed the negative regulatory relationship between local glucocorticoid action and IGF1 signaling in pancreas as well as the corresponding influence on insulin biosynthesis. Accordingly, we proposed that "GC-IGF1 axis programming" mechanism maybe mainly mediate the dysfunction of insulin biosynthesis after birth.

It should be noted that, in this study, the degradation of adult pancreatic tissues caused by ineligible preserve condition made RT-qPCR cannot be applied to accurately quantify the relative mRNA expression for GR, IGF1, ISL1 and insulin in pancreatic tissue of PW12 and PW24 animals. Therefore, IHC was chosen to semi-quantify these relative protein expression.

Ethanol May Also Have Direct Toxic Effects on the Pancreatic Development in Offspring

A series studies reveal that ethanol may also have direct toxic effects on the pancreatic development and function. The research from Kim et al (68) suggested that in PW7 mice, chronic ethanol exposure could induce down-regulation in glucokinases, thus induced β cell apoptosis and declined the β cell function. Researches in β-cell lines (69) and isolated murine islets (70) also suggested that ethanol reduced insulin content and caused ER stress, and resulted in β cell death by apoptosis. In the present study, we found the pancreatic proinsulin/insulin ratios of PEE male fetuses were unchanged with an equally decreased contents of pancreatic insulin and proinsulin, which may be due to the direct toxic effect of EtOH on the β cell function by reducing the production of all proteins including proinsulin and insulin equally. We should further study it in the future work.

CONCLUSION

In summary, we systematically confirmed the changes in glucose metabolism and pancreatic dysfunction before and after birth in the PEE male offspring rats with different ages, and we propose here for the first time a "GC-IGF1 axis programming" mechanism maybe mainly mediate the prenatal and postnatal pancreatic dysplasia and dysfunction of insulin biosynthesis (**Figure 8**). This study will help to clarify the pathophysiological mechanism and explore early prevention and treatment strategies for fetal-originated adult diabetes.

AUTHOR CONTRIBUTIONS

HK and DX were responsible for study design and data acquisition. SG and ZJ contributed to data analysis. YG and YW participated in data acquisition. DX and HW wrote and all the authors revised and approved the final manuscript.

FUNDING

This work was supported by grants from the National Natural Science Foundation of China (No. 81430089, 81673524, and 81703631), the National Key Research and Development Program of China (2017YFC1001300), Hubei Province Health and Family Planning Scientific Research Project (No. WJ2017C0003) and Outstanding Young Scholar Foundation of Hubei Province (2017CFA055).

SUPPLEMENTARY MATERIAL

The Supplementary Material for this article can be found online at: https://www.frontiersin.org/articles/10.3389/fendo.2019.00034/full#supplementary-material

Supplementary Figure 1 | Insulin immunohistochemistry and electron microscope images of pancreatic β cells of male fetal rats induced by prenatal ethanol exposure (PEE). **(A–D)** Representative images of pancreatic insulin immunohistochemical staining (×40 and ×400), and **(E,F)** electron microscope images of pancreatic β cells. $n = 5$ for insulin immunohistochemistry.

Supplementary Figure 2 | Insulin immunohistochemistry of prenatal ethanol exposure (PEE) male offspring rats at postnatal week (PW) 6, PW12 and PW24.**(A–D)** Representative images of insulin immunohistochemical staining at PW6 (×40 and ×400); **(E–H)** representative images of insulin immunohistochemical staining at PW12 (×40 and ×400); **(I–L)** representative images of insulin immunohistochemical staining at PW24 (×40 and ×400).

Supplementary Figure 3 | Glucocorticoid receptor (GR), insulin-like growth factor (IGF1) and insulin gene enhancer protein isl1 (ISL1) immunohistochemistry of prenatal ethanol exposure (PEE) male offspring rats at postnatal week (PW) 12 and PW24. **(A,B)** Representative images of GR at PW12, **(C,D)** representative images of IGF1 at PW12, **(E,F)** representative images of ISL1 at PW12, **(G,H)**

representative images of GR at PW24, **(I,J)** representative images of IGF1 at PW24, and **(K,L)** representative images of ISL1 at PW24.

Supplementary Figure 4 | Glucocorticoid receptor (GR), insulin-like growth factor (IGF1), insulin gene enhancer protein isl1 (ISL1) and INSULIN immunohistochemistry of prenatal ethanol exposure (PEE) male offspring rats at postnatal week (PW) 12 with chronic stress (CS). **(A,B)** Representative images of GR, **(C,D)** representative images of IGF1, **(E,F)** representative images of ISL1, and **(G,H)** representative images of INSULIN.

REFERENCES

1. Alati R, Betts KS, Williams GM, Najman JM, Hall WD. Generational increase in young women's drinking: a prospective analysis of mother-daughter dyads. *JAMA Psychiatry* (2014) 71:952–7. doi: 10.1001/jamapsychiatry.2014.513
2. Nizhnikov ME, Pautassi RM, Carter JM, Landin JD, Varlinskaya EI, Bordner KA, et al. Brief prenatal ethanol exposure alters behavioral sensitivity to the kappa opioid receptor agonist (U62,066E) and antagonist (Nor-BNI) and reduces kappa opioid receptor expression. *Alcohol Clin Exp Res.* (2014) 38:1630–8. doi: 10.1111/acer.12416
3. Chudley AE, Conry J, Cook JL, Loock C, Rosales T, LeBlanc N. Fetal alcohol spectrum disorder: canadian guidelines for diagnosis. *CMAJ* (2005) 172(5 Suppl.):S1–21. doi: 10.1503/cmaj.1040302
4. May PA, Gossage JP, Kalberg WO, Robinson LK, Buckley D, Manning M, et al. Prevalence and epidemiologic characteristics of FASD from various research methods with an emphasis on recent in-school studies. *Dev Disabil Res Rev.* (2009) 15:176–92. doi: 10.1002/ddrr.68
5. Clarren SK, Smith DW. The fetal alcohol syndrome. *N Engl J Med.* (1978) 298:1063–7. doi: 10.1056/NEJM197805112981906
6. Chen L, Nyomba BL. Effects of prenatal alcohol exposure on glucose tolerance in the rat offspring. *Metabol Clin Exp.* (2003) 52:454–62. doi: 10.1053/meta.2003.50073
7. Lopez-Tejero D, Llobera M, Herrera E. Permanent abnormal response to a glucose load after prenatal ethanol exposure in rats. *Alcohol* (1989) 6:469–73. doi: 10.1016/0741-8329(89)90054-2
8. Chen L, Nyomba BL. Glucose intolerance and resistin expression in rat offspring exposed to ethanol in utero: modulation by postnatal high-fat diet. *Endocrinology* (2003) 144:500–8. doi: 10.1210/en.2002-220623
9. Yao XH, Chen L, Nyomba BL. Adult rats prenatally exposed to ethanol have increased gluconeogenesis and impaired insulin response of hepatic gluconeogenic genes. *J Appl Physiol.* (2006) 100:642–8. doi: 10.1152/japplphysiol.01115.2005
10. Yao XH, Nguyen HK, Nyomba BL. Prenatal ethanol exposure causes glucose intolerance with increased hepatic gluconeogenesis and histone deacetylases in adult rat offspring: reversal by tauroursodeoxycholic acid. *PLoS ONE* (2013) 8:e59680. doi: 10.1371/journal.pone.0059680
11. Inoue T, Kido Y, Asahara S, Matsuda T, Shibutani Y, Koyanagi M, et al. Effect of intrauterine undernutrition during late gestation on pancreatic beta cell mass. *Biomed Res.* (2009) 30:325–30. doi: 10.2220/biomedres.30.325
12. Stoffers DA, Desai BM, DeLeon DD, Simmons RA. Neonatal exendin-4 prevents the development of diabetes in the intrauterine growth retarded rat. *Diabetes* (2003) 52:734–40. doi: 10.2337/diabetes.52.3.734
13. Nyirenda MJ, Lindsay RS, Kenyon CJ, Burchell A, Seckl JR. Glucocorticoid exposure in late gestation permanently programs rat hepatic phosphoenolpyruvate carboxykinase and glucocorticoid receptor expression and causes glucose intolerance in adult offspring. *J Clin Investig.* (1998) 101:2174–81. doi: 10.1172/JCI1567
14. Villarroya F, Mampel T. Glucose tolerance and insulin response in offspring of ethanol-treated pregnant rats. *Gen Pharmacol.* (1985) 16:415–7. doi: 10.1016/0306-3623(85)90208-3
15. Ting JW, Lautt WW. The effect of acute, chronic, and prenatal ethanol exposure on insulin sensitivity. *Pharmacol Ther.* (2006) 111:346–73. doi: 10.1016/j.pharmthera.2005.10.004
16. Gesina E, Tronche F, Herrera P, Duchene B, Tales W, Czernichow P, et al. Dissecting the role of glucocorticoids on pancreas development. *Diabetes* (2004) 53:2322–9. doi: 10.2337/diabetes.53.9.2322
17. Gesina E, Blondeau B, Milet A, Le Nin I, Duchene B, Czernichow P, et al. Glucocorticoid signalling affects pancreatic development through both direct and indirect effects. *Diabetologia* (2006) 49:2939–47. doi: 10.1007/s00125-006-0449-3
18. Blondeau B, Lesage J, Czernichow P, Dupouy JP, Breant B. Glucocorticoids impair fetal beta-cell development in rats. *Am J Physiol Endocrinol Metab.* (2001) 281:E592–9. doi: 10.1152/ajpendo.2001.281.3.E592
19. Smith FE, Rosen KM, Villa-Komaroff L, Weir GC, Bonner-Weir S. Enhanced insulin-like growth factor I gene expression in regenerating rat pancreas. *Proc Natl Acad Sci USA.* (1991) 88:6152–6. doi: 10.1073/pnas.88.14.6152
20. Hugl SR, White MF, Rhodes CJ. Insulin-like growth factor I (IGF-I)-stimulated pancreatic beta-cell growth is glucose-dependent. Synergistic activation of insulin receptor substrate-mediated signal transduction pathways by glucose and IGF-I in INS-1 cells. *J Biol Chem.* (1998) 273:17771–9. doi: 10.1074/jbc.273.28.17771
21. Lingohr MK, Dickson LM, McCuaig JF, Hugl SR, Twardzik DR, Rhodes CJ. Activation of IRS-2-mediated signal transduction by IGF-1, but not TGF-alpha or EGF, augments pancreatic beta-cell proliferation. *Diabetes* (2002) 51:966–76. doi: 10.2337/diabetes.51.4.966
22. Hill DJ, Petrik J, Arany E, McDonald TJ, Delovitch TL. Insulin-like growth factors prevent cytokine-mediated cell death in isolated islets of Langerhans from pre-diabetic non-obese diabetic mice. *J Endocrinol.* (1999) 161:153–65. doi: 10.1677/joe.0.1610153
23. Withers DJ, Burks DJ, Towery HH, Altamuro SL, Flint CL, White MF. Irs-2 coordinates Igf-1 receptor-mediated beta-cell development and peripheral insulin signalling. *Nat Genet.* (1999) 23:32–40. doi: 10.1038/12631
24. Hyatt MA, Budge H, Walker D, Stephenson T, Symonds ME. Ontogeny and nutritional programming of the hepatic growth hormone-insulin-like growth factor-prolactin axis in the sheep. *Endocrinology* (2007) 148:4754–60. doi: 10.1210/en.2007-0303
25. Inder WJ, Jang C, Obeyesekere VR, Alford FP. Dexamethasone administration inhibits skeletal muscle expression of the androgen receptor and IGF-1–implications for steroid-induced myopathy. *Clin Endocrinol.* (2010) 73:126–32. doi: 10.1111/j.1365-2265.2009.03683.x
26. Huang H, He Z, Zhu C, Liu L, Kou H, Shen L, et al. Prenatal ethanol exposure-induced adrenal developmental abnormality of male offspring rats and its possible intrauterine programming mechanisms. *Toxicol Appl Pharmacol.* (2015) 288:84–94. doi: 10.1016/j.taap.2015.07.005
27. Ni Q, Tan Y, Zhang X, Luo H, Deng Y, Magdalou J, et al. Prenatal ethanol exposure increases osteoarthritis susceptibility in female rat offspring by programming a low-functioning IGF-1 signaling pathway. *Sci Rep.* (2015) 5:14711. doi: 10.1038/srep14711
28. Shen L, Liu Z, Gong J, Zhang L, Wang L, Magdalou J, et al. Prenatal ethanol exposure programs an increased susceptibility of non-alcoholic fatty liver disease in female adult offspring rats *Toxicol Appl Pharmacol.* (2014) 274:263–73. doi: 10.1016/j.taap.2013.11.009
29. Phipps K, Barker DJ, Hales CN, Fall CH, Osmond C, Clark PM. Fetal growth and impaired glucose tolerance in men and women. *Diabetologia* (1993) 36:225–8. doi: 10.1007/BF00399954
30. Sugden MC, Holness MJ. Gender-specific programming of insulin secretion and action. *J Endocrinol.* (2002) 175:757–67. doi: 10.1677/joe.0.1750757
31. Fernandez-Twinn DS, Wayman A, Ekizoglou S, Martin MS, Hales CN, Ozanne SE. Maternal protein restriction leads to hyperinsulinemia and reduced insulin-signaling protein expression in 21-mo-old female rat offspring. *Am J Physiol Regul Integr Comp Physiol.* (2005) 288:R368–73. doi: 10.1152/ajpregu.00206.2004
32. Kind KL, Clifton PM, Grant PA, Owens PC, Sohlstrom A, Roberts CT, et al. Effect of maternal feed restriction during pregnancy on glucose tolerance in the adult guinea pig. *Am J Physiol Regul Integr Comp Physiol.* (2003) 284:R140–52. doi: 10.1152/ajpregu.00587.2001
33. Liu L, Liu F, Kou H, Zhang BJ, Xu D, Chen B, et al. Prenatal nicotine exposure induced a hypothalamic-pituitary-adrenal axis-associated neuroendocrine metabolic programmed alteration in intrauterine growth retardation offspring rats. *Toxicol Lett.* (2012) 214:307–13. doi: 10.1016/j.toxlet.2012.09.001
34. Xu D, Wu Y, Liu F, Liu YS, Shen L, Lei YY, et al. A hypothalamic-pituitary-adrenal axis-associated neuroendocrine metabolic programmed alteration in offspring rats of IUGR induced by prenatal caffeine ingestion. *Toxicol Appl Pharmacol.* (2012) 264:395–403. doi: 10.1016/j.taap.2012.08.016
35. Zhu Y, Zuo N, Li B, Xiong Y, Chen H, He H, et al. The expressional disorder of the renal RAS mediates nephrotic syndrome of male rat offspring

induced by prenatal ethanol exposure. *Toxicology* (2018) 400–401:9–19. doi: 10.1016/j.tox.2018.03.004
36. Manuel-Apolinar L, Zarate A, Rocha L, Hernandez M. Fetal malnutrition affects hypothalamic leptin receptor expression after birth in male mice. *Arch Med Res.* (2010) 41:240–5. doi: 10.1016/j.arcmed.2010.06.002
37. Linden MA, Fletcher JA, Morris EM, Meers GM, Laughlin MH, Booth FW, et al. Treating NAFLD in OLETF rats with vigorous-intensity interval exercise training. *Med Sci Sports Exerc.* (2015) 47:556–67. doi: 10.1249/MSS.0000000000000430
38. Zambrano E, Bautista CJ, Deas M, Martinez-Samayoa PM, Gonzalez-Zamorano M, Ledesma H, et al. A low maternal protein diet during pregnancy and lactation has sex- and window of exposure-specific effects on offspring growth and food intake, glucose metabolism and serum leptin in the rat. *J Physiol.* (2006) 571(Pt 1):221–30. doi: 10.1113/jphysiol.2005.100313
39. Valtat B, Riveline JP, Zhang P, Singh-Estivalet A, Armanet M, Venteclef N, et al. Fetal PGC-1alpha overexpression programs adult pancreatic beta-cell dysfunction. *Diabetes* (2013) 62:1206–16. doi: 10.2337/db12-0314
40. Garofano A, Czernichow P, Breant B. Beta-cell mass and proliferation following late fetal and early postnatal malnutrition in the rat. *Diabetologia* (1998) 41:1114–20. doi: 10.1007/s001250051038
41. Raab J, Haupt F, Kordonouri O, Scholz M, Wosch A, Ried C, et al. Continuous rise of insulin resistance before and after the onset of puberty in children at increased risk for type 1 diabetes - a cross-sectional analysis. *Diabetes Metab Res Rev.* (2013) 29:631–5. doi: 10.1002/dmrr.2438
42. Green AS, Rozance PJ, Limesand SW. Consequences of a compromised intrauterine environment on islet function. *J Endocrinol.* (2010) 205:211–24. doi: 10.1677/JOE-09-0399
43. Gatford KL, Simmons RA. Prenatal programming of insulin secretion in intrauterine growth restriction. *Clin Obstet Gynecol.* (2013) 56:520–8. doi: 10.1097/GRF.0b013e31829e5b29
44. Blondeau B, Avril I, Duchene B, Breant B. Endocrine pancreas development is altered in foetuses from rats previously showing intra-uterine growth retardation in response to malnutrition. *Diabetologia* (2002) 45:394–401. doi: 10.1007/s00125-001-0767-4
45. Van Assche FA, De Prins F, Aerts L, Verjans M. The endocrine pancreas in small-for-dates infants. *Br J obstetr Gynaecol.* (1977) 84:751–3
46. Nicolini U, Hubinont C, Santolaya J, Fisk NM, Rodeck CH. Effects of fetal intravenous glucose challenge in normal and growth retarded fetuses. *Horm Metab Res.* (1990) 22:426–30.
47. Beringue F, Blondeau B, Castellotti MC, Breant B, Czernichow P, Polak M. Endocrine pancreas development in growth-retarded human fetuses. *Diabetes* (2002) 51:385–91. doi: 10.2337/diabetes.51.2.385
48. Garofano A, Czernichow P, Breant B. In utero undernutrition impairs rat beta-cell development. *Diabetologia* (1997) 40:1231–4.
49. Limesand SW, Rozance PJ, Macko AR, Anderson MJ, Kelly AC, Hay WW Jr. Reductions in insulin concentrations and beta-cell mass precede growth restriction in sheep fetuses with placental insufficiency. *Am J physiol Endocrinol Metab.* (2013) 304:E516–23. doi: 10.1152/ajpendo.00435.2012
50. Bertin E, Gangnerau MN, Bellon G, Bailbe D, Arbelot De Vacqueur A, Portha B. Development of beta-cell mass in fetuses of rats deprived of protein and/or energy in last trimester of pregnancy. *Am J Physiol Regul Integr Comp Physiol.* (2002) 283:R623–30. doi: 10.1152/ajpregu.00037.2002
51. Limesand SW, Rozance PJ, Zerbe GO, Hutton JC, Hay WW Jr. Attenuated insulin release and storage in fetal sheep pancreatic islets with intrauterine growth restriction. *Endocrinology* (2006) 147:1488–97. doi: 10.1210/en.2005-0900
52. Reynolds RM. Glucocorticoid excess and the developmental origins of disease: two decades of testing the hypothesis—2012 Curt Richter Award Winner. *Psychoneuroendocrinology* (2013) 38:1–11. doi: 10.1016/j.psyneuen.2012.08.012
53. Yang Z, Zhang Q, Lu Q, Jia Z, Chen P, Ma K, et al. ISL-1 promotes pancreatic islet cell proliferation by forming an ISL-1/Set7/9/PDX-1 complex. *Cell cycle* (2015) 14:3820–9. doi: 10.1080/15384101.2015.1069926
54. Karlsson O, Thor S, Norberg T, Ohlsson H, Edlund T. Insulin gene enhancer binding protein Isl-1 is a member of a novel class of proteins containing both a homeo- and a Cys-His domain. *Nature* (1990) 344:879–82.
55. Liang G, Chen M, Pan XL, Zheng J, Wang H. Ethanol-induced inhibition of fetal hypothalamic-pituitary-adrenal axis due to prenatal overexposure to maternal glucocorticoid in mice. *Exp Toxicol Pathol.* (2011) 63:607–11. . doi: 10.1016/j.etp.2010.04.015
56. Lu J, Wen Y, Zhang L, Zhang C, Zhong W, Zhang L, et al. Prenatal ethanol exposure induces an intrauterine programming of enhanced sensitivity of the hypothalamic–pituitary–adrenal axis in female offspring rats fed with post-weaning high-fat diet. *Toxicol Res.* (2015) 4:1238–49. doi: 10.1039/C5TX00012B
57. He Z, Zhu C, Huang H, Liu L, Wang L, Chen L, et al. Prenatal caffeine exposure-induced adrenal developmental abnormality in male offspring rats and its possible intrauterine programming mechanisms. *Toxicol Res.* (2016) 5:388–98. doi: 10.1039/c5tx00265f
58. Xu D, Liang G, Yan YE, He WW, Liu YS, Chen LB, et al. Nicotine-induced over-exposure to maternal glucocorticoid and activated glucocorticoid metabolism causes hypothalamic-pituitary-adrenal axis-associated neuroendocrine metabolic alterations in fetal rats. *Toxicol Lett.* (2012) 209:282–90. doi: 10.1016/j.toxlet.2012.01.006
59. Matveyenko AV, Singh I, Shin BC, Georgia S, Devaskar SU. Differential effects of prenatal and postnatal nutritional environment on ss-cell mass development and turnover in male and female rats. *Endocrinology* (2010) 151:5647–56. doi: 10.1210/en.2010-0978
60. .Simmons RA, Templeton LJ, Gertz SJ. Intrauterine growth retardation leads to the development of type 2 diabetes in the rat. *Diabetes* (2001) 50:2279–86. doi: 10.2337/diabetes.50.10.2279
61. van Haeften TW, Twickler TB. Insulin-like growth factors and pancreas beta cells. *Eur J Clin Investig.* (2004) 34:249–55. doi: 10.1111/j.1365-2362.2004.01337.x
62. Fall CH, Pandit AN, Law CM, Yajnik CS, Clark PM, Breier B, et al. Size at birth and plasma insulin-like growth factor-1 concentrations. *Arch Dis Child.* (1995) 73:287–93.
63. Kahn SE, Prigeon RL, McCulloch DK, Boyko EJ, Bergman RN, Schwartz MW, et al. Quantification of the relationship between insulin sensitivity and beta-cell function in human subjects. Evidence for a hyperbolic function. *Diabetes* (1993) 42:1663–72.
64. Ueki K, Okada T, Hu J, Liew CW, Assmann A, Dahlgren GM, et al. Total insulin and IGF-I resistance in pancreatic beta cells causes overt diabetes. *Nat Genet.* (2006) 38:583–8. doi: 10.1038/ng1787
65. McGowan PO, Matthews SG. Prenatal stress, glucocorticoids, and developmental programming of the stress response. *Endocrinology* (2018) 159:69–82. doi: 10.1210/en.2017-00896
66. Tosh DN, Fu Q, Callaway CW, McKnight RA, McMillen IC, Ross MG, et al. Epigenetics of programmed obesity: alteration in IUGR rat hepatic IGF1 mRNA expression and histone structure in rapid vs. delayed postnatal catch-up growth. *Am J Physiol Gastrointest Liver Physiol.* (2010) 299:G1023–9. doi: 10.1152/ajpgi.00052.2010
67. Lu J, Jiao Z, Yu Y, Zhang C, He X, Li Q, et al. Programming for increased expression of hippocampal GAD67 mediated the hypersensitivity of the hypothalamic-pituitary-adrenal axis in male offspring rats with prenatal ethanol exposure. *Cell Death Dis.* (2018) 9:659. doi: 10.1038/s41419-018-0663-1
68. Kim JY, Song EH, Lee HJ, Oh YK, Park YS, Park JW, et al. Chronic ethanol consumption-induced pancreatic {beta}-cell dysfunction and apoptosis through glucokinase nitration and its down-regulation. *J Biol Chem.* (2010) 285:37251–62. doi: 10.1074/jbc.M110.142315
69. Dembele K, Nguyen KH, Hernandez TA, Nyomba BL. Effects of ethanol on pancreatic beta-cell death: interaction with glucose and fatty acids. *Cell Biol Toxicol.* (2009) 25:141–52. doi: 10.1007/s10565-008-9067-9
70. Nguyen KH, Lee JH, Nyomba BL. Ethanol causes endoplasmic reticulum stress and impairment of insulin secretion in pancreatic beta-cells. *Alcohol* (2012) 46:89–99. doi: 10.1016/j.alcohol.2011.04.001

Conflict of Interest Statement: The authors declare that the research was conducted in the absence of any commercial or financial relationships that could be construed as a potential conflict of interest.

frontiers in Neuroscience

REVIEW
published: 20 February 2019
doi: 10.3389/fnins.2019.00021

Intrapancreatic Ganglia and Neural Regulation of Pancreatic Endocrine Secretion

*Wenjing Li[1], Guangjiao Yu[2], Yudan Liu[1] and Lei Sha[1]**

[1] School of Pharmacy, China Medical University, Shenyang, China, [2] China Medical University-The Queen's University of Belfast Joint College, China Medical University, Shenyang, China

Extrapancreatic nerves project to pancreatic islets directly or converge onto intrapancreatic ganglia. Intrapancreatic ganglia constitute a complex information-processing center that contains various neurotransmitters and forms an endogenous neural network. Both intrapancreatic ganglia and extrapancreatic nerves have an important influence on pancreatic endocrine function. This review introduces the histomorphology, innervation, neurochemistry, and electrophysiological properties of intrapancreatic ganglia/neurons, and summarizes the modulatory effects of intrapancreatic ganglia and extrapancreatic nerves on endocrine function.

Keywords: intrapancreatic ganglia, extrapancreatic nerves, pancreas, islet, insulin

OPEN ACCESS

Edited by:
Lee E. Eiden,
National Institutes of Health (NIH), United States

Reviewed by:
Youssef Anouar,
Institut National de la Santé et de la Recherche Médicale (INSERM), France
Qingchun Tong,
The University of Texas Health Science Center at Houston, United States

****Correspondence:***
Lei Sha
lsha@cmu.edu.cn

Specialty section:
This article was submitted to Neuroendocrine Science, a section of the journal Frontiers in Neuroscience

Received: *12 July 2018*
Accepted: *10 January 2019*
Published: *20 February 2019*

Citation:
Li W, Yu G, Liu Y and Sha L (2019) Intrapancreatic Ganglia and Neural Regulation of Pancreatic Endocrine Secretion. Front. Neurosci. 13:21. doi: 10.3389/fnins.2019.00021

INTRODUCTION

Intrapancreatic ganglia were first described by Langerhans in 1869 and have been studied over several decades (Sha et al., 1995, 1996, 1997, 2001b; Liu and Kirchgessner, 1997; Love and Szebeni, 1999b; Sha and Szurszewski, 1999; Yi et al., 2005; Shen et al., 2016). While intrapancreatic ganglia have been traditionally considered to be simple parasympathetic relays, growing evidence suggests that, similar to the enteric nervous system (ENS), intrapancreatic ganglia may constitute a complex information-processing center containing various neurotransmitters and form an endogenous neural network (Gylfe and Tengholm, 2014; Shen et al., 2016; Tang et al., 2018b). Although the influence of extrapancreatic nerves, especially autonomic nerves, on pancreatic endocrine function has been extensively studied, the role of intrapancreatic ganglia in endocrine and exocrine functions has garnered far less attention (Sha et al., 2001b; Love et al., 2007; Gylfe and Tengholm, 2014; Rodriguez-Diaz and Caicedo, 2014). In this review, we will focus on research studies from the past 30 years. We will introduce the histomorphology, innervation, neurochemistry, and electrophysiological properties of intrapancreatic ganglia/neurons, and summarize the modulatory effects of intrapancreatic ganglia and extrapancreatic nerves on endocrine function.

ANATOMY AND MORPHOLOGY OF INTRAPANCREATIC GANGLIA

Intrapancreatic ganglia are composed of pancreatic neurons, glial cells, and extrinsic and intrinsic nerve fibers. They are located over or alongside nerve trunks in the interlobular, acinar, or insular connective tissues, or within lobules and islets (Liu and Kirchgessner, 1997; Tang et al., 2018a). Intrapancreatic ganglia can be oval, round, or polygonal in shape, and vary in size

(Shen et al., 2016). Most intrapancreatic ganglia are found alongside or inside nerve trunks that are branches of larger nerve trunks traveling along the pancreaticoduodenal artery in the head of the pancreas (Liu and Kirchgessner, 1997). Ganglia are also found along nerve bundles from the celiac and superior mesenteric plexuses, and the splenic nerves in the body and tail of the pancreas (Love et al., 2007). The ganglia in the head are larger and contain more neurons than those in the body and tail of the pancreas (Sha et al., 1996). In the rabbit pancreas, the larger ganglia (≥6 neurons) often appear to be encapsulated and connect to larger nerve trunks, while the smaller ganglia are similar to grape clusters; single pancreatic neurons are also found within islets (Love and Szebeni, 1999b). The peri-lobular ganglia are larger than intra-parenchymal ganglia. The ganglia of patients with type 2 diabetes are larger than those of individuals without diabetes (Tang et al., 2018a). The number of neurons in each pancreatic ganglion is different in different species. For example, rabbit ganglia contain 1 to 35 neurons per ganglion [mean ± standard error of the mean (SEM), 4 ± 1] (Love and Szebeni, 1999b), while rat ganglia contain 2–24 neurons per ganglion (mean ± SEM, 8.8 ± 0.5) (Shen et al., 2016). Although the neurons are typically oval or round, triangular neurons are also found. Most of the neurons are bipolar or multipolar, and unipolar neurons are rare. While the dendritic neuropil of neurons is variable in shape, most of the dendrites are typically short and stubby (Sha et al., 1996). Most nerve fibers of intrapancreatic ganglia are unmyelinated. The unmyelinated nerve bundles have a fine axonal structure, with a large number of microtubules present in the center. Some axons contain both small, clear vesicles and large dense-cored vesicles, while others appear to contain only small, clear vesicles (Love et al., 2007). The axons of pancreatic neurons project to all pancreatic effector cells, including islets, pancreatic ducts, acini, blood vessels, and other intrapancreatic ganglia, indicating that intrapancreatic ganglia may play an important role in pancreatic functions, including endocrine function (Niebergall-Roth and Singer, 2001; Love et al., 2007).

INNERVATION OF INTRAPANCREATIC GANGLIA

Sympathetic Efferent Fibers

Preganglionic efferent sympathetic fibers project from cell bodies in the lateral horn of the spinal cord (C_8-L_3) to paravertebral and prevertebral sympathetic ganglia (Llewellyn-Smith, 2009; **Figure 1**). The fibers projecting from the prevertebral ganglia (the celiac and superior mesenteric ganglia) enter the pancreas directly or with other autonomic nerves (Ahrén, 2000; Gilon and Henquin, 2001; Love et al., 2007). The celiac plexus mainly includes four branches: the anterior hepatic plexus, posterior hepatic plexus, splenic plexus, and plexus accompanying the transverse pancreatic artery (Dolensek et al., 2015). These branches are distributed in different locations of the human pancreas. The head of the pancreas receives the anterior and posterior hepatic plexuses, which are distributed along the hepatic artery and located in the dorsal aspect of the portal vein. The body and tail of the pancreas are innervated by the other two plexuses. Some nerves originate from the superior mesenteric ganglia and enter the uncinate process of the pancreas along the inferior pancreaticoduodenal artery. There also exist plexuses that surround the main pancreatic duct, but pass through the pancreas independently of the blood vessels (Yi et al., 2003). The postganglionic sympathetic fibers project to intrapancreatic ganglia, islets, ducts, and blood vessels, and release several neurotransmitters such as norepinephrine (NE), galanin, and neuropeptide Y (NPY) (Ahrén, 1999; Di Cairano et al., 2016). Preganglionic sympathetic fibers also enter the pancreas directly and terminate at the intrapancreatic ganglia (Havel et al., 1989).

Parasympathetic Efferent Fibers

Most preganglionic parasympathetic fibers supplying the pancreas originate from the dorsal motor nucleus of the vagus (DMV) in the medulla, and their cell bodies are rarely observed in the nucleus ambiguous (Love et al., 2007; Chandra and Liddle, 2013; Rodriguez-Diaz and Caicedo, 2014; Ma and Vella, 2018; **Figure 1**). Vagus nerve fibers pass through the hiatus of the esophagus into the abdomen and are divided into five distinct branches that subsequently innervate different organs. The vagus nerve fibers that innervate the pancreas include the hepatic and bilateral gastric branches (primary), and bilateral celiac branches (secondary) (Niebergall-Roth and Singer, 2001; Love et al., 2007; Chandra and Liddle, 2014).

A number of parasympathetic preganglionic fibers terminate at the intrapancreatic ganglia to form synapses (Chandra and Liddle, 2009). Acetylcholine (ACh) is released from both the preganglionic and postganglionic parasympathetic nerve terminals. In addition, vasoactive intestinal polypeptide (VIP), gastrin-releasing peptide (GRP), pituitary adenylate cyclase-activating polypeptide (PACAP), and nitric oxide (NO) are released from the postganglionic parasympathetic nerve fibers (Wang et al., 1999; Gilon and Henquin, 2001; Love et al., 2007; Di Cairano et al., 2016). NPY and galanin exist in both sympathetic and parasympathetic nerve fibers of the pancreas in pigs and mice (Pettersson et al., 1987; Sheikh et al., 1988; Ahrén, 2000).

Enteropancreatic Plexus

The ENS within the wall of the gastrointestinal tract is often considered to be the "local brain" that regulates gastrointestinal functions. Enteric neurons in the myenteric plexus of the gastric antrum and proximal duodenum also project out of the gut to the intrapancreatic ganglia (Kirchgessner and Gershon, 1990; Chandrasekharan and Srinivasan, 2007). Cholinergic enteropancreatic neurons form excitatory nicotinic synapses on pancreatic neurons. In addition, some enteropancreatic nerves, such as the PACAP-containing nerves, are peptidergic. PACAP is often considered as a neuromodulator that strengthens pancreatic secretion (Kirchgessner and Liu, 2001). The fibers of serotonergic enteropancreatic neurons form inhibitory axo-axonic synapses to inhibit amylase secretion (Kirchgessner and Gershon, 1995). Enteropancreatic neurons form nicotinic synapses in intrapancreatic ganglia; however, other excitatory pathways remain unknown. The role of enteric nerves in controlling the endocrine functions of the pancreas has not been

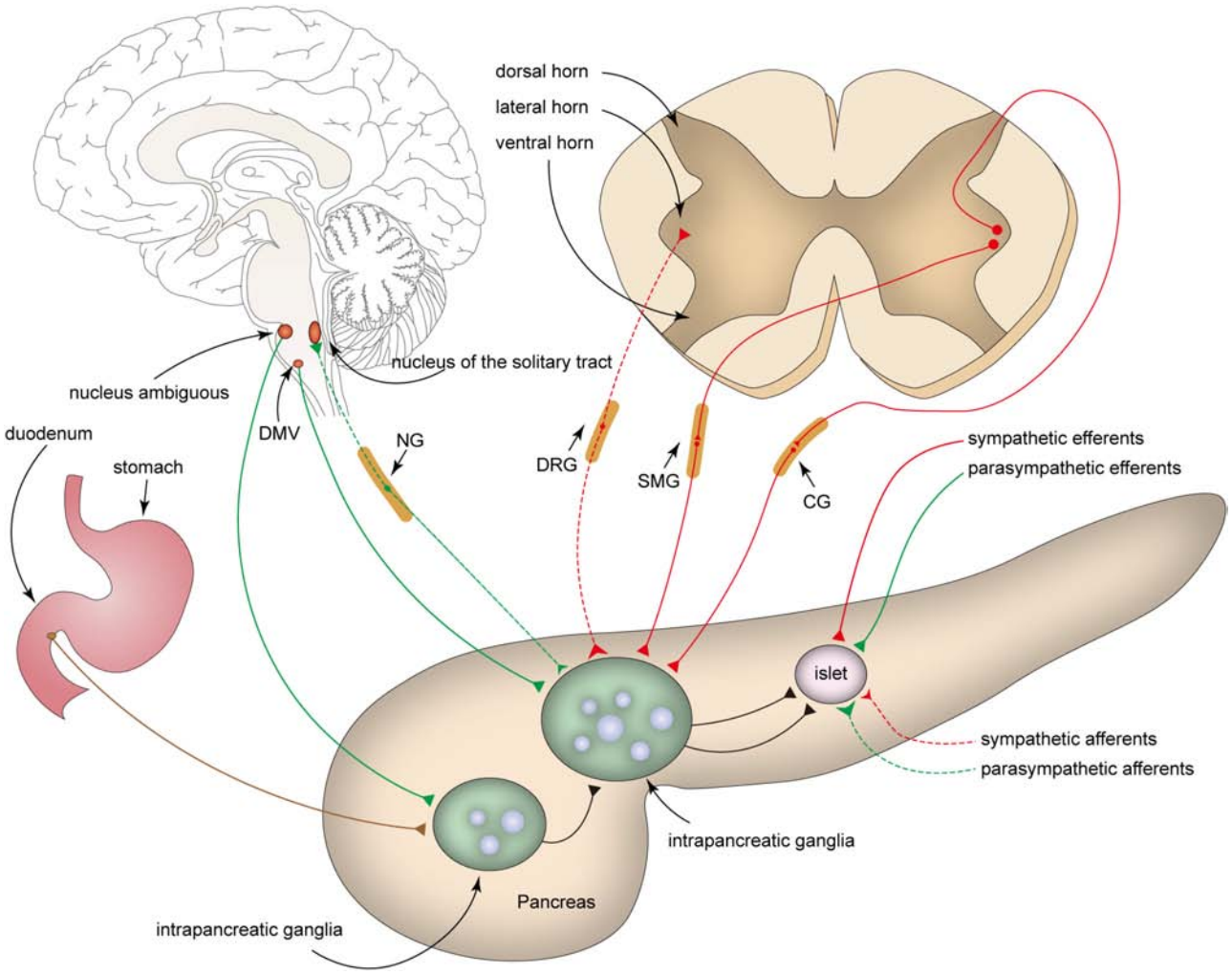

FIGURE 1 | Innervation of intrapancreatic ganglia. Intrapancreatic ganglia receive inputs from sympathetic fibers (red), parasympathetic fibers (green), enteric plexus (brown), and nerves of other intrapancreatic ganglia. The parasympathetic efferent fibers (green solid line) originate from the dorsal motor nucleus of the vagus (DMV) and ambiguous nucleus, whereas the cell bodies of sympathetic efferent fibers (red solid line) project from the lateral horn of the spinal cord to the celiac ganglia (CG), superior mesenteric ganglia (SMG), or paravertebral ganglia (not show in the Figure). The cell bodies of parasympathetic (green dashed line) and sympathetic (red dashed line) afferents are positioned in the nodose ganglia (NG) and the dorsal root ganglia (DRG), respectively.

completely elucidated. The ENS may be a therapeutic target for the regulation of glucose metabolism (Abot et al., 2018a,b).

Afferent Nerve Fibers

Intrapancreatic ganglia receive both sympathetic and parasympathetic afferents, most of which are sensitive to capsaicin. These afferent fibers transmit sensory information from the pancreas to the central nervous system (Dolensek et al., 2015).

Sympathetic afferents are thought to exit the pancreas along the postganglionic sympathetic fibers within the splanchnic nerves and the celiac plexus to the dorsal root ganglia (DRG, T_6-L_2) (Love et al., 2007; Rodriguez-Diaz and Caicedo, 2014; Dolensek et al., 2015). Pancreatic parasympathetic afferents originate from the nodose ganglia (NG) (Lartigue, 2016). While pancreatic parasympathetic afferent fibers primarily supply the blood vessels, ducts, acini, and islets, few parasympathetic afferents are found in intrapancreatic ganglia (Love et al., 2007). Although the central targets of vagal afferents remain largely unclear, the nucleus of the solitary tract (NTS) is considered to be the main relay center for vagal afferent nerves (Renehan et al., 1995; Dolensek et al., 2015). Sympathetic and parasympathetic afferent fibers contain either substance P (SP) or calcitonin gene-related peptide (CGRP), or both (Rodriguez-Diaz and Caicedo, 2014).

NEUROTRANSMITTERS OF INTRAPANCREATIC GANGLIA

A variety of neurotransmitters can be identified in the intrapancreatic ganglia (**Figure 2**). Studies show that choline

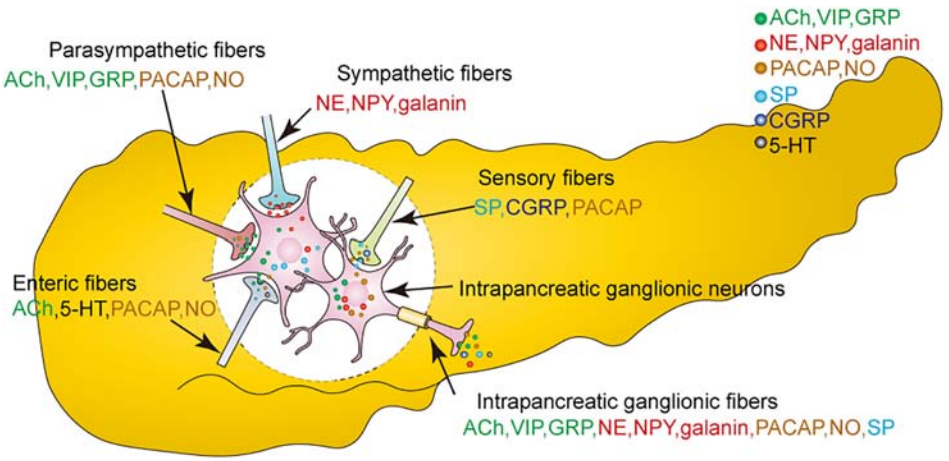

FIGURE 2 | Neurotransmitters are released from both extrinsic nerves and intrinsic intrapancreatic ganglia. Neurotransmitters are, respectively released from parasympathetic fibers, sympathetic fibers, sensory fibers, enteric fibers, the intrapancreatic ganglionic fibers. ACh, acetylcholine; GRP, gastrin-releasing peptide; VIP, vasoactive intestinal peptide; NO, nitric oxide; NE, noradrenaline; NPY, neuropeptide Y; PACAP, pituitary adenylate cyclase activating polypeptide; 5-HT, serotonin; CGRP, calcitonin gene-related peptide; SP, substance P.

acetyltransferase (CHAT)-immunopositive neuronal cell bodies and nerve fibers are present in the pancreas of many species (Liu et al., 1998; Love and Szebeni, 1999a; Wang et al., 1999), suggesting that ACh is not only released from parasympathetic efferents and enteropancreatic fibers, but also from the neurons in the intrapancreatic ganglia. However, intrapancreatic ganglia are not innervated by cholinergic nerve fibers in the sheep pancreas (Arciszewski and Zacharko-Siembida, 2007), which suggests that the cholinergic innervation of islets from pancreatic neurons is species-dependent.

It has been shown that intrinsic noradrenaline-containing neurons are present in the pancreases of rats and newborn guinea pigs. Dense catecholamine-containing nerves with few cell bodies are observed in the intrapancreatic ganglia of rabbits. Moreover, high performance liquid chromatography (HPLC) reveals higher levels of NE in the ganglia of the head and neck regions than in those of the body of the pancreas (Yi and Love, 2005a). It has also been reported that CHAT is colocalized with dopamine-β-hydroxylase (DβH), indicating that ACh and NE can be released from the same neurons. However, the origin of these fibers that release both ACh and NE remains unknown (Liu et al., 1998). Recent studies have also shown an increased density of noradrenergic nerve fibers in the islets of obese mice compared to control mice (Giannulis et al., 2014).

Apart from ACh and NE, many neuropeptides are also released from the intrapancreatic ganglia (De Giorgio et al., 1992a). VIP and GRP are located in both neuronal cell bodies and fibers of the intrapancreatic ganglia (De Giorgio et al., 1992b, 1993; Myojin et al., 2000). VIP is present in most intrapancreatic ganglionic cell bodies, while the number of neuronal cell bodies containing GRP is much lower (De Giorgio et al., 1992b). External PACAP originates from vagal nerves, sensory nerves, or enteropancreatic nerves, while intrinsic PACAP has been observed in the neurons of intrapancreatic ganglia (Hannibal and Fahrenkrug, 2000; Kirchgessner and Liu, 2001). PACAP is co-localized with VIP in the neurons of the rat pancreas (Hannibal and Fahrenkrug, 2000). PACAP is also co-localized with galanin, SP, and corticotrophin-releasing factor (CRF) in the intrapancreatic ganglia of the sheep pancreas (Arciszewski et al., 2015). Moreover, both galanin and NPY can be observed in intrapancreatic ganglia of the bovine pancreas (Furuzawa et al., 1996; Myojin et al., 2000; Adeghate et al., 2001), with galanin being more frequently observed than NPY (Myojin et al., 2000).

Besides sensory nerves, approximately 50% of the SP in the pancreas originates from intrapancreatic ganglia (Shen et al., 2016). CGRP-positive fibers are observed in intrapancreatic ganglia, but not in cell bodies (Silvestre et al., 1996; Myojin et al., 2000). Methionine-enkephalin-positive neurons are occasionally found in bovine intrapancreatic ganglia (Myojin et al., 2000).

Nicotinamide adenine dinucleotide phosphate (NADPH)-diaphorase (d) and nitric oxide synthase (NOS) levels have been used as markers of NO production in the intrapancreatic ganglia (Sha et al., 1995; Liu and Kirchgessner, 1997). This demonstrates that apart from enteric and vagal nerve fibers, nitrinergic nerves are also present in the intrapancreatic ganglia (Wang et al., 1999; Chaudhury, 2014). Most NADPH-d-positive neurons show immunoreactivity for VIP or galanin in the chicken pancreas (Hiramatsu et al., 1994). Moreover, ACh is co-localized with VIP or NOS or both in most cholinergic neurons (Myojin et al., 2000).

ELECTROPHYSIOLOGICAL PROPERTIES AND SYNAPTIC POTENTIALS OF PANCREATIC NEURONS

The electrophysiological properties of intrapancreatic ganglionic neurons have been characterized through intracellular recording in guinea pigs, rabbits, cats, and dogs (King et al., 1989; Sha et al., 1996; Liu and Kirchgessner, 1997; Sha and Szurszewski, 1999;

Love, 2000). The resting membrane potentials (RMP), input resistances (IR), action potential (AP) thresholds, AP amplitudes, time constant, and after-spike hyperpolarization (ASH) durations are similar in different species, as are the electrophysiological properties of pancreatic neurons in different regions of the pancreas (Sha et al., 1996). Electrophysiological properties of pancreatic neurons are summarized in **Table 1**. Pancreatic neurons have higher IR than other autonomic neurons. Most of the pancreatic neurons are classified as neurons with phasic firing patterns. A small number (9%) of rabbit pancreatic neurons show spontaneous low amplitude oscillations that resemble pacemaker potentials (Love, 2000).

Pancreatic neurons exhibit both fast and slow excitatory postsynaptic potentials (fEPSPs and sEPSPs). Stimulation of nerve bundles attached to intrapancreatic ganglia evokes multiple fEPSPs (Sha et al., 1996, 1997; Liu and Kirchgessner, 1997; Love, 2000) that are blocked by hexamethonium in 75% of the neurons, while non-cholinergic fEPSPs are observed in 25% of the neurons (Love, 2000). Repetitive stimulation evokes muscarinic and non-cholinergic sEPSPs, whose duration and amplitude are positively related to the stimulus trains; hexamethonium has no impact on the sEPSPs (Sha et al., 1996; Liu and Kirchgessner, 1997). sEPSPs are evoked by repetitive stimulation using atropine or BRL24924, a 5-HT_{1p} receptor antagonist (Sha et al., 1996, 1997). Spontaneous fEPSPs are usually observed at low frequency, and action potentials (APs) are also observed due to summation of subthreshold fEPSPs (King et al., 1989). Approximately 41% of the intrapancreatic neurons in the head and body of the pancreas show spontaneous fEPSPs and APs, while only 31% of the intrapancreatic neurons in the pancreatic tail show spontaneous fEPSPs and APs (Sha et al., 1996). Pancreatic neurons are capable of coordinating intrinsic activity owing to the rhythmic bursts of fEPSPs and APs in interconnected ganglia (Love, 2000). Inhibitory postsynaptic potentials (IPSPs) have not been reported yet. Intrapancreatic ganglia of rabbits in all three regions of pancreas exhibit paired-pulse facilitation (PPF) or depression (PPD) of fEPSPs. PPF peaking and disappearing have shorter inter-stimulus intervals than PPD. PPF is observed mainly in the pancreatic head and neck (60%), while PPD is observed in the body of the pancreas. In the head/neck region, facilitation during the initial 1–2 s of train stimulation is reduced by mid-train depression (2–5 s) of a greater magnitude. The frequency of postsynaptic APs is inversely related to the magnitude of mid-train depression, suggesting that the electrophysiological activities of pancreatic neurons can regulate synaptic strength. Train stimulation in the head or neck of the pancreas is seen to be followed by brief post-train augmentation of fEPSPs (Sha et al., 1996; Love, 2000; Yi and Love, 2005b). Presynaptic post-train depression results in a decrease in ACh release. Regional differences in electrophysiological activities may reflect regional differences in pancreatic function (Yi and Love, 2005b; Love et al., 2007).

Neurotransmitters of external or internal origin are observed to affect ganglionic transmission. In cats, ACh evokes fast depolarization with a decrease in IR, an effect mediated by nicotinic receptors. Most fEPSPs are activated by nicotinic receptor subunits in ganglionic neurons and few fEPSPs are not sensitive to hexamethonium, indicating that there exist non-cholinergic receptors in the ganglia. The slow transmission is mediated by M_1 receptors through an increase in the IR (Sha et al., 1997). However, muscarine can convert synaptic APs of rabbit pancreatic neurons into fEPSPs without any changes in the RMP or IR (Love, 2000). The electrical activity of intrapancreatic ganglia has a vital influence on amplitude regulation of pulsatile insulin secretion by isolated ganglia together with the adjacent pancreatic parenchyma (Sha et al., 2001b).

A higher percentage of neurons respond to adrenergic agonists in the pancreatic head than in the body or the tail of the pancreas, a finding consistent with the fact that the density of noradrenergic innervation to intrapancreatic ganglia in the pancreas head is higher than in the body or tail (Yi et al., 2004). A predominance of inhibitory α_2 receptors in the body of the pancreas contributes to the inhibition of ganglionic transmission, and excitatory α_1 receptors in the ganglia from the head/neck regions participate in the facilitation of ganglionic transmission. Presynaptic post-train depression (PTD) is mediated by NE and other unknown neurotransmitters (Yi and Love, 2005a).

PACAP depolarizes pancreatic neurons via the activation of ganglionic PAC_1 receptors and may enhance endocrine secretion (Kirchgessner and Liu, 2001).

TABLE 1 | Electrical properties of pancreatic neurons in different species.

	Guinea pigs Liu and Kirchgessner (1997)	**Rabbits** Love (2000)	**Dogs** Sha and Szurszewski (1999)	**Cats** King et al. (1989)	**Region of the cat pancreas** Sha et al. (1996)		
					Head	**Body**	**Tail**
RMP (mV)	−51.9 ± 0.6	−54 ± 0.4	−53.5 ± 1.6	−49 ± 2	−49.1 ± 7.1	−49.5 ± 7.2	−53.5 ± 1.6
IR (MΩ)	84 ± 2.3	106 ± 6	88.2 ± 1.9	46 ± 4	66.0 ± 31.6	69.1 ± 36.2	60.7 ± 28.4
AP threshold (mV)	−30.5 ± 0.8	−15 ± 1		−33 ± 1			
AP amplitude (mV)	53.2 ± 1.0	65 ± 1		60 ± 1			
Time constant (ms)	1.8 ± 0.1	2.0 ± 0.1		3.1 ± 0.2	3.0 ± 0.1	3.1 ± 0.1	3.1 ± 0.1
ASH amplitude (mV)	12.6 ± 1.1	11 ± 0.5		17 ± 1			
ASH duration (ms)	168.6 ± 23.6	210 ± 19					

RMP, resting membrane potentials; IR, input resistances; AP, action potential; ASH, after-spike hyperpolarization. All the values represent mean ± standard error of the data.

While NO evokes membrane hyperpolarization in neurons of the cat pancreas, the membrane IR does not markedly change. Inhibition of NO production may enhance release of ACh to evoke fEPSPs and increase the amplitude of sEPSPs (Sha et al., 1995).

Serotonergic nerve fibers are found in the intrapancreatic ganglia of guinea pigs and cats, but are rare or absent in rabbits (Ma and Szurszewski, 1996b; Liu and Kirchgessner, 1997; Yi et al., 2004). No 5-HT immunoreactive neurons are observed in cat intrapancreatic ganglia (Sha et al., 1996). Neurons in the pancreatic head have a higher excitability in response to 5-HT than those in the tail. The responses of neurons of the intrapancreatic ganglia to 5-HT with fast and slow depolarization are mediated by 5-HT_3 and 5-HT_1p receptors, respectively (Ma and Szurszewski, 1996b; Sha et al., 1996).

Cholecystokinin (CCK) has been shown to be present in nerve terminals which surround but are not in the intrapancreatic ganglia. The vagal and sympathetic nerve fibers may be the source of CCK in the pancreas. In cats, cholecystokinin octapeptide (CCK-8) can evoke slow depolarization by acting on CCK_B postsynaptic receptors, and amplify nicotinic transmission by facilitating the release of ACh from preganglionic nerve terminals or by increasing the sensitivity of postsynaptic membranes to ACh (Cantor and Rehfeld, 1984; Ma and Szurszewski, 1996a).

Investigation of electrophysiological effects of gamma-aminobutyric acid (GABA) on cat pancreatic neurons indicates that GABA acts on the ganglia through $GABA_A$ receptors, which can cause depolarization and inhibit fEPSPs (Sha et al., 2001a). While endogenous GABA has been shown to be stored in and released from the ganglionic glial cells, the origin of the GABA remains unclear (Sha et al., 2001a). Leptin promotes fast synaptic transmission by acting on presynaptic nerve terminals of intrapancreatic ganglia in dogs (Sha and Szurszewski, 1999).

NEURAL REGULATION OF ISLETS

Intrapancreatic ganglia are the integration center for extrinsic nerve inputs and intrinsic neuronal inputs. This integration center plays an important role in regulating pancreatic endocrine function. The extrinsic nerves modulate pancreatic endocrine function either directly at the islet level or by going through the integration center (Gylfe and Tengholm, 2014; Di Cairano et al., 2016; **Figure 3**).

Innervation of Islets

The modes of innervation of pancreatic islets vary across species. In mice, the postganglionic parasympathetic fibers contact all types of endocrine cells (α, β, δ, and PP cells) in the islets, while the postganglionic sympathetic fibers innervate α cells and smooth muscle cells of the blood vessels, but not the β cells (Dolensek et al., 2015). The islets are sparsely innervated in adult humans. Parasympathetic postganglionic fibers are observed to contact exocrine tissue preferentially. Most sympathetic nerves innervate smooth muscle cells of the blood vessels in the adult human pancreas. However, the human fetal pancreas is richly innervated (Taborsky, 2011; Krivova et al., 2016). Islet innervation is correlated with age and environmental factors in humans and rats (Proshchina et al., 2014; Mundinger et al., 2016; Tang et al., 2018b). The integration between epithelial cells

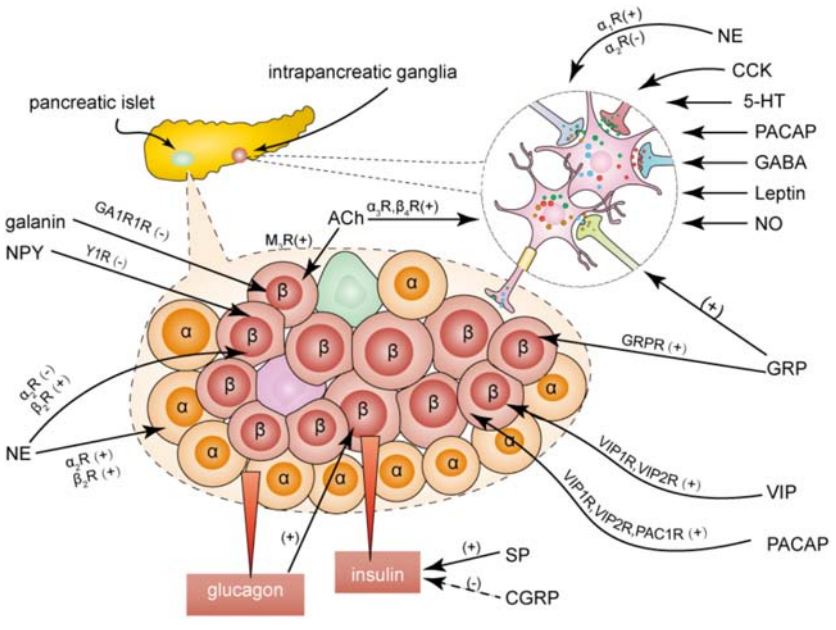

FIGURE 3 | Effects of neurotransmitters on insulin secretion. Neurotransmitters modulate the insulin secretion by activating different receptors both directly at the islets and indirectly at the ganglionic level. ACh, acetylcholine; GRP, gastrin-releasing peptide; VIP, vasoactive intestinal peptide; NO, nitric oxide; NE, noradrenaline; NPY, neuropeptide Y; PACAP, pituitary adenylate cyclase activating polypeptide; 5-HT, serotonin; CCK, cholecystokinin; CGRP, calcitonin gene-related peptide; SP, substance P.

and components of the nervous system may form the neuro-insular complexes seen during cellular differentiation (Krivova et al., 2016). In addition, the composition and cytoarchitecture of endocrine cells are also different in humans and rats (Rodriguez-Diaz and Caicedo, 2014; Thorens, 2014; Dolensek et al., 2015; Da Silva Xavier, 2018). Current findings indicate that different species may have different mechanisms for neural regulation of pancreatic endocrine function.

Intrapancreatic Ganglionic Regulation of Islets

As the integrated innervation enters the pancreas, intrapancreatic ganglia directly innervate islets, thereby modulating islet secretion.

Tract-tracing of intrapancreatic ganglionic neurons shows that intrapancreatic ganglia send nerve fibers directly to the islets (Kirchgessner and Pintar, 1991). This ganglion-islet association has been recently demonstrated by a three-dimensional panoramic histology study (Tang et al., 2018b). *In vivo* ganglionic nicotinic activation stimulates insulin and glucagon secretion in the mouse pancreas (Karlsson and Ahrén, 1998). Cholinergic nerves of the intrapancreatic ganglia regulate the oscillatory pattern of basal endocrine secretion (Karlsson and Ahrén, 1998; Fendler et al., 2009). Activation of postganglionic cholinergic nerves by GRP regulates insulin secretion *in vivo* (Karlsson et al., 1998). An electrophysiological study in a ganglion-islet attached preparation setting provides direct evidence for the modulation of insulin secretion by the intrapancreatic ganglia. The activity of intrapancreatic ganglionic neurons directly stimulates insulin secretion, while blockage of this activity removes the modulation (Sha et al., 2001b).

Sympathetic Regulation of Islets

Sympathetic nerves regulate pancreatic endocrine secretion with multiple direct and indirect mechanisms through their actions on islets, blood vessels, and intrapancreatic ganglia (Yi et al., 2005). Electrical stimulation of sympathetic nerves induces NE release and has an inhibitory effect on basal and glucose-stimulated insulin release by acting on the α_2-adrenoceptor of β cells in dogs and calves. Sympathetic nerves do not participate in the inhibition of basal insulin secretion in rats, pigs, and humans (Ahrén, 2000). NE can also stimulate insulin secretion by acting on the β_2-adrenoceptor of β cells or by acting on the α_2- and β_2-adrenoceptors of α cells, where glucagon secretion leads to an increase in insulin secretion (Ahrén, 2000). In general, the overall effect of NE is lowering the plasma insulin concentration (Rodriguez-Diaz and Caicedo, 2013). In humans, the primary targets of the sympathetic fibers are vascular smooth muscle cells, which can reduce blood flow to regulate secretion (Rodriguez-Diaz and Caicedo, 2013; Dolensek et al., 2015). Patients with type 1 diabetes show a severe loss of islet sympathetic nerves. Moreover, rats with short-term hyperglycemia show a dysfunction in the islet sympathetic innervation from the celiac ganglia, while hyperphagic weaning mice show markedly increased sympathetic innervation compared to control mice (Mundinger et al., 2015, 2016; Tang et al., 2018b).

Activation of the sympathetic pathway potentiates glucagon secretion and inhibits somatostatin secretion. However, the effects of sympathetic nerve activity on pancreatic polypeptide (PP) secretion are different across species, in that it enhances PP secretion in pig and human pancreases, but inhibits PP secretion in the dog pancreas (Ahrén, 1999; Gilon and Henquin, 2001; Rodriguez-Diaz and Caicedo, 2014).

Both NPY and galanin are known to mediate insulin secretion (Chandra and Liddle, 2013). NPY inhibits glucose-induced insulin secretion in rats and mice, but has no effect in dogs (Dunning et al., 1987; Pettersson et al., 1987; Morgan et al., 1998). Galanin inhibits insulin secretion in dogs but not in humans, as the innervation of galanin-containing nerves is abundant in dog islets, but rare in human pancreatic islets (Ahrén and Lindskog, 1992; Ahrén, 2000). Interestingly, both NPY and galanin have an insulinotropic effect on the pig pancreas (Sheikh et al., 1988). NPY binds to the Y1 receptor subtype, while galanin interacts with GA1R1 receptors in β cells to mediate insulin secretion (Parker et al., 1995; Morgan et al., 1998; Chandra and Liddle, 2009). Oral administration of galanin has been shown to improve insulin sensitivity by decreasing duodenal contraction in diabetic mice (Abot et al., 2018b).

Parasympathetic Regulation of Islets

Insulin secretion is stimulated by the electrical activation of parasympathetic fibers and inhibited by vagotomy (Ahrén, 2000; Teff, 2008; Balbo et al., 2016). The density of parasympathetic axons is lower in the exocrine tissue of the pancreas in individuals with new-onset type 1 diabetes (Lundberg et al., 2017) than in control individuals. ACh released by postganglionic nerve fibers acts on muscarinic receptors of β-cells and stimulates insulin secretion directly (Van der Zee et al., 1992). The M_3 receptor subtype plays an important role in regulating cholinergic nerves to induce secretion of islet hormones (Karlsson and Ahrén, 1993; Gautam et al., 2006; Miranda et al., 2016). ACh stimulates glucagon and PP secretion that can be blocked by atropine, and the effect of ACh on somatostatin secretion varies across species (Gilon and Henquin, 2001).

VIP, PACAP, and GRP can stimulate the secretion of glucagon and insulin. Given their similar structures, VIP and PACAP have common receptors called VIP_1 and VIP_2 receptors, whereas the PAC_1 receptor is specific for PACAP (Kirchgessner and Liu, 2001). GRP directly acts on the islets via the GRP receptors (Karlsson and Ahrén, 1998). As the nerves containing VIP are found very close to α cells in dogs, α cells are more sensitive to VIP than β cells (Havel et al., 1997).

Sensory Nerve-Mediated Regulation of Islets

Sensory nerves regulate endocrine secretion through two mechanisms: (a) direct action on the islet receptors, and (b) formation of neural circuits with adrenergic nerves (Ahrén, 2000). CGRP inhibits glucose-induced insulin release and stimulates glucagon secretion (Ahrén et al., 1987; Silvestre et al., 1996), but the specific CGRP receptor that mediates these processes has not yet been identified. There is

considerable variation in reports of the effects of SP on insulin release (Hermansen, 1980; Chiba et al., 1985; Shen et al., 2016). SP induces a marked increase in insulin secretion from the pancreas of healthy rats, but inhibits insulin secretion from the pancreas of diabetic rats, indicating that it may play a role in the onset of diabetes (Adeghate et al., 2001; Shen et al., 2016). It is generally considered that SP interacts with neurokinin G-protein-coupled receptors (NK-R) on islets. In rats, it is suggested that the role of vagal afferents is to suppress insulin secretion (Meyers et al., 2016). The role of sensory nerves in mediating glucose homeostasis remains unexplored.

CONCLUSION AND PERSPECTIVES

Intrapancreatic ganglia constitute endogenous neural networks and release various neurotransmitters. They integrate both intrinsic and external nerve inputs to play an important role in pancreatic endocrine secretion. The mechanisms underlying the role of intrapancreatic ganglia in islet function remain relatively unclear. Further studies are needed to elucidate the complete mechanisms underlying the functions of intrapancreatic ganglia in normal physiological and disease states of the pancreas. This may provide us with novel ways to treat diseases of the pancreas.

AUTHOR CONTRIBUTIONS

WL researched the articles and wrote the manuscript. GY, YL, and LS revised the draft before submission. All authors have made direct and intellectual contribution to the work, and approved it for publication.

ACKNOWLEDGMENTS

This work was supported by the National Natural Science Foundation of China (Grant Nos. 81270900 and 81670492).

REFERENCES

Abot, A., Cani, P. D., and Knauf, C. (2018a). Impact of intestinal peptides on the enteric nervous system: novel approaches to control glucose metabolism and food intake. *Front. Endocrinol.* 9:328. doi: 10.3389/fendo.2018.00328

Abot, A., Lucas, A., Bautzova, T., Bessac, A., Fournel, A., Le-Gonidec, S., et al. (2018b). Galanin enhances systemic glucose metabolism through enteric nitric oxide synthase-expressed neurons. *Mol. Metab.* 10, 100–108. doi: 10.1016/j.molmet.2018.01.020

Adeghate, E., Ponery, A. S., and Pallota, D. J. (2001). Distribution of vasoactive intestinal polypeptide, neuropeptide-Y and substance P and their effects on insulin secretion from the in vitro pancreas of normal and diabetic rats. *Peptides* 22, 99–107. doi: 10.1016/S0196-9781(00)00361-2

Ahrén, B. (1999). Regularion of insulin secretion by nerves and neuropeptides. *Ann. Acad. Med. Singapore* 28, 99–104.

Ahrén, B. (2000). Autonomic regulation of islet hormone secretion- implications for health and disease. *Diabetologia* 43, 393–410. doi: 10.1007/s001250051322

Ahrén, B., and Lindskog, S. (1992). Galanin and the regulation of islet hormone secretion. *Int. J. Pancreatol.* 11, 147–160.

Ahrén, B., Mårtensson, H., and Nobin, A. (1987). Effects of calcitonin gene-related peptide (CGRP) on islet hormone secretion in the pig. *Diabetologia* 30, 354–359. doi: 10.1007/BF00299030

Arciszewski, M., and Zacharko-Siembida, A. (2007). Cholinergic innervation of the pancreas in the sheep. *Acta Biol. Hungar.* 58, 151–161. doi: 10.1556/ABiol.58.2007.2.2

Arciszewski, M. B., Mozel, S., and Sienkiewicz, W. (2015). Pituitary adenylate cyclase-activating peptide-27 (PACAP-27) is co-stored with galanin, substance P and corticotropin releasing factor (CRF) in intrapancreatic ganglia of the sheep. *Pol. J. Vet. Sci.* 18, 343–350. doi: 10.1515/pjvs-2015-0044

Balbo, S. L., Ribeiro, R. A., Mendes, M. C., Lubaczeuski, C., Maller, A. C., Carneiro, E. M., et al. (2016). Vagotomy diminishes obesity in cafeteria rats by decreasing cholinergic potentiation of insulin release. *J. Physiol. Biochem.* 72, 625–633. doi: 10.1007/s13105-016-0501-9

Cantor, P., and Rehfeld, J. F. (1984). The molecular nature of cholecystokinin in the feline pancreas and related nervous structures. *Regul. Pept.* 8, 199–208. doi: 10.1016/0167-0115(84)90061-2

Chandra, R., and Liddle, R. A. (2009). Neural and hormonal regulation of pancreatic secretion. *Curr. Opin. Gastroenterol.* 25, 441–446. doi: 10.1097/MOG.0b013e32832e9c41

Chandra, R., and Liddle, R. A. (2013). Modulation of pancreatic exocrine and endocrine secretion. *Curr. Opin. Gastroenterol.* 29, 517–522. doi: 10.1097/MOG.0b013e3283639326

Chandra, R., and Liddle, R. A. (2014). Recent advances in the regulation of pancreatic secretion. *Curr. Opin. Gastroenterol.* 30, 490–494. doi: 10.1097/MOG.0000000000000099

Chandrasekharan, B., and Srinivasan, S. (2007). Diabetes and the enteric nervous system. *Neurogastroenterol. Motil.* 19, 951–960. doi: 10.1111/j.1365-2982.2007.01023.x

Chaudhury, A. (2014). Similarity in transcytosis of nNOSalpha in enteric nerve terminals and beta cells of pancreatic islet. *Front. Med.* 1:20. doi: 10.3389/fmed.2014.00020

Chiba, Y., Kawai, K., Okuda, Y., Munekata, E., and Yamashita, K. (1985). Effects of substance P and substance P-(6-11) on hormone release from isolated perfused pancreas- their opposite actions on rat and canine islets. *Endocrinology* 117, 1996–2000. doi: 10.1210/endo-117-5-1996

Da Silva Xavier, G. (2018). The cells of the islets of langerhans. *J. Clin. Med.* 7:54. doi: 10.3390/jcm7030054

De Giorgio, R., Sternini, C., Anderson, K., Brecha, N., and Go, V. (1992a). Tissue distribution and innervation pattern of peptide immunoreactivities in the rat pancreas. *Peptides* 13, 91–98. doi: 10.1016/0196-9781(92)90145-S

De Giorgio, R., Sternini, C., Brecha, N. C., Widdison, A. L., Karanjia, N. D., Reber, H. A., et al. (1992b). Patterns of innervation of vasoactive intestinal polypeptide, neuropeptide y, and gastrin-releasing peptide immunoreactive nerves in the feline pancreas. *Pancreas* 7, 376–384. doi: 10.1097/00006676-199205000-00016

De Giorgio, R., Sternini, C., Widdison, A., Alvarez, C., Brecha, N., Reber, H., et al. (1993). Differential effects of experimentally induced chronic pancreatitis on neuropeptide immunoreactivities in the feline pancreas. *Pancreas* 8, 700–710. doi: 10.1097/00006676-199311000-00006

Di Cairano, E. S., Moretti, S., Marciani, P., Sacchi, V. F., Castagna, M., Davalli, A., et al. (2016). Neurotransmitters and neuropeptides: new players in the control of islet of langerhans' cell mass and function. *J. Cell. Physiol.* 231, 756–767. doi: 10.1002/jcp.25176

Dolensek, J., Rupnik, M. S., and Stozer, A. (2015). Structural similarities and differences between the human and the mouse pancreas. *Islets* 7:e1024405. doi: 10.1080/19382014.2015.1024405

Dunning, B., Ahren, B., Böttcher, G., Sundler, F., and Taborsky, G. J. (1987). The presence and actions of NPY in the canine endocrine pancreas. *Regul. Pept.* 18, 253–265. doi: 10.1016/0167-0115(87)90183-2

Fendler, B., Zhang, M., Satin, L., and Bertram, R. (2009). Synchronization of pancreatic islet oscillations by intrapancreatic ganglia: a modeling study. *Biophys. J.* 97, 722–729. doi: 10.1016/j.bpj.2009.05.016

Furuzawa, Y., Ohmori, Y., and Watanabe, T. (1996). Immunohistochemical studies of neural elements in pancreatic islets of the cat. *J. Vet. Med. Sci.* 58, 641–646. doi: 10.1292/jvms.58.641

Gautam, D., Han, S. J., Hamdan, F. F., Jeon, J., Li, B., Li, J. H., et al. (2006). A critical role for beta cell M3 muscarinic acetylcholine receptors in regulating insulin release and blood glucose homeostasis in vivo. *Cell Metab.* 3, 449–461. doi: 10.1016/j.cmet.2006.04.009

Giannulis, I., Mondini, E., Cinti, F., Frontini, A., Murano, I., Barazzoni, R., et al. (2014). Increased density of inhibitory noradrenergic parenchymal nerve fibers in hypertrophic islets of Langerhans of obese mice. *Nutr. Metab. Cardiovasc. Dis.* 24, 384–392. doi: 10.1016/j.numecd.2013.09.006

Gilon, P., and Henquin, J. C. (2001). Mechanisms and physiological significance of the cholinergic control of pancreatic beta-cell function. *Endocr. Rev.* 22, 565–604.

Gylfe, E., and Tengholm, A. (2014). Neurotransmitter control of islet hormone pulsatility. *Diabetes Obes. Metab.* 16(Suppl. 1), 102–110. doi: 10.1111/dom.12345

Hannibal, J., and Fahrenkrug, J. (2000). Pituitary adenylate cyclase-activating polypeptide in intrinsic and extrinsic nerves of the rat pancreas. *Cell Tissue Res.* 299, 59–70. doi: 10.1007/s004410050006

Havel, P. J., Dunning, B. E., Vercherec, C. B., Baskin, D. G., Dorisio, T. O., and Taborsky, G. J. Jr. (1997). Evidence that vasoactive intestinal polypeptide is a parasympathetic neurotransmitter in the endocrine pancreas in dogs. *Regul. Pept.* 71, 163–170. doi: 10.1016/S0167-0115(97)01014-8

Havel, P. J., Gerald, J., and Taborsky, J. R. (1989). The contribution of the autonomic nervous system to changes of glucagon and insulin secretion during hypoglycemic stress. *Endocr. Soc.* 10, 332–350. doi: 10.1210/edrv-10-3-332

Hermansen, K. (1980). Effects of substance p and other peptides on the release of somatostatin, insulin, and glucagon in vitro. *Endocrinology* 107, 256–261. doi: 10.1210/endo-107-1-256

Hiramatsu, K., Ohshima, K., and Neurosci, L. (1994). Colocalization of NADPH-diaphorase with neuropeptides in the intrapancreatic neurons of the chicken. *Neurosci. Lett.* 182, 37–40. doi: 10.1016/0304-3940(94)90199-6

Karlsson, S., and Ahrén, B. (1993). Muscarinic receptor subtypes in carbachol-stimulated insulin and glucagon secretion in the mouse. *J. Auton. Pharmacol.* 13, 439–446. doi: 10.1111/j.1474-8673.1993.tb00291.x

Karlsson, S., and Ahrén, B. (1998). Insulin and glucagon secretion by ganglionic nicotinic activation in adrenalectomized mice. *Eur. J. Pharmacol.* 342, 291–295. doi: 10.1016/S0014-2999(97)01508-2

Karlsson, S., Sundler, F., and Ahrén, B. (1998). Insulin secretion by gastrin-releasing peptide in mice-ganglionic versus direct islet effect. *Am. Physiol. Soc.* 274, 124–129. doi: 10.1152/ajpendo.1998.274.1.E124

King, B. F., Love, J., and Szurszewski, J. (1989). Intracellular recordings from pancreatic ganglia of the cat. *J. Physiol.* 419, 379–403. doi: 10.1113/jphysiol.1989.sp017877

Kirchgessner, A. L., and Gershon, M. D. (1990). Innervation of the pancreas by neurons in the gut. *J. Neurosci.* 10, 1626–1642. doi: 10.1523/JNEUROSCI.10-05-01626.1990

Kirchgessner, A. L., and Gershon, M. D. (1995). Presynaptic inhibition by serotonin of nerve-mediated secretion of pancreatic amylase. *Am. Physiol. Soc.* 268, 339–345. doi: 10.1152/ajpgi.1995.268.2.G339

Kirchgessner, A. L., and Liu, M. T. (2001). Pituitary adenylate cyclase activating peptide (PACAP) in the enteropancreatic innervation. *Anatom. Rec.* 262, 91–100. doi: 10.1002/1097-0185(20010101)262:1<91::AID-AR1014>3.0.CO;2-2

Kirchgessner, A. L., and Pintar, J. E. (1991). Guinea pig pancreatic ganglia- projections, transmitter content, and the type-specific localization of monoamine oxidase. *J. Comp. Neurol.* 305, 613–631. doi: 10.1002/cne.903050407

Krivova, Y., Proshchina, A., Barabanov, V., Leonova, O., and Saveliev, S. (2016). Structure of neuro-endocrine and neuro-epithelial interactions in human foetal pancreas. *Tissue Cell* 48, 567–576. doi: 10.1016/j.tice.2016.10.005

Lartigue, G. D. (2016). Role of the vagus nerve in the development and treatment of diet-induced obesity. *J. Physiol.* 594, 5791–5815. doi: 10.1113/JP271538

Liu, H. P., Tay, S. S. W., Leong, S. K., and Schemann, M. (1998). Colocalization of ChAT, DbetaH and NADPH-d in the pancreatic neurons of the newborn guinea pig. *Cell Tissue Res.* 294, 227–231. doi: 10.1007/s004410051172

Liu, M. T., and Kirchgessner, A. L. (1997). Guinea pig pancreatic neurons: morphology, neurochemistry, electrical properties, and response to 5-HT. *Am. J. Physiol.* 273, 1273–1289. doi: 10.1152/ajpgi.1997.273.6.G1273

Llewellyn-Smith, I. J. (2009). Anatomy of synaptic circuits controlling the activity of sympathetic preganglionic neurons. *J. Chem. Neuroanat.* 38, 231–239. doi: 10.1016/j.jchemneu.2009.06.001

Love, J. A. (2000). Electrical properties and synaptic potentials of rabbit pancreatic neurons. *Auton. Neurosci.* 84, 68–77. doi: 10.1016/S1566-0702(00)00187-9

Love, J. A., and Szebeni, K. (1999a). Histochemistry and electrophysiology of cultured adult rabbit pancreatic neurons. *Pancreas* 18, 65–74.

Love, J. A., and Szebeni, K. (1999b). Morphology and histochemistry of the rabbit pancreatic innervation. *Pancreas* 18, 53–64. doi: 10.1097/00006676-199901000-00008

Love, J. A., Yi, E., and Smith, T. G. (2007). Autonomic pathways regulating pancreatic exocrine secretion. *Auton. Neurosci.* 133, 19–34. doi: 10.1016/j.autneu.2006.10.001

Lundberg, M., Lindqvist, A., Wierup, N., Krogvold, L., Dahl-Jorgensen, K., and Skog, O. (2017). The density of parasympathetic axons is reduced in the exocrine pancreas of individuals recently diagnosed with type 1 diabetes. *PLoS One* 12:e0179911. doi: 10.1371/journal.pone.0179911

Ma, J., and Vella, A. (2018). What has bariatric surgery taught us about the role of the upper gastrointestinal tract in the regulation of postprandial glucose metabolism? *Front. Endocrinol.* 9:324. doi: 10.3389/fendo.2018.00324

Ma, R. C., and Szurszewski, J. H. (1996a). Cholecystokinin depolarizes neurons of cat pancreatic ganglion. *Peptides* 17, 775–783.

Ma, R. C., and Szurszewski, J. H. (1996b). 5-Hydroxytryptamine depolarizes neurons of cat pancreatic ganglia. *J. Auton. Nerv. Syst.* 57, 78–86.

Meyers, E. E., Kronemberger, A., Lira, V., Rahmouni, K., and Stauss, H. M. (2016). Contrasting effects of afferent and efferent vagal nerve stimulation on insulin secretion and blood glucose regulation. *Physiol. Rep.* 4:e12718. doi: 10.14814/phy2.12718

Miranda, R. A., Torrezan, R., de Oliveira, J. C., Barella, L. F., da Silva Franco, C. C., Lisboa, P. C., et al. (2016). HPA axis and vagus nervous function are involved in impaired insulin secretion of MSG-obese rats. *J. Endocrinol.* 230, 27–38. doi: 10.1530/JOE-15-0467

Morgan, D., Kulkarni, R., Hurley, J., Wang, Z. L., Wang, R. M., Ghatei, M. A., et al. (1998). Inhibition of glucose stimulated insulin secretion by neuropeptide Y is mediated via the Y1 receptor and inhibition of adenylyl cyclase in RIN 5AH rat insulinoma cells. *Diabetologia* 41, 1482–1491. doi: 10.1007/s001250051095

Mundinger, T. O., Cooper, E., Coleman, M. P., and Taborsky, G. J. Jr. (2015). Short-term diabetic hyperglycemia suppresses celiac ganglia neurotransmission, thereby impairing sympathetically mediated glucagon responses. *Am. J. Physiol. Endocrinol. Metab.* 309, E246–E255. doi: 10.1152/ajpendo.00140.2015

Mundinger, T. O., Mei, Q., Foulis, A. K., Fligner, C. L., Hull, R. L., and Taborsky, G. J. Jr. (2016). Human type 1 diabetes is characterizedby an early,marked, sustained,and islet-selective loss of sympathetic nerves. *Diabetes* 65, 2322–2330. doi: 10.2337/db16-0284/-/DC1

Myojin, T., Kitamura, N., Hondo, E., Baltazar, E., Pearson, G., and Yamada, J. (2000). Immunohistochemical localization of neuropeptides in bovine pancreas. *Anat. Histol. Embryol.* 29, 167–172. doi: 10.1046/j.1439-0264.2000.00257.x

Niebergall-Roth, E., and Singer, M. V. (2001). Central and peripheral neural control of pancreatic exocrine secretion. *J. Physiol. Pharmacol.* 52, 523–538.

Parker, E. M., Izzarelli, D. G., Nowak, H. P., Mahle, C. D., Iben, L. G., Wang, J. C., et al. (1995). Cloning and characterization of the rat GALR1 galanin receptor from Rin14B insulinoma cells. *Brain Res.* 34, 179–189. doi: 10.1016/0169-328X(95)00159-P

Pettersson, M., Ahrén, B., Lundquist, I., Böttcher, G., and Sundler, F. (1987). Neuropeptide Y: intrapancreatic neuronal localization and effects on insulin secretion in the mouse. *Cell Tissue Res.* 248, 43–48. doi: 10.1007/BF01239960

Proshchina, A. E., Krivova, Y. S., Barabanov, V. M., and Saveliev, S. V. (2014). Ontogeny of neuro-insular complexes and islets innervation in the human pancreas. *Front. Endocrinol.* 5:57. doi: 10.3389/fendo.2014.00057

Renehan, W. E., Zhang, X., Beierwaltes, W. H., and Fogel, R. (1995). Neurons in the dorsal motor nucleus of the vagus may integrate vagal and spinal information from the GI tract. *Am. Physiol. Soc.* 268, 780–790. doi: 10.1152/ajpgi.1995.268.5.G780

Rodriguez-Diaz, R., and Caicedo, A. (2013). Novel approaches to studying the role of innervation in the biology of pancreatic islets. *Endocrinol. Metab. Clin. North Am.* 42, 39–56. doi: 10.1016/j.ecl.2012.11.001

Rodriguez-Diaz, R., and Caicedo, A. (2014). Neural control of the endocrine pancreas. *Best Pract. Res. Clin. Endocrinol. Metab.* 28, 745–756. doi: 10.1016/j.beem.2014.05.002

Sha, L., Love, J. A., Ma, R., and Szurszewski, J. H. (1997). Cholinergic transmission in pancreatic ganglia of the cat. *Pancreas* 14, 83–93. doi: 10.1097/00006676-199701000-00013

Sha, L., Miller, S., and Szurszewski, J. H. (2001a). Electrophysiological effects of GABA on cat pancreatic neurons. *Am. J. Physiol. Gastrointest. Liver Physiol.* 280, 324–331.

Sha, L., Westerlund, J., Szurszewski, J. H., and Bergsten, P. (2001b). Amplitude modulation of pulsatile insulin secretion by intrapancreatic ganglion neurons. *Diabetes* 50, 51–55.

Sha, L., Miller, S. M., and Szurszewski, J. H. (1995). Nitric oxide is a neuromodulator in cat pancreatic ganglia_ histochemical and electrophysiological study. *Neurosci. Lett.* 192, 77–80. doi: 10.1016/0304-3940(95)11614-3

Sha, L., Ou, L., Miller, S. M., Ma, R., and Szurszewski, J. H. (1996). Cat pancreatic neurons morphology, electrophysiological properties, and responses to 5-HT. *Pancreas* 13, 111–124. doi: 10.1097/00006676-199608000-00001

Sha, L., and Szurszewski, J. H. (1999). Leptin modulates fast synaptic transmission in dog pancreatic ganglia. *Neurosci. Lett.* 263, 93–96. doi: 10.1016/S0304-3940(99)00122-6

Sheikh, S. P., Holst, J. J., Skak-Nielsen, T., Knigge, U., Warberg, J., Theodorsson-Norheim, E., et al. (1988). Release of NPY in pig pancreas: dual parasympathetic and sympathetic regulation. *Am. J. Physiol.* 255(1 Pt 1), G46–G54. doi: 10.1152/ajpgi.1988.255.1.G46

Shen, Q., Wang, Y., Zhang, N., Gao, D., Liu, Y., and Sha, L. (2016). Substance P expresses in intrapancreatic ganglia of the rats. *Neuropeptides* 59, 33–38. doi: 10.1016/j.npep.2016.06.004

Silvestre, R. A., Salas, M., Rodriguez-Gallardo, J., Garcia-Hermida, O., Fontela, T., and Marco, J. (1996). Effect of (8 - 32) salmon calcitonin, an amylin antagonist, on insulin, glucagon and somatostatin release study in the perfused pancreas of the rat.pdf. *Br. J. Pharmacol.* 117, 347–350. doi: 10.1111/j.1476-5381.1996.tb15197.x

Taborsky, G. J. Jr. (2011). Islets have a lot of nerve! or do they? *Cell Metab.* 14, 5–6. doi: 10.1016/j.cmet.2011.06.004

Tang, S. C., Baeyens, L., Shen, C. N., Peng, S. J., Chien, H. J., Scheel, D. W., et al. (2018a). Human pancreatic neuro-insular network in health and fatty infiltration. *Diabetologia* 61, 168–181. doi: 10.1007/s00125-017-4409-x

Tang, S. C., Shen, C. N., Lin, P. Y., Peng, S. J., Chien, H. J., Chou, Y. H., et al. (2018b). Pancreatic neuro-insular network in young mice revealed by 3D panoramic histology. *Diabetologia* 61, 158–167. doi: 10.1007/s00125-017-4408-y

Teff, K. L. (2008). Visceral nerves_ vagal and sympathetic innervation. *J. Parenteral. Enteral. Nutr.* 32, 569–571. doi: 10.1177/0148607108321705

Thorens, B. (2014). Neural regulation of pancreatic islet cell mass and function. *Diabetes Obes. Metab.* 16(Suppl. 1), 87–95. doi: 10.1111/dom.12346

Van der Zee, E. A., Buwalda, B., Strubbe, J. H., Strosberg, A. D., and Luiten, P. G. M. (1992). Immunocytochemical localization of muscarinic acetylcholine receptors in the rat endocrine pancreas. *Cell Tissue Res.* 269, 99–106. doi: 10.1007/BF00384730

Wang, J., Zheng, H., and Berthoud, H. R. (1999). Functional vagal input to chemically identified neurons in pancreatic ganglia as revealed by Fos expression. *Am. Physiol. Soc.* 277, 958–964. doi: 10.1152/ajpendo.1999.277.5.E958

Yi, E., and Love, J. A. (2005a). Alpha-adrenergic modulation of synaptic transmission in rabbit pancreatic ganglia. *Auton. Neurosci* 122, 45–57. doi: 10.1016/j.autneu.2005.07.008

Yi, E., and Love, J. A. (2005b). Short-term synaptic plasticity in rabbit pancreatic ganglia. *Auton. Neurosci.* 119, 36–47. doi: 10.1016/j.autneu.2005.03.001

Yi, E., Smith, T. G., Baker, R. C., and Love, J. A. (2004). Catecholamines and 5-hydroxytryptamine in tissues of the rabbit exocrine pancreas. *Pancreas* 29, 218–224. doi: 10.1097/00006676-200410000-00007

Yi, E., Smith, T. G., and Love, J. A. (2005). Noradrenergic innervation of rabbit pancreatic ganglia. *Auton. Neurosci.* 117, 87–96. doi: 10.1016/j.autneu.2004.11.004

Yi, S. Q., Miwa, K., Ohta, T., Kayahara, M., Kitagawa, H., Tanaka, A., et al. (2003). Innervation of the pancreas from the perspective of perineural invasion of pancreatic cancer. *Pancreas* 27, 225–229. doi: 10.1097/00006676-200310000-00005

Conflict of Interest Statement: The authors declare that the research was conducted in the absence of any commercial or financial relationships that could be construed as a potential conflict of interest.

frontiers in Neuroscience

ORIGINAL RESEARCH
published: 26 February 2019
doi: 10.3389/fnins.2019.00150

Metabolite Profiles of the Cerebrospinal Fluid in Neurosyphilis Patients Determined by Untargeted Metabolomics Analysis

Li-Li Liu[1,2], Yong Lin[1], Wei Chen[3], Man-Li Tong[1,2], Xi Luo[1], Li-Rong Lin[1,2], Hui-Lin Zhang[1], Jiang-Hua Yan[4], Jian-Jun Niu[1,2]* and Tian-Ci Yang[1,2]**

[1] Center of Clinical Laboratory, Zhongshan Hospital, School of Medicine, Xiamen University, Xiamen, China, [2] Institute of Infectious Disease, School of Medicine, Xiamen University, Xiamen, China, [3] Shanghai Applied Protein Technology Co., Ltd., Shanghai, China, [4] Cancer Research Center, School of Medicine, Xiamen University, Xiamen, China

OPEN ACCESS

Edited by:
Leo T. O. Lee,
University of Macau, China

Reviewed by:
Qian-Qiu Wang,
Chinese Academy of Medical Sciences, China
Xuanxian Peng,
Sun Yat-sen University, China
Yimou Wu,
University of South China, China

***Correspondence:**
Jiang-Hua Yan
jhyan@xmu.edu.cn
Jian-Jun Niu
niujianjun211@xmu.edu.cn
Tian-Ci Yang
yangtianci@xmu.edu.cn

Specialty section:
This article was submitted to Neuroendocrine Science, a section of the journal Frontiers in Neuroscience

Received: 30 September 2018
Accepted: 11 February 2019
Published: 26 February 2019

Citation:
Liu L-L, Lin Y, Chen W, Tong M-L, Luo X, Lin L-R, Zhang H-L, Yan J-H, Niu J-J and Yang T-C (2019) Metabolite Profiles of the Cerebrospinal Fluid in Neurosyphilis Patients Determined by Untargeted Metabolomics Analysis. Front. Neurosci. 13:150. doi: 10.3389/fnins.2019.00150

The mechanism underlying the stealth property of neurosyphilis is still unclear. Global metabolomics analysis can provide substantial information on energy metabolism, physiology and possible diagnostic biomarkers and intervention strategies for pathogens. To gain better understanding of the metabolic mechanism of neurosyphilis, we conducted an untargeted metabolomics analysis of cerebrospinal fluid (CSF) from 18 neurosyphilis patients and an identical number of syphilis/non-neurosyphilis patients and syphilis-free patients using the Agilent, 1290 Infinity LC system. The raw data were normalized and subjected to subsequent statistical analysis by MetaboAnalyst 4.0. Metabolites with a variable importance in projection (VIP) greater than one were validated by Student's *T*-test. A total of 1,808 molecular features were extracted from each sample using XCMS software, and the peak intensity of each feature was obtained. Partial-least squares discrimination analysis provided satisfactory separation by comparing neurosyphilis, syphilis/non-neurosyphilis and syphilis-free patients. A similar trend was obtained in the hierarchical clustering analysis. Furthermore, several metabolites were identified as significantly different by Student's *T*-test, including L-gulono-gamma-lactone, D-mannose, N-acetyl-L-tyrosine, hypoxanthine, and *S*-methyl-5′-thioadenosine. Notably, 87.369-fold and 7.492-fold changes of N-acetyl-L-tyrosine were observed in neurosyphilis patients compared with syphilis/non-neurosyphilis patients and syphilis-free patients. These differential metabolites are involved in overlapping pathways, including fructose and mannose metabolism, lysosomes, ABC transporters, and galactose metabolism. Several significantly expressed metabolites were identified in CSF from neurosyphilis patients, including L-gulono-gamma-lactone, D-mannose, N-acetyl-L-tyrosine, and hypoxanthine. These differential metabolites could potentially improve neurosyphilis diagnostics in the future. The role of these differential metabolites in the development of neurosyphilis deserves further exploration.

Keywords: untargeted metabolomics, neurosyphilis, cerebrospinal fluid, *Treponema pallidum*, metabolites

INTRODUCTION

Syphilis is a common sexually transmitted disease worldwide, and the causative pathogen is the spirochete *Treponema pallidum* (Tong et al., 2013; Giacani and Lukehart, 2014). In China, the incidence of syphilis has demonstrated an increasing trend, with an annual growth percentage of 16.3% (Yang et al., 2017), and ranks first among 45 notifiable diseases (Yang et al., 2017). Although the significant growth in syphilis incidence in China can be partly attributed to the implementation of enhanced coverage and the completeness of nationwide, web-based and real-time reporting systems, syphilis is a sexually transmitted disease with a severe public health impact and should not be neglected.

Neurosyphilis refers to *T. pallidum* infection in the central nervous system, and it can occur at any stage of syphilis (Liu et al., 2017). In general, the most common form of neurosyphilis currently diagnosed in clinical practice is asymptomatic. The stealth property of *T. pallidum* is responsible for the obstacles currently encountered in the treatment and prevention of syphilis. To date, the mechanism underlying the stealth property has not yet been fully elucidated. Previous studies have proposed that the slow replication cycle of *T. pallidum in vivo* may be one of the reasons for the diminished immune response and clinical symptoms after infection (Wicher et al., 2000; Deka et al., 2013). Given a plentiful supply of glucose in the blood and interstitial fluids, *T. pallidum* requires approximately 33 to 44 h to double in number (Edmondson et al., 2018). The limited energy metabolic capacity of *T. pallidum* is responsible for the slow replication cycle and inability to survive outside mammalian cells of this pathogen (Deka et al., 2015). With the completion of whole genome sequencing of *T. pallidum*, the total size of 1.14 Mb and 1041 predicted open reading frames have been identified (Fraser et al., 1998). Compared with that of other bacterial pathogens, the genome of *T. pallidum* is several times smaller, and the absence of pathways related to the tricarboxylic acid cycle and components of oxidative phosphorylation in the limited genome have led to the major dependence on the host environment to perform the necessary biosynthetic functions (Tong et al., 2017). Endogenous metabolites are an excellent reflection of the metabolic process of pathogens in hosts.

Owing to the high sensitivity and specificity of state of the art ultra-high-performance liquid chromatography/quadrupole-time-of-flight-mass spectrometry (UHPLC-Q-TOF/MS), even tiny variations in metabolites can be detected (Zhu et al., 2016). Global metabolomics analysis has been widely applied in investigations of pathogen-related diseases (Wang et al., 2016; Du et al., 2017). For instance, a study conducted among 30 pairs of HCV-positive patients and healthy controls revealed several differentially excreted metabolites in urine, and after enrichment analysis, enhanced aldose reductase activity was identified as a hallmark among HCV patients (Semmo et al., 2015). Such studies are capable of providing substantial information on energy metabolism, physiology and possible diagnostic biomarkers and intervention strategies for the pathogen (Chen et al., 2017). To date, no publications on the metabolomics analysis of syphilis patients have been reported. To gain a better understanding of the metabolic changes of neurosyphilis patients, we conducted an untargeted metabolomics analysis on cerebrospinal fluid (CSF) samples collected from neurosyphilis patients, syphilis/non-neurosyphilis patients and syphilis-free patients. By conducting this study, we attempted to identify a few hallmark metabolites in the CSF among neurosyphilis patients and consequently reveal the physiology and possible diagnostic biomarkers in neurosyphilis for further investigation.

MATERIALS AND METHODS

Study Participants

Consecutive neurosyphilis patients (Group-1) were recruited from department of Neurology Zhongshan Hospital, Xiamen University between July 2017 and December 2017, with 18 cases. Considering sex- and age-matching with the neurosyphilis patients, syphilis/non-neurosyphilis patients (Group-2) and syphilis-free patients (Group-3) were selected from the department of Neurology department of Neurosurgery in the same period of the time with 18 cases in each group. According to the guidelines of the European Center for Disease Prevention and Control, the diagnosis of syphilis was established in the present study by employing treponemal tests, including chemiluminescence immunoassays and *T. pallidum* particle agglutination (TPPA) (French et al., 2009). The diagnostic criteria of neurosyphilis in our study complied with the guidelines of the Centers for Disease Control in America and Europe (Janier et al., 2014; Workowski and Bolan, 2015) as described in our previous study (Xiao et al., 2017a). Briefly, neurosyphilis was defined based on positive treponemal test results and one or more of the following findings: (i) positive CSF Venereal Disease Research Laboratory (VDRL) and/or rapid plasma reagin (RPR) tests; (ii) positive TPPA assay and elevated leukocyte count (>10 cells/μL) in CSF; and (iii) elevated CSF protein concentration (>500 mg/L) and/or leukocyte count (>10 cells/μL) in the absence of other known causes of these abnormalities and clinical symptoms or signs consistent with neurosyphilis without other known causes for these clinical abnormalities. Syphilis/non-neurosyphilis patients were diagnosed if (i) they were seropositive for treponemal tests, including chemiluminescence immunoassays and TPPA; and (ii) they had negative results on the CSF VDRL/RPR, CSF TPPA, and CSF fluorescent treponemal antibody absorption assays, without CSF pleocytosis and elevated CSF protein levels, and did not exhibit any characteristic symptoms or signs of neurosyphilis (Xiao et al., 2017a). Syphilis-free patients were recruited by the neurosurgery department, and these patients were hospitalized due to acute trauma which subjected to lumber puncture to exclude the possibility of infectious diseases. Potential participants were included in syphilis-free group if they showed all negative results in serum RPR, serum TPPA, CSF RPR, and CSF TPPA.

Ethics Statement

This study was carried out in accordance with the recommendations of the Institutional Ethics Committee of

Zhongshan Hospital, Medical College of Xiamen University with written informed consent from all subjects. All subjects gave written informed consent in accordance with the national legislation and the Declaration of Helsinki. The protocol was approved by the Institutional Ethics Committee of Zhongshan Hospital, Medical College of Xiamen University.

Sample Preparation

Approximately 2 mL of CSF was collected from each patient by conducting lumbar puncture from neurosyphilis patients and an identical number of syphilis/non-neurosyphilis patients and syphilis-free patients. After collection, the samples were immediately placed on ice for transportation; processed for syphilitic serological tests, CSF protein and leucocyte counted within 6 h of obtaining the CSF; and then stored at −80°C prior to further processing for UHPLC-Q-TOF/MS analysis. Before analysis, the samples were thawed at room temperature. Then, 100 μL of sample was transferred to EP tubes and mixed with 400 μL of methanol/acetonitrile (1:1, v/v). The tubes were vortexed for 30 s, incubated for 10 min at −20°C, and then centrifuged at 14000 g for 15 min at 4°C. The supernatants were collected and dried with nitrogen, and then, the lyophilized powder was stored at −80°C prior to analysis. Lyophilized samples were reconstituted by dissolving in 100 μL of solvent mixture containing water/acetonitrile (5:5, v/v). The samples were vortexed for 1 min and centrifuged at 14000 g for 15 min at 4°C. The supernatants were subjected to UHPLCQ-TOF/MS analysis. In parallel to the preparation of the test samples, pooled quality control (QC) samples were prepared by mixing equal amounts (30 μL) of each sample. The QC samples were utilized to monitor the LC-MS response in real time (Ma et al., 2017).

Laboratory Tests

The syphilitic serological tests for each sample were performed using RPR (InTec, Xiamen, China), Boson chemiluminescence immunoassays (Boson Biotechnology Co., Ltd., Xiamen, China), and TPPA (Fujirebio, Tokyo, Japan) tests according to the manufacturer's instructions and as previously reported (Xiao et al., 2017b). The protein in the CSF samples was measured using a Roche-Hitachi Modular P800 Analyzer (Roche Diagnostics, F. Hoffmann-La Roche, Ltd., Basel, Switzerland). The CSF leukocyte count was measured using an Automatic Blood Cell XE5000 Analyzer (Sysmex International Reagents, Co., Ltd., Japan).

UHPLC-Q-TOF/MS Analysis

Metabolic profiling of CSF samples was performed on an Agilent, 1290 Infinity LC system (Agilent Technologies, Santa Clara, California, CA, United States) coupled with an AB SCIEX Triple TOF 6600 System (AB SCIEX, Framingham, MA, United States) (Wang et al., 2017). Chromatographic separation was conducted on ACQUITY HSS T3 1.8 μm (2.1 × 100 mm) columns for both positive and negative models. The column temperature was set at 25°C for operation. The mobile phases of 0.1% formic acid in water (A) and 0.1% formic acid in acetonitrile (B) were used in positive ionization mode, while 0.5 mM ammonium fluoride in water (C) and acetonitrile (D) were used in negative ionization mode. In the positive (negative) model, the elution gradient initially started with 1% B (D) for 1 min, linearly increased to 100% B (D) at 8 min, was maintained for 2 min, and then returned to 1% B (D) for approximately 2 min of equilibrium. The delivery flow rate was 300 μL/min, and a 2 μL aliquot of each sample was injected onto the column. UHPLC-Q-TOF/MS was performed on both ionization modes. Electrospray ionization source conditions on Triple TOF were set as follows: the pressure for ion source gas 1 was 40 psi, and the pressure for ion source gas 2 was 60 psi; the pressure for curtain gas was 30 psi; source temperature, 650°C; ionspray voltage floating, 5000 V (+) and −4500 V (−). Information-dependent acquisition, an artificial intelligence-based product ion scan mode, was used to detect and identify MS/MS spectra. The parameters were set as follows: declustering potential, 60 V (+) and −60 V (−); collision energy, 50 V (+) and −20 V (−); exclude isotopes within 4 Da, candidate ions to monitor per cycle: 10. The analysis process was conducted with the assistance of Applied Protein Technology (Shanghai, China).

Data Analysis

The raw data generated by UPLC-Q-TOF/MS were converted into mzML format files using the Proteo Wizard MS converter tool and then subjected to data processing using XCMS online software (https://xcmsonline.scripps.edu/landing_page.php?pgcontent=mainPage). The non-linear alignment in the time domain, automatic integration, and extraction of the peak intensities were completed by XCMS, with default parameter settings. The data were subsequently processed using XCMS for peak alignment and data filtering. MetaboAnalyst 4.0 (http://www.metaboanalyst.ca) was employed for the statistical analysis (Chong et al., 2018). Principal component analysis (PCA) is initially applied to obtain an overview of the data, especially for the examination of QC data. Partial-least squares discrimination analysis (PLS-DA) was conducted as a supervised method to identify the important variables with discriminative power. PLS-DA models were validated based on the multiple correlation coefficient (R2), after that, we applied cross-validation on this R2 to calculate the cross-validated R2 (Q2); and permutation tests by applying 2000 iterations ($P < 0.001$). The significance of the biomarkers was evaluated by calculating the variable importance in projection (VIP) score (>1) from the PLS-DA model. For the univariate analysis, specific biomarkers were compared among the neurosyphilis, syphilis/non-neurosyphilis, and syphilis-free groups by employing Student's *T*-tests. Among the metabolites with a VIP greater than 1, those with a *P*-value ranging from 0.05 to 0.10 were considered differential metabolites, while a *P*-value less than 0.05 was considered significant (Luo et al., 2017). The heat map was created by using the embedded module of MetaboAnalyst 4.0, to be more specific, we applied Euclidean distance measure and ward clustering algorithm in creating the heat map. Meanwhile, based on the differentially expressed metabolites, we compared the groups, and KEGG pathway (http://www.genome.jp/kegg/) analysis was conducted to investigate the metabolomic pathways affected by *T. pallidum* infection. Briefly, the enrichment level of each metabolomic pathway was calculated by Fisher's exact test, and a *P*-value less than 0.05 was considered statistically significant.

RESULTS

Baseline Information of Study Participants

The demographic characteristics of all study participants are presented in **Table 1**. The three groups demonstrated a roughly equal distribution in gender. The average age of the neurosyphilis patients in the study was 56.2 years, and there were 10 males (55.6%) and 8 females (44.5%). The average age of the syphilis/non-neurosyphilis patients was 51.8 years, and there were 9 males (50.0%) and 9 females (50.0%). The average age of the syphilis-free patients was 50.7 years, and there were 9 males (50.0%) and 9 females (50.0%). For CSF RPR, 88.9% of neurosyphilis patients had positive results. We obtained all positive TPPA results in neurosyphilis cases.

Data Processing and Quality Control of Untargeted Metabolomics Analysis

The total ion chromatogram of the quality control sample showed that the overlaps of the spectral peak of the QC samples were within slight changes, suggesting that the method has good reproducibility overall. A total of 1,808 molecular features were extracted from each sample using XCMS software, and the peak intensity of each feature was obtained (**Figure 1**). Before the subsequent analysis, the data were subjected to a data integrity check, and no missing values were detected. We applied the log transformation and Pareto scaling to the data, and the metabolomics data presented a normal distribution after these processes (**Figure 2**). Principal component analysis (PCA) was carried out using the molecular features of all the groups from the study, including QC samples. The distribution of metabolic profiles for the test samples and QC samples in PCA are shown in **Figure 3**. All of the QC injections were clustered tightly in the PCA space. The consistency of the repeated QC injections and reliable data quality across all the samples revealed the potency of the method for metabolic profiling studies during the experiment.

TABLE 1 | Clinical information of study participants.

Variable	Syphilis/ Neurosyphilis patients (*n* = 18)	Syphilis-non-neurosyphilis patients (*n* = 18)	free patients (*n* = 18)	*P*-value
Age (Years)	58.5(21)	58.5(11.8)	53.0(27)	0.747
Gender				
Male n(%)	10 (55.6)	9 (50.0)	9 (50.0)	0.929
Female n(%)	8 (44.5)	9 (50.0)	9 (50.0)	
CSF RPR				
Negative n(%)	2 (11.1)	18 (100.0)	18 (100.0)	
Positive n(%)	16 (88.9)	0 (0.0)	0 (0.0)	
CSF TPPA				
Negative n(%)	0 (0.0)	18 (100.0)	18 (100.0)	
Positive n(%)	18 (100.0)	0 (0.0)	0 (0.0)	

CSF, cerebrospinal fluid; RPR, rapid plasma reagin; TPPA, T. pallidum particle agglutination.

Untargeted Metabolomics Analysis of CSF Obtained From Study Participants

To identify ion peaks that could possibly be used to differentiate the metabolite profiles among the three groups, we established a supervised PLS-DA model that was concentrated on the actual class discriminating variations. In 4A–4C, the multiple comparisons among the three groups all showed clear separation. The goodness of fit (R2) and prediction ability of the model (Q2) by the first three components were 0.985 and 0.5; 0.993 and 0.5; 0.986 and 0.339, respectively, for differentiating neurosyphilis patients and syphilis/non-neurosyphilis patients (**Figure 4A**); neurosyphilis patients and syphilis-free patients (**Figure 4B**); and syphilis/non-neurosyphilis patients and syphilis-free patients (**Figure 4C**).

Based on the VIP calculated by the PLS-DA model, the hierarchical analysis was conducted using Euclidean distance with an average clustering algorithm. Through this analysis and a heat map, the similarity of the metabolite abundance profiles was presented (**Figure 5**). The results showed a satisfactory discriminatory power between neurosyphilis patients and syphilis/non-neurosyphilis patients (**Figure 5A**) and between neurosyphilis patients and syphilis-free patients (**Figure 5B**). For discriminating syphilis/non-neurosyphilis patients and syphilis-free patients, the heat map showed a lower discriminatory power (**Figure 5C**).

Identification of Differential CSF Metabolites

We included metabolites with a VIP greater than 1 to conduct Student's *T*-test to verify whether they are differentially expressed or significantly different in CSF metabolites among neurosyphilis patients, syphilis/non-neurosyphilis patients and syphilis-free patients. A total of 1,808 metabolite components were obtained from each group. Differential metabolite components are described in **Table 2** according to the intersection of VIP >1.0 and *P*-value <0.1. The L-gulono-gamma-lactone, D-mannose, and hypoxanthine levels were significantly decreased in neurosyphilis patients compared with syphilis/non-neurosyphilis patients with fold changes of 0.517, 0.872, and 0.745 ($P < 0.05$), respectively. In contrast, an 87.369-fold change in N-acetyl-L-tyrosine levels was observed in neurosyphilis patients compared with syphilis/non-neurosyphilis patients ($P < 0.05$), and an approximately 7.5 times increase was found in neurosyphilis patients compared to syphilis-free patients ($0.05 < P < 0.1$). In addition, significant differences in L-gulono-gamma-lactone were found between the neurosyphilis patients and syphilis-free patients; syphilis/non-neurosyphilis patients and syphilis-free patients had fold changes of 0.646 and 1.591, respectively.

KEGG Pathway Analysis of Differential CSF Metabolites

The KEGG pathway analysis showed seven metabolic pathways that were enriched in neurosyphilis patients compared to syphilis/non-neurosyphilis patients; these pathways included tryptophan metabolism, biosynthesis of unsaturated fatty acids, fatty acid biosynthesis, lysosome, ABC transporters, fructose and

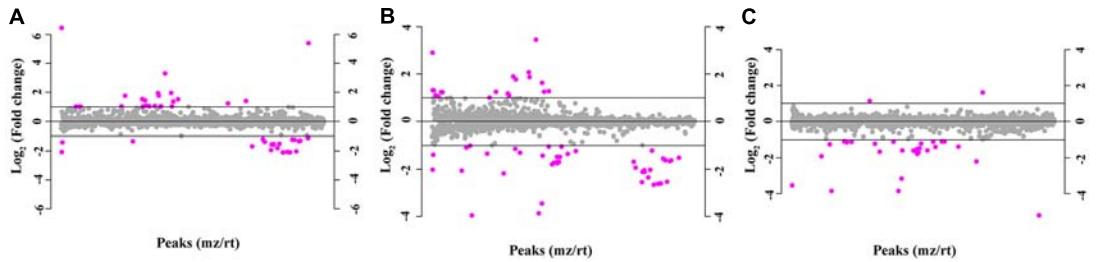

FIGURE 1 | The molecular features of 1,808 metabolite components based on the normalized peak intensity. Purple dots indicate metabolites with a fold change greater than 2, while the gray dots indicate the remaining metabolites. **(A)** Neurosyphilis patients vs. syphilis/non-neurosyphilis patients; **(B)** neurosyphilis patients vs. syphilis-free patients; **(C)** syphilis/non-neurosyphilis patients vs. syphilis-free patients.

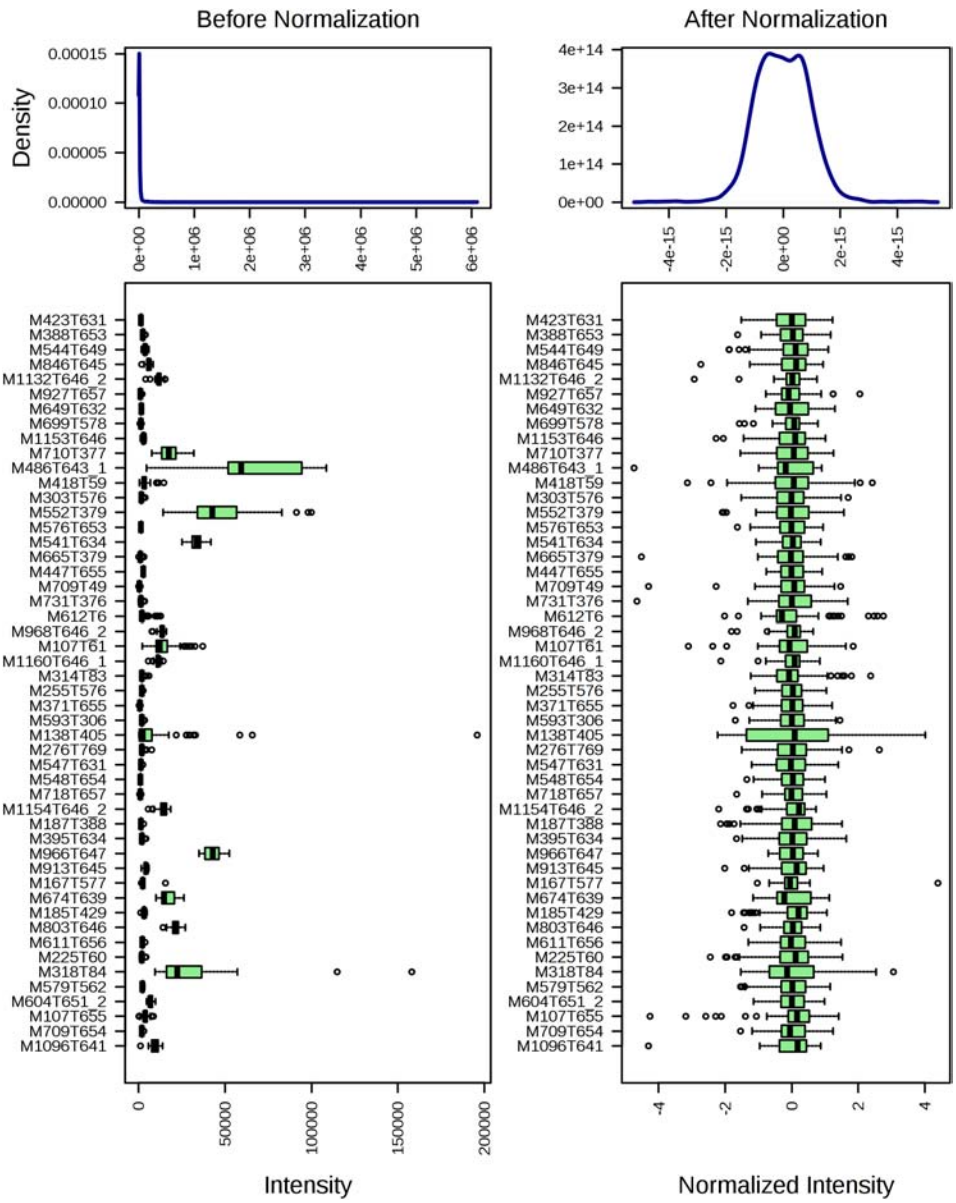

FIGURE 2 | The distribution of input data values before (left) and after (right) normalization.

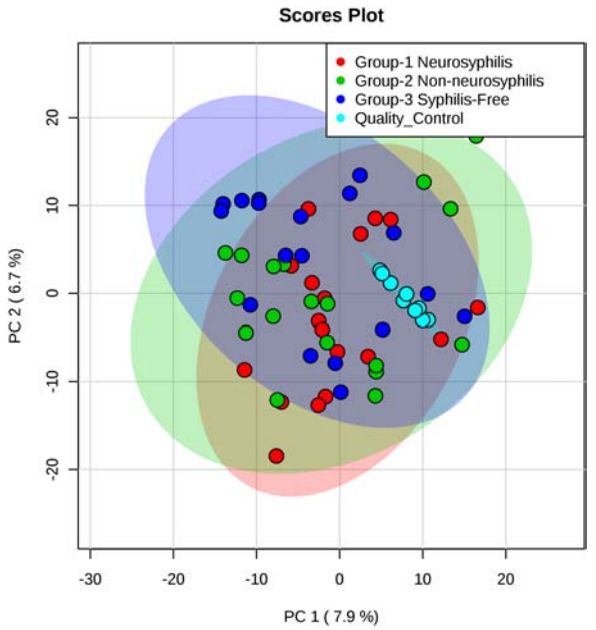

FIGURE 3 | PCA score plots based on the UHPLC-Q-TOF/MS data of CSF samples. Light red oval represents the 95% CI of score calculated from each neurosyphilis patient. Light green oval represents the 95% CI of score calculated from each syphilis/non-neurosyphilis patient. Light blue oval represents the 95% CI of score calculated from syphilis-free patient.

mannose metabolism, and galactose metabolism (**Figure 6A**). In a comparison of neurosyphilis patients and syphilis-free patients, there were only six pathways enriched, including proximal tubule bicarbonate reclamation, amino sugar and nucleotide sugar metabolism, lysosome, ABC transporters, fructose and mannose metabolism, and galactose metabolism (**Figure 6B**). In addition, 15 pathways were identified as enriched pathways when comparing syphilis/non-neurosyphilis patients and syphilis-free patients (**Figure 6C**). Among them, there were overlapping pathways with the former two comparisons, including fructose and mannose metabolism, lysosome, ABC transporters, and galactose metabolism.

DISCUSSION

Many studies have demonstrated that pathogens cause distinct host metabolomes, which show involvement of fructose and galactose metabolism, amino acid metabolism, lipid metabolism, and nucleotide metabolism, to adapt to their new environment (Langley et al., 2013; Semmo et al., 2015; Chen et al., 2017; Du et al., 2017). Metabolomics is a powerful tool for studying metabolic processes, identifying crucial biomarkers responsible for metabolic characteristics, and revealing metabolic mechanisms. CSF contains many metabolites, and their variations can offer biochemical clues into central nervous system diseases and possibly provide information on the physiology and diagnostic markers of diseases.

To the best of our knowledge, CSF metabolomics profiles have not previously been described for neurosyphilis. In the present study, we conducted an untargeted metabolomics analysis on CSF collected from neurosyphilis patients to gain a better understanding of the metabolic changes of neurosyphilis patients. We evaluated the experimental process by PLS-DA and hierarchical clustering analysis, and clear separation between groups was found. We verified the differential metabolites using Student's *T*-test, and several significantly differential metabolites were identified, including L-gulono-gamma-lactone, D-mannose, N-acetyl-L-tyrosine, and hypoxanthine, between neurosyphilis patients and syphilis/non-neurosyphilis patients. The differences in L-gulono-gamma-lactone, D-mannose, and hypoxanthine between neurosyphilis patients and syphilis/non-neurosyphilis patients were less than two times. More specifically, an 87.369-fold change was observed in neurosyphilis patients compared with syphilis/non-neurosyphilis patients, and a 7.492-fold change of N-acetyl-L-tyrosine was observed in neurosyphilis patients compared to syphilis-free patients. Currently, the diagnosis of neurosyphilis relies heavily on serological tests of CSF, such as VDRL and/or TPPA. However, the sensitivity and specificity of serological tests of CSF are not satisfactory based on the previous practices (Jiang et al., 2011). N-acetyl-L-tyrosine may be used as an indicator to distinguish neurosyphilis patients from syphilis/non-neurosyphilis patients. N-acetyl-L-tyrosine is a precursor of the essential neurotransmitter dopamine. Due to the absence of investigations into CSF metabolites in neurosyphilis patients, the role of tyrosine in neurosyphilis remains unknown. Similar to LPS, two purified *T. pallidum* lipoproteins (Tp47 and Tp17) induced NF-kB translocation in THP-1 human monocytoid cells (Norgard et al., 1996). There is considerable evidence for the involvement of tyrosine phosphorylation events (particularly mitogen-activated protein kinases) in LPS signaling and *T. pallidum* lipoproteins (English et al., 1997). However, elevated tyrosine levels may lead to increased formation of dopamine by the combined effects of tyrosine hydroxylase and tryptophan decarboxylase (Sehara et al., 2017). The enhanced level of dopamine would lead to neurobehavioural abnormalities, including increased psychomotor activity, hyperalertness, agitation, irritability, restlessness, combativeness, distractibility, and psychosis (Maldonado, 2008), and some of them overlap with the clinical symptom of neurosyphilis. Moreover, excessive dopamine is capable of inducing neuronal cell death and apoptosis via the caspase-3 pathway (Pedrosa and Soares-da-Silva, 2002). This change could partly explain the higher tyrosine levels in neurosyphilis patients compared to syphilis/non-neurosyphilis patients and syphilis-free patients and the neurobehavioural symptoms caused by *T. pallidum* infection in the central nervous system.

In addition, significantly different L-gulono-gamma-lactone levels were found not only between the neurosyphilis patients and syphilis/non-neurosyphilis patients but also between the neurosyphilis patients and syphilis-free patients, as well as the syphilis/non-neurosyphilis patients and syphilis-free patients. The fold change was less than two. The L-gulono-gamma-lactone levels were significantly decreased in neurosyphilis patients compared with syphilis/non-neurosyphilis patients.

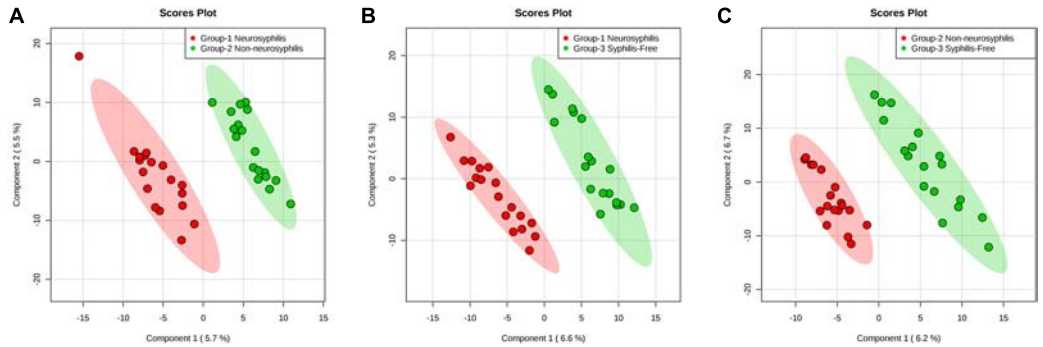

FIGURE 4 | PLS-DA plots based on the UHPLC-Q-TOF/MS data of CSF samples. **(A)** Neurosyphilis patients vs. syphilis/non-neurosyphilis patients (R2 = 0.985, Q2 = 0.5); **(B)** neurosyphilis patients vs. syphilis-free patients (R2 = 0.993, Q2 = 0.5); **(C)** syphilis/non-neurosyphilis patients vs. syphilis-free patients (R2 = 0.986, Q2 = 0.339).

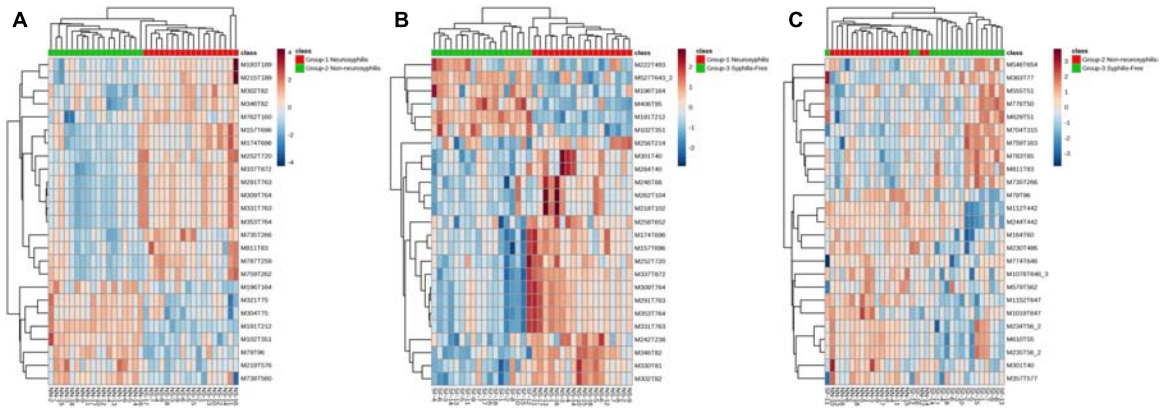

FIGURE 5 | Heatmap of clustering analysis of three groups. **(A)** Neurosyphilis patients vs. syphilis/non-neurosyphilis patients; **(B)** neurosyphilis patients vs. syphilis-free patients; **(C)** syphilis/non-neurosyphilis patients vs. syphilis-free patients.

TABLE 2 | List of differential CSF metabolites in three groups of study participants.

Comparison	Metabolite	Rt (sec)	m/z	VIP	Fold change	*P*-value
NS vs. Non-NS	L-gulono-gamma-lactone	206.4	196.0808	4.371	0.517	0.024*
	D-mannose	559.8	198.0968	3.142	0.872	0.020*
	N-acetyl-L-tyrosine	69.34	268.0621	5.156	87.369	0.019*
	Hypoxanthine	303.4	137.0447	2.042	0.765	0.002*
NS vs. syphilis-free	L-gulono-gamma-lactone	163.6	196.0808	2.342	0.646	< 0.001*
	D-mannose	559.8	198.0968	3.621	0.850	0.061
	N-acetyl-L-tyrosine	69.34	268.0621	4.791	7.492	0.069
NN cases VS NS cases	Hypoxanthine	303.366	137.0447	2.0645	0.765066	0.000692
Non-NS vs. syphilis free	L-gulono-gamma-lactone	206.4	196.0808	4.223	1.591	0.026*
	D-mannose	498.7	198.0966	1.078	0.797	0.071
	N-acetyl-L-tyrosine	69.34	268.0621	2.424	0.086	0.061
	S-methyl-5′-thioadenosine	144.7	298.0964	1.421	0.855	0.054
	L-Leucine	485.931	132.1009	1.32648	1.16155	0.071789

*NS, neurosyphilis; Non-NS, syphilis/non-neurosyphilis; Rt, retention time; VIP, variance importance for projection. *P < 0.05.*

L-gulono-gamma-lactone is an immediate precursor of Vitamin C, and its conversion into Vitamin C is catalyzed by L-gulono-1,4-lactone oxidase (Ching et al., 2014). Reduced levels of Vitamin C in the brain may trigger dangerous levels of oxidative stress during normal aging, particularly during inflammatory neurodegenerative diseases (Dixit et al., 2015).

We also observed decreased levels of D-mannose and hypoxanthine in neurosyphilis patients compared

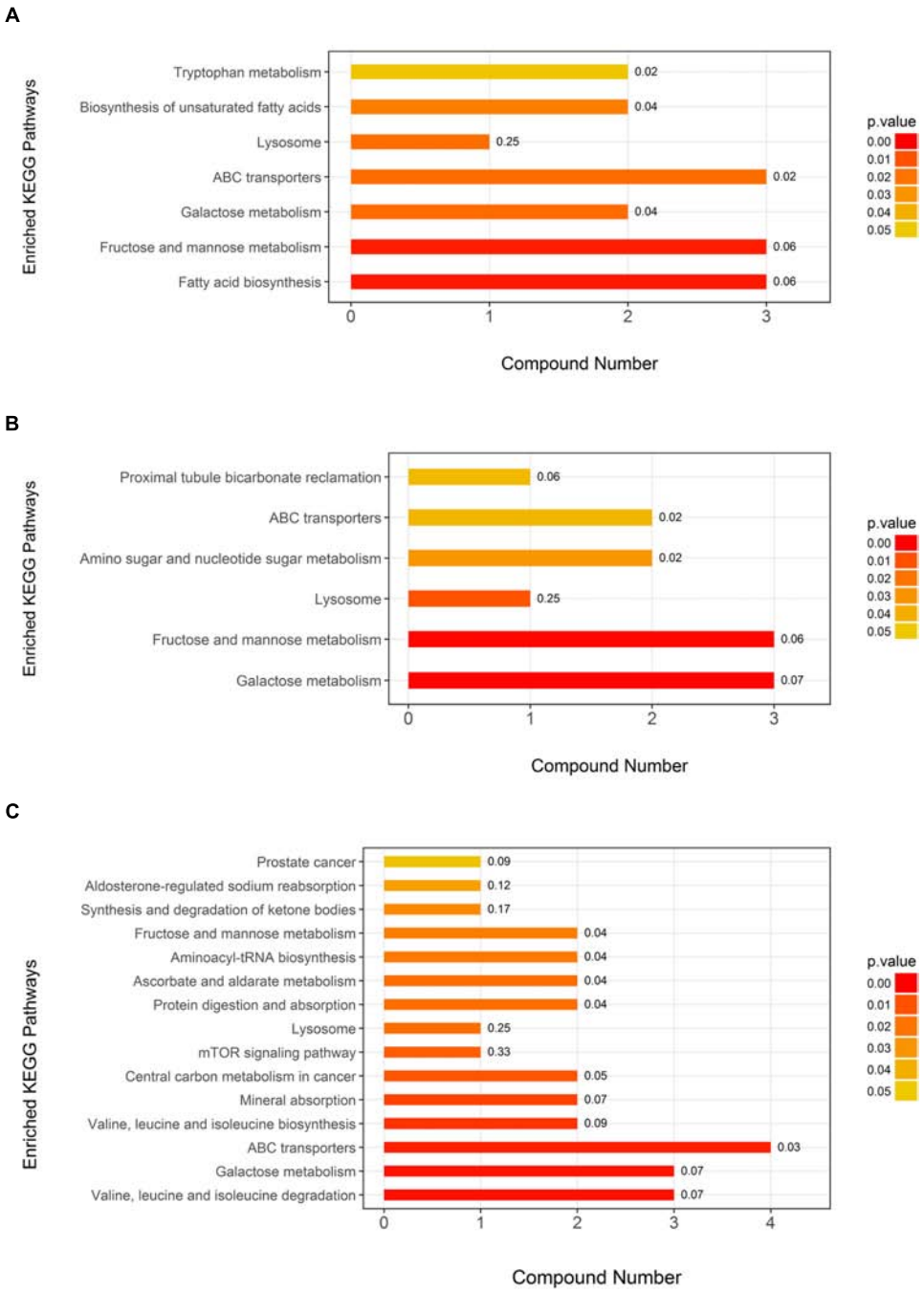

FIGURE 6 | KEGG pathway analysis of the differential metabolite components in the three groups. The *P*-value of each pathway was demonstrated by the color of bar, and the rich factor of each pathway generated by using KEGG analysis was presented in the number after the bar. **(A)** Neurosyphilis patients vs. syphilis/non-neurosyphilis patients; **(B)** neurosyphilis patients vs. syphilis-free patients; **(C)** syphilis/non-neurosyphilis patients vs. syphilis-free patients. The numbers presented in the bar were rich factors generated by using KEGG analysis.

with syphilis/non-neurosyphilis patients. The decrease in D-mannose may be due to *T. pallidum*, which is capable of metabolizing mannose as an alternative carbon source under insufficient glucose (Gonzalez et al., 2005). The reason for the decreased hypoxanthine levels in CSF in neurosyphilis patients compared to syphilis/non-neurosyphilis patients and its role in the development of neurosyphilis should be further explored.

We also conducted a metabolomics pathway analysis based on the differentially expressed metabolites identified by employing statistical analysis. Some overlapping pathways, including lysosome, ABC transporters, galactose metabolism

and fructose and mannose metabolism, were found in all comparisons. According to the previous literature, *T. pallidum* lacks tricarboxylic acid cycle enzymes and an electron transport chain (Fraser et al., 1998) but does carry enzymes for absorption of amino acids and fatty acids, which indicated that this pathogen has to derive some essential macromolecules from the host. The ABC transporter encoded by the *tro* operon plays an important role in this process and has been identified as an enriched pathway in the present study. Fructose and mannose metabolism was also found to be an enriched pathway. Under the circumstances of insufficient glucose, *T. denticola* is capable of metabolizing mannose as an alternative carbon source in an *in vitro* tissue culture system (Gonzalez et al., 2005). Therefore, *T. pallidum* may take up mannose in the CSF to reproduce itself, especially in a low-glucose environment, such as CSF. In the pathway analysis, most of the overlapping pathways are related to alternative carbon sources of *T. pallidum*.

There are some limitations in the present study. First, the sample size is limited. Second, further validation conducted on a larger population was absent. Whether the same changes take place in other neurological diseases, it need to do some experiments to verify that. Still, several metabolites were associated with neurological complications related to *T. pallidum* infection, and further investigation should be conducted to determine their exact function.

In summary, we conducted a metabolomics study on metabolites of CSF from neurosyphilis patients for the first time. Several significant differences in metabolites were identified, including differences in L-gulono-gamma-lactone, D-mannose, N-acetyl-L-tyrosine, and hypoxanthine. Among them, N-acetyl-L-tyrosine was 87.369 times more common in patients with neurosyphilis than syphilis/non-neurosyphilis patients. These differential metabolites could potentially improve neurosyphilis diagnostics in the future. In addition, the role of these differential metabolites in the development of neurosyphilis deserves further exploration.

AUTHOR CONTRIBUTIONS

L-LL, J-HY, and T-CY conceived and designed the experiments. L-LL, WC, M-LT, and H-LZ performed the experiments. YL, XL, and J-JN analyzed the data. WC, YL, and L-RL contributed to reagents, materials, and analysis tools. L-LL wrote the manuscript. J-HY, J-JN, and T-CY revised the manuscript critically for important intellectual content. All authors read and approved the final manuscript.

FUNDING

This work was supported by the National Natural Science Foundation (Grant Numbers 81771312, 81471231, 81101324, 81772260, 81471967, 81271335, 81672094, 81802089, 81871729, and 81171625). The funders played no role in the study design, data collection, or analyses, the decision to publish, or the manuscript preparation.

REFERENCES

Chen, X. H., Liu, S. R., Peng, B., Li, D., Cheng, Z. X., Zhu, J. X., et al. (2017). Exogenous l-valine promotes phagocytosis to kill multidrug-resistant bacterial pathogens. *Front. Immunol.* 8:207. doi: 10.3389/fimmu.2017.00207

Ching, B., Ong, J. L., Chng, Y. R., Chen, X. L., Wong, W. P., Chew, S. F., et al. (2014). L-gulono-gamma-lactone oxidase expression and vitamin C synthesis in the brain and kidney of the African lungfish, *Protopterus annectens*. *FASEB J.* 28, 3506–3517. doi: 10.1096/fj.14-249508

Chong, J., Soufan, O., Li, C., Caraus, I., Li, S., Bourque, G., et al. (2018). MetaboAnalyst 4.0: towards more transparent and integrative metabolomics analysis. *Nucleic Acids Res.* 46, W486–W494. doi: 10.1093/nar/gky310

Deka, R. K., Brautigam, C. A., Biddy, B. A., Liu, W. Z., and Norgard, M. V. (2013). Evidence for an ABC-type riboflavin transporter system in pathogenic spirochetes. *MBio* 4:e615-12. doi: 10.1128/mBio.00615-12

Deka, R. K., Brautigam, C. A., Liu, W. Z., Tomchick, D. R., and Norgard, M. V. (2015). Evidence for posttranslational protein flavinylation in the syphilis spirochete treponema pallidum: structural and biochemical insights from the catalytic core of a periplasmic flavin-trafficking protein. *MBio* 6:e519-15. doi: 10.1128/mBio.00519-15

Dixit, S., Bernardo, A., Walker, J. M., Kennard, J. A., Kim, G. Y., Kessler, E. S., et al. (2015). Vitamin C deficiency in the brain impairs cognition, increases amyloid accumulation and deposition, and oxidative stress in APP/PSEN1 and normally aging mice. *ACS Chem. Neurosci.* 6, 570–581. doi: 10.1021/cn500308h

Du, C. C., Yang, M. J., Li, M. Y., Yang, J., Peng, B., Li, H., et al. (2017). Metabolic mechanism for l-leucine-induced metabolome to eliminate streptococcus iniae. *J. Proteome Res.* 16, 1880–1889. doi: 10.1021/acs.jproteome.6b00944

Edmondson, D. G., Hu, B., and Norris, S. J. (2018). Long-term in vitro culture of the syphilis spirochete treponema pallidum subsp. pallidum. *MBio* 9:e1153-18. doi: 10.1128/mBio.01153-18

English, B. K., Orlicek, S. L., Mei, Z., and Meals, E. A. (1997). Bacterial LPS and IFN-gamma trigger the tyrosine phosphorylation of vav in macrophages: evidence for involvement of the hck tyrosine kinase. *J. Leukoc Biol.* 62, 859–864. doi: 10.1002/jlb.62.6.859

Fraser, C. M., Norris, S. J., Weinstock, G. M., White, O., Sutton, G. G., Dodson, R., et al. (1998). Complete genome sequence of *Treponema pallidum*, the syphilis spirochete. *Science* 281, 375–388. doi: 10.1126/science.281.5375.375

French, P., Gomberg, M., Janier, M., Schmidt, B., van Voorst Vader, P., and Young, H. (2009). IUSTI: 2008 European guidelines on the management of syphilis. *Int. J. STD AIDS* 20, 300–309. doi: 10.1258/ijsa.2008.008510

Giacani, L., and Lukehart, S. A. (2014). The endemic treponematoses. *Clin. Microbiol. Rev.* 27, 89–115. doi: 10.1128/cmr.00070-13

Gonzalez, C. F., Stonestrom, A. J., Lorca, G. L., and Saier, M. H. Jr. (2005). Biochemical characterization of phosphoryl transfer involving HPr of the phosphoenolpyruvate-dependent phosphotransferase system in *Treponema denticola*, an organism that lacks PTS permeases. *Biochemistry* 44, 598–608. doi: 10.1021/bi048412y

Janier, M., Hegyi, V., Dupin, N., Unemo, M., Tiplica, G. S., Potocnik, M., et al. (2014). 2014 European guideline on the management of syphilis. *J. Eur. Acad. Dermatol. Venereol.* 28, 1581–1593. doi: 10.1111/jdv.12734

Jiang, Y., Chen, X., Ma, X., Yang, Y., Peng, F., and Hu, X. (2011). The usefulness of toluidine red unheated serum test in the diagnosis of HIV-negative neurosyphilis. *Sex. Transm. Dis.* 38, 244–245. doi: 10.1097/OLQ.0b013e3181f42093

Langley, R. J., Tsalik, E. L., van Velkinburgh, J. C., Glickman, S. W., Rice, B. J., Wang, C. P., et al. (2013). An integrated clinico-metabolomic model improves prediction of death in sepsis. *Sci. Trans. Med.* 5:195ra195. doi: 10.1126/scitranslmed.3005893

Liu, L. L., Zhu, S. G., Jiang, X. Y., Ren, J., Lin, Y., Zhang, N. N., et al. (2017). LncRNA expression in CD4+T cells in neurosyphilis patients. *Front. Cell. Infect. Microbiol.* 7:461. doi: 10.3389/fcimb.2017.00461

Luo, D., Deng, T., Yuan, W., Deng, H., and Jin, M. (2017). Plasma metabolomic study in chinese patients with wet age-related macular degeneration. *BMC Ophthalmol.* 17:165. doi: 10.1186/s12886-017-0555-7

Ma, N., Karam, I., Liu, X. W., Kong, X. J., Qin, Z., Li, S. H., et al. (2017). UPLC-Q-TOF/MS-based urine and plasma metabonomics study on the ameliorative effects of aspirin eugenol ester in hyperlipidemia rats. *Toxicol. Appl. Pharmacol.* 332, 40–51. doi: 10.1016/j.taap.2017.07.013

Maldonado, J. R. (2008). Pathoetiological model of delirium: a comprehensive understanding of the neurobiology of delirium and an evidence-based approach to prevention and treatment. *Crit. Care Clin.* 24, 789–856, ix. doi: 10.1016/j.ccc.2008.06.004

Norgard, M. V., Arndt, L. L., Akins, D. R., Curetty, L. L., Harrich, D. A., and Radolf, J. D. (1996). Activation of human monocytic cells by Treponema pallidum and *Borrelia burgdorferi* lipoproteins and synthetic lipopeptides proceeds via a pathway distinct from that of lipopolysaccharide but involves the transcriptional activator NF-kappa B. *Infect. Immun.* 64, 3845–3852.

Pedrosa, R., and Soares-da-Silva, P. (2002). Oxidative and non-oxidative mechanisms of neuronal cell death and apoptosis by L-3,4-dihydroxyphenylalanine (L-DOPA) and dopamine. *Br. J. Pharmacol.* 137, 1305–1313. doi: 10.1038/sj.bjp.0704982

Sehara, Y., Fujimoto, K. I., Ikeguchi, K., Katakai, Y., Ono, F., Takino, N., et al. (2017). Persistent expression of dopamine-synthesizing enzymes 15 years after gene transfer in a primate model of parkinson's disease. *Hum. Gene. Ther. Clin. Dev.* 28, 74–79. doi: 10.1089/humc.2017.010

Semmo, N., Weber, T., Idle, J. R., and Beyoglu, D. (2015). Metabolomics reveals that aldose reductase activity due to AKR1B10 is upregulated in hepatitis C virus infection. *J. Viral Hepat.* 22, 617–624. doi: 10.1111/jvh.12376

Tong, M. L., Lin, L. R., Liu, G. L., Zhang, H. L., Zeng, Y. L., Zheng, W. H., et al. (2013). Factors associated with serological cure and the serofast state of HIV-negative patients with primary, secondary, latent, and tertiary syphilis. *PLoS One* 8:e70102. doi: 10.1371/journal.pone.0070102

Tong, M. L., Zhang, H. L., Zhu, X. Z., Fan, J. Y., Gao, K., Lin, L. R., et al. (2017). Re-evaluating the sensitivity of the rabbit infectivity test for *Treponema pallidum* in modern era. *Clin. Chim. Acta* 464, 136–141. doi: 10.1016/j.cca.2016.11.031

Wang, H., Liu, Z., Wang, S., Cui, D., Zhang, X., Liu, Y., et al. (2017). UHPLC-Q-TOF/MS based plasma metabolomics reveals the metabolic perturbations by manganese exposure in rat models. *Metallomics* 9, 192–203. doi: 10.1039/c7mt00007c

Wang, Z., Li, M. Y., Peng, B., Cheng, Z. X., Li, H., and Peng, X. X. (2016). GC-MS-based metabolome and metabolite regulation in serum-resistant *Streptococcus agalactiae*. *J. Proteome Res.* 15, 2246–2253. doi: 10.1021/acs.jproteome.6b00215

Wicher, K., Wicher, V., Abbruscato, F., and Baughn, R. E. (2000). Treponema pallidum subsp. pertenue displays pathogenic properties different from those of *T. pallidum* subsp. pallidum. *Infect. Immun.* 68, 3219–3225. doi: 10.1128/IAI.68.6.3219-3225.2000

Workowski, K. A., and Bolan, G. A. (2015). Sexually transmitted diseases treatment guidelines, 2015. *MMWR Recomm. Rep.* 64, 1–137.

Xiao, Y., Tong, M. L., Lin, L. R., Liu, L. L., Gao, K., Chen, M. J., et al. (2017a). Serological response predicts normalization of cerebrospinal fluid abnormalities at six months after treatment in HIV-negative neurosyphilis patients. *Sci. Rep.* 7, 9911–9917. doi: 10.1038/S41598-017-10387-X

Xiao, Y., Tong, M. L., Liu, L. L., Lin, L. R., Chen, M. J., Zhang, H. L., et al. (2017b). Novel predictors of neurosyphilis among HIV-negative syphilis patients with neurological symptoms: an observational study. *BMC Infect. Dis.* 17:310. doi: 10.1186/S12879-017-2339-3

Yang, S., Wu, J., Ding, C., Cui, Y., Zhou, Y., Li, Y., et al. (2017). Epidemiological features of and changes in incidence of infectious diseases in China in the first decade after the SARS outbreak: an observational trend study. *Lancet Infect. Dis.* 17, 716–725. doi: 10.1016/s1473-3099(17)30227-x

Zhu, Y., Li, L., Zhang, G., Wan, H., Yang, C., Diao, X., et al. (2016). Metabolic characterization of pyrotinib in humans by ultra-performance liquid chromatography/quadrupole time-of-flight mass spectrometry. *J. Chromatogr. B Analyt. Technol. Biomed. Life Sci.* 103, 117–127. doi: 10.1016/j.jchromb.2016.08.009

Conflict of Interest Statement: The authors declare that the research was conducted in the absence of any commercial or financial relationships that could be construed as a potential conflict of interest.

frontiers in Neuroscience

ORIGINAL RESEARCH
published: 26 February 2019
doi: 10.3389/fnins.2019.00122

Effects of Intranasal Oxytocin on Pup Deprivation-Evoked Aberrant Maternal Behavior and Hypogalactia in Rat Dams and the Underlying Mechanisms

Xiao Yu Liu[1†], Dongyang Li[1†], Tong Li[1], Haitao Liu[1], Dan Cui[1], Yang Liu[1], Shuwei Jia[1], Xiaoran Wang[1], Runsheng Jiao[1], Hui Zhu[1], Fengmin Zhang[2], Danian Qin[3] and Yu-Feng Wang[1]*

[1] Department of Physiology, School of Basic Medical Sciences, Harbin Medical University, Harbin, China, [2] Department of Pathogen, School of Basic Medical Sciences, Harbin Medical University, Harbin, China, [3] Department of Physiology, Shantou University of Medical College, Shantou, China

OPEN ACCESS

Edited by:
Sebastien G. Bouret,
University of Southern California,
United States

Reviewed by:
Françoise Muscatelli,
Institut National de la Santé et de la Recherche Médicale (INSERM),
France
Gábor B. Makara,
Hungarian Academy of Sciences (MTA), Hungary

***Correspondence:**
Yu-Feng Wang
yufengwang@ems.hrbmu.edu.cn

[†] These authors have contributed equally to this work

Specialty section:
This article was submitted to Neuroendocrine Science, a section of the journal Frontiers in Neuroscience

Received: 10 November 2018
Accepted: 04 February 2019
Published: 26 February 2019

Citation:
Liu XY, Li D, Li T, Liu H, Cui D, Liu Y, Jia S, Wang X, Jiao R, Zhu H, Zhang F, Qin D and Wang Y-F (2019) Effects of Intranasal Oxytocin on Pup Deprivation-Evoked Aberrant Maternal Behavior and Hypogalactia in Rat Dams and the Underlying Mechanisms. Front. Neurosci. 13:122. doi: 10.3389/fnins.2019.00122

Oxytocin (OT), a hypothalamic neuropeptide, applied through nasal approach (IAO), could improve maternal health during lactation that is disrupted by mother–baby separation; however, the regulation of IAO effects on maternal behaviors and lactation as well as the underlying mechanisms remain unclear. Using lactating rats, we observed effects of intermittent pup deprivation (PD) with and without IAO on maternal behaviors and lactation as well as the activity of OT neurons in the supraoptic nucleus (SON) and the activity of hypothalamic pituitary-adrenal axis, key factors determining the milk-letdown reflex during lactation and maternal behaviors. The results showed that PD reduced maternal behaviors and lactation efficiency of rat dams as indicated by significantly longer latency to retrieve their pups and low litter's body weight gains during the observation, respectively. In addition, PD caused early involution of the mammary glands. IAO partially improved these changes in rat dams, which was not as significant as IAO effects on control dams. In the SON, PD decreased c-Fos and increased glial fibrillary acidic protein (GFAP) filaments significantly; IAO made PD-evoked c-Fos reduction insignificant while reduced GFAP filament significantly in PD dams. IAO tended to increase the levels of phosphorylated extracellular signal-regulated kinases (pERK) 1/2 in PD dams. Moreover, PD+IAO significantly increased plasma levels of dam adrenocorticotropic hormone and corticosterone but not OT levels. Lastly, PD+IAO tended to increase the level of corticotropin-releasing hormone in the SON. These results indicate that PD disrupts maternal behaviors and lactation by suppressing the activity of hypothalamic OT-secreting system through expansion of

astrocytic processes, which are partially reversed by IAO through removing astrocytic inhibition of OT neuronal activity. However, the improving effect of IAO on the maternal health could be compromised by simultaneous activation of hypothalamic pituitary-adrenocortical axis.

Keywords: pup deprivation, intranasal drug application, lactation, maternal health, oxytocin

INTRODUCTION

Lactation is essential for maintaining the species of mammals and an irreplaceable factor for mental and physical health of mothers and the babies. However, lactation is vulnerable to many adverse factors, such as mother–baby separation (Wang and Hatton, 2009b), lacking social supports (Trickey and Newburn, 2014), obesity (Stuebe et al., 2014), babies' sickness (Lawrence, 2013), poor breast conditions (Tang et al., 2013), cesarean section (Orun et al., 2010), mothers' using drugs that are toxic to the babies (Varalda et al., 2012), early usages of bottle feeding and milk substitutes (Jiang et al., 2012), working requirements (Oslislo and Kaminski, 2000), and others (Seema et al., 1997; Berde and Yalcin, 2016). These factors often cause postpartum depression (Figueiredo et al., 2013) and insufficient breastfeeding (Stuebe et al., 2014), which are associated with high incidence of premenopausal breast cancer, diabetes, and obesity in the mothers and autism, sudden death, and deficiency in maternal behaviors in their offspring (Ip et al., 2007).

Oxytocin (OT), a neuropeptide produced in hypothalamic supraoptic nucleus (SON), paraventricular nucleus (PVN) and several accessory neuroendocrine nuclei, not only plays a major role in baby delivery and milk ejection, but is also pivotal in maintaining maternal mental health (Hou et al., 2016). It has been reported that OT knockout mice show a failure of the milk-ejection reflex (MER) and thus cannot rear their offsprings (Lee et al., 2008). In virgin ovariectomized female rats, intracerebroventricular administration of OT can induce a rapid onset of full maternal behavior (Pedersen et al., 1982); the expression of OT receptor (OTR) is associated with variations in maternal behaviors (Francis et al., 2000). Thus, OTR signaling is essential for normal maternal behavior and lactation. By contrast, pup deprivation (PD) can disrupt the activity of OT neurons and the MER (Wang and Hatton, 2009b) while OT applied through nasal approach (IAO) can activate OT neurons in the hypothalamus (Liu et al., 2017), thereby having the potential to promote maternal health. In parallel with OTR signaling, as a chronic stress, PD can activate the hypothalamic-pituitary-adrenocortical (HPA) axis (Russell et al., 2018), which in turn inhibits OT neuronal activity (Di et al., 2005) and maternal behaviors (Pereira et al., 2015) and IAO likely reverses this process. However, effects of PD and IAO on interactions of the two systems remain unclear, particularly at the early stage of lactation.

To clarify the effect of IAO on maternal behavior and lactation and identify its underlying mechanisms, a rat model of intermittent PD (Wang and Hatton, 2009b; Liu et al., 2016) was used. We observed effects of IAO on PD-evoked depression-like behaviors and hypogalactia, and then analyzed the neuroendocrine mechanisms underlying IAO effect on PD-evoked postpartum depression and hypogalactia. The results allow us to better understand the underlying mechanisms and to propose novel approaches to improve maternal health.

MATERIALS AND METHODS

Preparation of PD Model and IAO

Sprague-Dawley rats were used in this experiment. All the rats were housed and maintained on a 12–12 h light–dark cycle with free access to water and food. Two virgin females (180–250 g) and one proven breeder male (350–400 g) were housed in one cage for 1 week for making pregnant rats. The pregnant rats were randomly divided into control group, PD group and PD+IAO group. The PD model was made from lactating rats deprived 10 pups in the litter for 20 h/day from postpartum day 1 (PD1), continuously for 4 days (PD1 to PD4). All rat dams received 0.45% NaCl or 0.1 nmole OT in 0.45% NaCl nasally (Sigma-Aldrich, 10 μl for each naris), 3 times/day. During the separation from their biological mothers, the 10 pups in a litter were nursed by a foster mother. Control dams and pups received the same handling procedure as the PD dams did without the separation during observation. All the procedures were conducted in accordance with NIH Guidelines for the Care and Use of Animals and approved by the Animal Care and Use Committees of the Harbin Medical University.

Observation of Maternal Behaviors

Maternal behaviors and lactation performance were evaluated on PD1 and PD4 before the brain, blood and mammary glands were sampled for further examinations next day. Items of observations included the latency of pup retrieval and latency of suckling for judging maternal behaviors; litter's body weight gain (LBWG) was used for judging lactation efficiency. The whole procedure was video-taped for later analyses.

Western Blots

Methods for processing proteins were modified from previous reports (Wang et al., 2013b; Liu et al., 2017). On PD5, protein expression and immunohistochemistry of the hypothalamus were analyzed without suckling. Dams were decapitated and the hypothalamus were removed and cooled down in ice-cold artificial CSF for 1–2 min. Then, the SON and PVN were isolated and homogenized in a RIPA lysis buffer (Yeasen, Shanghai, CAS#20115ES60). In brief, 30 μg protein per lane was separated on a 10% SDS-PAGE gel and then transferred onto polyvinylidenefluoride membrane. The protein membranes

were incubated with TBS containing 5% dry milk (w/v) for 2 h at room temperature (21–23°C) and then incubated with primary antibodies (Santa Cruz Biotechnology, Shanghai) against glial fibrillary acidic protein (GFAP, SC6171, a marker of astrocytes), c-Fos (SC-7202), extracellular signal-regulated protein kinases (ERK) 1/2 (SC-514302), phosphorylated ERK (pERK) 1/2 (SC-136521, and Omnimabs, Shanghai, OM25780), corticotrophin-releasing hormone (CRH, SC-10718) and β-tubulin (Wanlei, Shanghai, WL-02296) in a dilution of 1:200 to 1:400 at 4°C for 12 h. ERK 1/2 and β-tubulin were used as loading controls. The protein membranes were further processed with horseradish peroxidase-conjugated secondary antibodies which matched with the species of corresponding primary antibodies and with an enhanced chemiluminescence detection kit (Tanon, Shanghai). Protein bands were visualized with an automated chemiluminescence imaging analysis system (Tanon 5200, Shanghai).

Immunohistochemistry of the Hypothalamus

Methods of immunostaining were the same as previously described (Wang et al., 2013b; Liu et al., 2017). In brief, the hypothalamus was fixed in 4% paraformaldehyde for 24 h, and then cut using a vibratome into 60 μm thick sections that contained the SON. The sections were treated with 0.3% Triton X-100 for 60 min to permeabilize cell membranes and then with 5% bovine serum albumin for 60 min to block non-specific binding sites. After incubation with primary antibodies against GFAP, pERK 1/2, c-Fos (see above) and OT-NP (SC-393907) in a dilution of 1:200 at 4°C overnight, species-matched secondary antibodies (1:1000) were applied for 1.5 h at room temperature to label the corresponding primary antibodies. Lastly, Hoechst staining (0.5 μg/ml, 15 min) was used to label nuclei. Sections were first examined with a fluorescence microscope (Eclipse FN1, Nikon) through a CCD camera (DS Ri2, Nikon), results of which were further compared with the images taken with a confocal microscope (Thorlabs). To avoid false positive or negative results of immunostaining, serial dilutions of the primary antibody, staining with pre-absorbed primary antibody, no-primary and no secondary antibody controls were applied.

Histochemistry of the Mammary Glands

In identification of the morphological features of mammary glands, conventional Hematoxylin and Eosin (H-E) staining was carried out after paraffin section (5 μm-thick) of the tissue. Images of the sections were taken using a Nikon microscopy and stored in computer for further analysis. To reduce the variability resulting from different loci, coronal sections of the middle part of the mammary glands from different groups were used for comparisons.

Assay of Plasma Levels of Adrenocorticotropic Hormone (ACTH), Corticosterone, and OT

Assaying plasma levels of different hormones was performed using enzyme linked immunosorbent assay (ELISA, for ACTH, HY-10057; corticosterone, HY-10063; OT, HY-10017) or radioimmunoassay (for OT only) by Beijing Sino-UK Institute of Biological technology (Beijing). Briefly, dams were decapitated after observations and trunk blood (0.5 ml) was collected in heparinized tubes; the plasma was separated by centrifugation (3,000 rpm, 4°C, 15 min), and aliquots were stored at −20°C. ELISA experiment was performed using the following method. In brief, the standard was prepared in a series (4, 8, 16, 32, 64, and 128 pg/ml for ACTH; 10, 20, 40, 80, 160, 320, 640 ng/ml for corticosterone and 60, 30, 15, 7.5, 3.75, and 1.875 pg/ml for OT). Samples were thawed and warmed to room temperature for assays in duplicates. The wells of a 96-well plate were coated with 100 μl antibody solution in each well for 2 h; after rinsing with washing buffer and drying, 200 μl blocking buffer was added and kept for 30 min; after rinsing with washing buffer, shaking and drying, 50 μl standard solutions or sample solution (25 μl coating solution plus 25 μl plasma sample) were added to designed wells, respectively; then, 100 μl enzyme-labeled agent HRP solution was added to each well and kept for 60 min; after rinsing and drying, 100 μl color substrate solution was added and kept for 15 min for coloration before the reaction was stopped by adding 100 μl stopping solution. Optical density for each well was measured at 450 nm within 15 min of reaction stopping. To confirm the result of ELISA assay of OT levels, radioimmunoassay was performed with conventional method with the kit containing OT antibody (ab212193, Abcam, Shanghai) by the same company. The average recovery rates were >96% in all assays. The sensitivities for OT, ACTH and corticosterone were <0.9 ng/ml, <0.4 pg/ml, and <0.5 ng/ml, respectively. Intra-group and inter-group variations were less than 5 and 9%, respectively. Negative controls were set with diluted plasma and final results were based on the average results of duplicated samples.

Data Collection and Analysis

Lactation failure was defined as a reduction in milk availability of more than 80% of the control. Signs of depression included those that showed loss of interests in the pups, such as delayed retrieval and suckling of pups (Wang et al., 2007). Data analyses of Western blots, and immunohistochemistry have been described in previous reports (Wang et al., 2013a). In brief, ImageJ or Photoshop was used for quantitation of protein bands (average luminosity multiply the total number of Pixels), which was further divided by the amount of their corresponding loading proteins; the protein amount of each bands in the control group was set as 1 or 100, and proteins in other groups were expressed as the fold or % of the control. In evaluation of confocal images, the fluorescence intensity in each channel was normalized to a standard curve (1–256) to allow for comparison between different experiments. The background level was set as 1 through minimum baseline correction. GFAP filaments were identified by fibrous GFAP positive staining that is an extension of astrocytic nucleus and longer than 20 μm (Wang and Hatton, 2009a). ANOVA, Kruskal–Wallis text or Wilcoxon rank test and χ^2 test were used for statistical analyses where appropriate as instructed by SigmaStat program (SPSS, Chicago, IL, United States), and $P < 0.05$ was considered significant. All graphs were represented

with box-whiskers with scattered plots indicating the median and the quartiles Q1 and Q3. All measures were also expressed as mean ± SEM in raw values or the percentage of controls.

RESULTS

In this study, we first tested the effect of PD and IAO on maternal behaviors and lactation efficiency in 63 dams and assayed plasma hormone levels. Then using Western blotting and immunohistochemistry, we identified activities of the OT-secreting system in 30 rats and assayed CRH contents in the PVN of 21 dams.

Effect of IAO on PD-Evoked Maternal Behaviors and Hypogalactia

PD reduces suckling stimulation, causes maternal stress, and likely evokes aberrant maternal behaviors and hypogalactia. To test this hypothesis, we observed effects of PD on maternal behaviors and lactation performance following parturition. Before observation, rat dams were put into the observation cages and their pups were put back to the cage 30 min later. In general, PD dams showed reduced interest toward the litters with certain time-dependence and individual variation (**Figure 1**). That is, on PD1, all dams retrieved and suckled their pups; on PD4, the number of dams retrieving pups (15/20) was significantly smaller than that in the control group (22/22, $P < 0.05$ by Fisher exact test), which became insignificant after IAO (17/20, **Figure 1Aa**). Similar trend was present in the number of dams suckling the pups (22/22 in control group, 16/20 in PD group, and 19/20 in PD+IAO group) (**Figure 1Ba**). The same change was also present in the dams that retrieved and suckled their pups. The average latency of retrieving the pups on PD4 was significantly longer in the PD dams than the control dams [PD: 115 (34, 510), $n = 15$; Control: 6 (3,21), $n = 22$; Kruskal–Wallis test, $P < 0.01$]. However, IAO in PD dams shortened the latency significantly, which made the difference in the latency become insignificant between the control group and PD+IAO group [PD+IAO: 34 (3.5, 207.5), $n = 17$; Kruskal–Wallis test, $P > 0.05$] (**Figure 1Ab**). Correspondingly, IAO also removed the trend of elongated latency of suckling in the PD group, but there was no statistical significance among the three groups [control: 11.5 (5.8, 24.3), $n = 22$; PD: 11.5 (8.3, 19.0), $n = 16$; PD+IAO: 8 (5, 21), $n = 19$, Kruskal–Wallis test, $P > 0.05$] (**Figure 1Bb**).

In evaluation of the lactation efficiency, we found that changes in the intramammary pressure of the dams were not as sharp as what we have observed in the dams at the middle stage (days 8–12) of lactation under urethane anesthesia although a slow rising and falling in the pressure could be evoked by intravenous injection of 1 mU OT in control dams but rarely in the PD dams at day 4 (data not shown). Instead, we evaluated lactation efficiency by daily measuring LBWGs in 4 h suckling during dam-pup reunion throughout PD1∼4. The result showed that on PD3, LBWGs in the PD dams were significantly lower than that in the control group (4.25 ± 0.0.4 *g*, $n = 6$, in the control; −1 ± 0.5 g, $n = 13$, in the PD, $P < 0.01$), which was partially weakened in PD+IAO group (1.28 ± 0.5 *g*, $n = 10$, $P < 0.01$ compared with the PD group). On PD4, both the PD and PD+IAO remained significantly lower than the control in the LBWGs; however, the difference between PD and PD+IAO group disappeared (**Figure 1C**). By contrast, in control dams, IAO significantly shortened the latency of lactation and increased the duration of suckling the pups (**Supplementary Figure S1**).

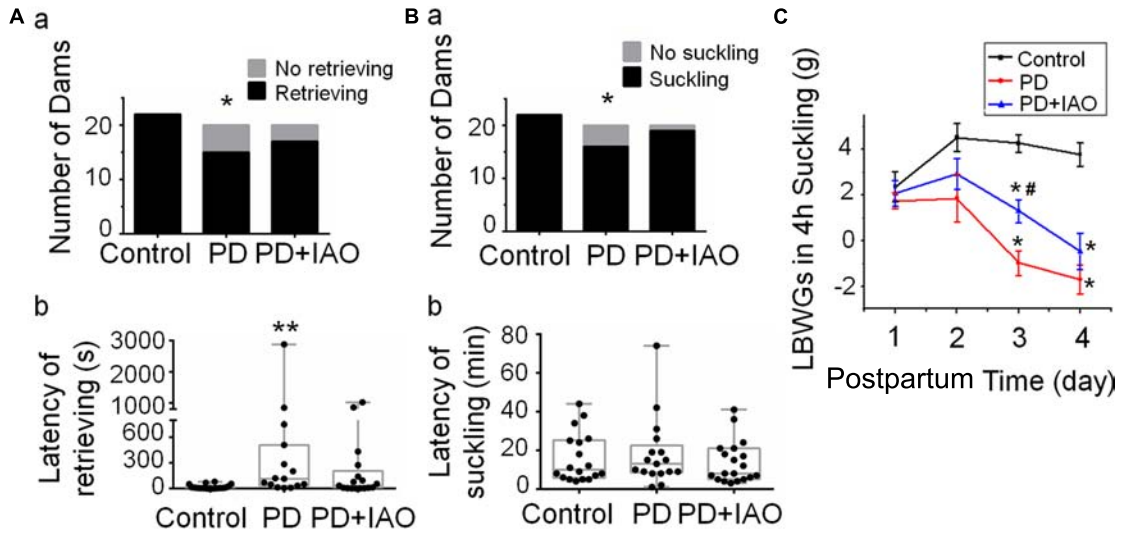

FIGURE 1 | Effects of PD and IAO on maternal behaviors and lactation. **(A,B)** The number of dams' retrieving **(Aa)** and suckling **(Ba)** their pups (black bars) or not (gray bars) during 1 h observation, and the average latency of dams' retrieving **(Ab)** and suckling **(Bb)** their pups among dams retrieving and suckling pups. Graphs of **(Ab,Bb)** were represented with box-whiskers with scattered plots indicating the median and the quartiles. **(C)** The litter's body weight gain (LBWG) in 4 h suckling throughout postpartum days 1–4 (PD1-4). PD, pup deprivation; IAO, oxytocin (OT) applied through nasal approach; $^{*}P < 0.05$, $^{**}P < 0.01$ compared with the control group; $^{\#}P < 0.05$ compared with the PD group.

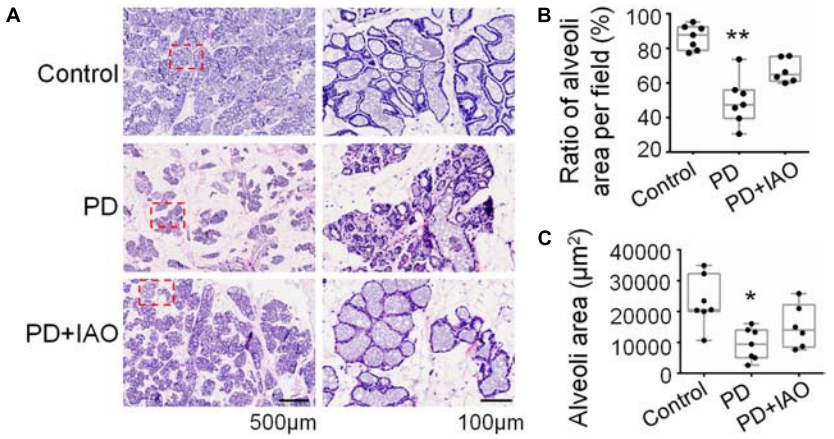

FIGURE 2 | Effects of PD and IAO on the development of mammary glands. **(A)** HE staining of the mammary glands, the right panels are the enlargements of red squares in left panels. Box-whiskers with scattered plots summarizing statistical analysis of the ratio of alveolar area per field **(B)** and the average area in five biggest alveoli in one filed **(C)**. Others refer to **Figure 1**.

Effects of IAO on PD-Evoked Involution of Mammary Glands

Upon pregnancy, the epithelium and lobule extensively proliferate and differentiate to meet the demand of milk production while weaning causes involution of them. The hypogalactia could be due to a failure of the milk production, secretion or ejection at the mammary glands. To test this hypothesis, we analyzed the histological feature of the mammary glands. Following 4 days of PD, relative to the enlarged and well-differentiated alveoli in control dams (**Figure 2A**), PD caused involution-like changes in the histology of the mammary glands. That is, the ratio between alveolar area and the total area of the mammary glands decreased [47.4% (39.6%, 56.0%) in PD vs. 87.8% (78.9%, 92.4%) in Control group, $n = 7$; Kruskal–Wallis test, $P < 0.01$]. The ratio remained lower in the PD+IAO group [64.9% (61.1%, 75.4%), $n = 6$, $P > 0.05$ compared with control group], but there was no statistically difference compared with PD groups, suggesting partial recovery.

Similarly, measuring the area of individual alveolar cavity revealed that PD dams [9413.1 (4985.1, 14029.5) μm^2, $n = 7$] had significantly smaller alveolar cavity than that in the control dams [20582.1 (20006.2, 32243.2) μm^2, $n = 7$, Kruskal–Wallis test, $P < 0.05$], and this difference became insignificant after IAO was applied to the PD dams [13993.9 (8445.1, 22183.0) μm^2, $n = 6$, Kruskal–Wallis test, $P > 0.05$ to the control]. This result is in agreement with the incomplete recovery of the depression-like behaviors and the LBWGs.

Effects of PD and IAO on Cellular Activities in the SON

The improving effect of IAO on maternal behaviors and lactation performance suggests involvement of the CNS, particularly the OT-secreting system, as suggested by the study on PD effects on maternal behaviors and lactation in the middle stage of suckling (Liu et al., 2016). To test this hypothesis, we first observed the expression of pERK 1/2, a marker of cellular activation in the SON (Wang and Hatton, 2007b), in OT neurons by immunohistochemistry (**Figure 3A**). The result showed that pERK 1/2-positive SON neurons were 29.3 ± 6.8 in control ($n = 6$), 35.3 ± 11.3 in PD ($n = 4$) and 32.5 ± 8.3 in PD+IAO ($n = 5$), respectively. By contrast, the ratio of neurons/pERK 1/2-positive neurons was 0.91 ± 0.10 in control ($n = 6$), 0.64 ± 0.10 in PD ($n = 4$) and 0.70 ± 0.07 in PD+IAO

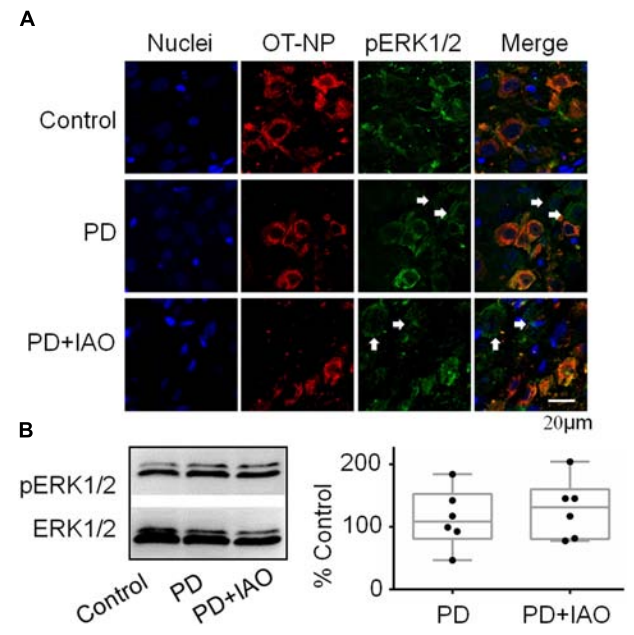

FIGURE 3 | Effects of PD and IAO on the expressions of pERK1/2 in the SON. **(A)** Fluorescent microscopy of immunostaining images of nuclei (in sky blue), OT-neurophysin (OT-NP, in red), pERK1/2 (in green), and their merges. The arrows point to non-OT neurons. **(B)** Western blot bands (left panel) and the summary graphs (right panel) showing the expression of pERK1/2 under different experimental conditions. Annotations are the same as **Figure 1**.

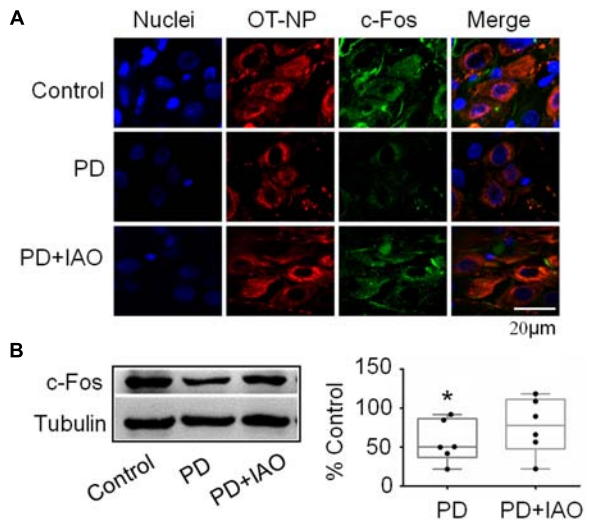

FIGURE 4 | Effects of PD and IAO on the expressions of c-Fos in the SON. **(A)** Fluorescent microscopy of immunostaining images of nuclei (in sky blue), OT-neurophysin (OT-NP, in red), c-Fos (in green), and their merges. **(B)** Western blotbands (left panel) and the summary graphs (right panel) showing the expression of c-Fos under different experimental conditions. Annotations are the same as **Figure 1**.

(n = 5), respectively. This result highlights a trend of reduction in pERK 1/2-positive OT neurons in PD and PD+IAO groups, which accompanied with an increase in pERK 1/2-positive vasopressin (VP) neurons, the only neuron that co-exists with OT neurons in the SON.

Moreover, we assayed protein levels of pERK1/2 in the SON following the 4 day PD. In Western blotting, there was no significant difference in the level of pERK 1/2 between the control and PD groups [108.3 (81.0, 152.6) % of the control, n = 6, Kruskal–Wallis test, $P > 0.05$]. Similar to PD group, the level of pERK 1/2 in the PD+IAO group showed an insignificant increase [131.2 (80.5, 160.1) % of the control, n = 6, Kruskal–Wallis test, $P > 0.05$] (**Figure 3B**).

By contrast, c-Fos expression in the SON decreased significantly in the PD group, which was partially blocked in the PD+IAO group in the immunohistochemical observation (**Figure 4A**). This finding was confirmed in Western blot analysis. As shown in **Figure 4B**, PD significantly decreased the protein levels of c-Fos [50.3 (36.8, 86.6) % of the control, n = 6, Kruskal–Wallis test, $P < 0.05$], which recovered partially in the PD+IAO group [77.8 (48.0, 111.3) % of control, n = 6, Kruskal–Wallis test, $P > 0.05$ compared to the control group]. As a strong marker of OT neuronal activation (Fenelon et al., 1993), the reduction in PD and the recovery in PD+IAO in c-Fos expression are consistent with the changes in maternal behaviors and lactation performance.

Effects of PD and IAO on Astrocytic Plasticity in the SON

There is a close interaction between neurons and astrocytes in activities of the OT-secreting system (Hou et al., 2016). PD-evoked alteration in OT neuronal activity could also result from aberrant astrocytic plasticity that is usually represented by GFAP, a cytoskeletal and scaffolding protein of astrocytes (Wang and Parpura, 2016). Thus, we observed GFAP plastic changes under PD without and with IAO (**Figure 5**). The result in immunohistochemistry showed that the length of GFAP filament increased significantly [62.8 (57.9, 77.0) μm, n = 5, Kruskal–Wallis test, $P < 0.05$] in PD compared with the control group [27.5 (18.7, 49.7) μm, n = 6]. With IAO, the elongation of GFAP filament attenuated [42.8 (33.5, 56.0) μm, n = 5, Kruskal–Wallis test, $P > 0.05$]. The representative images of fluorescent microscopy are shown in **Figure 5A**.

Corresponding to the morphological observation, we also analyzed levels of GFAP protein expression in the SON. As shown in **Figure 5B**, PD significantly reduced the level of GFAP monomers [59.7 (36.3, 89.5) % of control, n = 8, Kruskal–Wallis test, $P < 0.05$ compared to the control] and PD+IAO insignificantly reversed this trend [70.5 (34.0, 108.7) % of control, n = 8, Kruskal–Wallis test, $P > 0.05$]. **Supplementary Figure S2** shows a full panel of the blots in **Figures 3B**, **4B** and **5B**.

Effects of PD and IAO on Hormone Levels in the Plasma

Maternal behaviors and lactation are all associated with the production of OT; the depression-like behavior and hypogalactia possibly result from reduced OT secretion. To test this hypothesis, we assayed OT concentration in plasma with ELISA and then again using radioimmunoassay (**Figure 6A**). Unexpectedly, no obvious difference in the three groups was identified in the plasma although there was a trend of increased OT levels following PD and PD+IAO [Control: 17.3 (15.5, 20.1) pg/ml, n = 6; PD: 20.2 (11.5, 23.0) pg/ml, n = 7; PD+IAO: 21.2 (16.4, 25.5) pg/ml, n = 6, Kruskal–Wallis test, $P > 0.05$]. This is in agreement with the knowledge that OT functions during lactation are mainly at its pulsatile but not tonic pattern of secretion/action.

On the other hand, PD is a kind of chronic stress and unavoidably influences the activity of HPA axis. Thus, we assayed plasma concentration of stress hormones, ACTH, and corticosterone levels by ELISA. The results showed that PD+IAO evoked significant increase in ACTH [34.6 (33.6, 41.4) pg/ml, n = 4 in PD+IAO vs. 20.0 (16.5, 31.3) pg/ml, n = 6 in control, Kruskal–Wallis test, $P < 0.05$]. But in corticosterone, there was no difference [270.7 (254.7, 282.7) ng/ml, n = 6 in control group; 297.7 (266.9, 330.8) ng/ml, n = 5 in PD group; 346.1 (276.6, 355.6) ng/ml, n = 4 in PD+IAO group, Kruskal–Wallis test, $P > 0.05$] (**Figures 6B,C**). However, in an average level, PD+IAO did significantly increase corticosterone levels compared to the control (326.1 ± 24.3 ng/ml in BD+IAO vs. 268.4 ± 7.4 ng/ml in control, $P < 0.05$ by ANOVA).

Effects of PD and IAO on CRH Levels in the PVN

Increases in plasma ACTH and corticosterone levels suggest activation of the HPA axis, which is mainly assumed due to

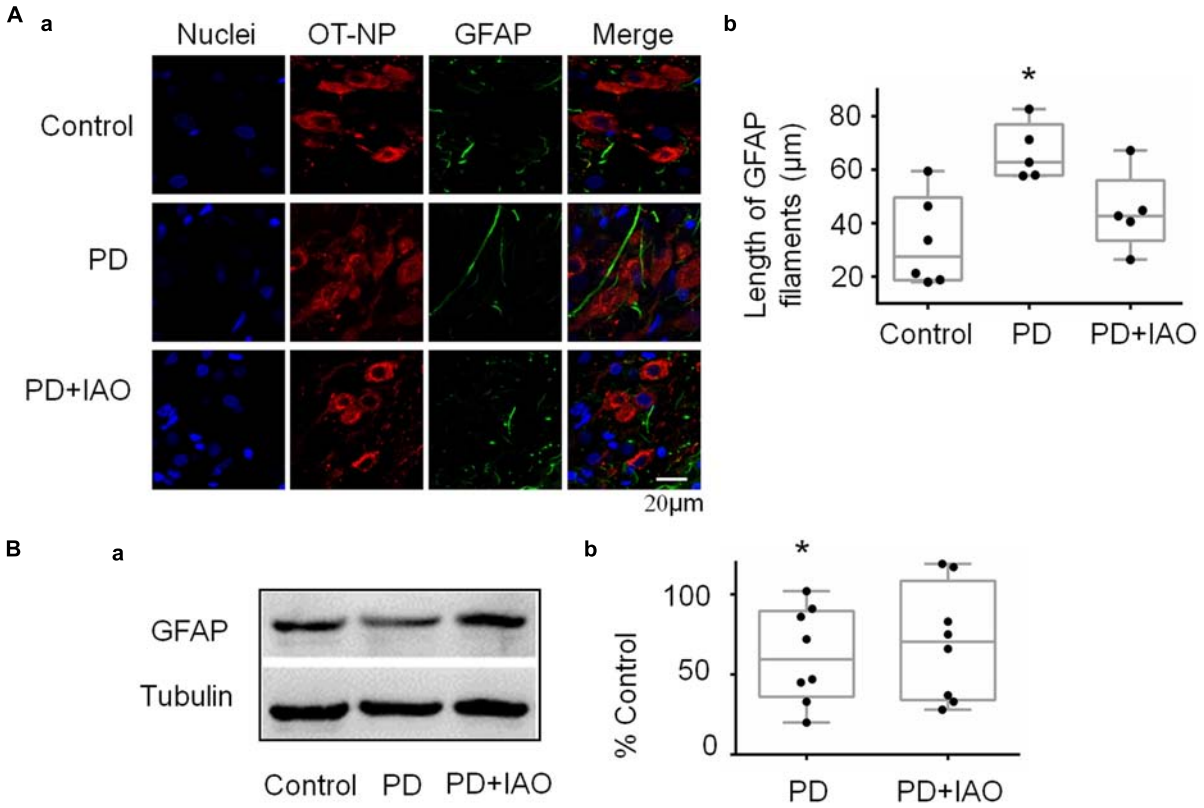

FIGURE 5 | Effects of PD and IAO on GFAP plasticity in the SON. **(A)** Fluorescent microscopy of immunostaining of GFAP filaments. From left to the right, the images show nuclei, OT-NP, GFAP, and their merges **(Aa)**; the right panel exhibiting the statistical result of average length of GFAP filaments **(Ab)**. **(B)** Western blot bands **(Ba)** and the summary graphs **(Bb)** showing the expression of GFAP under different experimental conditions. Annotations are the same as **Figure 1**.

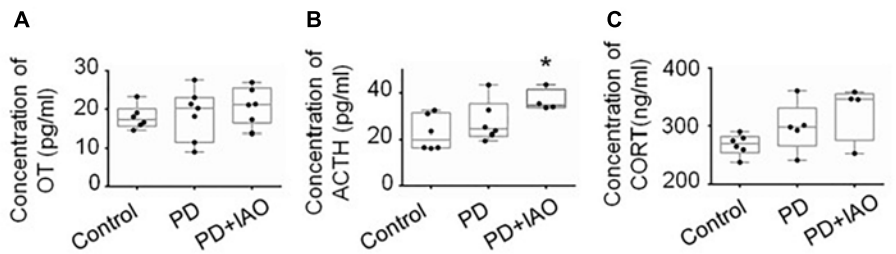

FIGURE 6 | Effects of PD and IAO on plasma levels of OT, ACTH, and corticosterone. **(A)** OT concentration. **(B)** Levels of ACTH. **(C)** Levels of corticosterone (CORT). Annotations are the same as **Figure 1**.

activation of CRH neurons in the PVN. To examine if IAO effect is also associated with CRH expression, we assayed the expression of CRH in Western blot (**Figure 7**). The result showed that PD and PD+IAO tended to increase CRH levels, particularly in PD+IAO dams (230.6 ± 63.2% of the control, $n = 7$, $P < 0.05$ by ANOVA); however, these did not reach statistically significant levels with non-parametric statistical analysis [126.0 (83.6, 187.9) % of the control, $n = 7$, $P > 0.05$ in PD; 162.6 (127.1, 433.7) % of the control, $n = 7$, in the PD+IAO group].

DISCUSSION

The present studies revealed that PD can cause postpartum depression-like maternal behaviors and hypogalactia with dramatic time dependence and certain individual variation. These effects are associated with reduced activity of the OT-secreting system, particularly astrocytes-associated inhibition of pulsatile OT secretion and early involution of the mammary glands for the MER. IAO can partially reverse these PD-evoked psycho-physical changes. However, activation of the HPA axis

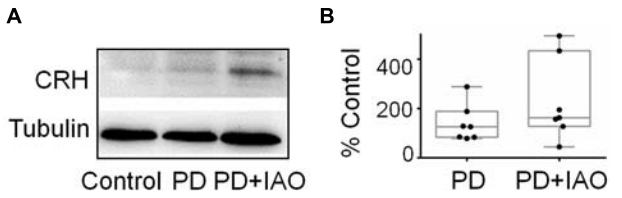

FIGURE 7 | Effects of PD and IAO on CRH expression in the PVN. **(A)** Western blot bands. **(B)** The summary graphs. Annotations are the same as **Figure 1**.

likely compromises the improving effects of IAO on PD-evoked changes. These findings highlight both the therapeutic potential of IAO in postpartum depression and hypogalactia and the challenges of integrative strategy of improving maternal health.

Effects of PD and PD Plus IAO on Maternal Behaviors and Lactation

Pup deprivation dams experience physical and psychological stress, which can be mimicked by the rat model of intermittent PD (Liu et al., 2016). It has been reported that maternal attachment behaviors and representations declined linearly with the duration of mother–infant separation (Feldman et al., 1999); early life stress due to maternal separation can induce anxiety- and aggressive-like behavior during adolescence (Shin et al., 2016). However, effects of PD on maternal behaviors have not been studied extensively. The present study revealed direct effects of PD on maternal behaviors of the dams. As presented in **Figure 1**, PD significantly reduced the ratio of retrieving and suckling pups while elongating the latency of pup retrieval by the dams that exhibited retrieval behaviors during observation, indicating reduced interest in pups, a critical sign of maternal depression (Wang et al., 2007). This finding is in agreement with a previous report that PD disrupted lactation while causing maternal depression in the rat dams at the middle stage of lactation (Liu et al., 2016) as well as clinical observations that OT can improve the mother's mood and the relationship between mother and baby (Mah et al., 2013; Mah, 2016) and that OT can mitigate the depressive-like behaviors of maternal separation stress through modulating mitochondrial function and neuroinflammation (Amini-Khoei et al., 2017).

Accompanying with the maternal depression, hypogalactia occurred in PD dams. As shown in **Figure 1**, PD reduced the LBWGs gradually during the 4 h dam-pup reunion, which became statistically significant on PD3 and PD4. Obviously, PD influence on lactation performance is associated with the length of separation, which not only causes the recession of the hypothalamic machinery for the MER, but also results in early involution-like changes in the histology of the mammary glands. As shown in **Figure 2**, PD dams had significantly smaller area of alveoli and increased fatty interstitial tissues compared to the control dams. Since we could not count all the alveoli, the increased fatty tissues did not exclude the possibility of reduction in total number of alveoli and thus, fully evaluating the features of PD-evoked changes in the mammary glands are needed. However, current finding of the histological alteration in the mammary glands could account for the hypogalactia, at least partially.

Different from the effect on maternal behaviors, IAO enhanced the LBWGs in PD dams particularly on PD3; however, this effect is short-lasting since there was no obvious effect of IAO on the PD4. Noteworthy is that plasma OT levels in the PD dams did not decrease compared to the control levels with or without IAO. Thus, the hypogalactia is likely a result of failure of the burst firing pattern of OT neurons and losses of pulsatile OT secretion that directly determine the milk ejection as previously identified in the middle stage of lactation (Wang and Hatton, 2009b; Liu et al., 2016). This finding is in agreement with the report of Fewtrell and colleagues that OT nasal spray in mothers with preterm babies could induce initial faster milk production but then convergence between groups (Fewtrell et al., 2006).

Effects of PD and IAO on Cellular Activities in the OT-Secreting System

OT can influence mental activity in the brain and milk letdown at the mammary glands by OT release from the hypothalamo-neurohypophysial system. The SON is a main source of OT in the brain and the blood (Hou et al., 2016). Therefore, we examined the cellular activity of the SON in PD dams. We found that PD significantly decreased the expression of c-Fos in the SON (**Figure 4**) although there was no significant change in pERK1/2 expression (**Figure 3**), an indicator of instant firing activity of OT neurons (Wang and Hatton, 2007b). An important contributor for the inhibition of OT neuronal activity is maladapted astrocytic plasticity. As shown in **Figure 5**, there was an expansion of GFAP filament in PD dams, suggesting expansion of astrocyte processes that is known as a key factor inhibiting OT neuronal activity (Wang and Hamilton, 2009; Wang and Zhu, 2014). Together with the previous finding (Liu et al., 2016), we can conclude that PD suppresses the activity of OT neurons and in turn reduces OT release into the brain and blood, leading to postpartum depression and hypogalactia.

In general, the effect of IAO on PD dams was similar to that on control dams (our unpublished data), i.e., increased the expression of both pERK 1/2 and c-Fos. In PD dams, IAO also tended to increase the expression of pERK 1/2 while made the reduction in c-Fos levels insignificantly different from the control. As a general inhibitory factor, the retraction of GFAP and its associated astrocyte processes can account for the weakened reduction of c-Fos, allowing OT neurons to regain its activity in response to suckling. As for the mechanisms underlying reduction in the expression of GFAP monomers, we currently do not have evidence to explain; however, different spatiotemporal distribution of pERK 1/2 and protein kinase A (Wang et al., 2017) could be a reason, which remains to be identified under PD condition.

Effects of PD and IAO on the Activity of HPA Axis

The possibility that HPA axis can be activated by chronic stress (Russell et al., 2018) is further tested in the present study.

We found that PD tended to increase the expression of CRH in the PVN in Western blots (5/7 rats showed an increase in CRH levels) as well as plasma ACTH and corticosterone levels although that did not reach a statistical significant levels due to big variation of one or two samples. Thus, the maternal depression and hypogalactia were not likely a result of tonic release of OT into the blood as evidenced in assaying plasma OT levels but possibly due to interrupting the burst firing ability of OT neurons by potentially increased activity of the HPA axis (Pereira et al., 2015), which should be verified in future study.

What come out unexpectedly are the increased plasma levels of ACTH and corticosterone by IAO in PD dams as well as CRH expression in the PVN. Appropriate and stable plasma corticosterone level is one of the essential factors for dams to take care of the offspring (Hasiec and Misztal, 2018); however, chronically increased corticosterone level could inhibit excitatory input on OT neurons (Di et al., 2005) and decreased maternal behaviors (Pereira et al., 2015), particularly a pulsatile pattern (Wang and Hatton, 2004, 2007a), thereby inhibited burst generation in OT neurons and the MER.

The increased activity of the HPA axis likely resulted from a general activation of both the SON and PVN including CRH neurons. As exhibited in the result, the expression of c-Fos became significantly high following IAO in PD dams involving OT neurons, VP neurons and likely astrocytes in the SON. The SON and PVN share many common structural and functional features and connect closely in the MER and thus, it is reasonable to believe that the two nuclei under went the same activation process during PD and following the IAO. Thus, CRH neurons could be activated in this process although that did not reach a statistical significant level due to big variation of one or two samples following the non-parametric analysis. We have to say that using Western blot to study on CRH expression allows only hemi-quantification; RIA or ELISA seems a better approach. Hopefully, a more trustable supplier would make all the assays more accurate in future study.

Alternatively, the activation of HPA axis could result from increased VP neuronal activity. As shown in **Figure 3**, PD+IAO also increased the number of VP neurons with pERK 1/2 staining, which reflects increased VP neuronal activity despite that could be differentiated in Western blotting. VP is generally believed to be an important activator of the ACTH cells and the HPA axis (Yayou et al., 2007). Thus, its activation should partially account for the increased plasma ACTH and the subsequently increased plasma corticosterone levels following IAO. In addition, because lactating rats exhibited a high degree of CRH and VP colocalization in parvocellular PVN neurons, hypothalamic projections, and median eminence terminals compared to virgins, it is possible for a simultaneous increase in VP and CRH in the PVN (Milewski et al., 2016).

CONCLUSION

The improving effect of IAO on the maternal health could be compromised by the simultaneous activation of HPA axis in association with potentially increased glutamatergic input from the olfactory bulbs (Hatton and Wang, 2008). Moreover, IAO can partially improve the activity of the OT-secreting system and prevents aberrant maternal behaviors, although it is not enough to reverse the reduced milk availability in PD dams due to the early involution-like alteration in the histology of the mammary glands. Thus, while using IAO, peripheral application of OT in a pulsatile manner (Liu et al., 2016) is also necessary to maintain the normal response of the MER and to reduce the risk of premenopausal breast cancer.

AUTHOR CONTRIBUTIONS

XL, DL, TL, and HL collected data. XL and DL analyzed data. XL wrote the first draft. Y-FW designed the study and made the final revision. All authors participated in discussion and revision.

FUNDING

This work was supported by the National Natural Science Foundation of China (Grant No. 31471113, Y-FW), the higher education talents funds of Heilongjiang Province (Grant No. 002000154, Y-FW), and the Postdoctoral Special Foundation of Heilongjiang Province.

ACKNOWLEDGMENTS

We thank Dr. Lei Sha for advice.

SUPPLEMENTARY MATERIAL

The Supplementary Material for this article can be found online at: https://www.frontiersin.org/articles/10.3389/fnins.2019.00122/full#supplementary-material

FIGURE S1 | Effects of IAO on the latency and duration of suckling in control dams. **(A)** Latency; **(B)** duration. Other annotations refer to **Figure 1**.

FIGURE S2 | Full blots showing the effect of PD and PD+IAO on the expression of pERK1/2, c-Fos and GFAP proteins in **Figures 3–5**, respectively. Other annotations refer to **Figures 1** and **3**.

REFERENCES

Amini-Khoei, H., Mohammadi-Asl, A., Amiri, S., Hosseini, M. J., Momeny, M., Hassanipour, M., et al. (2017). Oxytocin mitigated the depressive-like behaviors of maternal separation stress through modulating mitochondrial function and neuroinflammation. *Prog. Neuropsychopharmacol. Biol. Psychiatry* 76, 169–178. doi: 10.1016/j.pnpbp.2017.02.022

Berde, A. S., and Yalcin, S. S. (2016). Determinants of early initiation of breastfeeding in Nigeria: a population-based study using the 2013 demograhic and health survey data. *BMC Pregnancy Childbirth* 16:32. doi: 10.1186/s12884-016-0818-y

Di, S., Malcher-Lopes, R., Marcheselli, V. L., Bazan, N. G., and Tasker, J. G. (2005). Rapid glucocorticoid-mediated endocannabinoid release and opposing regulation of glutamate and gamma-aminobutyric acid inputs to hypothalamic

magnocellular neurons. *Endocrinology* 146, 4292–4301. doi: 10.1210/en.2005-0610

Feldman, R., Weller, A., Leckman, J. F., Kuint, J., and Eidelman, A. I. (1999). The nature of the mother's tie to her infant: maternal bonding under conditions of proximity, separation, and potential loss. *J. Child Psychol. Psychiatry* 40, 929–939. doi: 10.1017/S0021963099004308

Fenelon, V. S., Poulain, D. A., and Theodosis, D. T. (1993). Oxytocin neuron activation and Fos expression: a quantitative immunocytochemical analysis of the effect of lactation, parturition, osmotic and cardiovascular stimulation. *Neuroscience* 53, 77–89. doi: 10.1016/0306-4522(93)90286-O

Fewtrell, M. S., Loh, K. L., Blake, A., Ridout, D. A., and Hawdon, J. (2006). Randomised, double blind trial of oxytocin nasal spray in mothers expressing breast milk for preterm infants. *Arch. Dis. Child. Fetal Neonatal Ed.* 91, F169–F174.

Figueiredo, B., Dias, C. C., Brandao, S., Canario, C., and Nunes-Costa, R. (2013). Breastfeeding and postpartum depression: state of the art review. *J. Pediatr.* 89, 332–338. doi: 10.1016/j.jped.2012.12.002

Francis, D. D., Champagne, F. C., and Meaney, M. J. (2000). Variations in maternal behaviour are associated with differences in oxytocin receptor levels in the rat. *J. Neuroendocrinol.* 12, 1145–1148. doi: 10.1046/j.1365-2826.2000.00599.x

Hasiec, M., and Misztal, T. (2018). Adaptive modifications of maternal hypothalamic-pituitary-adrenal axis activity during lactation and salsolinol as a new player in this phenomenon. *Int. J. Endocrinol.* 2018:3786038. doi: 10.1155/2018/3786038

Hatton, G. I., and Wang, Y. F. (2008). Neural mechanisms underlying the milk ejection burst and reflex. *Prog. Brain Res.* 170, 155–166. doi: 10.1016/S0079-6123(08)00414-7

Hou, D., Jin, F., Li, J., Lian, J., Liu, M., Liu, X., et al. (2016). Model roles of the hypothalamo-neurohypophysial system in neuroscience study. *Biochem. Pharmacol.* 5:211. doi: 10.4172/2167-0501.1000211

Ip, S., Chung, M., Raman, G., Chew, P., Magula, N., Devine, D., et al. (2007). Breastfeeding and maternal and infant health outcomes in developed countries. *Evid. Rep. Technol. Assess.* 153, 1–186.

Jiang, H., Li, M., Yang, D., Wen, L. M., Hunter, C., He, G., et al. (2012). Awareness, intention, and needs regarding breastfeeding: findings from first-time mothers in Shanghai, China. *Breastfeed. Med.* 7, 526–534. doi: 10.1089/bfm.2011.0124

Lawrence, R. M. (2013). Circumstances when breastfeeding is contra-indicated. *Pediatr. Clin. North Am.* 60, 295–318. doi: 10.1016/j.pcl.2012.09.012

Lee, H. J., Caldwell, H. K., Macbeth, A. H., and Young, W. S. III (2008). Behavioural studies using temporal and spatial inactivation of the oxytocin receptor. *Prog. Brain Res.* 170, 73–77. doi: 10.1016/S0079-6123(08)00407-X

Liu, X., Jia, S., Zhang, Y., and Wang, Y.-F. (2016). Pulsatile but not tonic secretion of oxytocin plays the role of anti-precancerous lesions of the mammary glands in rat dams separated from the pups during lactation. *Mathews J. Neurol.* 1:002.

Liu, X. Y., Cui, D., Li, D., Jiao, R., Wang, X., Jia, S., et al. (2017). Oxytocin removes estrous female vs. male preference of virgin male rats: mediation of the supraoptic nucleus via olfactory bulbs. *Front. Cell. Neurosci.* 11:327. doi: 10.3389/fncel.2017.00327

Mah, B. L. (2016). Oxytocin, postnatal depression, and parenting: a systematic review. *Harv. Rev. Psychiatry* 24, 1–13. doi: 10.1097/HRP.0000000000000093

Mah, B. L., Van Ijzendoorn, M. H., Smith, R., and Bakermans-Kranenburg, M. J. (2013). Oxytocin in postnatally depressed mothers: its influence on mood and expressed emotion. *Prog. Neuropsychopharmacol. Biol. Psychiatry* 40, 267–272. doi: 10.1016/j.pnpbp.2012.10.005

Milewski, M., Goodey, A., Lee, D., Rimmer, E., Saklatvala, R., Koyama, S., et al. (2016). Rapid absorption of dry-powder intranasal oxytocin. *Pharm. Res.* 33, 1936–1944. doi: 10.1007/s11095-016-1929-x

Orun, E., Yalcin, S. S., Madendag, Y., Ustunyurt-Eras, Z., Kutluk, S., and Yurdakok, K. (2010). Factors associated with breastfeeding initiation time in a baby-friendly hospital. *Turk. J. Pediatr.* 52, 10–16.

Oslislo, A., and Kaminski, K. (2000). [Rooming-in: a new standard in obstetrics and neonatology]. *Ginekol. Pol.* 71, 202–207.

Pedersen, C. A., Ascher, J. A., Monroe, Y. L., and Prange, A. J. Jr. (1982). Oxytocin induces maternal behavior in virgin female rats. *Science* 216, 648–650. doi: 10.1126/science.7071605

Pereira, A. S., Giusti-Paiva, A., and Vilela, F. C. (2015). Central corticosterone disrupts behavioral and neuroendocrine responses during lactation. *Neurosci. Lett.* 606, 88–93. doi: 10.1016/j.neulet.2015.08.018

Russell, A. L., Tasker, J. G., Lucion, A. B., Fiedler, J., Munhoz, C. D., Wu, T. J., et al. (2018). Factors promoting vulnerability to dysregulated stress reactivity and stress-related disease. *J. Neuroendocrinol.* 30:e12641. doi: 10.1111/jne.12641

Seema, Patwari, A. K., and Satyanarayana, L. (1997). Relactation: an effective intervention to promote exclusive breastfeeding. *J. Trop. Pediatr.* 43, 213–216. doi: 10.1093/tropej/43.4.213

Shin, S. Y., Han, S. H., Woo, R. S., Jang, S. H., and Min, S. S. (2016). Adolescent mice show anxiety- and aggressive-like behavior and the reduction of long-term potentiation in mossy fiber-CA3 synapses after neonatal maternal separation. *Neuroscience* 316, 221–231. doi: 10.1016/j.neuroscience.2015.12.041

Stuebe, A. M., Horton, B. J., Chetwynd, E., Watkins, S., Grewen, K., and Meltzer-Brody, S. (2014). Prevalence and risk factors for early, undesired weaning attributed to lactation dysfunction. *J. Womens Health* 23, 404–412. doi: 10.1089/jwh.2013.4506

Tang, L., Lee, A. H., Qiu, L., and Binns, C. W. (2013). Mastitis in Chinese breastfeeding mothers: a prospective cohort study. *Breastfeed. Med.* 9, 35–38. doi: 10.1089/bfm.2013.0032

Trickey, H., and Newburn, M. (2014). Goals, dilemmas and assumptions in infant feeding education and support. Applying theory of constraints thinking tools to develop new priorities for action. *Matern. Child Nutr.* 10, 72–91. doi: 10.1111/j.1740-8709.2012.00417.x

Varalda, A., Coscia, A., Di Nicola, P., Sabatino, G., Rovelli, I., Giuliani, F., et al. (2012). Medication and breastfeeding. *J. Biol. Regul. Homeost. Agents* 26(3 Suppl.), 1–4.

Wang, D., Noda, Y., Tsunekawa, H., Zhou, Y., Miyazaki, M., Senzaki, K., et al. (2007). Behavioural and neurochemical features of olfactory bulbectomized rats resembling depression with comorbid anxiety. *Behav. Brain Res.* 178, 262–273. doi: 10.1016/j.bbr.2007.01.003

Wang, P., Qin, D., and Wang, Y. F. (2017). Oxytocin rapidly changes astrocytic GFAP plasticity by differentially modulating the expressions of pERK 1/2 and Protein kinase A. *Front. Mol. Neurosci.* 10:262. doi: 10.3389/fnmol.2017.00262

Wang, Y. F., and Hamilton, K. (2009). Chronic vs. acute interactions between supraoptic oxytocin neurons and astrocytes during lactation: role of glial fibrillary acidic protein plasticity. *ScientificWorldJournal* 9, 1308–1320. doi: 10.1100/tsw.2009.148

Wang, Y. F., and Hatton, G. I. (2004). Milk ejection burst-like electrical activity evoked in supraoptic oxytocin neurons in slices from lactating rats. *J. Neurophysiol.* 91, 2312–2321. doi: 10.1152/jn.00697.2003

Wang, Y. F., and Hatton, G. I. (2007a). Dominant role of betagamma subunits of G-proteins in oxytocin-evoked burst firing. *J. Neurosci.* 27, 1902–1912.

Wang, Y. F., and Hatton, G. I. (2007b). Interaction of extracellular signal-regulated protein kinase 1/2 with actin cytoskeleton in supraoptic oxytocin neurons and astrocytes: role in burst firing. *J. Neurosci.* 27, 13822–13834.

Wang, Y. F., and Hatton, G. I. (2009a). Astrocytic plasticity and patterned oxytocin neuronal activity: dynamic interactions. *J. Neurosci.* 29, 1743–1754. doi: 10.1523/JNEUROSCI.4669-08.2009

Wang, Y.-F., and Hatton, G. I. (2009b). Oxytocin, lactation and postpartum depression. *Front. Neurosci.* 3, 252–253.

Wang, Y.-F., and Parpura, V. (2016). Central role of maladapted astrocytic plasticity in ischemic brain edema formation. *Front. Cell. Neurosci.* 10:129. doi: 10.3389/fncel.2016.00129

Wang, Y. F., Sun, M. Y., Hou, Q., and Hamilton, K. A. (2013a). GABAergic inhibition through synergistic astrocytic neuronal interaction transiently decreases vasopressin neuronal activity during hypoosmotic challenge. *Eur. J. Neurosci.* 37, 1260–1269. doi: 10.1111/ejn.12137

Wang, Y. F., Sun, M. Y., Hou, Q., and Parpura, V. (2013b). Hyposmolality differentially and spatiotemporally modulates levels of glutamine synthetase and serine racemase in rat supraoptic nucleus. *Glia* 61, 529–538. doi: 10.1002/glia.22453

Wang, Y. F., and Zhu, H. (2014). [Mechanisms underlying astrocyte regulation of hypothalamic neuroendocrine neuron activity]. *Sheng Li Ke Xue Jin Zhan* 45, 177–184.

Yayou, K., Seo, T., Uetake, K., Ito, S., and Nakamura, M. (2007). Effects of intracerebroventricular infusions of arginine vasopressin in sheep. *Physiol. Behav.* 90, 376–381. doi: 10.1016/j.physbeh.2006.09.030

Conflict of Interest Statement: The authors declare that the research was conducted in the absence of any commercial or financial relationships that could be construed as a potential conflict of interest.

frontiers in Neuroscience

ORIGINAL RESEARCH
published: 08 March 2019
doi: 10.3389/fnins.2019.00188

Chronic Glucocorticoid Exposure Induces Depression-Like Phenotype in Rhesus Macaque (Macaca Mulatta)

Dongdong Qin[1,2,3,4†], Zhifei Li[1†], Zhaoxia Li[1], Limin Wang[1], Zhengfei Hu[5], Longbao Lü[5], Zhengbo Wang[1,4], Yun Liu[3], Yong Yin[6], Zhaofu Li[2*] and Xintian Hu[1,7*]*

[1] Key Laboratory of Animal Models and Human Disease Mechanisms of the Chinese Academy of Sciences and Yunnan Province, Kunming Institute of Zoology, Chinese Academy of Sciences, Kunming, China, [2] Yunnan University of Chinese Medicine, Kunming, China, [3] Department of Rehabilitation, Kunming Children's Hospital, Kunming, China, [4] Yunnan Key Laboratory of Primate Biomedicine Research, Institute of Primate Translational Medicine, Kunming University of Science and Technology, Kunming, China, [5] Kunming Primate Research Center, Kunming Institute of Zoology, Chinese Academy of Sciences, Kunming, China, [6] Department of Rehabilitation Medicine, the Fourth Affiliated Hospital of Kunming Medical University, Kunming, China, [7] Center for Excellence in Brain Science and Intelligence Technology, Chinese Academy of Sciences, Shanghai, China

OPEN ACCESS

Edited by:
Xue Qun Chen,
Zhejiang University, China

Reviewed by:
Balazs Gaszner,
University of Pécs, Hungary
Christina S. Barr,
National Institutes of Health (NIH), United States

***Correspondence:**
Yong Yin
yyinpmr@126.com
Zhaofu Li
lzf0817@126.com
Xintian Hu
xthu@mail.kiz.ac.cn

† These authors have contributed equally to this work

Specialty section:
This article was submitted to Neuroendocrine Science, a section of the journal Frontiers in Neuroscience

Received: *27 September 2018*
Accepted: *18 February 2019*
Published: *08 March 2019*

Citation:
Qin D, Li Z, Li Z, Wang L, Hu Z, Lü L, Wang Z, Liu Y, Yin Y, Li Z and Hu X (2019) Chronic Glucocorticoid Exposure Induces Depression-Like Phenotype in Rhesus Macaque (Macaca Mulatta). Front. Neurosci. 13:188. doi: 10.3389/fnins.2019.00188

It has long been observed in humans that the occurrence of depressive symptoms is often accompanied by the dysfunction of hypothalamic-pituitary-adrenal (HPA) axis. The rodent experiments also showed that chronic corticosterone exposure could induce depression-like phenotype. However, rodents are phylogenetically distant from humans. In contrast, non-human primates bear stronger similarities with humans, suggesting research on primates would provide an important complement. For the first time, we investigated the effects of chronic glucocorticoid exposure on rhesus macaques. Seven male macaques were selected and randomized to glucocorticoid or vehicle groups, which were subjected to either prednisolone acetate or saline injections, respectively. The depression-like behaviors were assessed weekly, and the body weights, HPA axis reactivity, sucrose solution consumption and monoaminergic neurotransmitters were further compared between these two groups. The glucocorticoid group was not found to display more depression-like behaviors than the vehicle group until 7 weeks after treatment. Chronic glucocorticoid exposure significantly decreased the levels of cortisol determined from blood (a biomarker for acute HPA axis reactivity) but increased the hair cortisol concentrations (a reliable indicator of chronic HPA axis reactivity) compared with controls. The glucocorticoid group was also found to consume less sucrose solution than controls, a good manifestation of anhedonia. This could be possibly explained by lower dopamine (DA) levels in cerebrospinal fluid induced by chronic glucocorticoid treatment. The results presented here indicate that chronic glucocorticoid exposure could disturb both the acute and chronic HPA axis reactivity, which eventually disturbed the neurotransmitter system and led monkeys to display depression-like phenotype.

Keywords: chronic, glucocorticoid, HPA axis, depression, rhesus macaque

INTRODUCTION

According to the World Health Organization (WHO), depression is estimated to become the second leading burden of illness in the world by 2020 (Mathers and Loncar, 2006). The core symptoms of depression include low mood and anhedonia (i.e., lack of interests in pleasurable activities), but it is always accompanied by a complex cluster of clinical symptoms that may include weight changes, sleep disturbances, psychomotor agitation or retardation, loss of energy, feelings of worthlessness, difficulty concentrating, and/or recurrent thoughts of death (American-Psychiatric-Association, 2013). In addition, depression can also cause increased physical illness, decreased social functioning, and a high mortality rate (Nemeroff, 1998). As is the case with other affective disorders, depression also has both a genetic and environmental basis. Twin studies revealed that about 25% of the variance was genetic and environmental factors accounted for about 75% of the variance (Henn et al., 2004). Further studies showed that stress was the most important environmental factor in the development of depression (Paykel, 2003; Charney and Manji, 2004).

The connection between stress and depression was initially drawn from clinical observations of abnormalities of stress reactivity in depressed patients, including dysfunction of hypothalamic–pituitary–adrenal (HPA) axis (Carroll and Curtis, 1976; Carroll et al., 1976b,c), disrupted cortisol rhythmicity (Sachar et al., 1973; Linkowski et al., 1985) and elevated cortisol levels in plasma (Carroll et al., 1976a), cerebrospinal fluid (Träskman et al., 1980), urine (Scott and Dinan, 1998), saliva (Vedhara et al., 2003), and hair samples (Staufenbiel et al., 2013). These findings solidly underpin a crucial role of cortisol in the development of depression. The link between disruption of the HPA axis and depression also comes from evidence that patients experiencing elevated cortisol levels as a result of Cushing's disease (Kelly et al., 1983; Sonino et al., 1998) or synthetic glucocorticoid therapy (Brown and Suppes, 1998; Antonijevic and Steiger, 2003; Brown et al., 2004) suffer from depressive episodes. Moreover, some effective antidepressant drugs were found to act on the function of glucocorticoid receptors (GR) to restore the function of HPA axis (Pariante et al., 2001; Okuyama-Tamura et al., 2003; Pariante et al., 2003).

Although dysfunction of the HPA axis has been verified to be closely related to the development of depression, it is still unknown that whether depression promotes dysfunction of the HPA axis or vice versa. In order to elucidate the causal relationship between them, animal models were developed. Among numerous animal models that currently exist, those involving repeated injection are the most promising as this paradigm could provide control over increases in circulating glucocorticoids to manipulate the function of HPA axis (Johnson et al., 2006), which cannot be achieved with other administration methods (e.g., corticosterone pellet implantation or corticosterone in drinking water).

However, previous animal studies involving glucocorticoids are mostly based on rodents, which may pose a major challenge. Rodent brain is phylogenetically distant from human brain (Piper et al., 2011), which makes them differ greatly from humans in anatomy, neurophysiology, function, and behavioral performance and thus limits the degree to which insights derived from the rodents can be applied to understanding human depression (Belmonte et al., 2015). There is another obvious limitation for rodent models that they cannot exhibit the core symptoms of depression (low mood and anhedonia) because of relatively simple brain structure (Song and Leonard, 2005), and they secrete corticosterone in response to stress (Wasser et al., 2000). Compared with cortisol, which is the primary glucocorticoid in both primates and humans, corticosterone has only weak glucocorticoid and mineralocorticoid potencies and is important mainly as an intermediate in the steroidogenic pathway from pregnenolone to aldosterone. By contrast, non-human primates share a common ancestry with humans, and bear strong similarities to humans, such as intricacy of brain organization, details of reproductive biology, complex cognitive capabilities, and great social complexity (Belmonte et al., 2015). As with human beings, non-human primates produce cortisol to cope with stress and can display core depression-like symptoms after exposed to chronic mild stress (Qin et al., 2015a). But what's even more crucial is that cortisol hyper-secretion can accelerate the occurrence of depressive behaviors in monkeys experiencing more stress (Qin et al., 2016).

Epidemiological studies have indicated that depression occurs nearly twice as frequently in females than in males, which can be ascribed to fluctuations in estrogen associated with reproductive function (Garde, 2007). Therefore, in order to avoid the disturbances of estrogen, male rhesus macaques (Macaca mulatta) were selected in this study and were injected repeatedly with synthetic glucocorticoid to characterize the behavioral and neurobiological consequences of prolonged glucocorticoid treatment, and to further provide insights into the biological mechanisms underlying the link between glucocorticoid and depression.

MATERIALS AND METHODS

Animals

Seven male rhesus macaques, aged 8–10 (8.60 ± 0.60) years old, were randomly selected from Kunming Primate Research Center of the Chinese Academy of Sciences. The animals were singly housed (0.80 × 0.80 × 0.80 m) in a controlled environment (temperature: 22 ± 1°C; humidity: 50 ± 5% RH), with 12 h light/12 h dark cycle (lights on at 07:00 h and lights off at 19:00 h). All monkeys were given commercial monkey biscuits twice a day and were fed with fruits and vegetables once daily. The animals were accommodated in their cages for at least 3 months prior to initial manipulation, and all efforts were made to minimize the monkeys' suffering. For example, hair samples were taken from the back of the monkeys' neck using an electric-razor without anesthetic and no animals were sacrificed in this study. Routine veterinary care was provided throughout the experiment by professional keepers and veterinarians.

All animal procedures were approved by the National Animal Research Authority (P.R. China) and the Institutional Animal Care and Use Committee (IACUC) of Kunming Institute of Zoology, Chinese Academy of Sciences.

Experimental Design

Animals were firstly habituated to experimental procedures to minimize the influences of stress, and then were randomized to glucocorticoid or vehicle group, which was subjected to either prednisolone acetate (3 monkeys) or saline (4 monkeys) treatment. Body weights, HPA axis reactivity and monoaminergic neurotransmitters as well as depression-like behaviors and anhedonia were assessed to analyze the effects of chronic glucocorticoid exposure on monkeys.

Injection of Prednisolone Acetate and Saline

After 3 months of acclimatization in single cages, the monkeys were injected intramuscularly with prednisolone acetate, which is a synthetic glucocorticoid. The injections (State Medical Permitment Number: H33020824, Drug Specifications: 25 mg/ml) were purchased from Zhejiang Xianju Pharmaceutical Co., Ltd. (China). According to previous studies, the injection dose for rats was 40 mg/kg and this dose reliably induced depression-like behavior in the forced swim test (Kalynchuk et al., 2004; Gregus et al., 2005; Johnson et al., 2006). Using the BSA (body surface area) method, the injection dose for monkeys was calculated (15.89 mg/kg). Saline was used as solvent of prednisolone acetate injection in this study, because it is less painful than sterile water for injection. As a result, the vehicle group was injected with equivalent does of saline. Throughout the experiment, all treatments were performed at 10:00 a.m.

Blood and Hair Samples Collection

In order to assess the acute HPA axis reactivity, each monkey was sampled 2 ml of blood. Each cage that monkeys lived was equipped with one locking push-pull device and the restraint could be achieved by reducing volumes of the cage. After 15 min of restraint, the blood was sampled from the femoral vein by pulling out the monkey's leg, with the restraint being the acute stressor. The blood samples were then put into a heparin lithium-treated vacuum collection tube. However, the stress of restraint, blood collection, and the limitation on the volume of blood that could be safely drawn from each monkey, precluded the possibility of repeated sampling of the same monkey. As a result, three blood samples were collected for each monkey every 14 days, with the first, second and third sample obtained on 14, 28, and 42 days after treatment, respectively. As there was an obvious rhythmic change in blood cortisol, all blood samples were obtained at the same time of the day (between 10:30 a.m. and 11:30 a.m.).

Hair samples from all monkeys were collected at the same time of the day (between 10:30 a.m. and 11:30 a.m.) to assess the chronic HPA axis reactivity. Before treatment, each monkey was captured by an experienced technician and taken out of the cage for hair sampling. The monkey was manually restrained, and the hair on the back of each animal's neck was shaved with an electric razor without the use of anesthetic, with particular attention paid by technicians not to break or damage the skin. After completion of treatment, newly grown hair was shaved as previously described and the hair samples were placed into a small pouch of aluminum foil for protection (Wennig, 2000; Davenport et al., 2006).

Measurement of Cortisol From Blood and Hair Samples

The blood samples were centrifuged at 8,000 $\times$ *g* for 10 min to isolate plasma, and the hair samples were ground to powder to break up the hair's protein matrix and to increase the surface area for the extraction of cortisol (Davenport et al., 2006; Feng et al., 2011; Qin et al., 2013, 2015a,b). The cortisol concentration in each blood and hair sample was quantified with a commercial cortisol radioimmunoassay (RIA) kit. In order to minimize the cross-reaction for prednisolone, the cortisol Kit "TFB" (Immunotech, Tokyo, Japan) was used because of its lowest cross-reaction (2.5%) for prednisolone (Horie et al., 2007). The cortisol RIA was performed in triplicate under a double-blind design at the Department of Nuclear Medicine of the Second Affiliated Hospital of the Kunming Medical College. The limit of detection for the cortisol assay was 0.5 μg/dL, and the intra-assay coefficient of variability (CV) for this assay was 2.08%. All the samples were assayed at the same time using the same kit.

Cerebrospinal Fluid Sampling and Measurement of Monoaminergic Neurotransmitters

Before and after the treatment, all monkeys were sampled cerebrospinal fluid (CSF) under ketamine anesthesia (15 mg/kg) within 10–20 min after their anesthesia. Using a spinal needle, the CSF was obtained through a lumbar puncture. During the procedure, the monkey was positioned in lateral recumbency and a needle was inserted usually between the 3rd and 4th lumbar vertebrae. The CSF fluid was collected into a polypropylene tube and immediately frozen in liquid nitrogen. For purposes of comparison, CSF samples were collected from the same sites. All the collected CSF samples were stored at −80°C until assayed.

Before analysis, CSF sample was centrifuged at 4°C in a high speed freezing centrifuge at 8,000 $\times$ *g* for 10 min. Homovanillic acid (HVA), 5-hydroxyindole acetic acid (5-HIAA) and dopamine (DA) concentrations in the supernatant was quantified by high performance liquid chromatography (HPLC) with electrochemical detection (Yang and Beal, 2011). The CSF samples from a given subject obtained before and after treatment were paired and run in a single assay.

The HPLC system was composed of an Antec LC-110 solvent delivery module, and an Antec Autoinjector AS-110. The separation of HVA and 5-HIAA was performed using an Antec ALF-115 column (C18, 3 μm, 150 $\times$ 1 mm). The mobile phase comprising 50 mM monobasic sodium phosphoric

acid, 8 mM Sodium chloride, 0.1 mM EDTA, 10.0% (v/v) methanol, 500 mg/L OSA with the final pH adjusted to 6.00 with phosphoric acid, was maintained at a flow rate of 40 μl/min. The separation of DA was performed using an Antec ALF-105 column (C18, 3 μm, 50 × 1 mm). The mobile phase comprising 50 mM phosphoric acid, 50 mM Citric acid, 8 mM Sodium chloride, 0.1 mM EDTA, 12.5% (v/v) methanol, 500 mg/L OSA with the final pH adjusted to 3.25 with phosphoric acid, was maintained at a flow rate of 40 μl/min. The optimal electrical potential settings were: E1 −700 mV and E2 +700 mV. For electrochemical detection, an Antec Decade-11 detector was used. Quantification of the detector signals was achieved by means of peak area integration. Data represent the average of at least two analysis.

Behavioral Sampling and Analysis

Animal behaviors were video-recorded using a focal follow technique (Altmann, 1974). Before the experiment, fourteen 1 h recordings were collected for each monkey, 1 h each day. Specifically, they were, respectively, collected from 7:00 a.m. to 8:00 a.m., 8:00 a.m. to 9:00 a.m., 9:00 a.m. to 10:00 a.m., 10:00 a.m. to 11:00 a.m., 11:00 a.m. to 12:00 p.m., 12:00 p.m. to 13:00 p.m., 13:00 p.m. to 14:00 p.m., 14:00 p.m. to 15:00 p.m., 15:00 p.m. to 16:00 p.m., 16:00 p.m. to 17:00 p.m., 17:00 p.m. to 18:00 p.m., 18:00 p.m. to 19:00 p.m., 9:00 a.m. to 10:00 a.m., and 14:00 p.m. to 15:00 p.m. After the start of the experiment, the monkeys' depression-like behaviors were assessed weekly. Once the monkey was observed to become obviously depressed, the treatment was finished and another fourteen 1 h recordings were collected for each monkey at the same time as before.

Each video-recording was scored simultaneously by three observers unaware of experimental design. During the scoring, the observers calculated the duration of specific behaviors by manually starting and stopping the video, and they all agreed on the definition of observed behaviors, including depression-like huddling behavior, environmental exploration, locomotion, stereotypic behaviors and self-grooming. All these behaviors were quantified as frequencies and seconds per hour. The inter-rater correlation coefficient was found to be > 0.90 through SPSS statistical analysis and there were no significant changes (Version 19.0 for the PC) after a period of training.

Depression-like huddling behavior was defined as a fetal-like, self-enclosed posture with the head at or below the shoulders during the waking state (Harlow and Suomi, 1971; Shively et al., 2005). Environmental exploration included tactile exploration of the cage or environments and oral exploration of the cage or environments (Davenport et al., 2008). The locomotion was divided into spontaneous locomotion (defined as any voluntary movement within the cage, including walking, running, jumping and climbing) and reactive locomotion (defined as the locomotion caused by external stimuli) (Rogers et al., 2008). The stereotypic behaviors were defined as frequent, repetitive, and constant postures or behaviors that appear to serve no purpose, including pacing, saluting, somersaulting, weaving and head tossing (Hugo et al., 2003). Self-grooming included any picking, scraping, spreading, mouth picking, or licking of the hair on monkey's own body (Parks and Novak, 1993).

Sucrose Preference Test

Anhedonia is a core symptom of depression (Gaillard et al., 2013), and can be evaluated in rhesus monkeys using the sucrose preference test (Paul et al., 2000). During the period of acclimatization, all animals were adapted to a 23 h/day water restriction schedule, and had access to water in two identical bottles for 1 h per day. During the test period, animals were supplied with 1.5% sucrose solution (SIGMA, Aldrich, China, dissolved in tap water) in one bottle, and tap water in the other one. Bottle positions were alternated daily to control for position preference, and the bottles were refilled 30 min after the start of the access period to accommodate the increased consumption. The sucrose concentration was selected based on previous experiments with rhesus monkeys (Paul et al., 2000). The test schedule included 14 days of continuous exposure to sucrose solution and tap water, corresponding to the behavioral sampling period. The test occurred between 9:00 a.m. and 10:00 a.m. The sucrose preference was calculated as ml consumed per kg body weight because the monkey's water consumption was correlated with its body weight (Paul et al., 2000).

Statistical Analysis

Data analysis was conducted with the SPSS software package (SPSS Inc., Chicago, IL, United States). The normality of the data was determined using the Kolmogorov-Smirnov test, the results of which demonstrate that they are normally distributed (all P-values > 0.05). And the data were further analyzed in separate 2 (groups: predonisolone versus vehicle) × 3 (time: 14th day, 28th day, and 42nd day) or 2 (time: pre-treatment and post-treatment) repeated-measures ANOVAs, with time being the repeated-measure. Further *post hoc* pairwise comparisons (Bonferroni correction) were also made. The alpha level was set at $P = 0.05$, and all P-values were generated using two-sided tests. All the data were presented as the mean ± SEM (standard error of the mean).

RESULTS

Body Weights

As shown in **Figure 1A**, no significant changes over time were observed in monkeys' body weights during the experiment ($F = 3.434$, $P = 0.073$, $\eta_p^2 = 0.407$) and there were no significant differences between the two groups ($F = 1.872$, $P = 0.230$, $\eta_p^2 = 0.272$), including on the 14th day ($F = 1.701$, $P = 0.249$), the 28th day ($F = 2.219$, $P = 0.197$) and the 42nd day ($F = 1.482$, $P = 0.278$) after treatment. The group by time interaction was also non-significant ($F = 0.626$, $P = 0.554$, $\eta_p^2 = 0.111$). Further *post hoc* pairwise comparisons (Bonferroni correction) showed no significant differences (all P-values > 0.05).

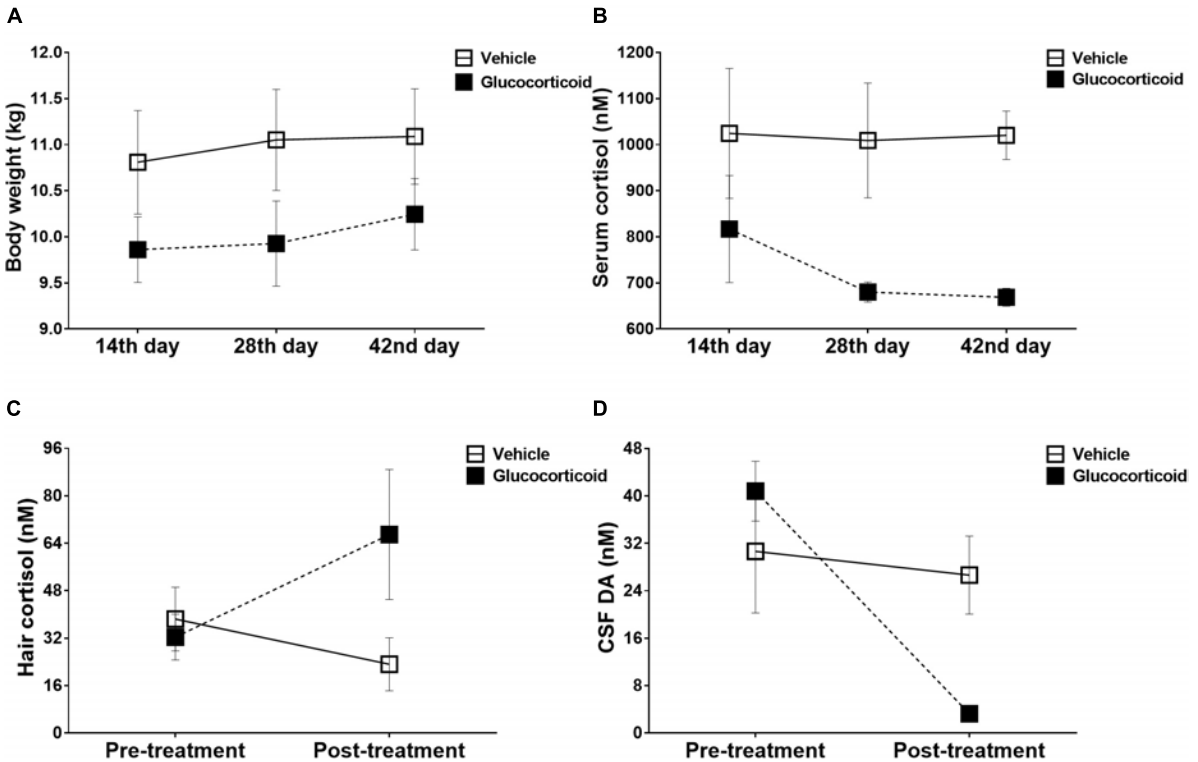

FIGURE 1 | Physiological changes induced by chronic glucocorticoid exposure. Mean (±SEM) physiological changes, including body weights **(A)** and plasma cortisol **(B)**, are depicted for the glucocorticoid and vehicle group on 14th day, 28th day, and 42nd day post-treatment. Chronic glucocorticoid exposure induced no significant changes in monkeys' body weights throughout the experiment, but the glucocorticoid group exhibited attenuated cortisol reactivity to the acute stressor than the vehicle group. Before and after treatment, the hair cortisol **(C)** and CSF DA **(D)** were also measured to assess the chronic stress reactivity and neurotransmitter function. The glucocorticoid group displayed exaggerated cortisol reactivity and neurotransmitter deficiency compared with the vehicle group.

Acute Stress Reactivity

The glucocorticoid group exhibited attenuated cortisol reactivity to the acute stressor compared with the vehicle group (**Figure 1B**, $F = 8.419$, $P = 0.034$, $\eta_p^2 = 0.627$), and on the 42nd day after treatment, the cortisol level was decreased significantly (**Figure 1B**, $F = 30.034$, $P = 0.003$). Further *post hoc* pairwise comparisons (Bonferroni correction) showed no significant differences (all P-values > 0.05).

Chronic Stress Reactivity

Although there was no significant difference between the two groups in cortisol reactivity to the chronic stress (**Figure 1C**, $F = 1.353$, $P = 0.297$, $\eta_p^2 = 0.213$), the glucocorticoid group displayed exaggerated cortisol reactivity as group by time interaction was significant ($F = 9.678$, $P = 0.027$, $\eta_p^2 = 0.659$).

Monoaminergic Transmitters

During the treatment, the monkeys displayed significant changes over time in the level of dopamine (**Figure 1D**, $F = 24.092$, $P = 0.004$, $\eta_p^2 = 0.828$), and the group by time interaction was also significant (**Figure 1D**, $F = 15.693$, $P = 0.011$, $\eta_p^2 = 0.758$). The level of dopamine was higher in the vehicle group than that of the glucocorticoid group on the 42nd day after treatment (**Figure 1D**, $F = 8.862$, $P = 0.031$). While, no significant differences were found in metabolites of the other two monoaminergic neurotransmitters, including HVA ($F = 1.334$, $P = 0.300$, $\eta_p^2 = 0.211$; vehicle group, pre-treatment versus post-treatment: 160.085 ± 23.278 versus 178.031 ± 41.083; glucocorticoid group, pre-treatment versus post-treatment: 121.236 ± 59.749 versus 95.602 ± 24.181) and 5-HIAA ($F = 0.138$, $P = 0.726$, $\eta_p^2 = 0.027$; vehicle group, pre-treatment versus post-treatment: 61.026 ± 4.987 versus 64.064 ± 5.417; glucocorticoid group, pre-treatment versus post-treatment: 76.099 ± 16.593 versus 87.030 ± 16.774).

Depression-Like Behavior

During the experiment, the monkeys' huddling behaviors exhibited significant changes over time, including frequencies (**Figure 2A**, $F = 6.368$, $P = 0.053$, $\eta_p^2 = 0.560$) and durations (**Figure 2B**, $F = 53.476$, $P = 0.001$, $\eta_p^2 = 0.914$), and the group by time interactions were also significant in frequencies (**Figure 2A**, $F = 7.003$, $P = 0.046$, $\eta_p^2 = 0.583$) and durations (**Figure 2B**, $F = 68.111$, $P = 0.0004$, $\eta_p^2 = 0.932$). The differences between the two groups were also found to be significant (frequencies: $F = 14.691$, $P = 0.012$, $\eta_p^2 = 0.746$; and durations: $F = 20.680$, $P = 0.006$, $\eta_p^2 = 0.805$). While

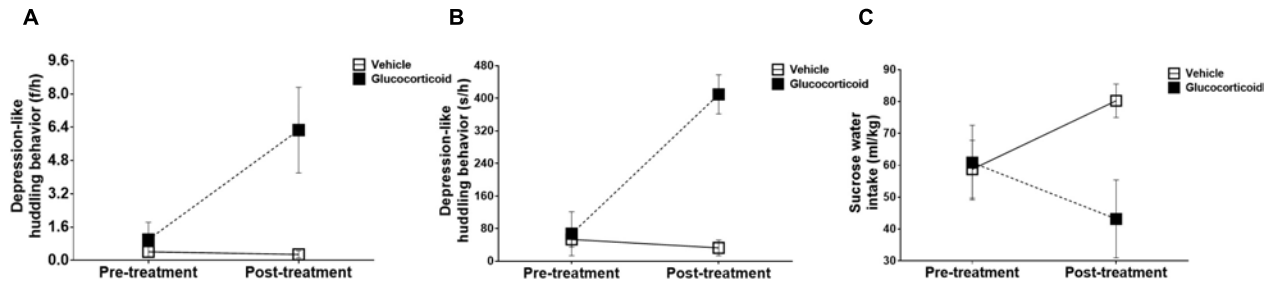

FIGURE 2 | Depression-like behaviors. The monkeys' depression-like behaviors, including the huddling behavior (**A:** frequencies per hour and **B:** seconds per hour) measuring depressed mood, and sucrose solution intake **(C)** assessing anhedonia, were recorded for 14 consecutive days and the changes before and after treatment were compared between the two groups. Chronic glucocorticoid exposure induced significant changes in external behavioral phenotype, such as increases in the huddling behavior and decreases in sucrose solution intake, which, respectively, represented two core symptoms of depression.

the frequencies and durations of other behaviors, including environmental exploration, spontaneous locomotion, passive locomotion, stereotyped behaviors and self-grooming, did not display significant changes (all *P*-values > 0.05) except for significant changes over time in durations of reactive locomotion ($F = 12.400$, $P = 0.017$, $\eta_p^2 = 0.713$).

Anhedonia

There were no significant changes over time in the preference of sucrose water (**Figure 2C**, $F = 0.102$, $P = 0.763$, $\eta_p^2 = 0.020$), but the group by time interaction was significant ($F = 10.610$, $P = 0.023$, $\eta_p^2 = 0.680$) with the glucocorticoid group consuming less sucrose solution than the vehicle group ($F = 9.640$, $P = 0.027$). However, no significant changes were found in the consumption of tap water (all *P*-values > 0.05).

Relations of HPA Reactivity and Neurotransmitters to Depression-Like Behaviors

There were no significant correlations between HPA axis reactivity and the levels of dopamine, including the acute stress reactivity (Pearson Correlation Coefficient = 0.470, $P = 0.288$), and chronic stress reactivity (Pearson Correlation Coefficient = 0.704, $P = 0.077$). Further analysis revealed that the acute stress reactivity was not related to the chronic stress reactivity (Pearson Correlation Coefficient = 0.328, $P = 0.472$).

Although plasma cortisol was not related to the frequencies of huddling behavior (**Figure 3A**, Pearson Correlation Coefficient = −0.516, $P = 0.059$), it was strongly related to the durations of huddling behavior (**Figure 3B**, Pearson Correlation Coefficient = −0.553, $P = 0.040$). Moreover, the plasma cortisol level showed a strong negative correlation with the severity of anhedonia symptoms (**Figure 3C**, Pearson Correlation Coefficient = 0.699, $P = 0.005$).

Further analysis revealed a moderate positive correlation between the huddling behavior and the cortisol reactivity to the chronic stressor as quantified by hair cortisol (**Figure 3D**, Pearson Correlation Coefficient = 0.582, $P = 0.029$). The hair cortisol was not found to be related to huddle frequencies (**Figure 3E**, Pearson Correlation Coefficient = 0.303, $P = 0.292$) and correlated with sucrose solution intake (**Figure 3F**, Pearson Correlation Coefficient = −0.233, $P = 0.422$), but these correlations displayed weak tendencies.

As analyzed above, the monkeys' depression-like phenotype was not only caused by abnormal HPA axis reactivity, including both the acute and chronic stress reactivity, but also was related to neurotransmitter deficiency, such as the lower level of dopamine in CSF (**Figure 3G**, huddle frequencies: Pearson Correlation Coefficient = −0.547, $P = 0.043$; **Figure 3H**, huddle durations: Pearson Correlation Coefficient = −0.670, $P = 0.009$; and **Figure 3I**, sucrose water intake: Pearson Correlation Coefficient = 0.422, $P = 0.133$).

DISCUSSION

It has long been recognized that glucocorticoid plays a crucial role in mediating the pathogenic effects of stress on depression, but clarifying mechanisms are still dependent upon the development of validated animal models. The majority of studies have been focused on rodents, and it has been consistently reported that chronic corticosterone (CORT) injections can induce depressive behavioral manifestations (Marks et al., 2009; Sterner and Kalynchuk, 2010; Xu et al., 2011). However, it is controversial that whether the results obtained from rodents can serve humans because rats and mice lack the enzyme 17 alpha-hydroxylase in their adrenal cortices, so that they produce CORT (Van Weerden et al., 1992). However, the CORT is of minor importance in humans, except in the very rare case of congenital adrenal hyperplasia due to 17 alpha-hydroxylase deficiency (D'armiento et al., 1983). This makes rodents dubious for experiments on the HPA axis, perhaps also for studying the relationship between glucocorticoid and human depression. In humans and other primates, cortisol is the most abundant and naturally occurring glucocorticoid, suggesting research on primates will provide a critical complement on previous rodents' studies. That is exactly why the macaques were chosen for this study.

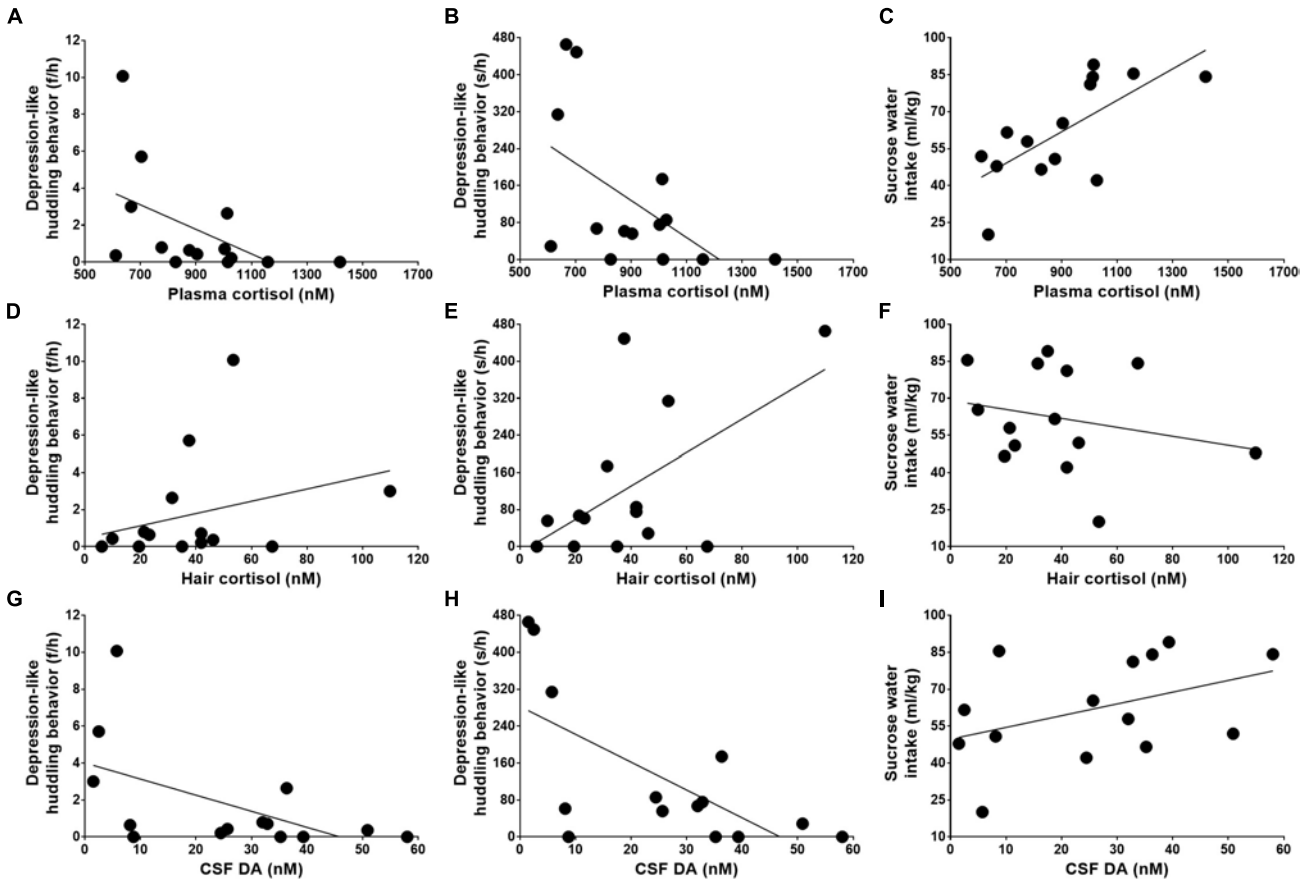

FIGURE 3 | Relations of stress reactivity and dopamine to depression-like behaviors. The depression-like behaviors, including huddling behavior and anhedonia, were caused by attenuated acute stress reactivity **(A–C)**, exaggerated chronic stress reactivity **(D–F)**, and neurotransmitter deficiency **(G–I)**.

To our knowledge, this is the first study using macaques to clarify the mechanisms underlying the causal relationship between glucocorticoid and depression. It was found that chronic glucocorticoid treatment can inflict severe damage on the monkeys' responses to stress, including both the acute and chronic HPA reactivity. When an organism undergoes stress, cortisol acts to mobilize energy stores and modulate the immune system, preparing it for fighting or fleeing. Blood samples provide a measurement of the cortisol secretion at the time of stress experiencing, and blood cortisol can therefore be used to test the acute HPA reactivity (Maidana et al., 2013). Hair of monkeys grows at an average speed of 1 cm/month, and the cortisol is constantly deposited in the growing hair shaft. This makes cortisol measurement from newly grown hair capturing systemic cortisol response over the period of hair growth, and therefore can serve as a biological marker for the chronic HPA reactivity (Russell et al., 2012). In this study, prolonged glucocorticoid exposure induced blunted cortisol reactivity in response to acute restraint stress but an exaggerated cortisol response to chronic stress experienced during the treatment. This indicated both the acute and chronic HPA reactivity were disturbed as a result of chronic glucocorticoid treatment.

The hyper-secreted cortisol can cross the blood brain barrier to rob the brain of dopamine, a neurotransmitter that plays a critical role in the subjective pleasure associated with positive rewards (Wise, 2008). This is also evidenced by our study that the monkeys exposed to chronic glucocorticoid treatment have decreased levels of dopamine in the cerebrospinal fluid, which induces them showing less of a preference for sucrose solution, a good manifestation of anhedonia. Postmortem investigations, especially the subjects with severe depression, have also demonstrated reduced concentrations of dopamine both in the cerebrospinal fluid and in brain regions that mediate mood and motivation (Dunlop and Nemeroff, 2007). It has also been found that drugs decreasing the dopamine level or the dopamine receptor antagonist can increase the duration of huddling behavior in monkeys (McKinney et al., 1971; Rosenzweig-Lipson et al., 1994).

Chronic glucocorticoid treatment caused severe damages on stress reactivity and neurotransmitter systems, which induced significant changes in external behavioral phenotype, such as increases in the huddling behavior reflecting depressed mood, and decreases in sucrose solution consumption reflecting anhedonia. These are two core symptoms of human depression. However, this behavioral depression was not induced by

decreases in exploration, locomotion, stereotyping and self-grooming, as these behaviors did not change significantly throughout the treatment. This was also not the result of poor health caused by glucocorticoid treatment as no significant changes over time were observed in monkeys' body weights. Although systemic glucocorticoids play an integral role in the management of many inflammatory and immunologic conditions, there are side effects. Prolonged glucocorticoids treatment commonly causes weight gain and redistribution of adipose tissue. The body weights of monkeys exhibited slight increases, but no significant changes were observed. This is possibly because the glucocorticoid treatment was relatively short in duration (only 7 weeks). The monkeys' depression had become obvious before a significant weight gain. Further correlation analysis showed that this behavioral depression was caused by abnormal HPA axis reactivity, including both acute and chronic stress reactivity, and it was also related to neurotransmitter deficiency, such as a decreased level of dopamine in CSF.

The behavioral alterations were not significant until 6 weeks after the first daily treatment, and the data justified the conclusion that prolonged glucocorticoid exposure can induce depression-like phenotype in rhesus macaques. The application of this primate model can help clarifying the role of glucocorticoid in stress-induced depressive disorders, as well as screening for novel therapeutic targets and specific preventive strategies for hypercortisolemia-induced depression.

AUTHOR CONTRIBUTIONS

All authors listed have made a substantial, direct and intellectual contribution to the work, and approved it for publication.

FUNDING

This research was supported by the National Natural Science Foundation of China (31700897, 81760868, 81471312, 81771387, 81460352, 81500983, 31700910, and 31800901), the Applied Basic Research Programs of Science and Technology Commission Foundation of Yunnan Province (2018FB053, 2018FB052, 2016FA037, 2017FB109, and 2014FA047), the China Postdoctoral Science Foundation (2018M631105), the Training Project for Yunnan Provincial Young and Middle-aged Leaders and Reserve Talents (2015HB052), the National Program for Key Basic Research Projects (973 Program: 2015CB755605), and the Strategic Priority Research Program of the Chinese Academy of Sciences (XDB32060200).

REFERENCES

Altmann, J. (1974). Observational study of behavior: sampling methods. *Behaviour* 49, 227–267. doi: 10.1163/156853974X00534

American-Psychiatric-Association (2013). *Diagnostic and Statistical Manual of Mental Disorders (DSM-5)*. Washington, DC: American Psychiatric Pub. doi: 10.1176/appi.books.9780890425596

Antonijevic, I. A., and Steiger, A. (2003). Depression-like changes of the sleep-EEG during high dose corticosteroid treatment in patients with multiple sclerosis. *Psychoneuroendocrinology* 28, 780–795. doi: 10.1016/S0306-4530(02)00085-9

Belmonte, J. C. I., Callaway, E. M., Churchland, P., Caddick, S. J., Feng, G., Homanics, G. E., et al. (2015). Brains, genes, and primates. *Neuron* 86, 617–631. doi: 10.1016/j.neuron.2015.03.021

Brown, E. S., and Suppes, T. (1998). Mood symptoms during corticosteroid therapy: a review. *Harv. Rev. Psychiatry* 5, 239–246. doi: 10.3109/10673229809000307

Brown, E. S. J., Woolston, D., Frol, A., Bobadilla, L., Khan, D. A., Hanczyc, M., et al. (2004). Hippocampal volume, spectroscopy, cognition, and mood in patients receiving corticosteroid therapy. *Biol. Psychiatry* 55, 538–545. doi: 10.1016/j.biopsych.2003.09.010

Carroll, B. J., and Curtis, G. C. (1976). Neuroendocrine identification of depressed patients. *Aust. N. Z. J. Psychiatry* 10, 13–20. doi: 10.3109/00048677609159480

Carroll, B. J., Curtis, G. C., and Mendels, J. (1976a). Cerebrospinal fluid and plasma free cortisol concentrations in depression. *Psychol. Med.* 6, 235–244. doi: 10.1017/S0033291700013775

Carroll, B. J., Curtis, G. C., and Mendels, J. (1976b). Neuroendocrine regulation in depression: I. Limbic system-adrenocortical dysfunction. *Arch. Gen. Psychiatry* 33, 1039–1044. doi: 10.1001/archpsyc.1976.01770090029002

Carroll, B. J., Curtis, G. C., and Mendels, J. (1976c). Neuroendocrine regulation in depression: Ii. discrimination of depressed from nondepressed patients. *Arch. Gen. Psychiatry* 33, 1051–1058.

Charney, D. S., and Manji, H. K. (2004). Life stress, genes, and depression: multiple pathways lead to increased risk and new opportunities for intervention. *Sci. Signal.* 2004:re5. doi: 10.1126/stke.2252004re5

D'armiento, M., Reda, G., Bisignani, G., Tabolli, S., Cappellaci, S., Lulli, P., et al. (1983). No linkage between HLA and congenital adrenal hyperplasia due to 17 alpha-hydroxylase deficiency. *N. Engl. J. Med.* 308, 970–971. doi: 10.1056/NEJM198304213081621

Davenport, M. D., Lutz, C. K., Tiefenbacher, S., Novak, M. A., and Meyer, J. S. (2008). A rhesus monkey model of self-injury: effects of relocation stress on behavior and neuroendocrine function. *Biol. Psychiatry* 63, 990–996. doi: 10.1016/j.biopsych.2007.10.025

Davenport, M. D., Tiefenbacher, S., Lutz, C. K., Novak, M. A., and Meyer, J. S. (2006). Analysis of endogenous cortisol concentrations in the hair of rhesus macaques. *Gen. Comp. Endocrinol.* 147, 255–261. doi: 10.1016/j.ygcen.2006.01.005

Dunlop, B. W., and Nemeroff, C. B. (2007). The role of dopamine in the pathophysiology of depression. *Arch. Gen. Psychiatry* 64, 327–337. doi: 10.1001/archpsyc.64.3.327

Feng, X., Wang, L., Yang, S., Qin, D., Wang, J., Li, C., et al. (2011). Maternal separation produces lasting changes in cortisol and behavior in rhesus monkeys. *Proc. Natl. Acad. Sci. U.S.A.* 108, 14312–14317. doi: 10.1073/pnas.1010943108

Gaillard, R., Gourion, D., and Llorca, P. M. (2013). Anhedonia in depression. *Encephale* 39, 296–305. doi: 10.1016/j.encep.2013.07.001

Garde, K. (2007). Depression–gender differences. *Ugeskrift Laeger* 169, 2422–2425.

Gregus, A., Wintink, A. J., Davis, A. C., and Kalynchuk, L. E. (2005). Effect of repeated corticosterone injections and restraint stress on anxiety and depression-like behavior in male rats. *Behav. Brain Res.* 156, 105–114. doi: 10.1016/j.bbr.2004.05.013

Harlow, H. F., and Suomi, S. J. (1971). Production of depressive behaviors in young monkeys. *J. Autism Dev. Disord.* 1, 246–255. doi: 10.1007/BF01557346

Henn, F., Vollmayr, B., and Sartorius, A. (2004). Mechanisms of depression: the role of neurogenesis. *Drug Discov. Today* 1, 407–411. doi: 10.1016/j.ddmec.2004.10.007

Horie, H., Kidowaki, T., Koyama, Y., Endo, T., Homma, K., Kambegawa, A., et al. (2007). Specificity assessment of immunoassay kits for determination of urinary free cortisol concentrations. *Clin. Chim. Acta* 378, 66–70. doi: 10.1016/j.cca.2006.10.018

Hugo, C., Seier, J., Mdhluli, C., Daniels, W., Harvey, B. H., Du Toit, D., et al. (2003). Fluoxetine decreases stereotypic behavior in primates. *Prog.*

Neuropsychopharmacol. Biol. Psychiatry 27, 639–643. doi: 10.1016/S0278-5846(03)00073-3

Johnson, S. A., Fournier, N. M., and Kalynchuk, L. E. (2006). Effect of different doses of corticosterone on depression-like behavior and HPA axis responses to a novel stressor. *Behav. Brain Res.* 168, 280–288. doi: 10.1016/j.bbr.2005.11.019

Kalynchuk, L. E., Gregus, A., Boudreau, D., and Perrot-Sinal, T. S. (2004). Corticosterone increases depression-like behavior, with some effects on predator odor-induced defensive behavior, in male and female rats. *Behav. Neurosci.* 118, 1365–1377. doi: 10.1037/0735-7044.118.6.1365

Kelly, W. F., Checkley, S. A., Bender, D. A., and Mashiter, K. (1983). Cushing's syndrome and depression–a prospective study of 26 patients. *Br. J. Psychiatry* 142, 16–19. doi: 10.1192/bjp.142.1.16

Linkowski, P., Mendlewicz, J., Leclercq, R., Brasseur, M., Hubain, P., Golstein, J., et al. (1985). The 24-Hour Profile of Adrenocorticotropin and Cortisol in Major Depressive Illness. *J. Clin. Endocrinol. Metab.* 61, 429–438. doi: 10.1210/jcem-61-3-429

Maidana, P., Bruno, O. D., and Mesch, V. (2013). A critical analysis of cortisol measurements: an update. *Medicina* 73, 579–584.

Marks, W., Fournier, N. M., and Kalynchuk, L. E. (2009). Repeated exposure to corticosterone increases depression-like behavior in two different versions of the forced swim test without altering nonspecific locomotor activity or muscle strength. *Physiol. Behav.* 98, 67–72. doi: 10.1016/j.physbeh.2009.04.014

Mathers, C. D., and Loncar, D. (2006). Projections of global mortality and burden of disease from 2002 to 2030. *PLoS Med.* 3:e442. doi: 10.1371/journal.pmed.0030442

McKinney, W. T. Jr., Eising, R. G., Moran, E. C., Suomi, S. J., and Harlow, H. F. (1971). Effects of reserpine on the social behavior of rhesus monkeys. *Dis. Nervous Syst.* 32, 735–741.

Nemeroff, C. (1998). The neurobiology of depression. *Sci. Am.* 278, 42–49. doi: 10.1038/scientificamerican0698-42

Okuyama-Tamura, M., Mikuni, M., and Kojima, I. (2003). Modulation of the human glucocorticoid receptor function by antidepressive compounds. *Neurosci. Lett.* 342, 206–210. doi: 10.1016/S0304-3940(03)00261-1

Pariante, C. M., Kim, R. B., Makoff, A., and Kerwin, R. W. (2003). Antidepressant fluoxetine enhances glucocorticoid receptor function in vitro by modulating membrane steroid transporters. *Br. J. Pharmacol.* 139, 1111–1118. doi: 10.1038/sj.bjp.0705357

Pariante, C. M., Makoff, A., Lovestone, S., Feroli, S., Heyden, A., Miller, A. H., et al. (2001). Antidepressants enhance glucocorticoid receptor function in vitro by modulating the membrane steroid transporters. *Br. J. Pharmacol.* 134, 1335–1343. doi: 10.1038/sj.bjp.0704368

Parks, K. A., and Novak, M. A. (1993). Observations of increased activity and tool use in captive rhesus monkeys exposed to troughs of water. *Am. J. Primatol.* 29, 13–25. doi: 10.1002/ajp.1350290103

Paul, I. A., English, J. A., and Halaris, A. (2000). Sucrose and quinine intake by maternally-deprived and control rhesus monkeys. *Behav. Brain Res.* 112, 127–134. doi: 10.1016/S0166-4328(00)00173-X

Paykel, E. S. (2003). Life events and affective disorders. *Acta Psychiatr. Scand.* 108, 61–66. doi: 10.1034/j.1600-0447.108.s418.13.x

Piper, M., Treuting, S., and Dintzis, M. (2011). *Comparative Anatomy and Histology: a Mouse and Human Atlas*. Amsterdam: Elsevier.

Qin, D., Rizak, J., Chu, X., Li, Z., Yang, S., Lü, L., et al. (2015a). A spontaneous depressive pattern in adult female rhesus macaques. *Sci. Rep.* 5:11267. doi: 10.1038/srep11267

Qin, D., Rizak, J., Feng, X., Yang, S., Yang, L., Fan, X., et al. (2015b). Cortisol responses to chronic stress in adult macaques: moderation by a polymorphism in the serotonin transporter gene. *Behav. Brain Res.* 278, 280–285. doi: 10.1016/j.bbr.2014.10.001

Qin, D. D., Dominic Rizak, J., Feng, X. L., Chu, X. X., Yang, S. C., Li, C. L., et al. (2013). Social rank and cortisol among female rhesus macaques (*Macaca mulatta*). *Zool. Res.* 34, E42–E49. doi: 10.3724/SP.J.1141.2013.E02E42

Qin, D. D., Rizak, J., Feng, X. L., Yang, S. C., Lü, L. B., Pan, L., et al. (2016). Prolonged secretion of cortisol as a possible mechanism underlying stress and depressive behaviour. *Sci. Rep.* 6:30187. doi: 10.1038/srep30187

Rogers, J., Shelton, S. E., Shelledy, W., Garcia, R., and Kalin, N. H. (2008). Genetic influences on behavioral inhibition and anxiety in juvenile rhesus macaques. *Genes Brain Behav.* 7, 463–469. doi: 10.1111/j.1601-183X.2007.00381.x

Rosenzweig-Lipson, S., Hesterberg, P., and Bergman, J. (1994). Observational studies of dopamine D1 and D2 agonists in squirrel monkeys. *Psychopharmacology* 116, 9–18. doi: 10.1007/BF02244865

Russell, E., Koren, G., Rieder, M., and Van Uum, S. (2012). Hair cortisol as a biological marker of chronic stress: current status, future directions and unanswered questions. *Psychoneuroendocrinology* 37, 589–601. doi: 10.1016/j.psyneuen.2011.09.009

Sachar, E. J., Hellman, L., Roffwarg, H. P., Halpern, F. S., Fukushima, D. K., and Gallagher, T. F. (1973). DIsrupted 24-hour patterns of cortisol secretion in psychotic depression. *Arch. Gen. Psychiatry* 28, 19–24. doi: 10.1001/archpsyc.1973.01750310011002

Scott, L., and Dinan, T. (1998). Urinary free cortisol excretion in chronic fatigue syndrome, major depression and in healthy volunteers. *J. Affect. Disord.* 47, 49–54. doi: 10.1016/S0165-0327(97)00101-8

Shively, C. A., Register, T. C., Friedman, D. P., Morgan, T. M., Thompson, J., and Lanier, T. (2005). Social stress-associated depression in adult female cynomolgus monkeys (Macaca fascicularis). *Biol. Psychol.* 69, 67–84. doi: 10.1016/j.biopsycho.2004.11.006

Song, C., and Leonard, B. E. (2005). The olfactory bulbectomised rat as a model of depression. *Neurosci. Biobehav. Rev.* 29, 627–647. doi: 10.1016/j.neubiorev.2005.03.010

Sonino, N., Fava, G. A., Raffi, A. R., Boscaro, M., and Fallo, F. (1998). Clinical correlates of major depression in cushing's disease. *Psychopathology* 31, 302–306. doi: 10.1159/000029054

Staufenbiel, S. M., Penninx, B. W., Spijker, A. T., Elzinga, B. M., and Van Rossum, E. F. (2013). Hair cortisol, stress exposure, and mental health in humans: a systematic review. *Psychoneuroendocrinology* 38, 1220–1235. doi: 10.1016/j.psyneuen.2012.11.015

Sterner, E. Y., and Kalynchuk, L. E. (2010). Behavioral and neurobiological consequences of prolonged glucocorticoid exposure in rats: relevance to depression. *Prog. Neuropsychopharmacol. Biol. Psychiatry* 34, 777–790. doi: 10.1016/j.pnpbp.2010.03.005

Träskman, L., Tybring, G., Åsberg, M., Bertilsson, L., Lantto, O., and Schalling, D. (1980). Cortisol in the CSF of depressed and suicidal patients. *Arch. Gen. Psychiatry* 37, 761–767. doi: 10.1001/archpsyc.1980.01780200039004

Van Weerden, W. M., Bierings, H. G., Van Steenbrugge, G. J., De Jong, F. H., and Schröder, F. H. (1992). Adrenal glands of mouse and rat do not synthesize androgens. *Life Sci.* 50, 857–861. doi: 10.1016/0024-3205(92)90204-3

Vedhara, K., Miles, J., Bennett, P., Plummer, S., Tallon, D., Brooks, E., et al. (2003). An investigation into the relationship between salivary cortisol, stress, anxiety and depression. *Biol. Psychol.* 62, 89–96. doi: 10.1016/S0301-0511(02)00128-X

Wasser, S. K., Hunt, K. E., Brown, J. L., Cooper, K., Crockett, C. M., Bechert, U., et al. (2000). A generalized fecal glucocorticoid assay for use in a diverse array of nondomestic mammalian and avian species. *Gen. Comp. Endocrinol.* 120, 260–275. doi: 10.1006/gcen.2000.7557

Wennig, R. (2000). Potential problems with the interpretation of hair analysis results. *Forensic Sci. Int.* 107, 5–12. doi: 10.1016/S0379-0738(99)00146-2

Wise, R. A. (2008). Dopamine and reward: the anhedonia hypothesis 30 years on. *Neurotox. Res.* 14, 169–183. doi: 10.1007/BF03033808

Xu, Z., Zhang, Y., Hou, B., Gao, Y., Wu, Y., and Zhang, C. (2011). Chronic corticosterone administration from adolescence through early adulthood attenuates depression-like behaviors in mice. *J. Affect. Disord.* 131, 128–135. doi: 10.1016/j.jad.2010.11.005

Yang, L., and Beal, M. (2011). Determination of neurotransmitter levels in models of parkinson's disease by HPLC-ECD. *Methods Mol. Biol.* 793, 401–415. doi: 10.1007/978-1-61779-328-8_27

Conflict of Interest Statement: The authors declare that the research was conducted in the absence of any commercial or financial relationships that could be construed as a potential conflict of interest.

frontiers in Neuroscience

ORIGINAL RESEARCH
published: 14 March 2019
doi: 10.3389/fnins.2019.00195

Expression of Dopamine Receptors in the Lateral Hypothalamic Nucleus and Their Potential Regulation of Gastric Motility in Rats With Lesions of Bilateral Substantia Nigra

Yan-Li Yang[1], Xue-Rui Ran[1], Yong Li[1], Li Zhou[1], Li-Fei Zheng[2], Yu Han[3], Qing-Qing Cai[1], Zhi-Yong Wang[1] and Jin-Xia Zhu[1,2]**

[1] Xinxiang Key Laboratory of Molecular Neurology, Department of Human Anatomy, School of Basic Medical Sciences, Xinxiang Medical University, Xinxiang, China, [2] Department of Physiology and Pathophysiology, School of Basic Medical Sciences, Capital Medical University, Beijing, China, [3] Department of Gastroenterology, The First Affiliated Hospital of Xinxiang Medical University, Xinxiang, China

OPEN ACCESS

Edited by:
Xue Qun Chen,
Zhejiang University, China

Reviewed by:
Sumei Liu,
University of Wisconsin–La Crosse, United States
Weifang Rong,
Shanghai Jiao Tong University, China

***Correspondence:**
Zhi-Yong Wang
wanliheng@vip.163.com
Jin-Xia Zhu
zhu_jx@ccmu.edu.cn

Specialty section:
This article was submitted to Neuroendocrine Science, a section of the journal Frontiers in Neuroscience

Received: *15 January 2019*
Accepted: *19 February 2019*
Published: *14 March 2019*

Citation:
Yang Y-L, Ran X-R, Li Y, Zhou L, Zheng L-F, Han Y, Cai Q-Q, Wang Z-Y and Zhu J-X (2019) Expression of Dopamine Receptors in the Lateral Hypothalamic Nucleus and Their Potential Regulation of Gastric Motility in Rats With Lesions of Bilateral Substantia Nigra. Front. Neurosci. 13:195. doi: 10.3389/fnins.2019.00195

Most Parkinson's Disease (PD) patients experience gastrointestinal (GI) dysfunction especially the gastroparesis, but its underlying mechanism is not clear. We have previously demonstrated that the neurons in the substantia nigra (SN) project to the lateral hypothalamic nucleus (LH) and the dorsal motor nucleus of vagus (DMV) receives the neural projection from LH by the means of anterograde and retrograde neural tracing technology. Orexin A (OXA) is predominately expressed in the LH. It has been reported that OXA can alter the gastric motility through the orexin receptor 1 (OX1R) in DMV. We speculated that this SN-LH-DMV pathway could modulate the motility of stomach because of the important role of LH and DMV in the regulation of gastric motility. However, the distribution and expression of dopamine receptors (DR) in the LH is unknown. In the present study, using a double-labeling immunofluorescence technique combined with confocal microscopy, we significantly extend our understanding of the SN-LH-DMV pathway by showing that (1) a considerable quantity of dopamine receptor 1 and 2 (D1 and D2) was expressed in the LH as well as the OX1R was expressed in the DMV; (2) Nearly all of the D1-immuoreactve (IR) neurons were also OXA-positive while only a few neurons express both D2 and OXA in the LH, and the DR-positive neurons were surrounded by the dopaminergic neural fibers; In the DMV, OX1R were colocalized with choline acetyltransferase (ChAT)-labeled motor neurons; (3) When the gastroparesis was induced by the destruction of dopaminergic neurons in the SN, the decreased expression of D1 and OXA was observed in the LH as well as the reduced OX1R and ChAT expression in the DMV. These findings suggest that SN might regulate the function of OXA-positive neurons via D1 receptor, which then affect the motor neurons in the DMV through OX1R. If the SN is damaged the vagal pathway would be affected, which may lead to gastric dysfunction. The present study raises the possibility that the SN-LH-DMV pathway can regulate the movement of stomach.

Keywords: dopamine receptor, lateral hypothalamic nucleus, orexin receptor 1, gastroparesis, Parkinson's disease

INTRODUCTION

Parkinson's disease (PD) is characterized by loss of dopaminergic neurons in the substantia nigra (SN) and decrease of dopamine level in the striatum of basal ganglia (Lees et al., 2009). Over 80% of PD patients experience gastrointestinal (GI) dysfunctions including gastroparesis (Jost and Eckardt, 2003; Jost, 2010). Accumulating evidence demonstrates that cholinergic neuron degeneration contributes to gastroparesis in PD (Travagli and Anselmi, 2016). We previously have reported the reduced cholinergic markers in the dorsal motor nucleus of vagus (DMV) and gastric muscularis in rats with bilateral SN lesion by 6-hydroxydopamine (6-OHDA). However, it is unknown how the SN influences the DMV.

The lateral hypothalamic nucleus (LH) in diencephalon has been identified as an important brain region that innervates multiple brain regions and regulates many important physiological processes including feeding, reward behaviors and autonomic function (Berthoud and Munzberg, 2011). Orexin (OX) neurons are primarily located in the LH (Sakurai et al., 1998; Takahashi et al., 2015). The OX neuropeptide family consists of orexin A (OXA) and B (OXB), which are encoded by the same pre-mRNA (Date et al., 1999; Sakurai et al., 1999). OXA regulates food intake (Dube et al., 1999) and gastric emptying in rats (Ehrstrom et al., 2005; Bulbul et al., 2010b). The OXA neurons stimulation or destruction will alter the movement of the stomach (Guo et al., 2018). Both the dopamine receptor 1 and 2 (D1 and D2) mRNA were reported to be expressed in LH neurons. OX neurons regulate GI functions through the brain-gut axis (Kirchgessner, 2002; Kukkonen et al., 2002). Microinjection of OXA into the DMV increased intragastric pressure and antral motility in anesthetized rats (Krowicki et al., 2002). Thus, OXA may regulate GI motility through the DMV (Grabauskas and Moises, 2003).

The DMV regulates upper GI functions, such as gastric motility. The orexin receptor 1 (OX1R) is highly expressed in the neurons of DMV, especially in the preganglionic neurons that innervate the stomach (Krowicki et al., 2002; Bulbul et al., 2010a). We previously have demonstrated that the SN and the DMV can contact with each other indirectly through the LH. By means of anterograde and retrograde neural tracing technology, we found that the neurons in the SN can project to the LH and the DMV receives neural projection from the LH (Wang et al., 2014). It is reported that a large number of OX neurons were lost in the LH of PD patients (Thannickal et al., 2007, 2008).

Based on the above results, we speculated that the OXA neurons in the LH could be regulated by dopaminergic projections from the SN through D1 or D2, destruction of the SN might change the expression of dopamine receptors (DR) in the LH and then orexin receptor (OXR) in the DMV. In the present study, double-labeling immunofluorescence procedures were performed to detect the distribution of tyrosine hydroxylase (TH), D1 and D2 in the LH and their co-localization with OXA neurons. The alternations of D1, D2, and OXA in the LH, and OX1R and choline acetyltransferase (ChAT) in the DMV were observed in the rats with bilateral SN injection of 6-OHDA. The present study may provide morphological evidences for DA/DR and OXA/OXR promoting gastric motility through SN-LH-DMV pathway.

MATERIALS AND METHODS

Animals

Twenty-five adult male Sprague-Dawley rats (180–220 g) were purchased from Beijing Vital River Laboratory Animal Technology Co., Ltd. All experiments were performed in accordance with the guidelines established by the National Institutes of Health (NIH, United States) and were approved by the Animal Care and Use Committee of Xinxiang Medical University, Xinxiang, China. All efforts were made to minimize animal suffering, and the minimal number of animals necessary to produce reliable scientific data was used.

6-OHDA Animal Models

The methods used have been previously described (Zheng et al., 2014). Rats were anesthetized by intraperitoneal injection with chloral hydrate (0.4 g/kg) and placed on stereotaxic instrument. Two small areas of the skull were exposed (coordinates: AP, −5.6 mm; ML, ± 2.0 mm; DV, −7.5 mm), and 6-OHDA (4 μg in 2 μl of 0.9% saline containing 0.05% ascorbic acid) was injected with a 10 μl Hamilton syringe. Control groups were injected with 0.05% ascorbic acid/saline. The rats injected with 6-OHDA in the SN were referred to as 6-OHDA rats. Subsequent experiments were conducted at 6 weeks after 6-OHDA administration.

Tissue Preparation

After deep anesthetization with chloral hydrate, rats received a thoracotomy and were perfused through the left ventricle with 250 ml of saline followed by 250 ml 4% paraformaldehyde in 0.01 M PBS (pH 7.4). The brains were immediately removed and immersed into 4% paraformaldehyde for a 12 h post-fixation period and then placed in 30% sucrose in 0.01 M PBS (pH 7.4) for at least 48 h until the dehydration achieved. The serial coronal sections which were 20 μm in thickness were made with a cryostat (Leica CM1850, St. Gallen, Switzerland). The tissue sections were air-dried overnight at room temperature and then stored at −80°C. In some experiments, the samples of dorsal medulla were collected (as descripted in our previous reports) on ice and immediately frozen in liquid nitrogen.

Immunofluorescence Staining

The methods used have been described previously (Wang et al., 2016). The brain sections were permeabilized with PBS containing 0.3% Triton X-100, then blocked for unspecific binding with 5% goat serum for 30 min. Sections were then incubated overnight in a mixture of two primary antibodies derived from different host species for 12–16 h at 4°C (**Table 1**, TH/D1, TH/D2, OXA/TH, OXA/D1, OXA/D2, and OX1R/ChAT) and then incubated with the secondary antibodies for 1 h at room temperature. Micrographs were obtained using a confocal microscope (Olympus, FV1000).

The OXA-IR, D1R-IR, and D2R-IR neurons in the LH were counted from every three LH-containing section per animal

($n = 3$). Five different fields (150 pixel *150 pixel) of each section (512 pixel *512 pixel, 200×) were selected randomly for the neuron count. The average number of neurons in each section was calculated from nine sections of three rats in total. To reduce the counting error, the number of line pressing cells was only counted on one side and moves arduously.

Western Blot Analysis

As in our previous reports (Zheng et al., 2014), tissues were homogenized in 300 μl cold lysis buffer supplemented with protease inhibitors for protein extraction. Proteins (100 μg) were loaded in a 10% SDS-PAGE gel and transferred onto a nitrocellulose membrane (NC membrane, Millipore, United States) at 4°C. After blocking with 10% non-fat dry milk in TBST for 2 h, the membranes were incubated with primary antibodies against ChAT (Rabbit polyclonal, Proteintech/20747-1-AP, 1:1,000), OX1R (Rabbit polyclonal, Abcam/ab68718, 1:500), or GAPDH (Rabbit polyclonal, Sigma/G9545, 1:5,000) overnight at 4°C. After washing, the membranes were incubated with horseradish-peroxidase-conjugated IgG (Pierce, Rockford, IL, United States) for 1 h at room temperature, then washed in TBST. Finally, the membranes were scanned with an Odyssey Infrared Imager (LI-COR, NE, United States), and analyzed using Odyssey software (version 1.2).

Gastric Emptying

The methods used have been described previously (Zheng et al., 2014). Following a 24-h fast, a 2.5 ml barium meal was administrated to each rat through oral gavage. Plain radiographs of the GI tract were obtained using a KODAK *in vivo* Imaging System FX with the focus distance manually fixed to 50 ± 1 cm. The exposure time was adjusted to 30 s. Images were recorded at different time points (30, 60, and 90 min) after the consumption of the barium meal. Gastric emptying (GE) was calculated according to the following formula:

$$GE(\%) = [1 - (\text{barium meal at Time 90 min} / \text{barium meal at Time zero})] \times 100.$$

TABLE 1 | Antibodies used in the immunofluorescent study.

Antigen	Antibody	Dilution	Source/Catalog No.
TH	Mouse monoclonal	1:5000	Sigma/T1299
TH	Rabbit polyclonal	1:500	Abcam/ab112
OXA	Mouse monoclonal	1:50	Santa cruz/SC-80263
ChAT	Mouse monoclonal	1:100	Abcam/ab35948
OX1R	Rabbit polyclonal	1:250	Abcam/ab68718
D1	Rabbit polyclonal	1:100	Alomone/ADR-001
D2	Rabbit polyclonal	1:100	Alomone/ADR-002
Alexa fluor 488-labeled anti-mouse IgG	Goat	1:500	Beyotime/A0428
Alexa fluor 488-labeled anti-rabbit IgG	Goat	1:500	Beyotime/A0423
Cy3-labeled anti-mouse IgG	Goat	1:500	Beyotime/A0521
Cy3-labeled anti-rabbit IgG	Goat	1:500	Beyotime/A0516

TH, tyrosine hydroxylase; ChAT, choline acetyltransferase; D1, dopamine 1 receptor; D2, dopamine 2 receptor; OXA, orexin A; OX1R, orexin receptor 1.

Anterograde Tracing

Approximately 4 μl of 20% Biotinylated Dextran Amines (BDA) (Eugene/n7167) (3 mg dissolved in 15 μl 0.01 M PBS, pH 7.4) was injected into the left SN (coordinates: AP, −5.6 mm; ML, −2.0 mm; DV, −7.5 mm) with the same Hamilton microsyringe. Seven days later, the animals were killed by decapitation, and the brains were removed for detection of the anterograde tracing fibers.

The sections from the anterograde tracing group were processed for observation of the injection site in the SN and the distribution of BDA-labeled fibers in the diencephalon and brainstem. The sections were incubated in 0.3% Triton X-100 in 0.01 M PBS (pH 7.6) for 15 min prior to incubation in fluorescent isothiocyanate (TEX RED)-labeled avidin D (1:200,A-2001,Vector Laboratories, Burlingame, CA, United States) at room temperature for 2 h. After incubation, all sections were rinsed in 0.01 M PBS, mounted onto gelatin-coated glass slides, air-dried, and cover-slipped with a mixture of 50% (v/v) glycerin and 2.5% (w/v) triethylene diamine (anti-fadingagent) in 0.01 M PBS. The injection sites and distribution of BDA-labeled fibers were examined under a fluorescence microscope.

Statistical Analysis

The values are presented as the means ± S.E.M. (standard error of the mean) from at least three independent experiments; "n" refers to the number of animals or tissue samples from different animals. Statistical analysis was conducted using unpaired *t*-tests. The level of significance was set at $P < 0.05$.

RESULTS

Neural Projection From the SN to the LH and the Distribution of TH-, D1-, D2-, and OXA-IR Neurons and Their Colocalization in the LH

The anterograde tracer BDA was microinjected into the left SN to determine whether BDA-labeled fibers could be observed in the DMV. After 7 days, a dense BDA stained area was located at the injection area, the left SN pars compacta (**Figure 1Aa**). Dense puncta and irregular curved BDA positive nerve fibers were observed in the LH (**Figures 1Ac,d**). However, no BDA positive fibers were found in the DMV (**Figure 1Ab**).

Double-label immunofluorescence was performed to assess the distribution patterns of OXA, TH, D1, and D2 in the LH. The results suggested that a considerable quantity OXA-IR, D1-IR, and D2-IR neurons were clearly observed throughout

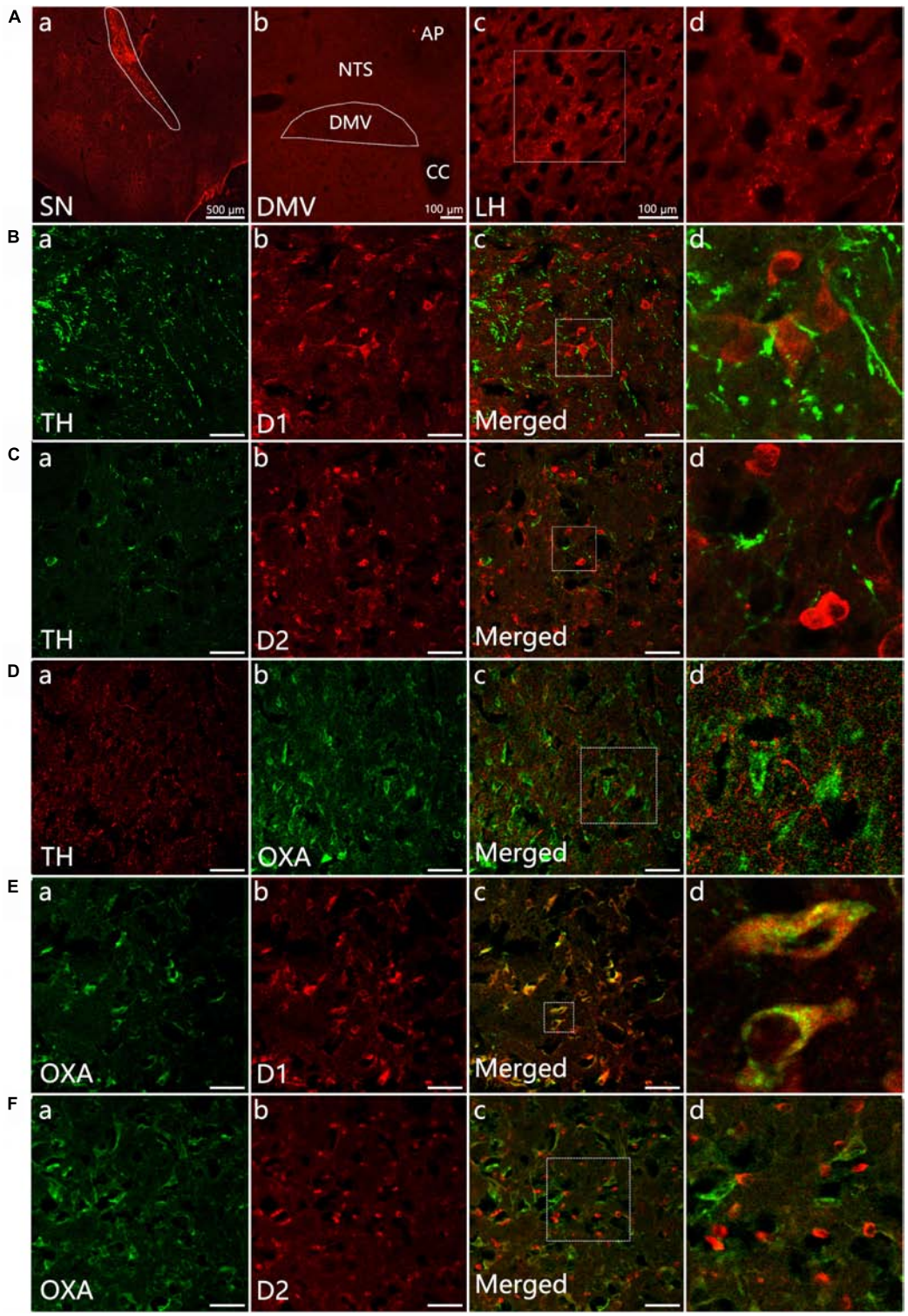

FIGURE 1 | Neural projection from the SN to the LH and distribution of TH-, D1-, D2- and OXA-IR neurons and their colocalization in the LH. **(Aa)** Injection site (white dotted lines) of BDA in the SN; **(b)** No BDA-labeled fibers were observed in the DMV; **(c)** The expression of BDA-stained anterograde traced fibers in the LH; **(d)** The magnified areas of the white dotted boxes in **(c)**. **(B–F)** Representative confocal photomicrographs of double-immunofluorescence of TH (green) and D1 (red), TH (green)and D2 (red), OXA (green), and TH (red), D1 and OXA, D2, and OXA in the LH. **(d)** Shows a magnified area of the white dotted box in **(c)**. Scale bars in **(B–F)**: 50 μm. TH, tyrosine hydroxylase; D1, dopamine 1 receptor; D2, dopamine 2 receptor; OXA, orexin A.

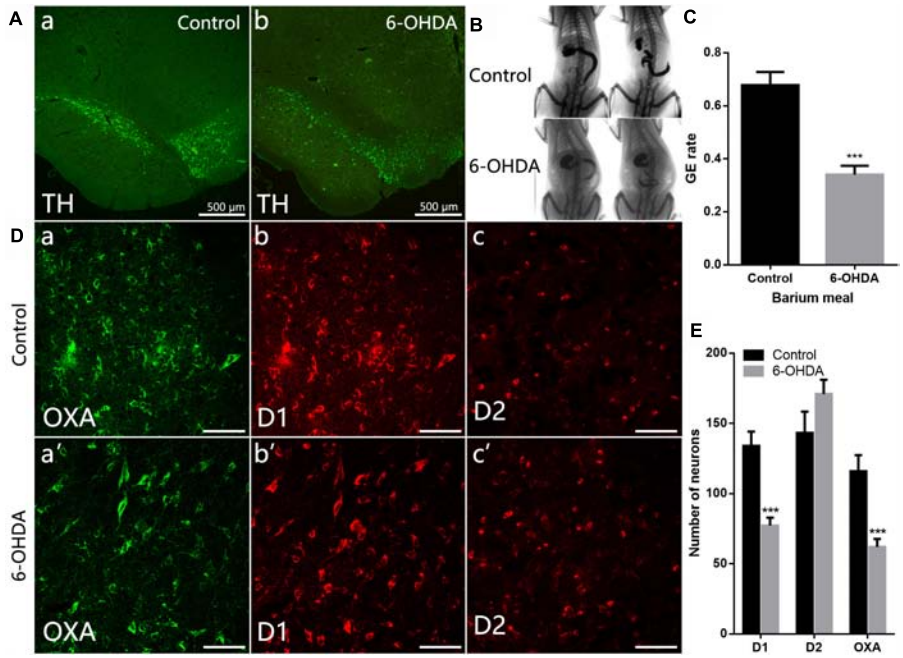

FIGURE 2 | Decreased expression of D1 and OXA in the LH of 6-OHDA rats. **(A)** Expression of TH-IR neurons within the SN in control and 6-OHDA rats; **(B)** Representative images of gastric emptying (GE) at 0 and 90 min after a barium meal in control and 6-OHDA rats; **(C)** GE of barium meals was significantly delayed in 6-OHDA rats compared to control animals; **(D)** Representative alterations in D1, D2, and OXA expression within the LH in control (upper panel) and 6-OHDA rats (lower panel); **(E)** Summary histogram shows a significant decrease number of D1-IR or OXA-IR neurons in the LH, while no significant change of D2-IR neurons in 6-OHDA rats. Scale bars in **(D)**: 50 μm. ***$P < 0.001$.

the LH and surrounded by TH-IR fibers. The TH-IR fibers were punctiform or short-bar in shape, and the distribution was not arranged in any particular manner (**Figures 1B–D**). The OXA was expressed in cytoplasm. We observed that OXA expression was cuneate, gracile, deltoid, buninoid or oval in shape (**Figures 1Db,Ea,Fa**). In the same slice, D1 expression displayed a similar shape as OXA (**Figures 1Bb,Eb**), while D2 expression was buninoid (**Figures 1Cb,Fb**). The numbers of D1-IR, OXA-IR and double-labeled neurons in the LH (n = 3) were 1206, 969, and 895, respectively, which were counted from nine sections of three rats in total. The double-labeled neurons accounted for 74.2% of total D1-labeled neurons and 92.3% of total OXA-labeled neurons. However, only a few neurons were both D2-IR and OXA-IR (**Figure 1F**). The numbers of D2-IR, OXA-IR and their double-labeled neurons in the LH were 1289, 1116, and 334, respectively. The double-labeled neurons accounted for 25.9% of total D2-labeled neurons and 29.9% of total OXA-labeled neurons.

Decreased Expression of D1 and OXA in the LH of 6-OHDA Rats

Distribution of TH-IR neurons in the SN was detected in control and 6-OHDA rats. TH-IR neurons in the SN was considerably reduced in 6-OHDA rats compared with control ones (**Figure 2A**). We further evaluated gastric emptying using an *in vivo* digital X-ray imaging system. The results showed that 67.78 ± 5.0% of the stomach contents were emptied at 90 min in control rats. Meanwhile, only 34.01 ± 3.3% was emptied in the 6-OHDA rats (n = 6, $P < 0.001$) (**Figures 2B,C**).

Compared with control rats (**Figures 2D,E**), the number of D1-IR neurons decreased from 134.0 ± 10.14 to 77.11 ± 5.69 in the 6-OHDA rats (n = 3, $P < 0.001$). The number of OXA-IR neurons was also decreased from 111.6 ± 10.38 to 62.00 ± 5.68 (n = 6, $P < 0.001$) in the LH of 6-OHDA rats. However, the change of D2-IR neurons number was not significant (n = 3, P = 0.14), slightly increased from 143.2 ± 15.21 to 170.9 ± 10.14 in 6-OHDA rats.

Reduced Expression of OX1R and ChAT Protein in the Dorsal Medulla of 6-OHDA Rats

ChAT-IR neurons were densely distributed throughout the DMV, and the distribution was not arranged in any particular manner. Nearly all ChAT-IR neurons were also OX1R-IR (**Figure 3A**). Western blot results showed a significant decrease in the level of OX1R and ChAT protein in the dorsal medulla of 6-OHDA rats, from 1.53 ± 0.07 to 0.42 ± 0.10 (n = 4, $P < 0.001$) and 0.62 ± 0.10 to 0.10 ± 0.01 (n = 4, $P < 0.01$), respectively (**Figures 3B,C**).

DISCUSSION

Most PD patients experience GI dysfunction especially the gastroparesis (Goetze et al., 2006), but its underlying mechanism

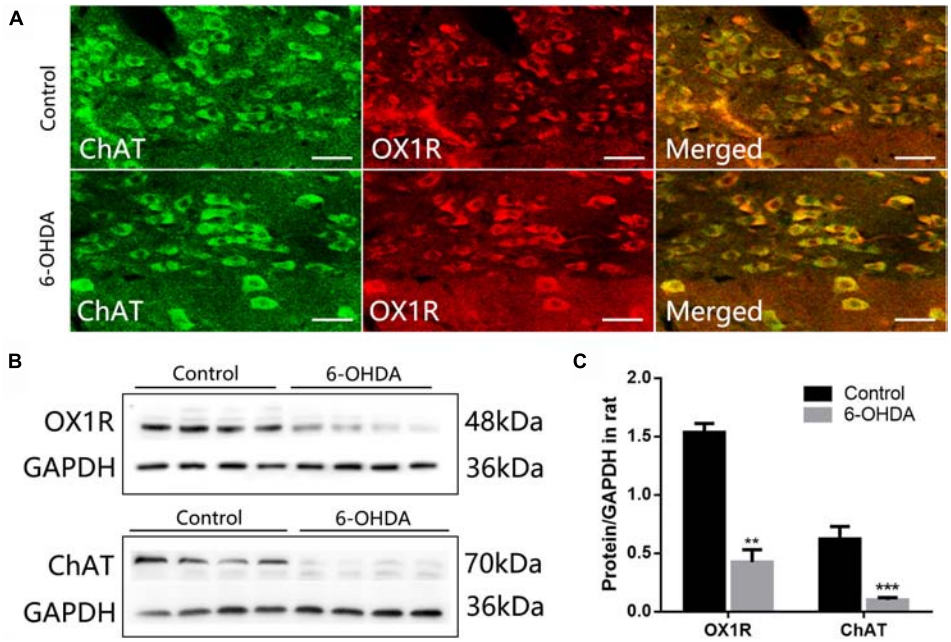

FIGURE 3 | Reduced expression of OX1R and ChAT protein in the dorsal medulla of 6-OHDA rats. **(A)** Colocalization of OX1R and ChAT in the DMV neurons; **(B)** Representative Western blot of OX1R and ChAT in the dorsal medulla from control and 6-OHDA rats. GAPDH was used as a loading control; **(C)** Summary histogram shows that the OX1R and ChAT expression in the dorsal medulla was significantly reduced in 6-OHDA rats. Scale bars: 100 μm. $^{**}P < 0.01$; $^{***}P < 0.001$.

is not clear. Our previous study has demonstrated that the neurons in the SN could project into the LH and the neurons in the DMV receives the neural projection from the LH (Wang et al., 2014). We speculate that this SN-LH-DMV pathway could modulate the gastric motility since the important role of LH and DMV in the regulation of gastric motility (Travagli et al., 2003, 2006; Stuber and Wiser, 2016). In the present study, we have demonstrated that a considerable quantity of D1 and few D2 was expressed in the OXA-positive neurons in the LH, and OX1R was expressed in the cholinergic neurons of the DMV.

Here we significantly extend our understanding of the SN-LH-DMV pathway by showing that (1) a considerable quantity of D1 and D2 was expressed in the LH, and the OX1R was expressed in the DMV; (2) Nearly all of the D1-IR neurons were also OXA-positive, while only a few neurons expressed both D2 and OXA in the LH, meanwhile the DR-positive neurons were surrounded by the catecholaminergic neural fibers; In the DMV, OX1R was colocalized with ChAT-labeled motor neurons; (3) When dopaminergic neurons in the SN were destroyed, the decreased expression of D1 and OXA in the LH, and the reduced OX1R and ChAT expression in the DMV were observed. These findings suggest that neurons from the SN might regulate the function of OXA-positive neurons in the LH via D1 receptor. The dysfunction of the OXA-positive neurons in turn affects the motor neurons in the DMV through OX1R, ultimately leads to the gastric dysmotility. This study provides a morphologic possibility for the SN-LH-DMV pathway in regulating gastric movement.

LH is one of the functional zones in the hypothalamus, and plays an important role in regulating feeding, sleep and wakefulness (Saper, 2002). A lot of OXA-IR neurons exist in the LH, and most of them are lost in the progression of PD (Thannickal et al., 2008). However, the underlying mechanism regulating OXA release from LH remnant neurons in PD patients is not clear. The SN-LH-DMV neural pathway has been observed in our previous study. In the present study, co-labeling of D1 with OXA in the LH provides an evidence that OXA-IR neurons in the LH might be regulated by the dopaminergic fibers from the SN via D1 receptors, which is further confirmed by surrounding dopaminergic fibers located around the D1-IR neurons in the LH. Moreover, OX1R was highly expressed in the DMV neurons. Specifically, it was presented in retrograde labeled preganglionic neurons from the DMV innervating the stomach. OXA can excite neurons by binding to OX1R of the DMV in rats (Krowicki et al., 2002). The OXA plays a stimulatory effect on the gastric emptying in rats (Ehrstrom et al., 2005; Bulbul et al., 2010b). These data support our idea that lesion of dopaminergic neurons in the SN impairs gastric motility might be mediated by the SN-LH-DMV pathway, in which OXA is a connecting factor between the LH and the DMV.

In the present study, after the dopaminergic neurons in the SN are destroyed by the 6-OHDA, the expressions of both D1 and OXA in the LH, and OX1R and ChAT in the DMV were significantly decrease, suggesting that the excitatory effect from the SN on OXA-positive neurons of the LH and in turn on the vagal cholinergic motor neurons of the DMV would be lowered, which subsequently resulted to gastroparesis in 6-OHDA rats. D1 receptor is a classic subtype of DR family that belongs to G protein-coupled receptors. D1 activates adenylyl cyclase and upregulates intracellular cAMP signaling pathway, whereas D2

inhibits the adenylyl cyclase and downregulates cAMP levels (Baldessarini and Tarazi, 1996). It seems that the decreased D1 in the LH and OX1R in the DMV, respectively, contribute to attenuated OXA and acetylcholine release, respectively. However, detailed mechanism of alteration of the D1, OX1R, OXA, and ChAT needs to be further studied.

In summary, our present study demonstrates that the down-regulated D1 and OX1R might be involved in the process of gastroparesis in PD through the SN-LH-DMV pathway. The SN-LH-DMV pathway has a potential effect on regulating gastric motility.

DATA AVAILABILITY

All datasets generated for this study are included in the manuscript and/or the supplementary files.

AUTHOR CONTRIBUTIONS

J-XZ and Z-YW designed the research and revised the paper. Y-LY performed the experiments and wrote the manuscript. Z-YW, LZ, and YH helped the data analysis. Q-QC, X-RR, and YL provided technical support. J-XZ, L-FZ, and LZ edited the manuscript.

FUNDING

The present study was supported by The National Key Research and Development Program of China (2016YFC1302203), National Natural Science Foundation of China (81570695, 31200897, and 31400991) and Henan Province Foundation for University Key Youth Scholars (2017GGJS107).

REFERENCES

Baldessarini, R. J., and Tarazi, F. I. (1996). Brain dopamine receptors: a primer on their current status, basic and clinical. *Harv. Rev. Psychiatry* 3, 301–325. doi: 10.3109/10673229609017200

Berthoud, H. R., and Munzberg, H. (2011). The lateral hypothalamus as integrator of metabolic and environmental needs: from electrical self-stimulation to opto-genetics. *Physiol. Behav.* 104, 29–39. doi: 10.1016/j.physbeh.2011.04.051

Bulbul, M., Babygirija, R., Ludwig, K., and Takahashi, T. (2010a). Central orexin-A increases gastric motility in rats. *Peptides* 31, 2118–2122. doi: 10.1016/j.peptides.2010.07.014

Bulbul, M., Tan, R., Gemici, B., Özdem, S., Üstünel, İ, Acar, N., et al. (2010b). Endogenous orexin-A modulates gastric motility by peripheral mechanisms in rats. *Peptides* 31, 1099–1108. doi: 10.1016/j.peptides.2010.03.007

Date, Y., Ueta, Y., Yamashita, H., Yamaguchi, H., Matsukura, S., Kangawa, K., et al. (1999). Orexins, orexigenic hypothalamic peptides, interact with autonomic, neuroendocrine and neuroregulatory systems. *Proc. Natl. Acad. Sci. U.S.A.* 96, 748–753. doi: 10.1073/pnas.96.2.748

Dube, M. G., Kalra, S. P., and Kalra, P. S. (1999). Food intake elicited by central administration of orexins/hypocretins: identification of hypothalamic sites of action. *Brain Res.* 842, 473–477. doi: 10.1016/S0006-8993(99)01824-7

Ehrstrom, M., Levin, F., Kirchgessner, A. L., Schmidt, P. T., Hilsted, L. M., Grybäck, P., et al. (2005). Stimulatory effect of endogenous orexin A on gastric emptying and acid secretion independent of gastrin. *Regul. Pept.* 132, 9–16. doi: 10.1016/j.regpep.2005.07.005

Goetze, O., Nikodem, A. B., Wiezcorek, J., Banasch, M., Przuntek, H., Mueller, T., et al. (2006). Predictors of gastric emptying in Parkinson's disease. *Neurogastroenterol. Motil.* 18, 369–375. doi: 10.1111/j.1365-2982.2006.00780.x

Grabauskas, G., and Moises, H. C. (2003). Gastrointestinal-projecting neurones in the dorsal motor nucleus of the vagus exhibit direct and viscerotopically organized sensitivity to orexin. *J. Physiol.* 549(Pt 1), 37–56. doi: 10.1113/jphysiol.2002.029546

Guo, F., Gao, S., Xu, L., Sun, X., Zhang, N., Gong, Y., et al. (2018). Arcuate nucleus orexin-A signaling alleviates cisplatin-induced nausea and vomiting through the paraventricular nucleus of the hypothalamus in rats. *Front. Physiol.* 9:1811. doi: 10.3389/fphys.2018.01811

Jost, W. H. (2010). Gastrointestinal dysfunction in Parkinson's Disease. *J. Neurol. Sci.* 289, 69–73. doi: 10.1016/j.jns.2009.08.020

Jost, W. H., and Eckardt, V. F. (2003). Constipation in idiopathic Parkinson's disease. *Scand. J. Gastroenterol.* 38, 681–686. doi: 10.1080/00365520310003200

Kirchgessner, A. L. (2002). Orexins in the brain-gut axis. *Endocr. Rev.* 23, 1–15. doi: 10.1210/edrv.23.1.0454

Krowicki, Z. K., Burmeister, M. A., Berthoud, H. R., Scullion, R. T., Fuchs, K., and Hornby, P. J. (2002). Orexins in rat dorsal motor nucleus of the vagus potently stimulate gastric motor function. *Am. J. Physiol. Gastrointest. Liver Physiol.* 283, G465–G472. doi: 10.1152/ajpgi.00264.2001

Kukkonen, J. P., Holmqvist, T., Ammoun, S., and Akerman, K. E. (2002). Functions of the orexinergic/hypocretinergic system. *Am. J. Physiol. Cell Physiol.* 283, C1567–C1591. doi: 10.1152/ajpcell.00055.2002

Lees, A. J., Hardy, J., and Revesz, T. (2009). Parkinson's disease. *Lancet* 373, 2055–2066. doi: 10.1016/S0140-6736(09)60492-X

Sakurai, T., Amemiya, A., Ishii, M., Matsuzaki, I., Chemelli, R. M., Tanaka, H., et al. (1998). Orexins and orexin receptors: a family of hypothalamic neuropeptides and G protein-coupled receptors that regulate feeding behavior. *Cell* 92, 573–585. doi: 10.1016/S0092-8674(00)80949-6

Sakurai, T., Moriguchi, T., Furuya, K., Kajiwara, N., Nakamura, T., Yanagisawa, M., et al. (1999). Structure and function of human prepro-orexin gene. *J. Biol. Chem.* 274, 17771–17776. doi: 10.1074/jbc.274.25.17771

Saper, C. B. (2002). The central autonomic nervous system: conscious visceral perception and autonomic pattern generation. *Annu. Rev. Neurosci.* 25, 433–469. doi: 10.1146/annurev.neuro.25.032502.111311

Stuber, G. D., and Wiser, R. A. (2016). Lateral hypothalamic circuits for feeding and reward. *Nat. Neurosci.* 19, 198–205. doi: 10.1038/nn.4220

Takahashi, K., Ohba, K., and Kaneko, K. (2015). Ubiquitous expression and multiple functions of biologically active peptides. *Peptides* 72, 184–191. doi: 10.1016/j.peptides.2015.04.004

Thannickal, T. C., Lai, Y. Y., and Siegel, J. M. (2007). Hypocretin (orexin) cell loss in Parkinson's disease. *Brain* 130(Pt 6), 1586–1595. doi: 10.1093/brain/awm097

Thannickal, T. C., Lai, Y. Y., and Siegel, J. M. (2008). Hypocretin (orexin) and melanin concentrating hormone loss and the symptoms of Parkinson's disease. *Brain* 131(Pt 1):e87.

Travagli, R. A., and Anselmi, L. (2016). Vagal neurocircuitry and its influence on gastric motility. *Nat. Rev. Gastroenterol. Hepatol.* 13, 389–401. doi: 10.1038/nrgastro.2016.76

Travagli, R. A., Hermann, G. E., Browning, K. N., and Rogers, R. C. (2003). Musings on the wanderer: what's new in our understanding of vago-vagal reflexes? III. Activity-dependent plasticity in vago-vagal reflexes controlling the stomach. *Am. J. Physiol. Gastrointest. Liver Physiol.* 284, G180–G187.

Travagli, R. A., Hermann, G. E., Browning, K. N., and Rogers, R. C. (2006). Brainstem circuits regulating gastric function. *Annu. Rev. Physiol.* 68, 279–305. doi: 10.1146/annurev.physiol.68.040504.094635

Wang, Z. Y., Lian, H., Cai, Q. Q., Song, H. Y., Zhang, X. L., Zhou, L., et al. (2014). No direct projection is observed from the substantia nigra to the dorsal

vagus complex in the rat. *J. Parkinsons Dis.* 4, 375–383. doi: 10.3233/JPD-130279

Wang, Z. Y., Lian, H., Zhou, L., Zhang, Y. M., Cai, Q. Q., Zheng, L. F., et al. (2016). Altered expression of D1 and D2 dopamine receptors in vagal neurons innervating the gastric muscularis externa in a parkinson's disease rat model. *J. Parkinsons Dis.* 6, 317–323. doi: 10.3233/JPD-160817

Zheng, L. F., Song, J., Fan, R. F., Chen, C. L., Ren, Q. Z., Zhang, X. L., et al. (2014). The role of the vagal pathway and gastric dopamine in the gastroparesis of rats after a 6-hydroxydopamine microinjection in the substantia nigra. *Acta Physiol.* 211, 434–446. doi: 10.1111/apha.12229

Conflict of Interest Statement: The authors declare that the research was conducted in the absence of any commercial or financial relationships that could be construed as a potential conflict of interest.

frontiers in Neuroscience

ORIGINAL RESEARCH
published: 26 March 2019
doi: 10.3389/fnins.2019.00264

Treadmill Exercise Ameliorates Depression-Like Behavior in the Rats With Prenatal Dexamethasone Exposure: The Role of Hippocampal Mitochondria

Tianwen Wu[1†], Yan Huang[1†], Yuxiang Gong[2†], Yongjun Xu[1,3], Jianqiang Lu[2], Hui Sheng[1] and Xin Ni[1,4*]*

[1] Department of Physiology, Second Military Medical University, Shanghai, China, [2] School of Kinesiology, Shanghai University of Sport, Shanghai, China, [3] Department of Clinical Genetics and Experimental Medicine, Fuzhou General Hospital, School of Medicine, Xiamen University, Fuzhou, China, [4] Research Center of Molecular Metabolomics, Xiangya Hospital, Central South University, Changsha, China

OPEN ACCESS

Edited by:
Xue Qun Chen,
Zhejiang University, China

Reviewed by:
Li-Tao Yi,
Huaqiao University, China
Jian Qiu,
Oregon Health & Science University, United States

***Correspondence:**
Hui Sheng
huisheng7979@126.com
Xin Ni
nixin@smmu.edu.cn;
nixinsmmu@hotmail.com

[†] These authors have contributed equally to this work

Specialty section:
This article was submitted to Neuroendocrine Science, a section of the journal Frontiers in Neuroscience

Received: 06 January 2019
Accepted: 06 March 2019
Published: 26 March 2019

Citation:
Wu T, Huang Y, Gong Y, Xu Y, Lu J, Sheng H and Ni X (2019) Treadmill Exercise Ameliorates Depression-Like Behavior in the Rats With Prenatal Dexamethasone Exposure: The Role of Hippocampal Mitochondria. Front. Neurosci. 13:264. doi: 10.3389/fnins.2019.00264

Prenatal exposure to synthetic glucocorticoids (sGCs) can increase the risk of affective disorders, such as depression, in adulthood. Given that exercise training can ameliorate depression and improve mitochondrial function, we sought to investigate whether exercise can ameliorate depression-like behavior induced by prenatal sGC exposure and mitochondria function contributes to that behavior. At first, we confirmed that prenatal dexamethasone (Dex) administration in late pregnancy resulted in depression-like behavior and elevated level of circulatory corticosterone in adult offspring. We then found that mRNA and protein expression of a number of mitochondrial genes was changed in the hippocampus of Dex offspring. Mitochondria in the hippocampus showed abnormal morphology, oxidative stress and dysfunction in Dex offspring. Intracerebroventricular (ICV) injection of the mitochondrial superoxide scavenger mitoTEMPO significantly alleviated depression-like behavior but did not significantly affect circulatory corticosterone level in Dex offspring. The adult Dex offspring treated with treadmill exercise starting at four-weeks of age showed ameliorated depressive-like behavior, improved mitochondrial morphology and function and reduced circulatory corticosterone level. Our data suggest mitochondria dysfunction contributes to depression-like behavior caused by prenatal sGC exposure. Intervention with exercise training in early life can reverse depression caused by prenatal Dex exposure, which is associated with improvement of mitochondrial function in the hippocampus.

Keywords: depression, hippocampus, glucocorticoid, mitochondria, exercise

INTRODUCTION

During late gestation, concentration of glucocorticoids (GCs) in the fetal circulation is exponentially increased, and this surge of GCs is critical for fetal organ development including the lungs and brain (Fowden and Forhead, 2009). Therefore, synthetic GCs (sGCs) are usually used to treat pregnant women at risk of preterm delivery in order to promote the development

of fetal organs and impede preterm delivery associated morbid symptoms, such as respiratory distress syndrome and intraventricular hemorrhage (Amiya et al., 2016). However, excess GC exposure can disturb normal fetal neurodevelopmental progress and impact lifelong programming of neuroendocrine function and behavior (Asztalos, 2012; O'Donnell and Meaney, 2017). Emerging epidemiological evidence has indicated that prenatal exposure to increased amounts of sGCs causes increased susceptibility to neuropsychiatric disorders, such as anxiety and depression, in adulthood (Khalife et al., 2013; Braithwaite et al., 2017). Many animal studies have also demonstrated that repeated exposure to sGCs in late gestation leads to depression-like behavior and other modified behavior in adult offspring (Hiroi et al., 2016; Conti et al., 2017; Xu et al., 2018). Although a number of genes have been found to be associated with depression-like behavior (McCoy et al., 2017; Xu et al., 2018), the mechanisms underlying the prenatal GC programming of depression-like behavior remain largely unknown.

Mitochondria are integral eukaryotic organelles that play major roles in numerous cellular processes, particularly in aerobic energy production and thermogenesis (Hadj-Moussa et al., 2018). Of note, mitochondria are particularly important for the brain because of both its high levels of energy use and its inability to store large amounts of energy reserves in the form of glycogen. Moreover, mitochondria can generate reactive oxygen species (ROS) that may have toxic effects in cells (Allen et al., 2018). Mitochondria are involved in many processes including apoptosis and calcium homeostasis, which is necessary for the proper functioning of the nervous tissue (MacAskill et al., 2010; Xavier et al., 2016). A growing body of evidence has indicated that mitochondrial dysfunction would be a crucial factor in the development and progress of depression (Marazziti et al., 2011). It has been reported that patients with major depression disease (MDD) display changed mitochondrial morphology and function as well as have abnormal expression of genes encoding for mitochondrial proteins in the brain (Gardner and Boles, 2011). More recently, a number of studies have demonstrated that mitochondrial abnormalities may contribute to the depression-like behavior induced by chronic stress or prenatal stress (Gong et al., 2011; Chakravarty et al., 2013; Glombik et al., 2016).

So far, the therapeutic strategy for MDD is antidepressant therapy although it is unsatisfactory since most patients are partial responder to the treatment (MacQueen et al., 2017). Therefore, much effort in the past decades has focused on seeking adjuvant therapeutic approaches. The evidence unearthed so far suggests that exercise training is an adjuvant treatment approach for MDD as many clinical data have demonstrated that physical exercise as a regular life style lead to improvements in depressive status (Null et al., 2017). Animal studies have also shown that exercise training ameliorates depression-like behavior (Chen et al., 2016; Morgan et al., 2018). Similarly, using several rodent models of depression, we have demonstrated that exercise training reduces depressive behavior (Wang et al., 2016; Liu et al., 2018). Up to now, the biological mechanisms by which exercise ameliorates depression are yet unclear. However, Aguiar et al. (2014) demonstrated that exercise engages mitochondrial pathways, which might be associated to the anti-depressive effect of exercise.

The objectives of the present study were to explore the role of mitochondria in the development of depression-like behavior induced by prenatal exposure to sGCs and to evaluate the impact of exercise on the depression-like behavior programmed by sGCs. To achieve these goals, we set up a series of experiments to confirm that depression-like behavior can be induced by prenatal exposure to dexamethasone (Dex) in late pregnancy in rats, then clarified the contribution of mitochondria dysfunction to prenatal Dex programming depression-like behavior, and finally elucidated the association of mitochondria function with excise intervention of depression-like behavior caused by prenatal Dex exposure.

MATERIALS AND METHODS

Animals

Adult Sprague Dawley rats weighing 220 ± 20 g were obtained from Shanghai Laboratory Animal (Shanghai, China). All animal procedures were carried out in accordance with the guidelines for the use of laboratory animals published by the People's Republic of China Ministry of Health (January 25, 1998), with the approval of the Ethical Committee of Experimental Animals of the Second Military Medical University. Procedures were designed to minimize the number of animals used and their suffering. The rats were housed in social groups of 3 to 5 in a cage with regular light–dark cycles (lights on at 7:00 AM, lights off at 7:00 PM) under controlled temperature (22 ± 2°C) and humidity (50 ± 10%), and were provided standard diet and water *ad libitum*. Breeding females were handled daily for 1 week. The female was placed with a male at 3:00 PM. The male was removed the next day at 8:00 AM to its social group, and the female was transferred to a new cage. Pregnant rats were confirmed by microscopic analysis of vaginal smears for the presence of sperm, then were assigned randomly to control (Con) and dexamethasone (Dex) groups. Dexamethasone-21-phosphate disodium salt (Sigma-Aldrich, St. Louis, MO, United States) was dissolved in saline to achieve the concentration as 100 μl containing 0.13 mg/kg body weight. The dosage of Dex was chosen on the basis of the literature (Hauser et al., 2006; Liu et al., 2018) and our preliminary study. During gestational days (GD) 14 to 21, rats of DEX group were subcutaneously administered with 0.13 mg/kg dexamethasone-21-phosphate disodium salt (equal to 0.1 mg/kg dexamethasone), while control rats were received vehicle (0.9% saline) once a day for 7 days. The pregnant rats delivered undisturbed to produce the offspring. Given that estrus cycle may have impact on the behavior tested and the expression of various factors, the male offspring were used in the following experiments.

Exercise Protocol

Twenty male offspring rats at 4 weeks of age were randomly selected from Dex group. They were then randomly assigned

to two groups (n = 10 for each group): sedentary and exercise. The exercise protocol for moderate physical activity was performed as described by prior studies (Ji et al., 2017; Shin et al., 2017). Briefly, animals were put on the treadmill at a speed of 2 m/min for the first 5 min, flow up a speed of 5 m/min for the next 5 min, and a speed of 8 m/min for the last 20 min, with the 0° inclination. The animals were adapted to the treadmill for a week, and then the above exercise was performed for 5 days a week for four weeks. After exercise, behavioral tests were examined on all of the animals. Then, rats were decapitated at 12:00 PM to 13:00 PM on the day of sacrifice for collection of blood and tissue. Hippocampi were rapidly and carefully separated on an ice-plate and then stored at −80°C until assays. The blood was collected and the serum was separated and stored at −80°C until assays.

Behavioral Tests

The behavior of offspring was monitored at 9 weeks. The forced swimming test (FST) and sucrose preference test were performed as previously described (Drake et al., 2005; Long et al., 2013). In the FST, each rat was introduced for 5 min into separate transparent cylindrical containers (diameter 30 cm, height 45 cm) that were filled with water to 30 cm so that rats could only touch the bottom with the tip of the tail. Water temperature was maintained at 24 ± 2°C. Duration of immobility was measured. The sucrose preference test was used to test behavioral anhedonia. Briefly, 2 bottles of 1% sucrose solution were placed in each cage, and 24 h later, one bottle was replaced with tap water for 24 h. After adaptation, rats were deprived of water and food for 24 h, followed by the sucrose preference test, in which rats housed in individual cages had free access to 2 bottles, one containing 200 ml of sucrose solution (1% w/v) and the other 200 ml of water. At the end of 24 h, sucrose and water consumption was measured, and the sucrose preference was calculated as the volume of 1% sucrose solution consumed expressed as a percentage of the total liquid intake.

Hormone Assays

Corticosterone levels in serum were measured using a commercially available radioimmunoassay kit (Sino-United Kingdom Institute of Biologic Technology, Beijing, China) according to the manufacturer's instructions. The specificity of the kit was 100% for corticosterone, and it did not cross react with progesterone, aldosterone, cortisol, testosterone, cortisone, dehydroepiandrosterone (DHEA), DHEA-sulfate, or pregnenolone. Intraassay variation was <7.5% and interassay variation <9.5%.

Microarray Analysis

The transcriptional profiles of hippocampal tissues from the male Dex offspring were characterized by Affymetrix v2 U133 plus 2 gene arrays using the One-Cycle Eukaryotic Target Labeling Assay protocol (Affymetrix, Santa Clara, CA, United States).

Total RNA Extraction and Real-Time Quantitative PCR

Total RNA of hippocampus of male offspring was extracted using Trizol reagent (Thermo Fisher Scientific, Waltham, MA, United States) following the manufacturer's instructions. Genomic contamination was removed by column treatment of RNA samples with DNase for 20 min at 20°C, using the DNAeasy cleanup protocol following the manufacturer's instructions (Qiagen, Germantown, MD, United States). RNA purity and concentrations were assessed using spectrophotometric analysis, and integrity was verified using gel electrophoresis. Briefly, 2 μg RNA was reverse transcribed with oligo(dT)12-18 primer using the Moloney murine leukemia virus reverse transcriptase (Promega, Madison, WI, United States). Real-time PCR was performed using SYBR green (Hoffmann-La Roche, Basel, Switzerland) incorporation with a CFX96 real-time detection system (Bio-Rad, Hercules, CA, United States). The reaction solution consisted of 2.0 μl diluted cDNA product, 0.1 μM of each paired primer, 100 μM deoxynucleotide triphosphates, 1 U Taq DNA polymerase (Promega), and 10.0 μl PCR buffer. The primer sequences for uncoupling protein 3 (UCP3), isocitrate dehydrogenase 2 (IDH2) and solute carrier family 25 member 21(Slc25a21), were designed based on cDNA sequences in GeneBank. The following primers were used: UCP3 (accession number NM_013167): sense 5′- CAAAGGAACGGACCACTCCA-3′ and anti-sense 5′- CTCCAGTTCCCAGGCGTATC-3′, IDH2 (accession number NM_001014161.1): sense 5′- AAGCCCATCACCATTGGCAG-3′ and anti-sense 5′- CCGAAATGGACTCGTCGGTG-3′, Slc25a21 (accession number NM_133614): sense5′- AGGAAGACTTAGG TATGAGTCAGAA-3′ and anti-sense 5′- TCACATTTTAAC TCAGCACTCACAA-3′, β-actin (accession number NM_001101): sense 5′- TGTGTTGGCGTACAGGTCTTTG-3′ and anti-sense 5′- GGGAAATCGTGCGTGACATTAAG-3′. The temperature range to detect the melting temperature of the PCR product was set from 60 to 95°C. The housekeeping gene β-actin was measured for each sample as an internal PCR control for sample loading and normalization. The specificity of the primers was verified by examining the melting curve as well as by subsequent sequencing of the PCR products. To determine the relative quantitation of genes expression for both target and housekeeping gene, the comparative C_t method with arithmetic formulae was used (Livak and Schmittgen, 2001). Subtracting the C_t of the housekeeping gene from the C_t of the target gene yields the ΔC_t in each group, which was entered into the equation $2^{-\Delta\Delta Ct}$ and calculated for the exponential amplification of PCR. β-Actin was used for calculation of ΔC_t in presentation of results.

Western Blotting Analysis

Hippocampal tissues of male offspring were homogenized in the presence of lysis buffer consisting of 60 mM Tris–HCl, 2% sodium dodecyl sulfate (SDS), 10% sucrose, 2 mM phenylmethylsulfonyl fluoride (Merck, Darmstadt, Germany), 1 mM sodium orthovanadate (Sigma-Aldrich) and 10 μg/ml aprotinin (Bayer, Leverkusen, Germany). The lysates were

quickly centrifuged at 4°C. The supernatant was collected and protein concentration was assayed using a modified Bradford assay. The samples were then diluted in sample buffer (250 mM Tris–HCl, 4% SDS, 10% glycerol, 2% β-mercaptoethanol and 0.002% bromophenol blue) and boiled for 10 min. Protein load was 30 μg per lane in 10% SDS-PAGE and subsequently transferred to nitrocellulose membranes. The blots were blocked with 5% skim milk powder in 0.1% Tris-buffered saline/Tween 20 at room temperature for 2 h, then incubated with antibodies against UCP3 (ab3477, Abcam), IDH2 (ab131263, Abcam) and Slc25a21(ab167033, Abcam) at a dilution 1:500 to 1:1000 overnight at 4°C. After 3 washes with Tris-buffered saline/Tween 20, the membrane was incubated with the secondary antibodies of horseradish peroxidase–conjugated antibody for 1 h at room temperature. Immunoreactive proteins were detected and visualized using the enhanced chemiluminescence western blot detection system (Santa Cruz Biotechnology). To control sampling errors, the ratio of band intensities to β-tubulin or GAPDH (Sigma-Aldrich) was obtained to quantify the relative protein expression level.

Isolation of Mitochondria

Mitochondria of hippocampus were isolated using Mitochondria Fractionation Kit (Beyotime) as previously described (Du et al., 2016). Briefly, the hippocampus tissues were quickly removed from adult male offspring and placed in chilled isolation media (0.25 M sucrose, 10 mM Tris–HCl buffer, pH 7.4, 1 m MEDTA, and 250 μg BSA/ml). The tissues were minced and washed with the isolation medium, and 10% (w/v) homogenates were ready. Nuclei and cell debris were sedimented by centrifugation at 600 *g* for 10 min at 4°C and discarded. The supernatant was subjected to centrifugation at 10,000 *g* for 10 min at 4°C. The resulting mitochondrial pellets were suspended in the isolation medium.

Detection of Mitochondrial Superoxide Production

MitoSOX (Molecular Probes, Invitrogen, Carlsbad, CA, United States), a cell-permeable probe, can accumulate specifically in mitochondria and become fluorescent after oxidation by superoxide. MitoSOX was dissolved in DMSO immediately before use, and then added into isolated mitochondria at a final concentration of 5 μM (DMSO diluted to less than 0.1%). After 30 min, the media were replaced with 100 μl HEPES buffered saline (10 mM HEPES, pH 7.4, 150 mM NaCl, 5 mM KCl, 1 mM $MgCl_2$, and 1.8 mM $CaCl_2$); then, red fluorescence was obtained at 485 nm excitation and 590 nm emission using a Synergy TM fluorescence plate reader (Bio-Tek Instruments).

Assessment of Mitochondrial Membrane Potential

Mitochondrial membrane potential was detected with the fluorescent probe JC-1 (Sigma-Aldrich), which exists predominantly in monomeric form in cells with depolarized mitochondria and displays fluorescent green. Cells with polarized mitochondria predominantly contain JC-1 in aggregate form and show fluoresced red. Loading was done by incubating isolated mitochondria with 2 μM JC-1 for 15 min. After staining, the red fluorescent signals were excited at 530 nm and detected at 630 nm, and the green fluorescence was excited at 488 nm and detected at 530 nm using a Synergy TM fluorescence plate reader. The ratio of red and green fluorescence indicates mitochondrial membrane depolarization.

Measurement of Mitochondrial ATP Concentration

Isolated mitochondria were homogenized in a protein extraction solution (Pierce). The supernatant after centrifugation at 10,000 *g* for 10 min was subject to determination of ATP concentration, using an ATP bioluminescence assay (Beyotime). Light emitted from a luciferase-mediated reaction was measured by a tube luminometer (Tecan).

Intracerebroventricular (ICV) Injection

Eighteen male offspring were randomly picked up from Dex group and then randomly divided into 3 groups (n = 6 in each group): vehicle and mitoTEMPO (0.02 and 0.2 μmol/kg). They were anesthetized with 10% chloral hydrate (0.33 mg/kg, i.p.) and placed in a stereotaxic apparatus (Stoelting Co., Wood Dale, IL, United States). At first, stainless steel guide cannulas were implanted in lateral ventricle using stereotactic co-ordinates (AP = –0.8 mm, L = +1.5 mm, and DV = –3.6 mm) (Stengel et al., 2011), and fixed to the skull with dental cement and one metal screw. After one week recovery, the rats were anesthetized continuously with 2.5% halothane, and then mitoTEMPO (Sigma-Aldrich) at the dosage 0.02 or 0.2 μmol/kg (5 μL) was injected into the left ventricle at the rate of 1 μL/min by Hamilton syringe. Equal volume of saline was injected into the left ventricle of the vehicle animals. The infusion needle was left in place for an additional 5 min after each infusion and then slowly withdrawn. This injection was taken once a day for 4 days. Then, behavioral tests were performed on all of animals.

Electron Microscopy

Hippocampus specimens were immediately placed in 2.5% glutaraldehyde in 0.1 M cacodylate buffer, sectioned to ∼1 mm^2, and incubated in the same glutaraldehyde solution for 12 h at room temperature. Samples were postfixed in 1% osmium tetroxide for 1.5 h, then dehydrated in increasing concentrations of alcohol, immersed in propylene oxide, and embedded in Araldite 502 resin at 60°C. Ultrathin sections were placed on grids and stained with uranyl acetate and lead citrate. The ultrastructure of hippocampus was observed under a transmission electron microscope (JEOL 1010; JEOL, Akishima, Japan).

Statistics

Data were presented as mean ± SEM. All data were tested for homogeneity of variance by the Bartlett test at first, and then analyzed using one or two-way ANOVA followed by Dunnett's or LSD *post hoc* test, where appropriate. $P < 0.05$ was considered significant.

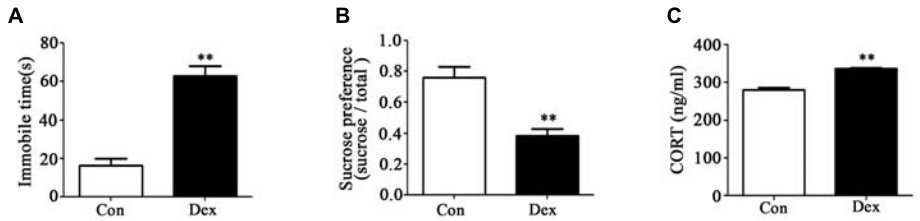

FIGURE 1 | Prenatal Dex exposure induces depression-like behavior and increases circulatory GC level in adult offspring. Pregnant rats were administered Dex at 0.1 mg/kg/d during GD14 to 21. Behavioral tests and determination of corticosterone concentration in blood were performed on male offspring rats at adult (9-week old). Immobile time of FST **(A)**; sucrose preference test **(B)**; corticosterone level **(C)**. Data are presented as means ± SEM (n = 10). $^{**}P < 0.01$ vs. control. Con, control; Dex, dexamethasone.

RESULTS

Prenatal Dex Exposure Induces Depression-Like Behavior and Increases Circulatory Corticosterone Level

As shown in **Figures 1A,B**, immobile time in the FST was significantly increased whilst sucrose preference was significantly reduced in male Dex offspring compared with control offspring ($P < 0.01$).

It has been reported that increased hypothalamic–pituitary–adrenal (HPA) activity contributes to depression-like behavior induced by prenatal GC exposure (Shoener et al., 2006; Xu et al., 2018). We therefore examined circulating corticosterone level in offspring with prenatal Dex exposure. As shown in **Figure 1C**, corticosterone level in circulation was significantly higher in Dex offspring than that in control offspring ($P < 0.01$).

Prenatal Dex Exposure Leads to Mitochondrial Dysfunction in Hippocampus

The hippocampus is the key brain region responsible for affective and behavioral functions and is sensitive to steroid hormones (Miller and O'Callaghan, 2005; Snyder et al., 2011). To identify the key genes in hippocampus that mediate depression-like behavior, we performed microarray analysis to compare the gene expression profiles in hippocampus of Dex offspring and control offspring (Xu et al., 2018). Among the regulated genes, UCP3, Slc25a21 and IDH2 are the genes related to mitochondrial function. Using Q-PCR, we confirmed that UCP3 expression was significantly upregulated whilst Slc25a21 and IDH2 expression was significantly downregulated in Dex offspring compared with control offspring ($P < 0.01$, **Figures 2A–C**). Consistently, western blotting analysis showed that the protein level of UCP3 was significantly increased whilst the levels Slc25a21 and IDH2 were significantly decreased in Dex offspring compared with control offspring ($P < 0.05$, **Figures 2D–F**).

Next, we assessed the effect of prenatal Dex exposure on mitochondrial function in the hippocampus. As shown in **Figures 3A–C**, prenatal Dex exposure resulted in a significant decrease in ATP production ($P < 0.01$ vs. control) and mitochondrial membrane potential ($P < 0.05$ vs. control), as well as a significant increase in mitochondrial superoxide production ($P < 0.01$ vs. control).

The ultrastructure of mitochondria in hippocampus was then determined by transmission electron microscopy. As shown in **Figure 3D**, male Dex offspring showed mitochondrial damage, including a decrease in cristae density or even disappearance, vacuole formation by mitochondrial outer membrane extension, and intermembrane space expansion (**Figure 3D**).

MitoTEMPO Administration Ameliorates Depression-Like Behavior in Dex Offspring

MitoTEMPO is a mitochondria-targeted antioxidant with superoxide and alkyl radical scavenging properties (Hu and Li, 2016). We then examined the effect of MitoTEMPO administration on depression-like behavior in Dex offspring. Adult Dex rats were received ICV injection of MitoTEMPO (0.02 or 0.2 μmol/kg, 5 μL) for 4 days prior to behavioral tests. As shown in **Figures 4A,B**, injection of MitoTEMPO at the dosage of 0.02 μmol/kg had no significant effect on depression-like behavior, while administration of 0.2 μmol/kg MitoTEMPO significantly decreased depression-like behavior as evidenced by increased sucrose preference and a decrease in immobile time in FST compared to those with vehicle injection.

Given that increased corticosterone level in circulation contributes to depression-like behavior, we examined the level of corticosterone in response to MitoTEMPO administration. As shown in **Figure 4C**, there was no significant difference in corticosterone level among injection with 0.2 μmol/kg MitoTEMPO and vehicle injection groups.

Treadmill Exercise Ameliorates Depression-Like Behavior, Reduces Circulatory Level of Corticosterone and Improves Mitochondrial Function in Dex Offspring

As mentioned, exercise could be an adjuvant treatment approach for depression, we therefore applied treadmill exercise to 4-week old Dex offspring in order to determine the impact of exercise on depression-like behavior in early life. As shown in **Figures 5A,B**, these rats with exercise training displayed

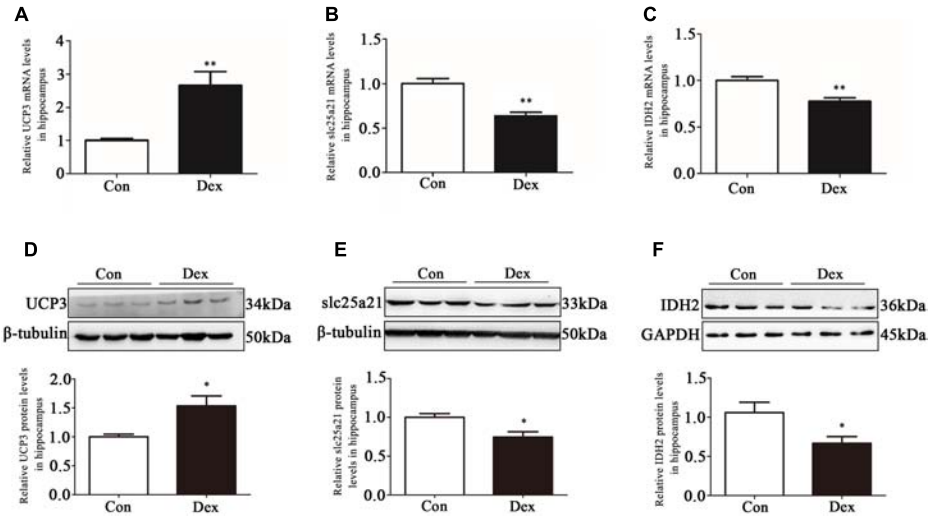

FIGURE 2 | Effects of prenatal Dex exposure on hippocampal UCP3, Slc25a21 and IDH2 expression in adult offspring. Pregnant rats at GD 14 to 21 were subcutaneously administered either 0.1 mg/kg/d Dex or vehicle (0.9% saline) once a day for 7 days. Hippocampal tissues were obtained from adult offspring rats (9-week old). UCP3 **(A)**, Slc25a21 **(B)**, and IDH2 **(C)** mRNA level was determined by Q-PCR. Protein level of UCP3 **(D)**, Slc25a21 **(E)**, and IDH2 **(F)** was determined by western blot analysis. Representative protein bands are presented above corresponding histogram. Data are presented as means ± SEM (n = 10/group). $^{*}P < 0.05$, $^{**}P < 0.01$ vs. control. Con, control; Dex, dexamethasone.

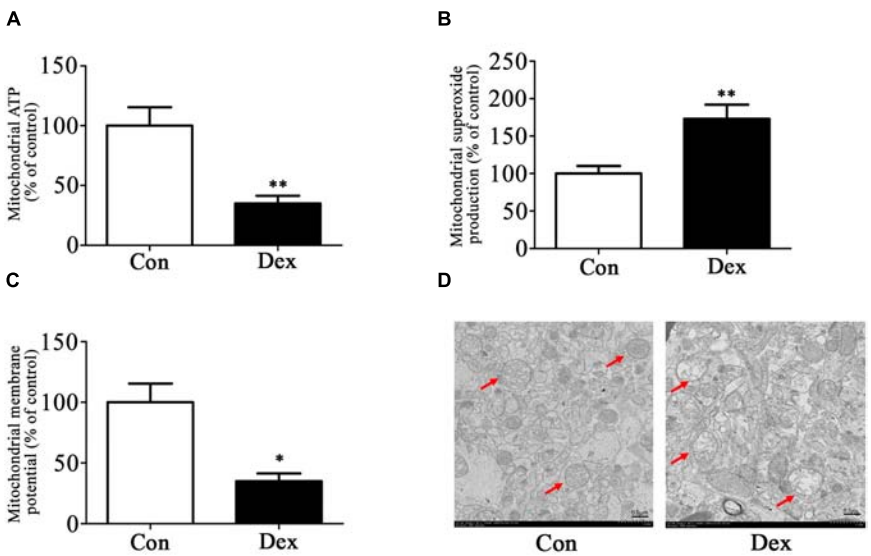

FIGURE 3 | Effects of prenatal Dex exposure on mitochondrial function and morphology in hippocampus of adult offspring. Pregnant rats at GD 14 to 21 were subcutaneously administered either 0.1 mg/kg/d Dex or vehicle (0.9% saline) once a day for 7 days. Mitochondria were isolated from the hippocampus of adult offspring rats (9-week old) for determination of ATP production **(A)**, mitochondrial superoxide production **(B)**, and membrane potential **(C)** as described in Section "Materials and Methods". Mitochondrial morphology **(D)** was determined by transmission electron microscopy. Data are presented as means ± SEM (n = 10/group). $^{*}P < 0.05$, $^{**}P < 0.01$ vs. control. Con, control; Dex, dexamethasone.

improvement of depression-like behavior in adult. Sucrose preference was significantly increased and the immobile time in FST was significantly decreased in Dex offspring with exercise training compared those in Dex offspring without exercise training. In addition, circulatory level of corticosterone was lower in Dex offspring with exercise than that in Dex offspring without exercise (**Figure 5C**).

We then assessed the effect of treadmill exercise on mitochondrial function and morphology in hippocampus. As shown in **Figures 6A–C**, Dex offspring with treadmill exercise showed a significant increase in ATP production and mitochondrial membrane potential and a significant decrease in mitochondrial superoxide production compared with those without exercise ($P < 0.01$).

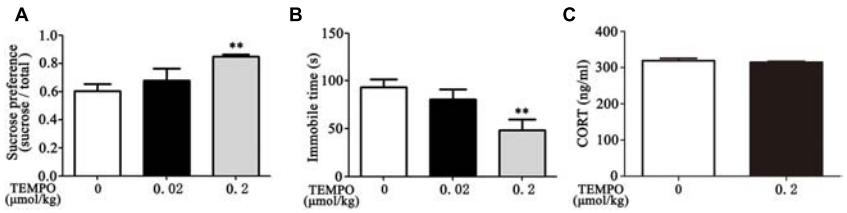

FIGURE 4 | ICV administration of MitoTEMPO improves depression-like behavior and reduces circulatory corticosterone level in Dex offspring. Male Dex offspring received ICV administration of MitoTEMPO (0.02 or 0.2 μmol/kg, 5 μL/day) for 4 days. Sucrose preference test **(A)**, FST **(B)** and corticosterone concentration in blood **(C)** were then determined. Data are presented as means ± SEM (n = 6/group). $^{**}P < 0.01$ vs. control.

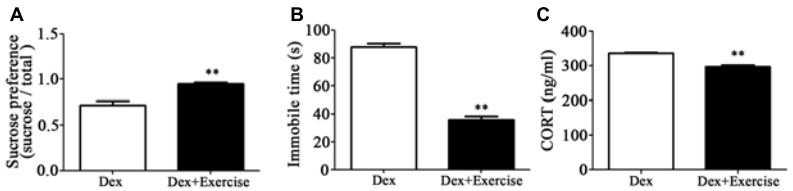

FIGURE 5 | Effects of treadmill exercise on depression-like behaviors and circulatory corticosterone level in Dex offspring. Dex offspring at 4-week old received 4 weeks of treadmill exercise. Then, sucrose preference test **(A)** and FST **(B)**, and corticosterone concentration in blood **(C)** were determined. Data are presented as means ± SEM (n = 6/group). $^{**}P < 0.01$ vs. Dex. Dex, dexamethasone; CORT, corticosterone.

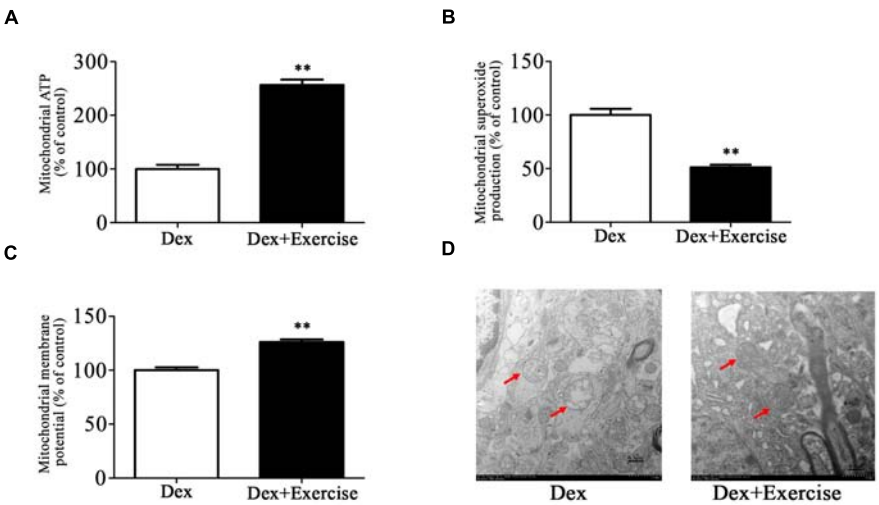

FIGURE 6 | Effects of treadmill exercise on mitochondrial function and morphology in Dex offspring. Dex offspring at 4-week old received 4 weeks of treadmill exercise. Then, mitochondria were isolated from hippocampus for the determination of ATP production **(A)**, mitochondrial superoxide production **(B)**, and membrane potential **(C)** as described in Section "Materials and Methods". Mitochondrial morphology **(D)** was determined by transmission electron microscopy. Data are presented as means ± SEM (n = 10/group). $^{**}P < 0.01$ vs. Dex. Dex, dexamethasone.

Electron microscopy analysis showed that mitochondrial morphology in hippocampus was greatly improved in Dex offspring with exercise compared with those without exercise (**Figure 6D**).

DISCUSSION

In the present study, we confirmed that prenatal GCs exposure induces depression-like behavior and increases HPA activity, demonstrated that mitochondrial dysfunction in hippocampus occurred in Dex offspring, and found that depression-like behavior was ameliorated by administration of a mitochondria-targeted antioxidant into the brain. Moreover, we also showed that treadmill exercise intervention in early life can reverse the above behavior outcome and mitochondrial alternations in brain. Our data indicates that mitochondria dysfunction contributes to Dex programming behavior and that exercise reversion of this behavior outcome is associated with recovery of mitochondrial function and morphology in the hippocampus.

As mentioned previously, the hippocampus is the key brain region in cognitive, affective and behavioral functions and is a highly plastic structure that is sensitive to steroid hormones (Miller and O'Callaghan, 2005; Snyder et al., 2011). Our previous study has shown that prenatal Dex exposure leads to significant changes in 149 genes in hippocampus (Xu et al., 2018). We noted that several genes including UCP3, IDH2 and Slc25a21 are the regulators of mitochondrial function, glycolysis and oxidative stress. UCP3 belongs to a family of mitochondrial transporter proteins that mediates a regulated permeabilization of the mitochondrial inner membrane to protons (Chakravarty et al., 2013; Giralt and Villarroya, 2017). IDH2 is an NADP(+)-dependent mitochondrial protein that regulates mitochondrial redox status through its role in intermediary metabolism and energy production (Han et al., 2017). Slc25a21 is a member of the mitochondrial carrier subfamily of solute carrier protein genes and functions as a gated pore, translocating ADP from the mitochondrial matrix into the cytoplasm to maintain the cytoplasmic phosphorylation potential for cell growth (Gutierrez-Aguilar and Baines, 2013). Consistent with the functional role of these factors, we found that hippocampal mitochondria exhibited oxidative stress and impairment of energy production as evidenced by an increase in ROS production and a decrease in ATP production and reduced mitochondrial membrane potential in Dex offspring. It is known that increased ROS content would cause mitochondria damage such as leading to swollen and reduction of cristae density (Wang et al., 2012). Consistently, morphology of mitochondria showed a dramatic reduction of cristae density and vacuole formation by mitochondrial outer membrane extension and intermembrane space expansion in Dex offspring. As UCP3 plays an important role in permeabilization of the mitochondrial inner membrane to protons, the above morphological changes are at least partly attributed to changed UCP3 expression in Dex offspring.

Mitochondria are essential for the life of the cell as they are well-known ATP producers. In the brain, mitochondria are also crucial for the processes of neuroplasticity, including neural differentiation, neurite outgrowth, neurotransmitter release and dendritic remodeling (Mattson et al., 2008). Given that depression development is associated with abnormal neurogenesis and synaptic formation in some brain regions (Pilar-Cuellar et al., 2014; Gulbins et al., 2015), increasing lines of evidence have indicated that mitochondrial disturbances are involved in the development and progress of depression (Gardner and Boles, 2011; Marazziti et al., 2011). In animal models of depression induced by chronic mild stress, the collapse of mitochondrial membrane potential, inhibited mitochondrial respiration rates and destroyed mitochondrial ultrastructure have been reported (Gong et al., 2011). In the model of LPS-induced depression, mitochondrial dysfunction is believed to play a central role in the pathogenesis of depressive behavior (Chen et al., 2017). Some studies have also shown that prenatal stress resulted in mitochondrial malfunction, which may play a role in depression (Chakravarty et al., 2013; Glombik et al., 2016). In the present study, we have also provided the evidence that mitochondria dysfunction contributes to depression-like behavior caused by prenatal Dex exposure.

There is now substantial evidence that exercise could effectively ameliorate depressive symptoms (Chen et al., 2016; Null et al., 2017; Morgan et al., 2018). Our previous studies also showed that swimming exercise is beneficial to depression-like behavior induced by prenatal Dex exposure (Liu et al., 2013). The present study showed that treadmill exercise can also improve depression-like behavior induced by prenatal Dex exposure. Studies from Wen et al. (2014) have indicated that anti-depressive actions of exercise may, in part, be due to a reversal of mitochondrial dysfunction. Moreover, a number of studies have shown that exercise could improve mitochondrial function and increased anti-oxidant enzymes in the nervous tissue. For instance, Dos Santos et al. (2017) showed physical exercise during the developmental period may protect against brain oxidative damage caused by chronic stress exposure later in life. In the present study, we showed that exercise ameliorates depression-like behavior whilst improves mitochondrial function in Dex offspring, indicating that improvement of mitochondrial function contributes to exercise ameliorating the behavior programmed by prenatal sGC exposure.

Many studies have demonstrated that prenatal sGC exposure programs the HPA axis and subsequently leads to increased HPA activity (Liu et al., 2013; van Bodegom et al., 2017). It is known that increased HPA activity is one of key factors responsible for development of depression (Keller et al., 2017; Juruena et al., 2018). Here, we showed that exercise also reduced circulatory level of corticosterone in Dex offspring, which suggests that exercise improvement of depression-like behavior is also associated with reversion of higher HPA activity in Dex offspring. Of note, we found that administration of the mitochondria-targeted antioxidant MitoTEMPO could not reduce circulatory level of corticosterone in Dex offspring, suggesting that mitochondria dysfunction may not be involved in increased HPA activity caused by prenatal Dex exposure. The mechanisms underlying prenatal sGC programming HPA activity remain to be further investigated.

In conclusion, we found that prenatal sGC exposure results in depression-like behavior, accompanied by alterations in mitochondrial function, and that intervention with exercise improves both depression-like behavior and mitochondrial dysfunction. Our results suggest that exercise may recover mitochondrial function, thereby ameliorating depression caused by prenatal sGC exposure.

DATA AVAILABILITY

Publicly available datasets were analyzed in this study. This data can be found here: https://doi.org/10.1096/fj.201700948RR.

AUTHOR CONTRIBUTIONS

TW, YH, and YG performed the experiments and analyses. TW wrote the manuscript. XN and HS designed the experiments and made the final revision. YX and JL participated in discussions and revisions of the article.

FUNDING

This work was supported by Key State Research and Development Program of China 2017YFC1001404 and 2018YFC1002802, Natural Science Foundation of China (Nos. 81620108013, 81741011, and 81671176), and Technology Commission of Shanghai Municipals (1814090300).

REFERENCES

Aguiar, A. S. Jr., Stragier, E., da Luz Scheffer, D., Remor, A. P., Oliveira, P. A., Prediger, R. D., et al. (2014). Effects of exercise on mitochondrial function, neuroplasticity and anxio-depressive behavior of mice. *Neuroscience* 271, 56–63. doi: 10.1016/j.neuroscience.2014.04.027

Allen, J., Romay-Tallon, R., Brymer, K. J., Caruncho, H. J., and Kalynchuk, L. E. (2018). Mitochondria and mood: mitochondrial dysfunction as a key player in the manifestation of depression. *Front. Neurosci.* 12:386. doi: 10.3389/fnins.2018.00386

Amiya, R. M., Mlunde, L. B., Ota, E., Swa, T., Oladapo, O. T., and Mori, R. (2016). Antenatal corticosteroids for reducing adverse maternal and child outcomes in special populations of women at risk of imminent preterm birth: a systematic review and meta-analysis. *PLoS One* 11:e0147604. doi: 10.1371/journal.pone.0147604

Asztalos, E. (2012). Antenatal corticosteroids: a risk factor for the development of chronic disease. *J. Nutr. Metab.* 2012:930591. doi: 10.1155/2012/930591

Braithwaite, E. C., Pickles, A., Sharp, H., Glover, V., O'Donnell, K. J., Tibu, F., et al. (2017). Maternal prenatal cortisol predicts infant negative emotionality in a sex-dependent manner. *Physiol. Behav.* 175, 31–36. doi: 10.1016/j.physbeh.2017.03.017

Chakravarty, S., Reddy, B. R., Sudhakar, S. R., Saxena, S., Das, T., Meghah, V., et al. (2013). Chronic unpredictable stress (CUS)-induced anxiety and related mood disorders in a zebrafish model: altered brain proteome profile implicates mitochondrial dysfunction. *PLoS One* 8:e63302. doi: 10.1371/journal.pone.0063302

Chen, C., Nakagawa, S., Kitaichi, Y., An, Y., Omiya, Y., Song, N., et al. (2016). The role of medial prefrontal corticosterone and dopamine in the antidepressant-like effect of exercise. *Psychoneuroendocrinology* 69, 1–9. doi: 10.1016/j.psyneuen.2016.03.008

Chen, W. J., Du, J. K., Hu, X., Yu, Q., Li, D. X., Wang, C. N., et al. (2017). Protective effects of resveratrol on mitochondrial function in the hippocampus improves inflammation-induced depressive-like behavior. *Physiol. Behav.* 182, 54–61. doi: 10.1016/j.physbeh.2017.09.024

Conti, M., Spulber, S., Raciti, M., and Ceccatelli, S. (2017). Depressive-like phenotype induced by prenatal dexamethasone in mice is reversed by desipramine. *Neuropharmacology* 126, 242–249. doi: 10.1016/j.neuropharm.2017.09.015

Dos Santos, T. M., Kolling, J., Siebert, C., Biasibetti, H., Berto, C. G., Grun, L. K., et al. (2017). Effects of previous physical exercise to chronic stress on long-term aversive memory and oxidative stress in amygdala and hippocampus of rats. *Int. J. Dev. Neurosci.* 56, 58–67. doi: 10.1016/j.ijdevneu.2016.12.003

Drake, A. J., Walker, B. R., and Seckl, J. R. (2005). Intergenerational consequences of fetal programming by in utero exposure to glucocorticoids in rats. *Am. J. Physiol. Regul. Integr. Comp. Physiol.* 288, R34–R38. doi: 10.1152/ajpregu.00106.2004

Du, J. K., Cong, B. H., Yu, Q., Wang, H., Wang, L., Wang, C. N., et al. (2016). Upregulation of microRNA-22 contributes to myocardial ischemia-reperfusion injury by interfering with the mitochondrial function. *Free Radic. Biol. Med.* 96, 406–417. doi: 10.1016/j.freeradbiomed.2016.05.006

Fowden, A. L., and Forhead, A. J. (2009). Endocrine regulation of feto-placental growth. *Horm Res.* 72, 257–265. doi: 10.1159/000245927

Gardner, A., and Boles, R. G. (2011). Beyond the serotonin hypothesis: mitochondria, inflammation and neurodegeneration in major depression and affective spectrum disorders. *Prog. Neuropsychopharmacol. Biol. Psychiatry* 35, 730–743. doi: 10.1016/j.pnpbp.2010.07.030

Giralt, M., and Villarroya, F. (2017). Mitochondrial uncoupling and the regulation of glucose homeostasis. *Curr. Diabetes Rev.* 13, 386–394. doi: 10.2174/1573399812666160217122707

Glombik, K., Stachowicz, A., Olszanecki, R., Slusarczyk, J., Trojan, E., Lason, W., et al. (2016). The effect of chronic tianeptine administration on the brain mitochondria: direct links with an animal model of depression. *Mol. Neurobiol.* 53, 7351–7362. doi: 10.1007/s12035-016-9807-4

Gong, Y., Chai, Y., Ding, J. H., Sun, X. L., and Hu, G. (2011). Chronic mild stress damages mitochondrial ultrastructure and function in mouse brain. *Neurosci. Lett.* 488, 76–80. doi: 10.1016/j.neulet.2010.11.006

Gulbins, E., Walter, S., Becker, K. A., Halmer, R., Liu, Y., Reichel, M., et al. (2015). A central role for the acid sphingomyelinase/ceramide system in neurogenesis and major depression. *J. Neurochem.* 134, 183–192. doi: 10.1111/jnc.13145

Gutierrez-Aguilar, M., and Baines, C. P. (2013). Physiological and pathological roles of mitochondrial SLC25 carriers. *Biochem. J.* 454, 371–386. doi: 10.1042/bj20121753

Hadj-Moussa, H., Green, S. R., and Storey, K. B. (2018). The living dead: mitochondria and metabolic arrest. *IUBMB Life* 70, 1260–1266. doi: 10.1002/iub.1910

Han, S. J., Jang, H. S., Noh, M. R., Kim, J., Kong, M. J., Kim, J. I., et al. (2017). Mitochondrial NADP(+)-dependent isocitrate dehydrogenase deficiency exacerbates mitochondrial and cell damage after kidney ischemia-reperfusion injury. *J. Am. Soc. Nephrol.* 28, 1200–1215. doi: 10.1681/asn.2016030349

Hauser, J., Feldon, J., and Pryce, C. R. (2006). Prenatal dexamethasone exposure, postnatal development, and adulthood prepulse inhibition and latent inhibition in Wistar rats. *Behav. Brain Res.* 175, 51–61. doi: 10.1016/j.bbr.2006.07.026

Hiroi, R., Carbone, D. L., Zuloaga, D. G., Bimonte-Nelson, H. A., and Handa, R. J. (2016). Sex-dependent programming effects of prenatal glucocorticoid treatment on the developing serotonin system and stress-related behaviors in adulthood. *Neuroscience* 320, 43–56. doi: 10.1016/j.neuroscience.2016.01.055

Hu, H., and Li, M. (2016). Mitochondria-targeted antioxidant mitotempo protects mitochondrial function against amyloid beta toxicity in primary cultured mouse neurons. *Biochem. Biophys. Res. Commun.* 478, 174–180. doi: 10.1016/j.bbrc.2016.07.071

Ji, E. S., Lee, J. M., Kim, T. W., Kim, Y. M., Kim, Y. S., and Kim, K. (2017). Treadmill exercise ameliorates depressive symptoms through increasing serotonin expression in postpartum depression rats. *J. Exerc. Rehabil.* 13, 130–135. doi: 10.12965/jer.1734968.484

Juruena, M. F., Bocharova, M., Agustini, B., and Young, A. H. (2018). Atypical depression and non-atypical depression: is HPA axis function a biomarker? A systematic review. *J. Affect. Disord.* 233, 45–67. doi: 10.1016/j.jad.2017.09.052

Keller, J., Gomez, R., Williams, G., Lembke, A., Lazzeroni, L., Murphy, G. M., et al. (2017). HPA axis in major depression: cortisol, clinical symptomatology and genetic variation predict cognition. *Mol. Psychiatry* 22, 527–536. doi: 10.1038/mp.2016.120

Khalife, N., Glover, V., Taanila, A., Ebeling, H., Jarvelin, M. R., and Rodriguez, A. (2013). Prenatal glucocorticoid treatment and later mental health in children and adolescents. *PLoS One* 8:e81394. doi: 10.1371/journal.pone.0081394

Liu, W., Sheng, H., Xu, Y., Liu, Y., Lu, J., and Ni, X. (2013). Swimming exercise ameliorates depression-like behavior in chronically stressed rats: relevant to proinflammatory cytokines and IDO activation. *Behav. Brain Res.* 242, 110–116. doi: 10.1016/j.bbr.2012.12.041

Liu, W., Wang, H., Xue, X., Xia, J., Liu, J., Qi, Z., et al. (2018). OGT-related mitochondrial motility is associated with sex differences and exercise effects in depression induced by prenatal exposure to glucocorticoids. *J. Affect. Disord.* 226, 203–215. doi: 10.1016/j.jad.2017.09.053

Livak, K. J., and Schmittgen, T. D. (2001). Analysis of relative gene expression data using real-time quantitative PCR and the 2(-Delta Delta C(T)) Method. *Methods* 25, 402–408. doi: 10.1006/meth.2001.1262

Long, N. M., Ford, S. P., and Nathanielsz, P. W. (2013). Multigenerational effects of fetal dexamethasone exposure on the hypothalamic-pituitary-adrenal axis of first- and second-generation female offspring. *Am. J. Obstet. Gynecol.* 208, 217.e1–217.e8. doi: 10.1016/j.ajog.2012.12.014

MacAskill, A. F., Atkin, T. A., and Kittler, J. T. (2010). Mitochondrial trafficking and the provision of energy and calcium buffering at excitatory synapses. *Eur. J. Neurosci.* 32, 231–240. doi: 10.1111/j.1460-9568.2010.07345.x

MacQueen, G., Santaguida, P., Keshavarz, H., Jaworska, N., Levine, M., Beyene, J., et al. (2017). Systematic review of clinical practice guidelines for failed antidepressant treatment response in major depressive disorder, dysthymia, and subthreshold depression in adults. *Can. J. Psychiatry* 62, 11–23. doi: 10.1177/0706743716664885

Marazziti, D., Baroni, S., Picchetti, M., Landi, P., Silvestri, S., Vatteroni, E., et al. (2011). Mitochondrial alterations and neuropsychiatric disorders. *Curr. Med. Chem.* 18, 4715–4721. doi: 10.2174/092986711797379221

Mattson, M. P., Gleichmann, M., and Cheng, A. (2008). Mitochondria in neuroplasticity and neurological disorders. *Neuron* 60, 748–766. doi: 10.1016/j.neuron.2008.10.010

McCoy, C. R., Jackson, N. L., Day, J., and Clinton, S. M. (2017). Genetic predisposition to high anxiety- and depression-like behavior coincides with diminished DNA methylation in the adult rat amygdala. *Behav. Brain Res.* 320, 165–178. doi: 10.1016/j.bbr.2016.12.008

Miller, D. B., and O'Callaghan, J. P. (2005). Aging, stress and the hippocampus. *Ageing Res. Rev.* 4, 123–140. doi: 10.1016/j.arr.2005.03.002

Morgan, J. A., Singhal, G., Corrigan, F., Jaehne, E. J., Jawahar, M. C., and Baune, B. T. (2018). The effects of aerobic exercise on depression-like, anxiety-like, and cognition-like behaviours over the healthy adult lifespan of C57BL/6 mice. *Behav. Brain Res.* 337, 193–203. doi: 10.1016/j.bbr.2017.09.022

Null, G., Pennesi, L., and Feldman, M. (2017). Nutrition and lifestyle intervention on mood and neurological disorders. *J. Evid. Based Complement. Altern. Med.* 22, 68–74. doi: 10.1177/2156587216637539

O'Donnell, K. J., and Meaney, M. J. (2017). Fetal origins of mental health: the developmental origins of health and disease hypothesis. *Am. J. Psychiatry* 174, 319–328. doi: 10.1176/appi.ajp.2016.16020138

Pilar-Cuellar, F., Vidal, R., Diaz, A., Castro, E., dos Anjos, S., Vargas, V., et al. (2014). Signaling pathways involved in antidepressant-induced cell proliferation and synaptic plasticity. *Curr. Pharm. Des.* 20, 3776–3794. doi: 10.2174/13816128113196660736

Shin, M. S., Park, S. S., Lee, J. M., Kim, T. W., and Kim, Y. P. (2017). Treadmill exercise improves depression-like symptoms by enhancing serotonergic function through upregulation of 5-HT1A expression in the olfactory bulbectomized rats. *J. Exerc. Rehabil.* 13, 36–42. doi: 10.12965/jer.1734918.459

Shoener, J. A., Baig, R., and Page, K. C. (2006). Prenatal exposure to dexamethasone alters hippocampal drive on hypothalamic-pituitary-adrenal axis activity in adult male rats. *Am. J. Physiol. Regul. Integr. Comp. Physiol.* 290, R1366–R1373. doi: 10.1152/ajpregu.00757.2004

Snyder, J. S., Soumier, A., Brewer, M., Pickel, J., and Cameron, H. A. (2011). Adult hippocampal neurogenesis buffers stress responses and depressive behaviour. *Nature* 476, 458–461. doi: 10.1038/nature10287

Stengel, A., Goebel-Stengel, M., Wang L., Luckey, A., Hu, E., Rivier, J., et al. (2011). Central administration of pan-somatostatin agonist ODT8-SST prevents abdominal surgery-induced inhibition of circulating ghrelin, food intake and gastric emptying in rats. *Neurogastroenterol. Motil.* 23, e294–e308. doi: 10.1111/j.1365-2982.2011.01721.x

van Bodegom, M., Homberg, J. R., and Henckens, M. J. A. G. (2017). Modulation of the hypothalamic-pituitary-adrenal axis by early life stress exposure. *Front. Cell Neurosci.* 11:87. doi: 10.3389/fncel.2017.00087

Wang, Y., Nartiss, Y., Steipe, B., McQuibban, G. A., and Kim, P. K. (2012). ROS-induced mitochondrial depolarization initiates PARK2/PARKIN-dependent mitochondrial degradation by autophagy. *Autophagy* 8, 1462–1476. doi: 10.4161/auto.21211

Wang, Y., Xu, Y., Sheng, H., Ni, X., and Lu, J. (2016). Exercise amelioration of depression-like behavior in OVX mice is associated with suppression of NLRP3 inflammasome activation in hippocampus. *Behav. Brain Res.* 307, 18–24. doi: 10.1016/j.bbr.2016.03.044

Wen, L., Jin, Y., Li, L., Sun, S., Cheng, S., Zhang, S., et al. (2014). Exercise prevents raphe nucleus mitochondrial overactivity in a rat depression model. *Physiol. Behav.* 132, 57–65. doi: 10.1016/j.physbeh.2014.04.050

Xavier, J. M., Rodrigues, C. M., and Sola, S. (2016). Mitochondria: major regulators of neural development. *Neuroscientist* 22, 346–358. doi: 10.1177/1073858415585472

Xu, Y. J., Sheng, H., Wu, T. W., Bao, Q. Y., Zheng, Y., Zhang, Y. M., et al. (2018). CRH/CRHR1 mediates prenatal synthetic glucocorticoid programming of depression-like behavior across 2 generations. *FASEB J.* 32, 4258–4269. doi: 10.1096/fj.201700948RR

Conflict of Interest Statement: The authors declare that the research was conducted in the absence of any commercial or financial relationships that could be construed as a potential conflict of interest.

frontiers in Neuroscience

ORIGINAL RESEARCH
published: 04 April 2019
doi: 10.3389/fnins.2019.00256

Voluntary Wheel Running Reverses Deficits in Social Behavior Induced by Chronic Social Defeat Stress in Mice: Involvement of the Dopamine System

Jing Zhang, Zhi-xiong He, Li-min Wang, Wei Yuan, Lai-fu Li, Wen-juan Hou, Yang Yang, Qian-qian Guo, Xue-ni Zhang, Wen-qi Cai, Shu-cheng An and Fa-dao Tai**

Institute of Brain and Behavioral Sciences, College of Life Sciences, Shaanxi Normal University, Xi'an, China

OPEN ACCESS

Edited by:
Xue Qun Chen, Zhejiang University, China

Reviewed by:
Tetsuya Shiuchi, Tokushima University Graduate School of Biomedical Sciences, Japan
Chun-lei Jiang, The Second Military Medical University, China

***Correspondence:**
Shu-cheng An
shuchengan@snnu.edu.cn
Fa-dao Tai
taifadao@snnu.edu.cn

Specialty section:
This article was submitted to Neuroendocrine Science, a section of the journal Frontiers in Neuroscience

Received: *14 January 2019*
Accepted: *05 March 2019*
Published: *04 April 2019*

Citation:
Zhang J, He Z-x, Wang L-m, Yuan W, Li L-f, Hou W-j, Yang Y, Guo Q-q, Zhang X-n, Cai W-q, An S-c and Tai F-d (2019) Voluntary Wheel Running Reverses Deficits in Social Behavior Induced by Chronic Social Defeat Stress in Mice: Involvement of the Dopamine System. Front. Neurosci. 13:256. doi: 10.3389/fnins.2019.00256

Voluntary exercise has been reported to have a therapeutic effect on many psychiatric disorders and social stress is known to impair social interaction. However, whether voluntary exercise could reverse deficits in social behaviors induced by chronic social defeat stress (CSDS) and the underlying mechanism remain unclear. The present study shows CSDS impaired social preference and induced social interaction deficiency in susceptible mice. Voluntary wheel running (VWR) reversed these effects. In addition, CSDS decreased the levels of tyrosine hydroxylase in the ventral tegmental area and the D2 receptor (D2R) in the nucleus accumbens (NAc) shell. These changes can be recovered by VWR. Furthermore, the recovery effect of VWR on deficits in social behaviors in CSDS mice was blocked by the microinjection of D2R antagonist raclopride into the NAc shell. Thus, these results suggest that the mechanism underlying CSDS-induced social interaction disorder might be caused by an alteration of the dopamine system. VWR may be a novel means to treat CSDS-induced deficits in social behaviors via modifying the dopamine system.

Keywords: voluntary wheel running, chronic social defeat stress, dopamine system, D2 receptors, nucleus accumbens

INTRODUCTION

Social interaction disorders such as social avoidance and lack of desire for social interaction are common symptoms of psychiatric disorders (Miyoshi and Morimura, 2010; Rosa et al., 2018). Social interaction disorders can be induced by social stress such as bullying and workplace harassment (Bonafons et al., 2009; Halabi et al., 2018). Chronic social defeat stress (CSDS) is widely used for research on the social stress in animal models (Krishnan et al., 2007; Rosa et al., 2018). In general, mice show a tendency to investigate novel same-sex conspecifics (Murugan et al., 2017). Previous reports showed that CSDS can reduce the tendency to interact with other individuals in susceptible mice, and symptoms include social avoidance and decreased social sniffing (Jin et al., 2015; Huang et al., 2016). This effect can last at least 3 weeks after the last day of CSDS (Krishnan et al., 2007; Razzoli et al., 2011). However, the mechanisms in the brain underlying the changes induced by CSDS in these social behaviors are currently poorly understood. An improved

understanding of these mechanisms is critical in finding novel treatment options for these social interaction disorders.

Growing evidence shows that the dysfunction of mesolimbic dopamine (DA) neurons negatively impacts behavioral responses to social stress (Trainor, 2011). The mesolimbic DA pathway is composed of several brain regions, including the ventral tegmental area (VTA), the nucleus accumbens (NAc), and the medial prefrontal cortex (mPFC). The VTA and its projections to NAc allow an organism to identify and learn about outcomes that are associated with stimuli, as well as to initiate appropriate approaches or avoidance responses (Wise, 2004). CSDS decreases social sniffing in susceptible mice in social interaction tests, which might involve a dysfunction of the DA receptor (Jin et al., 2015; Huang et al., 2016). In addition, injection of DA can rescue such deficits in social interaction in Dcf1 (dendritic cell factor 1, also known as TMEM59) mice, which are gene knockout mice with social interaction disorder (Liu et al., 2017). Thus, we hypothesize that CSDS-induced social interaction disorder might involve alterations in the DA system.

The NAc is a major projection site of dopaminergic neurons, which contain high levels of D1 and D2 dopamine receptors (D1R and D2R). Recent findings show that D2R in the NAc core increases only when exposed to social defeat stress in adolescent rats; however, no significant D2R alteration was observed in the same region in adolescent rats exposed to foot-shock stress (Burke et al., 2011). A further report showed that chronic passive exposure to aggression decreases D2R densities in the NAc shell in rats (Suzuki et al., 2010). In addition, only a significant decrease of D1R was observed in the prefrontal cortex (PFC) in CSDS mice, while no significant difference of D2R was observed (Huang et al., 2016). Another study reported that CSDS exerts no significant effects on D1R and D2R expression in PFC in CSDS mice (Jin et al., 2015). Thus, effects of CSDS on the levels of D1R and D2R are region-specific and stress-type-dependent. More studies are required to investigate the effects of CSDS on levels of D1R and D2R in different brain regions.

Clinical studies showed that exercise has significant effects in ameliorating psychiatric disorders, the efficacy of which is as good as that of the drug sertraline, which is used to treat psychiatric disorders. Moreover, exercise treatments have lower recurrence rates of psychiatric disorders and side effects than sertraline (Blumenthal et al., 2007; Hoffman et al., 2011). Voluntary wheel running (VWR) is a type of voluntary exercise that is regularly used in pre-clinical studies. VWR is a natural exercise intervention (Mul, 2018), similar to human motivation to exercise. A recent report showed that VWR reverses high levels of defensive/submissive behaviors induced by a single social defeat stress in Syrian hamsters (Kingston et al., 2018). Otsuka et al. pointed out that voluntary running on a wheel for 2 h can reduce the social avoidance behavior induced by CSDS (Otsuka et al., 2015). However, whether brain monoamine levels are altered by VWR remains unclear. The activation of DA receptors was found to contribute to VWR (Correa et al., 2016; Zhu et al., 2016). Thus, whether VWR can treat social interaction disorder induced by CSDS remains largely unknown. Furthermore, it remains unclear whether VWR ameliorates social interaction disorder via alteration of the DA system.

Hence, this study first examined the effects of VWR on CSDS-induced alterations of the social behavior and DA system in mice. Second, this study investigated whether VWR can reverse the CSDS-induced alteration of the DA system. Lastly, this study explored whether DA receptors play an essential role in the reversal of CSDS-induced alteration of social interaction via VWR.

MATERIALS AND METHODS

Animals

Healthy male C57BL/6J mice (7–8 week) and retired breeding mice of CD1 male mice (6 months) were purchased from the Laboratory Animal Breeding and Research Center of The Fourth Military Medical University and from Xi'an Jiaotong University (Xi'an, China), respectively. Mice were fed in a controlled room (Temperature: 22 ± 2°C, Humidity: 60 ± 5%, 12 h/12 h: light/dark cycle, 06:30/18:30) with access to food and water *ad libitum*. All procedures were approved by the Animal Care and Use Committee of Shaanxi Normal University and were in accordance with the Guide for the Care and Use of Laboratory Animals of China.

CSDS Paradigm

After 7 days of acclimation, C57BL/6J mice were randomly assigned to two groups: control group (NC, n = 12) and CSDS group (SD, n = 38). Mice from the SD group underwent a repeated social defeat stress paradigm (**Figures 1A,B**). The resident-intruder social stress paradigm was applied as previously reported with a slight modification (Golden et al., 2011). CD1 mice were selected on the basis of their attack latency (shorter than 30 s on three consecutive screening tests) and were classified as aggressive residents. The resident CD1 mouse remained solely in its own home cage. A C57BL/6J mouse as an intruder was exposed to a strange resident CD1 mouse. After 10 min of confrontation, they were separated via holed clear perforated acrylic glass (allowing the animals to see, hear, and smell each other, but preventing physical contact). They were exposed to chronic stress in the form of this threat for the next 24 h. In case the CD1 severely attacked the C57BL/6J, the defeat bout was immediately interrupted by the experimenter (**Figure 1B**). After 24 h, the intruder mouse was exposed to another strange resident CD1 mouse. The paradigm was consistently conducted between 2 pm and 5 pm for 10 days. Control group mice were pair-housed in similar cages and took turns in different cages every day; however, these were not treated to CSDS.

Social Avoidance Test

The social approach and avoidance behaviors of mice in the SD group (n = 38) were observed 1 day after CSDS. Before the tests, experimental mice were placed into the behavioral testing room for at least 1 h. The social approach and avoidance test consisted of a two-trial procedure under dimly lit conditions: during the first 2.5 min of the test (target absent condition), the experimental mouse was allowed to freely explore a square shaped open filed arena (48 × 48 cm) containing a mesh cage

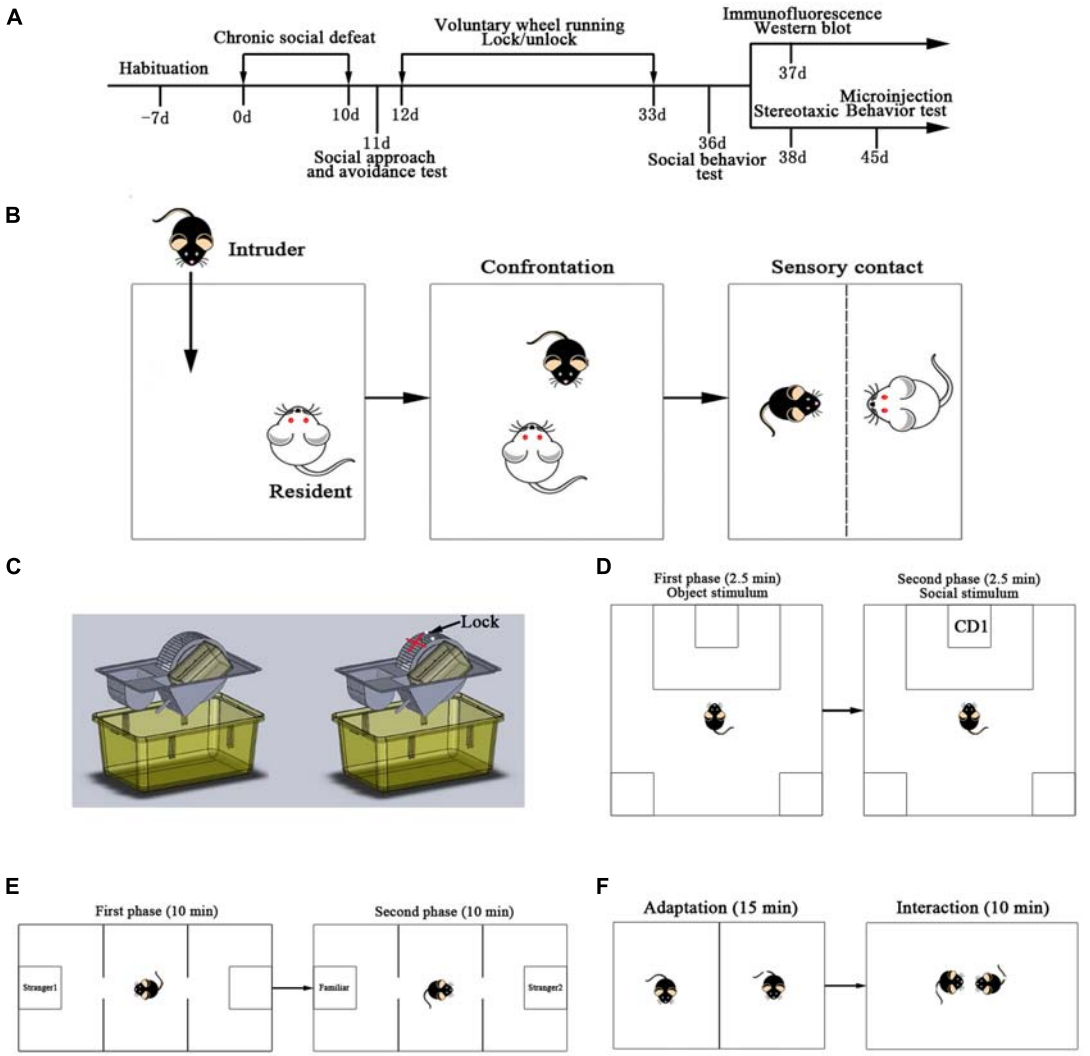

FIGURE 1 | Experiment design. **(A)** Time-line showing all the steps of the experimental manipulations. **(B)** Resident-intruder paradigm was used as chronic social defeat stress. **(C)** Voluntary wheel running was used in this study. **(D)** Scheme of the social approach and avoidance test. **(E)** Scheme of the three-chambered social test. **(F)** Scheme of the social interaction test.

(7 cm × 7 cm × 14 cm high) placed on one side of the interactive arena. The experimental C57BL/6J mouse was then removed from the testing arena for 1 min and placed into a separate cage. In the second 2.5 min of the test (target present condition), the experimental mouse was reintroduced into the arena, which contained a novel CD1 mouse in a mesh cage. "Interaction Zone" (16 × 28.8 cm) and "Corner Zone" (9.6 × 9.6 cm) were assigned as previously reported with a slight modification (Golden et al., 2011; **Figure 1D**). The duration was also recorded and scored using an automated video tracking system (Shanghai Xinruan Information Technology Co., Ltd., China). The interaction ratio was calculated as (interaction time, target present)/(interaction time, target absent) and normalized to 100. Susceptible and unsusceptible mice were separated based on the interaction ratio: mice with scores <100 were defined as "susceptible" and those with scores ≥100 were defined as "unsusceptible" or resilient (Chaudhury et al., 2013). Between sessions, the box was cleaned with 70% ethanol and dried with paper towels. From the 38 mice exposed to CSDS, 24 were susceptible and 14 were unsusceptible. Susceptible animals were used for the following study.

Exercise Protocol

To test the effects of voluntary exercise on behavioral alteration induced by CSDS, susceptible animals were separated into SD group and SD + VWR group. Mice from the SD group were CSDS mice that were exposed to a locked wheel for 21 days. The mice from the SD + VWR group were CSDS mice that were constantly exposed to VWR for 21 days (**Figures 1A,C**). Control group mice were normally fed for 21 days. Exercise training was performed using a wheel with a diameter of 160 mm, corresponding to 0.5 m per revolution (Shanghai minlylab hi-tech development, Shanghai, China).

Behavioral Test

Three-Chambered Social Test

After 21 days of VWR, the experimental mice were moved to the behavioral testing room for an adaptation of at least 1 h. The social test apparatus consisted of a box with three chambers (60 cm × 40 cm × 22 cm) under dimly lit conditions. First, the mouse was placed into the middle chamber and allowed to habituate for 10 min to three-chambers containing two empty mesh cages (7 cm × 7 cm × 14 cm) in each side-chamber. For the sociability test, an unfamiliar mouse (Stranger 1) was introduced into one of the mesh cages in one of the side chambers, leaving an empty mesh cage in the other side chamber. Then, the mouse was allowed to freely explore all three chambers for 10 min. Next, for the social preference test, a novel stranger mouse (Stranger 2) was introduced into the mesh cage that was previously empty, and the test mouse was again allowed to explore for 10 min (**Figure 1E**). The duration of the investigation was also recorded and scored using an automated video tracking system (Shanghai Xinruan Information Technology Co., Ltd., Shanghai, China).

Social Interaction Test

Behaviors of mice from different groups were observed during the social interaction test. The social interaction apparatus consisted of an open opaque acrylic box (37 × 27.5 × 18 cm). Each test mouse and an unfamiliar mouse of the same genetic background with similar weight and age were carefully and individually placed in the cage. They were separated via a paperboard to adapt to the new surroundings for 15 min. Then, the paperboard was removed and the following behaviors were recorded for 10 min using a digital video camera (**Figure 1F**): aggression, climbing (or mounting, crawling under or over), defensive (including escaping and surrender), exploration, freeze, and grooming. The total duration and frequency of these behaviors were scored using J Watch software[1] by a researcher who was blind to the experimental design. All behavioral analyses have been described previously (Jia et al., 2009; Zeng et al., 2010; Huang et al., 2016; Wang et al., 2018).

Immunofluorescence

Mice from different groups (n = 6 for each group) were anesthetized with pentobarbital sodium and transcardially perfused with 0.1 M PBS buffer (pH 7.4) followed by 4% paraformaldehyde. The brains were rapidly removed and immersed in 4% paraformaldehyde for 5–7 days, following 20% and 30% sucrose solution until saturated at 4°C. Afterward, the brains were sectioned at 30 μm thickness on a freezing microtome (CM1950, Leica, Germany) and used in the following experiment.

These slices were dried for 10 min at room temperature, then washed with 0.01 M PBS for 10 min, following incubation with 0.3% H_2O_2 for 20 min, and washed for 3 × 5 min with 0.01 M PBS. Next, sections were blocked in 5% BSA blocking solution (containing 0.2% Triton X-100, Boster, China) for 30 min, then preincubated for 60 min in blocking solution (normal goat serum, AR0009, Boster Company, China). All incubations were conducted in a dark humidifying box. After that, sections were incubated overnight at 4°C. Tyrosine hydroxylase (TH) immunofluorescence used purified rabbit polyclonal antibody of TH (1:500, ab112, Abcam, United States) diluted in antibody diluent (0.1 M PBS containing 60% bovine serum albumin). On the second day, sections were washed 3 × 5 min, and incubated in the goat anti-rabbit secondary antibody (SA1022, Boster Company, China) for 60 min in a dark humidifying box. All sections were visualized and images were captured with a fluorescent microscope (FV-1000, Olympus, Japan). Then, TH-immunoreactive (TH-ir) neurons in the VTA were bilaterally measured using the Image-Pro Plus software (V6.0, Media Cybernetics, United States).

Western Blot Analysis

The mice of different groups (n = 6 for each group) were sacrificed with an overdose of sodium pentobarbital 24 h after the behavioral tests. The mPFC, core and shell regions of the NAc and VTA were bilaterally punched out using a 1.0 mm Harris Uni-Core micropuncher (Electron Microscopy Sciences, Hatfield, PA, United States) according to the mice brain atlases (Paxinos and Franklin, 2001). These regions were then stored at −80°C until further processing. Brain tissues were homogenized in ice-cold RIPA lysis buffer. Protein concentrations were quantified with the BCA protein assay kit (Thermo Fisher Scientific). Equal amounts of total protein were separated via SDS-PAGE on 8–12% polyacrylamide gels and transferred to a nitrocellulose membrane. The immunoblots were incubated with primary antibodies overnight at 4°C followed by incubation with the corresponding secondary antibodies (1:10000, Zhong Shan Golden bridge Biotechnology, China) at room temperature for 1 h. The blots were visualized with ECL-plus reagent and the results were quantified with a fully automatic chemiluminescence image analysis system (Tanon2000). Quantification was conducted using the Image Pro Plus software, and target protein data were normalized to GAPDH band. The following primary antibodies were used: D1R (1:500, ab81296, abcam), D2R (1:1000, ab85367, abcam, United States), TH (1:1000, ab112, abcam, United States), and GAPDH (1:8000, NC020, Zhuangzhibio, China).

Stereotaxic Cannulation and Microinjection

The additional C57BL/6J mice (SD + VWR group, n = 24) received stereotaxic cannulation surgery following anesthesia with pentobarbital sodium combined with a mixture of isoflurane and oxygen under sterile conditions. 26-gauge stainless steel guide cannulae (RWD, China) were implanted bilaterally, aimed at the NAc shell (1.4 mm rostral, ± 0.5 mm bilateral, and −4.5 mm ventral to the bregma). Finally, the cannulae were affixed to the skull using dental cement. The D2R antagonist raclopride (abcam, United States) was diluted in sterile saline to obtain final concentrations of 5, 25, and 50 μg/μl. After 3 days of recovery, each mouse with normal activity (similar to that of animals without surgery) received microinjection of bilateral raclopride 1 μg/0.2 μl (n = 6), 5 μg/0.2 μl (n = 6),

[1] http://www.jwatcher.ucla.edu/

and 10 μg/0.2 μl ($n = 6$) or the same volume of saline ($n = 6$). The volume of injection was 0.1 μl for each NAc shell. The speed of injection was 0.1 μl/min and required about 1 min. The injection cannula was left in position for an additional 1 min after drug infusion. These doses were selected on the basis of previous studies with a slight modification (van den Boss et al., 1988; Miller and Lonstein, 2005; Benedetto et al., 2017; Steidl et al., 2017). The three-chambered social test and social interaction test were conducted within 30 min after microinjection. After the behavioral tests were completed, all subjects were anesthetized, and the brains were harvested. Then, the brains were cut into 30-μm sections on a cryostat to histologically verify the injection sites. The experimental data of animals in which the cannula tips were successfully located in the NAc shell were analyzed.

Statistical Analyses

According to one-sample Kolmogorov-Smirnov tests, all data were normally distributed; therefore, parametric tests were used for in statistical analyses. The results are presented as mean ± SEM. Statistical analyses were performed using SPSS version 20.0 (SPSS Institute, Chicago, IL, United States). A paired sample *t*-test was used for analysis of data from sociality and social preference tests. Multivariate analysis of variance (ANOVA) was used to analyze the behavioral data of the social interaction test. One-way ANOVA was employed to evaluate the existence of differences among three or more groups. Once a significant difference was detected, Tukey's multiple comparisons test was used to determine the significance between every two groups. A p-value <0.05 was considered statistically significant.

RESULTS

VWR Improves CSDS-Induced Deficits in Social Preference and Social Interaction

The three-chambered social test was used to investigate the effect of VWR on the levels of sociability and social preference in CSDS-induced mice. Paired-samples *t*-test showed that the mice from all three groups spent more time investigating the chamber with the strange mouse than the empty chamber, showing similar levels of sociability (NC: t (11) = 4.384, $p < 0.01$; SD: t (11) = 2.724, $p < 0.05$; SD + VWR: t (11) = 6.938, $p < 0.01$) (**Figure 2A**). However, when faced with the choice of either entering a familiar chamber or a strange chamber, mice in the NC group and SD + VWR group spent less time investigating the chamber with familiar mice than the chamber with strange mice (NC: t (11) = −2.376, $p < 0.05$; SD + VWR: t (11) = −4.707, $p < 0.01$). However, there was no significant difference in the time spent by mice of the SD group in chambers with familiar mice and strange mice (t (11) = 0.157, $p = 0.878$), suggesting that VWR improved CSDS-induced deficiency of social preference (**Figure 2B**).

The social interaction test was used to evaluate the effect of VWR on social behaviors of CSDS mice. Multivariate ANOVA showed that the total durations and frequency of aggression (duration: $F_{2,\ 33} = 5.132$, $p < 0.05$; frequency: $F_{2,33} = 3.436$, $p < 0.05$), climbing (duration: $F_{2,33} = 5.351$, $p < 0.05$; frequency: $F_{2,33} = 4.595$, $p < 0.05$), defensive (duration: $F_{2,33} = 5.78$, $p < 0.01$; frequency: $F_{2,33} = 5.768$, $p < 0.01$), exploration (duration: $F_{2,33} = 6.424$, $p < 0.01$; frequency: $F_{2,33} = 4.69$, $p < 0.05$), and freeze (duration: $F_{2,33} = 8.078$, $p < 0.01$; frequency: $F_{2,33} = 10.428$, $p < 0.01$) were significantly different between groups. CSDS significantly decreased the duration of aggression ($p < 0.05$), climbing ($p < 0.05$), and exploration behavior ($p < 0.05$), while increasing the levels of defensive behavior ($p < 0.01$) and freeze ($p < 0.01$) compared to NC groups. VWR significantly reversed the effects of CSDS on aggression ($p < 0.05$), climbing ($p < 0.05$), exploration behavior ($p < 0.01$), defensive behavior ($p < 0.05$), and freeze ($p < 0.01$) compared to the SD group (**Figure 2C**). CSDS significantly decreased the frequency of climbing ($p < 0.05$) and exploration behavior ($p < 0.05$), while increasing the levels of defensive behavior ($p < 0.05$) and freeze ($p < 0.01$) compared to the NC group. VWR significantly reversed the effects of CSDS climbing ($p < 0.05$), exploration behavior ($p < 0.05$), defensive behavior ($p < 0.05$), and freeze ($p < 0.01$) compared to SD groups (**Figure 2D**). This result suggests that VWR improved CSDS-induced deficiency in social interaction.

VWR Increases TH Levels in VTA of CSDS Mice

Western blot analysis and immunofluorescence were used to investigate the effect of VWR on TH levels in CSDS mice. As shown in **Figure 3**, the expression of TH ($F_{2,15} = 8.722$, $p < 0.05$) and the numbers of TH positive neurons ($F_{2,15} = 36.341$, $p < 0.01$) in the VTA showed significant differences between the three groups. The expression of TH and the numbers of TH positive neurons in the VTA in the SD groups were significantly lower than those in the NC groups (expression of TH: $p < 0.01$, numbers of TH positive neurons: $p < 0.01$), and significantly lower than those in the SD + VWR groups (expression of TH: $p < 0.05$, numbers of TH positive neurons: $p < 0.01$) (**Figure 3**). These results indicate that TH in the VTA might be involved in the reverse effects of VWR on deficits in CSDS-induced social interaction.

VWR Increases Expressions of D2R in NAc Shell of CSDS-Induced Mice

Western blot analysis was used to evaluate the effect of VWR on expression levels of dopamine receptors in the mPFC and NAc of CSDS mice. As shown in **Figure 4**, expression levels of D1R in the mPFC ($F_{2,15} = 1.884$, $p = 0.754$), NAc core ($F_{2,15} = 0.675$, $p = 0.505$), and NAc shell ($F_{2,15} = 1.034$, $p = 0.561$) were not significantly different among the three groups. Expressions of D2R in the mPFC ($F_{2,15} = 2.796$, $p = 0.083$) and NAc core ($F_{2,15} = 0.61$, $p = 0.26$) were not significantly different among the three groups. However, D2R levels in the NAc shell of mice in the SD group ($p < 0.01$) were significantly lower compared to the NC group, and VWR up-regulated CSDS-induced decrease in D2R expression in the NAc shell ($p < 0.01$) (**Figure 4**). These results suggest that D2R in the NAc shell might be involved in

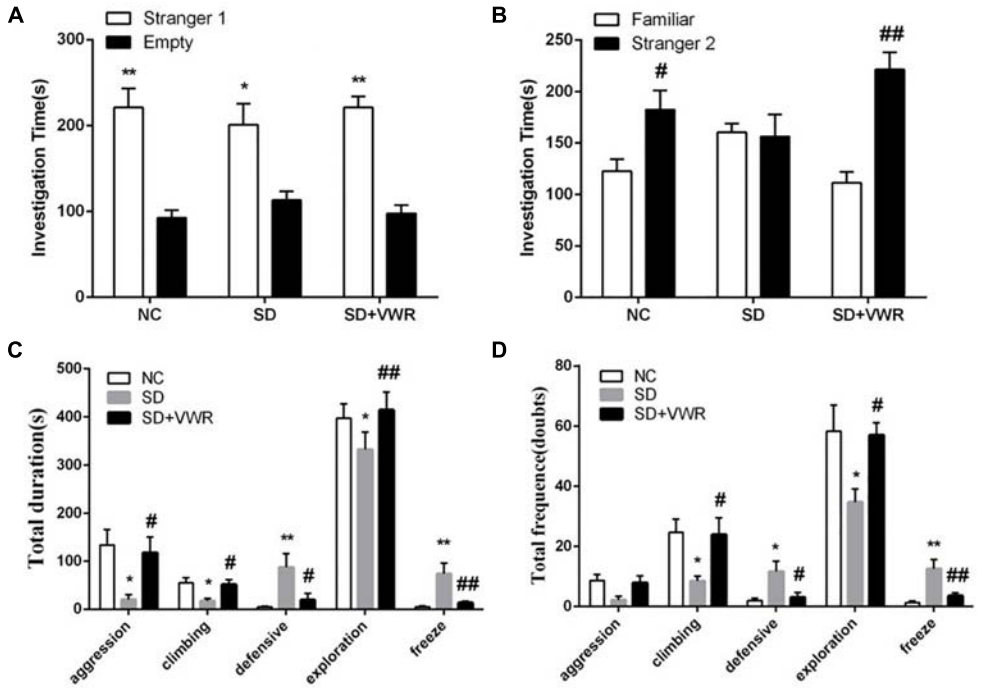

FIGURE 2 | The effect of VWR on CSDS-induced alteration in sociability and social interaction. The sociability **(A)** and social preference **(B)** of mice were detected by three-chambered social test. **(A)** $^{*}p < 0.05$ and $^{**}p < 0.01$, stranger 1 vs. empty. **(B)** $^{\#}p < 0.05$ and $^{\#\#}p < 0.01$, stranger 2 vs. familiar. The total durations **(C)** and frequency **(D)** of social interaction behaviors were tested by social interaction test. $n = 12$. $^{*}p < 0.05$ and $^{**}p < 0.01$, vs. NC. $^{\#}p < 0.05$ and $^{\#\#}p < 0.01$, vs. SD. NC, control group; SD, chronic social defeat stress; SD + VWR, SD + voluntary wheel running.

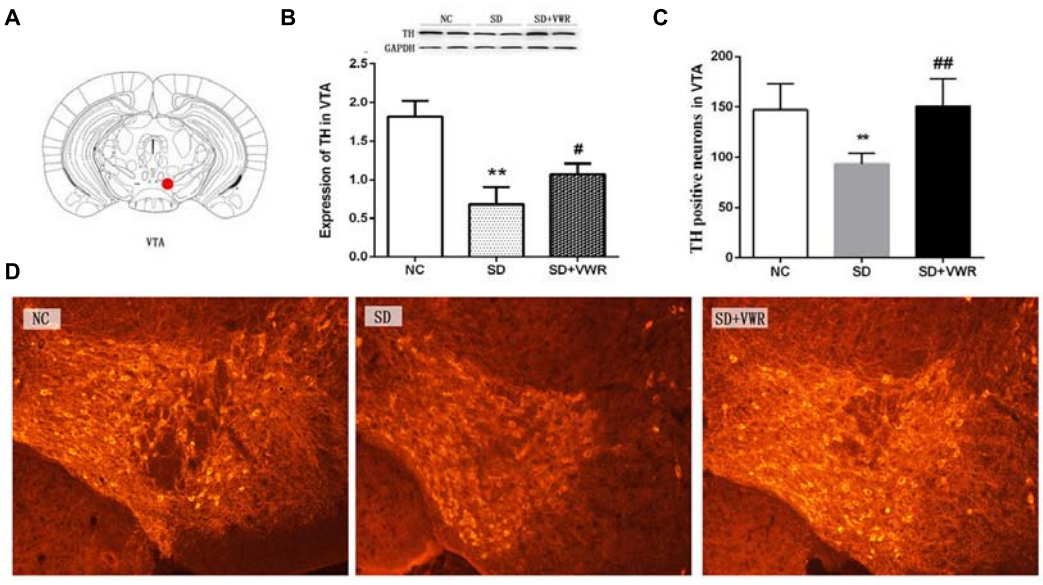

FIGURE 3 | The effect of VWR on CSDS-induced changes in TH levels in the VTA. **(A)** Location of the VTA. **(B)** The expression of TH in the VTA was measured by western blot. **(C,D)** The numbers of TH positive neurons in the VTA was detected by immunofluorescence. Bar = 100 μm. $n = 6$. $^{**}p < 0.01$, vs. NC. $^{\#}p < 0.05$, and $^{\#\#}p < 0.01$, vs. SD. TH, tyrosine hydroxylase; NC, control group; SD, chronic social defeat stress; SD + VWR, SD + voluntary wheel running.

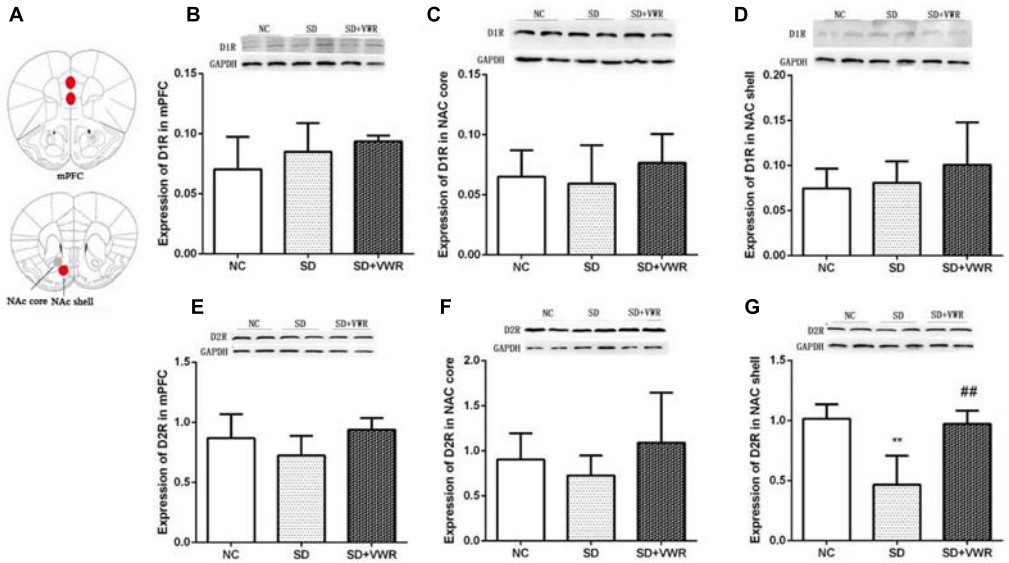

FIGURE 4 | The effect of VWR on CSDS-induced changes in D1R and D2R levels in the mPFC and NAc. **(A)** Locations of the mPFC, NAc core and NAc shell. The expressions of D1R in the mPFC **(B)**, NAc core **(C)** and NAc shell **(D)** were measured by western blot. The expression levels of D2R in mPFC **(E)**, NAc core **(F)** and NAc shell **(G)** were measured by western blot. $n = 6$. $^{**}p < 0.01$, vs. NC. $^{\#\#}p < 0.01$, vs. SD. D1R, dopamine D1 receptor; D2R, dopamine D2 receptor; NC, control group; SD, chronic social defeat stress; SD + VWR, SD + voluntary wheel running.

the reversal of the effects of VWR on deficits in social interaction induced by CSDS.

Raclopride Induced D2R Blockages in the NAc Shell Induce Deficits in Social Interaction in Mice of the SD + VWR Group

To explore the involvement of D2R in the NAc shell on social behaviors in mice of the SD + VWR group, raclopride (a D2R specific antagonist) at dosages of 1, 5, and 10 μg were microinjected into the NAc of mice with SD + VWR via stereotaxic apparatus (**Figure 5A**). Then, the three-chambered social test and social interaction test were used to evaluate social behaviors of mice after D2R blockage. In the three-chambered social test, paired-samples *t*-test showed that mice spent more time investigating the chamber with strange mice than the empty chamber (saline: $t\ (5) = 4.161$, $p < 0.01$, 1 μg: ($t\ (5) = 4.356$, $p < 0.01$), 5 μg: ($t\ (5) = 7.635$, $p < 0.01$), and 10 μg ($t\ (5) = 3.24$, $p < 0.05$), showing similar levels of sociability among all four groups of mice (**Figure 5B**). However, when faced with the choice of entering a familiar chamber or a strange chamber, only mice microinjected with 10 μg of raclopride ($t\ (5) = 5.795$, $p < 0.01$) showed a preference for familiar mice, while other groups showed a significant preference for strange mice (saline: $t\ (5) = -3.565$, $p < 0.05$; 1 μg/μl: $t\ (5) = -2.913$, $p < 0.05$; 5 μg, $t\ (5) = -2.767$, $p < 0.05$) (**Figure 5C**). These results suggest that D2R blockage caused by 10 μg of raclopride induced a social preference deficit in mice with SD + VWR.

In the social interaction test, multivariate ANOVA showed that the total duration of aggression ($F_{3,20} = 3.159$, $p < 0.05$), defensive behavior ($F_{3,20} = 8.234$, $p < 0.01$), exploration ($F_{3,20} = 3.303$, $p < 0.05$), and freeze ($F_{3,20} = 3.435$, $p < 0.05$) were differed significantly among groups. No significant difference in the total duration of climbing was found ($F_{3,20} = 0.123$, $p = 0.946$). Tukey *post hoc* tests showed that the 10 μg group spent less time engaging in aggression ($p < 0.05$), exploration ($p < 0.05$), and grooming ($p < 0.05$), but spent more time engaging with defensive behavior ($p < 0.01$) and freeze ($p < 0.05$) than the saline group. Mice of the 10 μg group spent more time engaging in defensive behavior than mice of the 1 μg group ($p < 0.01$) and the 5 μg group ($p < 0.01$) (**Figure 5D**). Multivariate ANOVA showed that the D2 receptors antagonists significantly changed the frequency of aggression ($F_{3,20} = 3.492$, $p < 0.05$), defensive behavior ($F_{3,20} = 7.518$, $p < 0.01$), and grooming ($F_{3,20} = 3.402$, $p < 0.05$). Tukey *Post hoc* tests showed that mice of the 10 μg group exhibited a lower frequency of aggression ($p < 0.05$) and a higher frequency of defensive behavior ($p < 0.01$) than the saline group. Mice from the 10 μg group engaged in defensive behavior more frequently than those of the 1 μg group ($p < 0.01$) and the 5 μg group ($p < 0.01$). No significant differences were found in the total frequency of climbing ($F_{3,20} = 0.066$, $p = 0.978$), exploration ($F_{3,20} = 0.593$, $p = 0.627$), and freeze ($F_{3,20} = 0.829$, $p = 0.493$) (**Figure 5E**). These data show that D2R blockage via 10 μg raclopride induced deficiency in social interaction in mice with SD + VWR.

DISCUSSION

In this study, VWR reversed the impairment of social preference and deficiency in social interaction induced by CSDS in susceptible mice. In addition, the decreased levels of TH in the

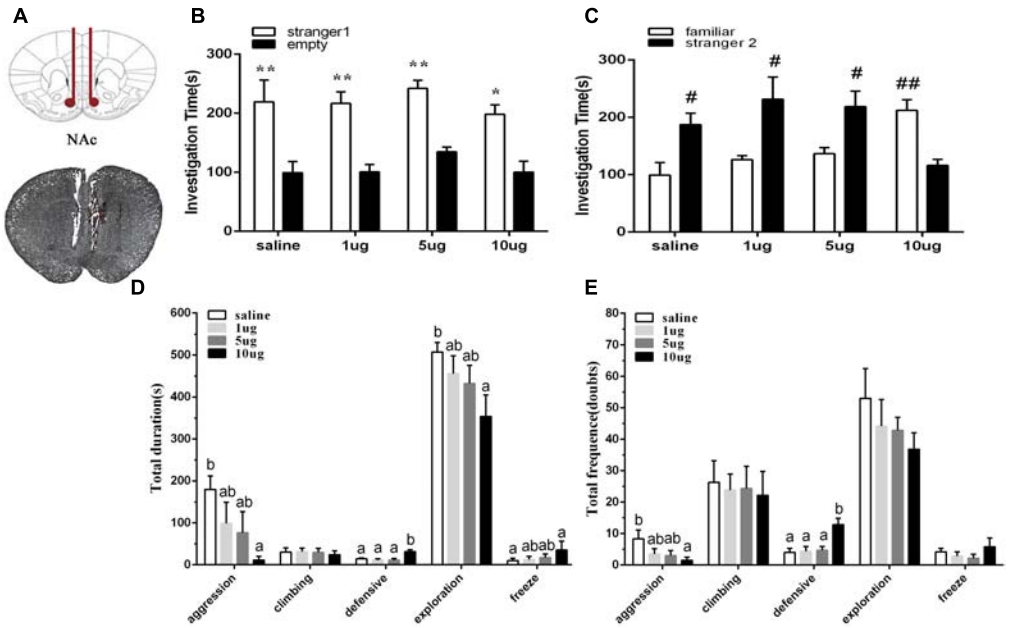

FIGURE 5 | Effect of D2R blockage in the NAc shell on social behaviors in mice with SD + VWR. **(A)** Histological verification of injection sites located in the NAc shell. The sociability **(B)** and social preference **(C)** of mice were detected by three-chambered social test after microinjection of saline and 1, 5, 10 μg raclopride into the NAc shell. **(B)** $^{*}p < 0.05$ and $^{**}p < 0.01$, stranger 1 vs. empty. **(C)** $^{\#}p < 0.05$ and $^{\#\#}p < 0.01$, stranger 2 vs. familiar. The total durations **(D)** and frequency **(E)** of social interaction behaviors were tested by social interaction test after microinjection of saline and 1, 5, 10 μg raclopride into the NAc shell. $n = 6$. Groups not sharing the same letters are significantly different from each other in each behavior ($p < 0.05$). NC, control group; SD, chronic social defeat stress; SD + VWR, SD + voluntary wheel running.

VTA and D2R in the NAc shell induced by CSDS were also up-regulated by VWR. Furthermore, the recovery effect of VWR in CSDS mice with regard to deficits in social interaction was blocked by microinjection of the D2R antagonist raclopride into the NAc shell. Thus, this study provides a novel method to treat CSDS-induced social interaction disorder and verifies the involvement of the dopamine system in this process.

VWR Reversed Impairment of Social Preference and Deficiency in Social Interaction Induced by CSDS

This study showed that CSDS impaired social preferences and induced deficiency in social interaction. In the social preference test, CSDS mice spent more time with familiar than novel mice. These results are consistent with a previous report where defeated mice exposed to aggressive CD1 mice did not display social avoidance behavior toward a conspecific mouse (Desbonnet et al., 2012). However, in this social preference test, CSDS mice spent more time with familiar mice. In general, rodents tend to investigate novel same-sex conspecifics (Murugan et al., 2017). However, following exposure to social stress, rodents choose familiar mice (Hammels et al., 2015). This is also in agreement with previous studies where CSDS female mandarin voles (*Microtus mandarinus*) showed avoidance behavior to novel same-sex conspecifics (Wang et al., 2018). This suggests that SD group mice had an increased amount of vigilance when faced with novel mice and even displayed decreased curiosity. In social interaction tests, the SD group showed higher levels of defensive, freeze behavior, aggression, climbing, and exploration compared to controls, which indicates a lack of desire for social interaction. Disruption of natural social behavior is a common symptom of neuropsychiatric disorder (Miyoshi and Morimura, 2010). Previous studies showed that CSDS could induce a deficiency in social interaction (Iniguez et al., 2014; Yin et al., 2015). This result is also consistent with previous reports indicating that CSDS induces social interaction disorder in susceptible mice (Gray et al., 2015; Jin et al., 2015; Huang et al., 2016). Therefore, these findings support the CSDS impaired social preference and induced deficiency in social interaction.

Interestingly, VWR could reverse the impairment of social preference and deficiency in social interaction induced by CSDS. This is consistent with previous studies where exercise before or in the process of CSDS can reverse social avoidance of defeated mice (Otsuka et al., 2015; Mul et al., 2018). The time of VWR in the present study is more similar to the treatment of psychiatric disorders using antidepressants in human. This finding is supported by several lines of evidence, reporting that physical exercise can effectively relieve psychopathological disorders, and the effect of exercise is similar to or more significant than that of a psychological intervention and antidepressant treatment (Blumenthal et al., 2007; Hoffman et al., 2011; Otsuka et al., 2015; Kingston et al., 2018). These results suggest that voluntary exercise is an effective way to treat social interaction disorders induced by social stress.

Effect of VWR on Levels of VTA TH in CSDS Mice

Chronic social defeat stress also reduced the levels of TH in the VTA. VWR reversed this alteration. The up-regulated levels of TH might increase DA synthesis in the VTA, and increased its release in dopaminergic neuron projection areas, such as the NAc. VTA is the origin of dopaminergic neurons. Tyrosine hydroxylase is a speed-limiting enzyme in dopamine synthesis from tyrosine. Previous findings indicate that dopaminergic neurons in the VTA and their projections to the NAc (but not the mPFC) induced susceptibility to CSDS (Nestler and Carlezon, 2006; Chaudhury et al., 2013). A further report also showed that dopaminergic neurons in the VTA project to the shell of the NAc (Lammel et al., 2011). In addition, optogenetic phasic stimulation of VTA DA neurons also induced a susceptible phenotype in previously resilient TH-Cre mice that have been subjected to CSDS (Chaudhury et al., 2013). The results of the present study agree with these previous findings. Although these results show that VWR reversed the decrease of both TH positive neurons and TH expression in the VTA induced by CSDS, the reversing effect of VWR on the decrease of TH positive neurons in the VTA is more significant than the reversing effect on the decrease of TH expression in the VTA. This discrepancy may be due to methodological differences (immunofluorescence vs. Western blot). The recovery effect of VWR on deficits in social interaction of CSDS mice was related to the levels of TH in the VTA and their projections areas.

Effect of VWR on Levels of NAc Shell D2R in CSDS Mice

Western blot showed that CSDS decreased D2R protein expression in the NAc shell. No significant difference in D1R expression was observed between control and CSDS groups in the mPFC, NAc core, and shell. These results are consistent with a previous study where CSDS was reported to only alter the dopaminergic projection from VTA to NAc, but had no significant effects on projection from VTA to mPFC (Chaudhury et al., 2013). An increasing number of studies showed that the dysfunction of dopamine and its receptors is an important cause of social defeat stress (Trainor, 2011; Huang et al., 2016). Previous results showed that changes in D1R and D2R expression induced by social stress are inconsistent. For example, D2R density was reported to be elevated in the NAc after single and repeated visible burrow system treatments (a chronic social stress paradigm), but no change in D1R binding was observed (Lucas et al., 2004). Eight weeks of social isolation did not change the D2R expression in the NAc core or shell (Malone et al., 2008). No significant change was observed in adolescent rats in the expression of D2R in the NAc after CSDS (Burke et al., 2011). The results of this study are inconsistent with these previous studies. Although caution needs to be applied in the interpretation of these results, one possible explanation for this inconsistency may be that the levels of the D2R fluctuation depend on different stress. Another possible explanation is that adolescent and adult animals may have different changes of DA receptors in the brain after CSDS. However, the result of the present study is supported by a previous study where chronic passive exposure to aggression was reported to decrease D2R densities in the cortical-accumbal regions (shell of the NAc and cingulate and motor cortices) (Suzuki et al., 2010). Another interesting finding is that 3 week of VWR in mice could increase D2R levels in the NAc shell. Using the running wheel may be a natural reward (Novak et al., 2012), and both genders displayed a strong conditioned place preference associated with running (Basso and Morrell, 2015). Young et al. pointed out that the DA receptor in the NAc plays an important role in the motor motivation underlying voluntary exercise (Park et al., 2016). The results of the present study are inconsistent with a previous report where the activation of dopamine D2/D3 receptors was reported to contribute to the motivation for mice during VWR training (Ebada et al., 2016). The strategy of direct control of neural activity by using designer receptors exclusively activated by designer drugs (DREADD) showed that manipulation of NAc D2R neuron influences the running distance (Zhu et al., 2016). A further possibility suggests that VWR or exercise training increases daily food intake and this increased appetite may possibly induce elevation of D2R expression in NAc. This is possibly also associated with the observed reversal of VWR effects in the present study since it has been reported that increased food intake can also reduce social avoidance behavior induced by mild chronic stress (Otsuka et al., 2015). The results obtained in the present study agree with these previous studies, showing that VWR increased the D2R expression in the NAc shell. An increased running distance may improve the therapeutic effect of voluntary exercise on social interaction disorders. The effects of VWR on social interaction deficits induced by CSDS may be initiated via the upregulation of D2R in the NAc shell.

D2R Blockage in the NAc Shell Induces Social Interaction Deficits in Mice With SD+VWR

Consistent with the hypothesis of this study, the recovery effect of VWR to CSDS mice on social interaction deficits was blocked via microinjection of the D2R antagonist raclopride into the NAc shell. The results that the VWR reverses CSDS-induced social interaction deficit is consistent with effects reported for antidepressants, which predominantly increase D2R mRNA in the NAc shell (Ainsworth et al., 1998). In addition, activation of D2R in the NAc also has an antidepressant effect (Gershon et al., 2007). Increase of D2R expression in the NAc of adult mice enhances motivation (Trifilieff et al., 2013). However, mice exposed to CSDS displayed a lack of desire for social interaction (Miyoshi and Morimura, 2010; Rosa et al., 2018). Injection of a D2R agonist in the CSDS group might improve deficits in social behavior. Therefore, it can be inferred that impairments in social preference and deficiency in social interaction could be reversed by voluntary exercise via activation of D2R in the NAc shell.

Despite this clear result, this study has several limitations. First, CSDS may affect the level of spontaneous running, and therefore, a control group without CSDS should be included in

future research. Second, DA agonist microinjection in the SD group should be included in further investigations to confirm whether exercising decreases CSDS-induced social interaction disorder by increasing D2R in the NAc. Third, although a number of studies reported that CSDS could increase depression-like behaviors in rodents (Garcia-Garcia et al., 2017; Fukumoto et al., 2018), future studies should better test whether VWR could also reverse CSDS-induced depression-like behaviors and whether the 5-HT system is involved in this process.

CONCLUSION

In conclusion, this study showed that CSDS can impair social preference and induce a deficiency in social interaction. These effects could be reversed by VWR. Both the TH in the VTA and D2R in the NAc shell may be involved in the processes underlying the reversal of CSDS-induced social interaction deficit mediated by voluntary exercise. This finding suggests that voluntary exercise has positive efficacy in the treatment of CSDS-induced social interaction disorder via alteration of the levels of D2R in the NAc shell. This result indicates that voluntary exercise can treat social interaction disorder induced by CSDS, and its underlying mechanism may be the activation of the DA system. These results suggest that voluntary exercise can be used as a complementary therapy method to treat psychiatric disorders.

DATA AVAILABILITY

All datasets generated for this study are included in the manuscript.

AUTHOR CONTRIBUTIONS

JZ, F-dT, and S-cA designed the experiments. JZ, WY, YY, Q-qG, W-qC, and L-fL performed the experiments. JZ, W-jH, X-nZ, Z-xH, and L-mW analyzed the data and prepared the figures. JZ and F-dT wrote the manuscript. All authors approved the final version of the manuscript.

FUNDING

This research was supported by the National Natural Science Foundation of China (Grant Nos. 31670421 and 31372213) and Fundamental Research Funds for Central University (GK201102018).

REFERENCES

Ainsworth, K., Smith, S. E., Zetterstrom, T. S., Pei, Q., Franklin, M., and Sharp, T. (1998). Effect of antidepressant drugs on dopamine D1 and D2 receptor expression and dopamine release in the nucleus accumbens of the rat. *Psychopharmacology* 140, 470–477. doi: 10.1007/s002130050791

Basso, J. C., and Morrell, J. I. (2015). The medial prefrontal cortex and nucleus accumbens mediate the motivation for voluntary wheel running in the rat. *Behav. Neurosci.* 129, 457–472. doi: 10.1037/bne0000070

Benedetto, L., Rivas, M., Cavelli, M., Pena, F., Monti, J., Ferreira, A., et al. (2017). Microinjection of the dopamine D2-receptor antagonist raclopride into the medial preoptic area reduces REM sleep in lactating rats. *Neurosci. Lett.* 659, 104–109. doi: 10.1016/j.neulet.2017.08.077

Blumenthal, J. A., Babyak, M. A., Doraiswamy, P. M., Watkins, L., Hoffman, B. M., Barbour, K. A., et al. (2007). Exercise and pharmacotherapy in the treatment of major depressive disorder. *Psychosom. Med.* 69, 587–596. doi: 10.1097/psy.0b013e318148c19a

Bonafons, C., Jehel, L., and Coroller-Bequet, A. (2009). Specificity of the links between workplace harassment and PTSD: primary results using court decisions, a pilot study in France. *Int. Arch. Occup. Environ. Health* 82, 663–668. doi: 10.1007/s00420-008-0370-379

Burke, A. R., Watt, M. J., and Forster, G. L. (2011). Adolescent social defeat increases adult amphetamine conditioned place preference and alters D2 dopamine receptor expression. *Neuroscience* 197, 269–279. doi: 10.1016/j.neuroscience.2011.09.008

Chaudhury, D., Walsh, J. J., Friedman, A. K., Juarez, B., Ku, S. M., Koo, J. W., et al. (2013). Rapid regulation of depression-related behaviours by control of midbrain dopamine neurons. *Nature* 493, 532–536. doi: 10.1038/nature11713

Correa, M., Pardo, M., Bayarri, P., Lopez-Cruz, L., San Miguel, N., Valverde, O., et al. (2016). Choosing voluntary exercise over sucrose consumption depends upon dopamine transmission: effects of haloperidol in wild type and adenosine A(2)AKO mice. *Psychopharmacology* 233, 393–404. doi: 10.1007/s00213-015-4127-3

Desbonnet, L., O'Tuathaigh, C., Clarke, G., O'Leary, C., Petit, E., Clarke, N., et al. (2012). Phenotypic effects of repeated psychosocial stress during adolescence in mice mutant for the schizophrenia risk gene neuregulin-1: a putative model of gene x environment interaction. *Brain Behav. Immun.* 26, 660–671. doi: 10.1016/j.bbi.2012.02.010

Ebada, M. E., Kendall, D. A., and Pardon, M. C. (2016). Corticosterone and dopamine D2/D3 receptors mediate the motivation for voluntary wheel running in C57BL/6J mice. *Behav. Brain Res.* 311, 228–238. doi: 10.1016/j.bbr.2016.05.051

Fukumoto, K., Iijima, M., Funakoshi, T., and Chaki, S. (2018). Role of 5-HT1A receptor stimulation in the medial prefrontal cortex in the sustained antidepressant effects of ketamine. *Int. J. Neuropsychopharmacol.* 21, 371–381. doi: 10.1093/ijnp/pyx116

Garcia-Garcia, A. L., Meng, Q., Canetta, S., Gardier, A. M., Guiard, B. P., Kellendonk, C., et al. (2017). Serotonin signaling through prefrontal cortex 5-HT1A receptors during adolescence can determine baseline mood-related behaviors. *Cell Rep.* 18, 1144–1156. doi: 10.1016/j.celrep.2017.01.021

Gershon, A. A., Vishne, T., and Grunhaus, L. (2007). Dopamine D2-like receptors and the antidepressant response. *Biol. Psychiatry* 61, 145–153. doi: 10.1016/j.biopsych.2006.05.031

Golden, S. A., Covington, H. E. III, Berton, O., and Russo, S. J. (2011). A standardized protocol for repeated social defeat stress in mice. *Nat. Protoc.* 6, 1183–1191. doi: 10.1038/nprot.2011.361

Gray, C. L., Norvelle, A., Larkin, T., and Huhman, K. L. (2015). Dopamine in the nucleus accumbens modulates the memory of social defeat in Syrian hamsters (*Mesocricetus auratus*). *Behav. Brain Res.* 286, 22–28. doi: 10.1016/j.bbr.2015.02.030

Halabi, F., Ghandour, L., Dib, R., Zeinoun, P., and Maalouf, F. T. (2018). Correlates of bullying and its relationship with psychiatric disorders in lebanese adolescents. *Psychiatry Res.* 261, 94–101. doi: 10.1016/j.psychres.2017.12.039

Hammels, C., Pishva, E., De Vry, J., van den Hove, D. L., Prickaerts, J., van Winkel, R., et al. (2015). Defeat stress in rodents: From behavior to molecules. *Neurosci. Biobehav. Rev.* 59, 111–140. doi: 10.1016/j.neubiorev.2015.10.006

Hoffman, B. M., Babyak, M. A., Craighead, W. E., Sherwood, A., Doraiswamy, P. M., Coons, M. J., et al. (2011). Exercise and pharmacotherapy in patients with major depression: one-year follow-up of the SMILE study. *Psychosom. Med.* 73, 127–133. doi: 10.1097/PSY.0b013e31820433a5

Huang, G. B., Zhao, T., Gao, X. L., Zhang, H. X., Xu, Y. M., Li, H., et al. (2016). Effect of chronic social defeat stress on behaviors and dopamine receptor in adult mice. *Prog. Neuropsychopharmacol. Biol. Psychiatry* 66, 73–79. doi: 10.1016/j.pnpbp.2015.12.002

Iniguez, S. D., Riggs, L. M., Nieto, S. J., Dayrit, G., Zamora, N. N., Shawhan, K. L., et al. (2014). Social defeat stress induces a depression-like phenotype in adolescent male c57BL/6 mice. *Stress* 17, 247–255. doi: 10.3109/10253890.2014.910650

Jia, R., Tai, F., An, S., Zhang, X., and Broders, H. (2009). Effects of neonatal paternal deprivation or early deprivation on anxiety and social behaviors of the adults in mandarin voles. *Behav. Process.* 82, 271–278. doi: 10.1016/j.beproc.2009.07.006

Jin, H. M., Shrestha Muna, S., Bagalkot, T. R., Cui, Y., Yadav, B. K., and Chung, Y. C. (2015). The effects of social defeat on behavior and dopaminergic markers in mice. *Neuroscience* 288, 167–177. doi: 10.1016/j.neuroscience.2014.12.043

Kingston, R. C., Smith, M., Lacey, T., Edwards, M., Best, J. N., and Markham, C. M. (2018). Voluntary exercise increases resilience to social defeat stress in Syrian hamsters. *Physiol. Behav.* 188, 194–198. doi: 10.1016/j.physbeh.2018.02.003

Krishnan, V., Han, M. H., Graham, D. L., Berton, O., Renthal, W., Russo, S. J., et al. (2007). Molecular adaptations underlying susceptibility and resistance to social defeat in brain reward regions. *Cell* 131, 391–404. doi: 10.1016/j.cell.2007.09.018

Lammel, S., Ion, D. I., Roeper, J., and Malenka, R. C. (2011). Projection-specific modulation of dopamine neuron synapses by aversive and rewarding stimuli. *Neuron* 70, 855–862. doi: 10.1016/j.neuron.2011.03.025

Liu, Q., Shi, J., Lin, R., and Wen, T. (2017). Dopamine and dopamine receptor D1 associated with decreased social interaction. *Behav. Brain Res.* 324, 51–57. doi: 10.1016/j.bbr.2017.01.045

Lucas, L. R., Celen, Z., Tamashiro, K. L., Blanchard, R. J., Blanchard, D. C., Markham, C., et al. (2004). Repeated exposure to social stress has long-term effects on indirect markers of dopaminergic activity in brain regions associated with motivated behavior. *Neuroscience* 124, 449–457. doi: 10.1016/j.neuroscience.2003.12.009

Malone, D. T., Kearn, C. S., Chongue, L., Mackie, K., and Taylor, D. A. (2008). Effect of social isolation on CB1 and D2 receptor and fatty acid amide hydrolase expression in rats. *Neuroscience* 152, 265–272. doi: 10.1016/j.neuroscience.2007.10.043

Miller, S. M., and Lonstein, J. S. (2005). Dopamine d1 and d2 receptor antagonism in the preoptic area produces different effects on maternal behavior in lactating rats. *Behav. Neurosci.* 119, 1072–1083. doi: 10.1037/0735-7044.119.4.1072

Miyoshi, K., and Morimura, Y. (2010). Clinical manifestations of neuropsychiatric disorders. *Neuropsychiatr. Disord.* 1–14. doi: 10.1007/978-4-431-53871-4_1

Mul, J. D. (2018). Voluntary exercise and depression-like behavior in rodents: are we running in the right direction? *J. Mol. Endocrinol.* 60, R77–R95. doi: 10.1530/JME-17-0165

Mul, J. D., Soto, M., Cahill, M. E., Ryan, R. E., Takahashi, H., So, K., et al. (2018). Voluntary wheel running promotes resilience to chronic social defeat stress in mice: a role for nucleus accumbens DeltaFosB. *Neuropsychopharmacology* 43, 1934–1942. doi: 10.1038/s41386-018-0103-z

Murugan, M., Jang, H. J., Park, M., Miller, E. M., Cox, J., Taliaferro, J. P., et al. (2017). Combined social and spatial coding in a descending projection from the prefrontal cortex. *Cell* 171, 1663.e16–1677.e16. doi: 10.1016/j.cell.2017.11.002

Nestler, E. J., and Carlezon, W. A. Jr. (2006). The mesolimbic dopamine reward circuit in depression. *Biol. Psychiatry* 59, 1151–1159. doi: 10.1016/j.biopsych.2005.09.018

Novak, C. M., Burghardt, P. R., and Levine, J. A. (2012). The use of a running wheel to measure activity in rodents: relationship to energy balance, general activity, and reward. *Neurosci. Biobehav. Rev.* 36, 1001–1014. doi: 10.1016/j.neubiorev.2011.12.012

Otsuka, A., Shiuchi, T., Chikahisa, S., Shimizu, N., and Sei, H. (2015). Voluntary exercise and increased food intake after mild chronic stress improve social avoidance behavior in mice. *Physiol. Behav.* 151, 264–271. doi: 10.1016/j.physbeh.2015.07.024

Park, Y. M., Kanaley, J. A., Padilla, J., Zidon, T., Welly, R. J., Will, M. J., et al. (2016). Effects of intrinsic aerobic capacity and ovariectomy on voluntary wheel running and nucleus accumbens dopamine receptor gene expression. *Physiol. Behav.* 164(Pt A), 383–389. doi: 10.1016/j.physbeh.2016.06.006

Paxinos, G., and Franklin, K. B. J. (2001). *The Mouse Brain in Stereotaxic Coordinates*, 2nd edn. San Diego: Academic Press.

Razzoli, M., Andreoli, M., Michielin, F., Quarta, D., and Sokal, D. M. (2011). Increased phasic activity of VTA dopamine neurons in mice 3 weeks after repeated social defeat. *Behav. Brain Res.* 218, 253–257. doi: 10.1016/j.bbr.2010.11.050

Rosa, S. G., Pesarico, A. P., and Nogueira, C. W. (2018). m-Trifluoromethyl-diphenyl diselenide promotes resilience to social avoidance induced by social defeat stress in mice: contribution of opioid receptors and MAPKs. *Prog. Neuropsychopharmacol. Biol. Psychiatry* 82, 123–135. doi: 10.1016/j.pnpbp.2017.11.021

Steidl, S., O'Sullivan, S., Pilat, D., Bubula, N., Brown, J., and Vezina, P. (2017). Operant responding for optogenetic excitation of LDTg inputs to the VTA requires D1 and D2 dopamine receptor activation in the NAcc. *Behav. Brain Res.* 333, 161–170. doi: 10.1016/j.bbr.2017.06.045

Suzuki, H., Han, S. D., and Lucas, L. R. (2010). Chronic passive exposure to aggression decreases D2 and 5-HT 1B receptor densities. *Physiol. Behav.* 99, 562–570. doi: 10.1016/j.physbeh.2010.01.018

Trainor, B. C. (2011). Stress responses and the mesolimbic dopamine system: social contexts and sex differences. *Horm. Behav.* 60, 457–469. doi: 10.1016/j.yhbeh.2011.08.013

Trifilieff, P., Feng, B., Urizar, E., Winiger, V., Ward, R. D., Taylor, K. M., et al. (2013). Increasing dopamine D2 receptor expression in the adult nucleus accumbens enhances motivation. *Mol. Psychiatry* 18, 1025–1033. doi: 10.1038/mp.2013.57

van den Boss, R., Cools, A. R., and Ogren, S. O. (1988). Differential effects of the selective D2-antagonist raclopride in the nucleus accumbens of the rat on spontaneous and d-amphetamine-induced activity. *Psychopharmacology* 95, 447–451. doi: 10.1007/BF00172953

Wang, L., Hou, W., He, Z., Yuan, W., Yang, J., Yang, Y., et al. (2018). Effects of chronic social defeat on social behaviors in adult female mandarin voles (*Microtus mandarinus*): involvement of the oxytocin system in the nucleus accumbens. *Prog. Neuropsychopharmacol. Biol. Psychiatry* 82, 278–288. doi: 10.1016/j.pnpbp.2017.11.002

Wise, R. A. (2004). Dopamine, learning and motivation. *Nat. Rev. Neurosci.* 5, 483–494. doi: 10.1038/nrn1406

Yin, Y. Q., Zhang, C., Wang, J. X., Hou, J., Yang, X., and Qin, J. (2015). Chronic caffeine treatment enhances the resilience to social defeat stress in mice. *Food Funct.* 6, 479–491. doi: 10.1039/c4fo00702f

Zeng, S., Tai, F., Zhai, P., Yuan, A., Jia, R., and Zhang, X. (2010). Effect of daidzein on anxiety, social behavior and spatial learning in male Balb/cJ mice. *Pharmacol. Biochem. Behav.* 96, 16–23. doi: 10.1016/j.pbb.2010.03.015

Zhu, X., Ottenheimer, D., and DiLeone, R. J. (2016). Activity of D1/2 receptor expressing neurons in the nucleus accumbens regulates running, locomotion, and food intake. *Front. Behav. Neurosci.* 10:66. doi: 10.3389/fnbeh.2016.00066

Conflict of Interest Statement: The authors declare that the research was conducted in the absence of any commercial or financial relationships that could be construed as a potential conflict of interest.

frontiers in Neuroscience

REVIEW
published: 03 May 2019
doi: 10.3389/fnins.2019.00378

Role of Leptin in Mood Disorder and Neurodegenerative Disease

Xiaohan Zou[1], Lili Zhong[1], Cuilin Zhu[1], Haisheng Zhao[1], Fangyi Zhao[1], Ranji Cui[1], Shuohui Gao[2] and Bingjin Li[1]**

[1] Jilin Provincial Key Laboratory on Molecular and Chemical Genetic, The Second Hospital of Jilin University, Changchun, China, [2] Department of Gastrointestinal Colorectal Surgery, China-Japan Union Hospital of Jilin University, Changchun, China

The critical regulatory role of leptin in the neuroendocrine system has been widely reported. Significantly, leptin can improve learning and memory, affect hippocampal synaptic plasticity, exert neuroprotective efficacy and reduce the risk of several neuropsychiatric diseases. In terms of depression, leptin could modulate the levels of neurotransmitters, neurotrophic factors and reverse the dysfunction in the hypothalamic-pituitary-adrenal axis (HPA). At the same time, leptin affects neurological diseases during the regulation of metabolic homeostasis. With regards to neurodegenerative diseases, leptin can affect them via neuroprotection, mainly including Alzheimer's disease and Parkinson's disease. This review will summarize the mechanisms of leptin signaling within the neuroendocrine system with respect to these diseases and discuss the therapeutic potential of leptin.

Keywords: leptin, neurodegeneration, mood disorders, depression, neuroprotection

OPEN ACCESS

Edited by:
Yu-Feng Wang,
Harbin Medical University, China

Reviewed by:
Taixing Cui,
University of South Carolina, United States
Chun-Ping Chu,
Yanbian University, China

****Correspondence:***
Bingjin Li
libingjin@jlu.edu.cn
Shuohui Gao
gaoshuohui@foxmail.com

Specialty section:
This article was submitted to Neuroendocrine Science, a section of the journal Frontiers in Neuroscience

Received: *04 September 2018*
Accepted: *02 April 2019*
Published: *03 May 2019*

Citation:
Zou X, Zhong L, Zhu C, Zhao H, Zhao F, Cui R, Gao S and Li B (2019) Role of Leptin in Mood Disorder and Neurodegenerative Disease. Front. Neurosci. 13:378. doi: 10.3389/fnins.2019.00378

INTRODUCTION

Leptin is an adipocyte-derived hormone which is encoded by the obese gene (Zhang et al., 1994). Receptors of leptin are expressed in many brain regions, such as the arcuate nucleus of the hypothalamus, olfactory bulb, the dorsal raphe nucleus, hippocampus, the cortex and the nucleus of the solitary tract (Tartaglia et al., 1995). Recently, growing experimental results indicate that leptin also plays a significant regulatory role in the central nervous system (CNS) and is associated with several pathological and physiological mechanisms of neurological diseases, including neurodegenerative diseases and mood disorders (Lee et al., 2015; Kurosawa et al., 2016). It was found that neurological diseases occurred alongside leptin level alterations, indicating that leptin might be a critical modulator of these diseases and studying the specific relationship is of significance. In this article, we mainly discuss the role of leptin in mood disorder and neurodegenerative diseases and try to interpret the potential mechanisms.

THE ROLE OF LEPTIN IN DEPRESSION

Depression is one of the most prevalent mental illnesses, with high morbidity and suicide rates (Milaneschi et al., 2017). Due to the serious side-effects and long onset time of traditional antidepressants, recent investigations focus on neuropeptides' antidepressant effects and potential mechanisms, such as leptin and ghrelin (Kormos and Gaszner, 2013). Clinical studies investigating the relationship of depression and leptin levels yielded inconsistent results. Lower leptin levels were reported in depressive patients compared to controls in earlier studies. However, there is also research demonstrating that patients with major depression disorder have higher leptin

levels (Milaneschi et al., 2017). The confounding factors, including age, gender, and medication history of depressive patients, might impact periphery leptin levels (Ge et al., 2018). Several animal studies demonstrated lower leptin levels in rats with chronic unpredictable stress (Ozsoy et al., 2015). Pharmacological studies have shown that intra-hippocampus administration of leptin could exert an antidepressant-like effect, while no positive efficacy has been detected when leptin was injected into the hypothalamus (Finn et al., 2001; Lu et al., 2006). Leptin can also increase the activation of neurons in hippocampal limbic structures which contribute to a delayed long-lasting antidepressant-like effect in force swim test (Kurosawa et al., 2016). Deletion of leptin receptor (LepRb) is sufficient to induce depression-like behavioral impairments, indicating that leptin-lepRb signaling is involved in the molecular mechanism of leptin's antidepressant action (Guo et al., 2013). However, the possible molecular and cellular mechanisms of leptin's antidepressant actions are still obscure.

LEPTIN'S ROLE IN NEUROTRANSMISSION

Both basic and clinical investigations demonstrate that the brains of patients with depression are characterized by disturbances of the neurotransmitter system, including 5-hydroxytryptamine (5-HT), dopamine (DA) and γ-aminobutyric acid (GABA). Traditional depression theories propose that a lack of 5-HT leads to depression, and monoaminergic drugs can alleviate behavior impairments (Aberg-Wistedt et al., 1998). It was reported that leptin administration decreases the binding site density of the selective 5-HT transporter inhibitor paroxetine (Aberg-Wistedt et al., 1998; Charnay et al., 2000). The 5-HT transporter mRNA levels are lower in leptin-deficient ob/ob mice (Collin et al., 2000). These results suggest that leptin can promote the 5-HT transporter functionally and enhance the expression in protein levels. DA has the potential to be an antidepressant drug (Jay et al., 2004). Double-labeling fluorescence immunohistochemistry suggests that dopamine neurons also express leptin receptors in the brain (Figlewicz et al., 2003). Leptin can impact motivated behavior and reward-seeking behavior via the midbrain DA pathway (Fulton et al., 2006). In addition, the level of GABA in depressed patients is lower than that in healthy subjects (Sanacora et al., 1999). Antidepressants drugs can alleviate depressive phenotypes via activation of the GABA transmission system (Garcia-Garcia et al., 2009; Fuchs et al., 2017). As there is expression of LepRb on GABAergic neurons, leptin potentially exerts regulatory effects via the GABAergic system (Fuchs et al., 1984; Francis et al., 2004).

LEPTIN'S NEUROTROPHIC EFFECT

The current neurotrophic hypothesis of depression proposed that a deficit of neurotrophic factors or disturbance of neurotrophic factor signaling pathways is the primary cause of depression (Gulyaeva, 2017). Brain-derived neurotrophic factor (BDNF) is a member of the neurotrophin protein family and is involved in the pathophysiological symptoms of depression (Novkovic et al., 2015; Huang et al., 2017). BDNF could influence hippocampal synaptic plasticity through down-regulating 5-HT3 receptors (Hao et al., 2017).

Leptin was reported to increase the expression of BDNF mRNA (Komori et al., 2006). Leptin can also activate BDNF-expressing hypothalamic neurons through activating neural circuits that stimulate dendritic BDNF synthesis (Liao et al., 2012). BDNF plays a key role in the CNS through binding its receptor. Administration of leptin to the hindbrain significantly increases the level of BDNF within the dorsal vagal complex (Sahu et al., 2016; Kim et al., 2017).

Leptin can significantly improve cAMP-response element binding protein (CREB) phosphorylation via the MAP kinase/extracellular signal-regulated protein kinase (ERK1/2) pathway (Dhar et al., 2014). ERK1/2 phosphorylation (pERK1/2) can directly activate the protein signaling cascade to regulate a series of cellular processes, such as nerve growth, survival and neuroplasticity. Leptin can induce ERK1/2 phosphorylation in a time-dependent manner (Kim et al., 2017; Ghasemi et al., 2018; Han et al., 2018). The increase in pERK1/2 can phosphorylate CREB and alter its transcriptional activity, which is considered a key event of cell survival and cognition (Liu et al., 2015) and in the case of cocultured neurons and astrocytes, leptin exerts an anti-apoptotic effect in astrocytes against glutamate toxicity (Park et al., 2017).

The BDNF and phosphatidylinositol 3 kinase (PI3K)/protein kinase B (AKT) pathways not only regulate the growth and survival of neurons in the hippocampus, but also regulate stress-induced depression and antidepressant response. Several recent studies have found that the antidepressant effect of antidepressants may be related to the PI3K-AKT-mammalian target of rapamycin (mTOR) pathway. Treatment with leptin activates the PI3K-AKT-mTOR pathway (Fazolini et al., 2015; Gui et al., 2018). BDNF increased outgrowth of hippocampal neurites though PI3K pathway signaling (Park et al., 2013). Administration of exogenous leptin to SD rats induced up-regulation of Janus Kinase 2 (JAK2)-signal transducers, and activators of transcription 3 (STAT3) signaling (Wu et al., 2017). To summarize, the protein levels of pSTAT3, AKT, and ERK are all up-regulated by leptin (Kim et al., 2017).

LEPTIN AND HYPOTHALAMIC-PITUITARY-ADRENAL AXIS

Elevation of hypothalamic-pituitary-adrenal axis (HPA) activity is one of the most common neurobiological abnormalities in patients with depression. Studies have shown that the most important factor in the increase of hypothalamic-pituitary activity is the excessive secretion of corticotropin-releasing hormone (CRH) (Plotsky et al., 1998; Morris et al., 2012). CRH induces pituitary adrenal corticotropic hormone (ACTH) secretion; in turn, ACTH causes the adrenal cortex to secrete glucocorticoids (GC). When the concentration of GC increases (e.g., during stress), GC binds to the glucocorticoid receptor (GR), causing negative feedback to inhibit CRH in the

hypothalamus. Finally, the hyperactive HPA axis is restored to the level at baseline (Juruena, 2014). However, hypersecretion of GC constantly stimulates GR, leading to GR desensitization (Board et al., 1957; Cowen, 2010).

Leptin leads to the down-regulation of CRH in the paraventricular hypothalamic nucleus (PVH), and small doses of leptin can also down-regulate CRH mRNA expression. This function of leptin demonstrates that it is a regulator of the HPA axis (Arvaniti et al., 2001). In a starvation model leptin is used to change HPA axis activity. Leptin prevents the synthesis of CRH in PVN and inhibits the activation of the CRH neurons (Huang et al., 1998). Plasma leptin inhibits the expression of the ACTH receptor (ACTH-R) (Su et al., 2012). Furthermore, an injection of leptin to the sheep fetus inhibits the rise in ACTH and cortisol concentration (Howe et al., 2002). Besides the known effects of leptin on ACTH, ACTH can modulate leptin secretion in plasma. Increased plasma ACTH concentrations cause a decrease in leptin output (Spinedi and Gaillard, 1998).

LEPTIN AND METABOLIC ABNORMALITIES IN NEUROLOGICAL DISEASES

Metabolic homeostasis is a complicated regulation process that implicates regulatory signals from both CNS and peripheral systems (Procaccini et al., 2016). As leptin is an important peripheral signal molecule, it is necessary to take metabolic factors into account. Leptin resistance, manifesting as feedback elevated peripheral levels, is defined as a hallmark of metabolic disorders (Talton et al., 2016; Szkudelski et al., 2017; Wang et al., 2018). Recent studies gave the explanation that leptin resistance is caused by leptin signaling disruption, which implicates LepRb deficiency, leptin transport dysfunction through the blood–brain barrier (BBB) and intracellular leptin signaling pathways defects (Wang et al., 2014). Obesity is the most prevalent side-effect of present therapeutic drugs for neurological diseases (Maayan and Correll, 2010). Long-lasting metabolic abnormalities lead to leptin resistance and leptin signaling disruption (Pan et al., 2014). In turn, epidemiological studies showed that diabetes patients have an increased risk of depression and Alzheimer's disease (AD) compared to people without diabetes (Anderson et al., 2001; Arvanitakis et al., 2004; Ernst et al., 2013). These results suggest that neurological diseases, especially mood disorders and metabolism abnormalities, might share overlapping brain circuitries integrating homeostatic and mood regulatory responses and genetic susceptibility factors. As a neuroendocrine regulator of energy metabolism, circulating leptin levels appear to change immediately, which is correlated with central leptin signaling disruption.

Ottaway et al. (2015) found that obese animals retain their sensitivity to endogenous leptin; however, that does not argue against the presence of leptin resistance, based on the most recent reports. For instance, there are increases in plasma leptin concentrations during the initial stage of pregnancy, down-regulation of hypothalamic long form of the leptin receptor in the ventro- and dorso-medial nuclei during the second half of gestation and suppressor of cytokine signaling-3 up-regulation in the arcuate nucleus in late-pregnant ewes (Szczesna et al., 2019). In studying age-related obesity, celastrol, a leptin sensitizer, can induce weight loss in aged animals but not in young controls (Chellappa et al., 2019). In addition, gene expression of leptin receptor in the hypothalamus was found significantly down-regulated in a high-fat diet group (Zhao et al., 2018). These findings support the presence of a relative "leptin resistance" despite partial activity of endogenous leptin signaling in obese animals.

In addition, several experiments *in vivo* and *in vitro* confirmed that leptin itself could exert neuroprotective and neurotrophic actions via promoting BDNF signaling and reduction of neuronal apoptotic and loss (Spina et al., 1992; Komori et al., 2006; Novkovic et al., 2015). These might explain why leptin can improve cognitive and behavior impairments. Contradictory observations exist showing that fasting and calorie restriction, contributing to a decreased leptin level, have an anti-depressant effect (Alzoghaibi et al., 2014; Zhang et al., 2015). Since most animal studies use a few hours of fasting as an experimental process, leptin's antidepressant action is a comparably long-term process. It can be inferred that they may exert antidepressant actions via different molecular ways, while the clear mechanisms are still obscure. In conclusion, leptin might be a potential combination therapeutic target but still not sensitive enough to be a biomarker of neurological diseases at present.

LEPTIN'S NEUROPROTECTIVE EFFECT IN NEURODEGENERATIVE DISEASE

Leptin and Alzheimer's Disease

Alzheimer's disease is one of the most common chronic neurodegenerative diseases and mainly occurs in the elderly (Mangialasche et al., 2010). Amyloid-β, neurofibrillary tangles, synaptic loss and reactive gliosis are the major neuropathological hallmarks of AD (Rockenstein et al., 1995; Alpár et al., 2006).

Previous studies demonstrated that neurotrophic and neuroprotective effects have been induced by leptin in Alzheimer's patients (Pérez-González et al., 2011). Amyloid-β, the main component of amyloid plaques, is highly expressed in the brains of AD patients. It has been observed that the amyloid-β level is decreased in both brain extracts and the serum of transgenic mice after treatment with leptin (Xing et al., 2015). Immunocytochemistry analysis also revealed a decrease in amyloid-β levels in the hippocampus (Greco et al., 2010; Xing et al., 2015). The phosphorylation of JAK2, STAT3 and the consequent activation of adenosine 5′-monophosphate (AMP)-activated protein kinase (AMPK) are involved, whereas it has also been found that primary neurons exhibit increased amyloid-β levels following leptin antagonist treatment (Liu et al., 2017). As showed in **Table 1**, several animal studies reported leptin have significant regulatory role in AD and depression. Leptin phosphorylates PI3K/AKT/mTOR to decrease the expression of GM1 ganglioside in the detergent-resistant membrane microdomains (DRMs) of the neuronal surface. Subsequently, the decrease of GM1 ganglioside (GM1) inhibits

TABLE 1 | Role of leptin in neurological diseases.

Disease	References	Model	Role of leptin
AD	Dudek and Bear, 1992; Mulkey and Malenka, 1992	Long-term potentiation and high-frequency stimulation in hippocampal synapses	Enhances NMDA receptor
AD	Dicou et al., 2001	Ibotenate increase cortical lesions and white matter cysts	Activates its receptor and JAK2
AD	Yamamoto et al., 2014	GM1 ganglioside in the detergent-resistant membrane microdomains (DRMs) of neuronal surface	Decreases GM1 and inhibits the assembly of amyloid-β
Depression	Kurosawa et al., 2016	Forced swim test	Increases the activation of neurons in hippocampus limbic structures
Depression	Park et al., 2017	Coculture neurons and astrocytes	Exerts an anti-apoptotic effect in astrocytes, acting against glutamate

the assembly of amyloid-β (Yamamoto et al., 2014). In addition, outgrowth of neurites in primary neuronal cultures is influenced by leptin. Leptin can rescue the neurite from amyloid-β toxicity (Pérez-González et al., 2014). Chronic leptin treatment is able to recover the deficits caused by amyloid-β. Leptin rescues deficits in spatial memory induced by amyloid-β and long-term potentiation *in vivo* in the hippocampal late-phase. Chronic intracerebroventricular injection of leptin alleviates spatial memory impairment (Tong et al., 2015). Administration of leptin also reverses amyloid-β-induced suppression of hippocampal late-phase long-term potentiation in rats (Tong et al., 2015).

Leptin can affect hippocampus-dependent learning and memory processes (Kiliaan et al., 2014). With regards to long-term potentiation and high-frequency stimulation in hippocampal synapses, synaptic activation of *N*-methyl-D-aspartate (NMDA) receptors is important (Dudek and Bear, 1992; Mulkey and Malenka, 1992). Leptin affects hippocampal synaptic plasticity by enhancing the expression of NMDA receptors (Kiliaan et al., 2014). It has also been shown that AβPP/PS1 double transgenic mice, a mouse model for AD, display increased caspase-3 expression and a reduction in synapse number, which can be reversed to the previous state by leptin treatment (Pérez-González et al., 2014). At the same time, leptin can reduce cortical lesions and white matter cysts. Results from *in vitro* experiments showed that leptin might act as a potential neuroprotective factor. Activation of the leptin receptor and consequent JAK2 are involved in this process (Dicou et al., 2001). In addition, leptin can stimulate neuronal proliferation. It has been reported that chronic leptin administration increases BrdU-positive cells in the dentate gyrus subgranular zone of the hippocampus which indicates a neurogenesis-stimulated benefit of leptin (Pérez-González et al., 2011).

Microglial cells are classes of immune cells that modulate homeostasis in the brain. In the brain of patients with AD, the level of microglia clearance tends to be insufficient (Bacskai et al., 2001; Napoli and Neumann, 2009). On the other hand, some studies have suggested that phagocytosis of microglia leads to the death of neurons. Lipoteichoic acid and lipopolysaccharide (agonists of glial TLR2 and TLR4, respectively) also activate microglia phagocytes, leading to inflammatory neurodegeneration (Neher et al., 2011). It has been shown that leptin deficiency or leptin antagonists inhibit the development of microgliosis in the brain. Thus, leptin is involved in the proliferation of microglia (Fernández-Martos et al., 2012; Gao et al., 2014; Chang et al., 2017). However, the association of leptin's effect on microglia and development of AD needs further exploration.

Several animal studies have confirmed leptin's effect on AD, such as its neurotrophic and neuroprotective effects, its decreasing amyloid-β level, its rescuing the neurites from amyloid-βtoxicity, its influencing hippocampus-dependent learning and memory processes and so on. However, some results from human studies have shown that plasma leptin level has no effect on cognitive ability. It has therefore been suggested that plasma leptin is not an appropriate clinical biomarker for AD at this stage (Oania and McEvoy, 2015; Teunissen et al., 2015).

Leptin and Parkinson's Disease

Parkinson's disease, another common neurodegenerative disease, is characterized by classical motor function deficits due to loss of dopaminergic neurons in the substantia nigra and is induced by a complicated interplay between genetic and environmental factors (Kalia and Lang, 2015).

It was well-known that Parkinson's disease (PD) was mainly characterized by death of dopaminergic neurons in substantia nigra and the accumulation of proteins into Lewy bodies in the neurons (Cosgrove et al., 2015; Duda et al., 2016). Studies of 6-hydroxydopamine (6-OHDA)-induced PD animal models showed that leptin can reverse behavioral abnormalities and reduced dopaminergic cell death (Weng et al., 2007). In the process of leptin-induced neuroprotection, extracellular regulated pERK1/2 plays a key role as a survival factor of dopaminergic neurons, which caused subsequently a MEK-dependent increase in CREB (Weng et al., 2007). Furthermore, another downstream product of leptin is BDNF, which can preserve the survival of dopaminergic neurons via activation of the ERK/CREB pathway (Spina et al., 1992). Though some human studies showed that there's no significant correlation of

peripheral leptin levels and PD, it was found that circulating leptin levels of unintended weight loss PD patients were lower than those with stable weight (Evidente et al., 2001; Fiszer et al., 2010). Different selection criteria for inclusion might explain the contradictory conclusions.

Leptin can also preserve neuronal survival via increased uncoupling protein-2 (UCP2) expression in neuronal cultures. UCP2 could maintain the level of ATP and mitochondrial membrane potential (MMP). At the same time, it preserves cell survival against MPP+ toxicity, which has been widely used in producing Parkinsonism models (Ho et al., 2010; Procaccini et al., 2016). These results suggest that leptin might have potential to be a therapeutic target. However, at this stage, the research is relatively limited. More research will be needed to address this issue.

The Therapeutic Potential of Leptin

In the context of increasing incidence of neurological diseases, it is important to explore the pathogenesis of these diseases and to find effective treatments. It has been shown that leptin has an effect on the nervous system. Leptin could modulate the levels of neurotransmitters, promote the 5-HT transporter functionally and enhance the expression in protein levels (Collin et al., 2000). Also, there is expression of LepRb on GABAergic neurons and dopamine neurons in the brain (Fuchs et al., 1984; Figlewicz et al., 2003; Francis et al., 2004). Leptin can also increase the expression of BDNF mRNA, activate BDNF-expressing neurons (Komori et al., 2006; Liao et al., 2012), activate the PI3K-AKT-mTOR pathway to regulate the growth of neurons and regulate stress-induced depression and antidepressant response (Fazolini et al., 2015; Gui et al., 2018) while reversing the dysfunction in the HPA axis. These functions of leptin reflect its potential to treat depression. In neurodegenerative disease, leptin has neurotrophic and neuroprotective effects (Pérez-González et al., 2011), it affects hippocampal synaptic plasticity and improves learning and memory processes (Kiliaan et al., 2014).

However, some experiments from human studies have shown that plasma leptin levels are not associated with these diseases. Studies have shown that leptin levels are higher in depression patients than in control groups (Milaneschi et al., 2017). Moreover, leptin has no effect on human cognition and memory ability (Oania and McEvoy, 2015; Teunissen et al., 2015). Thus, despite the fact that leptin has the potential to be a therapeutic drug for neurological diseases through different molecular mechanisms and a target for combination therapy, it is not a clinical biomarker for neurological diseases before a clear mechanism is explored.

CONCLUSION

Since the prevalence of neurodegenerative disorders and mood disorders has ascended in recent years, investigating the radical cellular and molecular mechanisms of these diseases and finding out a novel therapeutic target is important. In this article, we discussed the effects of adipocyte-derived hormone leptin in depression, AD, PD and its possible modulatory role. Antidepressant effects of leptin have been observed in recent studies. The mechanism might implicate leptin's role in neurotransmission, neurotrophic factors and the HPA axis. Furthermore, an inescapable issue is that neurological diseases and metabolism abnormalities might share overlapping brain circuitries integrating homeostatic and regulatory responses and genetic susceptibility factors. Still, increasing evidence indicates a potential effect of leptin in reversing AD symptoms. The effect of leptin might be based on the mechanism that increases the activation of neurons in the hippocampus, reduces the levels of amyloid-β and tau and modulates the microglia. As for PD, leptin can preserve dopaminergic neurons via several pathways. Leptin appears to exert neuroprotective effects on neurodegenerative disorders. More investigation is required to understand the association between leptin and neurological diseases.

AUTHOR CONTRIBUTIONS

XZ, LZ, and CZ wrote the first draft. XZ, LZ, CZ, HZ, FZ, RC, SG, and BL participated in the discussion of the manuscript. SG and BL provided the critical revisions. All authors approved the final version of the manuscript for submission.

FUNDING

This study was financially supported by the Natural Science Foundation of China (NSFC) (grant nos. 81871070, 31571126, 81772291) and the Jilin Science and Technology Agency (grant nos. 20180519003JH, 20180414050GH).

REFERENCES

Aberg-Wistedt, A., Hasselmark, L., Stain-Malmgren, R., Apéria, B., Kjellman, B. F., and Mathé, A. A. (1998). Serotonergic 'vulnerability' in affective disorder: a study of the tryptophan depletion test and relationships between peripheral and central serotonin indexes in citalopram-responders. *Acta Psychiatr. Scand.* 97, 374–380.

Alpár, A., Ueberham, U., Brückner, M. K., Seeger, G., Arendt, T., and Gärtner, U. (2006). Different dendrite and dendritic spine alterations in basal and apical arbors in mutant human amyloid precursor protein transgenic mice. *Brain Res.* 1099, 189–198. doi: 10.1016/j.brainres.2006.04.109

Alzoghaibi, M. A., Pandi-Perumal, S. R., Sharif, M. M., and BaHammam, A. S. (2014). Diurnal intermittent fasting during Ramadan: the effects on leptin and ghrelin levels. *PLoS One* 9:e92214. doi: 10.1371/journal.pone.0092214

Anderson, R. J., Freedland, K. E., Clouse, R. E., and Lustman, P. J. (2001). The prevalence of comorbid depression in adults with diabetes: a meta-analysis. *Diabetes Care* 24, 1069–1078.

Arvanitakis, Z., Wilson, R. S., Bienias, J. L., Evans, D. A., and Bennett, D. A. (2004). Diabetes mellitus and risk of Alzheimer disease and decline in cognitive function. *Arch. Neurol.* 61, 661–666. doi: 10.1001/archneur.61.5.661

Arvaniti, K., Huang, Q., and Richard, D. (2001). Effects of leptin and corticosterone on the expression of corticotropin-releasing hormone, agouti-related protein, and proopiomelanocortin in the brain of ob/ob mouse. *Neuroendocrinology* 73, 227–236. doi: 10.1159/000054639

Bacskai, B. J., Kajdasz, S. T., Christie, R. H., Carter, C., Games, D., Seubert, P., et al. (2001). Imaging of amyloid-beta deposits in brains of living mice permits direct observation of clearance of plaques with immunotherapy. *Nat. Med.* 7, 369–372. doi: 10.1038/85525

Board, F., Wadeson, R., and Persky, H. (1957). Depressive affect and endocrine functions; blood levels of adrenal cortex and thyroid hormones in patients suffering from depressive reactions. *AMA Arch. Neurol. Psychiatry* 78, 612–620.

Chang, K. T., Lin, Y. L., Lin, C. T., Hong, C. J., Tsai, M. J., Huang, W. C., et al. (2017). Leptin is essential for microglial activation and neuropathic pain after preganglionic cervical root avulsion. *Life Sci.* 187, 31–41. doi: 10.1016/j.lfs.2017.08.016

Charnay, Y., Cusin, I., Vallet, P. G., Muzzin, P., Rohner-Jeanrenaud, F., and Bouras, C. (2000). Intracerebroventricular infusion of leptin decreases serotonin transporter binding sites in the frontal cortex of the rat. *Neurosci. Lett.* 283, 89–92.

Chellappa, K., Perron, I. J., Naidoo, N., and Baur, J. A. (2019). The leptin sensitizer celastrol reduces age-associated obesity and modulates behavioral rhythms. *Aging Cell* doi: 10.1111/acel.12874 [Epub ahead of print].

Collin, M., Håkansson-Ovesjö, M. L., Misane, I., Ogren, S. O., and Meister, B. (2000). Decreased 5-HT transporter mRNA in neurons of the dorsal raphe nucleus and behavioral depression in the obese leptin-deficient ob/ob mouse. *Brain Res. Mol. Brain Res.* 81, 51–61.

Cosgrove, J., Alty, J. E., and Jamieson, S. (2015). Cognitive impairment in Parkinson's disease. *Postgrad. Med. J.* 91, 212–220. doi: 10.1136/postgradmedj-2015-133247

Cowen, P. J. (2010). Not fade away: the HPA axis and depression. *Psychol. Med.* 40, 1–4. doi: 10.1017/S0033291709005558

Dhar, M., Zhu, M., Impey, S., Lambert, T. J., Bland, T., Karatsoreos, I. N., et al. (2014). Leptin induces hippocampal synaptogenesis via CREB-regulated microRNA-132 suppression of p250GAP. *Mol. Endocrinol.* 28, 1073–1087. doi: 10.1210/me.2013-1332

Dicou, E., Attoub, S., and Gressens, P. (2001). Neuroprotective effects of leptin in vivo and in vitro. *Neuroreport* 12, 3947–3951.

Duda, J., Pötschke, C., and Liss, B. (2016). Converging roles of ion channels, calcium, metabolic stress, and activity pattern of Substantia nigra dopaminergic neurons in health and Parkinson's disease. *J. Neurochem.* 139(Suppl. 1), 156–178. doi: 10.1111/jnc.13572

Dudek, S. M., and Bear, M. F. (1992). Homosynaptic long-term depression in area CA1 of hippocampus and effects of N-methyl-D-aspartate receptor blockade. *Proc. Natl. Acad. Sci. U.S.A.* 89, 4363–4367.

Ernst, A., Sharma, A. N., Elased, K. M., Guest, P. C., Rahmoune, H., and Bahn, S. (2013). Diabetic db/db mice exhibit central nervous system and peripheral molecular alterations as seen in neurological disorders. *Transl. Psychiatry* 3:e263. doi: 10.1038/tp.2013.42

Evidente, V. G., Caviness, J. N., Adler, C. H., Gwinn-Hardy, K. A., and Pratley, R. E. (2001). Serum leptin concentrations and satiety in Parkinson's disease patients with and without weight loss. *Mov. Disord.* 16, 924–927.

Fazolini, N. P., Cruz, A. L., Werneck, M. B., Viola, J. P., Maya-Monteiro, C. M., and Bozza, P. T. (2015). Leptin activation of mTOR pathway in intestinal epithelial cell triggers lipid droplet formation, cytokine production and increased cell proliferation. *Cell Cycle* 14, 2667–2676. doi: 10.1080/15384101.2015.1041684

Fernández-Martos, C. M., González, P., and Rodriguez, F. J. (2012). Acute leptin treatment enhances functional recovery after spinal cord injury. *PLoS One* 7:e35594. doi: 10.1371/journal.pone.0035594

Figlewicz, D. P., Evans, S. B., Murphy, J., Hoen, M., and Baskin, D. G. (2003). Expression of receptors for insulin and leptin in the ventral tegmental area/substantia nigra (VTA/SN) of the rat. *Brain Res.* 964, 107–115.

Finn, P. D., Cunningham, M. J., Rickard, D. G., Clifton, D. K., and Steiner, R. A. (2001). Serotonergic neurons are targets for leptin in the monkey. *J. Clin. Endocrinol. Metab.* 86, 422–426. doi: 10.1210/jcem.86.1.7128

Fiszer, U., Michałowska, M., Baranowska, B., Wolińska-Witort, E., Jeske, W., Jethon, M., et al. (2010). Leptin and ghrelin concentrations and weight loss in Parkinson's disease. *Acta Neurol. Scand.* 121, 230–236. doi: 10.1111/j.1600-0404.2009.01185.x

Francis, J., MohanKumar, S. M., and MohanKumar, P. S. (2004). Leptin inhibits norepinephrine efflux from the hypothalamus in vitro: role of gamma aminobutyric acid. *Brain Res.* 1021, 286–291. doi: 10.1016/j.brainres.2004.07.010

Fuchs, E., Mansky, T., Stock, K. W., Vijayan, E., and Wuttke, W. (1984). Involvement of catecholamines and glutamate in GABAergic mechanism regulatory to luteinizing hormone and prolactin secretion. *Neuroendocrinology* 38, 484–489. doi: 10.1159/000123937

Fuchs, T., Jefferson, S. J., Hooper, A., Yee, P. H., Maguire, J., and Luscher, B. (2017). Disinhibition of somatostatin-positive GABAergic interneurons results in an anxiolytic and antidepressant-like brain state. *Mol. Psychiatry* 22, 920–930. doi: 10.1038/mp.2016.188

Fulton, S., Pissios, P., Manchon, R. P., Stiles, L., Frank, L., Pothos, E. N., et al. (2006). Leptin regulation of the mesoaccumbens dopamine pathway. *Neuron* 51, 811–822. doi: 10.1016/j.neuron.2006.09.006

Gao, Y., Ottaway, N., Schriever, S. C., Legutko, B., García-Cáceres, C., de la Fuente, E., et al. (2014). Hormones and diet, but not body weight, control hypothalamic microglial activity. *Glia* 62, 17–25. doi: 10.1002/glia.22580

Garcia-Garcia, A. L., Elizalde, N., Matrov, D., Harro, J., Wojcik, S. M., Venzala, E., et al. (2009). Increased vulnerability to depressive-like behavior of mice with decreased expression of VGLUT1. *Biol. Psychiatry* 66, 275–282. doi: 10.1016/j.biopsych.2009.02.027

Ge, T., Fan, J., Yang, W., Cui, R., and Li, B. (2018). Leptin in depression: a potential therapeutic target. *Cell Death Dis.* 9:1096. doi: 10.1038/s41419-018-1129-1

Ghasemi, A., Hashemy, S. I., Aghaei, M., and Panjehpour, M. (2018). Leptin induces matrix metalloproteinase 7 expression to promote ovarian cancer cell invasion by activating ERK and JNK pathways. *J. Cell. Biochem.* 119, 2333–2344. doi: 10.1002/jcb.26396

Greco, S. J., Bryan, K. J., Sarkar, S., Zhu, X., Smith, M. A., Ashford, J. W., et al. (2010). Leptin reduces pathology and improves memory in a transgenic mouse model of Alzheimer's disease. *J. Alzheimers Dis.* 19, 1155–1167. doi: 10.3233/JAD-2010-1308

Gui, X., Chen, H., Cai, H., Sun, L., and Gu, L. (2018). Leptin promotes pulmonary fibrosis development by inhibiting autophagy via PI3K/Akt/mTOR pathway. *Biochem. Biophys. Res. Commun.* 498, 660–666. doi: 10.1016/j.bbrc.2018.03.039

Gulyaeva, N. V. (2017). Interplay between brain BDNF and glutamatergic systems: a brief state of the evidence and association with the pathogenesis of depression. *Biochem. Mosc.* 82, 301–307. doi: 10.1134/S0006297917030087

Guo, M., Huang, T. Y., Garza, J. C., Chua, S. C., and Lu, X. Y. (2013). Selective deletion of leptin receptors in adult hippocampus induces depression-related behaviours. *Int. J. Neuropsychopharmacol.* 16, 857–867. doi: 10.1017/S1461145712000703

Han, Y. C., Ma, B., Guo, S., Yang, M., Li, L. J., Wang, S. J., et al. (2018). Leptin regulates disc cartilage endplate degeneration and ossification through activation of the MAPK-ERK signalling pathway in vivo and in vitro. *J. Cell. Mol. Med.* 22, 2098–2109. doi: 10.1111/jcmm.13398

Hao, R., Qi, Y., Hou, D. N., Ji, Y. Y., Zheng, C. Y., Li, C. Y., et al. (2017). BDNF val66met polymorphism impairs hippocampal long-term depression by down-regulation of 5-HT3 receptors. *Front. Cell. Neurosci.* 11:306. doi: 10.3389/fncel.2017.00306

Ho, P. W., Liu, H. F., Ho, J. W., Zhang, W. Y., Chu, A. C., Kwok, K. H., et al. (2010). Mitochondrial uncoupling protein-2 (UCP2) mediates leptin protection against MPP+ toxicity in neuronal cells. *Neurotox. Res.* 17, 332–343. doi: 10.1007/s12640-009-9109-y

Howe, D. C., Gertler, A., and Challis, J. R. (2002). The late gestation increase in circulating ACTH and cortisol in the fetal sheep is suppressed by intracerebroventricular infusion of recombinant ovine leptin. *J. Endocrinol.* 174, 259–266.

Huang, Q., Rivest, R., and Richard, D. (1998). Effects of leptin on corticotropin-releasing factor (CRF) synthesis and CRF neuron activation in the paraventricular hypothalamic nucleus of obese (ob/ob) mice. *Endocrinology* 139, 1524–1532. doi: 10.1210/endo.139.4.5889

Huang, X., Huang, X., Zhou, Y., He, H., Mei, F., Sun, B., et al. (2017). Association of serum BDNF levels with psychotic symptom in chronic patients with treatment-resistant depression in a Chinese Han population. *Psychiatry Res.* 257, 279–283. doi: 10.1016/j.psychres.2017.07.076

Jay, T. M., Rocher, C., Hotte, M., Naudon, L., Gurden, H., and Spedding, M. (2004). Plasticity at hippocampal to prefrontal cortex synapses is impaired by loss of dopamine and stress: importance for psychiatric diseases. *Neurotox. Res.* 6, 233–244.

Juruena, M. F. (2014). Early-life stress and HPA axis trigger recurrent adulthood depression. *Epilepsy Behav.* 38, 148–159. doi: 10.1016/j.yebeh.2013.10.020

Kalia, L. V., and Lang, A. E. (2015). Parkinson's disease. *Lancet* 386, 896–912. doi: 10.1016/S0140-6736(14)61393-3

Kiliaan, A. J., Arnoldussen, I. A., and Gustafson, D. R. (2014). Adipokines: a link between obesity and dementia. *Lancet Neurol.* 13, 913–923. doi: 10.1016/S1474-4422(14)70085-7

Kim, H. G., Jin, S. W., Kim, Y. A., Khanal, T., Lee, G. H., Kim, S. J., et al. (2017). Leptin induces CREB-dependent aromatase activation through COX-2 expression in breast cancer cells. *Food Chem. Toxicol.* 106, 232–241. doi: 10.1016/j.fct.2017.05.058

Komori, T., Morikawa, Y., Nanjo, K., and Senba, E. (2006). Induction of brain-derived neurotrophic factor by leptin in the ventromedial hypothalamus. *Neuroscience* 139, 1107–1115. doi: 10.1016/j.neuroscience.2005.12.066

Kormos, V., and Gaszner, B. (2013). Role of neuropeptides in anxiety, stress, and depression: from animals to humans. *Neuropeptides* 47, 401–419. doi: 10.1016/j.npep.2013.10.014

Kurosawa, N., Shimizu, K., and Seki, K. (2016). The development of depression-like behavior is consolidated by IL-6-induced activation of locus coeruleus neurons and IL-1β-induced elevated leptin levels in mice. *Psychopharmacology* 233, 1725–1737. doi: 10.1007/s00213-015-4084-x

Lee, J. Y., Lim, O. K., Lee, J. K., Park, Y., Kim, C., Yoon, J. W., et al. (2015). The Association between serum leptin levels and post-stroke depression: a retrospective clinical study. *Ann. Rehabil. Med.* 39, 786–792. doi: 10.5535/arm.2015.39.5.786

Liao, G. Y., An, J. J., Gharami, K., Waterhouse, E. G., Vanevski, F., Jones, K. R., et al. (2012). Dendritically targeted Bdnf mRNA is essential for energy balance and response to leptin. *Nat. Med.* 18, 564–571. doi: 10.1038/nm.2687

Liu, B. B., Luo, L., Liu, X. L., Geng, D., Li, C. F., Chen, S. M., et al. (2015). Essential oil of Syzygium aromaticum reverses the deficits of stress-induced behaviors and hippocampal p-ERK/p-CREB/brain-derived neurotrophic factor expression. *Planta Med.* 81, 185–192. doi: 10.1055/s-0034-1396150

Liu, Z., Zhang, Y., Liu, J., and Yin, F. (2017). Geniposide attenuates the level of Aβ1-42 via enhancing leptin signaling in cellular and APP/PS1 transgenic mice. *Arch. Pharm. Res.* 40, 571–578. doi: 10.1007/s12272-016-0875-9

Lu, X. Y., Kim, C. S., Frazer, A., and Zhang, W. (2006). Leptin: a potential novel antidepressant. *Proc. Natl. Acad. Sci. U.S.A.* 103, 1593–1598. doi: 10.1073/pnas.0508901103

Maayan, L., and Correll, C. U. (2010). Management of antipsychotic-related weight gain. *Expert Rev. Neurother.* 10, 1175–1200. doi: 10.1586/ern.10.85

Mangialasche, F., Solomon, A., Winblad, B., Mecocci, P., and Kivipelto, M. (2010). Alzheimer's disease: clinical trials and drug development. *Lancet Neurol.* 9, 702–716. doi: 10.1016/S1474-4422(10)70119-8

Milaneschi, Y., Lamers, F., Bot, M., Drent, M. L., and Penninx, B. W. (2017). Leptin dysregulation is specifically associated with major depression with atypical features: evidence for a mechanism connecting obesity and depression. *Biol. Psychiatry* 81, 807–814. doi: 10.1016/j.biopsych.2015.10.023

Morris, M. C., Compas, B. E., and Garber, J. (2012). Relations among posttraumatic stress disorder, comorbid major depression, and HPA function: a systematic review and meta-analysis. *Clin. Psychol. Rev.* 32, 301–315. doi: 10.1016/j.cpr.2012.02.002

Mulkey, R. M., and Malenka, R. C. (1992). Mechanisms underlying induction of homosynaptic long-term depression in area CA1 of the hippocampus. *Neuron* 9, 967–975.

Napoli, I., and Neumann, H. (2009). Microglial clearance function in health and disease. *Neuroscience* 158, 1030–1038. doi: 10.1016/j.neuroscience.2008.06.046

Neher, J. J., Neniskyte, U., Zhao, J. W., Bal-Price, A., Tolkovsky, A. M., and Brown, G. C. (2011). Inhibition of microglial phagocytosis is sufficient to prevent inflammatory neuronal death. *J. Immunol.* 186, 4973–4983. doi: 10.4049/jimmunol.1003600

Novkovic, T., Mittmann, T., and Manahan-Vaughan, D. (2015). BDNF contributes to the facilitation of hippocampal synaptic plasticity and learning enabled by environmental enrichment. *Hippocampus* 25, 1–15. doi: 10.1002/hipo.22342

Oania, R., and McEvoy, L. K. (2015). Plasma leptin levels are not predictive of dementia in patients with mild cognitive impairment. *Age Ageing* 44, 53–58. doi: 10.1093/ageing/afu160

Ottaway, N., Mahbod, P., Rivero, B., Norman, L. A., Gertler, A., D'Alessio, D. A., et al. (2015). Diet-induced obese mice retain endogenous leptin action. *Cell Metab.* 21, 877–882. doi: 10.1016/j.cmet.2015.04.015

Ozsoy, S., Besirli, A., Unal, D., Abdulrezzak, U., and Orhan, O. (2015). The association between depression, weight loss and leptin/ghrelin levels in male patients with head and neck cancer undergoing radiotherapy. *Gen. Hosp. Psychiatry* 37, 31–35. doi: 10.1016/j.genhosppsych.2014.09.002

Pan, H., Guo, J., and Su, Z. (2014). Advances in understanding the interrelations between leptin resistance and obesity. *Physiol. Behav.* 130, 157–169. doi: 10.1016/j.physbeh.2014.04.003

Park, H., Ahn, S. H., Jung, Y., Yoon, J. C., and Choi, Y. H. (2017). Leptin suppresses glutamate-induced apoptosis through regulation of ERK1/2 signaling pathways in rat primary astrocytes. *Cell. Physiol. Biochem.* 44, 2117–2128. doi: 10.1159/000485950

Park, S. W., Lee, C. H., Cho, H. Y., Seo, M. K., Lee, J. G., Lee, B. J., et al. (2013). Effects of antipsychotic drugs on the expression of synaptic proteins and dendritic outgrowth in hippocampal neuronal cultures. *Synapse* 67, 224–234. doi: 10.1002/syn.21634

Pérez-González, R., Alvira-Botero, M. X., Robayo, O., Antequera, D., Garzón, M., Martín-Moreno, A. M., et al. (2014). Leptin gene therapy attenuates neuronal damages evoked by amyloid-β and rescues memory deficits in APP/PS1 mice. *Gene Ther.* 21, 298–308. doi: 10.1038/gt.2013.85

Pérez-González, R., Antequera, D., Vargas, T., Spuch, C., Bolós, M., and Carro, E. (2011). Leptin induces proliferation of neuronal progenitors and neuroprotection in a mouse model of Alzheimer's disease. *J. Alzheimers Dis.* 24(Suppl. 2), 17–25. doi: 10.3233/JAD-2011-102070

Plotsky, P. M., Owens, M. J., and Nemeroff, C. B. (1998). Psychoneuroendocrinology of depression. Hypothalamic-pituitary-adrenal axis. *Psychiatr. Clin. North Am.* 21, 293–307.

Procaccini, C., Santopaolo, M., Faicchia, D., Colamatteo, A., Formisano, L., de Candia, P., et al. (2016). Role of metabolism in neurodegenerative disorders. *Metab. Clin. Exp.* 65, 1376–1390. doi: 10.1016/j.metabol.2016.05.018

Rockenstein, E. M., McConlogue, L., Tan, H., Power, M., Masliah, E., and Mucke, L. (1995). Levels and alternative splicing of amyloid beta protein precursor (APP) transcripts in brains of APP transgenic mice and humans with Alzheimer's disease. *J. Biol. Chem.* 270, 28257–28267.

Sahu, S., Ganguly, R., and Raman, P. (2016). Leptin augments recruitment of IRF-1 and CREB to thrombospondin-1 gene promoter in vascular smooth muscle cells in vitro. *Am. J. Physiol. Cell Physiol.* 311, C212–C224. doi: 10.1152/ajpcell.00068.2016

Sanacora, G., Mason, G. F., Rothman, D. L., Behar, K. L., Hyder, F., Petroff, O. A., et al. (1999). Reduced cortical gamma-aminobutyric acid levels in depressed patients determined by proton magnetic resonance spectroscopy. *Arch. Gen. Psychiatry* 56, 1043–1047.

Spina, M. B., Squinto, S. P., Miller, J., Lindsay, R. M., and Hyman, C. (1992). Brain-derived neurotrophic factor protects dopamine neurons against 6-hydroxydopamine and N-methyl-4-phenylpyridinium ion toxicity: involvement of the glutathione system. *J. Neurochem.* 59, 99–106.

Spinedi, E., and Gaillard, R. C. (1998). A regulatory loop between the hypothalamo-pituitary-adrenal (HPA) axis and circulating leptin: a physiological role of ACTH. *Endocrinology* 139, 4016–4020. doi: 10.1210/endo.139.9.6291

Su, Y., Carey, L. C., Rose, J. C., and Pulgar, V. M. (2012). Leptin alters adrenal responsiveness by decreasing expression of ACTH-R, StAR, and P450c21 in hypoxemic fetal sheep. *Reprod. Sci.* 19, 1075–1084. doi: 10.1177/1933719112442246

Szczesna, M., Kirsz, K., Misztal, T., and Zieba, D. A. (2019). Downregulation of LRb in VMH/DMH during the second half of gestation and upregulation of SOCS-3 in ARC in late-pregnant ewes - Implications for leptin resistance. *Gen. Comp. Endocrinol.* 274, 73–79. doi: 10.1016/j.ygcen.2019.01.003

Szkudelski, T., Dłużewicz, K., Sadoch, J., and Szkudelska, K. (2017). Effects of the activation of heme oxygenase-1 on hormonal and metabolic changes in rats fed a high-fat diet. *Biomed. Pharmacother.* 87, 375–380. doi: 10.1016/j.biopha.2016.12.060

Talton, O. O., Pennington, K. A., Pollock, K. E., Bates, K., Ma, L., Ellersieck, M. R., et al. (2016). Maternal hyperleptinemia improves offspring

insulin sensitivity in mice. *Endocrinology* 157, 2636–2648. doi: 10.1210/en.2016-1039

Tartaglia, L. A., Dembski, M., Weng, X., Deng, N., Culpepper, J., Devos, R., et al. (1995). Identification and expression cloning of a leptin receptor, OB-R. *Cell* 83, 1263–1271.

Teunissen, C. E., van der Flier, W. M., Scheltens, P., Duits, A., Wijnstok, N., Nijpels, G., et al. (2015). Serum leptin is not altered nor related to cognitive decline in Alzheimer's disease. *J. Alzheimers Dis.* 44, 809–813. doi: 10.3233/JAD-141503

Tong, J. Q., Zhang, J., Hao, M., Yang, J., Han, Y. F., Liu, X. J., et al. (2015). Leptin attenuates the detrimental effects of β-amyloid on spatial memory and hippocampal later-phase long term potentiation in rats. *Horm. Behav.* 73, 125–130. doi: 10.1016/j.yhbeh.2015.06.013

Wang, B., Chandrasekera, P. C., and Pippin, J. J. (2014). Leptin- and leptin receptor-deficient rodent models: relevance for human type 2 diabetes. *Curr. Diabetes Rev.* 10, 131–145.

Wang, Y., Xu, J., Liu, Y., Li, Z., and Li, X. (2018). TLR4-NF-κB signal involved in depressive-like behaviors and cytokine expression of frontal cortex and hippocampus in stressed C57BL/6 and ob/ob Mice. *Neural Plast.* 2018:7254016. doi: 10.1155/2018/7254016

Weng, Z., Signore, A. P., Gao, Y., Wang, S., Zhang, F., Hastings, T., et al. (2007). Leptin protects against 6-hydroxydopamine-induced dopaminergic cell death via mitogen-activated protein kinase signaling. *J. Biol. Chem.* 282, 34479–34491. doi: 10.1074/jbc.M705426200

Wu, L., Chen, G., Liu, W., Yang, X., Gao, J., Huang, L., et al. (2017). Intramuscular injection of exogenous leptin induces adiposity, glucose intolerance and fatty liver by repressing the JAK2-STAT3/PI3K pathway in a rat model. *Gen. Comp. Endocrinol.* 252, 88–96. doi: 10.1016/j.ygcen.2017.02.012

Xing, Y., Liu, J., Xu, J., Yin, L., Wang, L., Li, J., et al. (2015). Association between plasma leptin and estrogen in female patients of amnestic mild cognitive impairment. *Dis. Mark.* 2015:450237. doi: 10.1155/2015/450237

Yamamoto, N., Tanida, M., Kasahara, R., Sobue, K., and Suzuki, K. (2014). Leptin inhibits amyloid β-protein fibrillogenesis by decreasing GM1 gangliosides on the neuronal cell surface through PI3K/Akt/mTOR pathway. *J. Neurochem.* 131, 323–332. doi: 10.1111/jnc.12828

Zhang, Y., Liu, C., Zhao, Y., Zhang, X., Li, B., and Cui, R. (2015). The effects of calorie restriction in depression and potential mechanisms. *Curr. Neuropharmacol.* 13, 536–542.

Zhang, Y., Proenca, R., Maffei, M., Barone, M., Leopold, L., and Friedman, J. M. (1994). Positional cloning of the mouse obese gene, and its human homologue. *Nature* 372, 425–432.

Zhao, Y., Chen, L. B., Mao, S. S., Min, H. X., and Cao, J. (2018). Leptin resistance was involved in susceptibility to overweight in the striped hamster re-fed with high fat diet. *Sci. Rep.* 8:920. doi: 10.1038/s41598-017-18158-4

Conflict of Interest Statement: The authors declare that the research was conducted in the absence of any commercial or financial relationships that could be construed as a potential conflict of interest.

frontiers in Neuroscience

ORIGINAL RESEARCH
published: 08 May 2019
doi: 10.3389/fnins.2019.00436

Exposure of Hyperandrogen During Pregnancy Causes Depression- and Anxiety-Like Behaviors, and Reduced Hippocampal Neurogenesis in Rat Offspring

*Juan Cheng[1,2], Haojuan Wu[1,2], Huawei Liu[1], Hua Li[1], Hua Zhu[1], Yongmei Zhou[1], Hongxia Li[1], Wenming Xu[3,4] and Jiang Xie[1]**

[1] Chengdu Third People's Hospital, Affiliated Hospital of Southwest JiaoTong University Medical School, Chengdu, China, [2] Department of Clinical Medicine, Southwest Medical University, Luzhou, China, [3] Department of Obstetrics and Gynecology, West China Second University Hospital, Key Laboratory of Birth Defects and Related Diseases of Women and Children, Ministry of Education, Sichuan University, Chengdu, China, [4] Joint Laboratory of Reproductive Medicine, SCU-CUHK, West China Second University Hospital, Sichuan University, Chengdu, China

OPEN ACCESS

Edited by:
Keith Maurice Kendrick, University of Electronic Science and Technology of China, China

Reviewed by:
Jane Elizabeth Robinson, University of Glasgow, United Kingdom
Rosalinda Guevara-Guzmán, National Autonomous University of Mexico, Mexico

***Correspondence:**
Jiang Xie
909380599@qq.com

Specialty section:
This article was submitted to Neuroendocrine Science, a section of the journal Frontiers in Neuroscience

Received: *13 December 2018*
Accepted: *16 April 2019*
Published: *08 May 2019*

Citation:
Cheng J, Wu H, Liu H, Li H, Zhu H, Zhou Y, Li H, Xu W and Xie J (2019) Exposure of Hyperandrogen During Pregnancy Causes Depression- and Anxiety-Like Behaviors, and Reduced Hippocampal Neurogenesis in Rat Offspring. Front. Neurosci. 13:436. doi: 10.3389/fnins.2019.00436

The hippocampus is a region in which neurogenesis persists and retains substantial plasticity throughout lifespan. Accumulating evidences indicate an important role of androgens and androgenic signaling in the regulation of offspring hippocampal neurogenesis and the survival of mature or immature neurons and gliocyte. Hyperandrogenic disorders have been associated with depression and anxiety. Previous studies have found that pregnant hyperandrogenism may increase the susceptibility of the offspring to depression or anxiety and lead to abnormal hippocampal neurogenesis in rats. In this study, pregnant rats were given subcutaneous injection of aromatase inhibitor letrozole in order to establish a maternal hyperandrogenic environment for the fetal rats. The lithium chloride (LICl) was used as an intervention agent since a previous study has shown that lithium chloride could promote neurogenesis in the hippocampus. The results revealed that pregnant administration of letrozole resulted in depressive- and anxious-like behaviors in the adolescent period. A remarkable decrease in immature nerve cells marked by doublecortin and mature neurons co-expressed by Brdu and NeuN in adult years were detected in the hippocampal dentate gyrus of adolescent rats. Lithium chloride alleviated the effects on neurobehavioral and promoted the differentiation and proliferation of neural progenitor cells, while a hyperandrogenic intrauterine environment had no effects on astrocytes marked by GFAP in the dentate gyrus. Furthermore, the Wnt/β-catenin signaling pathway related to normal development of hippocampus was examined but there was no significant changes in Wnt signaling pathway members. Our study provides evidence that exposure of androgen during pregnancy leads to alterations in depressive, anxious and stereotypical behaviors and these phenotypes are possibly associated with changes in neurogenesis in the dentate gyrus.

Keywords: androgen, neurogenesis, hippocampus, depression, lithium chloride

INTRODUCTION

In mammals, sex steroid hormones are synthesized in the gonads: ovary for 17β estradiol (E2) and progesterone (P), and in the Leydig cells of testes for testosterone (T) and have effects on many tissues, including the gonads, the liver, and the nervous system. Such steroids, either via *de novo* synthesis from cholesterol or from local metabolism of steroid intermediate produced in the periphery, can rapidly modulate neuronal excitability and functions, control brain plasticity, and behavior. The *de novo* steroid synthesis occurs in the brains of mammals, called neurosteroids. Neurosteroidogenesis maintains an intense neurogenic activity during adulthood in numerous regions, one of key regions for neurobehavior is hippocampus.

The hippocampus is a region in which neurogenesis persists (Eriksson et al., 1998; Spalding et al., 2013; Woodward et al., 2018) and retains substantial plasticity for the whole life including in humans (Jessberger et al., 2007; Wainwright et al., 2016; Hall et al., 2018). Much research has shown that the compromised hippocampal neurogenesis is attributed to multiple neuropsychiatric diseases, including depression (McKinnon et al., 2009) and dementia (Henneman et al., 2009). Hippocampus neurogenesis also has effect on cognition (Sweatt, 2004) and mood regulation (Campbell and Macqueen, 2004), dysregulation of which is particularly susceptible to depression (Liu et al., 2017). Therefore, the behavior change is often related to the compromised neurogenesis.

Accumulating evidences indicate that androgens and androgenic signaling modulate the hippocampal neurogenesis (Galea et al., 2013). Androgens are the crucial gonadal hormones in men, derived from cholesterol via progestins, including testosterone and androstenedione, which may also be converted to 17β-estradiol via aromatase. Previous evidences show that exposure to androgens for a long time increase hippocampal neurogenesis via modulating the survival of new neurons (Nelson, 2011) within the dentate gyrus (DG), which have been specifically contributed to the activation of the androgen receptor (AR) in rodents, while estradiol has no significant effect on them (Spritzer and Galea, 2007; Carrier and Kabbaj, 2012). A recent study shows that the AR is widely expressed in the developing cortex and hippocampus in mice, and their sexual dimorphism of expression indicates the sex-specific role in behavior regulation (Tsai et al., 2015). Pregnancy and the postpartum period are accompanied with a significant change in steroid levels and peptide hormones, which are necessary for offspring survival (Kinsley and Lambert, 2008). Studies have shown that Wnt plays an important regulatory role in the normal development of the cerebral cortex and hippocampus (Li and Pleasure, 2005; Machon et al., 2007), and can promote the self-renewal and differentiation of prostate cancer cells with stem cell characteristics (Bisson and Prowse, 2009). Wnt signaling in the early stage of neurogenesis plays a role in regulating the self-renewal and survival of neural progenitor cells and inducing the differentiation of neural progenitor cells at later stage. Interestingly, AR can form complexes with β-catenin, a key effector protein of the Wnt/β-catenin signaling pathway, and in prostate tumors β-catenin regulates activation of downstream AR pathways (Lee et al., 2013). Therefore, the dysregulation of androgen production could have a significant impact on neurodevelopment in the offspring.

In this study, we investigated the effects of the prenatal hyperandrogenic environment on neurobehavioral abnormality and hippocampal neurogenesis in offspring. An aromatase inhibitor was used to elevate testosterone since it has been shown that pregnant treatment leads to elevated testosterone level as well autism-like behavior in rat offspring (Xu et al., 2015). In addition, chronic lithium chloride (LICl), a widely prescribed psychological drug, was given to investigate whether it has an alleviating effect on neurobehavioral and neurogenic abnormalities, providing an experimental and theoretical basis for early clinical intervention.

Abbreviations: AR, androgen receptor; BSA, bovine serum albumin; DCX, doublecortin; DG, dentate gyrus; E2, estradiol; GSK-3β, glycogen synthase kinase 3β; LICl, lithium chloride; P, progesterone; SDS-PAGE, sodium dodecyl sulfate-polyacrylamide gel electrophoresis; T, testosterone; TBST, Tris-buffered saline Tween-20.

MATERIALS AND METHODS

Animals

This study was carried out according to the recommendations of the Experimental Animal Management and Ethics Committee of West China Second University Hospital. The protocol was approved by the Committee of West China Second University Hospital. Adult Sprague-Dawley (SD, weighing 220–240 g) rats were ordered from the Chengdu Dashuo Experimental Animals Co., Ltd. The animals were housed at 24 ± 1°C, in a 12 h light/dark cycle (light on at 7:00 AM) with full food and water. All animal experiments were performed in accordance with the recommendation of The Guide for the Care and Use of Laboratory Animals of Sichuan University. In order to have timed mating, virgin female rats were individually mated overnight with one or two adult males. Detection of the vaginal plug was named as the day gestation day 0 (G0). Pregnant female rats were randomly assigned into four groups as described below.

Experimental Groups

The pregnant female rats were divided into four groups: control group (CTL group, $n = 6$), high androgen exposure group (HA group, $n = 6$), lithium chloride treatment group (LICl group, $n = 6$), and high androgen exposure with lithium chloride treatment group (HA+LICL group, $n = 6$). Similarly, after delivery, the offspring were grouped accordingly (CTL group, $n = 6$, male 4, female 2; HA group, $n = 4$, male 2, female 2; LICl group, $n = 7$, male 1, female 6; HA+LICl group, $n = 4$, male 3, female 1). Letrozole (Novartis Pharma Stein AG, Switzerland) at 1 μg/ml was dissolved in 20% ethanol in sesame oil, in accordance with the method established by Moradi-Azani et al. (2011). Pregnant female rats in the HA group and HA+LICl group received subcutaneous injection of letrozole at 1 μg/kg from G0 to G20, while CTL group and LICl group rats received only the vehicle with the same volume at the same time. The LICl group and HA+LICl group treated offspring were given intraperitoneal

injection of lithium chloride (Sigma-Aldrich, United States) 2 mmol/kg at postnatal 9 days (from PND 1 to PND 9), while the CTL group and HA group were given intraperitoneal injection of saline solution of the same volume. At PND45-55 (adolescent rats), behavioral tests were examined as following described. After neurobehavioral detection, Brdu (100 mg/kg) was injected intraperitoneally once a day for three consecutive days. At postnatal day 60 (PND60), immunofluorescence staining and western blot were conducted.

Cesarean Section From Decapitated Rats and Blood Sampling

All the rats' brains were removed on G21 and blood serum were collected for ELISA analysis. As described by Vaillancourt et al. (1999), an incision is made through the midsection of the abdomen after removed from the brain and pups were quickly delivered from the isolated uterus. The whole operation was conducted under warm conditions to maintain the pups' body temperature. After delivery, the pups were placed in standard conditions and raised separately until the weaned females and males on the postnatal day 21 (PND21).

Detection of Testosterone and Estradiol

All blood samples were centrifuged at 3000 rpm for 10 min. ELISA Kit (MSK, Wuhan, China) was used to examine the testosterone and estradiol concentrations in the serum samples of the pregnant rats. The procedure was conducted according to the manufacturer's instructions. Briefly, the collected condition medium was added to a well coated with testosterone/estradiol polyclonal antibody and then immunosorbented by biotinylated monoclonal anti-rat testosterone/estradiol antibody at 37°C for 2 h. The color development, catalyzed by horseradish peroxidase, was terminated with 2.5 mol/l sulfuric acid, and the absorption was measured at 450 nm. The protein concentration was calculated by comparing the relative absorbance of the samples with the standards. There was less than 10% cross-reactivity with other steroid hormones, and the information was stated in the manual of the company (MSK, Wuhan, China). The *r*-values of standard curves were greater than 0.99 for both assays.

Neurobehavioral Detection

At PND45-55 (adolescent) behavioral tests were examined as following described.

Forced Swimming Test

The depression status of rats was determined by the forced swimming test device (20 cm in diameter, 40 cm in height). Before the trial, the device was filled with water maintained at 25°C, the height of which meant that rats could not reach the bottom or the upper edge of the cylinder to escape. The camera recorded for 10 min including the time of immobility whenever rats aborted all active behaviors and spent for strongly swimming. After each experiment, the rats should be kept dry on a heater before making their way back to cages. The device was cleaned before next animal.

Elevated Plus Maze

The animals' anxious-like behaviors were detected using the elevated cross maze experimental device, which had two open arms and two closed arms (two arms with 20 cm high walls on both sides, a length of 50 cm). There was a connected platform (10 × 10 cm) in the middle. The rats were placed on the intermediate platform of the device, and the cameras were used to record 10 min, including the time and times of their entering the open arms.

Three-Chamber Sociability Test

The three-chamber device was used to test the social communication ability of SD rats. The apparatus consisted of three Plexiglas chambers (40 cm × 20 cm × 20 cm) with each of the side chambers connected to the middle chamber by a corridor (10 cm × 10 cm × 15 cm). One side of the compartment was set up with unfamiliar rats of the same sex and age which had no previous contact, while the other side was set up with a toy. At the beginning of the test, the rat was placed into the middle chamber and allowed the exploration of the three chambers for 5 min. Then a model rat, locked in a small cage, was placed in one of the side chambers and a toy was placed in the other side chamber. The testing rat was allowed to freely explore the apparatus and interact with the model rat for 10 min. The activity of rats in the set was recorded, and the time of communication with unfamiliar rats and the object was counted. All behavioral experiments were carried out during the dark period of the light cycle under dim red illumination.

Self-Grooming Test

The open-field experiment device (60 × 60 cm) was used to detect the rats' repetitive or stereotypical self-combing behavior. Before the test, the rats were placed in the device for 5 min, and the rats were put into the device on the day of the experiment. The activity of the rats was recorded for 15 min and their self-grooming behaviors were counted. Before the next experimental rat, 75% ethanol was used to clean the facility.

Immunofluorescence Staining

After neurobehavioral evaluation, Brdu (100 mg/kg) was injected intraperitoneally once a day for three consecutive days. At postnatal day 60 (PND60), rats were deeply anesthetized with chloral hydrate. After anesthesia, rats were perfused pericardially with saline and 4% paraformaldehyde buffer. Then, the removed brain tissues were fixed in 4% paraformaldehyde for 48 h, next dehydrated with 10, 20, and 30% sucrose consecutively for 24 h, respectively. After treatment with sucrose solution, the tissues were embedded in paraffin. 30 μm paraffinic cross sections were prepared and examined, and each group were 10 brain slices at the same level. All sections were permeabilized with 0.5% Triton X-100, then blocked with 5% bovine serum albumin (BSA) and incubated with anti-Brdu and NeuN antibody (1:1000; Cell Signaling) mix diluents, anti-Brdu and GFAP (1:1000; Cell Signaling) mix diluents or anti-doublecortin antibody (1:1000; Cell Signaling) overnight at 4°C. Secondary antibodies (1:1000, Thermo Fisher Scientific) were added for 1 h and then incubated with 4,6-diamidino-2-phenylindole (DAPI, Sigma-Aldrich) to

label the nuclei, respectively at RT. Finally, confocal microscope (Olympus) was used to acquire the images. At least six sections were used for staining of each rat, and the sequential sections were used in each condition.

Western Blotting

Hippocampus Collection

Approximately at postnatal day 60 (PND60), the rats' brains of each group were rapidly removed from the skull and dissected brain tissue on ice. At least three rat tissues were extracted in every group. The whole hippocampus was quickly dissected and stored at −80°C for further protein extraction.

Protein Extraction

The hippocampal tissue samples were weighed (30 mg) and placed onto a filter cartridge. The tissue was then grounded using the plastic rod for 1–2 min. 100 μl buffer A was added to the filter and mixed well, placing the filter with cap open on ice for 5 min. Next, the proteins of the nuclei, cytosol and plasma membrane were extracted according to the instructions of Minute™ Plasma Membrane Protein Isolation and Cell Fractionation Kit (Beyotime Institute of Biotechnology). The concentration of protein was detected by the BCA Protein Assay Kit (Beyotime Institute of Biotechnology).

Western Blotting

The proteins were adjusted to the same concentration with RIPA lysis buffer and added 5× sample loading buffer. 40 μg total protein was separated on a 10% SDS-polyacrylamide gel (SDS-PAGE) and transferred to polyvinylidene difluoride (PVDF) membranes (Millipore, MA). After blocking in 5% BSA for 1 h at RT, the membranes were incubated overnight at 4°C with the following antibodies: anti-GAPDH (1:5000, Zen Bioscience, China), anti-β-catenin (1:400, Abcam, United States), anti-GSK-3β (1:500, Abcam, United States), anti-DVL2 (1:500, Bioss, China), anti-TCF-4 (1:500, Bioss, China). β-catenin, GSK-3β, DVL2, TCF-4 are the main members of Wnt/β-catenin signaling pathway. On the next day, the membranes were washed by Tris-buffered saline Tween-20 (TBST) (3 × 5 min), then incubated with anti-mouse or rabbit secondary antibodies for 1 h at RT. Protein bands on the membrane were detected using an chemiluminescence detection system (Millipore Corporation, United States), following the manufacturer's instructions. The relative densities of each band were measured using ImageJ (Schneider et al., 2012). All the antibodies were either validated by other studies or by ourselves in a preliminary experiment.

Statistics

The results were analyzed by SPSS version 19.0 and GraphPad Prism version 5.0. Data were presented as mean ± SEM and comparisons among groups used one-way analysis of variance (ANOVA). For all tests, it is considered as statistically significant for a probability (p) value below 0.05 (two-tailed).

RESULTS

Serum Testosterone and Estradiol Levels in Pregnant Rats

Serum samples from blood of the pregnant rats were collected on G21 before the Cesarean sections. ELISA measurement shows that serum testosterone levels of the pregnant rats were higher in the HA and HA+LICL groups (mean ± SEM: 283.65 ± 46.05 nmol/L, 199.04 ± 10.52 nmol/L, respectively), as compared to the CTL group (113.36 ± 19.39 nmol/L, $p < 0.05$) and LICL group (127.07 ± 13.74 nmol/L, $p < 0.05$). No significant difference was found in serum estradiol levels between the four groups (**Figure 1**).

Behavioral Detection of the Offspring

The behavior test was examined in the offspring, and the results show that the time spent in struggling significantly decreased in HA group (38.38 ± 9.36 s) compared to CTL group (123.58 ± 30.39 s, $p < 0.01$) (**Figure 2A**). No significant difference was found in the time of latency to immobility between the four groups (**Figure 2B**). Both the time and times for them to enter the open arms were higher in the HA group as compared to the CTL group ($p < 0.05$) (**Figure 2C**), and lower in the HA+LICL group as compared to the HA group (**Figure 2D**). The time of communication with unfamiliar rats and object had no significant difference between the four groups (**Figures 2E,F**). The times spent in grooming were less in the HA group as compared to the CTL group (**Figure 2G**), and the times spent in standing were lower in the HA+LICL group as compared to the HA group ($p < 0.05$) (**Figure 2H**). The results show that HA treatment could alter some parameters of behavior and lithium chloride could rescue the phenotypes related to depression and anxiety.

The Neurogenesis of DG Area

The rat DG area Doublecortin (DCX) positive expression of immature neurons in HA group (n = 6, 387 ± 53) was significantly decreased compared to CTL group (n = 6, 553 ± 54, $p < 0.05$), and after lithium chloride treatment, the number of DCX positive cells increased significantly between HA and HA+LICL group (n = 6, 618 ± 59, $p < 0.05$) (**Figures 3A,B**). In the HA group (n = 6, 264 ± 20), both Brdu and NeuN positive neurons in the DG region were more reduced than in the CTL group (n = 6,526 ± 19, $p < 0.05$), whereas, after LICl treatment, Brdu and NeuN positive cells increased in HA+LICL group (n = 6, 516 ± 21, $p < 0.05$) (**Figures 3C,D**). There was no significant difference in Brdu and GFAP positive neurons among the four groups ($p > 0.05$) (**Figures 3E,F**).

Western Blotting of Wnt/β-Catenin Signaling Pathway

The β-catenin protein was detected in the cytoplasm, TCF-4 detected in nucleus, and GSK-3β and DVL2 in the cell membrane. The results show that there was no significant difference after letrozole or LICl treatment (**Figures 4A–F**).

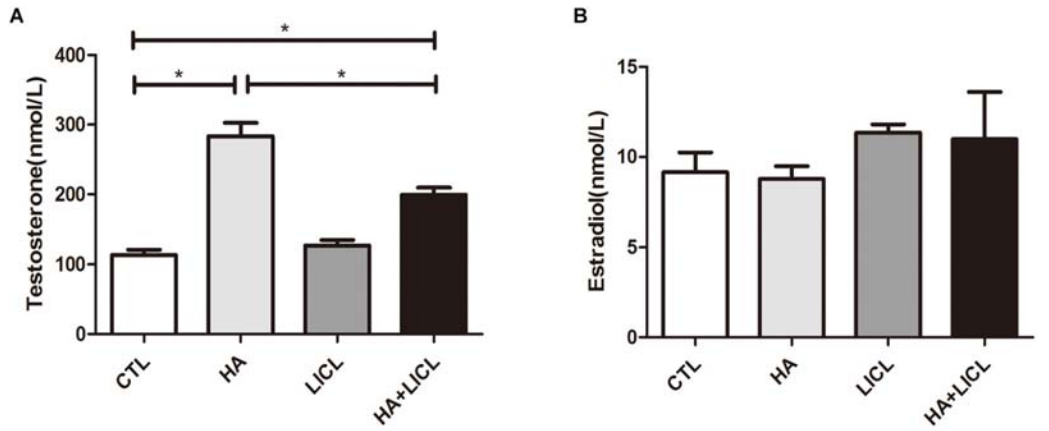

FIGURE 1 | Higher levels of serum testosterone in pregnant rats after letrozole treatment. **(A)** Pregnant rats in the HA and HA+LICl groups ($n = 6$) had higher levels of serum testosterone as compared to the CTL group ($n = 6$), **(B)** There was no significant difference in serum estradiol levels among the four groups. $^*p < 0.05$.

DISCUSSION

The current study shows that after exposure of the mother to hyperandrogenic environment, the offspring presented more depressive- and anxious-like behaviors. This is consistent with previous studies in animal models (Meng et al., 2011; Hernández and Fernández-Guasti, 2018).

Many studies have already shown that chronic stress produces decreased grooming activities (Yalcin et al., 2007), meanwhile in chronic social crowding and isolation stress (Pan et al., 2006; Dronjak et al., 2007). In line with these observations, our studies also indicate the reduced grooming behavior in depression or anxiety condition in our model. Clinical researches have suggested that testosterone administration may alleviate the social anxiety symptoms (Terburg et al., 2016). Prenatal intrauterine exposure to the hyperandrogenic environment of female rats resulted in less time of adolescent offspring in social interaction (Xu et al., 2015). In terms of the impact of androgen on the neurogenesis, one previous study is also controversial as it shows that androgens increase survival of neurons in the dentate gyrus through AR dependent mechanism in male rats (Hamson et al., 2013), while our results indicate the opposite effects in the same region of offspring. Furthermore, our results show that exposure to a maternal hyperandrogenic environment, induced by letrozole, may contribute to neurobehavioral abnormalities, and lithium chloride could rescue the neurogenesis defects in our rat model. It has been shown that the neurogenesis of the hippocampus is compromised in post-mortem tissue of patients accompanied with depression (Boldrini et al., 2012) and Alzheimer's disease (Crews et al., 2010), as well as in animal models (Mu and Gage, 2011; Wainwright et al., 2011). Therefore, the prenatal hyperandrogenic environment should be regarded as an important etiological factor in neurodevelopmental diseases. Furthermore, studies on patients of Polycystic Ovary Syndrome and Congenital Adrenal Hyperplasia show that they are often more likely to be accompanied with neurobehavior abnormalities (Hamson et al., 2013). Therefore, the study in the current research has broad clinical implications.

One of key findings from the current study is that the reduction of neurogenesis caused by exposure to high testosterone can be restored to a normal level with lithium chloride, supporting an important role of lithium chloride effect in different conditions of neurogenesis defects (Bianchi et al., 2010; Kitamura et al., 2011; Qi et al., 2017; Lewin et al., 2018; Zhang et al., 2018). Lithium chloride has been used as a mood stabilizer for a long time as a clinical treatment of bipolar disorder with mania and depression and for prevention of their recurrence (Manji et al., 2000). In animal models, lithium chloride has therapeutic effects on neurodevelopmental diseases such as Down syndrome (Bianchi et al., 2010) and neurodegenerative diseases such as Alzheimer's disease (AD) (De Ferrari et al., 2003), as it has the function of protecting and nourishing nerves. It may play a role in promoting the proliferation and differentiation of neural progenitor cells, reducing the apoptosis of neurons and up-regulating the level of neurotrophic factors (Chen et al., 2000; Son et al., 2003). Neurogenesis refers to the proliferation and division of neural stem cells into differentiating progenitor cells, which become mature neurons when migrating to functional areas and establish synaptic connections with other neurons to support neurogenesis (Vogel, 2013; Paridaen and Huttner, 2014). Doublecortin (DCX) functions in the stabilizing microtubules in early mitotic neurons as a marker of immature neurons and is often used to evaluate immature neuronal morphology (Bechstedt et al., 2014), which is expressed in the hippocampus of rat from P0 to P21 after the birth (Brown et al., 2003). NeuN expressed in most mature neurons functions in RNA splicing at the nucleus (Kim et al., 2009; Duan et al., 2016), which is not expressed in certain neuronal populations such as the cerebellar purkinje cells (Mullen et al., 1992). Previous studies have confirmed that neuropsychiatric diseases are often associated with neurological damage of different degrees (Ruksee et al., 2014; Zhang et al., 2014). The current result shows that maternal rats exposed to the hyperandrogenic environment were

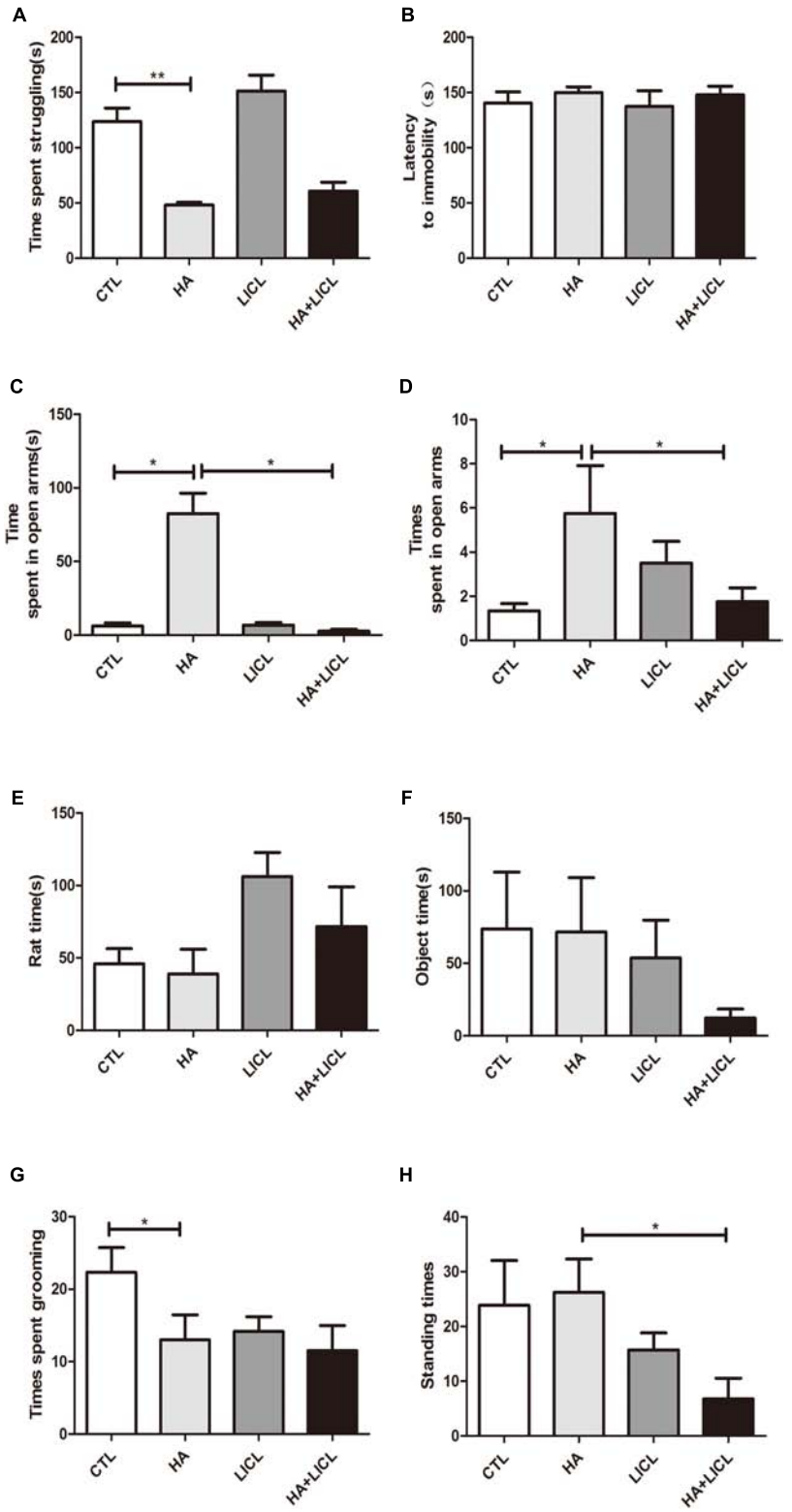

FIGURE 2 | Behavioral test of the offspring. **(A)** Time spent in struggling was significantly decreased after HA treatment **(B)** No significant difference was found on the time of latency to immobility in treatment group. **(C,D)** Both the time and times of their entering the open arms were higher in the HA group as compared to the CTL group and lower in the HA+LICl group as compared to the HA group. **(E,F)** The time of communication with unfamiliar rats and object showed no significant difference following letrozole and lithium chloride treatment. **(G)** The stereotyped behavior of grooming were decreased, **(H)** and the standing behavior were not improved after lithium chloride intervention. $*p < 0.05$, $**p < 0.01$.

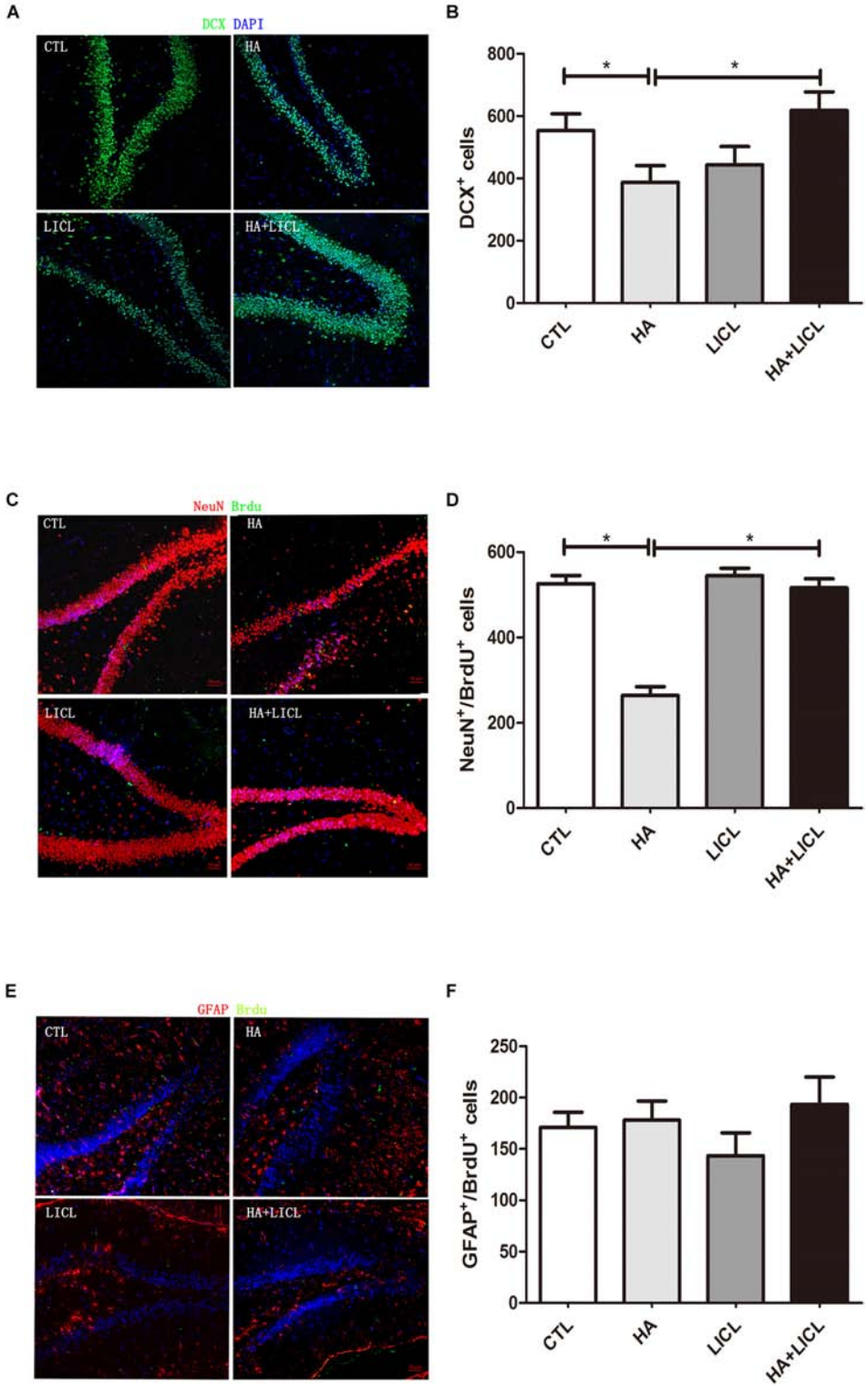

FIGURE 3 | The neurogenesis of DG area among different treatment groups. **(A,B)** The number of DCX positive neurons of the rat DG area was significantly decreased in HA group as compared to CTL group, and after lithium chloride treatment the number of DCX positive neurons increased in HA+LICl group. **(C,D)** Brdu and NeuN neurons in the DG region were reduced, while lithium chloride promoted the proliferation of NPCS in HA+LICl group. **(E,F)** No significant difference was found in Brdu and GFAP neurons among the four groups. $^{*}p < 0.05$.

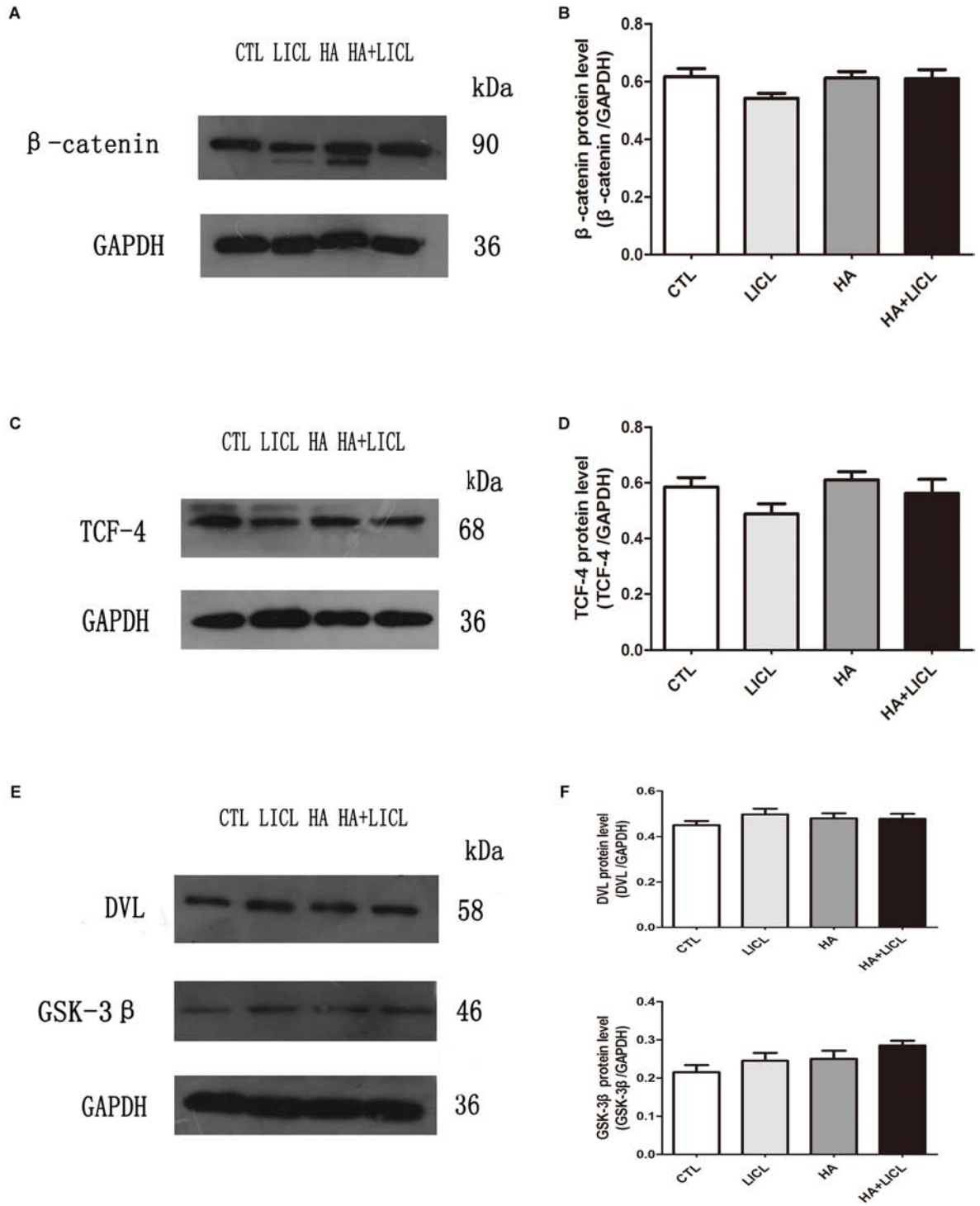

FIGURE 4 | The expression of Wnt/β-catenin signaling pathway proteins. **(A–F)** After letrozole exposure there was no significant difference of β-catenin, TCF-4, GSK-3β and DVL2 between CTL group and HA group. Furthermore, single lithium chloride or co-letrozole treatment had no effects on the expression of four proteins in LICl group and HA+LICl group.

found to have a reduced number of immature nerve cells marked by DCX and mature neurons co-expressed by Brdu and NeuN during their adult years. Meanwhile, lithium chloride promoted the proliferation and differentiation of neural progenitor cells. The effects of lithium chloride on the neurogenesis support its potential role in neurobehavior intervention.

Letrozole, an aromatase inhibitor was used to elevate testosterone in the current study. Letrozole decreases estrogen expression levels and accumulates androgen in the body (Haynes et al., 2003). This is similar to the results of hyperandrogen, except without any apparent effect on the level of estrogen (Xu et al., 2015), although it contradicts previous research showing a lower concentration after letrozole treatment (Rashid et al., 2015).

The exact pathway of how androgen exposure reduce neurogenesis is not clear, as studies have reported that glycogen synthase kinase 3β (GSK-3β) activation leads to neurogenic damage (Chao et al., 2014; Trazzi et al., 2014). It has also been shown that lithium chloride promoted the proliferation and differentiation of neural progenitor cells through regulating Wnt pathway. However, in the current study, we have detected Wnt signaling molecules using Western blot and found no significant change of Wnt signal molecules. Although the current result did not find any significant change in Wnt molecules after the treatment in the hippocampus, a subtle change in the Wnt pathway, such as β-catenin phosphorylation, cannot be ruled out since more sensitive methods are needed to clarify the issue. In this regard, further experimental studies are needed to explore the underlying mechanism of defective neurogenesis caused by exposure to hyperandrogen during pregnancy and the alleviation of lithium chloride intervention.

CONCLUSION

The present study demonstrated that pregnant administration of letrozole resulted in depressive and anxious -like behaviors of rats in the adolescent period. A remarkable decrease in immature nerve cells marked by DCX and mature neurons co-expressed by Brdu and NeuN during adult years were detected in the hippocampus of rats, which indicated that the hyperandrogenic intrauterine environment could induce depression and abnormal hippocampal neurogenesis in rats, and lithium chloride alleviated the effects on neurobehavioral and hippocampal abnormalities. Wnt/β-catenin signaling pathway seems not to be related to this regulation process.

ETHICS STATEMENT

This study was carried out in accordance with the recommendations of the Experimental Animal Management and Ethics Committee of West China Second University Hospital. The protocol was approved by the Experimental Animal Management and Ethics Committee of West China Second University Hospital.

AUTHOR CONTRIBUTIONS

JX and WX involved in research design and data interpretation. JC performed the majority of the experimental work and analysis of data, and contributed to writing of the manuscript. HW, HuawL, HuaL, HZ, YZ, and HoL were responsible for the experimental progress.

FUNDING

This work was supported by funding from the Science and Technology Bureau of Chengdu (No. 2014-HM01-00232-SF); Department of Science and Technology of Sichuan Province, China (No. 2016JY0185).

REFERENCES

Bechstedt, S., Lu, K., and Brouhard, G. J. (2014). Doublecortin recognizes the longitudinal curvature of the microtubule end and lattice. *Curr. Biol.* 24, 2366–2375. doi: 10.1016/j.cub.2014.08.039

Bianchi, P., Ciani, E., Contestabile, A., Guidi, S., and Bartesaghi, R. (2010). Lithium restores neurogenesis in the subventricular zone of the Ts65Dn mouse, a model for Down syndrome. *Brain Pathol.* 20, 106–118. doi: 10.1111/j.1750-3639.2008.00246.x

Bisson, I., and Prowse, D. M. (2009). WNT signaling regulates self-renewal and differentiation of prostate cancer cells with stem cell characteristics. *Cell Res.* 19, 683–697. doi: 10.1038/cr.2009.43

Boldrini, M., Hen, R., Underwood, M. D., Rosoklija, G. B., Dwork, A. J., Mann, J. J., et al. (2012). Hippocampal angiogenesis and progenitor cell proliferation are increased with antidepressant use in major depression. *Biol. Psychiatry* 72, 562–571. doi: 10.1016/j.biopsych.2012.04.024

Brown, J. P., Couillard-Despres, S., Cooper-Kuhn, C. M., Winkler, J., Aigner, L., and Kuhn, H. G. (2003). Transient expression of doublecortin during adult neurogenesis. *J. Comp. Neurol.* 467, 1–10. doi: 10.1002/cne.10874

Campbell, S., and Macqueen, G. (2004). The role of the hippocampus in the pathophysiology of major depression. *J. Psychiatry Neurosci.* 29, 417–426.

Carrier, N., and Kabbaj, M. (2012). Extracellular signal-regulated kinase 2 signaling in the hippocampal dentate gyrus mediates the antidepressant effects of testosterone. *Biol. Psychiatry* 71, 642–651. doi: 10.1016/j.biopsych.2011.11.028

Chao, J., Yang, L., Yao, H., and Buch, S. (2014). Platelet-derived growth factor-BB restores HIV Tat -mediated impairment of neurogenesis: role of GSK-3β/β-catenin. *J. Neuroimmune Pharmacol.* 9, 259–268. doi: 10.1007/s11481-013-9509-x

Chen, G., Rajkowska, G., Du, F., Seraji-Bozorgzad, N., and Manji, H. K. (2000). Enhancement of hippocampal neurogenesis by lithium. *J. Neurochem.* 75, 1729–1734. doi: 10.1046/j.1471-4159.2000.0751729.x

Crews, L., Adame, A., Patrick, C., Delaney, A., Pham, E., Rockenstein, E., et al. (2010). Increased BMP6 levels in the brains of Alzheimer's disease patients and APP transgenic mice are accompanied by impaired neurogenesis. *J. Neurosci.* 30, 12252–12262. doi: 10.1523/JNEUROSCI.1305-10.2010

De Ferrari, G. V., Chacón, M. A., Barría, M. I., Garrido, J. L., Godoy, J. A., Olivares, G., et al. (2003). Activation of Wnt signaling rescues neurodegeneration and behavioral impairments induced by beta-amyloid fibrils. *Mol. Psychiatry* 8, 195–208. doi: 10.1038/sj.mp.4001208

Dronjak, S., Spasojevic, N., Gavrilovic, L., and Varagic, V. (2007). Behavioural and endocrine responses of socially isolated rats to long-term diazepam treatment. *Acta Vet.* 57, 291–302. doi: 10.2298/avb0704291d

Duan, W., Zhang, Y. P., Hou, Z., Huang, C., Zhu, H., Zhang, C. Q., et al. (2016). Novel insights into neun: from neuronal marker to splicing regulator. *Mol. Neurobiol.* 53, 1637–1647. doi: 10.1007/s12035-015-9122-5

Eriksson, P. S., Perfilieva, E., Björk-Eriksson, T., Alborn, A. M., Nordborg, C., Peterson, D. A., et al. (1998). Neurogenesis in the adult human hippocampus. *Nat. Med.* 4, 1313–1317. doi: 10.1038/3305

Galea, L. A. M., Wainwright, S. R., Roes, M. M., Duarte-Guterman, P., Chow, C., and Hamson, D. K. (2013). Sex, hormones and neurogenesis in the hippocampus: hormonal modulation of neurogenesis and potential functional implications. *J. Neuroendocrinol.* 25, 1039–1061. doi: 10.1111/jne.12070

Hall, J. M., Gomez-Pinilla, F., and Savage, L. M. (2018). Nerve growth factor is responsible for exercise-induced recovery of septohippocampal cholinergic structure and function. *Front. Neurosci.* 12:773. doi: 10.3389/fnins.2018.00773

Hamson, D. K., Wainwright, K. S., Taylor, J. R., Jones, B. A., Watson, N. V., and Galea, L. A. (2013). Androgens increase survival of adult-born neurons in the dentate gyrus by an androgen receptor-dependent mechanism in male rats. *Endocrinology* 154, 3294–3304. doi: 10.1210/en.2013-1129

Haynes, B. P., Dowsett, M., Miller, W. R., Dixon, J. M., and Bhatnagar, A. S. (2003). The pharmacology of letrozole. *J. Steroid Biochem. Mol. Biol.* 87, 35–45.

Henneman, W. J. P., Sluimer, J. D., Barnes, J., van der Flier, W. M., Sluimer, I. C., Fox, N. C., et al. (2009). Hippocampal atrophy rates in Alzheimerdisease: added value over whole brain volume measures. *Neurology* 72, 999–1007. doi: 10.1212/01.wnl.0000344568.09360.31

Hernández, A., and Fernández-Guasti, A. (2018). Male rats with same-sex preference show higher immobility in the forced swim test, but similar effects of fluoxetine and desipramine than males that prefer females. *Pharmacol. Biochem. Behav.* 171, 39–45. doi: 10.1016/j.pbb.2018.05.017

Jessberger, S., Nakashima, K., Clemenson, G. D., Mejia, E., Mathews, E., Ure, K., et al. (2007). Epigenetic modulation of seizure-induced neurogenesis and cognitive decline. *J. Neurosci.* 27, 5967–5975. doi: 10.1523/JNEUROSCI.0110-07.2007

Kim, K. K., Adelstein, R. S., and Kawamoto, S. (2009). Identification of neuronal nuclei (NeuN) as Fox-3, a new member of the Fox-1 gene family of splicing factors. *J. Biol. Chem.* 284, 31052–31061. doi: 10.1074/jbc.M109.052969

Kinsley, C. H., and Lambert, K. G. (2008). Reproduction-induced neuroplasticity: natural behavioural and neuronal alterations associated with the production and care of offspring. *J. Neuroendocrinol.* 20, 515–525. doi: 10.1111/j.1365-2826.2008.01667.x

Kitamura, Y., Doi, M., Kuwatsuka, K., Onoue, Y., Miyazaki, I., Shinomiya, K., et al. (2011). Chronic treatment with imipramine and lithium increases cell proliferation in the hippocampus in adrenocorticotropic hormone-treated rats. *Biol. Pharm. Bull.* 34, 77–81. doi: 10.1248/bpb.34.77

Lee, E., Madar, A., David, G., Garabedian, M. J., Dasgupta, R., and Logan, S. K. (2013). Inhibition of androgen receptor and β-catenin activity in prostate cancer. *Proc. Natl. Acad. Sci. U.S.A.* 110, 15710–15715. doi: 10.1073/pnas.1218168110

Lewin, M., Ilina, M., Betz, J., Masiello, K., Hui, M., Wilson, D. A., et al. (2018). Developmental ethanol-induced sleep fragmentation, behavioral hyperactivity, cognitive impairment and parvalbumin cell loss are prevented by lithium co-treatment. *Neuroscience* 369, 269–277. doi: 10.1016/j.neuroscience.2017.11.033

Li, G., and Pleasure, S. J. (2005). Morphogenesis of the dentate gyrus: what we are learning from mouse mutants. *Dev. Neurosci.* 27, 93–99. doi: 10.1159/000085980

Liu, W., Ge, T., Leng, Y., Pan, Z., Fan, J., Yang, W., et al. (2017). The role of neural plasticity in depression: from hippocampus to prefrontal cortex. *Neural Plast.* 2017:6871089. doi: 10.1155/2017/6871089

Machon, O., Backman, M., Machonova, O., Kozmik, Z., Vacik, T., Andersen, L., et al. (2007). A dynamic gradient of Wnt signaling controls initiation of neurogenesis in the mammalian cortex and cellular specification in the hippocampus. *Dev. Biol.* 311, 223–237. doi: 10.1016/j.ydbio.2007.08.038

Manji, H. K., Moore, G. J., and Chen, G. (2000). Clinical and preclinical evidence for the neurotrophic effects of mood stabilizers: implications for the pathophysiolo gy and treatment of manic-depressive illness. *Biol. Psychiatry.* 48, 740–754. doi: 10.1016/s0006-3223(00)00979-3

McKinnon, M. C., Yucel, K., Nazarov, A., and MacQueen, G. M. (2009). A meta-analysis examining clinical predictors of hippocampal volume in patients with major depressive disorder. *J. Psychiatry Neurosci.* 34, 41–54.

Meng, F. T., Ni, R. J., Zhang, Z., Zhao, J., Liu, Y. J., and Zhou, J. N. (2011). Inhibition of oestrogen biosynthesis induces mild anxiety in C57BL/6J ovariectomized female mice. *Neurosci. Bull.* 27, 241–250. doi: 10.1007/s12264-011-1014-8

Moradi-Azani, M., Ahmadiani, A., and Amini, H. (2011). Increase in formalin-induced tonic pain by 5alpha-reductase and aromatase inhibition in female rats. *Pharmacol. Biochem. Behav.* 98, 62–66. doi: 10.1016/j.pbb.2010.12.016

Mu, Y., and Gage, F. H. (2011). Adult hippocampal neurogenesis and its role in Alzheimer's disease. *Mol. Neurodegener.* 6:85. doi: 10.1186/1750-1326-6-85

Mullen, R. J., Buck, C. R., and Smith, A. M. (1992). NeuN, a neuronal specific nuclear protein in vertebrates. *Development* 116, 201–211.

Nelson, R. J. (2011). *An Introduction to Behavioral Endocrinology*, 4th Edn. Sunderland, MA: Sinauer Associates.

Pan, F. L. C., Song, J., Hong, J., Li, Q., Yu, H. I., and Chen, X. Y. (2006). Different duration of crowding and noise exposure effects on exploratory behavior, cellular immunity and hsp70 expression in rats. *Stress Health* 22, 257–262. doi: 10.1002/smi.1103

Paridaen, J. T., and Huttner, W. B. (2014). Neurogenesis during development of the vertebrate central nervous system. *EMBO Rep.* 15, 351–364. doi: 10.1002/embr.201438447

Qi, L., Tang, Y., He, W., Pan, H., Jiang, W., Wang, L., et al. (2017). Lithium chloride promotes neuronal differentiation of rat neural stem cells and enhances neural regeneration in Parkinson's disease model. *Cytotechnology* 69, 277–287. doi: 10.1007/s10616-016-0056-1

Rashid, D., Panda, B. P., and Vohora, D. (2015). Reduced estradiol synthesis by letrozole, an aromatase inhibitor, is protective against development of pentylenetetrazole-induced kindling in mice. *Neurochem. Int.* 90, 271–274. doi: 10.1016/j.neuint.2015.10.001

Ruksee, N., Tongjaroenbuangam, W., Mahanam, T., and Govitrapong, P. (2014). Melatonin pretreatment prevented the effect of dexamethasone negative alterations on behavior and hippocampal neurogenesis in the mouse brain. *J. Steroid Biochem. Mol. Biol.* 143, 72–80. doi: 10.1016/j.jsbmb.2014.02.011

Schneider, C. A., Rasband, W. S., and Eliceiri, K. W. (2012). NIH Image to ImageJ: 25 years of image analysis. *Nat. Methods* 9, 671–675. doi: 10.1038/nmeth.2089

Son, H., Yu, I. T., Hwang, S. J., Kim, J. S., Lee, S. H., Lee, Y. S., et al. (2003). Lithium enhances long-term potentiation independently of hippocampal neurogenesis in the rat dentate gyrus. *J. Neurochem.* 85, 872–881. doi: 10.1046/j.1471-4159.2003.01725.x

Spalding, K. L., Bergmann, O., Alkass, K., Bernard, S., Salehpour, M., Huttner, H. B., et al. (2013). Dynamics of hippocampal neurogenesis in adult humans. *Cell* 153, 1219–1227. doi: 10.1016/j.cell.2013.05.002

Spritzer, M. D., and Galea, L. A. (2007). Testosterone and dihydrotestosterone, but not estradiol, enhance survival of new hippocampal neurons in adult male rats. *Dev. Neurobiol.* 67, 1321–1333. doi: 10.1002/dneu.20457

Sweatt, J. D. (2004). Hippocampal function in cognition. *Psychopharmacology* 174, 99–110. doi: 10.1007/s00213-004-1795-9

Terburg, D., Syal, S., Rosenberger, L. A., Heany, S. J., Stein, D. J., and Honk, J. V. (2016). Testosterone abolishes implicit subordination in social anxiety. *Psychoneuroendocrinology* 72, 205–211. doi: 10.1016/j.psyneuen.2016.07.203

Trazzi, S., Fuchs, C., De Franceschi, M., Mitrugno, V. M., Bartesaghi, R., and Ciani, E. (2014). APP-dependent alteration of GSK3β activity impairs neurogenesis in the Ts65Dn mouse model of Down syndrome. *Neurobiol. Dis.* 67, 24–36. doi: 10.1016/j.nbd.2014.03.003

Tsai, H. W., Taniguchi, S., Samoza, J., and Ridder, A. (2015). Age- and sex-dependent changes in androgen receptor expression in the developing mouse cortex and hippocampus. *Neurosci. J.* 2015:525369. doi: 10.1155/2015/525369

Vaillancourt, C., Berger, N., and Boksa, P. (1999). Effects of vaginal birth versus caesarean section birth with general anesthesia on blood gases and brain energy metabolism in neona- tal rats. *Exp. Neurol.* 160, 142–150. doi: 10.1006/exnr.1999.7201

Vogel, G. (2013). Neurodevelopment. Lab dishes up mini-brains. *Science* 341, 946–947. doi: 10.1126/science.341.6149.946

Wainwright, S. R., Barha, C. K., Hamson, D. K., Epp, J. R., Chow, C., Lieblich, S. E., et al. (2016). Enzymatic depletion of the polysialic acid moiety associated with the neural cell adhesion molecule inhibits antidepressant efficacy. *Neuropsychopharmacology* 41, 1670–1680. doi: 10.1038/npp.2015.337

Wainwright, S. R., Lieblich, S. E., and Galea, L. A. M. (2011). Hypogonadism predisposes males to the development of behavioural and neuroplastic depressive phenotypes. *Psychoneuroendocrinology* 36, 1327–1341. doi: 10.1016/j.psyneuen.2011.03.004

Woodward, N. C., Haghani, A., Johnson, R. G., Hsu, T. M., Saffari, A., Sioutas, C., et al. (2018). Prenatal and early life exposure to air pollution induced hippocampal vascular leakage and impaired neurogenesis in association with behavioral deficits. *Transl. Psychiatry* 8:261. doi: 10.1038/s41398-018-0317-1

Xu, X. J., Zhang, H. F., Shou, X. J., Li, J., Jing, W. L., Zhou, Y., et al. (2015). Prenatal hyperandrogenic environment induced autistic-like behavior in rat offspring. *Physiol. Behav.* 138, 13–20. doi: 10.1016/j.physbeh.2014.09.014

Yalcin, I., Aksu, F., Bodard, S., Chalon, S., and Belzung, C. (2007). Antidepressant-like effect of tramadol in the unpredictable chronic mild stress procedure: possible involvement of the noradrenergic system. *Behav. Pharmacol.* 18, 623–631. doi: 10.1097/fbp.0b013e3282eff109

Zhang, L. Q., Zhang, W. M., Deng, L., Xu, Z. X., Lan, W. B., and Lin, J. H. (2018). Transplantation of a peripheral nerve with neural stem cells plus lithium chloride injection promote the recovery of rat spinal cord injury. *Cell Transplant.* 27, 471–484. doi: 10.1177/0963689717752945

Zhang, Y., Mao, R. R., Chen, Z. F., Tian, M., Tong, D. L., Gao, Z. R., et al. (2014). Deep-brain magnetic stimulation promotes adult hippocampal neurogenesis and alleviates stress-related behaviors in mouse models for neuropsychiatric disorders. *Mol. Brain* 7:11. doi: 10.1186/1756-6606-7-1

Conflict of Interest Statement: The authors declare that the research was conducted in the absence of any commercial or financial relationships that could be construed as a potential conflict of interest.

frontiers in Neuroscience

REVIEW
published: 21 May 2019
doi: 10.3389/fnins.2019.00454

Therapeutic Potential of Oxytocin in Atherosclerotic Cardiovascular Disease: Mechanisms and Signaling Pathways

Ping Wang[1†], Stephani C. Wang[2†], Haipeng Yang[3], Chunmei Lv[4], Shuwei Jia[4], Xiaoyu Liu[4], Xiaoran Wang[4], Dexin Meng[5], Danian Qin[6], Hui Zhu[4] and Yu-Feng Wang[4]**

[1] Department of Genetics, School of Basic Medical Sciences, Harbin Medical University, Harbin, China, [2] Department of Medicine, Albany Medical Center, Albany, NY, United States, [3] Department of Pediatrics, The Forth Affiliated Hospital, Harbin Medical University, Harbin, China, [4] Department of Physiology, School of Basic Medical Sciences, Harbin Medical University, Harbin, China, [5] Department of Physiology, Jiamusi University, Jiamusi, China, [6] Department of Physiology, Shantou University of Medical College, Shantou, China

OPEN ACCESS

Edited by:
Pierrette Gaudreau,
Université de Montréal, Canada

Reviewed by:
Marta Busnelli,
Italian National Research Council (CNR), Italy
Philip M. McCabe,
University of Miami, United States

***Correspondence:**
Yu-Feng Wang
yufengwang@ems.hrbmu.edu.cn
Hui Zhu
dzhuhui@aliyun.com

[†]These authors have contributed equally to this work

Specialty section:
This article was submitted to Neuroendocrine Science, a section of the journal Frontiers in Neuroscience

Received: 14 December 2018
Accepted: 23 April 2019
Published: 21 May 2019

Citation:
Wang P, Wang SC, Yang H, Lv C, Jia S, Liu X, Wang X, Meng D, Qin D, Zhu H and Wang Y-F (2019) Therapeutic Potential of Oxytocin in Atherosclerotic Cardiovascular Disease: Mechanisms and Signaling Pathways. Front. Neurosci. 13:454. doi: 10.3389/fnins.2019.00454

Coronary artery disease (CAD) is a major cardiovascular disease responsible for high morbidity and mortality worldwide. The major pathophysiological basis of CAD is atherosclerosis in association with varieties of immunometabolic disorders that can suppress oxytocin (OT) receptor (OTR) signaling in the cardiovascular system (CVS). By contrast, OT not only maintains cardiovascular integrity but also has the potential to suppress and even reverse atherosclerotic alterations and CAD. These protective effects of OT are associated with its protection of the heart and blood vessels from immunometabolic injuries and the resultant inflammation and apoptosis through both peripheral and central approaches. As a result, OT can decelerate the progression of atherosclerosis and facilitate the recovery of CVS from these injuries. At the cellular level, the protective effect of OT on CVS involves a broad array of OTR signaling events. These signals mainly belong to the reperfusion injury salvage kinase pathway that is composed of phosphatidylinositol 3-kinase-Akt-endothelial nitric oxide synthase cascades and extracellular signal-regulated protein kinase 1/2. Additionally, AMP-activated protein kinase, Ca^{2+}/calmodulin-dependent protein kinase signaling and many others are also implicated in OTR signaling in the CVS protection. These signaling events interact coordinately at many levels to suppress the production of inflammatory cytokines and the activation of apoptotic pathways. A particular target of these signaling events is endoplasmic reticulum (ER) stress and mitochondrial oxidative stress that interact through mitochondria-associated ER membrane. In contrast to these protective effects and machineries, rare but serious cardiovascular disturbances were also reported in labor induction and animal studies including hypotension, reflexive tachycardia, coronary spasm or thrombosis and allergy. Here, we review our current understanding of the protective effect of OT against varieties of atherosclerotic etiologies as well as the approaches and underlying mechanisms of these effects. Moreover, potential cardiovascular disturbances following OT application are also discussed to avoid unwanted effects in clinical trials of OT usages.

Keywords: atherosclerosis, coronary artery disease, etiology, oxytocin, signaling pathways

INTRODUCTION

Cardiovascular disease (CVD) is responsible for both high morbidity and mortality worldwide with coronary artery disease (CAD) being the leading cause of death (45.1%) (Cassar et al., 2009). In the United States, the prevalence of CVD comprising chronic heart disease, heart failure, and hypertension in adults (≥20 years of age) was 121.5 million in 2016 and increases with advancing age in both males and females (Benjamin et al., 2019). The major pathological basis of CAD is atherosclerosis that affects various components of the cardiovascular system (CVS), particularly the coronary artery. Over the past decades, identifying and reversing the pathogenesis of CAD and preventing myocardial infarction (MI) remain a major challenge for clinical management of CAD (Koton et al., 2014).

Oxytocin (OT), a nonapeptide synthesized in hypothalamic magnocellular neuroendocrine cells in the supraoptic and paraventricular nuclei (SON and PVN) (Yang et al., 2013; Johnson and Young, 2017), has emerged as an efficient cardioprotective agent in animal studies (Jankowski et al., 2016). However, due to the lack of deep knowledge of its involvement in the pathogenesis of atherosclerosis, therapeutic potential of OT in treating CAD is largely unexplored in clinical studies. In this review, we summarize our current understanding of the pathogenetic involvement of OT in atherosclerosis, the cellular/molecular mechanisms underlying OT suppression of atherosclerosis development and current challenges in clinical trials of OT.

ATHEROSCLEROSIS AND CARDIOPROTECTIVE EFFECT OF OT

Atherosclerosis can occur in the coronary artery, renal and cerebral circulation, and peripheral and mesenteric vasculature, largely due to metabolic disorders and immunological injuries (Rahman and Woollard, 2017). CVDs are often accompanied by disruption of OT/OT receptor (OTR) signaling. For instance, particulate matter 2.5 exposure resulted in global adult cardiac dysfunction (Tanwar et al., 2017) while reduced OTR mRNA expression (Iobst et al., 2019). Moreover, endoplasmic reticulum (ER) stress, a common cause of cardiovascular disorders (Wang S.C. et al., 2018), significantly reduced the levels of OT mRNA (Morishita et al., 2011); in ischemia/reperfusion (I/R) injury in C57B6 mice, OTR expression decreased in the heart by 40% (Indrambarya et al., 2009). By contrast, OT can exert cardiovascular protective function through suppressing the development of atherosclerosis and repairing the injured heart following myocardial infarction as shown in mice (Plante et al., 2015).

Atherosclerosis and Its Etiology

Cardiovascular health is largely determined by mechanisms of vascular endothelial defenses. This defense involves oxygen utilization, tension on the wall and flow resistance, local regulation of vascular tone and contractility, control of inflammatory cell adhesion, and anti-thrombotic nature of the endothelial surfaces. These factors together support normal circulatory function and its adaptive response to adverse environmental challenges, disturbance of which can predispose to atherosclerosis (Kim et al., 2013; Lee et al., 2013). Factors leading to atherosclerosis include consumption of high-fat and cholesterol diet (Marir et al., 2013), dyslipidemia (Sanin et al., 2017), diabetes (Lehrke and Marx, 2017), chronic inflammation (Lee et al., 2018), genetic risk (WhayneJr., and Saha, 2019), lack of exercise (Yang J. et al., 2017), hypertension (Hurtubise et al., 2016), social stress (Meng et al., 2019), smoking and other unhealthy life-styles or environmental factors (Niemann et al., 2017). As shown in a cohort study in Mexico, the coronary risk factors observed were dyslipidemia (100%), hypertension (86%), obesity/overweight (75%), metabolic syndrome (71%), smoking (68%), and diabetes (58%) (Rettori et al., 2014). Moreover, coronary artery spasm and embolism could be evoked by emotional or physical stress due to increased sympathetic output (Kc and Dick, 2010; Mori et al., 2012). Thus, immunometabolic disorders and abnormal cerebral-cardiovascular communication are the major etiology of CAD in association with atherosclerosis.

In general, the development of atherosclerosis begins with the attachment and invasion of leukocytes to the endothelium of the artery under the drive of oxidized lipoprotein particles within the wall or injuries of epithelial cells. The ensuing inflammation causes adhesion of platelets, leading to formation of atheromatous plaques in the arterial tunica intima. This process involves precipitation and oxidization of cholesterol released from circulating low density lipoprotein, inflammation-stimulated proliferation and migration of smooth muscle from the tunica media into the intima, followed by the formation of fibrous capsule and calcification of the arterial walls. As the plaques grow, wall thickening and narrowing can affect any arteries, particularly the coronary artery, resulting in a shortage of blood and oxygen delivery to various tissues. Pieces of plaque can also break off, and lead to MI, stroke, or heart failure if left untreated (Crea and Libby, 2017).

In the pathogenesis of atherosclerosis, different etiologies work through different mechanisms. For example, high blood cholesterol and fat can deposit in the wall of arteries, which reduces the flexibility of blood vessels, stimulates inflammation and restricts, even blocks blood circulation to the heart and other organs (Garrott et al., 2017). Hypertension can damage the endothelium of blood vessels in heart, increase shear and tear forces on vessel walls that change cell osmotic stability (Jiao et al., 2017) and fasten lipid deposition in arteries (Lawes et al., 2008). Cigarette smoking can damage the endothelium of arteries, stimulate inflammation (Hussien and Mousa, 2016), increase blood pressure (BP) and cause cardiac hypertrophy (Guasch and Gilsanz, 2016). People with diabetes have a much higher incidence of CAD because of dyslipidemia and metabolic disorders, particularly the formation of glycated proteins that cause inflammation, stiffening arteries, trapping other macromolecules, and disrupting enzyme activities, hormone regulation, immune function and activities of dendritic cells (Price and Knight, 2007). Furthermore, lack of social support or mental stress is etiologically related to coronary artery lesion through sympathetic-adrenomedullary influences on platelet

function, heart rate, and BP in the initial endothelial injury, and the hypothalamic-pituitary-adrenocortical (HPA) axis that is involved in smooth muscle cell proliferation during progression of vascular lesion (Dupont et al., 2014). With increase in age, arteries become less elastic and are more susceptible to plaque buildup (Rahman and Woollard, 2017; Sanin et al., 2017). Correspondingly, prevention of CAD involves changing lifestyle to limit the amount of fat and cholesterol intake and increase their utilization through exercise. In the treatment, cholesterol-lowering medication statins, antiplatelet and anticoagulants, β-blockers, calcium channel blockers, diuretics, or angiotensin converting enzyme inhibitors can be recommended. In some cases, interventions may be necessary such as percutaneous coronary intervention, bypass surgery, thrombolytic therapy, angioplasty, and endarterectomy (Lee et al., 2013; Lindahl et al., 2017). These measures could slow down injuries to the arteries but with various side effects and complications. Thus, agents targeting multiple aspects of atherosclerotic pathogenesis or CAD but having minimal side-effects are especially critical, and OT is one potential agent with such properties.

Cardiovascular Protective Effect of OT

Oxytocin has multiple cardiovascular protective functions, which are achieved through both central and peripheral approaches (Viero et al., 2010). OT terminals were found on large intracerebral (Zimmerman et al., 1984) and other large blood vessels (Jankowski et al., 2000) as well as neural structures regulating cardiac activity (Yang et al., 2013). OTR was localized in microvessels expressing CD31 marker and co-localized with endothelial NO synthase (eNOS) (Jankowski et al., 2010b). OTR mRNA was found in the vena cava, pulmonary veins, and pulmonary artery with lower levels in the aorta in the rats (Jankowski et al., 2000; Wsol et al., 2016). Thus, OT may modulate cardiac activity by activating OTRs on CVS.

OT and Ischemic Cardiomyopathy

Ischemic cardiomyopathy involves poor perfusion and oxygenation to the myocardium, mainly due to CAD. OTR signaling is closely associated with the development of CAD and its complications. As previously reviewed (Li et al., 2017), plasma OT levels or hypothalamic OT neuronal activities were significantly increased at the early stage of sepsis, advanced cancer patients, adjuvant arthritis and pancreatic injury, which in turn changed the activity of immune system to initiate immune defense, thereby playing the role of immune surveillance. In CVS, OT plasma levels and the activity of the intracardiac OT system significantly increased at 4 weeks after MI in the rats survived from the coronary artery ligation (Ciosek and Drobnik, 2012); post-infarction heart failure was associated with an increased activity of the intracardiac OTergic system (Wsol et al., 2016). Moreover, MI activates parvocellular OT neurons projecting to the rostral ventral lateral medulla (Roy et al., 2018). Thus, changes in the activity of the OT-secreting system in the brain and the heart can be a biomarker of immune disturbance in CVD while exerting the function of adaptive cardioprotection (Jankowski et al., 2010a).

The cardioprotective effect of OT has been proven by many experimental observations. OT administration significantly inhibited myocardial injury in rats (Moghimian et al., 2012; Polshekan et al., 2016); however, blocking OTRs with atosiban increased infarct size and levels of creatine kinase MB isoenzyme and lactate dehydrogenase (Moghimian et al., 2012; Houshmand et al., 2015). In rabbits with I/R of the left coronary artery, OT pretreatment significantly decreased infarct size and yielded antiarrhythmic effects including ventricular tachycardia and fibrillation (Faghihi et al., 2012); however, atosiban abolished the beneficial effects of this ischemic preconditioning of OT (Das and Sarkar, 2012). Lastly, in the post-ischemia repair of a rabbit model, post-infarction group treated with OT had reduced infarct size and improved left ventricular function by enhancing anti-fibrotic and angiogenic effects via activating OTRs (Kobayashi et al., 2009). Importantly, the cardioprotective effect of OT can be achieved in doses of 8×10^{-12} to 2×10^{-11}M as shown in rat I/R heart (Anvari et al., 2012), a physiological level in the plasma (Hirst et al., 1991), indicating that the protective role can be physiological.

The protective effect of OT is first attributable to its negative chronotropic and inotropic roles in cardiac activity following the activation of cardiac OTR (Costa E Sousa et al., 2005) in association with the release of protective atrial natriuretic peptide (ANP) and nitric oxide (NO) (Houshmand et al., 2015) and increase in parasympathetic output (Sun et al., 2015), decrease in the activity of renin-angiotensin-aldosterone system (Nielsen et al., 1997) and reduction of sympathetic outflow (Olszewski et al., 2010). In addition, OT also decreased cardiac preload and afterload through its diuresis and natriuretic effect (Nielsen et al., 1997). As a result, OT can reduce oxygen consumption while increasing the cardiac output during I/R injury.

Vascular Protection

Oxytocin is synthesized and released in the heart and vasculature that express OTRs, and is important in normal homeostatic regulation of cardiac and vascular systems (Japundzic-Zigon, 2013). It is well-known that OT preconditioning increased expression of genes associated with angiogenic, antiapoptotic, and cardiac antiremodeling properties (Noiseux et al., 2012). OT promoted angiogenic behaviors of human umbilical vein endothelial cells through activating OTRs (Cattaneo et al., 2008) by increasing hypoxia-inducible factor-1α mRNA and protein expression (Zhu et al., 2017). In rats of sinoaortic denervation, intravenous application of OT induced an enhanced initial pressor effect with much reduced reflex bradycardia and fall in cardiac output. A larger and more prolonged delayed fall in mean arterial pressure was apparent with both OT and its specific agonist [Thr4,Gly7]OT (Busnelli et al., 2013) although supraphysiological doses of OT caused transient pressor reaction by activating vasopressin (VP) receptors (Petty et al., 1985). Moreover, OT could antagonize the pressor effect of VP through reflexively activating cholinergic neurons (Mukaddam-Daher et al., 2001). These effects allow OT to reduce the pre- and after-load of CVS.

The protective effect of OT is closely associated with its suppression of immunological disorders. In rat heart,

angiogenic and antiapototic effects of OT were mediated by upregulating vascular endothelial growth factor (VEGF) and prosurvival B-cell lymphoma-2 protein (Kobayashi et al., 2009), with decreasing apoptosis caused by neutrophils (Al-Amran and Shahkolahi, 2013). Moreover, incubation of cells at physiological levels of OT significantly decreased basal and stimulated NADPH-dependent superoxide activity in vascular cells, monocytes, and macrophages that express OTR protein and mRNA. OT can decrease NADPH-dependent superoxide production and pro-inflammatory cytokine release from vascular endothelial cells and macrophages, and thus, inhibit inflammation and atherosclerotic lesion development (Wang P. et al., 2015). In Watanabe Heritable Hyperlipidemic rabbit, a model of dyslipidemia and atherosclerosis, chronic OT-treatment significantly reduced plasma C-reactive protein levels, atherosclerosis formation in the thoracic aorta and cytokine gene expression in visceral adipose tissues; however, body weight, serum lipids, plasma/urinary measures of oxidative stress, plasma cortisol, or urinary catecholamines did not change (Szeto et al., 2013). Thus, attenuating vascular oxidative stress and inflammation are important mechanisms for OT to antagonize the pathogenesis of atherosclerosis.

Cardioprotection in Post-menopausal Women

Coronary artery disease is generally considered the pathology of aging and gender with strong correlation with the activity of OT neurons. Between age 45 to 65, approximately 10% women developed CAD, while the incidence increased to 33% after age 65 (Benjamin et al., 2019). Correspondingly, heart disease was the leading cause of death for women in the United States, killing 289,758 women in 2013 (Xu et al., 2016). CAD-associated hypertension increased dramatically in women after menopause due to reduction in ovarian hormone in older women (McLeod et al., 2010), which could impair baroreflex and autonomic balance by negatively impacting OTergic drive and OT levels in pre-autonomic neurons in rats (De Melo et al., 2016). Declines in OT and OTRs were related to aging-associated acceleration of inflammation and oxidative injuries in the CVS, particularly after menopause (Light et al., 2005). Consistently, plasma OT level experienced a threefold decline in aged mice compared with young, and this decline was accompanied by similar decrease in levels of OTRs in muscle stem cells (Elabd et al., 2014). Exogenous estrogen application was found to increase OT secretion in both rodents (Quinones-Jenab et al., 1997) and women (Chiodera et al., 1991), and increase in OTR mRNA expression in mouse brain (Quinones-Jenab et al., 1997) as well as intracardiac OTR signaling (Jankowski et al., 2010b). The pro-synthetic function of estrogen in OT expression may also explain the lower CAD prevalence among women before menopause. Hence, OT has special potential in treating female patients with CAD.

MECHANISMS UNDERLYING THE PROTECTIVE EFFECTS OF OT

Oxytocin exerts much protective functions on the CVS through suppressing atherosclerosis-evoking factors and reducing the injury following MI. These protective effects of OT are based on its direct CVS effects and its modulation of the regulatory system of CVS activity (**Figure 1**).

Peripheral Effect

In response to environmetal challenges, OT in the hypothalamus can be released into the blood stream in various amounts and patterns (Hatton and Wang, 2008; Hou et al., 2016) and modulate activities of the heart and blood vessels by activating OTRs along with intracardiac OT (Wsol et al., 2016). OT has both chronotropic and inotropic effects on cardiac activity, which can protect the heart from I/R-induced myocardial injury by reducing oxygen consumption. OT also regulates lipid metabolism, and exerts the effect of anti-diabetes, anti-inflammation, and anti-apoptosis while promotes angiogenesis and regeneration of cardiomyocytes as further stated below.

Regulation of Lipid Metabolism

Among many factors contributing to atherosclerosis, disorders in the regulation of lipid metabolism and obesity are major etiologies (Schinzari et al., 2017) and thus the target of cardioprotective effect of OT. As reported that hyperlipidemia disrupted OTR signaling (Padol et al., 2017), that serum OT levels were decreased in obese group (Qian et al., 2014), and that mice with OT- or OTR-deficiency developed late-onset obesity (Takayanagi et al., 2008) which was associated with type 2 diabetes and CAD (Amri and Pisani, 2016). Consistently, blood OT concentration was inversely correlated to serum triglyceride, low-density lipoprotein and total cholesterol levels (Qian et al., 2014). It was also found that cholesterol levels in rats displayed a tendency to fall in response to subcutaneous injection of OT (Suva et al., 1980); chronic systemic treatment with OT largely reproduced the effects of central administration of OT by reducing weight gain in obese rodents; chronic subcutaneous or intranasal OT treatment was sufficient to elicit body weight loss in obese subjects (Blevins and Baskin, 2015). Thus, increasing OTR signaling is an important step in prevention of atherosclerosis and OT has therapeutic potential in reducing obesity, atherosclerosis, and the incidence of CAD through regulating lipid metabolism.

Anti-diabetic Effects

Population with diabetes mellitus has high prevalence of CAD, peripheral vascular disease and heart failure (Lehrke and Marx, 2017). In type 2 diabetes mellitus, serum OT levels were decreased (Qian et al., 2014). Similarly, in a mouse model of type 2 diabetes mellitus, there was a significant down-regulation of OT, OTRs, ANP, and eNOS gene expressions in the heart, and chronic OT treatment prevented the development of diabetic cardiomyopathy in these animals (Plante et al., 2015). Consistently, OT administered to fasted male subjects via intranasal approach attenuated the peak excursion of plasma glucose (Klement et al., 2017). These findings support that disruption of OTR signaling is closely related to the occurrence of diabetes mellitus.

Further studies revealed that the anti-diabetic effect of OT is closely related to its regulation of glucose metabolism. OT

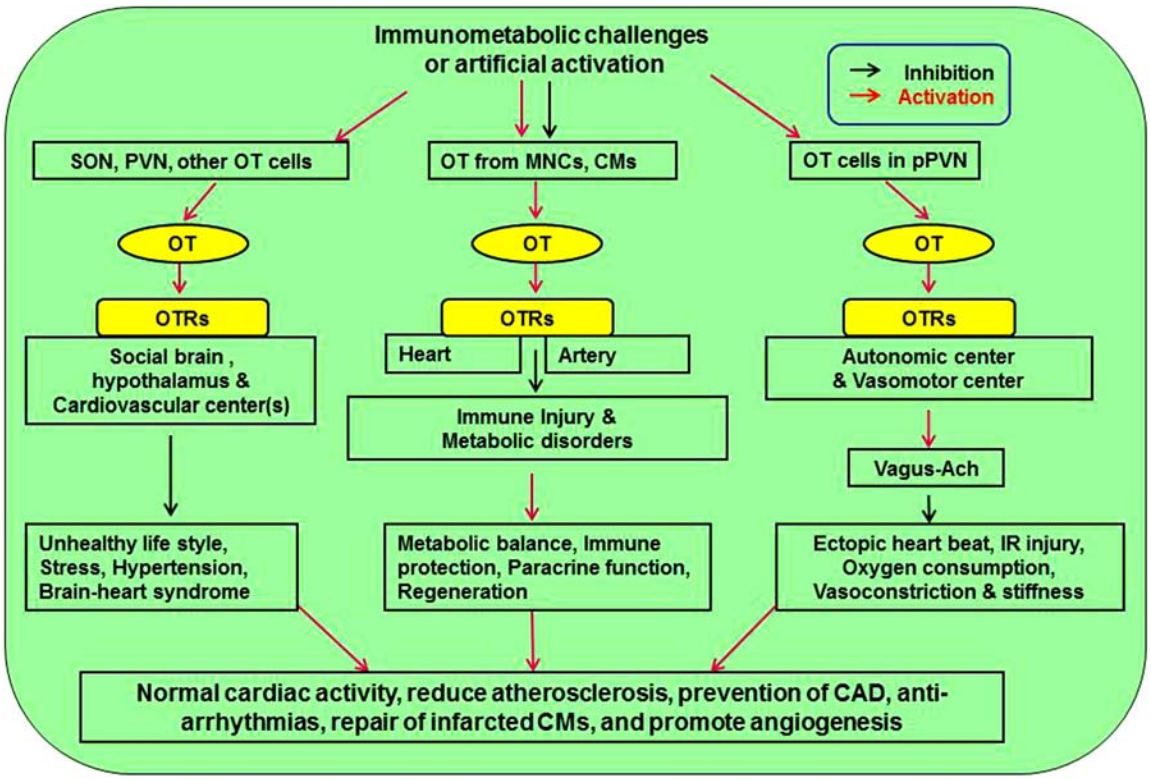

FIGURE 1 | Approaches mediating cardiovascular protective effect of OT. There are three pathways affecting cardiovascular activity. Neuronal activation of SON and PVN can counteract stress, hypertension, and brain-heart syndrome. Release of OT from MNCs and CMs inhibits atherosclerotic injuries of heart and artery by inhibiting immunological injuries and metabolic disorders through immune protection, paracrine function, and CM regeneration. Finally, activation of OT in pPVN regulates autonomic and vasomotor center activity, leading to inhibition of cardiac arrhythmia, ischemia-reperfusion injury, oxygen demand, and vasoconstriction. Ach, acetylcholine; CM, cardiomyocyte; MNCs, magnocellular neuroendocrine cells; OT, oxytocin; OTR, oxytocin receptor; pPVN, parvocellular division of the PVN; PVN, paraventricular nucleus; SON, supraoptic nucleus.

could promote glucose metabolism in cultured cardiomyocytes from newborn and adult rats (Florian et al., 2010), in myocardial cells during hypoxia and other physiological stressors (Shioi et al., 2000) and in mesenchymal stem cells (Noiseux et al., 2012). These findings are consistent with the report that OT stimulated glucose oxidation in myometrial tissue (Okabe et al., 1985) and glucose oxidation and lipogenesis in rat epididymal adipocytes (Goren et al., 1986). This effect was mediated through tricarboxylic acid cycle (Okabe et al., 1985) in an extracellular Ca^{2+}-dependent manner (Bonne et al., 1978). On the other hand, OT contributes to metabolic control of glucose by directly improving pancreatic functions. In mice, OTR signaling reduced the death of pancreatic β-cells in islets exposed to cytotoxic stresses, which was diminished in islets isolated from OTR knockout mice (Watanabe et al., 2016). In fasted male subjects, OT was also found to augment the early increases in insulin and C-peptide concentrations in response to glucose challenge due to a pronounced increase in β-cell sensitivity (Klement et al., 2017). These facts indicate that OT exerts anti-diabetic effect by regulating glucose metabolism and protecting pancreatic β-cells in islets, thereby rendering the OT system a potential target of anti-diabetic treatment and prevention of CAD.

Anti-inflammation

One of the critical factors involved in the development of CAD is chronic inflammation in association with oxidative stress and the release of pro-inflammatory cytokines (Mullenix et al., 2005). Early atherosclerosis formation is based on leukocyte accumulation and atheroma-activating cells, such as macrophages, dendritic cells, and T- and B-lymphocytes. Pro-inflammatory cytokines enhance leukocyte adhesion molecule expression, leading to leukocyte penetration into the endothelial layer and accumulation in intima. Other molecules, such as interleukin-6, that affect lipid metabolism (Yudkin, 2003) are associated with increased level of C-reactive protein production, which changes inversely to serum OT levels (Qian et al., 2014). OT was also identified as an agent that suppresses the production of inflammatory cytokines (Wang, 2016), including smooth muscle and vascular endothelial cells (Szeto et al., 2013). Moreover, OT could down-regulate neutrophil chemotactic molecules and myocardial neutrophil infiltration, and prevent myocardial injury by reducing inflammatory reaction and reactive oxygen species (ROS) produced by neutrophils (Al-Amran and Shahkolahi, 2013). Thus, along with the general immunological regulatory functions (Wang P. et al., 2015; Wang, 2016), OT could be a potentially preventative agent in those at

high-risk for atherosclerosis development and further limit the progression in those with existing disease.

Regeneration of Cardiomyocytes

In MI, an initial ischemic event can lead to either reversible or irreversible myocardial injury based on the duration and size of ischemia, and subsequent damages by reperfusion. Prolonged ischemia caused dysfunction in ATPase-dependent ion transport, cellular swelling and rupture, intracellular ion dysregulation and cellular apoptosis; reperfusion caused transient elevation in levels of ROS and inflammatory neutrophils, leading to exacerbation of initial ischemic event; following an ischemic attack, up to 1-billion cardiac cells died but humans had a limited ability to regenerate myocardial cells and injured cells were often replaced by fibrotic scars, leading to conduction abnormalities and heart failure (Rahman and Woollard, 2017; Sanin et al., 2017). For this reason, regeneration of cardiomyocytes is extremely important in long-term prognosis.

Along with the anti-inflammatory and anti-apoptotic effects of OT on the CVS (Kobayashi et al., 2009; Noiseux et al., 2012; Al-Amran and Shahkolahi, 2013), OTR signaling can exert cardioprotective function by promoting regeneration of injured cardiomyocytes. OT stimulated *in situ* differentiation of cardiac stem cells into functionally matured cardiomyocytes by replacing lost cells from ischemic events. When OT-treated mesenchymal stem cells were co-cultured with I/R rat cardiomyocytes, there were decreased cardiac fibrosis, macrophage infiltration, restoration of connexin 43, and increased overall cardiac ejection fraction (Kim et al., 2012). OT preconditioning was also known to increase expression of genes involved in angiogenesis, anti-apoptosis, and anti-cardiac remodeling, such as HSP 27, HSP 32, and VEGF (Gutkowska et al., 2009). Thus, OT treatment can evoke mesenchymal stem cell differentiation to replace the lost cardiac cells, which endows OT the potential of reversing injuries from atherosclerotic CVD.

Effects of Intracardiac OT via ANP

In rat heart (Wsol et al., 2016), the right atrium has the highest OT concentration (∼2.128 ng/mg protein) (Jankowski et al., 1998), comparable with OT content in the hypothalamus wherein different regions have OT concentrations varying from >0.1∼228 ng/mg protein (Gainer, 2011). Thus, when OT is released from the atrium, dramatic changes in the cardiac activity can be elicited through paracrine functions, in which ANP serves as cardioprotective mediators of OT in the heart. Upon activation of OTRs, intracellular Ca^{2+} mobilization occurred in the right atrium, which caused ANP release from cardiomyocytes (Gutkowska et al., 2014) whereas, application of OT antagonist blocked basal ANP release (Paquin et al., 2002) and caused a significant decline in ejection fraction and increased cardiac fibrosis (Jankowski et al., 2010b).

Similarly, OTR signaling also increased NO production (Polshekan et al., 2019) that exerted cardiovascular protective effect (Jackson et al., 2017). This action is likely mediated by ANP (Menaouar et al., 2014). Moreover, OT-evoked release of ANP into the blood during expansion of blood volume could also reduce BP through its diuresis and natriuresis effects (Soares et al., 1999). The natriuretic effect helps to remove excess volume and thus reduces BP. These features allow OT to modulate cardiovascular activity through changing ANP secretion.

Central Effect

Cardiovascular activity is under intense regulation of the central nervous system. CVDs can be caused by disorders in the cardiovascular regulation involving disrupting normal neuroendocrine, autonomic, and behavioral responses. By antagonizing these responses, OT can counteract the deleterious effects of stress, hypertension, unhealthy life-style, and brain-heart syndrome on the CVS.

Neural Regulation of Cardiovascular Activity

Vasomotor center(s) in the brainstem are the key structure in neural regulation of cardiovascular activity and are also the target of OT protection of cardiovascular activity. In response to physiological challenges, OT in the hypothalamus can change vasotone through autonomic nerves and in turn modulate cardiovascular activity.

The pumping effectiveness of the heart and contractility of blood vessels are primarily regulated by the autonomic nervous system including excitatory sympathetic and inhibitory parasympathetic nerves. As evidenced in trained rats, there were an increased gain of baroreflex control of heart rate, markedly elevated OT mRNA expression and OT peptide density in PVN neurons, which were blocked with sinoaortic denervation (Cavalleri et al., 2011). OT neurons and their terminals are present in both intra- and extra-hypothalamic sites (Hou et al., 2016), through which OT can change the activity of the neural centers controlling CVS at different levels. The descending fibers from hypothalamic OT cells were found to innervate the locus coeruleus and dorsal vagal complex in the brainstem of the rat (Swanson and Hartman, 1980; Llewellyn-Smith et al., 2012). Through them, OT increased parasympathetic cardiac control and decreased sympathetic cardiac control by activating brainstem vagal neurons (Olszewski et al., 2010), resulting in the slowing down of the heart rate (Higa et al., 2002).

It is worth noting that acute MI could activate microglial P2X7R in the PVN that mediates sympatho-excitatory responses and the production of proinflammatory cytokines in rats. In addition, pro-inflammatory cytokines subsequently increased OT release (Du et al., 2015), thereby limiting the damaging effect of sympathetic outflows (Nielsen et al., 1997; Roy et al., 2018).

OT and Hypertension

Hypertension was one of the most significant risk factors for atherosclerosis and the development of CVD, and responsible for 54% of all strokes and 47% of ischemic cardiomyopathy (Lawes et al., 2008). In a cohort study on patients without baseline CVD, about 63% of those with baseline hypertension developed CVD while only 46% in those with normal baseline BP developed CVD (Rapsomaniki et al., 2014).

Oxytocin is deeply involved in body defense against hypertension. As reported, intrauterine growth restriction, caused by excessive glucocorticoid exposure to the fetus, produced hypertension later in life due to damages to

OTR signaling (Vargas-Martinez et al., 2017). In hypertensive rats, a decreased expression of OT mRNA and protein was found in hypothalamus. This is consistent with an earlier finding that when OT was injected subcutaneously or intracerebroventricularly for 5 day, BP decreased in rats (Petersson and Uvnas-Moberg, 2008). Moreover, centrally released OT was also found to reduce the cardiovascular responses in BP and heart rate to the acute stressor significantly, which were reversed by OTR antagonist applied through brain ventricular system (Wsol et al., 2009).

The central anti-hypertensive effect of OT is mediated by PVN-brainstem-autonomic nervous system. It has been known for long that OT could reduce overall sympathetic activation of vessel contraction (Olszewski et al., 2010), and selectively dilate blood vessels that were innervated by parasympathetic nerves (Nielsen et al., 1997). Chronic activation of OT neurons restored the release of OT from PVN fibers in the dorsal motor nucleus of the vagus, and prevented the hypertension that occurred with 3 weeks of chronic intermittent hypoxia-hypercapnia exposure (Jameson et al., 2016). Thus, promoting OTergic drive from PVN to brainstem could improve autonomic control of the circulation to maintain stability of the BP.

Lastly, disorder of the immune system in the pathogenesis of hypertension has been firmly established by a large number of investigations (Rodriguez-Iturbe et al., 2017); hence, OT could also reduce hypertension through its immune homeostatic functions (Wang P. et al., 2015; Wang, 2016). Thus, OT can exert anti-hypertensive effects through multiple approaches.

Cardiovascular Protection Through Anti-stress Effects

Both positive and negative social stimuli can modify the activity of HPA axis and thus, affect body recovery from acute illnesses including stress, wounds, stroke, and cardiovascular complications (Dupont et al., 2014). OT can exert cardiovascular protection through its anti-stress effects. It has been demonstrated that Watanabe Heritable Hyperlipidemic rabbits exposed to a consistent, stable social experience in association with higher blood OT levels exhibited more affiliative social behavior and less aortic atherosclerosis (Szeto et al., 2013). Social stress promoted the progression of atherosclerosis in these rabbits in association with increased urinary norepinephrine, plasma cortisol and splenic weight as well as less affiliative behavior and more stressful physiological and tissue responses (Noller et al., 2013). In human being, OT was positively associated with diminished stress among securely attached participants and had an attenuating effect on perceived stress due to adverse life events in old age (Emeny et al., 2015). Moreover, in adult mice grouped into isolated or paired environment, social pairing enhanced hypothalamic OT gene expression and that was associated with smaller infarct size, and reduced neuroinflammation and oxidative stress following stroke. In contrast, administration of OT to socially isolated mice reproduced the neuroprotection conferred by social housing, and this effect was associated with the suppressive action of OT on microglia, a source of brain inflammatory cytokines (Karelina et al., 2011). By acting on many brain sites, OT could reduce stress-elicited neuroendocrine, autonomic, and behavioral responses (Li et al., 2017) wherein OT reduced stress-associated release of epinephrine (Wronska et al., 2017), which can reduce cardiac consumption of oxygen and thus endow OT the ability to oppose the injury from stress on the CVS.

Suppression of Smoking and Alcohol Craving

Healthy behaviors including moderate alcohol consumption, smoking abstinence, lack of abdominal adiposity, decreased sedentarism, and adherence to Alternate Mediterranean Dietary Index that is characterized by high intakes of fruit, vegetables, fish, and whole grains, moderate amounts of alcohol and dairy products, and low amounts of red or processed meats and sweets, could significantly reduce the presence of coronary artery calcium and plaques in femoral and carotid arteries; adoption of multiple healthy lifestyle behaviors early in life could be a key strategy in tackling the onset of atherosclerosis and reducing the burden of CVD (Dennis and Gerstman, 2014). However, cigarette smoking and alcoholism remain significant problems among population that is at high-risk for atherogenesis.

In a well-characterized, multi-ethnic United States cohort, it has been found that coronary artery calcium was predictive of atherosclerotic CVD in 6.7% of all smokers and in 14.2% of lung cancer screening eligible smokers (Kenkel et al., 2014). Cigarette smoking decreased OT secretion while worsening CAD (Vardavas and Panagiotakos, 2009). Smoking in men inhibited OT release by the mediation of endogenous opioids (Seckl et al., 1988) and GABA (Chiodera et al., 1993). In contrast, nasal application of OT significantly reduced levels of cue-induced smoking craving that often led to smoking relapse (Miller et al., 2016). In addition, OT could decrease withdrawal signs in rats and somatic component of the nicotine withdrawal syndrome (Manbeck et al., 2014). Thus, OT is helpful in reducing these detrimental behaviors.

Similar to the effect on smoking, OT can also inhibit craving for alcohol. The primary metabolite of alcohol, acetaldehyde, stimulated vascular smooth muscle cell Notch signaling and muscle growth, and mediated the ultimate effects of drinking on CVD (Patrick and Ames, 2014). Animal studies support OT as a potential treatment in reducing alcohol consumption. For example, intraperitoneal application of OT (3.0 mg/kg) significantly reduced alcohol (15%) consumption in the first-hour after treatment (Stevenson et al., 2017). Moreover, acute intracerebroventricular infusion of OT attenuated voluntary alcohol self-administration (20%) in male rats. Furthermore, intracerebroventricular application of OT completely blocked alcohol-induced dopamine release within the nucleus accumbens (Peters et al., 2017) that is a well-known nucleus of rewarding. Mechanistically, OT was considered to act by inhibiting the effects of the corticotropin-releasing factor on GABAergic interneurons in the amygdala and PVN, which suppressed the mechanisms of relapse and craving by reducing anxiety, stress vulnerability, and social withdrawal in abstinent alcohol-dependent patients (Faehrmann et al., 2018). By improving these life-styles, OT may also help to suppress the development of atherosclerotic CVD.

Protection From Brain-Heart Syndrome

Brain-heart syndrome is reversible acute heart diseases caused by acute encephalopathy involving the regulatory centers of the CVS. Many autonomic brain regions, including insula cortex, amygdala complex, anterior cingulate cortex, ventral medial prefrontal cortex, hypothalamus, and pineal gland are involved in the regulation of cardiovascular activity. At the cellular level, the disturbance of autonomic regulation resulted in catecholamine excitotoxicity, oxidative stress, and free radical myocardium injury (Gotovina et al., 2018). The damage of these structures leads to arrhythmia in previously intact myocardium, systolic and diastolic dysfunction, and ischemic changes. Although it does not cause CAD directly, it often occurs on the basis of atherosclerosis and worsens the CAD.

In association with the stress-relieving effect, OT could also alleviate brain-heart syndrome through its neuroprotective functions. As reported that in a rat model of transient middle cerebral artery occlusion, OT significantly reduced the infarct volume of the cerebral cortex and striatum (Reed et al., 2019). Moreover, intracerebroventricular infusion of OT and centrally released OT induced a preconditioning effect in I/R rat heart via brain receptors (Moghimian et al., 2013). Thus, while OT system dysfunction serves as one common mechanism underlying metabolic syndrome and psychotic disorders (Quintana et al., 2017), brain OT can exert cardiovascular protective effect by suppressing the brain-heart syndrome in cerebrovascular accidents.

SIGNALING PATHWAYS MEDIATING THE CARDIOVASCULAR PROTECTIVE EFFECT OF OT

Oxytocin is known to exert its biological functions through both OTR and VP receptors (Song and Albers, 2017). Although supraphysiological doses of OT could also activate VP receptors, OTR is the mediator of OT effects in terms of cardiovascular protection (Wsol et al., 2014). Understanding of the signaling pathway through OTR signaling is crucial in understanding of its cardiovascular protection and identifying novel targets of treatment.

OTR and G Proteins

Oxytocin receptors are typical class I G protein-coupled receptors (GPCRs). The binding of OT to OTRs activates its primary downstream effector Gq protein via RVSSVKL segment in the COOH-terminal region of the third intracellular domain of OTR (Zhong et al., 2007); however, Gi/o family members can also mediate the cardioprotective effects of OT directly as stated below.

In general, the effect of OTR activation is mediated by phospholipase C (PLC)-β downstream to the α-subunit of both Gq and Gi/o proteins (Busnelli et al., 2013; Jurek and Neumann, 2018). In the early stage of cardiac injury, the activity of PLC-β1b was elevated selectively, which caused dephosphorylation of phospholamban and depletion of the Ca^{2+} stores in the sarcoplasmic reticulum (SR), leading to cytosolic Ca^{2+} oscillation, mitochondrial Ca^{2+}overload, and oxidative stress (Abdallah et al., 2011). Thus, it is not likely for OTR to activate PLC-β1 signaling to exert the cardioprotective function. Instead, PLC-β3 could be a mediator of OTR signaling (Yue and Sanborn, 2001). The differential effects of downstream signals to OTR are in agreement with the findings that biological effects of OT depended on OTR localization in caveolin-1 enriched domains (Rimoldi et al., 2003) and that angiotensin and OT respectively caused injury and protective effects by activating different signaling pathways downstream to their corresponding Gq proteins (Natochin et al., 2018).

The activation of OTRs can also protect cardiomyocytes through Gβγ subunits of OTR-coupled G proteins and the crosstalk between this GPCR and receptor tyrosine kinase signaling pathways, which has been identified in myometrial cells (Zhong et al., 2003) and HEK293 cells (Rimoldi et al., 2003) wherein Gβγ subunits could increase phosphorylation of extracellular signal-regulated protein kinase (ERK) 1/2, the critical component of cardioprotective reperfusion injury salvage kinase (RISK) pathway (Polshekan et al., 2016). The RISK pathway involves phosphatidylinositol 3-kinase (PI3K)-protein kinase B (Akt)-eNOS cascades and ERK 1/2. In addition, AMP-activated protein kinase (AMPK), Ca^{2+}/calmodulin-dependent protein kinase (CaMK) signaling and others are also implicated, disruption of which has been implicated in immunometabolic dysregulation-associated pathogenesis of cardiac arrhythmias as recently reviewed (Wang S.C. et al., 2018). The activation of OTR-Gq and Gi/o proteins could regulate these and other signaling pathways to suppress immunometabolic dysregulation-associated CAD.

Between the signaling events downstream to α-subunit and Gβγ subunits of OTR-coupled G proteins, there is also crosstalk. Indeed, the activation of PLC could be generated by the βγ complexes released by Gαi of the OTR/Gi coupled receptor and by transactivating tyrosine kinase receptor EGFR via MAPK cascade (Rimoldi et al., 2003).

It is important to note that there are rapid and extensive internalization and desensitization of the OTR upon agonist exposure, which is determined by several signaling molecules in a cascade. For example, stable OTR/beta-arrestin2 interaction played an important role in determining the rate of recycling of human OTRs; OTRs were localized in vesicles containing Rab5 and Rab4 small GTPases, the markers for direct receptor recycling without decomposition (Conti et al., 2009). In human embryonic kidney cells, OTR internalization was unaffected by inhibitors of protein kinase C (PKC) or CaMK-II but was significantly reduced after transfection with dominant-negative mutant cDNAs of GPCR kinase (GRK)2, β-arrestin 2, dynamin, and Eps15 (a component of clathrin-coated pits) (Patel and Radeos, 2018); GRK-evoked OTR phosphorylation was a prerequisite for β-arrestin-mediated internalization and OTR desensitization (Wang C. et al., 2018). In uterus, knockdown of GRK6 largely prevented OT-induced OTR desensitization; in contrast, selective depletion of GRKs 2, 3, or 5 was without effect (Denson et al., 2018; Liu et al., 2018). This signaling feature highlights a potentially beneficial effect of using intermittent OT application pattern in treating CVDs, the power of which has

been well-discussed about studies on the milk-letdown reflex (Hatton and Wang, 2008; Hou et al., 2016).

PI3K/Akt Cascades

Disruption of PI3K/Akt cascade is a major pathological event for CAD occurrence, which has been observed in smoking interference of the cardioprotective signaling by post-conditioning (Guasch and Gilsanz, 2016) and many other etiologies as recently reviewed (Wang S.C. et al., 2018). The protective effect of this pathway is supported by the findings of myocardial protection through hydrogen sulfate (H_2S) (Jin et al., 2017), isoflurane-induced myocardial post-conditioning under acute hyperglycemia (Raphael et al., 2015), the protection of the heart against I/R injury by limb remote ischemia preconditioning through the opioid system (Zhang et al., 2017), post-reperfusion administration of granulocyte colony-stimulating factor (Sumi et al., 2010) and others (Zhou et al., 2015; Zafirovic et al., 2017). The protective effect of this pathway is likely associated with its critical roles in cellular proliferation, migration, and protection against apoptotic and cytotoxic effects due to hypoxia (Wang S.C. et al., 2018). Consistently, PI3K/Akt cascade is also implicated in the cardioprotective effect of OT. For example, activating PI3K/Akt signaling was responsible for the post-conditioning and the anti-apoptotic effect of OT (Gonzalez-Reyes et al., 2015) whereas, PI3K/Akt inhibitors and OTR blocker atosiban blocked the protective effect in rats (Polshekan et al., 2016).

Oxytocin activation of PI3K/Akt signaling could be achieved through a crosstalk between Gq protein and epidermal growth factor receptor (Zhong et al., 2003) that is an upstream signal of PI3K/Akt as demonstrated in the action of protease-activated receptor 2 (Wang and DeFea, 2006; Wang et al., 2010). In OTR signaling, PI3K/Akt signaling-mediated protection is achieved through eNOS that subsequently activates mitochondrial ATP-dependent potassium (mKATP) channels (Das and Sarkar, 2012) to reduce mitochondrial oxidative stress (MOS) as discussed in previous review in detail (Wang S.C. et al., 2018).

Between NO and mKATP channels, the involvement of NO-soluble guanylyl cyclase has been found in OT-evoked differentiation of porcine bone marrow stem cells into cardiomyocytes and cell proliferation (Ybarra et al., 2011). In cells treated with OT, activated Akt and eNOS were translocated into the nuclear and perinuclear area to protect heart from I/R injury, which was abrogated by inhibition of OTR signaling, PI3K, cGMP-dependent protein kinase as well as soluble guanylate cyclase (Gonzalez-Reyes et al., 2015). Downstream to the eNOS-cGMP-dependent protein kinase is the mKATP channels, inhibition of which is a pivotal mechanism in immunometabolic disorder-evoked CVDs (Wang S.C. et al., 2018). In addition, cyclic AMP response element-binding protein (CREB) signaling could also be a mediator of PI3K/Akt signaling, which has been shown in the nervous system (Da Silva et al., 2013).

ERK 1/2 Pathway

Following the activation of OTRs, the release of Gβγ subunits from OTR-associated Gq protein can activate ERK 1/2 as shown in myometrial cells (Zhong et al., 2003) and in OT neurons (Wang and Hatton, 2007a,b). As a major component of the RISK pathway, ERK 1/2 signaling is also implicated in OT-mediated cardiovascular protection. For example, the cardioprotective effect of OT post-conditioning on isolated ischemic rat heart depended on the activation of ERK1/2 signaling (Gonzalez-Reyes et al., 2015) since that was blocked by ERK1/2 inhibitors and atosiban (Polshekan et al., 2016).

Studies further revealed that the protective effect of ERK1/2 signaling is mediated through CREB signaling. Reduced expression of genes regulated by the transcription factor CREB is linked to atrial fibrillation susceptibility in patients, which has been verified in transgenic mouse model recently (Seidl et al., 2017). CREB is responsible for the expression of potassium channel Kv1.5 that was impaired in diet-induced obese in mice (Huang et al., 2013). Thus, this signaling cascade is critical in pathophysiology of atrial fibrillation, ventricular ectopy, insulin secretion, hypoxic pulmonary vasoconstriction and sudden cardiac death. Moreover, CREB is also associated with peroxisome proliferator-activated receptor signaling known to regulate lipid metabolism and insulin sensitivity, integrity of sarcomeres and mitochondria, and the deposition of collagen and glycogen in the heart (Seidl et al., 2017). In addition, GRK2 may participate in OT regulation of CVS activity although the expression level of GRK2 was dependent on the tissues and their functional status (Montgomery et al., 2018). Importantly, high fat-diet caused marked intracellular lipid accumulation and significantly increased cardiac GRK2 levels in mice, which promoted obesity-induced cardiac remodeling and steatosis. In contrast, low GRK2 protein levels were able to keep the PKA/CREB pathway active and prevented a high fat diet-induced down-regulation of key fatty acid metabolism modulators such as peroxisome proliferator-activated receptor gamma co-activators, thus preserving the expression of cardioprotective proteins such as mitochondrial fusion markers mitofusin (Marir et al., 2013).

Mitofusin was known as an inhibitor of mitochondrial membrane depolarization and ROS production by acting on the mitochondria-associated ER membrane (MAM) to inhibit mitochondrial Ca^{2+} overloading, a function opposite to glycogen synthase kinase-3β (GSK-3β) (Jankowski et al., 2010b). Thus, by activating CREB signaling, OT-activated ERK 1/2 can suppress ER stress response (Watanabe et al., 2016) and the associated MOS (Wang S.C. et al., 2018), thereby exerting cardiovascular protective effects. Interestingly, the protective effect of CREB signaling might not work in low potassium diet since elevated autophagy and CREB signaling were found to promote calcification of arteries from low potassium diet-fed mice as well as aortic arteries exposed to low potassium *ex vivo* (Brown et al., 2013).

CaMK Signaling

Another important signaling molecule in OT protective effect is CaMK-II. CaMK II is important for Ca^{2+} homeostasis of cardiomyocytes. In infarcted heart, cardiac SR Ca^{2+} uptake and release activities were depressed significantly due to a decrease in SR CaMK-II phosphorylation of the SR proteins, ryanodine receptor, Ca^{2+} pump ATPase/ER Ca^{2+} ATPase, and phospholamban (Araujo et al., 2013), leading to ER stress and

MOS. Thus, CaMK could be an important mediator of the cardiovascular protection of OT.

Following the activation of OTRs, mobilization of Gαq or Gβγ caused intracellular Ca^{2+} release and subsequent activation of CaMK-II (Yue and Sanborn, 2001), likely mediated by PLC-β3 signaling pathway. The intracellular Ca^{2+} could also come from other sources. For instance, L-type Ca^{2+} channels, IP3-RyR-gated, and store-operated Ca^{2+} channels including transient receptor potential channel pathways played significant roles in OT-induced contractions of myometrium of buffaloes (Borrow et al., 2018). CaMK-II can further phosphorylate PLC-β3 but not PLC-β1 (Yue and Sanborn, 2001) that was a known as a deteriorating signal in heart (Abdallah et al., 2011). The activation of CaMK-II was associated with OT-elicited activation of AMPK (Lee et al., 2008), release of ANP (Gutkowska et al., 2014) and NO (Lee et al., 2008; Menaouar et al., 2014), and they are all known to play important roles in OT protection of CVS.

It has been demonstrated that OT could antagonize endothelin-1 or angiotensin II-evoked cardiomyocyte hypertrophy though ANP and NO release in the developing rat heart, which was mediated by CaMK-II and AMPK pathways and by normalization of the reduced Akt phosphorylation (Menaouar et al., 2014). Moreover, CaMK II was involved in NO-elicited relaxation of endothelium-intact rat aortic rings as a result of Ca^{2+}-dependent activation of eNOS in cultured porcine aortic endothelial cells (Alizadeh and Mirzabeglo, 2013). Thus, CaMK signaling is an important approach for OT protection of arteries.

AMPK Pathway

In parallel with the RISK pathway, AMPK signaling pathway is also involved in OT function in anti-inflammation and promotion of metabolic homeostasis (Mancini et al., 2017) through multiple approaches. As reported that OT stimulated and activated AMPK in C2C12 myoblast cells in a time/dose-dependent manner. This process also depends on the activation of CaMK since it was blocked by inhibition of either CaMK or AMPK (Lee et al., 2008). In db/db mice, OT treatment normalized cardiac structure and function, cardiac OTRs, ANP, and AMPK while reducing body fat accumulation, fasting blood glucose levels and improving glucose tolerance and insulin sensitivity (Plante et al., 2015). Moreover, AMPK could inhibit HMG-CoA reductase to reduce cholesterol synthesis and inflammation (Vilahur et al., 2014). Thus, inhibition of multiple pro-inflammatory signaling pathways and metabolic disorders by AMPK should be an important mechanism of the cardiovascular protective functions by OT.

Other Signals

Oxytocin protection of the CVS was associated with its activation of PKC (Faghihi et al., 2012), likely PKC-ε signaling in the mitochondria. In cardioprotection, PKC-ε, a downstream effector of PLC-β and NO generated by eNOS, increased the stability of gap junctions and suppressed ventricular fibrillation by antioxidant-increased connexin-43 in rats (Bacova et al., 2017; Lee et al., 2017). In contrast, activation of PKC-α, a downstream event of PLC-β1b that is a heart-specific signaling, led to cardiac injury by increasing inducible NOS (iNOS) expression, concomitant to enhanced apoptotic cell percentage, and molecular interaction between apoptotic protease activating factor-1 and cytochrome C (Qiu et al., 2012). These findings indicate that PLC-β1b-PKC-α-iNOS signaling pathway activates mitochondrial apoptotic pathways while PKC-ε is protective. In contrast to the effect of OT, norepinephrine, angiotensin II, and endothelin 1 and phorbol ester could activate and translocate protein kinase D1 to the Z-disks in rat cardiomyocytes in a PKC-ε-dependent manner, which process was essential to induce hypertrophic responses (Iwata et al., 2005). Thus, protein kinase D1 and PKC-ε interaction may also induce cardiac hypertrophy. Moreover, ERK1/2 activation by metabotropic glutamate receptor 1 induced melanoma development and was also PKC-ε-dependent, but cAMP and PKA-independent. Thus, the proliferating effect of PKC-ε downstream to OTRs either functions during regeneration of injured cardiomyocytes or is linked to different signaling events from those that are used by the GPCRs of "stress hormones." Nevertheless, experimental evidence remains to be collected.

In parallel with NO, H_2S is also a well-known cardioprotective gaseous signal (Raphael et al., 2015; Jin et al., 2017). H_2S is mainly converted from cysteine catalyzed by cystathionine-γ-lyase (CSE) that was present in OTR-expressing supraoptic neurons (Coletti et al., 2019) and could be activated by CaMK, PI3K and NO. H_2S could also suppress inflammation by activating KATP channel, PI3K, and pERK1/2 signaling (You et al., 2017). Importantly, CSE can regulate OTR expression in tissue- and function-dependent manner. In isolated human uterine smooth muscle cells, CSE had negative correlation with the expression of OTR in pregnant myometrial tissues (You et al., 2017). By contrast, myocardial injury evoked by contusion of the thorax in mice was found to reduce myocardial OTR expression, and that was aggravated in CSE(−/−) mice; exogenous H_2S administration restored myocardial OTR protein expression to wild-type levels (Merz et al., 2018). This study suggests that cardiac CSE can exert cardioprotective function by activating RISK pathway and up-regulating cardiac OTR expression.

In addition, OT-evoked protection was also related to increases in VEGF, B-cell lymphoma 2 and matrix metalloproteinase-1 (Kobayashi et al., 2009) along with aforementioned signals that opened mKATP channels (Alizadeh et al., 2010). Among them, serum levels of VEGF had negative association with atrial fibrillation episode duration (Peller et al., 2017) and exerted antifibrotic and angiogenic effects, which were associated with the activation of matrix metalloproteinase-1 and eNOS (Kobayashi et al., 2009).

Signaling Network

In cardiovascular protection, different signaling pathways function interactively and coordinately to suppress immunometabolic disorders. For instance, exercise in mice reduced infarct size by 60% while increasing phosphorylation of Akt, ERK1/2, and AMPK; however, the level of corresponding phosphatases PTEN, MKP-3, and PP2C were decreased in both wild-type and obese mice (Danalache et al., 2014). Moreover, different signaling pathways have close interactions as shown in the following studies. In vascular endothelial cells in mice

(Chen et al., 2009) and human umbilical vein endothelial cells (Huang et al., 2017), AMPK served as an upstream enzyme of the Akt-NO pathway. These signals are known to activate mKATP channels via activation of eNOS-NO-protein kinase G pathway and CREB, thereby protecting the CVS from the damaging effect of ER stress and MOS as previously discussed (Wang S.C. et al., 2018). Another example is that H_2S-evoked activation of ERK 1/2 PI3K depended on mKATP channel activation (You et al., 2017).

Together with other evidence, such as the mediation of statin protection by the phosphorylated Akt, GSK-3β (inhibition), and CREB and the functions of OT at other tissues (Klein et al., 2014; Watanabe et al., 2016), we propose the presence of an OTR signaling network that protects the CVS from atherosclerotic injury and CAD (**Figure 2**).

PROTECTION BY ALLEVIATING ER STRESS AND MOS

Coronary atherosclerosis and CAD are largely caused by immunometabolic disorders and the resultant ER stress and MOS (Wang S.C. et al., 2018). In agreement with the common machinery of immunometabolic regulation, the cardioprotective effect of OT is also dependent on its suppression of immunometabolic disorders involving "ER-mitochondrial syncytium."

Reducing ER Stress

The ER is an essential organelle for protein synthesis, folding, translocation, calcium homoeostasis, and lipid biosynthesis. Stimuli that disrupt ER homoeostasis and functions can cause the accumulation of misfolded and unfolded proteins that disrupt ER membrane structure and functions. As an adaptive strategy to restore ER homoeostasis, an unfolded protein response (UPR) occurs following ER stress through activating transcriptional and translational pathways. Maladapted ER stress could worsen ER functions, trigger inflammatory reaction and damage membrane structure, leading to cell dysfunction and apoptosis (Wang et al., 2017). In the CVS, ER stress causes the development and progression of various CVDs. Suppression of ER stress has been shown to promote angiogenesis (Pohl et al., 2018), reduce cardiomyocyte apoptosis, improve heart function in diabetic rats (Rabow et al., 2018) and decrease cell death in ER stress models of cultured neonatal rat cardiomyocytes and in acute MI in mice (Ding et al., 2019). In OT-elicited cardiovascular protection, suppression of ER stress is also an important mechanism.

It has been reported that OT in the colostrum attenuated the impact of inflammation on postnatal gut villi and enhanced autophagy to protect against amino acid insufficiency-induced ER stress during the interval between birth and the first feeding (Klein et al., 2017). OT reduced ER stress by reducing the burden of protein synthesis and processes in the ER through rapamycin complex 1 (mTORC1) signaling that was up-regulated in CVDs (Yano et al., 2016). In gut cells, OT was found to downregulate anabolic effects induced by fresh growth medium catalyzed by mTORC1 through regulation of PI3K/Akt/mTORC1 pathway, which has been identified in mice with malignant arrhythmias, heart failure, and premature death (Cao et al., 2013). Consistently, through activating inositol requiring enzyme (IRE), OT increased the UPR and a chaperone protein, immunoglobulin binding protein while decreased translation initiation factors (Klein et al., 2017). Through this chaperone approach, OT could inhibit lipopolysaccharide-evoked ER stress (Klein et al., 2017). Mechanistic studies revealed that the enhancement of IRE1α (IRE1α)/X box-binding protein-1 (XBP1) activity in turn increased ER-associated degradation-mediated clearance of misfolded proteins and autophagy (Ding et al., 2019). Another line of evidence showed that following the activation of OTRs, IRE1α activation was mediated by OT-elicited VEGF release, which together with sliced XBP1 could carry out the protective functions of OT in a PI3K/Akt/GSK-3β/β-catenin/E2F2-dependent manner (Pohl et al., 2018). Thus, OT can reduce translation of proteins, increase their export and clearance of misfolded proteins during ER stress and thus protect cardiomyocytes from injuries of immunometabolic stress.

Inhibition of the MOS

The mKATP channel is a key carrier in the cardioprotective effect of OT and a downstream signal in the RISK pathway (Raphael et al., 2015; Jin et al., 2017; You et al., 2017) and AMPK signaling (Chen et al., 2009; Huang et al., 2017). In OT-stimulated cells, activated Akt accumulated intracellularly close to mitochondria in mesenchymal stem cells that have therapeutic potential in I/R heart, and allowed NO-dependent activation of protein kinase G to open mKATP channels (Faghihi et al., 2012). Moreover, OT could activate mKATP channels in the heart of anesthetized rats that were subject to I/R injury and thus significantly decreased infarct size, creatine kinase-MB isoenzyme plasma level, severity and incidence of ventricular arrhythmia. These effects were blocked by atosiban (Alizadeh et al., 2010). These findings are consistent with the cardioprotective effect of activating mKATP channels under other conditions (Das and Sarkar, 2012).

What needs to be note is that the protective effect of OT in mitochondria is achieved in an "oxidative preconditioning" manner. In a simulated I/R experiment using heart-derived H9c2 cells, OT was shown to trigger a short-lived burst in ROS production but reduced I/R-evoked remarkable ROS production (Gonzalez-Reyes et al., 2015). This "oxidative preconditioning" blocks I/R-evoked MOS, thereby exerting the protective effect. By suppressing the MOS, OT also restores tricarboxylic acid cycle and normal ATP production that are critical in cardiac protection (Wang S.C. et al., 2018).

OT Suppression of Ca^{2+} Overload Through SR/ER-Mitochondrial Network

It is of interest to note that ER stress and MOS do not occur independently in CAD-associated immunometabolic disorders. The two organelles are interconnected through MAM in the heart, which was responsible for Ca^{2+} signaling between ER and mitochondria following the activation of inositol 1,4,5-trisphosphate receptor (IP_3R) (Wu et al., 2017), thereby forming an ER-mitochondrial channel.

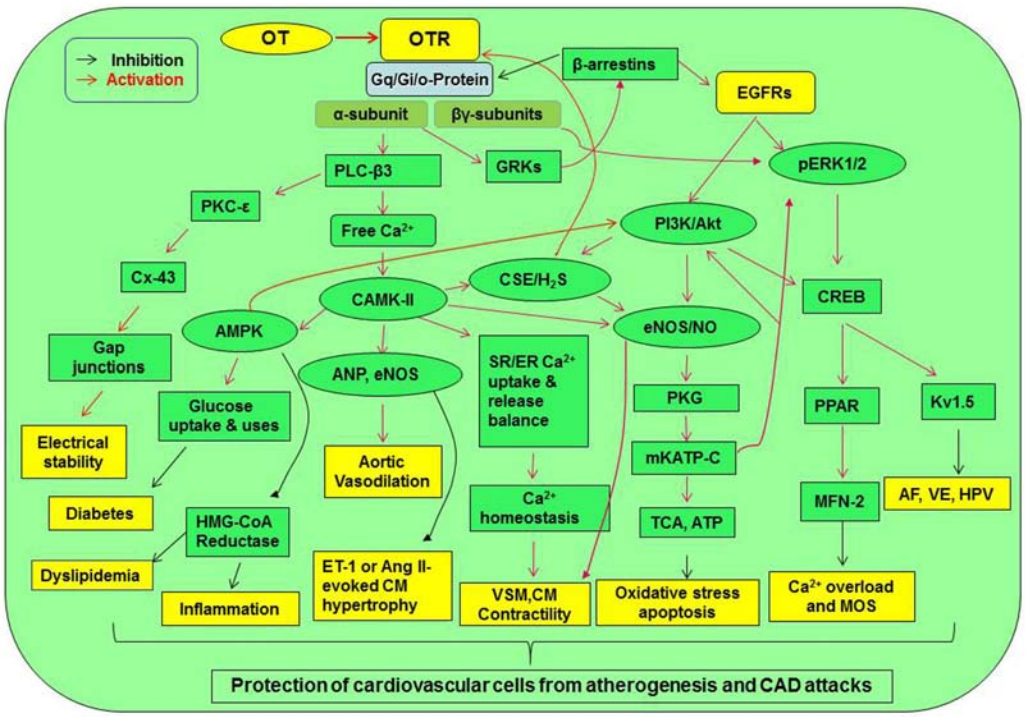

FIGURE 2 | Signaling pathway mediating cardiovascular protection of OT. Activation of OTR-Gq and Gi/o proteins can directly increase Gqα subunit and Gβγ subunit signaling. These signals can cross-activate EGFR while activating their downstream signaling molecules, resulting in the activation of CaMK-AMPK, PKC-ε, PI3K/Akt-eNOS, H_2S, and ERK1/2-CREB signaling cascades. These signaling cascades lead to the activation of a variety of cardioprotective functions including electrical stability, metabolic arrangement, inhibition of inflammation or oxidative stress, and others. AF, atrial fibrillation; Akt, protein kinase B; AMPK, AMP-activated protein kinase; Ang, angiotensin; CaMK, Ca^{2+}/calmodulin-dependent protein kinase; CREB, cyclic AMP response element-binding protein; CSE, cystathionine-γ-lyase; Cx-43, connexin-43; EGFR, epidermal growth factor receptor; eNOS, endothelial nitric oxide synthase; ER, endoplasmic reticulum; ERK1/2, extracellular signal-regulated protein kinase 1/2; ET-1, endothelin-1; GRK, G protein-coupled receptor kinase; HMG-CoA reductase, 3-hydroxy-3-methyl-glutaryl-coenzyme A reductase; HPV, hypoxic pulmonary vasoconstriction; H_2S, hydrogen sulfate; Kv1.5, voltage-gated potassium channel Kv1.5; MFN-2, mitofusin-2; mKATP C, mitochondrial ATP-dependent potassium channels; MOS, mitochondrial oxidative stress; PI3K, phosphatidylinositol 3-kinases; PKC, protein kinase C; PKG, protein kinase G; PLC-β3, phospholipase C-β3; PPAR, peroxisome proliferator-activated receptor; SR, sarcoplasmic reticulum; TCA cycle, tricarboxylic acid cycle; VSM, vascular smooth muscle; VE, ventricular ectopy. Other annotations refer to **Figure 1**.

This Ca^{2+} signaling in the heart is regulated by GSK-3β protein in the ER. Dephosphorylation/activation of GSK-3β occurs following the activation of JNK which could be induced by advanced glycation end-products in diverse pathological settings including diabetes, inflammation and acute I/R injury in the heart (Wang S.C. et al., 2018). During I/R, increased GSK-3β activity leads to enhanced transfer of Ca^{2+} from ER to mitochondria by interacting with the IP_3R Ca^{2+} channeling complex in MAM, leading to cytosolic and mitochondrial Ca^{2+} overload and the resultant cell death. Inhibition of GSK-3β reduced both IP_3R phosphorylation and ER Ca^{2+} release, which consequently diminished both cytosolic and mitochondrial Ca^{2+}concentrations as well as mitochondrial sensitivity to apoptosis (Gomez et al., 2016). Activation of the mKATP channels reversely induced inhibitory phosphorylation of GSK-3β and suppressed substantial ROS production, lactate dehydrogenase release and apoptosis after antimycin washout (Sunaga et al., 2014). Another key molecule regulating the interaction between mitochondria and ER is mitofusin-2. Mitofusin-2 has been identified to suppress the interaction between the ER and mitochondrial apoptotic pathway (Guan et al., 2016; Yang F. et al., 2017), a function opposite to GSK-β.

In addition to the ER, SR is also an important source of mitochondrial Ca^{2+} overload in myocardiac pathogenesis. Ca^{2+} transient from SR could also contribute to the MOS. For example, fructose-rich diet induced decrease in SR-mitochondrial distance, SR Ca^{2+} leak, and Ca^{2+} transit between the two organelles, which resulted in mitochondrial membrane depolarization and oxidative stress, thereby activating the apoptotic pathway and diabetic heart injury (Federico et al., 2017).

Oxytocin could protect the heart by blocking the activity of malfunctioned ER-mitochondrial syncytium through the following approaches. (1) OT can increase cardiac expression of connexin 43 (Gassanov et al., 2008; Kim et al., 2012), which was known to inhibit GSK-3β signaling in cardiomyocytes (Ishikawa et al., 2012). (2) OT can activate PI3K/Akt pathway (Gonzalez-Reyes et al., 2015) that is known to exert antiapoptosis in association with upregulation of mitofusin 2 (Zhang et al., 2014). (3) By activating AMPK, OT can decrease the Ca^{2+} oscillation through increasing mitofusin 2 expression (Wang F. et al., 2015) and suppressing GSK-3β by activation of insulin receptor

(Chopra et al., 2012) that was known to increase mitofusin 2 and decrease GSK-3β (Litwiniuk et al., 2016). This possibility is supported by the fact that OT stimulated PKC activity in adipocyte plasma membranes, an effect similar to that of insulin (Egan et al., 1990); however, direct evidence remains to be collected. **Figure 3** presents a working model of OT suppression of the malfunctioned ER-mitochondrial communication.

LIMITATION FOR THERAPEUTIC USE OF OT

Oxytocin was generally considered a safe agent in clinical usage (Alfirevic et al., 2016). A daily treatment with 40 IU intranasal OT for 4 months did not impact on OT and VP plasma levels nor on cardiovascular, body fluids and food intake parameters in healthy humans (Busnelli et al., 2015). Similarly, intranasal OT strengthened the bonding between male resident and its female partner in rats without changing cardiovascular activity (Calcagnoli et al., 2015). Moreover, OT has the beneficial effects of insulin, antioxidants, and corticosteroids but not their side effects (Hou et al., 2016). Thus, its clinical trial is tempting.

It is important to note that some animal studies administer supraphysiological levels of OT (e.g., micromolar concentrations rather than picomolar levels) and at that dosage, OT has affinity for VP receptors and VP-like effect, such as pressor effect of OT at its initial actions (Petty et al., 1985). Moreover, cardiovascular side effects and allergy to OT have been found in gynecological practice although quite rare. Thus, it is necessary to address these negative sides in clinical trials of OT in prevention and treatment of the CVD.

Exogenous OT Application

Since chronic CVDs are associated with declines in OT/OTR signaling, restoring OTR signaling with OT becomes a natural selection. To simulate physiological and natural labor, pulsatile application of intravenous OT was commonly used (Saccone et al., 2017). Pulsatile application was associated with lower total dose of OT and less incidence of tachy-systole; however, cardiovascular disturbances like hypotension and reflexive tachycardia were sometimes observed when 5∼10 IU OT was given as a rapid intravenous bolus (Lin et al., 2007; Saccone et al., 2017). In pregnant women with MI, coronary spasm or thrombosis could occur in response to the intravenous bolus

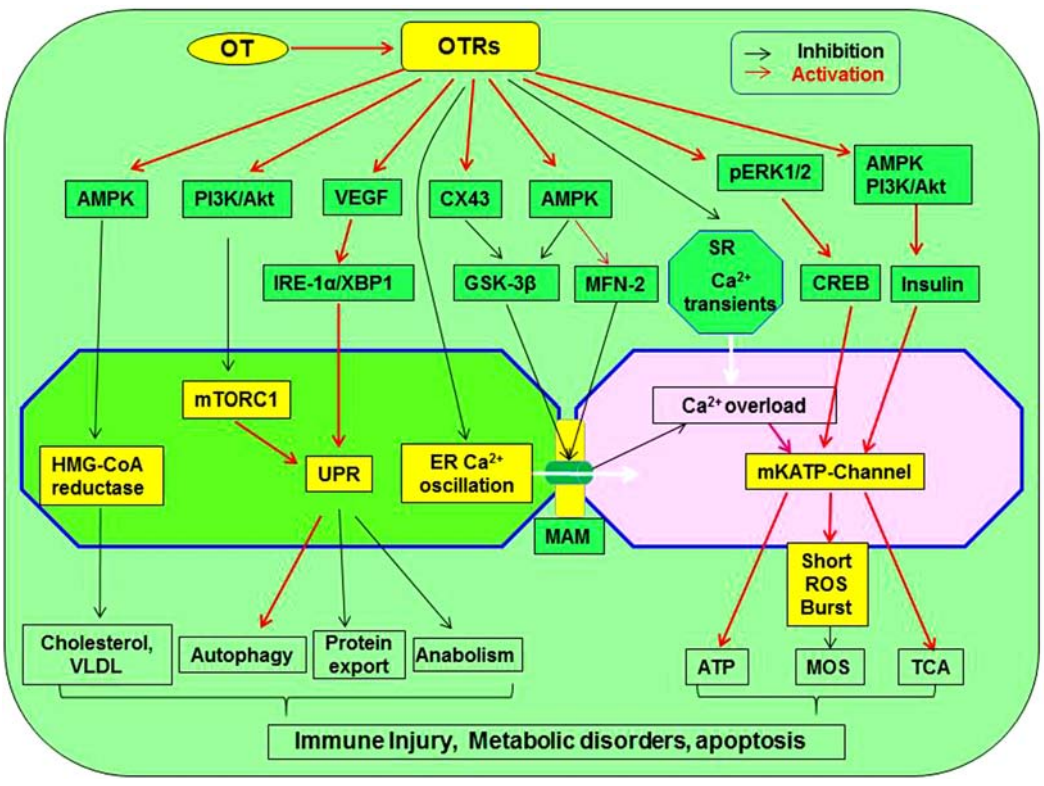

FIGURE 3 | Working model of OT suppression of the malfunctioned ER-mitochondrial communication. OTR activation can inhibit inflammation, ER stress, restore UPR and chaperone functions, reduce the production of cholesterol and VLDL, inhibit ER-mitochondrial Ca^{2+} oscillation and overload through MAM, precondition MOS, restore TCA cycle, and suppress inflammatory and apoptotic pathways, leading to regeneration and repair of injured cardiomyocytes. These processes are signaling through activating AMPK, pERK1/2, PI3K/Akt, VEGF, and CX43 while inhibiting mTORC1, HMG-CoA reductase, GSK-3β, and calcium oscillation. As a result, lipotoxicity and formation of atherosclerosis are inhibited. GSK-3β, glycogen synthase kinase-3β; IRE1α, inositol-requiring enzyme 1α; pERK1/2, extracellular signal-regulated protein kinase 1/2; MAM, mitochondria-associated ER membrane; ROS, reactive oxygen species; mTORC1, rapamycin complex 1; UPR, unfolded protein response; VEGF, vascular endothelial growth factor; VLDL, low-density lipoproteins; XBP1, X box-binding protein-1. Other annotations refer to **Figure 2**.

of OT. By contrast, there were only modest cardiovascular disturbances during slow infusion (Svanstrom et al., 2008). This fact highlights the necessity to reconsider the optimal drug, dose, and administration route in clinical trials of OT.

It is known that the beneficial effect of OT on cardioprotection is correlated with the basal levels of endogenous OT (Hirst et al., 1991). OT administration to individuals with a low pretreatment OT levels could be beneficial whereas, individuals with an elevated basal OT levels would be prone to adverse effects, which has been shown in swine (Jacquenod et al., 2015). It is likely that during parturition the basal OT levels are already very high, a bolus injection of OT in large amount may reversely decrease OTR signaling by reducing OTR protein expression (Authier et al., 2010). Moreover, high doses of OT also activated VP receptors (Wang and Hatton, 2006), thereby evoking MI (Ying et al., 2015). These facts highlight the necessity to assay the basal levels of blood OT in the induction of labor, particularly in those with CAD, and use drugs like prostaglandins (Mahomed et al., 2018) and misoprostol (Pimentel et al., 2018) to replace OT in those who have higher basal OT levels.

In using exogenous OT to treat CAD, pre-existing neuroendocrine conditions of the patients should also be considered. It has been observed that chronic application of OT and angiotensin-II together increased mean arterial pressure, and caused left ventricular hypertrophy and renal damage in male rats (Phie et al., 2015). It is likely that prolonged administration of OT in CAD patients with elevated basal angiotensin-II levels accelerated angiotensin-II-induced hypertension and renal damage (Gu et al., 2016). Since elevated basal levels of angiotensin-II is common among patients with CAD complications (Schuh et al., 2017), alternative approaches of OT application should be considered.

In addition, anaphylaxis to OT was occasionally observed in delivering women with latex allergy and bronchial asthma (Liccardi et al., 2013). Thus, special attention in exogenous OT application should be paid to patients who have the history of latex allergy as well as history of hypotension, reflexive tachycardia, and high angiotensin levels in delivering women.

Intranasal OT Delivery

Circulating OT could modulate cardiovascular activity directly (Alfirevic et al., 2016); however, intravenous application of OT is inaccessible to the brain sites that are involved in neural regulation of CVS activity. Thus, intranasal OT application had been tested in heart rate variability-an index of autonomic cardiac control (Quintana et al., 2013). Although intranasally-applied OT usually does not evoke significant change in plasma OT levels (Leng and Ludwig, 2016), it could exert antiarrhythmic effect in human being as reported (Jain et al., 2017; Sack et al., 2017).

Intranasal administration of OT could regulate brain activities including hypothalamic sites (Delorme and Garabedian, 2018) without side effects of peripheral exposure (Busnelli et al., 2015; Calcagnoli et al., 2015). Intranasal delivery of OT had been considered in relieving brain-associated etiologies of CAD, such as obesity, Alzheimer's disease, depression, anxiety, seizure, and stroke (Chapman et al., 2013). In CAD patients, intranasal OT also exerted the protective effect (Zhang et al., 2013) by suppressing the activity of HPA axis and adrenaline secretion (Yee et al., 2016) and reducing sympathetic output (Tracy et al., 2018). However, intranasal OT may act on multiple brain sites though different nose-brain routes (Veening and Olivier, 2013) that may impose additional complications, such as co-activation of VP neurons, thereby compromising the protective effect of OT (Bartekova et al., 2015). In addition, responsive activation of parvocellular OT neurons during MI could drive cardiac sympathetic nerve activation as observed in rats (Roy et al., 2018), which could worsen the decompensated heart functions. Although it remains to study if intranasal OT application could activate this sympathetic pathway, caution should be taken in using this approach to deliver OT in acute phase of MI. As a whole, how to let OT activate the descending vagal pathway to minimize cardiac injury remains a puzzle in exploring the therapeutic potential of intranasal OT.

SUMMARY

In varieties of etiologies of atherosclerosis and the resultant CAD, deficits in OTR signaling are an important one. Although the presence of some rare side effects and optimal approaches of OT application remain to be clarified, the perspective to reduce the morbidity and mortality of atherosclerosis and CAD by targeting OTR signaling is highly desirable, which can at least avoid the compromising effect of VP receptor signaling while efficiently blocking the key pathological link in CAD development. To exert the therapeutic potential of OT, questions remain to be answered include but not limit to understandings of the signaling processes from OTR activation to its downstream signals, including CaMK, AMPK, PI3K/Akt, pERK 1/2, PKC-ε, NO and H_2S, and the details of inter-organelle Ca^{2+}transfer and its regulation, and so on. With careful monitoring of both the positive and negative effects of OT, particularly in delivering women (Weissman et al., 2017), future clinical trials of OT therapies would contribute significantly to the translational study in curbing the development of atherosclerosis and the CAD complications.

AUTHOR CONTRIBUTIONS

PW and SW wrote the first draft. HZ and Y-FW conceived the study. Y-FW edited the draft. All authors made critical discussion.

FUNDING

This work was supported by the National Natural Science Foundation of China (Grant No. 31471113, Y-FW), Fund of "Double-First-Class" Construction of Harbin Medical University (HZ), and the higher education talents funds of Heilongjiang Province (Grant No. 002000154, Y-FW).

ACKNOWLEDGMENTS

We thank Drs B. Yang, R. Lyubarova, and C. Xu for advice.

REFERENCES

Abdallah, Y., Kasseckert, S. A., Iraqi, W., Said, M., Shahzad, T., Erdogan, A., et al. (2011). Interplay between Ca2+ cycling and mitochondrial permeability transition pores promotes reperfusion-induced injury of cardiac myocytes. *J. Cell. Mol. Med.* 15, 2478–2485. doi: 10.1111/j.1582-4934.2010.01249.x

Al-Amran, F., and Shahkolahi, M. (2013). Oxytocin ameliorates the immediate myocardial injury in rat heart transplant through downregulation of neutrophil-dependent myocardial apoptosis. *Transplant. Proc.* 45, 2506–2512. doi: 10.1016/j.transproceed.2013.03.022

Alfirevic, Z., Keeney, E., Dowswell, T., Welton, N. J., Medley, N., Dias, S., et al. (2016). Which method is best for the induction of labour? A systematic review, network meta-analysis and cost-effectiveness analysis. *Health Technol. Assess.* 20, 1–584. doi: 10.3310/hta20650

Alizadeh, A. M., Faghihi, M., Sadeghipour, H. R., Mohammadghasemi, F., Imani, A., Houshmand, F., et al. (2010). Oxytocin protects rat heart against ischemia-reperfusion injury via pathway involving mitochondrial ATP-dependent potassium channel. *Peptides* 31, 1341–1345. doi: 10.1016/j.peptides.2010.04.012

Alizadeh, A. M., and Mirzabeglo, P. (2013). Is oxytocin a therapeutic factor for ischemic heart disease? *Peptides* 45, 66–72. doi: 10.1016/j.peptides.2013.04.016

Amri, E. Z., and Pisani, D. F. (2016). Control of bone and fat mass by oxytocin. *Horm. Mol. Biol. Clin. Investig.* 28, 95–104.

Anvari, M. A., Imani, A., Faghihi, M., Karimian, S. M., Moghimian, M., and Khansari, M. (2012). The administration of oxytocin during early reperfusion, dose-dependently protects the isolated male rat heart against ischemia/reperfusion injury. *Eur. J. Pharmacol.* 682, 137–141. doi: 10.1016/j.ejphar.2012.02.029

Araujo, I. G., Elias, L. L., Antunes-Rodrigues, J., Reis, L. C., and Mecawi, A. S. (2013). Effects of acute and subchronic AT1 receptor blockade on cardiovascular, hydromineral and neuroendocrine responses in female rats. *Physiol. Behav.* 122, 104–112. doi: 10.1016/j.physbeh.2013.08.018

Authier, S., Tanguay, J. F., Geoffroy, P., Gauvin, D., Bichot, S., Ybarra, N., et al. (2010). Cardiovascular effects of oxytocin infusion in a porcine model of myocardial infarct. *J. Cardiovasc. Pharmacol.* 55, 74–82. doi: 10.1097/fjc.0b013e3181c5e7d4

Bacova, B. S., Vinczenzova, C., Zurmanova, J., Kasparova, D., Knezl, V., Benova, T. E., et al. (2017). Altered thyroid status affects myocardial expression of connexin-43 and susceptibility of rat heart to malignant arrhythmias that can be partially normalized by red palm oil intake. *Histochem. Cell Biol.* 147, 63–73. doi: 10.1007/s00418-016-1488-6

Bartekova, M., Barancik, M., Pokusa, M., Prokopova, B., Radosinska, J., Rusnak, A., et al. (2015). Molecular changes induced by repeated restraint stress in the heart: the effect of oxytocin receptor antagonist atosiban. *Can. J. Physiol. Pharmacol.* 93, 827–834. doi: 10.1139/cjpp-2015-0096

Benjamin, E. J., Muntner, P., Alonso, A., Bittencourt, M. S., Callaway, C. W., and Carson, A. P. (2019). Heart disease and stroke statistics-2019 update: a report from the american heart association. *Circulation* 139, e56–e66.

Blevins, J. E., and Baskin, D. G. (2015). Translational and therapeutic potential of oxytocin as an anti-obesity strategy: insights from rodents, nonhuman primates and humans. *Physiol. Behav.* 152(Pt B), 438–449.

Bonne, D., Belhadj, O., and Cohen, P. (1978). Calcium as modulator of the hormonal-receptors-biological-response coupling system. Effects of Ca2+ ions on the insulin activated 2-deoxyglucose transport in rat fat cells. *Eur. J. Biochem.* 86, 261–266. doi: 10.1111/j.1432-1033.1978.tb12307.x

Borrow, A. P., Bales, N. J., Stover, S. A., and Handa, R. J. (2018). Chronic variable stress induces sex-specific alterations in social behavior and neuropeptide expression in the mouse. *Endocrinology* 159, 2803–2814.

Brown, C. H., Bains, J. S., Ludwig, M., and Stern, J. E. (2013). Physiological regulation of magnocellular neurosecretory cell activity: integration of intrinsic, local and afferent mechanisms. *J. Neuroendocrinol.* 25, 678–710. doi: 10.1111/jne.12051

Busnelli, M., Bulgheroni, E., Manning, M., Kleinau, G., and Chini, B. (2013). Selective and potent agonists and antagonists for investigating the role of mouse oxytocin receptors. *J. Pharmacol. Exp. Ther.* 346, 318–327. doi: 10.1124/jpet.113.202994

Busnelli, M., Dagani, J., De Girolamo, G., Balestrieri, M., Pini, S., Saviotti, F. M., et al. (2015). Unaltered oxytocin and vasopressin plasma levels in patients with schizophrenia after 4 months of daily treatment with intranasal oxytocin. *J. Neuroendocrinol.* doi: 10.1111/jne.12359 [Epub ahead of print].

Calcagnoli, F., Kreutzmann, J. C., De Boer, S. F., Althaus, M., and Koolhaas, J. M. (2015). Acute and repeated intranasal oxytocin administration exerts anti-aggressive and pro-affiliative effects in male rats. *Psychoneuroendocrinology* 51, 112–121. doi: 10.1016/j.psyneuen.2014.09.019

Cao, Y., Tao, L., Shen, S., Xiao, J., Wu, H., Li, B., et al. (2013). Cardiac ablation of Rheb1 induces impaired heart growth, endoplasmic reticulum-associated apoptosis and heart failure in infant mice. *Int. J. Mol. Sci.* 14, 24380–24398. doi: 10.3390/ijms141224380

Cassar, A., Holmes, D. R. Jr., Rihal, C. S., and Gersh, B. J. (2009). Chronic coronary artery disease: diagnosis and management. *Mayo Clin. Proc.* 84, 1130–1146.

Cattaneo, M. G., Chini, B., and Vicentini, L. M. (2008). Oxytocin stimulates migration and invasion in human endothelial cells. *Br. J. Pharmacol.* 153, 728–736. doi: 10.1038/sj.bjp.0707609

Cavalleri, M. T., Burgi, K., Cruz, J. C., Jordao, M. T., Ceroni, A., and Michelini, L. C. (2011). Afferent signaling drives oxytocinergic preautonomic neurons and mediates training-induced plasticity. *Am. J. Physiol. Regul. Integr. Comp. Physiol.* 301, R958–R966.

Chapman, C. D., Frey, W. H. II, Craft, S., Danielyan, L., Hallschmid, M., Schioth, H. B., et al. (2013). Intranasal treatment of central nervous system dysfunction in humans. *Pharm. Res.* 30, 2475–2484. doi: 10.1007/s11095-012-0915-1

Chen, Z., Peng, I. C., Sun, W., Su, M. I., Hsu, P. H., Fu, Y., et al. (2009). AMP-activated protein kinase functionally phosphorylates endothelial nitric oxide synthase Ser633. *Circ. Res.* 104, 496–505. doi: 10.1161/circresaha.108.187567

Chiodera, P., Volpi, R., Capretti, L., Bocchi, R., Caffarri, G., Marcato, A., et al. (1993). Gamma-aminobutyric acid mediation of the inhibitory effect of endogenous opioids on the arginine vasopressin and oxytocin responses to nicotine from cigarette smoking. *Metabolism* 42, 762–765. doi: 10.1016/0026-0495(93)90246-k

Chiodera, P., Volpi, R., Capretti, L., Marchesi, C., D'amato, L., De Ferri, A., et al. (1991). Effect of estrogen or insulin-induced hypoglycemia on plasma oxytocin levels in bulimia and anorexia nervosa. *Metabolism* 40, 1226–1230. doi: 10.1016/0026-0495(91)90220-q

Chopra, I., Li, H. F., Wang, H., and Webster, K. A. (2012). Phosphorylation of the insulin receptor by AMP-activated protein kinase (AMPK) promotes ligand-independent activation of the insulin signalling pathway in rodent muscle. *Diabetologia* 55, 783–794. doi: 10.1007/s00125-011-2407-y

Ciosek, J., and Drobnik, J. (2012). Function of the hypothalamo-neurohypophysial system in rats with myocardial infarction is modified by melatonin. *Pharmacol. Rep.* 64, 1442–1454. doi: 10.1016/s1734-1140(12)70942-8

Coletti, R., De Lima, J. B. M., Maria, F., Vechiato, V., De Oliveira, F. L., Debarba, L. K., et al. (2019). Nitric oxide acutely modulates hypothalamic and neurohypophyseal carbon monoxide and hydrogen sulphide production to control vasopressin, oxytocin and atrial natriuretic peptide release in rats. *J. Neuroendocrinol.* 31:e12686. doi: 10.1111/jne.12686

Conti, F., Sertic, S., Reversi, A., and Chini, B. (2009). Intracellular trafficking of the human oxytocin receptor: evidence of receptor recycling via a Rab4/Rab5 "short cycle". *Am. J. Physiol. Endocrinol. Metab.* 296, E532–E542.

Costa E Sousa, R. H., Pereira-Junior, P. P., Oliveira, P. F., Olivares, E. L., Werneck-De-Castro, J. P., Mello, D. B., et al. (2005). Cardiac effects of oxytocin: is there a role for this peptide in cardiovascular homeostasis? *Regul. Pept.* 132, 107–112. doi: 10.1016/j.regpep.2005.09.011

Crea, F., and Libby, P. (2017). Acute coronary syndromes: the way forward from mechanisms to precision treatment. *Circulation* 136, 1155–1166. doi: 10.1161/circulationaha.117.029870

Da Silva, A. L., Ruginsk, S. G., Uchoa, E. T., Crestani, C. C., Scopinho, A. A., Correa, F. M., et al. (2013). Time-course of neuroendocrine changes and its correlation with hypertension induced by ethanol consumption. *Alcohol Alcohol.* 48, 495–504. doi: 10.1093/alcalc/agt040

Danalache, B. A., Yu, C., Gutkowska, J., and Jankowski, M. (2014). Oxytocin-Gly-Lys-Arg stimulates cardiomyogenesis by targeting cardiac side population cells. *J. Endocrinol.* 220, 277–289. doi: 10.1530/joe-13-0305

Das, B., and Sarkar, C. (2012). Is preconditioning by oxytocin administration mediated by iNOS and/or mitochondrial K(ATP) channel activation in the in vivo anesthetized rabbit heart? *Life Sci.* 90, 763–769. doi: 10.1016/j.lfs.2012.03.030

De Melo, V. U., Saldanha, R. R., Dos Santos, C. R., De Campos Cruz, J., Lira, V. A., Santana-Filho, V. J., et al. (2016). Ovarian hormone deprivation reduces oxytocin expression in paraventricular nucleus preautonomic neurons and correlates with baroreflex impairment in rats. *Front. Physiol.* 7:461. doi: 10.3389/fphys.2016.00461

Delorme, P., and Garabedian, C. (2018). [Modalities of birth in case of uncomplicated preterm premature rupture of membranes: CNGOF Preterm Premature Rupture of Membranes Guidelines]. *Gynecol. Obstet. Fertil. Senol.* 46, 1068–1075.

Dennis, A. T., and Gerstman, M. D. (2014). Management of labour and delivery in a woman with refractory supraventricular tachycardia. *Int. J. Obstet. Anesth.* 23, 80–85. doi: 10.1016/j.ijoa.2013.08.012

Denson, T. F., O'dean, S. M., Blake, K. R., and Beames, J. R. (2018). Aggression in women: behavior, brain and hormones. *Front. Behav. Neurosci.* 12:81. doi: 10.3389/fnbeh.2018.00081

Ding, C., Leow, M. K., and Magkos, F. (2019). Oxytocin in metabolic homeostasis: implications for obesity and diabetes management. *Obes. Rev.* 20, 22–40. doi: 10.1111/obr.12757

Du, D., Jiang, M., Liu, M., Wang, J., Xia, C., Guan, R., et al. (2015). Microglial P2X(7) receptor in the hypothalamic paraventricular nuclei contributes to sympathoexcitatory responses in acute myocardial infarction rat. *Neurosci. Lett.* 587, 22–28. doi: 10.1016/j.neulet.2014.12.026

Dupont, C., Ducloy-Bouthors, A. S., and Huissoud, C. (2014). [Clinical and pharmacological procedures for the prevention of postpartum haemorrhage in the third stage of labor]. *J. Gynecol. Obstet. Biol. Reprod.* 43, 966–997.

Egan, J. J., Saltis, J., Wek, S. A., Simpson, I. A., and Londos, C. (1990). Insulin, oxytocin, and vasopressin stimulate protein kinase C activity in adipocyte plasma membranes. *Proc. Natl. Acad. Sci. U.S.A.* 87, 1052–1056. doi: 10.1073/pnas.87.3.1052

Elabd, C., Cousin, W., Upadhyayula, P., Chen, R. Y., Chooljian, M. S., Li, J., et al. (2014). Oxytocin is an age-specific circulating hormone that is necessary for muscle maintenance and regeneration. *Nat. Commun.* 5:4082.

Emeny, R. T., Huber, D., Bidlingmaier, M., Reincke, M., Klug, G., and Ladwig, K. H. (2015). Oxytocin-induced coping with stressful life events in old age depends on attachment: findings from the cross-sectional KORA Age study. *Psychoneuroendocrinology* 56, 132–142. doi: 10.1016/j.psyneuen.2015.03.014

Faehrmann, T., Zernig, G., and Mechtcheriakov, S. (2018). [Oxytocin and the mechanisms of alcohol dependence]. *Neuropsychiatrie* 32, 1–8.

Faghihi, M., Alizadeh, A. M., Khori, V., Latifpour, M., and Khodayari, S. (2012). The role of nitric oxide, reactive oxygen species, and protein kinase C in oxytocin-induced cardioprotection in ischemic rat heart. *Peptides* 37, 314–319. doi: 10.1016/j.peptides.2012.08.001

Federico, M., Portiansky, E. L., Sommese, L., Alvarado, F. J., Blanco, P. G., Zanuzzi, C. N., et al. (2017). Calcium-calmodulin-dependent protein kinase mediates the intracellular signalling pathways of cardiac apoptosis in mice with impaired glucose tolerance. *J. Physiol.* 595, 4089–4108. doi: 10.1113/jp273714

Florian, M., Jankowski, M., and Gutkowska, J. (2010). Oxytocin increases glucose uptake in neonatal rat cardiomyocytes. *Endocrinology* 151, 482–491. doi: 10.1210/en.2009-0624

Gainer, H. (2011). *Peptides in Neurobiology*.<publoc>New York, NY: Springer.

Garrott, K., Dyavanapalli, J., Cauley, E., Dwyer, M. K., Kuzmiak-Glancy, S., Wang, X., et al. (2017). Chronic activation of hypothalamic oxytocin neurons improves cardiac function during left ventricular hypertrophy-induced heart failure. *Cardiovasc. Res.* 113, 1318–1328. doi: 10.1093/cvr/cvx084

Gassanov, N., Devost, D., Danalache, B., Noiseux, N., Jankowski, M., Zingg, H. H., et al. (2008). Functional activity of the carboxyl-terminally extended oxytocin precursor Peptide during cardiac differentiation of embryonic stem cells. *Stem Cells* 26, 45–54. doi: 10.1634/stemcells.2007-0289

Gomez, L., Thiebaut, P. A., Paillard, M., Ducreux, S., Abrial, M., Crola Da Silva, C., et al. (2016). The SR/ER-mitochondria calcium crosstalk is regulated by GSK3beta during reperfusion injury. *Cell Death Differ.* 23, 313–322. doi: 10.1038/cdd.2015.101

Gonzalez-Reyes, A., Menaouar, A., Yip, D., Danalache, B., Plante, E., Noiseux, N., et al. (2015). Molecular mechanisms underlying oxytocin-induced cardiomyocyte protection from simulated ischemia-reperfusion. *Mol. Cell. Endocrinol.* 412, 170–181. doi: 10.1016/j.mce.2015.04.028

Goren, H. J., Hanif, K., Dudley, R., Hollenberg, M. D., and Lederis, K. (1986). Adenosine modulation of fat cell responsiveness to insulin and oxytocin. *Regul. Pept.* 16, 125–134. doi: 10.1016/0167-0115(86)90056-x

Gotovina, J., Pranger, C. L., Jensen, A. N., Wagner, S., Kothgassner, O. D., Mothes-Luksch, N., et al. (2018). Elevated oxytocin and noradrenaline indicate higher stress levels in allergic rhinitis patients: implications for the skin prick diagnosis in a pilot study. *PLoS One* 13:e0196879. doi: 10.1371/journal.pone.0196879

Gu, J., Cai, Y., Liu, B., and Lv, S. (2016). Anesthetic management for cesarean section in a patient with uncorrected double-outlet right ventricle. *Springerplus* 5:415.

Guan, X., Wang, L., Liu, Z., Guo, X., Jiang, Y., Lu, Y., et al. (2016). miR-106a promotes cardiac hypertrophy by targeting mitofusin 2. *J. Mol. Cell. Cardiol.* 99, 207–217. doi: 10.1016/j.yjmcc.2016.08.016

Guasch, E., and Gilsanz, F. (2016). Massive obstetric hemorrhage: current approach to management. *Med. Intensiva* 40, 298–310. doi: 10.1016/j.medine.2016.02.003

Gutkowska, J., Broderick, T. L., Bogdan, D., Wang, D., Lavoie, J. M., and Jankowski, M. (2009). Downregulation of oxytocin and natriuretic peptides in diabetes: possible implications in cardiomyopathy. *J. Physiol.* 587, 4725–4736. doi: 10.1113/jphysiol.2009.176461

Gutkowska, J., Jankowski, M., and Antunes-Rodrigues, J. (2014). The role of oxytocin in cardiovascular regulation. *Braz. J. Med. Biol. Res.* 47, 206–214. doi: 10.1590/1414-431x20133309

Hatton, G. I., and Wang, Y. F. (2008). Neural mechanisms underlying the milk ejection burst and reflex. *Prog. Brain Res.* 170, 155–166. doi: 10.1016/s0079-6123(08)00414-7

Higa, K. T., Mori, E., Viana, F. F., Morris, M., and Michelini, L. C. (2002). Baroreflex control of heart rate by oxytocin in the solitary-vagal complex. *Am. J. Physiol. Regul. Integr. Comp. Physiol.* 282, R537–R545.

Hirst, J. J., Haluska, G. J., Cook, M. J., Hess, D. L., and Novy, M. J. (1991). Comparison of plasma oxytocin and catecholamine concentrations with uterine activity in pregnant rhesus monkeys. *J. Clin. Endocrinol. Metab.* 73, 804–810. doi: 10.1210/jcem-73-4-804

Hou, D., Jin, F., Li, J., Lian, J., Liu, M., Liu, X., et al. (2016). Model roles of the hypothalamo-neurohypophysial system in neuroscience study. *Biochem. Pharmacol.* 5:211.

Houshmand, F., Faghihi, M., and Zahediasl, S. (2015). Role of atrial natriuretic Peptide in oxytocin induced cardioprotection. *Heart Lung Circ.* 24, 86–93. doi: 10.1016/j.hlc.2014.05.023

Huang, H., Amin, V., Gurin, M., Wan, E., Thorp, E., Homma, S., et al. (2013). Diet-induced obesity causes long QT and reduces transcription of voltage-gated potassium channels. *J. Mol. Cell. Cardiol.* 59, 151–158. doi: 10.1016/j.yjmcc.2013.03.007

Huang, L. Y., Yen, I. C., Tsai, W. C., Ahmetaj-Shala, B., Chang, T. C., Tsai, C. S., et al. (2017). Rhodiola crenulata attenuates high glucose induced endothelial dysfunction in human umbilical vein endothelial cells. *Am. J. Chin. Med.* 45, 1201–1216. doi: 10.1142/s0192415x17500665

Hurtubise, J., Mclellan, K., Durr, K., Onasanya, O., Nwabuko, D., and Ndisang, J. F. (2016). The different facets of dyslipidemia and hypertension in atherosclerosis. *Curr. Atheroscler. Rep.* 18:82.

Hussien, N. I., and Mousa, A. M. (2016). Could nitric oxide be a mediator of action of oxytocin on myocardial injury in rats? (Biochemical, histological and immunohistochemical study). *Gen. Physiol. Biophys.* 35, 353–362. doi: 10.4149/gpb_2015049

Indrambarya, T., Boyd, J. H., Wang, Y., Mcconechy, M., and Walley, K. R. (2009). Low-dose vasopressin infusion results in increased mortality and cardiac dysfunction following ischemia-reperfusion injury in mice. *Crit. Care* 13:R98.

Iobst, S. E., Breman, R. B., Bingham, D., Storr, C. L., Zhu, S., and Johantgen, M. (2019). Associations among cervical dilatation at admission, intrapartum care, and birth mode in low-risk, nulliparous women. *Birth* [Epub ahead of print].

Ishikawa, S., Kuno, A., Tanno, M., Miki, T., Kouzu, H., Itoh, T., et al. (2012). Role of connexin-43 in protective PI3K-Akt-GSK-3beta signaling in cardiomyocytes. *Am. J. Physiol. Heart Circ. Physiol.* 302, H2536–H2544.

Iwata, M., Maturana, A., Hoshijima, M., Tatematsu, K., Okajima, T., Vandenheede, J. R., et al. (2005). PKCepsilon-PKD1 signaling complex at Z-discs plays a pivotal role in the cardiac hypertrophy induced by G-protein coupling receptor agonists. *Biochem. Biophys. Res. Commun.* 327, 1105–1113. doi: 10.1016/j.bbrc.2004.12.128

Jackson, J., Patterson, A. J., Macdonald-Wicks, L., and Mcevoy, M. (2017). The role of inorganic nitrate and nitrite in CVD. *Nutr. Res. Rev.* 30, 247–264. doi: 10.1017/s0954422417000105

Jacquenod, P., Cattenoz, M., Canu, G., Bois, E., and Lieutaud, T. (2015). [Acute coronary syndrome following a 100 microg carbetocin injection during an emergency Cesarean delivery]. *Can. J. Anaesth.* 62, 513–517.

Jain, V., Marbach, J., Kimbro, S., Andrade, D. C., Jain, A., Capozzi, E., et al. (2017). Benefits of oxytocin administration in obstructive sleep apnea. *Am. J. Physiol. Lung Cell. Mol. Physiol.* 313, L825–L833.

Jameson, H., Bateman, R., Byrne, P., Dyavanapalli, J., Wang, X., Jain, V., et al. (2016). Oxytocin neuron activation prevents hypertension that occurs with chronic intermittent hypoxia/hypercapnia in rats. *Am. J. Physiol. Heart Circ. Physiol.* 310, H1549–H1557.

Jankowski, M., Bissonauth, V., Gao, L., Gangal, M., Wang, D., Danalache, B., et al. (2010a). Anti-inflammatory effect of oxytocin in rat myocardial infarction. *Basic Res. Cardiol.* 105, 205–218. doi: 10.1007/s00395-009-0076-5

Jankowski, M., Wang, D., Danalache, B., Gangal, M., and Gutkowska, J. (2010b). Cardiac oxytocin receptor blockade stimulates adverse cardiac remodeling in ovariectomized spontaneously hypertensive rats. *Am. J. Physiol. Heart Circ. Physiol.* 299, H265–H274.

Jankowski, M., Broderick, T. L., and Gutkowska, J. (2016). Oxytocin and cardioprotection in diabetes and obesity. *BMC Endocr. Disord.* 16:34. doi: 10.1186/s12902-016-0110-1

Jankowski, M., Hajjar, F., Kawas, S. A., Mukaddam-Daher, S., Hoffman, G., Mccann, S. M., et al. (1998). Rat heart: a site of oxytocin production and action. *Proc. Natl. Acad. Sci. U.S.A.* 95, 14558–14563. doi: 10.1073/pnas.95.24.14558

Jankowski, M., Wang, D., Hajjar, F., Mukaddam-Daher, S., Mccann, S. M., and Gutkowska, J. (2000). Oxytocin and its receptors are synthesized in the rat vasculature. *Proc. Natl. Acad. Sci. U.S.A.* 97, 6207–6211. doi: 10.1073/pnas.110137497

Japundzic-Zigon, N. (2013). Vasopressin and oxytocin in control of the cardiovascular system. *Curr. Neuropharmacol.* 11, 218–230. doi: 10.2174/1570159x11311020008

Jiao, R., Cui, D., Wang, S. C., Li, D., and Wang, Y. F. (2017). Interactions of the mechanosensitive channels with extracellular matrix, integrins, and cytoskeletal network in osmosensation. *Front. Mol. Neurosci.* 10:96. doi: 10.3389/fnmol.2017.00096

Jin, S., Teng, X., Xiao, L., Xue, H., Guo, Q., Duan, X., et al. (2017). Hydrogen sulfide ameliorated L-NAME-induced hypertensive heart disease by the Akt/eNOS/NO pathway. *Exp. Biol. Med.* 242, 1831–1841. doi: 10.1177/1535370217732325

Johnson, Z. V., and Young, L. J. (2017). Oxytocin and vasopressin neural networks: implications for social behavioral diversity and translational neuroscience. *Neurosci. Biobehav. Rev.* 76, 87–98. doi: 10.1016/j.neubiorev.2017.01.034

Jurek, B., and Neumann, I. D. (2018). The oxytocin receptor: from intracellular signaling to behavior. *Physiol. Rev.* 98, 1805–1908. doi: 10.1152/physrev.00031.2017

Karelina, K., Stuller, K. A., Jarrett, B., Zhang, N., Wells, J., Norman, G. J., et al. (2011). Oxytocin mediates social neuroprotection after cerebral ischemia. *Stroke* 42, 3606–3611. doi: 10.1161/strokeaha.111.628008

Kc, P., and Dick, T. E. (2010). Modulation of cardiorespiratory function mediated by the paraventricular nucleus. *Respir. Physiol. Neurobiol.* 174, 55–64. doi: 10.1016/j.resp.2010.08.001

Kenkel, W. M., Suboc, G., and Carter, C. S. (2014). Autonomic, behavioral and neuroendocrine correlates of paternal behavior in male prairie voles. *Physiol. Behav.* 128, 252–259. doi: 10.1016/j.physbeh.2014.02.006

Kim, Y. S., Ahn, Y., Kwon, J. S., Cho, Y. K., Jeong, M. H., Cho, J. G., et al. (2012). Priming of mesenchymal stem cells with oxytocin enhances the cardiac repair in ischemia/reperfusion injury. *Cells Tissues Organs* 195, 428–442. doi: 10.1159/000329234

Kim, Y. S., Kwon, J. S., Hong, M. H., Kang, W. S., Jeong, H. Y., Kang, H. J., et al. (2013). Restoration of angiogenic capacity of diabetes-insulted mesenchymal stem cells by oxytocin. *BMC Cell Biol.* 14:38. doi: 10.1186/1471-2121-14-38

Klein, B. Y., Tamir, H., Hirschberg, D. L., Glickstein, S. B., Ludwig, R. J., and Welch, M. G. (2014). Oxytocin modulates markers of the unfolded protein response in Caco2BB gut cells. *Cell Stress Chaperones* 19, 465–477. doi: 10.1007/s12192-013-0473-4

Klein, B. Y., Tamir, H., Ludwig, R. J., Glickstein, S. B., and Welch, M. G. (2017). Colostrum oxytocin modulates cellular stress response, inflammation, and autophagy markers in newborn rat gut villi. *Biochem. Biophys. Res. Commun.* 487, 47–53. doi: 10.1016/j.bbrc.2017.04.011

Klement, J., Ott, V., Rapp, K., Brede, S., Piccinini, F., Cobelli, C., et al. (2017). Oxytocin improves beta-cell responsivity and glucose tolerance in healthy men. *Diabetes* 66, 264–271. doi: 10.2337/db16-0569

Kobayashi, H., Yasuda, S., Bao, N., Iwasa, M., Kawamura, I., Yamada, Y., et al. (2009). Postinfarct treatment with oxytocin improves cardiac function and remodeling via activating cell-survival signals and angiogenesis. *J. Cardiovasc. Pharmacol.* 54, 510–519. doi: 10.1097/fjc.0b013e3181bfac02

Koton, S., Schneider, A. L., Rosamond, W. D., Shahar, E., Sang, Y., Gottesman, R. F., et al. (2014). Stroke incidence and mortality trends in US communities, 1987 to 2011. *JAMA* 312, 259–268.

Lawes, C. M., Vander Hoorn, S., and Rodgers, A. (2008). Global burden of blood-pressure-related disease, 2001. *Lancet* 371, 1513–1518. doi: 10.1016/s0140-6736(08)60655-8

Lee, E. S., Uhm, K. O., Lee, Y. M., Kwon, J., Park, S. H., and Soo, K. H. (2008). Oxytocin stimulates glucose uptake in skeletal muscle cells through the calcium-CaMKK-AMPK pathway. *Regul. Pept.* 151, 71–74. doi: 10.1016/j.regpep.2008.05.001

Lee, H. C., Chen, C. C., Tsai, W. C., Lin, H. T., Shiao, Y. L., Sheu, S. H., et al. (2017). Very-low-density lipoprotein of metabolic syndrome modulates gap junctions and slows cardiac conduction. *Sci. Rep.* 7:12050.

Lee, K. S., Kronbichler, A., Eisenhut, M., Lee, K. H., and Shin, J. I. (2018). Cardiovascular involvement in systemic rheumatic diseases: an integrated view for the treating physicians. *Autoimmun. Rev.* 17, 201–214.

Lee, S. K., Ryu, P. D., and Lee, S. Y. (2013). Differential distributions of neuropeptides in hypothalamic paraventricular nucleus neurons projecting to the rostral ventrolateral medulla in the rat. *Neurosci. Lett.* 556, 160–165. doi: 10.1016/j.neulet.2013.09.070

Lehrke, M., and Marx, N. (2017). Diabetes mellitus and heart failure. *Am. J. Cardiol.* 120, S37–S47.

Leng, G., and Ludwig, M. (2016). Intranasal oxytocin: myths and delusions. *Biol. Psychiatry* 79, 243–250. doi: 10.1016/j.biopsych.2015.05.003

Li, T., Wang, P., Wang, S. C., and Wang, Y. F. (2017). Approaches mediating oxytocin regulation of the immune system. *Front. Immunol.* 7:693. doi: 10.3389/fimmu.2016.00693

Liccardi, G., Bilo, M., Mauro, C., Salzillo, A., Piccolo, A., D'amato, M., et al. (2013). Oxytocin: an unexpected risk for cardiologic and broncho-obstructive effects, and allergic reactions in susceptible delivering women. *Multidiscip. Respir. Med.* 8:67.

Light, K. C., Grewen, K. M., Amico, J. A., Brownley, K. A., West, S. G., Hinderliter, A. L., et al. (2005). Oxytocinergic activity is linked to lower blood pressure and vascular resistance during stress in postmenopausal women on estrogen replacement. *Horm. Behav.* 47, 540–548. doi: 10.1016/j.yhbeh.2004.12.010

Lin, M. C., Hsieh, T. K., Liu, C. A., Chu, C. C., Chen, J. Y., Wang, J. J., et al. (2007). Anaphylactoid shock induced by oxytocin administration–a case report. *Acta Anaesthesiol. Taiwan.* 45, 233–236.

Lindahl, B., Baron, T., Erlinge, D., Hadziosmanovic, N., Nordenskjold, A., Gard, A., et al. (2017). Medical therapy for secondary prevention and long-term outcome in patients with myocardial infarction with nonobstructive coronary artery disease. *Circulation* 135, 1481–1489. doi: 10.1161/circulationaha.116.026336

Litwiniuk, A., Pijet, B., Pijet-Kucicka, M., Gajewska, M., Pajak, B., and Orzechowski, A. (2016). FOXO1 and GSK-3beta are main targets of insulin-mediated myogenesis in C2C12 muscle cells. *PLoS One* 11:e0146726. doi: 10.1371/journal.pone.0146726

Liu, R., Yuan, X., Chen, K., Jiang, Y., and Zhou, W. (2018). Perception of social interaction compresses subjective duration in an oxytocin-dependent manner. *eLife* 7:e32100.

Llewellyn-Smith, I. J., Kellett, D. O., Jordan, D., Browning, K. N., and Travagli, R. A. (2012). Oxytocin-immunoreactive innervation of identified neurons in the rat dorsal vagal complex. *Neurogastroenterol. Motil.* 24, e136–146.

Mahomed, K., Wild, K., and Weekes, C. R. (2018). Prostaglandin gel versus oxytocin - prelabour rupture of membranes at term - A randomised controlled trial. *Aust. N. Z. J. Obstet. Gynaecol.* 58, 654–659.

Manbeck, K. E., Shelley, D., Schmidt, C. E., and Harris, A. C. (2014). Effects of oxytocin on nicotine withdrawal in rats. *Pharmacol. Biochem. Behav.* 116, 84–89. doi: 10.1016/j.pbb.2013.11.002

Mancini, S. J., White, A. D., Bijland, S., Rutherford, C., Graham, D., Richter, E. A., et al. (2017). Activation of AMP-activated protein kinase rapidly suppresses multiple pro-inflammatory pathways in adipocytes including IL-1 receptor-associated kinase-4 phosphorylation. *Mol. Cell. Endocrinol.* 440, 44–56. doi: 10.1016/j.mce.2016.11.010

Marir, R., Virsolvy, A., Wisniewski, K., Mion, J., Haddou, D., Galibert, E., et al. (2013). Pharmacological characterization of FE 201874, the first selective high affinity rat V1A vasopressin receptor agonist. *Br. J. Pharmacol.* 170, 278–292. doi: 10.1111/bph.12249

McLeod, G., Munishankar, B., Macgregor, H., and Murphy, D. J. (2010). Maternal haemodynamics at elective caesarean section: a randomised comparison of oxytocin 5-unit bolus and placebo infusion with oxytocin 5-unit bolus and 30-unit infusion. *Int. J. Obstet. Anesth.* 19, 155–160. doi: 10.1016/j.ijoa.2009.08.005

Menaouar, A., Florian, M., Wang, D., Danalache, B., Jankowski, M., and Gutkowska, J. (2014). Anti-hypertrophic effects of oxytocin in rat ventricular myocytes. *Int. J. Cardiol.* 175, 38–49. doi: 10.1016/j.ijcard.2014.04.174

Meng, L. B., Shan, M. J., Yu, Z. M., Lv, J., Qi, R. M., Guo, P., et al. (2019). Chronic stress: a crucial promoter of cell apoptosis in atherosclerosis. *J. Int. Med. Res.* doi: 10.1177/0300060518814606 [Epub ahead of print].

Merz, T., Lukaschewski, B., Wigger, D., Rupprecht, A., Wepler, M., Groger, M., et al. (2018). Interaction of the hydrogen sulfide system with the oxytocin system in the injured mouse heart. *Intensive Care Med. Exp.* 6:41.

Miller, M. A., Bershad, A., King, A. C., Lee, R., and De Wit, H. (2016). Intranasal oxytocin dampens cue-elicited cigarette craving in daily smokers: a pilot study. *Behav. Pharmacol.* 27, 697–703. doi: 10.1097/fbp.0000000000000260

Moghimian, M., Faghihi, M., Karimian, S. M., and Imani, A. (2012). The effect of acute stress exposure on ischemia and reperfusion injury in rat heart: role of oxytocin. *Stress* 15, 385–392. doi: 10.3109/10253890.2011.630436

Moghimian, M., Faghihi, M., Karimian, S. M., Imani, A., Houshmand, F., and Azizi, Y. (2013). Role of central oxytocin in stress-induced cardioprotection in ischemic-reperfused heart model. *J. Cardiol.* 61, 79–86. doi: 10.1016/j.jjcc.2012.08.021

Montgomery, T. M., Pendleton, E. L., and Smith, J. E. (2018). Physiological mechanisms mediating patterns of reproductive suppression and alloparental care in cooperatively breeding carnivores. *Physiol. Behav.* 193(Pt A), 167–178.

Mori, R., Nardin, J. M., Yamamoto, N., Carroli, G., and Weeks, A. (2012). Umbilical vein injection for the routine management of third stage of labour. *Cochrane Database Syst. Rev.* 14:CD006176.

Morishita, Y., Arima, H., Hiroi, M., Hayashi, M., Hagiwara, D., Asai, N., et al. (2011). Poly(A) tail length of neurohypophysial hormones is shortened under endoplasmic reticulum stress. *Endocrinology* 152, 4846–4855. doi: 10.1210/en.2011-1415

Mukaddam-Daher, S., Yin, Y. L., Roy, J., Gutkowska, J., and Cardinal, R. (2001). Negative inotropic and chronotropic effects of oxytocin. *Hypertension* 38, 292–296. doi: 10.1161/01.hyp.38.2.292

Mullenix, P. S., Andersen, C. A., and Starnes, B. W. (2005). Atherosclerosis as inflammation. *Ann. Vasc. Surg.* 19, 130–138.

Natochin, Y. V., Golosova, D. V., and Shakhmatova, E. I. (2018). A new functional role of oxytocin: participation in osmoregulation. *Dokl. Biol. Sci.* 479, 60–63. doi: 10.1134/s0012496618020096

Nielsen, S. H., Magid, E., Spannow, J., Christensen, S., Lam, H. R., and Petersen, J. S. (1997). Renal function after myocardial infarction and cardiac arrest in rats: role of ANP-induced albuminuria? *Acta Physiol. Scand.* 160, 301–310. doi: 10.1046/j.1365-201x.1997.00162.x

Niemann, B., Rohrbach, S., Miller, M. R., Newby, D. E., Fuster, V., and Kovacic, J. C. (2017). Oxidative stress and cardiovascular risk: obesity, diabetes, smoking, and pollution: part 3 of a 3-part series. *J. Am. Coll. Cardiol.* 70, 230–251. doi: 10.1016/j.jacc.2017.05.043

Noiseux, N., Borie, M., Desnoyers, A., Menaouar, A., Stevens, L. M., Mansour, S., et al. (2012). Preconditioning of stem cells by oxytocin to improve their therapeutic potential. *Endocrinology* 153, 5361–5372. doi: 10.1210/en.2012-1402

Noller, C. M., Szeto, A., Mendez, A. J., Llabre, M. M., Gonzales, J. A., Rossetti, M. A., et al. (2013). The influence of social environment on endocrine, cardiovascular and tissue responses in the rabbit. *Int. J. Psychophysiol.* 88, 282–288. doi: 10.1016/j.ijpsycho.2012.04.008

Okabe, T., Goren, H. J., Lederis, K., and Hollenberg, M. D. (1985). Oxytocin and glucose oxidation in the rat uterus. *Regul. Pept.* 10, 269–279. doi: 10.1016/0167-0115(85)90039-4

Olszewski, P. K., Klockars, A., Schioth, H. B., and Levine, A. S. (2010). Oxytocin as feeding inhibitor: maintaining homeostasis in consummatory behavior. *Pharmacol. Biochem. Behav.* 97, 47–54. doi: 10.1016/j.pbb.2010.05.026

Padol, A. R., Sukumaran, S. V., Sadam, A., Kesavan, M., Arunvikram, K., Verma, A. D., et al. (2017). Hypercholesterolemia impairs oxytocin-induced uterine contractility in late pregnant mouse. *Reproduction* 153, 565–576. doi: 10.1530/rep-16-0446

Paquin, J., Danalache, B. A., Jankowski, M., Mccann, S. M., and Gutkowska, J. (2002). Oxytocin induces differentiation of P19 embryonic stem cells to cardiomyocytes. *Proc. Natl. Acad. Sci. U.S.A.* 99, 9550–9555. doi: 10.1073/pnas.152302499

Patel, N., and Radeos, M. (2018). Severe delayed postpartum hemorrhage after cesarean section. *J. Emerg. Med.* 55, 408–410.

Patrick, R. P., and Ames, B. N. (2014). Vitamin D hormone regulates serotonin synthesis. Part 1: relevance for autism. *FASEB J.* 28, 2398–2413. doi: 10.1096/fj.13-246546

Peller, M., Lodzinski, P., Ozieranski, K., Tyminska, A., Balsam, P., Kajurek, K., et al. (2017). The influence of the atrial fibrillation episode duration on the endothelial function in patients treated with pulmonary veins isolation. *Adv. Clin. Exp. Med.* 26, 109–113. doi: 10.17219/acem/66995

Peters, S. T., Bowen, M. T., Bohrer, K., Mcgregor, I. S., and Neumann, I. D. (2017). Oxytocin inhibits ethanol consumption and ethanol-induced dopamine release in the nucleus accumbens. *Addict. Biol.* 22, 702–711. doi: 10.1111/adb.12362

Petersson, M., and Uvnas-Moberg, K. (2008). Postnatal oxytocin treatment of spontaneously hypertensive male rats decreases blood pressure and body weight in adulthood. *Neurosci. Lett.* 440, 166–169. doi: 10.1016/j.neulet.2008.05.091

Petty, M. A., Lang, R. E., Unger, T., and Ganten, D. (1985). The cardiovascular effects of oxytocin in conscious male rats. *Eur. J. Pharmacol.* 112, 203–210. doi: 10.1016/0014-2999(85)90497-2

Phie, J., Haleagrahara, N., Newton, P., Constantinoiu, C., Sarnyai, Z., Chilton, L., et al. (2015). Prolonged subcutaneous administration of oxytocin accelerates angiotensin II-induced hypertension and renal damage in male rats. *PLoS One* 10:e0138048. doi: 10.1371/journal.pone.0138048

Pimentel, V. M., Arabkhazaeli, M., Moon, J. Y., Wang, A., Kapedani, A., Bernstein, P. S., et al. (2018). Induction of labor using one dose versus multiple doses of misoprostol: a randomized controlled trial. *Am. J. Obstet. Gynecol.* 218, 614.e1–614.e8.

Plante, E., Menaouar, A., Danalache, B. A., Yip, D., Broderick, T. L., Chiasson, J. L., et al. (2015). Oxytocin treatment prevents the cardiomyopathy observed in obese diabetic male db/db mice. *Endocrinology* 156, 1416–1428. doi: 10.1210/en.2014-1718

Pohl, O., Chollet, A., Kim, S. H., Riaposova, L., Spezia, F., Gervais, F., et al. (2018). OBE022, an oral and selective prostaglandin F2alpha receptor antagonist as an effective and safe modality for the treatment of preterm labor. *J. Pharmacol. Exp. Ther.* 366, 349–364. doi: 10.1124/jpet.118.247668

Polshekan, M., Jamialahmadi, K., Khori, V., Alizadeh, A. M., Saeidi, M., Ghayour-Mobarhan, M., et al. (2016). RISK pathway is involved in oxytocin postconditioning in isolated rat heart. *Peptides* 86, 55–62. doi: 10.1016/j.peptides.2016.10.001

Polshekan, M., Khori, V., Alizadeh, A. M., Ghayour-Mobarhan, M., Saeidi, M., Jand, Y., et al. (2019). The SAFE pathway is involved in the postconditioning mechanism of oxytocin in isolated rat heart. *Peptides* 111, 142–151. doi: 10.1016/j.peptides.2018.04.002

Price, C. L., and Knight, S. C. (2007). Advanced glycation: a novel outlook on atherosclerosis. *Curr. Pharm. Des.* 13, 3681–3687. doi: 10.2174/138161207783018608

Qian, W., Zhu, T., Tang, B., Yu, S., Hu, H., Sun, W., et al. (2014). Decreased circulating levels of oxytocin in obesity and newly diagnosed type 2 diabetic patients. *J. Clin. Endocrinol. Metab.* 99, 4683–4689. doi: 10.1210/jc.2014-2206

Qiu, Z., Zhang, W., Fan, F., Li, H., Wu, C., Ye, Y., et al. (2012). Rosuvastatin-attenuated heart failure in aged spontaneously hypertensive rats via PKCalpha/beta2 signal pathway. *J. Cell. Mol. Med.* 16, 3052–3061. doi: 10.1111/j.1582-4934.2012.01632.x

Quinones-Jenab, V., Jenab, S., Ogawa, S., Adan, R. A., Burbach, J. P., and Pfaff, D. W. (1997). Effects of estrogen on oxytocin receptor messenger ribonucleic acid expression in the uterus, pituitary, and forebrain of the female rat. *Neuroendocrinology* 65, 9–17. doi: 10.1159/000127160

Quintana, D. S., Dieset, I., Elvsashagen, T., Westlye, L. T., and Andreassen, O. A. (2017). Oxytocin system dysfunction as a common mechanism underlying metabolic syndrome and psychiatric symptoms in schizophrenia and bipolar disorders. *Front. Neuroendocrinol.* 45, 1–10. doi: 10.1016/j.yfrne.2016.12.004

Quintana, D. S., Kemp, A. H., Alvares, G. A., and Guastella, A. J. (2013). A role for autonomic cardiac control in the effects of oxytocin on social behavior and psychiatric illness. *Front. Neurosci.* 7:48. doi: 10.3389/fnins.2013.00048

Rabow, S., Hjorth, U., Schonbeck, S., and Olofsson, P. (2018). Effects of oxytocin and anaesthesia on vascular tone in pregnant women: a randomised double-blind placebo-controlled study using non-invasive pulse wave analysis. *BMC Pregnancy Childbirth* 18:453. doi: 10.1186/s12884-018-2029-1

Rahman, M. S., and Woollard, K. (2017). Atherosclerosis. *Adv. Exp. Med. Biol.* 1003, 121–144.

Raphael, J., Gozal, Y., Navot, N., and Zuo, Z. (2015). Activation of adenosine triphosphate-regulated potassium channels during reperfusion restores isoflurane postconditioning-induced cardiac protection in acutely hyperglycemic rabbits. *Anesthesiology* 122, 1299–1311. doi: 10.1097/aln.0000000000000648

Rapsomaniki, E., Timmis, A., George, J., Pujades-Rodriguez, M., Shah, A. D., Denaxas, S., et al. (2014). Blood pressure and incidence of twelve cardiovascular diseases: lifetime risks, healthy life-years lost, and age-specific associations in 1.25 million people. *Lancet* 383, 1899–1911. doi: 10.1016/s0140-6736(14)60685-1

Reed, S. C., Haney, M., Manubay, J., Campagna, B. R., Reed, B., Foltin, R. W., et al. (2019). Sex differences in stress reactivity after intranasal oxytocin in recreational cannabis users. *Pharmacol. Biochem. Behav.* 176, 72–82. doi: 10.1016/j.pbb.2018.11.008

Rettori, E., De Laurentiis, A., Dees, W. L., Endruhn, A., and Rettori, V. (2014). Host neuro- immuno-endocrine responses in periodontal disease. *Curr. Pharm. Des.* 20, 4749–4759. doi: 10.2174/1381612820666140130204043

Rimoldi, V., Reversi, A., Taverna, E., Rosa, P., Francolini, M., Cassoni, P., et al. (2003). Oxytocin receptor elicits different EGFR/MAPK activation patterns depending on its localization in caveolin-1 enriched domains. *Oncogene* 22, 6054–6060. doi: 10.1038/sj.onc.1206612

Rodriguez-Iturbe, B., Pons, H., and Johnson, R. J. (2017). Role of the immune system in hypertension. *Physiol. Rev.* 97, 1127–1164.

Roy, R. K., Augustine, R. A., Brown, C. H., and Schwenke, D. O. (2018). Activation of oxytocin neurons in the paraventricular nucleus drives cardiac sympathetic nerve activation following myocardial infarction in rats. *Commun. Biol.* 1:160.

Saccone, G., Ciardulli, A., Baxter, J. K., Quinones, J. N., Diven, L. C., Pinar, B., et al. (2017). Discontinuing oxytocin infusion in the active phase of labor: a systematic review and meta-analysis. *Obstet. Gynecol.* 130, 1090–1096. doi: 10.1097/aog.0000000000002325

Sack, M., Spieler, D., Wizelman, L., Epple, G., Stich, J., Zaba, M., et al. (2017). Intranasal oxytocin reduces provoked symptoms in female patients with posttraumatic stress disorder despite exerting sympathomimetic and positive chronotropic effects in a randomized controlled trial. *BMC Med.* 15:40. doi: 10.1186/s12916-017-0801-

Sanin, V., Pfetsch, V., and Koenig, W. (2017). Dyslipidemias and cardiovascular prevention: tailoring treatment according to lipid phenotype. *Curr. Cardiol. Rep.* 19:61.

Schinzari, F., Tesauro, M., and Cardillo, C. (2017). Endothelial and perivascular adipose tissue abnormalities in obesity-related vascular dysfunction: novel targets for treatment. *J. Cardiovasc. Pharmacol.* 69, 360–368.

Schuh, A. K., Sheybani, B., Jortzik, E., Niemann, B., Wilhelm, J., Boening, A., et al. (2017). Redox status of patients before cardiac surgery. *Redox Rep.* 23, 83–93. doi: 10.1080/13510002.2017.1418620

Seckl, J. R., Johnson, M., Shakespear, C., and Lightman, S. L. (1988). Endogenous opioids inhibit oxytocin release during nicotine-stimulated secretion of vasopressin in man. *Clin. Endocrinol.* 28, 509–514. doi: 10.1111/j.1365-2265.1988.tb03685.x

Seidl, M. D., Stein, J., Hamer, S., Pluteanu, F., Scholz, B., Wardelmann, E., et al. (2017). Characterization of the genetic program linked to the development of atrial fibrillation in CREM-IbDeltaC-X mice. *Circ. Arrhythm. Electrophysiol.* 10:e005075.

Shioi, T., Kang, P. M., Douglas, P. S., Hampe, J., Yballe, C. M., Lawitts, J., et al. (2000). The conserved phosphoinositide 3-kinase pathway determines heart size in mice. *EMBO J.* 19, 2537–2548. doi: 10.1093/emboj/19.11.2537

Soares, T. J., Coimbra, T. M., Martins, A. R., Pereira, A. G., Carnio, E. C., Branco, L. G., et al. (1999). Atrial natriuretic peptide and oxytocin induce natriuresis by release of cGMP. *Proc. Natl. Acad. Sci. U.S.A.* 96, 278–283. doi: 10.1073/pnas.96.1.278

Song, Z., and Albers, H. E. (2017). Cross-talk among oxytocin and arginine-vasopressin receptors: relevance for basic and clinical studies of the brain and periphery. *Front. Neuroendocrinol.* 51, 14–24.

Stevenson, J. R., Wenner, S. M., Freestone, D. M., Romaine, C. C., Parian, M. C., Christian, S. M., et al. (2017). Oxytocin reduces alcohol consumption in prairie voles. *Physiol. Behav.* 179, 411–421. doi: 10.1016/j.physbeh.2017.07.021

Sumi, S., Kobayashi, H., Yasuda, S., Iwasa, M., Yamaki, T., Yamada, Y., et al. (2010). Postconditioning effect of granulocyte colony-stimulating factor is mediated through activation of risk pathway and opening of the mitochondrial KATP channels. *Am. J. Physiol. Heart Circ. Physiol.* 299, H1174–H1182.

Sun, J., Lu, Y., Huang, Y., and Wugeti, N. (2015). Unilateral vagus nerve stimulation improves ventricular autonomic nerve distribution and functional imbalance in a canine heart failure model. *Int. J. Clin. Exp. Med.* 8, 9334–9340.

Sunaga, D., Tanno, M., Kuno, A., Ishikawa, S., Ogasawara, M., Yano, T., et al. (2014). Accelerated recovery of mitochondrial membrane potential by GSK-3beta inactivation affords cardiomyocytes protection from oxidant-induced necrosis. *PLoS One* 9:e112529. doi: 10.1371/journal.pone.0112529

Suva, J., Caisova, D., and Stajner, A. (1980). Modification of fat and carbohydrate metabolism by neurohypophyseal hormones. III. Effect of oxytocin on non-esterified fatty acid, glucose, triglyceride and cholesterol levels in rat serum. *Endokrinologie* 76, 333–339.

Svanstrom, M. C., Biber, B., Hanes, M., Johansson, G., Naslund, U., and Balfors, E. M. (2008). Signs of myocardial ischaemia after injection of oxytocin: a randomized double-blind comparison of oxytocin and methylergometrine during Caesarean section. *Br. J. Anaesth.* 100, 683–689. doi: 10.1093/bja/aen071

Swanson, L. W., and Hartman, B. K. (1980). Biochemical specificity in central pathways related to peripheral and intracerebral homeostatic functions. *Neurosci. Lett.* 16, 55–60. doi: 10.1016/0304-3940(80)90100-7

Szeto, A., Rossetti, M. A., Mendez, A. J., Noller, C. M., Herderick, E. E., Gonzales, J. A., et al. (2013). Oxytocin administration attenuates atherosclerosis and inflammation in Watanabe Heritable Hyperlipidemic rabbits. *Psychoneuroendocrinology* 38, 685–693. doi: 10.1016/j.psyneuen.2012.08.009

Takayanagi, Y., Kasahara, Y., Onaka, T., Takahashi, N., Kawada, T., and Nishimori, K. (2008). Oxytocin receptor-deficient mice developed late-onset obesity. *Neuroreport* 19, 951–955. doi: 10.1097/wnr.0b013e3283021ca9

Tanwar, V., Gorr, M. W., Velten, M., Eichenseer, C. M., Long, V. P. III, Bonilla, I. M., et al. (2017). In utero particulate matter exposure produces heart failure, electrical remodeling, and epigenetic changes at adulthood. *J. Am. Heart Assoc.* 6:e005796.

Tracy, L. M., Gibson, S. J., Labuschagne, I., Georgiou-Karistianis, N., and Giummarra, M. J. (2018). Intranasal oxytocin reduces heart rate variability during a mental arithmetic task: a randomised, double-blind, placebo-controlled cross-over study. *Prog. Neuropsychopharmacol. Biol. Psychiatry* 81, 408–415. doi: 10.1016/j.pnpbp.2017.08.016

Vardavas, C. I., and Panagiotakos, D. B. (2009). The causal relationship between passive smoking and inflammation on the development of cardiovascular disease: a review of the evidence. *Inflamm. Allergy Drug Targets* 8, 328–333. doi: 10.2174/187152811090805032 8

Vargas-Martinez, F., Schanler, R. J., Abrams, S. A., Hawthorne, K. M., Landers, S., Guzman-Barcenas, J., et al. (2017). Oxytocin, a main breastfeeding hormone, prevents hypertension acquired in utero: a therapeutics preview. *Biochim. Biophys. Acta* 1861, 3071–3084. doi: 10.1016/j.bbagen.2016.09.020

Veening, J. G., and Olivier, B. (2013). Intranasal administration of oxytocin: behavioral and clinical effects, a review. *Neurosci. Biobehav. Rev.* 37, 1445–1465. doi: 10.1016/j.neubiorev.2013.04.012

Viero, C., Shibuya, I., Kitamura, N., Verkhratsky, A., Fujihara, H., Katoh, A., et al. (2010). REVIEW: oxytocin: crossing the bridge between basic science

and pharmacotherapy. *CNS Neurosci. Ther.* 16, e138–e156. doi: 10.1111/j.1755-5949.2010.00185.x

Vilahur, G., Casani, L., Pena, E., Juan-Babot, O., Mendieta, G., Crespo, J., et al. (2014). HMG-CoA reductase inhibition prior reperfusion improves reparative fibrosis post-myocardial infarction in a preclinical experimental model. *Int. J. Cardiol.* 175, 528–538. doi: 10.1016/j.ijcard.2014.06.040

Wang, C., Fujita, T., and Kumamoto, E. (2018). Orexin B modulates spontaneous excitatory and inhibitory transmission in lamina II neurons of adult rat spinal cord. *Neuroscience* 383, 114–128. doi: 10.1016/j.neuroscience.2018.04.048

Wang, S. C., Meng, D., Yang, H., Wang, X., Jia, S., Wang, P., Wang, Y.-F., et al. (2018). Pathological basis of cardiac arrhythmias: vicious cycle of immune-metabolic dysregulation. *Cardiovasc. Disord. Med.* 3, 1–7.

Wang, F., Yang, J., Sun, J., Dong, Y., Zhao, H., Shi, H., et al. (2015). Testosterone replacement attenuates mitochondrial damage in a rat model of myocardial infarction. *J. Endocrinol.* 225, 101–111. doi: 10.1530/joe-14-0638

Wang, P., Yang, H. P., Tian, S., Wang, L., Wang, S. C., Zhang, F., et al. (2015). Oxytocin-secreting system: a major part of the neuroendocrine center regulating immunologic activity. *J. Neuroimmunol.* 289, 152–161. doi: 10.1016/j.jneuroim.2015.11.001

Wang, P., and DeFea, K. A. (2006). Protease-activated receptor-2 simultaneously directs beta-arrestin-1-dependent inhibition and Galphaq-dependent activation of phosphatidylinositol 3-kinase. *Biochemistry* 45, 9374–9385. doi: 10.1021/bi0602617

Wang, P., Jiang, Y., Wang, Y., Shyy, J. Y., and Defea, K. A. (2010). Beta-arrestin inhibits CAMKKbeta-dependent AMPK activation downstream of protease-activated-receptor-2. *BMC Biochem.* 11:36. doi: 10.1186/1471-2091-11-36

Wang, S., Binder, P., Fang, Q., Wang, Z., Xiao, W., Liu, W., et al. (2017). Endoplasmic reticulum stress in the heart: insights into mechanisms and drug targets. *Br. J. Pharmacol.* 175, 1293–1304.

Wang, Y.-F. (2016). Center role of the oxytocin-secreting system in neuroendocrine-immune network revisited. *J. Clin. Exp. Neuroimmunol.* 1:102.

Wang, Y. F., and Hatton, G. I. (2006). Mechanisms underlying oxytocin-induced excitation of supraoptic neurons: prostaglandin mediation of actin polymerization. *J. Neurophysiol.* 95, 3933–3947. doi: 10.1152/jn.01267.2005

Wang, Y. F., and Hatton, G. I. (2007a). Dominant role of betagamma subunits of G-proteins in oxytocin-evoked burst firing. *J. Neurosci.* 27, 1902–1912. doi: 10.1523/jneurosci.5346-06.2007

Wang, Y. F., and Hatton, G. I. (2007b). Interaction of extracellular signal-regulated protein kinase 1/2 with actin cytoskeleton in supraoptic oxytocin neurons and astrocytes: role in burst firing. *J. Neurosci.* 27, 13822–13834. doi: 10.1523/jneurosci.4119-07.2007

Watanabe, S., Wei, F. Y., Matsunaga, T., Matsunaga, N., Kaitsuka, T., and Tomizawa, K. (2016). Oxytocin protects against stress-induced cell death in murine pancreatic beta-cells. *Sci. Rep.* 6:25185.

Weissman, A., Tobia, R. S., Burke, Y. Z., Maxymovski, O., and Drugan, A. (2017). The effects of oxytocin and atosiban on the modulation of heart rate in pregnant women. *J. Matern. Fetal Neonatal Med.* 30, 329–333. doi: 10.3109/14767058.2016.1172564

Whayne, T. F. Jr., and Saha, S. P. (2019). Genetic risk, adherence to a healthy lifestyle, and ischemic heart disease. *Curr. Cardiol. Rep.* 21:1.

Wronska, D., Kania, B. F., and Blachuta, M. (2017). Direct effect of hypothalamic neuropeptides on the release of catecholamines by adrenal medulla in sheep - study ex vivo. *Pol. J. Vet. Sci.* 20, 339–346. doi: 10.1515/pjvs-2017-0041

Wsol, A., Cudnoch-Je Drzejewska, A., Szczepanska-Sadowska, E., Kowalewski, S., and Dobruch, J. (2009). Central oxytocin modulation of acute stress-induced cardiovascular responses after myocardial infarction in the rat. *Stress* 12, 517–525. doi: 10.3109/10253890802687688

Wsol, A., Kasarello, K., Kuch, M., Gala, K., and Cudnoch-Jedrzejewska, A. (2016). Increased activity of the intracardiac oxytocinergic system in the development of postinfarction heart failure. *Biomed Res. Int.* 2016:3652068.

Wsol, A., Szczepanska-Sadowska, E., Kowalewski, S., Puchalska, L., and Cudnoch-Jedrzejewska, A. (2014). Oxytocin differently regulates pressor responses to stress in WKY and SHR rats: the role of central oxytocin and V1a receptors. *Stress* 17, 117–125. doi: 10.3109/10253890.2013.872620

Wu, S., Lu, Q., Wang, Q., Ding, Y., Ma, Z., Mao, X., et al. (2017). Binding of FUN14 domain containing 1 with inositol 1,4,5-trisphosphate receptor in mitochondria-associated endoplasmic reticulum membranes maintains mitochondrial dynamics and function in hearts in vivo. *Circulation* 136, 2248–2266. doi: 10.1161/circulationaha.117.030235

Xu, J. Q., Murphy, S. L., Kochanek, K. D., and Bastian, B. A. (2016). Deaths: final data for 2013. *Natl. Vital Stat. Rep.* 64, 1–119.

Yang, F., Yu, X., Li, T., Wu, J., Zhao, Y., Liu, J., et al. (2017). Exogenous H2S regulates endoplasmic reticulum-mitochondria cross-talk to inhibit apoptotic pathways in STZ-induced type I diabetes. *Am. J. Physiol. Endocrinol. Metab.* 312, E190–E203.

Yang, J., Cao, R. Y., Gao, R., Mi, Q., Dai, Q., and Zhu, F. (2017). Physical exercise is a potential "Medicine" for atherosclerosis. *Adv. Exp. Med. Biol.* 999, 269–286. doi: 10.1007/978-981-10-4307-9_15

Yang, H. P., Wang, L., Han, L., and Wang, S. C. (2013). Nonsocial functions of hypothalamic oxytocin. *ISRN Neurosci.* 2013:179272.

Yano, T., Shimoshige, S., Miki, T., Tanno, M., Mochizuki, A., Fujito, T., et al. (2016). Clinical impact of myocardial mTORC1 activation in nonischemic dilated cardiomyopathy. *J. Mol. Cell. Cardiol.* 91, 6–9. doi: 10.1016/j.yjmcc.2015.12.022

Ybarra, N., Del Castillo, J. R., and Troncy, E. (2011). Involvement of the nitric oxide-soluble guanylyl cyclase pathway in the oxytocin-mediated differentiation of porcine bone marrow stem cells into cardiomyocytes. *Nitric Oxide* 24, 25–33. doi: 10.1016/j.niox.2010.09.008

Yee, J. R., Kenkel, W. M., Frijling, J. L., Dodhia, S., Onishi, K. G., Tovar, S., et al. (2016). Oxytocin promotes functional coupling between paraventricular nucleus and both sympathetic and parasympathetic cardioregulatory nuclei. *Horm. Behav.* 80, 82–91. doi: 10.1016/j.yhbeh.2016.01.010

Ying, L., Becard, M., Lyell, D., Han, X., Shortliffe, L., Husted, C. I., et al. (2015). The transient receptor potential vanilloid 4 channel modulates uterine tone during pregnancy. *Sci. Transl. Med.* 7:319ra204. doi: 10.1126/scitranslmed.aad0376

You, X., Chen, Z., Zhao, H., Xu, C., Liu, W., Sun, Q., et al. (2017). Endogenous hydrogen sulfide contributes to uterine quiescence during pregnancy. *Reproduction* 153, 535–543. doi: 10.1530/rep-16-0549

Yudkin, J. S. (2003). Adipose tissue, insulin action and vascular disease: inflammatory signals. *Int. J. Obes. Relat. Metab. Disord.* 27(Suppl. 3), S25–S28.

Yue, C., and Sanborn, B. M. (2001). KN-93 inhibition of G protein signaling is independent of the ability of Ca2+/calmodulin-dependent protein kinase II to phosphorylate phospholipase Cbeta3 on 537-Ser. *Mol. Cell. Endocrinol.* 175, 149–156. doi: 10.1016/s0303-7207(01)00383-5

Zafirovic, S., Obradovic, M., Sudar-Milovanovic, E., Jovanovic, A., Stanimirovic, J., Stewart, A. J., et al. (2017). 17beta-Estradiol protects against the effects of a high fat diet on cardiac glucose, lipid and nitric oxide metabolism in rats. *Mol. Cell. Endocrinol.* 446, 12–20. doi: 10.1016/j.mce.2017.02.001

Zhang, H., Wu, C., Chen, Q., Chen, X., Xu, Z., Wu, J., et al. (2013). Treatment of obesity and diabetes using oxytocin or analogs in patients and mouse models. *PLoS One* 8:e61477. doi: 10.1371/journal.pone.0061477

Zhang, H. M., Qiu, Y., Ye, X., Hemida, M. G., Hanson, P., and Yang, D. (2014). P58(IPK) inhibits coxsackievirus-induced apoptosis via the PI3K/Akt pathway requiring activation of ATF6a and subsequent upregulation of mitofusin 2. *Cell. Microbiol.* 16, 411–424. doi: 10.1111/cmi.12229

Zhang, L., Guo, H., Yuan, F., Hong, Z. C., Tian, Y. M., Zhang, X. J., et al. (2017). Limb remote ischemia per-conditioning protects the heart against ischemia-reperfusion injury through the opioid system in rats. *Can. J. Physiol. Pharmacol.* 96, 68–75. doi: 10.1139/cjpp-2016-0585

Zhong, M., Parish, B., Murtazina, D. A., Ku, C. Y., and Sanborn, B. M. (2007). Amino acids in the COOH-terminal region of the oxytocin receptor third intracellular domain are important for receptor function. *Am. J. Physiol. Endocrinol. Metab.* 292, E977–E984.

Zhong, M., Yang, M., and Sanborn, B. M. (2003). Extracellular signal-regulated kinase 1/2 activation by myometrial oxytocin receptor involves Galpha(q)Gbetagamma and epidermal growth factor receptor tyrosine kinase activation. *Endocrinology* 144, 2947–2956. doi: 10.1210/en.2002-221039

Zhou, M., Bao, Y., Li, H., Pan, Y., Shu, L., Xia, Z., et al. (2015). Deficiency of adipocyte fatty-acid-binding protein alleviates

myocardial ischaemia/reperfusion injury and diabetes-induced cardiac dysfunction. *Clin. Sci.* 129, 547–559. doi: 10.1042/cs20150073

Zhu, J., Wang, H., Zhang, X., and Xie, Y. (2017). Regulation of angiogenic behaviors by oxytocin receptor through Gli1-indcued transcription of HIF-1alpha in human umbilical vein endothelial cells. *Biomed. Pharmacother.* 90, 928–934. doi: 10.1016/j.biopha.2017.04.021

Zimmerman, E. A., Nilaver, G., Hou-Yu, A., and Silverman, A. J. (1984). Vasopressinergic and oxytocinergic pathways in the central nervous system. *Fed. Proc.* 43, 91–96.

Conflict of Interest Statement: The authors declare that the research was conducted in the absence of any commercial or financial relationships that could be construed as a potential conflict of interest.

frontiers in Neuroscience

ORIGINAL RESEARCH
published: 29 May 2019
doi: 10.3389/fnins.2019.00529

Primary Age-Related Tauopathy in Human Subcortical Nuclei

Keqing Zhu[1,2], Xin Wang[1,2], Bing Sun[1], Juanli Wu[1], Hui Lu[1], Xiaoling Zhang[1], Huazheng Liang[3,4], Dandan Zhang[2] and Chong Liu[1,2]*

[1] China Brain Bank and Department of Neurology in Second Affiliated Hospital, Key Laboratory of Medical Neurobiology of Zhejiang Province, and Department of Neurobiology, Zhejiang University School of Medicine, Hangzhou, China, [2] Department of Pathology, Zhejiang University School of Medicine, Hangzhou, China, [3] Brain Structure and Function, Neuroscience Research Australia, Randwick, NSW, Australia, [4] Department of Neurology, Shanghai Fourth People's Hospital, Tongji University, Shanghai, China

The present study aimed to determine the spatial distribution patterns of hyperphosphorylated tau-immunoreactive cells in subcortical nuclei of post-mortem human brain with primary age-related tauopathy (PART). Subcortical tauopathy has important pathological and clinical implications. Expression of tau was examined in different subcortical regions of definite PART cases with a Braak neurofibrillary tangle stage >0 and ≤IV, and with a Thal phase 0 (no beta-amyloid present). Post-mortem brain tissue of PART was studied using immunohistochemistry and subsequent semi-quantitative assessment with Braak NFT stage -matched pre-Alzheimer's disease (AD) and AD cases as a control. Expression of tau was frequently found in subcortical nuclei including the substantia nigra, inferior colliculus, locus coeruleus, medulla oblongata in the brainstem, the caudate, putamen, nucleus globus pallidus in the striatum, the hypothalamus, thalamus, subthalamus in the diencephalon, and the cervical spinal cord in both PART and AD, but not in the dentate nucleus of the cerebellum. A positive correlation was found between the Braak NFT stage and the tau distribution (qualitative)/tau density (quantitative) in PART and AD. Brainstem nuclei were commonly involved in early PART with NFT Braak stage I/II, there was no preference among the substantia nigra, inferior colliculus, locus caeruleus and medulla oblongata. The prevalence and severity of tau pathology in subcortical nuclei of PART and AD were positively correlated with NFT Braak stage, suggesting that these nuclei were increasingly involved as PART and AD progressed. Subcortical nuclei were likely the sites initially affected by aging associated tau pathology, especially the brainstem nuclei including the substantia nigra, inferior colliculus, locus caeruleus and medulla oblongata.

Keywords: primary age-related tauopathy, subcortical nuclei, Alzheimer's disease, neurofibrillary tangle, brainstem, brain bank

OPEN ACCESS

Edited by:
Lee E. Eiden,
National Institutes of Health (NIH),
United States

Reviewed by:
Erwin Lemche,
King's College London,
United Kingdom
Ben Nephew,
Worcester Polytechnic Institute,
United States

****Correspondence:***
Keqing Zhu
zhukeqing@zju.edu.cn

Specialty section:
This article was submitted to Neuroendocrine Science, a section of the journal Frontiers in Neuroscience

Received: *20 September 2018*
Accepted: *07 May 2019*
Published: *29 May 2019*

Citation:
Zhu K, Wang X, Sun B, Wu J, Lu H, Zhang X, Liang H, Zhang D and Liu C (2019) Primary Age-Related Tauopathy in Human Subcortical Nuclei. Front. Neurosci. 13:529. doi: 10.3389/fnins.2019.00529

INTRODUCTION

The stepwise progression of tau pathology in Alzheimer's disease (AD) is reflected by NFT Braak stages and this pathology is generally assumed to begin from the *trans*-entorhinal region (Braak et al., 2006). However, it has been shown that some subcortical nuclei are involved early, even at NFT Braak stage I or 0 (Braak et al., 2011; Attems et al., 2012b; Stratmann et al., 2016).

Specifically, it has been shown recently that tau pathology is frequently seen in locus caeruleus (LC), suggesting that AD-associated tau pathology may begin from LC rather than from the *trans*-entorhinal region (Braak and Del Tredici, 2011; Braak et al., 2011). It is noted that LC was recently considered as the pretangle stage b before Braak stage I (Braak et al., 2011; Braak and Del Tredici, 2015), whereas the subcortical nuclei are in general not considered in the basic scheme of Braak staging. In fact, a number of other subcortical nuclei were reported to be involved in AD, including the hypothalamus, thalamus, and the substantia nigra (SN) (Mattila et al., 2002; Arendt et al., 2015; Theofilas et al., 2015). The studies have shown that these nuclei were involved early in the progression of the disease and the lesions had important clinical consequences (Rüb et al., 2017). Further studies are thus needed to determine how early and consistently these nuclei are affected (Braak and Del Tredici, 2012).

Primary age-related tauopathy (PART) is characterized neuropathologically by the presence of AD-type neurofibrillary changes without, or with few Aβ plaques. Definite PART has recently been defined by the absence of Aβ plaques (Crary et al., 2014). Whether PART is a subtype of early AD, or an individual aging related change, is still controversial (Duyckaerts et al., 2015; Jellinger et al., 2015). Due to the absence of Aβ plaques, PART shows a pure tauopathy. This is helpful for seeking the starting point of NFT "seeding" and the NFT progression mechanism (Crary, 2016). Subcortical tauopathy has been described in AD in the medulla oblongata (MO), SN, LC, and some other subcortical nuclei (Arendt et al., 2015). Tauopathy was also reported in the aging brain (Wharton et al., 2016), but this phenomenon has not been comprehensively described in PART. To address this issue, we examined tau pathology in the subcortical nuclei of definite PART cases that met the pathological criteria, Braak NFT stage-matched pre-AD, and AD cases. We found that tauopathy was frequently observed in the subcortical nuclei of PART, pre-AD, and AD, including SN, colliculus inferior, LC, MO in the brainstem; the caudatum, putamen, globus pallidus (GP) in the striatum; the hypothalamus, thalamus, subthalamus in the diencephalon. The severity (distribution and density) of tau pathology in these subcortical nuclei was significantly correlated with Braak stages and tauopathy in nuclei of the brainstem, striatum and diencephalon has important pathological and clinical consequences (Theofilas et al., 2015).

MATERIALS AND METHODS

Materials

Two independent groups, including 16 neuropathologically confirmed definite PART brains, 7 AD (Braak NFT stage ≥V and CERAD plaque density C) and 5 pre-AD (Braak NFT stage Ø/IV and CERAD plaque density C) brains were selected for this study. All cases were obtained from the China Brain Bank, Zhejiang University School of Medicine. Subcortical nuclei were checked in five major brain areas: SN, colliculus inferior/pons (CIP), locus caeruleus/pons (LCP), and MO in the brainstem; the caudatum, putamen, and globus pallidus in the basal gangalia; the hypothalamus, thalamus, subthalamus in the diencephalon; the cerebellum (dentate nuclei) and cervical spinal cord (SCC).

The study included 16 PART cases: their age was 78.5 ± 9.17 years in the range of 60–98 years; 12 were male and 4 were female; their average brain weight was 1240 ± 70.71 g. 7 neuropathologically confirmed definite Pre-AD cases: their age was 80.9 ± 6.67 years in the range of 69–90 years; 2 were male and 5 were female; their average brain weight was 1152 ± 73.05 g. 5 neuropathologically confirmed definite AD cases: their age was 86.8 ± 6.94 years in the range of 79–99 years; 3 were male and 2 were female; their average brain weight was 1235 ± 136.73 g.

Immunohistochemistry

Immunohistochemistry was performed on formalin-fixed, paraffin-embedded tissue from all autopsy cases. Small blocks of brain were dissected at autopsy and fixed in 4% paraformaldehyde (PFA) in 0.1 M phosphate buffer (pH 7.4) for 2 days. Following cryoprotection in 15% sucrose in 0.01 M phosphate-buffered saline (PBS, pH 7.4), blocks were cut at 3 μm thickness using a microtome. Free floating sections were incubated with 3% H_2O_2 for 10 min to eliminate endogenous peroxidase activity in the tissue. Prior to immunostaining, sections underwent microwave antigen retrieval for 15 min in the citrate buffer (pH 6.0). After washing with PBS containing 0.3% Triton X-100 (Tx-PBS) for 30 min, sections were blocked with 10% normal goat serum, and then incubated with the primary antibody (anti-hyperphosphorylated-tau, AT8: Mouse monoclonal, 1:200, Thermo Fisher Scientific, Rockford, United States; anti-amyloid β protein: Mouse monoclonal, 1:200, Sigma-Aldrich, St. Louis, United States) for 24 h in a cold room. Following treatment with the appropriate secondary antibody (anti-mouse), labeling was detected using the avidin–biotinylated HRP complex (ABC) system (Vector Laboratories, Burlingame, CA). The peroxidase reaction was carried out using a developer solution containing 0.4 mg/ml DAB and 0.0006% hydrogen peroxide in TBS. For negative control, the primary antibodies were omitted and all other steps carried out as described above. After the staining procedures, sections were mounted onto gelatin coated slides and dehydrated before being coverslipped with the DPX mounting medium.

The severity of tau pathology was semi-quantitatively scored based on a four-point grading scale (−/0, none; +/1, mild; ++/2, moderate; +++/3, severe). Of note, all cases initially were checked using the routine protocol for the Braak stage system.

Data Analysis

The hyperphosphorylated-tau immunochemistry results were analyzed using the semi-quantitative tau score index (severity) and the qualitative tau score index (distribution). The quantitative tau score index was evaluated using a four-point grading scale, and the qualitative tau score index is evaluated using a two-point grading scale (negative, 0; positive, 1). For inter-group comparison of means, the Kruskal-Wallis H test was used. Statistical comparison between variables was performed using the Mann-Whitney test.

TABLE 1 | Subcortical nuclei tau distribution in PART.

PART	Age	Sex	Striatum			Diencephalon			Brainstem				CD	SCC
			Ca	Pu	Pa	HT	T	ST	SN	CIP	LCP	MO		
I	60	M	–	–	–	–	–	–	–	–	–	–	–	+
	74	F	–	–	–	–	–	–	–	–	–	–	–	–
	76	M	–	–	–	–	–	–	+	+	+	–	–	+
	80	M	–	–	–	–	+	+	+	–	++	–	–	+
	84	M	–	–	–	–	–	–	–	–	–	+	–	–
	91	M	+	+	+	–	–	–	+	+	–	–	–	–
II	70	M	+	–	–	–	–	–	+	+	+	–	–	+
	83	M	+	–	–	–	+	–	–	+	–	+	–	N
	65	M	–	–	–	–	–	–	–	+	+	–	–	–
III	80	F	N	–	–	++	+	+	++	+	N	+	–	+
	81	F	–	–	–	+	+	–	+	+	+	+	–	+
	83	F	–	+	+	+	+	–	+	++	+	+	–	–
IV	74	M	–	+	+	+	+		+	+	+	+	–	–
	78	M	+	–	+	+	–	+	+	+	–	+	–	N
	79	M	–	+	+	++	–	–	–	+	+	–	–	N
	98	M	+	+	+	++	+	+	+	+	+	+	–	+

NFT, neurofibrillary tangle; Ca, caudate; Pu, putamen; Pa, globus pallidus; HT, hypothalamus; Th, thalamus; ST, subthalamus; SN, substantia nigra; CIP, colliculus inferior/pons; LCP, locus caeruleus/pons; MO, medulla oblongata; CD, cerebellum/dentate nuclei; SCC, cervical spinal cord. –, None; +/1, mild; ++/2, moderate; +++/3, severe. N not examined.

RESULTS

We investigated both the prevalence and severity of subcortical tau pathology in PART brains and compared them with those of pre-AD and AD brains. The present study correlated tau pathology in the subcortical nuclei with their Braak stages.

Tau Pathology in Subcortical Nuclei in PART (Table 1)

Among 16 PART cases, 15 cases (15/16) had tau-positive pathology in the subcortical regions. The region affected most frequently by tau pathology in the PART cohort was the brainstem including CIP (12 out of the 16 cases), SN (10/16), MO (9/16), and LCP (8/16); followed by the diencephalon including the thalamus (7/16), subthalamus (7/16), and hypothalamus (4/16); and the striatum including the caudatum (5/16), putamen (5/16), globus pallidus (6/16) (**Figure 1**). The SCC showed AT8 immunoreactivity (AT8-ir) in 7 out of the 16 cases (7/16). None of the cerebellum showed tau pathology (0/16).

The same regions were assessed using NFT Braak staging. In PART with Braak stage I, subcortical tauopathy was present in the brainstem (SN 3/6, CIP 2/6, LCP 2/6, MO 1/6), basal ganglia (caudatum 1/6, putamen 1/6, globus pallidus 1/6), thalamus 1/6, subthalamus 1/6 and SCC 3/6. PART cases with NFT Braak stage III/IV showed more AT8-ir in the brainstem (SN 6/7, CIP 7/7, LCP 5/7, MO 6/7), followed by the diencephalon (hypothalamus 7/7, thalamus 5/7, subthalamus 3/7), and the striatum (caudatum 2/7, putamen 4/7, globus pallidus 5/7). SCC showed AT8-ir in 3 out of 7 cases (3/7). Notably, the hypothalamus was consistently affected at Braak stage III /IV, but not at Braak stage I/II. None of the cerebellum showed tauopathy in PART cases.

In terms of tau distribution sites, the low grade (Braak stage I/II) PART showed AT8-ir in fewer subcortical sites (within 0–5 brain nuclei) than in the high grade (Braak stage III /IV) PART cases (between 5 and 11 nuclei). There was a statistical difference in the means of NFT distribution sites between PART with Braak NFT stage I/II and PART with Braak NFT stage Ø/IV ($p < 0.01$) (**Figure 3A**). The total tau IHC scores (four-point grading scale) were low in all subcortical nuclei of PART, below 1 at Braak stage I/II, and 1–2 at Braak stage III/IV. The tau score means of PART with Braak NFT stage III/IV cases were significantly higher than those of PART with Braak NFT stage I/II ($P < 0.01$) (**Figure 3D**).

Tau Pathology in Subcortical Brain Sites in Pre-AD and AD (Table 2)

In all AD individuals, nearly all of the subcortical nuclei showed a marked to severe AT8-ir tau pathology (**Figure 2**). Compared with PART, the subcortical regions were frequently affected by tau pathology in pre-AD and AD cases. Tauopathy was frequently observed in the striatum (caudatum 10/12, putamen 10/12, globus pallidus 10/12), diencephalon (thalamus 8/12, subthalamus 5/12, hypothalamus 11/12), and brainstem (SN 8/12, CIP 9/12, LCP 11/12, MO 7/12). In pre-AD cases, fewer brain sites showed HP-tau immunoreactivity (i.e., within 2–8 sites) than in AD (10–11 sites). A significant difference was found in the number of sites affected between pre-AD and AD ($p < 0.01$), between PART with Braak NFT stage I/II and pre-AD/AD ($p < 0.05$), and between PART with Braak NFT stage III/IV and AD ($p < 0.05$). There was no significant difference in the number of sites affected between pre-AD and PART with Braak NFT stage III/IV ($P > 0.05$) (**Figure 3A**).

In terms of tau density, similar to late PART with Braak stage III/IV, Pre-AD cases showed minimal AT8-ir with a total tau

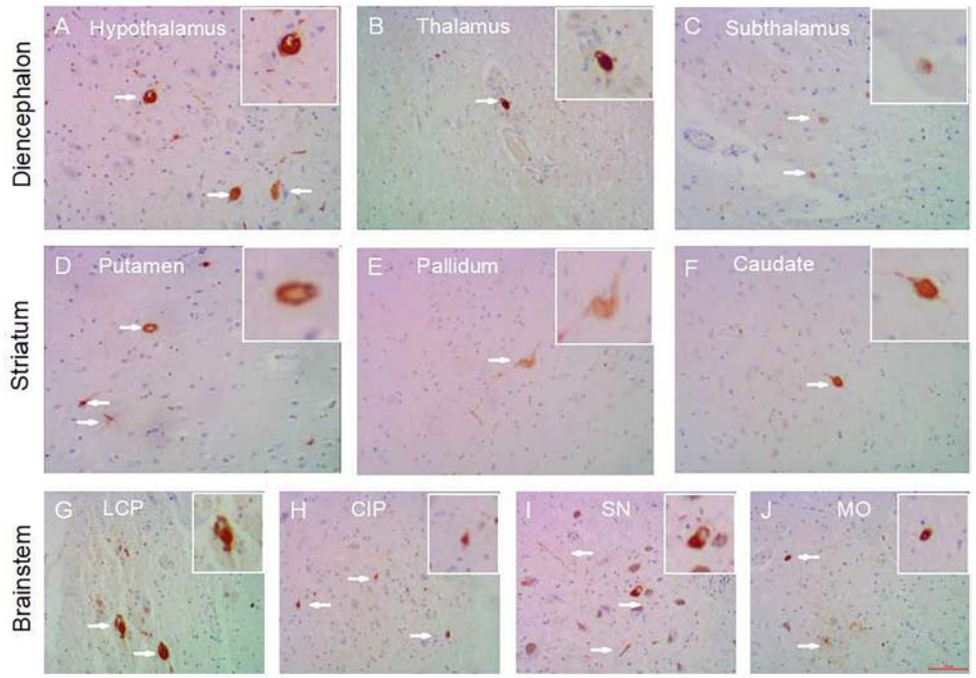

FIGURE 1 | Subcortical nuclei tau distribution in PART. Tau pathology in the subcortical nuclei in PART cases: hypothalamus **(A)**, thalamus **(B)**, subthalamus **(C)** in the diencephalon; caudatum **(F)**, putamen **(D)**, globus pallidus **(E)** in the striatum; substantia nigra **(I)**, colliculus inferior/pons **(H)**, locus caeruleus/pons **(G)**, medulla oblongata **(J)** in the brainstem. All images are of the same magnification × 100. scale bars, 100 μm.

TABLE 2 | Subcortical nuclei tau distribution in AD and pre-AD.

AD NFT (Braak)	Age	Sex	SP (CERAD)	Striatum			Diencephalon			Brainstem				CD	SCC
				Ca	Pu	Pa	HT	T	ST	SN	CIP	LCP	MO		
III	69	F	C	–	–	–	+	–	–	–	–	+	–	–	–
	79	F	c	+	+	+	+	+	+	–	++	+	–	–	–
	90	M	c	+	+	+	+	–	–	–	–	+	+	–	–
IV	78	F	c	–	–	+	–	–	–	–	++ +	++	–	–	–
	81	F	c	+	+	–	++	–	–	+	+	–	–	–	–
	83	M	c	+	+	+	+	+		+		+	+	–	–
	86	F	c	+	+	++	++	++	–	+	++	+	++	–	++
V	85	M	c	++	++	+++	++	++	++	++	+	+	–	–	+++
	99	F	c	+	+	+	+++	+	–	+	+	++	+	–	+
VI	79	M	c	++	++	++	+++	++	++	++	++	++	++	–	+
	86	F	c	++	++	+	+++	++	+++	++	++	++	++	–	N
	85	M	c	+	+	+	+	++	+	++	++	++	+	–	+

AD, Braak NFT stage ≥IV and CERAD SP density = C; Pre-AD, Braak NFT stage III/IV and CERAD SP density = C or B. SP, Senile plaque; NFT, neurofibrillary tangle; Ca, caudate; Pu, putamen; Pa, globus pallidus; HT, hypothalamus; Th, thalamus; ST, subthalamus; SN, substantia nigra; CIP, colliculus inferior/pons; LCP, locus caeruleus/pons; MO, medulla oblongata; CD, cerebellum/dentate nuclei; SCC, cervical spinal cord. –, None; +/1, mild; ++/2, moderate; +++/3, severe. N not examined.

score of 1–2 in subcortical nuclei, whereas nearly all AD cases showed a higher tau score of 2–3 in the majority of subcortical nuclei. A statistical difference in the means of tau scores was observed between pre-AD and AD ($p < 0.01$), between PART with Braak NFT stage I/II and pre-AD/AD ($p < 0.01$), between PART with Braak NFT stage III/IV and AD ($p < 0.01$). There was no statistical difference in the means of tau scores between pre-AD and PART with Braak NFT stage III/IV (**Figure 3D**). Similarly, total tau scores increased with the increasing NFT Braak stages in SCC, scoring 1 in pre-AD and 3 in AD. No AT8-ir was seen in the cerebellum of either AD or pre-AD cases.

The tauopathy distribution scores of the striatum, diencephalon and brainstem showed no significant difference between AD and pre-AD cases ($P > 0.05$). In PART, especially

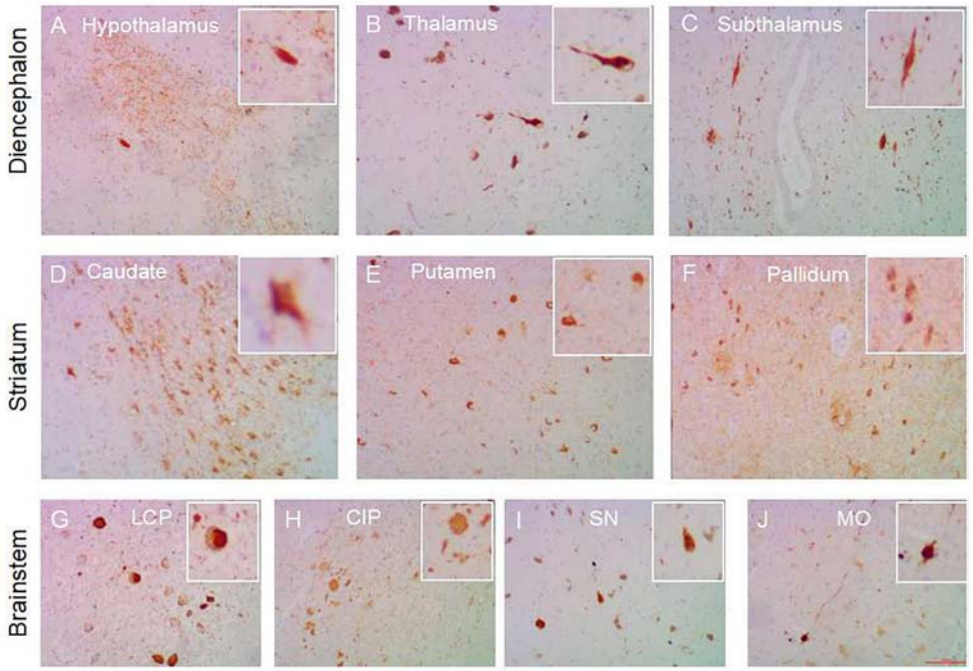

FIGURE 2 | Subcortical nuclei tau distribution in AD. Tau pathology in the subcortical nuclei in AD cases: hypothalamus **(A)**, thalamus **(B)**, subthalamus **(C)** in the diencephalon; caudate **(D)**, putamen **(E)**, globus pallidum **(F)** in the striatum; substantia nigra **(I)**, colliculus inferia/pons **(H)**, locus ceruleus/pons **(G)**, medulla oblongata **(J)** in the brainstem. All images are the same magnification × 100. scale bars, 100 μm.

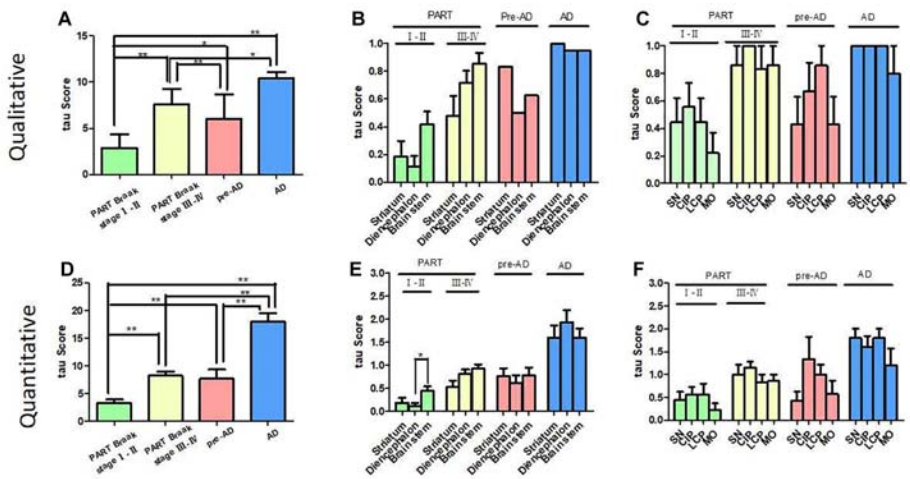

FIGURE 3 | Correlation of Braak NFT stages with tau scores in PART and pre-AD/AD. **(A)** The qualitative tau score means (tau distribution pathology) in PART and AD/pre-AD. There was a statistical difference in NFT distribution score means between PART with Braak NFT stage I/II, PART with Braak NFT stage Ø/IV, pre-AD, and AD ($p < 0.01$). **(B)** The qualitative tau score means (tau distribution pathology) in the striatum, diencephalon, and brainstem in PART and AD/pre-AD. **(C)** The qualitative tau score means (tau distribution pathology) in SN, CIP, LCP, and MO in PART and AD/pre-AD. **(D)** The quantitative tau score means (tau density pathology) in PART and AD/pre-AD. There was a statistical difference in the tau score means between PART with Braak NFT stage I/II and PART with Braak NFT stage Ø/IV cases ($p < 0.01$) as well as pre-AD/AD ($p < 0.01$). **(E)** The quantitative tau score means (tau density pathology) in the striatum, diencephalon, and brainstem in PART and AD/pre-AD. **(F)** The quantitative tau score means (tau density pathology) in SN, CIP, LCP, and MO in PART and AD/pre-AD.

in the early Braak stage I/II, many brainstem nuclei showed tauopathy (**Figure 3B**) with a moderate to high severity score. Because of the limitated number of cases, a statistical difference was only found between the brainstem and the diencephalon in PART with Braak stage I/II (**Figure 3E**). There was no significant difference in the distribution (**Figure 3C**) and severity (**Figure 3F**) scores between brainstem nuclei including SN, CIP, LC, and MO.

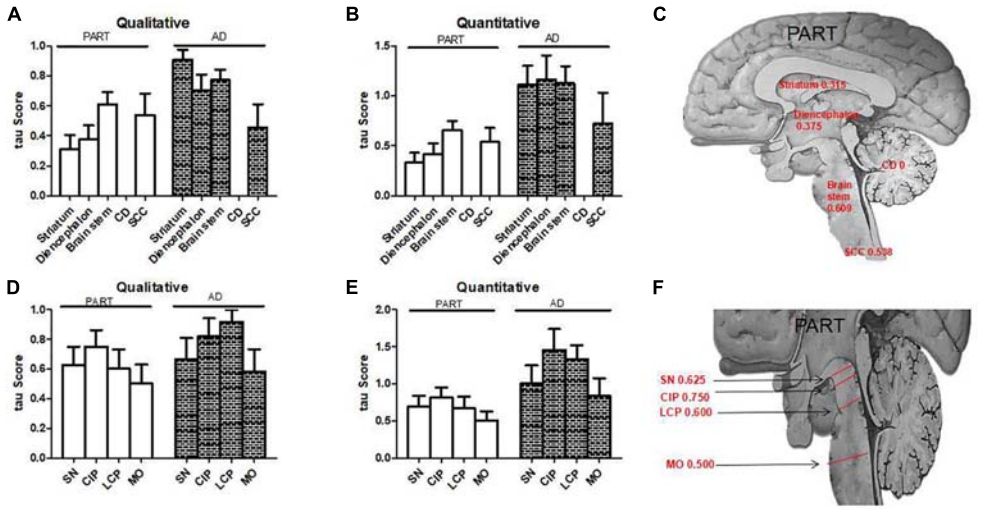

FIGURE 4 | The qualitative and quantitative tau scores in PART and AD. **(A)** The qualitative tau score means in subcortical nuclei in PART and AD. **(B)** The quantitative tau score means in subcortical nuclei in PART and AD. **(C)** The qualitative tau score means in the striatum, diencephalon, brainstem, and cervical spinal cord in PART. **(D)** The qualitative tau score means in brainstem nuclei in PART and AD. **(E)** The quantitative tau score means in brainstem nuclei in PART and AD. **(F)**. The qualitative tau score means in SN, CIP, LCP, and MO in PART.

DISCUSSION

Recent studies indicated that tau pathology in AD did not initially manifest in the cerebral cortex but in selected subcortical nuclei, including the thalamus, striatum and brainstem, in particular LC (Elobeid et al., 2012). Structural brain imaging studies also found changes in subcortical regions in early stage AD (Tentolouris-Piperas et al., 2017). For example, the thalamus and striatum were found to be atrophied in symptomatic patients, with an altered caudate volume implicated in early stage AD (Leh et al., 2016). Without Aβ deposition, PART represents a pure tau pathology at the early stage of neurodegeneration and is a good model of studying the mechanism for NFT Braak staging. In a previous study (Attems et al., 2012a), we addressed the question whether degeneration of subcortical nuclei occurred early during the progression of PART. In the present study, we systematically assessed the subcortical nuclei in PART and per-AD/AD patients ranging from preclinical stages to severe dementia. In the five brain regions we checked, tau became detectable in the brainstem, diencephalon, striatum, and spinal cord in PART and pre-AD, but not in the cerebellum. Tauopathy was more pronounced in these regions in more advanced AD with higher NFT Braak stages.

Primary Age-Related Tauopathy in the Brainstem

It was reported that brainstem nuclei were affected by early AD before the supratentorial regions, including the LC, SN and the nucleus basalis of Meynert (NbM). Some normal aging subjects without NFTs (Braak 0) in LC showed NFTs in the dorsal raphe nucleus (DR) (Grinberg et al., 2011). In the present study, LC showed tau pathology in early PART with NFT Braak stage I, other brainstem nuclei including SN, CIP and MO also showed tau pathology at the same time. In some PART cases with NFT Braak stage I, a few brainstem nuclei, such as the MO (**Table 1**/ case 5), SN, and CIP (**Table 1**/case 6), but not LC, showed tau pathology. So at least, when LC was involved, some other brainstem nuclei have already manifested tauopathy in early PART with NFT Braak stage I. Compared with the striatum and the diencephalon, brainstem nuclei were the most commonly affected region at the early stage of PART with NFT Braak stage I/II, which supports that tauopathy may begin from the brainstem (Simic et al., 2009; Lee et al., 2015; Rüb et al., 2016b). In pre-AD and AD brains, tau pathology was severe and evenly distributed in these nuclei without a clear preference (**Figures 3B,E**).

Primary Age-Related Tauopathy in Striatum and Diencephalon

In our study cohort, tauopathy was also positive in the other subcortical nuclei including the caudate nucleus, putamen, globus pallidus in the striatum, the thalamus and subthalamus in the diencephalon in early PART with NFT Braak stage I. Early tauopathy is not confined to a single subcortical nucleus. The possibility that neurodegeneration occurs independently at a number of sites in parallel cannot be ruled out (Rüb et al., 2016a). Moreover, more subcortical nuclei were positive for tau in PART with higher Braak stages like III/IV. Tau pathology (both distribution and density) in the diencephalon and striatum showed a nearly identical pattern as that shown in the brainstem. In the hypothalamus, thalamus, and subthalamus, tau pathology (density and distribution) was negative or mild in early PART (NFT Braak stage I/II), moderate in late PART (NFT Braak stage III/IV) and pre-AD (NFT Braak stage III/IV), and severe in AD brains. Nuclei in the striatum (caudatum, putamen, globus pallidus) showed a similar pattern. We propose, therefore, that the subcortical nuclei should be

considered in the basic scheme of Braak NFT staging in the future as others suggested (Paskavitz et al., 1995; Mattila et al., 2002; Pievani et al., 2013; Kawakami et al., 2014).

Primary Age-Related Tauopathy in the Spinal Cord and the Cerebellum

To date, there are few studies having examined deposition of abnormally phosphorylated tau in the spinal cord of normal aging subjects or AD patients. A study showed that the cervical cord segments were affected in 96% AD vs. in 27% non-demented individuals (Dugger et al., 2013). We found that SCC was frequently positive for tau pathology (11/12, 92% in AD vs. 7/16, 44% in PART) in both AD and PART brains, and was even positive in early PART with Braak stage I. No tauopathy was observed in the cerebellum/dentate nuclei in our PART and AD brains.

Subcortical Tauopathy Has Important Clinical Implications

In the present study, tauopathy was observed in subcortical nuclei of PART brains. Based on the tau score (both qualitative and quantitative scores), brainstem was the most frequently affected region by tauopathy, followed by the diencephalon, striatum and SCC in PART (**Figures 4A–C**). Among these brainstem nuclei, there was no evident prevalence tendency observed (**Figures 4D–F**). The presence of tau pathology in subcortical nuclei has important implications for both the pathogenesis and clinical manifestations of PART and AD. As tau immunoreactivity is present in the subcortical regions of PART as well as pre-AD subjects, it could explain some clinical symptoms prior to typical dementia symptoms manifest (Besser et al., 2017; Josephs et al., 2017). The density (tau score) of AT8-ir cells increased in all regions investigated as the NFT Braak stage increased in AD, which could explain symptoms frequently found in AD. But this has not been correlated with tau pathology in the subcortical nuclei such as SN or LC in PART (Giaccone, 2015). Tau pathology in the brainstem is severe in AD, which may explain clinical symptoms due to serotonergic deficit found in AD, and a variety of less well-understood symptoms of AD patients. For example, parkinsonian extrapyramidal motor signs, depression, hallucinations, dysfunctions of the sleep/wake cycle, etc. (Attems et al., 2007).

Although there are some reports about the subcortical tauopathy in AD, the extent of the subcortical tauopathy in aging and AD has been underestimated (Janocko et al., 2012; Lemche, 2018). To our knowledge, this is the first systemic report on the occurrence of tau accumulation in the subcortical regions in PART. Our findings showed that tau pathology began from the subcortical nuclei in PART as early as NFT Braak stage I. The distribution and density of tau pathology in the subcortical nuclei significantly increased as the NFT Braak stage increased in both PART and AD. These observations indicate that subcortical nuclei are inflicted by neurofibrillary changes as early as the *trans*-entorhinal cortex in both PART and AD. Study of tau pathology in the subcortical nuclei improves our understanding about the evolution of clinical manifestations of AD and provides a simple and early structural indicator of PART and AD development. Prevalence of abnormal tau accumulation in the subcortical regions in PART and AD may support the hypothesis that abnormal tau aggregation propagates via neural circuits. PART will be an optimal disease model for testing hypotheses related to tau propagation in the brain.

ETHICS STATEMENT

The research was given ethical approval by Medical Ethics Committee of Zhejiang University School of Medicine.

AUTHOR CONTRIBUTIONS

XW, BS, JW, XZ, and HL did the immunohistochemistry analysis and tissue preparation. KZ and XW contributed to statistical assessment and data processing. KZ designed the study, supervised the results, and wrote the first advanced version of the manuscript which was circulated among all the contributors for comments and suggestions. HL, DZ, and CL contributed to the final version of the manuscript.

FUNDING

This research was supported by the National Natural Science Foundation of China (91632109) (to Zhong and KZ), the Zhejiang Provincial Natural Science Foundation (LY16H090013) (to KZ), and the Zhejiang Medical and Health Science and Technology Plan Project (WKJ2013-2-009) (to KZ).

ACKNOWLEDGMENTS

We wish to thank the families of the patients who donated their brains to China Brain Bank in School of Medicine, Zhejiang University, to allow the completion of this study.

REFERENCES

Arendt, T., Brückner, M. K., Morawski, M., Jäger, C., and Gertz, H. J. (2015). Early neurone loss in Alzheimer's disease: cortical or subcortical? *Acta Neuropathol. Commun.* 3:10.

Attems, J., Quass, M., and Jellinger, K. A. (2007). Tau and alpha-synuclein brainstem pathology in Alzheimer disease: relation with extrapyramidal signs. *Acta Neuropathol.* 113, 53–62. doi: 10.1007/s00401-006-0146-9

Attems, J., Thal, D. R., and Jellinger, K. A. (2012a). The relationship between subcortical tau pathology and Alzheimer's disease. *Biochem. Soc. Trans.* 40, 711–715. doi: 10.1042/BST20120034

Attems, J., Thomas, A., and Jellinger, K. (2012b). Correlations between cortical and subcortical tau pathology. *Neuropathol. Appl. Neurobiol.* 38, 582–590. doi: 10.1111/j.1365-2990.2011.01244.x

Besser, L. M., Crary, J. F., Mock, C., and Kukull, W. A. (2017). Comparison of symptomatic and asymptomatic persons with primary age-related tauopathy. *Neurology* 89, 1707–1715. doi: 10.1212/WNL.0000000000004521

Braak, H., Alafuzoff, I., Arzberger, T., Kretzschmar, H., and Del Tredici, K. (2006). Staging of Alzheimer disease-associated neurofibrillary pathology using paraffin sections and immunocytochemistry. *Acta Neuropathol.* 112, 389–404. doi: 10.1007/s00401-006-0127-z

Braak, H., and Del Tredici, K. (2011). The pathological process underlying Alzheimer's disease in individuals under thirty. *Acta Neuropathol.* 121, 171–181. doi: 10.1007/s00401-010-0789-4

Braak, H., and Del Tredici, K. (2012). Where, when, and in what form does sporadic Alzheimer's disease begin? *Curr. Opin. Neurol.* 25, 708–714. doi: 10.1097/WCO.0b013e32835a3432

Braak, H., and Del Tredici, K. (2015). The preclinical phase of the pathological process underlying sporadic Alzheimer's disease. *Brain* 138, 2814–2833. doi: 10.1093/brain/awv236

Braak, H., Thal, D. R., Ghebremedhin, E., and Del Tredici, K. J. (2011). Neuropathol Stages of the pathologic process in Alzheimer disease: age categories from 1 to 100 years. *Exp. Neurol.* 70, 960–969. doi: 10.1097/NEN.0b013e318232a379

Crary, J. F. (2016). Primary age-related tauopathy and the amyloid cascade hypothesis: the exception that proves the rule? *J. Neurol. Neuromed.* 1, 53–57. doi: 10.29245/2572.942x/2016/6.1059

Crary, J. F., Trojanowski, J. Q., Schneider, J. A., Abisambra, J. F., Abner, E. L., and Alafuzoff, I. (2014). Primary age-related tauopathy (PART): a common pathology associated with human aging. *Acta Neuropathol.* 128, 755–766. doi: 10.1007/s00401-014-1349-0

Dugger, B. N., Hidalgo, J. A., Chiarolanza, G., Mariner, M., Henry-Watson, J., Sue, L. I., et al. (2013). The distribution of phosphorylated tau in spinal cords of Alzheimer's disease and non-demented individuals. *J. Alzh. Dis.* 34, 529–536. doi: 10.3233/JAD-121864

Duyckaerts, C., Braak, H., Brion, J. P., Buée, L., Del Tredici, K., Goedert, M., et al. (2015). PART is part of Alzheimer disease. *Acta Neuropathol.* 129, 749–756. doi: 10.1007/s00401-015-1390-7

Elobeid, A., Soininen, H., and Alafuzoff, I. (2012). Hyperphosphorylated tau in young and middle-aged subjects. *Acta Neuropathol.* 123, 97–104. doi: 10.1007/s00401-011-0906-z

Giaccone, G. (2015). The existence of primary age-related tauopathy suggests that not all the cases with early braak stages of neurofibrillary pathology are alzheimer's disease. *J. Alzh. Dis.* 48, 919–921. doi: 10.3233/JAD-150435

Grinberg, L. T., Rueb, U., and Heinsen, H. (2011). Brainstem: neglected locus in neurodegenerative diseases. *Front. Neurol.* 2:42. doi: 10.3389/fneur.2011.00042

Janocko, N. J., Brodersen, K. A., Soto-Ortolaza, A. I., Ross, O. A., Liesinger, A. M., and Duara, R. (2012). Neuropathologically defined subtypes of Alzheimer's disease differ significantly from neurofibrillary tangle-predominant dementia. *Acta Neuropathol.* 124, 681–692. doi: 10.1007/s00401-012-1044-y

Jellinger, K. A., Alafuzoff, I., Attems, J., Beach, T. G., Cairns, N. J., Crary, J. F., et al. (2015). PART, a distinct tauopathy, different from classical sporadic Alzheimer disease. *Acta Neuropathol.* 129, 757–762. doi: 10.1007/s00401-015-1407-2

Josephs, K. A., Murray, M. E., Tosakulwong, N., Whitwell, J. L., Knopman, D. S., and Machulda, M. M. (2017). Tau aggregation influences cognition and hippocampal atrophy in the absence of beta-amyloid: a clinico-imaging-pathological study of primary age-related tauopathy (PART). *Acta Neuropathol.* 133, 705–715. doi: 10.1007/s00401-017-1681-2

Kawakami, I., Hasegawa, M., Arai, T., Ikeda, K., Oshima, K., and Niizato, K. (2014). Tau accumulation in the nucleus accumbens in tangle-predominant dementia. *Acta Neuropathol. Commun.* 2:40. doi: 10.1186/2051-5960-2-40

Lee, J. H., Ryan, J., Andreescu, C., Aizenstein, H., and Lim, H. K. (2015). Brainstem morphological changes in Alzheimer's disease. *Neuroreport* 26, 411–415. doi: 10.1097/WNR.0000000000000362

Leh, S. E., Kälin, A. M., Schroeder, C., Park, M. T., Chakravarty, M. M., Freund, P., et al. (2016). Volumetric and shape analysis of the thalamus and striatum in amnestic mild cognitive impairment. *J Alzheimers Dis.* 49, 237–249. doi: 10.3233/JAD-150080

Lemche, E. (2018). Early life stress and epigenetics in late-onset alzheimer's dementia: a systematic review. *Curr. Genomics* 19, 522–602. doi: 10.2174/1389202919666171229145156

Mattila, P., Togo, T., and Dickson, D. W. (2002). The subthalamic nucleus has neurofibrillary tangles in argyrophilic grain disease and advanced Alzheimer's disease. *Neurosci. Lett.* 320, 81–85. doi: 10.1016/s0304-3940(02)00006-x

Paskavitz, J. F., Lippa, C. F., Hamos, J. E., Pulaski-Salo, D., and Drachman, D. A. (1995). Role of the dorsomedial nucleus of the thalamus in Alzheimer's disease. *J. Geriatr. Psychiatry Neurol.* 8, 32–37.

Pievani, M., Bocchetta, M., Boccardi, M., Cavedo, E., Bonetti, M., Thompson, P. M., et al. (2013). Striatal morphology in early-onset and late-onset Alzheimer's disease: a preliminary study. *Neurobiol. Aging* 34, 1728–1739. doi: 10.1016/j.neurobiolaging.2013.01.016

Rüb, U., Stratmann, K., Heinsen, H., Del Turco, D., Ghebremedhin, E., Seidel, K., et al. (2016a). Hierarchical distribution of the tau cytoskeletal pathology in the thalamus of alzheimer's disease patients. *J. Alzheimers Dis.* 49, 905–915. doi: 10.3233/JAD-150639

Rüb, U., Stratmann, K., Heinsen, H., Turco, D. D., Seidel, K., Dunnen, W. D., et al. (2016b). The Brainstem tau cytoskeletal pathology of alzheimer's disease: a brief historical overview and description of its anatomical distribution pattern, evolutional features, pathogenetic and clinical relevance. *Curr. Alzheimer Res.* 13, 1178–1197. doi: 10.2174/1567205013666160606100509

Rüb, U., Stratmann, K., Heinsen, H., Seidel, K., Bouzrou, M., and Korf, H. W. (2017). Alzheimer's disease: characterization of the brain sites of the initial tau cytoskeletal pathology will improve the success of novel immunological anti-tau treatment approaches. *J. Alzheimers Dis.* 57, 683–696. doi: 10.3233/JAD-161102

Simic, G., Stanic, G., Mladinov, M., Jovanov-Milosevic, N., Kostovic, I., and Hof, P. R. (2009). Does Alzheimer's disease begin in the brainstem? *Neuropathol. Appl. Neurobiol.* 35, 532–554. doi: 10.1111/j.1365-2990.2009.01038.x

Stratmann, K., Heinsen, H., Korf, H. W., Del Turco, D., Ghebremedhin, E., Seidel, K., et al. (2016). Precortical phase of Alzheimer's disease (AD)-related tau cytoskeletal pathology. *Brain Pathol.* 26, 371–386. doi: 10.1111/bpa.12289

Tentolouris-Piperas, V., Ryan, N. S., Thomas, D. L., and Kinnunen, K. M. (2017). Brain imaging evidence of early involvement of subcortical regions in familial and sporadic Alzheimer's disease. *Brain Res.* 1655, 23–32. doi: 10.1016/j.brainres.2016.11.011

Theofilas, P., Dunlop, S., Heinsen, H., and Grinberg, L. T. (2015). Turning on the light within: subcortical nuclei of the isodentritic core and their role in alzheimer's disease pathogenesis. *J. Alzheimers* 46, 17–34. doi: 10.3233/jad-142682

Wharton, S. B., Minett, T., Drew, D., Forster, G., Matthews, F., and Brayne, C. (2016). Epidemiological pathology of Tau in the ageing brain: application of staging for neuropil threads (BrainNet Europe protocol) to the MRC cognitive function and ageing brain study. *Acta Neuropathol. Commun.* 4:11. doi: 10.1186/s40478-016-0275-x

Conflict of Interest Statement: The authors declare that the research was conducted in the absence of any commercial or financial relationships that could be construed as a potential conflict of interest.

frontiers in Neuroscience

ORIGINAL RESEARCH
published: 23 July 2019
doi: 10.3389/fnins.2019.00751

Downregulated Dopamine Receptor 2 and Upregulated Corticotrophin Releasing Hormone in the Paraventricular Nucleus Are Correlated With Decreased Glucose Tolerance in Rats With Bilateral Substantia Nigra Lesions

Li Zhou[1†], Xue-Rui Ran[2], Feng Hong[1], Guang-Wen Li[1] and Jin-Xia Zhu[1]*

[1] Department of Physiology and Pathophysiology, School of Basic Medical Sciences, Capital Medical University, Beijing, China, [2] Xinxiang Key Laboratory of Molecular Neurology, Department of Human Anatomy, Xinxiang Medical University, Xinxiang, China

OPEN ACCESS

Edited by:
Lei Sha,
China Medical University, China

Reviewed by:
Sumei Liu,
University of Wisconsin–La Crosse, United States
Guo-Du Wang,
Tulane Medical Center, United States

***Correspondence:**
Jin-Xia Zhu
zhu_jx@ccmu.edu.cn

†Present address:
Li Zhou,
Department of Human Anatomy, Xinxiang Medical University, Xinxiang, China

Specialty section:
This article was submitted to Neuroendocrine Science, a section of the journal Frontiers in Neuroscience

Received: 07 May 2019
Accepted: 08 July 2019
Published: 23 July 2019

Citation:
Zhou L, Ran X-R, Hong F, Li G-W and Zhu J-X (2019) Downregulated Dopamine Receptor 2 and Upregulated Corticotrophin Releasing Hormone in the Paraventricular Nucleus Are Correlated With Decreased Glucose Tolerance in Rats With Bilateral Substantia Nigra Lesions. Front. Neurosci. 13:751. doi: 10.3389/fnins.2019.00751

Patients with Parkinson's disease (PD) have a high prevalence of glucose metabolism abnormalities. However, the mechanism underlying these symptoms remains unclear. The hypothalamic-pituitary-adrenal (HPA) axis is the major neuroendocrine axis that regulates homeostasis in mammals, including glucose metabolism. Corticotrophin releasing hormone (CRH), which is synthesized in the paraventricular nucleus (PVN) of the hypothalamus, plays an important role in the regulation of blood glucose levels via the HPA axis. Our previous studies have reported that PVN neurons express numerous dopamine receptors (DRs) and accept direct projections from the substantia nigra (SN). We hypothesize that damage to dopaminergic neurons in the SN might influence the blood glucose level through the HPA system. Rats with bilateral SN lesions induced by 6-hydroxydopamine (6-OHDA) (referred to as 6-OHDA rats) were used to investigate alterations in the levels of blood glucose, CRH, and factors related to the HPA axis and to explore possible mechanisms. Blood glucose levels were detected at different time points after the glucose solution was intraperitoneally administered. CRH and DRs in the PVN were evaluated by immunofluorescence and western blot analysis. Adrenocorticotropic hormone (ACTH) in the pituitary and plasma corticosterone (CORT) was evaluated by radioimmunoassay (RIA). The results showed that 6-OHDA rats exhibited significantly decreased tyrosine hydroxylase (TH) in the SN and decreased glucose tolerance at 6 weeks, but not at 4 weeks. In the PVN, dopamine receptor 2 (D2) was expressed on CRH-positive neurons, and D2-positive neurons were surrounded by TH-positive fibers. Additionally, the expression of CRH was upregulated, whereas the expression of D2 and TH were downregulated in 6-OHDA rats compared with control rats. In D2 knock-out mice, the significantly enhanced expression of CRH and reduced expression of D2 were detected in the PVN. Furthermore, RIA revealed increased ACTH

in the pituitary and elevated CORT in the blood. In summary, the present study suggests that the dopaminergic neurons in the SN are involved in the regulation of body glucose metabolism through CRH neurons that express D2 in the hypothalamic PVN. SN lesions decrease glucose tolerance mainly by downregulating D2 and upregulating CRH in the PVN through the HPA neuroendocrine system.

Keywords: glucose metabolism, Parkinson's disease, dopamine receptor, corticotrophin releasing hormone, hypothalamic-pituitary-adrenal axis

INTRODUCTION

Parkinson's disease (PD) is a common neurodegenerative disorder characterized by the progressive loss of dopaminergic neurons in the substantia nigra (SN), which manifests both motor and non-motor symptoms (NMS) (Stern et al., 2012). While the classic motor features are due to the loss of nigrostriatal dopaminergic cells, the spectrum of NMS reflects a more complex etiology, including neuroendocrine and metabolic abnormalities (De Pablo-Fernandez et al., 2017). People realize that NMS play a tremendously important role in the management and even the diagnosis of the disorder (Pfeiffer, 2016). Here, we focused on the high prevalence of glucose metabolism abnormalities observed in patients with PD, which have been extensively studied (Lipman et al., 1974; Dunn et al., 2014; De Pablo-Fernandez et al., 2017; Biosa et al., 2018). It is important to elucidate the mechanism of impaired glucose metabolism in patients with PD for controlling and delaying the onset and progression of disease-related complications in the early stage of the disease. However, the underlying pathogenesis remains unclear.

The hypothalamic-pituitary-adrenal (HPA) axis is the major neuroendocrine axis that regulates homeostasis in mammals, including glucose metabolism (Si et al., 2015). Corticotrophin releasing hormone (CRH), which is synthesized in the paraventricular nucleus (PVN) of the hypothalamus, plays an important role in regulating blood glucose via the HPA axis (Lu et al., 2018). CRH is released into the hypophyseal portal capillaries in the median eminence and stimulates the secretion of adrenocorticotropic hormone (ACTH) in the pituitary gland. Then, ACTH arrives at the adrenal cortex through the systemic blood circulation and promotes the synthesis and secretion of glucocorticoid hormones, cortisol or corticosterone (CORT), in the adrenal cortex, participating in the regulation of blood sugar (Spencer and Deak, 2017).

Reduced PVN function has been reported in patients with PD (Mann and Yates, 1983; Jellinger, 1991). Our previous studies have shown that the PVN receives a direct projection from the SN by neural tracing technology (Wang et al., 2014), and a large number of dopamine receptors 1 and 2 (D1 and D2) are distributed throughout the PVN (Ran et al., 2019). We hypothesized that the CRH-positive neurons in the PVN express dopamine receptors (DRs) and that dopamine from the SN could influence the synthesis and secretion of CRH via DRs in the PVN, which in turn regulate the blood glucose level via the HPA system.

The present study aimed to explore the relationship between PD and glucose metabolism and its underlying mechanism by using a classic animal model established with the neurotoxin 6-hydroxydopamine (6-OHDA), which cannot cross the blood-brain barrier and therefore requires direct administration on the SN (Jackson-Lewis et al., 2012). Our findings provide direct evidence that the loss of dopamine in the SN leads to decreased glucose tolerance, which is correlated with the altered HPA neuroendocrine system.

MATERIALS AND METHODS

Animals

Male Sprague–Dawley rats (Laboratory Animal Services Center of Capital Medical University, Beijing, China) that ranged in weight from 210 to 230 g (7∼8 weeks) were used. All animals were housed in animal care facilities at 22 ± 1°C on a 12:12 h light–dark cycle. Food and water were provided *ad libitum*.

Global D2 knock-out mice were generated and purchased from the Institute of Laboratory Animals Science, the Chinese Academy of Medical Sciences & Peking Union Medical College. Sex- and age-matched wild-type littermates were used as controls. All male mice used had a C57BL/6 background, were 8 weeks of age and were housed under the same environmental conditions as the rats.

Every procedure was approved by the Animal Care and Use Committee of Capital Medical University and was conducted according to the established guidelines of the National Institutes of Health (NIH, United States).

6-OHDA Animal Models

The animal model of PD was made by bilaterally microinjecting the SN with 6-OHDA (Sigma, United States) (referred to as 6-OHDA rats) as previously reported (Zheng et al., 2011). Briefly, all animals were anesthetized with an intraperitoneal (i.p.) injection of chloral hydrate (0.4 g/kg) and placed on a stereotaxic instrument. Two holes were drilled into the skull (coordinates: anterior-posterior (AP), −5.6 mm; medial-lateral (ML), ± 2.0 mm; dorsal-ventral (DV), −7.5 mm), and 6-OHDA (4 μg in μl of 0.9% saline containing 0.05% ascorbic acid) was bilaterally injected with a 10-μl Hamilton syringe. Control groups were injected with saline containing 0.2% ascorbic acid. Subsequent experiments were performed 4 and 6 weeks after 6-OHDA administration.

ipGTT

At 4 and 6 weeks, the intraperitoneal glucose tolerance test (ipGTT) was performed in fasted (8 h) rats at approximately 16:00. The tips of the tails of the rats were cut (less than

1 mm) for blood collection. The first drop was discarded, and the second drop was used for the determination of blood glucose (time 0) using a glucometer (Accu-Chek Performa; Roche Diagnostics, GmbH, Mannheim, Germany). Immediately afterward, a 20% glucose solution prewarmed at 37°C (2 g/kg) was intraperitoneally injected, and blood samples were collected at 15, 30, 60, and 120 min for blood glucose measurements as previously described (Oh et al., 2013).

Tissue Preparation

For brain sections, the animals were perfused through the left ventricle according to the previous method (Zhou et al., 2014). The brains were then quickly removed and kept in 4% paraformaldehyde for 24 h after fixation. After dehydration with 15 and 30% sucrose in 0.01 M PBS (pH 7.4), coronal frozen sections including the SN and PVN were cut to a thickness of 20 μm with a cryostat (Leica CM1950, Switzerland). The brain sections were air-dried overnight at room temperature and stored at −80°C.

For western blot analysis and radioimmunoassay, samples of the SN, hypothalamus, pituitary gland and adrenal gland were collected on ice and immediately frozen in liquid nitrogen. The tissues were stored at −80°C until further testing.

IF and IHC Staining

For immunofluorescence (IF), as described in our previous report (Zhou et al., 2014). Briefly, after retrieving antigens by heating to 95°C–100°C in a beaker containing citrate buffer (0.01 M, pH 6.0) for 15 min, the sections were incubated with 10% normal goat serum for 1 h at room temperature. Then, the sections were incubated with primary antibodies (**Table 1**) at 4°C overnight, and subsequently incubated with secondary antibodies (**Table 2**) for 1 h at room temperature. Photomicrographs were obtained using a confocal microscope (Olympus, FV1000).

For immunohistochemistry (IHC), in contrast with IF, the slices were quenched in endogenous peroxidase using 0.3% H_2O_2 before antigen retrieval. After incubation with primary antibody (**Table 1**) at 4°C overnight, immunostaining was performed using a PV-9002 Polymer Detection System (ZSGB-Bio, China) with diaminobenzidine according to the manufacturer's protocol. The sections were photographed with a light microscope (Nikon E80i, Japan).

Western Blot Analysis

The frozen brain tissues were homogenized in 300 μl of cold lysis buffer supplemented with protease inhibitors for protein extraction. Proteins (100 μg) were separated by 10% SDS-PAGE and transferred to a nitrocellulose membrane. After blocking with 5% skim milk in PBS for 1 h, the membranes were incubated with primary antibodies (**Table 1**) overnight at 4°C. Then, the membranes were incubated with the appropriate secondary antibodies (**Table 2**) for 1 h at room temperature. After the final wash, the membrane was scanned and quantified with an Odyssey Infrared Image system (LI-COR, United States). The integrated intensity of the bands was analyzed by Odyssey software (version 3.0).

Radioimmunoassay

Under anesthesia, blood samples were collected into cold EDTA tubes from the heart and centrifuged at 3000 rpm (4°C) for 10 min to isolate the plasma. The supernatant was transferred to new Eppendorf tubes and stored at −80°C. Then, homogenates of hypothalamus, pituitary gland and adrenal gland samples were also centrifuged to obtain the supernatant. ACTH and CORT levels in the blood samples and brain tissue homogenates were detected by Beijing Furunruize Biotechnology Co., Ltd.

Statistical Analysis

The results are presented as the mean ± SEM from at least three experiments. Statistical analyses were performed using the unpaired Student's *t* test (GraphPad Software 5.0, La Jolla, CA, United States). Differences were considered significant at $p < 0.05$.

RESULTS

SN Lesions and Attenuated Glucose Tolerance in 6-OHDA-Induced Rats

As a rate-limiting enzyme in catecholamine synthesis, tyrosine hydroxylase (TH) is normally used as a marker for intrinsic catecholaminergic neurons (Zheng and Travagli, 2007). The majority of TH-immunoreactive (TH-IR) neurons in the SN are dopaminergic; thus, TH-IR neurons were observed to indirectly

TABLE 1 | First antibodies used in this study.

Antigen	Antibody	Dilution		Source/catalog no.
		IHC/IF	Western blot	
TH	Mouse monoclonal	1:5000	1:10000	Sigma/T1299
D1	Rabbit polyclonal	1:100	1:500	Alomone/ADR-001
D2	Rabbit polyclonal	1:100	1:500	Alomone/ADR-002
D2	Mouse monoclonal	1:100	1:500	Santa Cruz/sc-5303
CRH	Rabbit polyclonal	1:100	1:500	Cloud-clone corp/PAA853Hu01
GAPDH	Rabbit polyclonal	N/A	1:5000	Sigma/G9545

TH, tyrosine hydroxylase; D1, dopamine 1 receptor; D2, dopamine 2 receptor; CRH, corticotrophin releasing hormone.

TABLE 2 | Secondary antibodies used in this study.

Antigen	Conjugation	Dilution	Source/Catalog no.
anti-mouse IgG (IHC)	HRP	HRP	ZSGB-Bio/PV-9002
Goat anti-mouse IgG (IF)	Alexa Fluor 488	1:1000	Invitrogen/A11017
Goat anti-mouse IgG (IF)	Alexa Fluor 594	1:1000	Invitrogen/A11020
Donkey anti-rabbit IgG (IF)	Alexa Fluor 488	1:1000	Invitrogen/A21206
Donkey anti-rabbit IgG (IF)	Alexa Fluor 594	1:1000	Invitrogen/A21207
Goat anti-rabbit IgG (WB)	IRDye800	1:10000	Rockland/611-132-122
Sheep anti-mouse IgG (WB)	IRDye800	1:10000	Rocklane/610-632-002

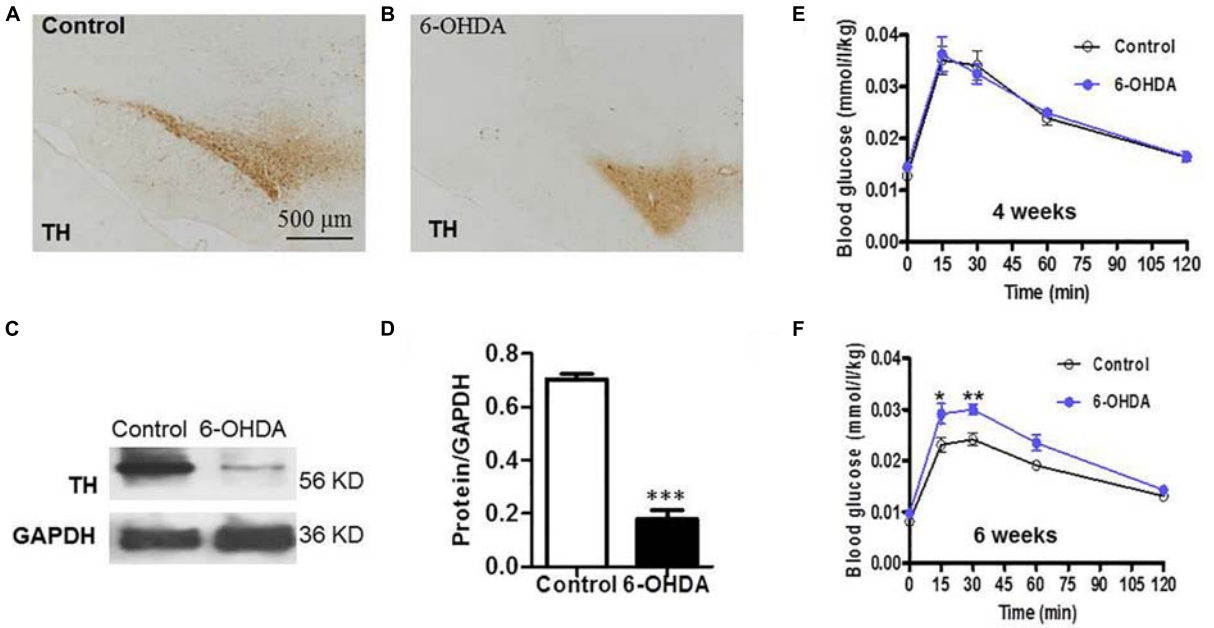

FIGURE 1 | SN lesions and attenuated glucose tolerance in 6-OHDA-induced rats. **(A)** (Control group) and **(B)** (6-OHDA group): Representative images of TH-IR neurons in the SN, Scale bar, 500 μm; **(C)** Representative western blot of TH in the SN of control and 6-OHDA rats. **(D)** Summary histogram of C, $^{*}p < 0.05$, $^{**}p < 0.01$, and $^{***}p < 0.001$ ($n = 6$). **(E,F)** Blood glucose values during the ipGTT on the 4th and 6th weeks, respectively, ($n = 10$).

detect the dopaminergic neurons in the SN. Six weeks after injecting 6-OHDA into the SN, IHC analysis showed that the field number of TH-IR neurons in the SN was significantly reduced in 6-OHDA rats (**Figure 1B**) compared with control rats (**Figure 1A**). Western blot analysis showed that the protein level of TH in the SN was markedly decreased in 6-OHDA rats compared with control rats, from 0.70 ± 0.02 to 0.18 ± 0.04 ($n = 6$, $p < 0.001$, **Figures 1C,D**).

To verify whether the loss of dopaminergic neurons in the SN caused by 6-OHDA may be associated with glucose homeostasis disturbances; blood sugar analysis was performed to identify the possible alterations associated with dopamine loss. Considering that glucose intolerance may reflect an elevation in blood glucose, glucose tolerance was assessed on the 4th and 6th weeks of the experiment. At 30 min after i.p. injecting a glucose solution, the blood glucose level of the rats treated with 6-OHDA was significantly increased compared with that of the control rats at the 6th week ($n = 10$, $p < 0.01$, **Figure 1F**), which revealed attenuated glucose tolerance in the 6-OHDA rats. The blood glucose values at 30 min were 0.02 ± 0.00 (mmol/L/kg) in the control group and 0.03 ± 0.00 (mmol/L/kg) in the 6-OHDA group after normalization to body weight. However, this difference between the two groups was not observed at the 4th week (**Figure 1E**).

Decreased Expression of D2 and TH in the PVN of 6-OHDA-Induced Rats

To evaluate the effect of the degeneration of dopaminergic neurons in the SN on the DRs in the PVN and their relationship with dopaminergic fibers, double IF and western blot were used. Both TH-IR neurons and nerve fibers were observed in the PVN (**Figures 2Ab,Bb**). D1-IR and D2-IR neurons were also detected in the PVN (**Figures 2Aa,Ba**), which was consistent with our previous study (Ran et al., 2019). Double labeling experiments showed that TH-IR neurons were also D1/D2-IR (**Figures 2Ac,d,Bc,d**), while the D1/D2-IR neurons were surrounded by the majority of the TH-IR fibers (**Figures 2Ad,d′,Bd,d′**) in the PVN. However, nearly all the TH-IR neurons were lost in the 6-OHDA rats, and only TH-IR fibers were left (**Figures 2Ab,b′,c,c′,Bb,b′,c,c′**). In addition, after the destruction of dopamine in the SN, the expression of D2 also significantly decreased (**Figures 2Ba,a′**), whereas there was no change in D1 expression (**Figures 2Aa,a′**). The western blot results were consistent with the IF results, which further confirmed the reality of the expression of TH and D1/D2 (**Figures 2C,D**).

Increased Expression of CRH, ACTH, and CORT in the HPA System of 6-OHDA Rats

The CRH-related HPA axis in the rat consists of CRH in the PVN, ACTH in the pituitary gland and glucocorticoids (mainly CORT) in the adrenal gland, which are eventually released into the blood. To investigate the role of the HPA axis in the decreased glucose tolerance of 6-OHDA rats, hypothalamus, pituitary gland, and blood samples were collected to perform histological and immunological tests. As illustrated in **Figure 3A**, compared with control rats, the 6-OHDA rats had enhanced expression of CRH in the PVN (**Figure 3A**), and this result was

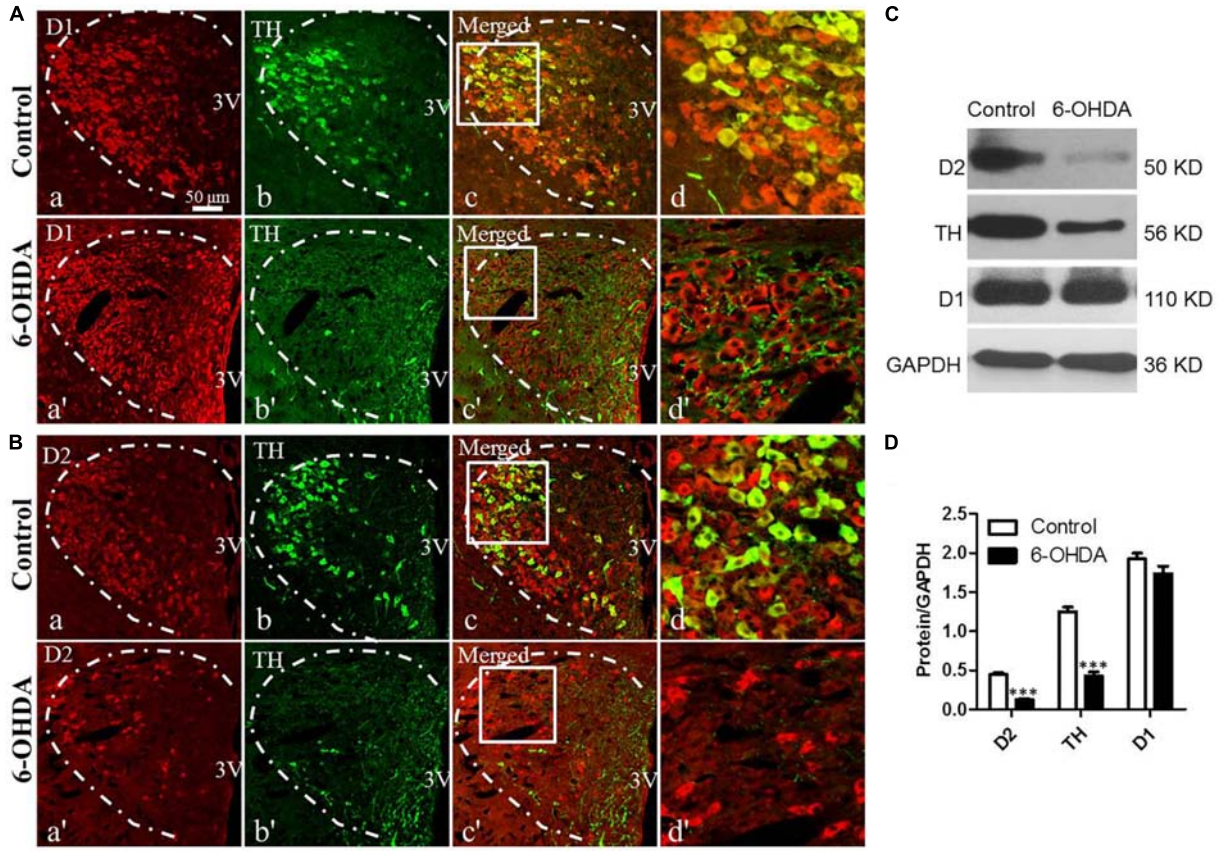

FIGURE 2 | Decreased expression of D2 and TH in the PVN of 6-OHDA-induced rats. **(A,B)** Double-labeling immunofluorescence of D1 (Aa and Aa′) or D2 (Ba and Ba′) (red) and TH (green, Control group: Ab and Bb; 6-OHDA group: Ab′ and Bb′) in the PVN neurons (white dashed frame) of the control and 6-OHDA groups; **(d,d′)** are the enlargement of the white frame in **(c,c′)**, respectively. Scale bar is 50 μm; **(C)** Representative western blot of TH, D1, and D2 in the hypothalamus of control and 6-OHDA rats. **(D)** Summary histogram of **C**, $^{***}p < 0.001$ ($n = 6$). 3v: Third ventricle.

further confirmed by western blot analysis (**Figures 3B,C**). To further confirm the correlation of D2 expression with CRH in the PVN, we employed D2 knock-out mice. We found that the CRH expression in the PVN was significantly increased in the D2 knock-out mice compared with the control mice (**Figures 3D,E**). Moreover, morphological analysis also revealed the coexpression of CRH and D2 in the PVN (**Figure 3Ad**). As expected, the contents of ACTH in the pituitary gland and CORT in the blood were significantly increased by radioimmunoassay (**Table 3**).

DISCUSSION

In the present study, we demonstrated that the central administration of 6-OHDA attenuated glucose tolerance and activated the HPA system, as evidenced by the upregulated expression of CRH in the PVN, the increased content of ACTH in the pituitary gland and the increased content of CORT in the blood in the 6-OHDA group compared with the control group. In addition, we showed that D2 was expressed on CRH-IR neurons and that when the SN was destroyed, D2 expression was downregulated. Furthermore, the D2 knock-out mice had significantly upregulated CRH in the PVN.

The dysregulation of glucose metabolism can occur early in the course of sporadic PD (Dunn et al., 2014). Several studies have suggested that type 2 diabetes mellitus (T2DM) is a risk factor for the development of PD (Hu et al., 2007; Pagano et al., 2018). An association between a gene involved in glucose metabolism control and PD was found in genetic microarray studies (Zheng et al., 2010). In addition, a high prevalence of T2DM was also reported in patients with PD (Pressley et al., 2003). The present study showed decreased glucose tolerance after the central destruction of SN dopaminergic neurons by 6-OHDA, which was consistent with the aforementioned studies and provided animal-based experimental evidence that the central dopaminergic system could influence glucose metabolism. However, the underlying pathophysiological mechanisms remain unclear.

Parkinson's disease is known to damage several brain areas and may affect the regions involved in metabolic control, such as the hypothalamus (Dayan et al., 2018) and especially the PVN (Mann and Yates, 1983; Jellinger, 1991). We previously reported that SN dopaminergic neurons directly

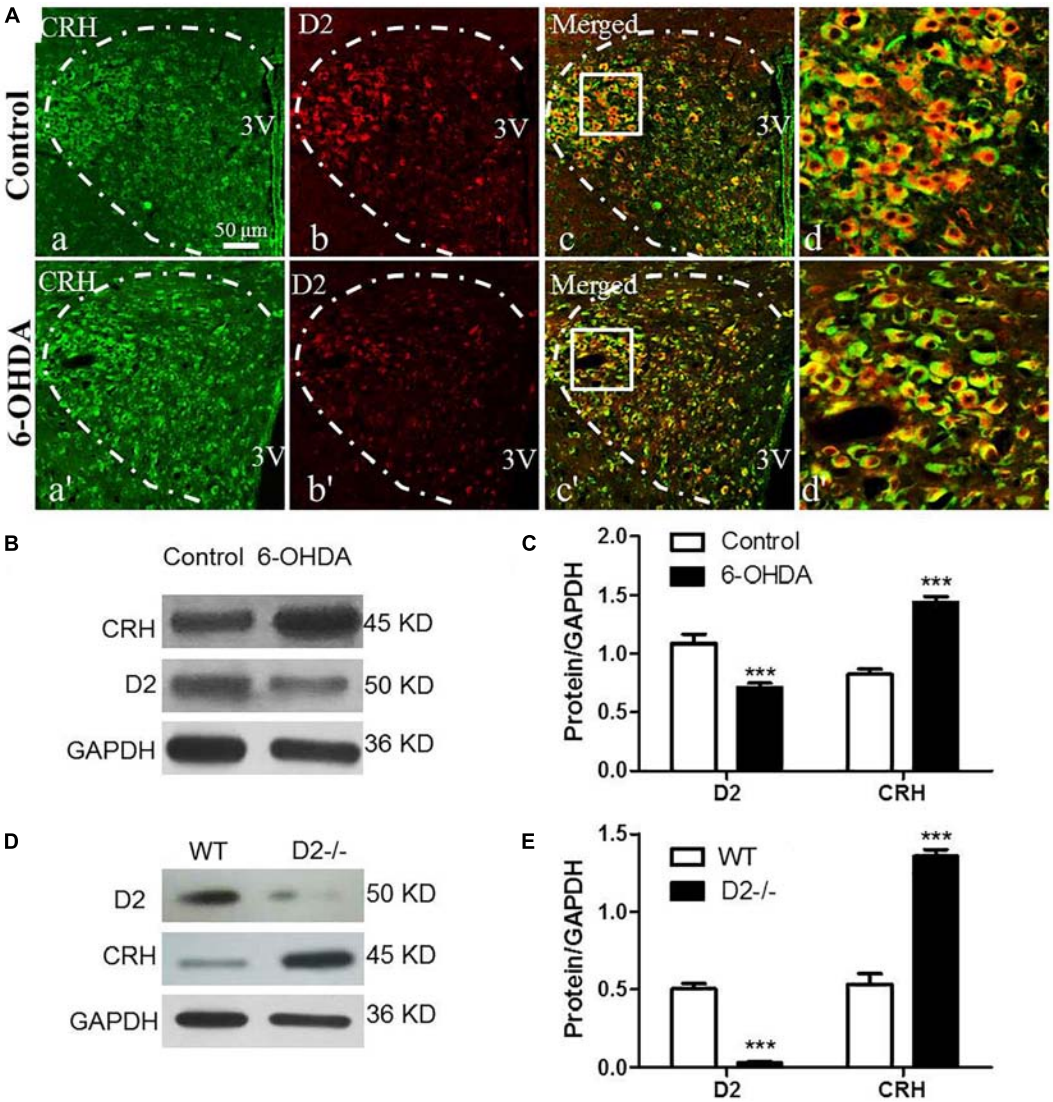

FIGURE 3 | Upregulated CRH and downregulated D2 in the PVN of 6-OHDA-induced rats. **(A)** Double-labeling immunofluorescence of CRH (green: a,a′) and D2 (red: b,b′) in the PVN neurons (white dashed frame) of the control and 6-OHDA groups; **d** and **d′** are the enlargement of the white frame in **c** and **c′**, respectively. Scale bar is 50 μm; **(B)** Representative western blot of D2 and CRH in the hypothalamus of control and 6-OHDA rats. **(C)** Summary histogram of B ($n = 6$). **(D)** Representative western blot of D2 and CRH in the hypothalamus of wild type (WT) and D2−/− mice. **(E)** Summary histogram of D. ***$p < 0.001$ ($n = 6$).

TABLE 3 | Hormone contents in blood and brain tissues of rats (mean ± SD, $n = 6$).

Group	Pituitary gland	Blood
	ACTH (pg.ml^{-1})	CORT (ng.ml^{-1})
Control	2768.91 ± 290.57	82.07 ± 12.1
6-OHDA	3363.76 ± 316.56*	124.61 ± 19.1*

*ACTH, adrenocorticotropic hormone; CORT, corticosterone; *$p < 0.05$.*

project to the PVN by the neural tracing method (Wang et al., 2014). Recently, we further confirmed the expression and distribution of DRs in the PVN (Ran et al., 2019). In the present study, the coexpression of D2 and CRH in the same neurons and the surrounding TH-IR fibers provide the morphological basis for our speculation that the SN in the midbrain could regulate the function of CRH-IR neurons in the PVN of the hypothalamus via DRs. D1 and D2 are the representative subtypes of the DR family that are G protein-coupled receptors. D1 activates adenylyl cyclase and upregulates the intracellular cAMP signaling pathway, whereas D2 inhibits the adenylyl cyclase and downregulates cAMP levels (Baldessarini and Tarazi, 1996). In the present study, after the central destruction of SN dopamine by 6-OHDA, downregulated D2 was observed in the PVN and D1 was not altered, which indicates that the inhibition of CRH-IR neurons by the D2 signaling pathway was attenuated. In other words, the synthesis of CRH in the PVN was upregulated when D2 was

downregulated, which was further confirmed in D2 knock-out mice. The altered expression of D2 and CRH in the PVN provides clues for exploring HPA axis-based glucose metabolism in PD.

The HPA neuroendocrine system consists of three populations of cells, and each population of cells secretes specialized hormones. The neurons in the PVN secrete CRH (Hauger et al., 2003), the endocrine cells (corticotrophs) in the anterior pituitary secrete ACTH (Allen and Sharma, 2019), and the endocrine cells primarily in the zona fasciculata of the adrenal cortex secrete the glucocorticoid hormones cortisol and/or CORT. CORT is secreted into the systemic circulation and affects the cells throughout the body (Spencer and Deak, 2017). Glucocorticoid hormones can increase the synthesis of hepatic glycogen, reduce the utilization and decomposition of glycogen in tissues, and elevate blood sugar (Si et al., 2015). In the present study, we observed increased CRH expression in the PVN, elevated ACTH in the pituitary and increased CORT content in the blood in 6-OHDA rats. The increased CORT level in the 6-OHDA rat is possibly due to the altered HPA axis activity because of the enhanced CRH expression in the PVN and increased ACTH content in pituitary (Spencer and Deak, 2017). This hypothesis means that the dopamine in the SN could regulate the function of the HPA axis via DRs in the PVN through the SN-PVN dopaminergic nerve pathway.

The interaction between neurodegeneration and metabolic disorders is complex and is influenced by many factors, which in turn make it difficult to define causal factor(s) (Yang et al., 2017; Biosa et al., 2018; De Pablo-Fernandez et al., 2018). In the present study, it seemed that the decreased glucose tolerance was due to the loss of dopaminergic neurons in the SN, which suggests that neurodegeneration occurred first and then influenced metabolism. Patients with PD have glucose intolerance (Lipman et al., 1974). Elevated plasma cortisol is strongly associated with glucose intolerant (Reynolds et al., 2001). It is well established that cortisol excess causes insulin resistance in man (Conn and Fajans, 1956; Rooney et al., 1993), which in turn impairs the ability of insulin to suppress glucose production and glucose utilization resulted from glucocorticoid excess (Munck, 1971). It has been reported that cortisol-induced insulin resistance is due to a decrease in both hepatic and extrahepatic sensitivity to insulin which can be explained on the basis of post-receptor defect (Rizza et al., 1982). Therefore, in our present study, the observed glucose intolerance accompanied by the activated HPA axis in 6-OHDA rats could be associated with the insulin resistance. However, CORT induces the direct negative feedback of corticotrophs in the anterior pituitary and in the CRH neurons in the PVN. The activity of the HPA axis is directly and indirectly controlled by various neural activities present throughout the forebrain and brainstem. Therefore, the underlying mechanism of the abnormality of the HPA axis in patients with PD or in PD animal models remains to be elucidated.

DATA AVAILABILITY

All datasets generated for this study are included in the manuscript and/or the supplementary files.

ETHICS STATEMENT

Every procedure was approved by the Animal Care and Use Committee of Capital Medical University and was conducted according to the established guidelines of the National Institutes of Health (NIH, United States).

AUTHOR CONTRIBUTIONS

J-XZ designed the research. LZ and X-RR performed the experiments. FH and G-WL helped the data analysis and provided the technical support. LZ wrote the manuscript. J-XZ revised the manuscript.

FUNDING

This present study was supported by the National Key Research and Development Program of China (2016YFC1302203) and the National Natural Science Foundation of China (81570695, 7182014, and 31400991).

REFERENCES

Allen, M. J., and Sharma, S. (2019). *Physiology, Adrenocorticotropic Hormone (ACTH)*. Treasure Island : StatPearls Publishing LLC.

Baldessarini, R. J., and Tarazi, F. I. (1996). "Brain dopamine receptors: a primer on their current status, basic and clinical." *Harv. Rev. Psychiatry* 3, 301–325.

Biosa, A., Outeiro, T. F., Bubacco, L., and Bisaglia, M. (2018). "Diabetes Mellitus as a risk factor for parkinson's disease: a molecular point of view." *Mol. Neurobiol.* 55, 8754–8763. doi: 10.1007/s12035-018-1025-9

Conn, J. W., and Fajans, S. S. (1956). Influence of adrenal cortical steroids on carbohydrate metabolism in man. *Metabolism* 5, 114–127.

Dayan, E., Sklerov, M., and Browner, N. (2018). Disrupted hypothalamic functional connectivity in patients with PD and autonomic dysfunction. *Neurology* 90, e2051–e2058. doi: 10.1212/WNL.0000000000005641

De Pablo-Fernandez, E., Courtney, R., Holton, J. L., and Warner, T. T. (2017). "Hypothalamic alpha-synuclein and its relation to weight loss and autonomic symptoms in Parkinson's disease." *Mov. Disord.* 32, 296–298.

De Pablo-Fernandez, E., Goldacre, R., Pakpoor, J., Noyce, A. J., and Warner, T. T. (2018). Association between diabetes and subsequent Parkinson disease: a record-linkage cohort study. *Neurology* 91, e139–e142. doi: 10.1212/WNL.0000000000005771

Dunn, L., Allen, G. F., Mamais, A., Ling, H., Li, A., Duberley, K. E., et al. (2014). "Dysregulation of glucose metabolism is an early event in sporadic Parkinson's disease." *Neurobiol. Aging* 35, 1111–1115. doi: 10.1016/j.neurobiolaging.2013.11.001

Hauger, R. L., Grigoriadis, D. E., Dallman, M. F., Plotsky, P. M., Vale, W. W., and Dautzenberg, F. M. (2003). International Union of Pharmacology. XXXVI. current status of the nomenclature for receptors for corticotropin-releasing factor and their ligands. *Pharmacol. Rev.* 55, 21–26.

Hu, G., Jousilahti, P., Bidel, S., Antikainen, R., and Tuomilehto, J. (2007). Type 2 diabetes and the risk of Parkinson's disease. *Diabetes Care* 30, 842–847.

Jackson-Lewis, V., Blesa, J., and Przedborski, S. (2012). "Animal models of Parkinson's disease." *Parkinsonism Relat. Disord.* 18(Suppl. 1), S183–S185. doi: 10.1016/S1353-8020(11)70057-8

Jellinger, K. A. (1991). Pathology of Parkinson's disease. changes other than the nigrostriatal pathway. *Mol. Chem. Neuropathol.* 14, 153–197.

Lipman, I. J., Boykin, M. E., and Flora, R. E. (1974). Glucose intolerance in Parkinson's disease. *J. Chronic. Dis.* 27, 573–579.

Lu, J., Montgomery, B. K., Chatain, G. P., Bugarini, A., Zhang, Q., Wang, X., et al. (2018). "Corticotropin releasing hormone can selectively stimulate glucose uptake in corticotropinoma via glucose transporter 1." *Mol. Cell. Endocrinol.* 470, 105–114. doi: 10.1016/j.mce.2017.10.003

Mann, D. M., and Yates, P. O. (1983). "Pathological basis for neurotransmitter changes in Parkinson's disease." *Neuropathol. Appl. Neurobiol.* 9, 3–19.

Munck, A. (1971). "Glucocorticoid inhibition of glucose uptake by peripheral tissues: old and new evidence, molecular mechanisms, and physiological significance." *Perspect. Biol. Med.* 14, 265–269.

Oh, T. J., Shin, J. Y., Kang, G. H., Park, K. S., and Cho, Y. M. (2013). "Effect of the combination of metformin and fenofibrate on glucose homeostasis in diabetic Goto-Kakizaki rats." *Exp. Mol. Med.* 45:e30. doi: 10.1038/emm.2013.58

Pagano, G., Polychronis, S., Wilson, H., Giordano, B., Ferrara, N., Niccolini, F., et al. (2018). Diabetes mellitus and Parkinson disease. *Neurology* 90, e1654–e1662. doi: 10.1212/WNL.0000000000005475

Pfeiffer, R. F. (2016). "Non-motor symptoms in Parkinson's disease." *Parkinsonism. Relat. Disord.* 22(Suppl. 1), S119–S122. doi: 10.1016/j.parkreldis.2015.09.004

Pressley, J. C., Louis, E. D., Tang, M. X., Cote, L., Cohen, P. D., Glied, S., et al. (2003). The impact of comorbid disease and injuries on resource use and expenditures in parkinsonism. *Neurology* 60, 87–93.

Ran, X., Yang, Y., Meng, Y., Li, Y., Zhou, L., Wang, Z., et al. (2019). Distribution of D1 and D2 receptor- immunoreactive neurons in the paraventricular nucleus of the hypothalamus in the rat. *J. Chem. Neuroanat.* 98, 97–103. doi: 10.1016/j.jchemneu.2019.04.002

Reynolds, R. M., Walker, B. R., Syddall, H. E., Whorwood, C. B., Wood, P. J., and Phillips, D. I. (2001). "Elevated plasma cortisol in glucose-intolerant men: differences in responses to glucose and habituation to venepuncture." *J. Clin. Endocrinol. Metab.* 86, 1149–1153.

Rizza, R. A., Mandarino, L. J., and Gerich, J. E. (1982). "Cortisol-induced insulin resistance in man: impaired suppression of glucose production and stimulation of glucose utilization due to a postreceptor detect of insulin action." *J. Clin. Endocrinol. Metab.* 54, 131–138.

Rooney, D. P., Neely, R. D., Cullen, C., Ennis, C. N., Sheridan, B., Atkinson, A. B., et al. (1993). "The effect of cortisol on glucose/glucose-6-phosphate cycle activity and insulin action." *J. Clin. Endocrinol. Metab.* 77, 1180–1183.

Si, M. W., Yang, M. K., and Fu, X. D. (2015). "Effect of hypothalamic-pituitary-adrenal axis alterations on glucose and lipid metabolism in diabetic rats." *Genet. Mol. Res.* 14, 9562–9570. doi: 10.4238/2015.August.14.19

Spencer, R. L., and Deak, T. (2017). "A users guide to HPA axis research." *Physiol. Behav.* 178, 43–65. doi: 10.1016/j.physbeh.2016.11.014

Stern, M. B., Lang, A., and Poewe, W. (2012). "Toward a redefinition of Parkinson's disease." *Mov. Disord.* 27, 54–60.

Wang, Z. Y., Lian, H., Cai, Q. Q., Song, H. Y., Zhang, X. L., Zhou, L., et al. (2014). No direct projection is observed from the substantia nigra to the dorsal vagus complex in the rat. *J. Parkinsons. Dis.* 4, 375–383. doi: 10.3233/JPD-130279

Yang, Y. W., Hsieh, T. F., Li, C. I., Liu, C. S., Lin, W. Y., Chiang, J. H., et al. (2017). Increased risk of Parkinson disease with diabetes mellitus in a population-based study. *Medicine* 96:e5921. doi: 10.1097/MD.0000000000005921

Zheng, B., Liao, Z., Locascio, J. J., Lesniak, K. A., Roderick, S. S., Watt, M. L., et al. (2010). PGC-1alpha, a potential therapeutic target for early intervention in Parkinson's disease. *Sci Transl Med* 2:52ra73. doi: 10.1126/scitranslmed.3001059

Zheng, L., Wang, Z., Li, X., Song, J., Hong, F., Lian, H., et al. (2011). Reduced expression of choline acetyltransferase in vagal motoneurons and gastric motor dysfunction in a 6-OHDA rat model of Parkinson's disease. *Brain Res.* 1420, 59–67. doi: 10.1016/j.brainres.2011.09.006

Zheng, Z., and Travagli, R. A. (2007). Dopamine effects on identified rat vagal motoneurons. *Am. J. Physiol. Gastrointest. Liver Physiol.* 292, G1002–G1008.

Zhou, L., Wang, Z. Y., Lian, H., Song, H. Y., Zhang, Y. M., Zhang, X. L., et al. (2014). Altered expression of dopamine receptors in cholinergic motoneurons of the hypoglossal nucleus in a 6-OHDA-induced Parkinson's disease rat model. *Biochem. Biophys. Res. Commun.* 452, 560–566. doi: 10.1016/j.bbrc.2014.08.104

Conflict of Interest Statement: The authors declare that the research was conducted in the absence of any commercial or financial relationships that could be construed as a potential conflict of interest.

frontiers in Endocrinology

ORIGINAL RESEARCH
published: 16 August 2019
doi: 10.3389/fendo.2019.00564

Association of Cortisol Levels With Neuropsychiatric Functions: A Mendelian Randomization Analysis

Xiang Zhou[1] *and Nidan Qiao*[1,2]*

[1] Department of Neurosurgery, Huashan Hospital, Fudan University, Shanghai, China, [2] Neuroendocrine Unit, Massachusetts General Hospital, Harvard Medical School, Boston, MA, United States

Aim: The conflicting evidence as to whether a real association exists between cortisol levels and depression lends support to adopting a Mendelian randomization approach to investigate whether cortisol levels have a causal effect with depression.

Methods: Single nucleotide polymorphisms (SNPs) associated with serum morning plasma cortisol level and salivary cortisol level from CORNET consortium (12,597 participants) were proposed as instrumental variables. The primary outcome was depression, and the secondary outcomes were neuroticism and cognitive performance. Summary-level statistics were extracted from the Social Science Genetic Association Consortium including the United Kingdom Biobank cohort (105,739 subjects). Multiple analysis methods (inverse-variance weighted method, max likelihood method, weighted median estimator, model-based estimation, heterogeneity-penalized method, and MR-Egger regression) were applied to test the stability of the summary causal estimate.

Results: Weighted median analysis estimated that the effect of serum morning cortisol on depression score was 0.027 per standard deviation increase of cortisol (95% CI, 0.000–0.054; $p = 0.043$). Other sensitivity analysis suggested similar results suggesting the result was robust. No evidence of pleiotropy (MR-Egger intercept, −0.002; $p = 0.739$) was observed. The effect of serum cortisol on neuroticism was 0.030 (95% CI, 0.008–0.052; $p = 0.006$) by weighted median estimator. None of the methods observed the effect of serum cortisol level on cognitive function. As for the effect of salivary cortisol level, no method obtained a p-value lower than 0.05 in any of the outcomes.

Conclusion: Mendelian randomization analysis provided evidence that a genetic predisposition to higher serum morning cortisol level was associated with increased depression score.

Keywords: Cushing's syndrome, depression, neuroendocrinology, single nucleotide polymorphisms, cortisol

OPEN ACCESS

Edited by:
Xue Qun Chen,
Zhejiang University, China

Reviewed by:
Yu-Feng Wang,
Harbin Medical University, China
Nicolas Ramoz,
Institut National de la Santé et de la Recherche Médicale (INSERM), France
Yudan Liu,
China Medical University, China

***Correspondence:**
Nidan Qiao
norikaisa@gmail.com;
nidan_qiao@hms.harvard.edu

Specialty section:
This article was submitted to Neuroendocrine Science, a section of the journal Frontiers in Endocrinology

Received: *05 December 2018*
Accepted: *02 August 2019*
Published: *16 August 2019*

Citation:
Zhou X and Qiao N (2019) Association of Cortisol Levels With Neuropsychiatric Functions: A Mendelian Randomization Analysis. Front. Endocrinol. 10:564. doi: 10.3389/fendo.2019.00564

INTRODUCTION

One of the most common psychiatric diseases in Cushing's syndrome is major depression with the prevalence of 50–81% (1). Some studies have reported an improvement in neuropsychiatric disorders after the resolution of hypercortisolism, suggesting the causal effect of cortisol on depression (2).

Morning serum cortisol and salivary cortisol levels are two diagnostic tools for Cushing's syndrome. Studies about the causaleffect of cortisol levels on depression varied among studies. The

positive association between cortisol measures with overall depressive symptoms was observed in the TRAILS cohort (3).

Midnight salivary cortisol was associated with self-reported depression in patients with type 1 diabetes (4). Caparros-Gonzalez et al. (5) used hair cortisol level as a positive predictor for postpartum depression. On the contrary, several studies observed a negative association of cortisol levels and depression. Lower cortisol awakening response correlated with subclinical depression in young subjects (6). Rhebergen et al. (7) found a blunted cortisol awakening response in older people with the depressive disorder. Low salivary cortisol concentration is a risk factor of depression recurrence in another 2-year follow-up study (8).

Neuroticism and cognitive performance are two other neuropsychiatric assessment in patients with Cushing's syndrome. Increased prevalence of neuroticism was observed in patients with Cushing's disease but without knowing the effect size (9, 10). Studies on cognitive performance in chronic exposure of cortisol were controversial with both positive and negative results (11, 12).

Mendelian randomization is an analytic method that involves finding genetic proxies for a target exposure and then testing the association with the outcome (13) (**Figure 1**). This approach avoids some of the limitations of observational studies (free from measured or unmeasured confounding) and is not affected by the disease, thereby avoiding reverse causation bias (14). On the other hand, summary-level data of large genome-wide association studies (GWAS) are increasingly available and allow the use of combinations of single nucleotide polymorphisms (SNPs) in Mendelian randomization analyses.

The conflicting evidence of whether a real association exists between cortisol levels and depression and if so, the magnitude of that association lends support to adopting a Mendelian randomization approach. We hypothesized that cortisol levels have a causal effect on depression as well as neuroticism and cognitive performance. We conducted a Mendelian randomization study, using summary-level data from publicly available GWAS to investigate the causal relationship of cortisol levels with depression as well as neuroticism and cognitive performance.

METHODS

Study Design and Data Sources

The mendelian randomization approach used in this study builds on three assumptions (13, 15) (**Figure 1**). First, the genetic variants [instrumental variables: single nucleotide polymorphisms (SNPs)] are predictive of the exposure (cortisol levels); second, the genetic variants are only associated with the outcome (neuropsychiatric functions) through the variants-exposure-outcome pathway; third, the variants do not share common causes with the outcomes. This study involved analysis of publicly available, summary-level data; specific ethical review and informed consent were obtained in all of the original studies. Ethical approval of this study was not required due to not involving human subjects.

Instrumental Variables

CORNET consortium was a genome-wide association study (GWAS) for genetic association with serum morning cortisol and salivary cortisol levels (16, 17). The GWAS was conducted in 12,597 individuals of European ancestry (established in a cohort of 74.9 $\pm$ 5.7 years old with 45.4% of male and validated in a cohort of 60.9 $\pm$ 5.7 years old with 77.7% of male). Eighteen SNPs associated with serum morning cortisol level at the genome-wide significance level ($p < 5.0 \times 10^{-8}$) in the discovery cohorts (**Supplement Table 1**). Effect alleles in these SNPs associated with at least 0.07 standard deviation (SD) increase of serum morning cortisol level in the log scale.

Though no SNPs associated with salivary cortisol levels at the genome-wide significance level were identified, we still extracted two SNPs at the significance level of $p < 5.0 \times 10^{-7}$ (**Supplement Table 2**). Effect alleles in these two SNPs were associated with at least 0.12 SD increase of salivary cortisol level in the log scale.

Outcomes

The primary outcome was depression. We extracted summary-level statistics for the associations of the cortisol-associated SNPs from the study conducted by Okbay et al. (18) in 105,739 subjects. The population came from UK Biobank (UKB) cohorts. The outcome used a continuous measure by combining responses to two questions. The first question was: "Over the past 2 weeks, how often have you felt down, depressed or hopeless?" The second question was: "Over the past 2 weeks, how often have you had little interest or pleasure in doing things?" Answers were categorized into: (1) "Not at all," (2) "Several days," (3) "More than half the days," and (4) "Nearly every day."

The secondary outcomes were neuroticism and cognitive performance. We extracted summary-level statistics of neuroticism from a population of 168,105 subjects with the population coming from the Genetics of Personality Consortium (GPC) and UKB data (18). The outcome used in UKB cohort was summing response of a 12-item version of the Eysenck Personality Inventory (mean: 4.16, SD: 3.23). The outcome used in GPC was harmonized different neuroticism batteries. The summary-level statistics of cognitive performance were obtained from a recently published study (19) using the respondent's score on a test of verbal cognition.

Sensitivity Analyses

We used multiple analysis methods (inverse-variance weighted method, max likelihood method, weighted median estimator, model-based estimation, and heterogeneity-penalized method) to test the stability of the summary causal estimate. We used MR-Egger regression to test pleiotropy. In the absence of statistical evidence for horizontal pleiotropy (the intercept from MR-Egger not differed from zero), we used the conventional Mendelian randomization analyses as they retain greater power (20). We further examined the stability of the summary causal estimate by excluding SNPs with high linkage disequilibrium with each other from the instrumental variables.

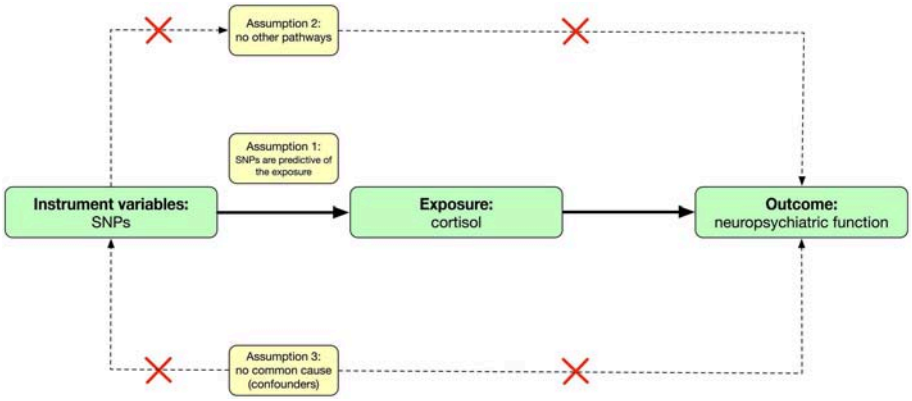

FIGURE 1 | Causal diagram and three assumptions in mendelian randomization.

Statistical Analysis

The SD for cortisol in the GWAS cohorts was around 200 nmol/L, with a SD of 1 for depression symptom score. Assuming that the lowest observational causal effect is 0.003 depression score increase per 1 nmol/L cortisol increase based on observational studies (21, 22), and also assuming that the genetic instrument explains only 1% of variation in cortisol level (16, 17), the calculated power of this Mendelian randomization study in 100,000 subjects was 35% (23). If we assume that the causal effect is 0.01 depression score increase per 1 nmol/L cortisol increase, the calculated power will be 100%.

SNPs were matched across the data sources by assigning them to the same effect allele. The association of each SNP with primary or secondary outcomes was weighted by its association with cortisol levels. The effect of cortisol levels on primary or secondary outcomes was scaled per SD increase. Statistical tests for the Mendelian randomization analyses were considered significant at $p = 0.05$. All analyses were conducted in R version 3.2.5.

RESULTS

In the UKB cohort (British population-based cohort focused on individuals in the age range 40–69) for depression, the average score of the first question was 1.29 ± 0.61, the average score of the second question was 1.27 ± 0.60. The combination of those two questions achieved an average score of 2.56 ± 1.09 (18).

In the inverse-variance weighted analysis, the effect of serum morning cortisol on depression score was 0.014 per SD increase of cortisol (95% CI, −0.002–0.030; $p = 0.081$) (**Figure 2**). Max likelihood method obtained almost the same estimation and confidence interval. Weighted median estimated the effect to be 0.027 (95% CI, 0.000–0.054; $p = 0.043$). Model-based estimation also obtained almost the same estimation and confidence interval with weighted median estimator. The effect was 0.014 (95% CI, −0.001–0.029) using the heterogeneity-penalized method. The association between serum cortisol levels and depression score was consistent in MR-Egger regression, although with a wider confidence interval (0.042, [95% CI, −0.125–0.209]). There was no evidence of pleiotropy (MR-Egger intercept, −0.002; $p = 0.739$, **Figure 3**). No heterogeneity was observed between the estimates from different methods ($I^2 = 0\%$, $p = 0.76$ for heterogeneity).

Inverse-variance weighted and max likelihood estimation obtained null results (0.011, [95% CI, −0.011–0.032, $p = 0.322$] and 0.012, [95% CI, −0.011–0.034, $p = 0.563$], respectively) regarding the effect of serum cortisol on neuroticism (**Figure 2**). The effect using weighted median estimator, model-based estimation and heterogeneity-penalized method were 0.030 (95% CI, 0.008–0.052, $p = 0.006$), 0.042 (95% CI, 0.011–0.073, $p = 0.008$) and 0.028 (95% CI, 0.002–0.047), respectively. None of the method observed effect of serum cortisol level on cognitive function, p-values ranged from 0.277 to 0.674 (**Figure 2**).

As for the effect of salivary cortisol level, no method obtained a p-value lower than 0.05 in any of the outcomes (**Figure 4**).

In the sensitivity analysis excluding SNPs with high linkage disequilibrium with each other, which provided 8 SNPs in the remaining instrumental variables, the effect of serum morning cortisol level on depression score using weighted median estimator was 0.026 (95% CI, −0.002–0.055, $p = 0.072$, **Supplement Figure 1**).

DISCUSSION

To reveal the causal effects of cortisol levels on the depression, we conducted this Mendelian randomization analysis using public available summary-level data in Caucasian subjects. We observed positive associations of serum morning cortisol with self-report depression score and neuroticism score.

Among three assumptions of Mendelian randomization, using serum cortisol associated SNPs as instrumental variables in this study probably meet the first assumption. Effect alleles in each SNP were associated with at least 0.07 SD increase of cortisol level. Proposed salivary cortisol associated SNPs as instrumental variables may violate this assumption due to failing the genome-wide significant level. This may explain that no causal effect was observed between salivary cortisol and the outcomes.

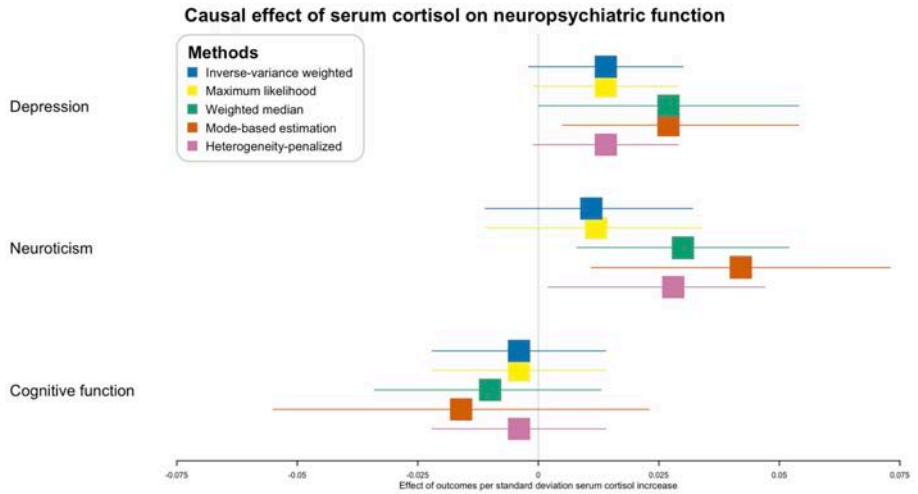

FIGURE 2 | Causal effect of serum morning cortisol level on neuropsychiatric functions. X-axis represents the effect of per standard deviation of serum cortisol increase on the neuropsychiatric outcomes. Boxes represent point estimations of the effect with the 95% confidence interval. Different colors represent different statistical methods.

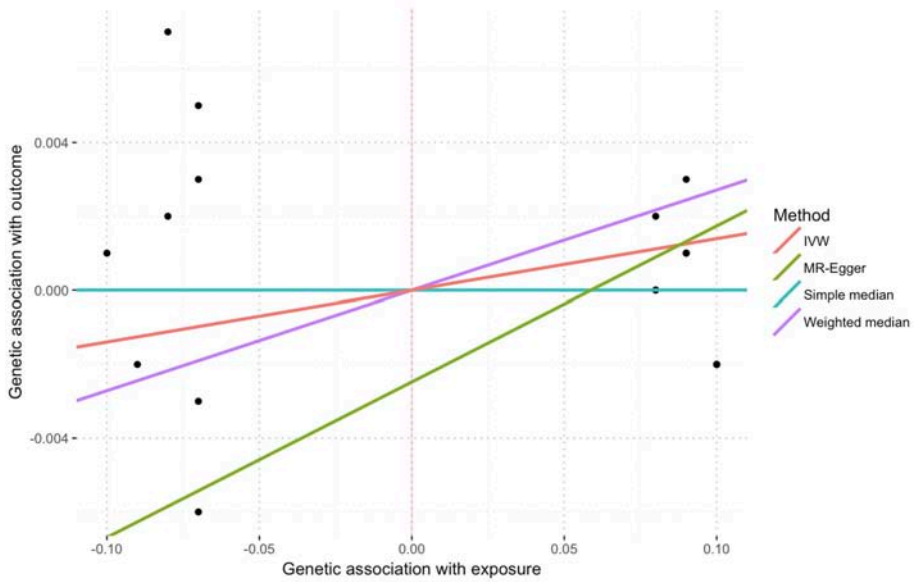

FIGURE 3 | Sensitivity plot of genetic association with exposure vs. with outcome using multiple methods. Points represent SNPs. There was no evidence of pleiotropy represent by the intercept of MR-Egger (-0.002, $p = 0.739$).

The second Mendelian randomization assumption may be violated when instrumental variables display associations with the outcome through pathways that are distinct to the one from exposure through to outcome (15). Though the second assumption was not verifiable, we adopted several approaches to minimize the originated bias. We evaluated each cortisol-associated SNP for pleiotropic associations with potential known confounders, including body mass index and diabetes. None of these SNPs had pleiotropic associations at the Bonferroni-corrected significance threshold [($p < 0.05$)/18 SNPs = 0.003, **Supplement Table 3**]. We used MR-Egger regression as one of the sensitivity tests, which provided a valid test of pleiotropy (no evidence of pleiotropy) and a valid test of the causal null hypothesis. The slope of MR-Egger regression (0.042, **Figure 4**) provided a consistent estimate of the true causal effect (20).

The third mendelian randomization assumption may also be violated when instrumental variables and outcomes share common causes (15). This may be the case in population stratification and linkage disequilibrium. We restricted the study in the frame of the European population, which minimized the risk of population stratification. We also searched SNPs in the same linkage disequilibrium block but not included in the

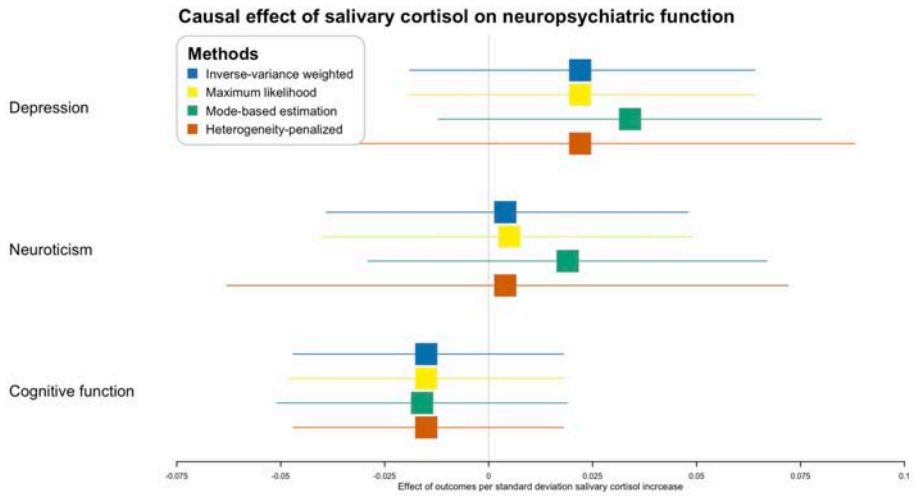

FIGURE 4 | Causal effect of salivary cortisol level on neuropsychiatric functions. X-axis represents the effect of per standard deviation of salivary cortisol increase on the neuropsychiatric outcomes. Boxes represent point estimations of the effect with the 95% confidence interval. Different colors represent different statistical methods.

instrumental variables (261 SNPs). No association of those SNPs with the outcomes (**Supplement Table 4**) was observed at the Bonferroni-corrected significance level [$(p < 0.05)/261$ SNPs $= 0.0002$]. In the sensitivity analysis, we removed SNPs with high association with each other. The point estimations almost unchanged, though the confidence intervals of most methods included the null hypothesis, which was caused by decreased number of instrumental variables.

SNPs associated with serum cortisol level and saliva cortisol level were established and validated in two different cohorts with different ages and different gender proportion, which suggests age and gender do not influence the association between SNPs and cortisol levels. On the other hand, UKB is a relatively younger cohort comparing to the two discovering cohorts, but we argue that even though age is associated with the outcomes, there is no evidence that age would be associated with the SNPs.

We used five different statistical methods to estimate the causal effect because either method had its own advantage. Inverse-variance weighted method is biased when one genetic variant is an invalid instrument variable (24). Weighted median gives consistent estimation when 50% of the genetic variants is valid (24). Maximum likelihood method has been encouraged especially in weak instruments due to the unbiased estimation (25). The model base estimation and heterogeneity-penalized method presented less bias and lower type-I error rates than other methods under the null (26, 27). MR-Egger method is consistent even when 100% of genetic variants are invalid but has wider confidence interval than inverse-variance weighted or median-based methods (24).

In patients with Cushing's syndrome, morning serum cortisol level may increase by 10 standard deviations in certain patients, which may result in the depression score increase by approximately 0.2 (roughly half day of depression according to the question and answer in the phenotype). The finding from this study supports results from several observational studies showing a positive association of serum cortisol levels with risk of depression (3–5). Different scales used in the outcome among studies increase the difficulty of comparison. Findings from observational studies further show that recovery of hypercortisolemia is associated with recovery of depression (1, 28). The positive association between serum cortisol and neuroticism also supports previous observational studies (9, 10, 29–31).

This was the first study to investigate the causal relation of cortisol levels with depression using a very large sample and a method that may allow for unbiased estimates. The results in this study were robust with multiple sensitivity analysis indicating that confounding is unlikely to explain the observed association.

This study has some limitations. First, although we used several approaches in an attempt to rule out pleiotropy, it was still possible that the association of SNPs and depression were through other pathways. A shared genetic basis between SNPs and depression cannot be ruled out either. Second, outcomes derived from self-report answers. Although the continuous outcomes were more likely to increase power than binomial diagnostic data in this study, their clinical use has not been validated. The DSM diagnosis can be used for depression in future studies. Third, only two SNPs were associated with salivary cortisol levels in the original GWAS which made the analysis not robust on the effect of salivary cortisol levels. Besides, neither individual-level SNP data nor a replication data set with a similarly large number of depression cohort were not available. Fourth, this analysis was restricted to individuals of European ancestry, thus hindering the generalizability in the whole population. The results were derived from only statistical analyses and thus, they have to be presented with more cautions. Future studies may investigate cortisol level and genotyping from subjects with depression from the UKB cohorts to see if the genetic

variants confirm the association of the cortisol exposure with the disease.

CONCLUSIONS

Mendelian randomization analysis provided evidence that a genetic predisposition to higher serum morning cortisol level was associated with increased depression score.

AUTHOR CONTRIBUTIONS

NQ: conception and design of the study. XZ: acquisition and analysis of data and drafting the manuscript.

FUNDING

This study was supported by Shanghai Committee of Science and Technology, China (grant nos. 17JC1402100 and 17YF1426700). NQ was supported by 2018 Milstein Medical Asian American Partnership Foundation Fellowship Award in Translational Medicine.

SUPPLEMENTARY MATERIAL

The Supplementary Material for this article can be found online at: https://www.frontiersin.org/articles/10.3389/fendo.2019.00564/full#supplementary-material

REFERENCES

1. Pivonello R, Isidori AM, De Martino MC, Newell-Price J, Biller BMK, Colao A. Complications of Cushing's syndrome: state of the art. *Lancet Diab Endocrinol.* (2016) 4:611–29. doi: 10.1016/S2213-8587(16)00086-3
2. Pivonello R, Simeoli C, De Martino MC, Cozzolino A, De Leo M, Iacuaniello D, et al. Neuropsychiatric disorders ex Cushing's syndrome. *Front Neurosci.* (2015) 9:129. doi: 10.3389/fnins.2015.00129
3. Dietrich A, Ormel J, Buitelaar JK, Verhulst FC, Hoekstra PJ, Hartman CA. Cortisol in the morning and dimensions of anxiety, depression, and aggression in children from a general population and clinic-referred cohort: an integrated analysis. The TRAILS study. *Psychoneuroendocrinology.* (2013) 38:1281–98. doi: 10.1016/j.psyneuen.2012.11.013
4. Melin EO, Thunander M, Landin-Olsson M, Hillman M, Thulesius HO. Depression, smoking, physical inactivity and season independently associated with midnight salivary cortisol in type 1 diabetes. *BMC Endocr Disord.* (2014) 14:75. doi: 10.1186/1472-6823-14-75
5. Caparros-Gonzalez RA, Romero-Gonzalez B, Strivens-Vilchez H, Gonzalez-Perez R, Martinez-Augustin O, Peralta-Ramirez MI. Hair cortisol levels, psychological stress and psychopathological symptoms as predictors of postpartum depression. *PLoS ONE.* (2017) 12:e0182817. doi: 10.1371/journal.pone.0182817
6. Dedovic K, Engert V, Duchesne A, Lue SD, Andrews J, Efanov SI, et al. Cortisol awakening response and hippocampal volume: vulnerability for major depressive disorder? *Biol Psychiatry.* (2010) 68:847–53. doi: 10.1016/j.biopsych.2010.07.025
7. Rhebergen D, Korten NCM, Penninx BWJH, Stek ML, van der Mast RC, Oude Voshaar R, et al. Hypothalamic-pituitary-adrenal axis activity in older persons with and without a depressive disorder. *Psychoneuroendocrinology.* (2015) 51:341–50. doi: 10.1016/j.psyneuen.2014.10.005
8. Grynderup MB, Kolstad HA, Mikkelsen S, Andersen JH, Bonde JP, Buttenschøn HN, et al. A two-year follow-up study of salivary cortisol concentration and the risk of depression. *Psychoneuroendocrinology.* (2013) 38:2042–50. doi: 10.1016/j.psyneuen.2013.03.013
9. Kelly WF, Kelly MJ, Faragher B. A prospective study of psychiatric and psychological aspects of Cushing's syndrome. *Clin Endocrinol.* (1996) 45:715–20.
10. Dimopoulou C, Ising M, Pfister H, Schopohl J, Stalla GK, Sievers C. Increased prevalence of anxiety-associated personality traits in patients with Cushing's disease: a cross-sectional study. *Neuroendocrinology.* (2013) 97:139–45. doi: 10.1159/000338408
11. Forget H, Lacroix A, Bourdeau I, Cohen H. Long-term cognitive effects of glucocorticoid excess in Cushing's syndrome. *Psychoneuroendocrinology.* (2016) 65:26–33. doi: 10.1016/j.psyneuen.2015.11.020
12. Heald A, Parr C, Gibson C, O'driscoll K, Fowler H. A cross-sectional study to investigate long-term cognitive function in people with treated pituitary Cushing's disease. *Exp Clin Endocrinol Diab.* (2006) 114:490–7. doi: 10.1055/s-2006-924332
13. Thanassoulis G, O'Donnell CJ. Mendelian randomization: nature's randomized trial in the post-genome era. *JAMA.* (2009) 301:2386–8. doi: 10.1001/jama.2009.812
14. Haycock PC, Burgess S, Wade KH, Bowden J, Relton C, Davey Smith G. Best (but oft-forgotten) practices: the design, analysis, and interpretation of Mendelian randomization studies. *Am J Clin Nutr.* (2016) 103:965–78. doi: 10.3945/ajcn.115.118216
15. Smith GD, Ebrahim S. "Mendelian randomization": can genetic epidemiology contribute to understanding environmental determinants of disease? *Int J Epidemiol.* (2003) 32:1–22. doi: 10.1093/ije/dyg070
16. Velders FP, Kuningas M, Kumari M, Dekker MJ, Uitterlinden AG, Kirschbaum C, et al. Genetics of cortisol secretion and depressive symptoms: a candidate gene and genome wide association approach. *Psychoneuroendocrinology.* (2011) 36:1053–61. doi: 10.1016/j.psyneuen.2011.01.003
17. Neumann A, Direk N, Crawford AA, Mirza S, Adams H, Bolton J, et al. The low single nucleotide polymorphism heritability of plasma and saliva cortisol levels. *Psychoneuroendocrinology.* (2017) 85:88–95. doi: 10.1016/j.psyneuen.2017.08.011
18. Okbay A, Baselmans BML, De Neve J-E, Turley P, Nivard MG, Fontana MA, et al. Genetic variants associated with subjective well-being, depressive symptoms, and neuroticism identified through genome-wide analyses. *Nat Genet.* (2016) 48:624–33. doi: 10.1038/ng.3552
19. Lee JJ, Wedow R, Okbay A, Kong E, Maghzian O, Zacher M, et al. Gene discovery and polygenic prediction from a genome-wide association study of educational attainment in 1.1 million individuals. *Nat Genet.* (2018) 50:1112–21. doi: 10.1038/s41588-018-0147-3
20. Bowden J, Davey Smith G, Burgess S. Mendelian randomization with invalid instruments: effect estimation and bias detection through Egger regression. *Int J Epidemiol.* (2015) 44:512–25. doi: 10.1093/ije/dyv080
21. Xu Y, Yao S, Wei H, Zhu X, Yu M, Li Y. Application value of selected serum indicators in the differential diagnosis of geriatric depression and transient depressive state. *NDT.* (2018) 14:459–65. doi: 10.2147/NDT.S152247
22. Doolin K, Farrell C, Tozzi L, Harkin A, Frodl T, O'Keane V. Diurnal hypothalamic-pituitary-adrenal axis measures and inflammatory marker correlates in major depressive disorder. *Int J Mol Sci.* (2017) 18:2226. doi: 10.3390/ijms18102226
23. Brion M-JA, Shakhbazov K, Visscher PM. Calculating statistical power in Mendelian randomization studies. *Int J Epidemiol.* (2013) 42:1497–501. doi: 10.1093/ije/dyt179
24. Bowden J, Davey Smith G, Haycock PC, Burgess S. Consistent estimation in Mendelian randomization with some invalid instruments using a weighted median estimator. *Genet Epidemiol.* (2016) 40:304–14. doi: 10.1002/gepi.21965
25. Burgess S, Small DS, Thompson SG. A review of instrumental variable estimators for Mendelian randomization. *Stat Methods Med Res.* (2017) 26:2333–55. doi: 10.1177/0962280215597579
26. Hartwig FP, Davey Smith G, Bowden J. Robust inference in summary data Mendelian randomization via the zero modal pleiotropy

assumption. *Int J Epidemiol.* (2017) 46:1985–98. doi: 10.1093/ije/dyx102
27. Burgess S, Zuber V, Gkatzionis A, Rees JMB, Foley C. Improving on a modal-based estimation method: model averaging for consistent and efficient estimation in Mendelian randomization when a plurality of candidate instruments are valid. *Epidemiology*. (2017) 2017:1–28. doi: 10.1101/175372
28. Dorn LD, Burgess ES, Friedman TC, Dubbert B, Gold PW, Chrousos GP. The longitudinal course of psychopathology in Cushing's syndrome after correction of hypercortisolism. *J Clin Endocrinol Metab.* (1997) 82:912–9. doi: 10.1210/jcem.82.3.3834
29. Rietschel L, Streit F, Zhu G, McAloney K, Kirschbaum C, Frank J, et al. Hair cortisol and its association with psychological risk factors for psychiatric disorders: a pilot study in adolescent twins. *Twin Res Hum Genet*. (2016) 19:438–46. doi: 10.1017/thg.2016.50
30. Garcia-Banda G, Chellew K, Fornes J, Perez G, Servera M, Evans P. Neuroticism and cortisol: pinning down an expected effect. *Int J Psychophysiol.* (2014) 91:132–8. doi: 10.1016/j.ijpsycho.2013.12.005
31. Hauner KKY, Adam EK, Mineka S, Doane LD, DeSantis AS, Zinbarg R, et al. Neuroticism and introversion are associated with salivary cortisol patterns in adolescents. *Psychoneuroendocrinology*. (2008) 33:1344–56. doi: 10.1016/j.psyneuen.2008.07.011

Conflict of Interest Statement: The authors declare that the research was conducted in the absence of any commercial or financial relationships that could be construed as a potential conflict of interest.

frontiers in Endocrinology

ORIGINAL RESEARCH
published: 28 August 2019
doi: 10.3389/fendo.2019.00594

The Role of Insulin Glargine and Human Insulin in the Regulation of Thyroid Proliferation Through Mitogenic Signaling

Xiaoli Sheng[1†], Kannan Yao[2†], Anwen Shao[3†], Sheng Tu[4], Xinxia Zhang[5], Ting Chen[6] and Dingguo Yao[7*]*

[1] Department of Obstetrics, The First Affiliated Hospital, School of Medicine, Zhejiang University, Hangzhou, China, [2] The Second Central Laboratory, The First Affiliated Hospital of Zhejiang Chinese Medical University, Hangzhou, China, [3] Department of Neurosurgery, Second Affiliated Hospital, School of Medicine, Zhejiang University, Hangzhou, China, [4] Department of Infectious Diseases, Collaborative Innovation Center for Diagnosis and Treatment of Infectious Diseases, The First Affiliated Hospital, School of Medicine, Zhejiang University, Hangzhou, China, [5] Department of Geriatrics, The First Affiliated Hospital, School of Medicine, Zhejiang University, Hangzhou, China, [6] Department of Ultrasonography, The First Affiliated Hospital of Zhejiang Chinese Medical University, Hangzhou, China, [7] Department of Endocrinology, The First Affiliated Hospital of Zhejiang Chinese Medical University, Hangzhou, China

OPEN ACCESS

Edited by:
Lei Sha,
China Medical University, China

Reviewed by:
Haim Werner,
Tel Aviv University, Israel
Derek LeRoith,
Icahn School of Medicine at Mount Sinai, United States

***Correspondence:**
Sheng Tu
tusheng118@163.com
Dingguo Yao
cndingguoyao@163.com

[†]These authors have contributed equally to this work

Specialty section:
This article was submitted to Neuroendocrine Science, a section of the journal Frontiers in Endocrinology

Received: *14 April 2019*
Accepted: *13 August 2019*
Published: *28 August 2019*

Citation:
Sheng X, Yao K, Shao A, Tu S, Zhang X, Chen T and Yao D (2019) The Role of Insulin Glargine and Human Insulin in the Regulation of Thyroid Proliferation Through Mitogenic Signaling. Front. Endocrinol. 10:594. doi: 10.3389/fendo.2019.00594

Our aim was to investigate whether human insulin (HI) or insulin glargine treatment could promote the proliferation of thyroid cells and determine the association between type 2 diabetes and thyroid disease. Rats were treated with different doses of HI and insulin glargine. Plasma glucose and the phosphorylation levels of the insulin receptor (IR), insulin-like growth factor 1 receptor (IGF-1R), protein kinase B (Akt), and extracellular signal-regulated kinase 1/2 (ERK1/2) were measured. A total of 105 rats were randomly assigned to three groups as follows: control group, HI group, and glargine group. Both drugs promoted the phosphorylation of IR, Akt, and ERK1/2 in a dose-dependent manner ($p < 0.05$), and the effect of glargine persisted for longer period. Treatment with ultra-therapeutic doses of HI or glargine ($p < 0.05$) increased the expression of Ki-67 in thyroid cells. The results demonstrated that therapeutic doses of glargine have a longer-lasting hypoglycemic control than HI. Based on the results, HI or glargine did not stimulate thyroid cell proliferation at therapeutic doses, but high doses did.

Keywords: insulin, glargine, thyroid disease, proliferation, insulin receptor

INTRODUCTION

Over the past few decades, it has emerged that diabetes increases the risk of many types of cancer, including thyroid cancer, colon cancer, pancreatic cancer, breast cancer, bladder cancer, and non-Hodgkin lymphoma (1). Among these cancers, thyroid cancer is the most common in diabetic patients. From a 5-years longitudinal study of over 200,000 men and women, it was concluded that diabetes increases the risk of thyroid cancer by 25%, and that the rate of thyroid cancer in women with diabetes is on the rise (2). An endocrine research institute in Copernicus University (Poland) found that patients with type 1 diabetes or type 2 diabetes have a larger thyroid volume than healthy patients, and that the incidence of thyroid diseases (such as thyroid nodules or thyroid tumors) is significantly higher in type 2 diabetes mellitus patients compared to the general population (3).

A study conducted at the American Veterans' Affairs Medical Center suggested that diabetes has a profound impact on the risk of developing thyroid nodules and cancer. Currently, five hypotheses have been proposed to explain the increased risk of thyroid nodules and tumors in diabetic patients. The hypotheses suggest that increased risk of thyroid disease could result from: (1) elevated levels of insulin, insulin resistance, insulin injections, or the use of sulfonylurea drugs; (2) increased BMI; (3) increased thyroid-stimulating hormone levels; (4) chronically elevated blood sugar and triglyceride levels; or (5) vitamin D deficiency (1). Among these hypotheses, previous research has focused on the role of high insulin levels. Diabetic patients have elevated levels of insulin, either due to the injection of exogenous drugs (insulin and its analogs), or as a secondary consequence of resistance to endogenous insulin. Moreover, it should be noted that exogenous drugs play an important role in the late stages of the disease. In the treatment of type 1 and type 2 diabetes, insulin analogs have shown high efficacy and easy application than human insulin (4). However, *in vitro* experiments (5, 6) show that protamine zinc insulin promotes proliferation of breast cancer and bladder cancer cells by increasing phosphorylation of the insulin receptor (IR) and insulin-like growth factor 1 receptor (IGF-1R), also by activating downstream phosphatidylinositol 3-kinase/mitogen-activated protein kinase (PI3K/MAPK) signaling pathways. In 2009, the Diabetologia published four epidemiological studies on diabetic patients and emphasized the potential link between glargine treatment and increased risk of cancer. This concept has caused tremendous controversy in academia regarding the safety of glargine to patients (7–10).

Endogenous human insulin and glargine can bind to IR, and high doses of insulin can also cross-react with IGF-1R. This results in the activation of the PI3K/MAPK signal pathway, which leads to increased metabolism, cell proliferation, and inhibition of apoptosis (11).

Activation of IGF-1R promotes mitosis and reduces apoptosis of tumor cells. These changes are prerequisites to tumor formation. IGF-1R is highly expressed in many cancers, and this is linked to tumor development, invasion, and metastasis. Glargine increases the affinity of endogenous insulin for IGF-1R and enhances its effects on mitosis by 6- to 8-folds (12). Glargine also increases the phosphorylation and activation of known regulators of the insulin-signaling pathway that promote cell proliferation, such as protein kinase B (Akt) and ERK1/2 (13). In this study, we examined the effect of therapeutic doses and supra-pharmacological doses of human insulin (HI) and glargine on the phosphorylation levels of IR, Akt, and ERK1/2 in rats. We also detected the pro-proliferation marker Ki-67 to explore whether HI and glargine promote thyroid cell proliferation.

MATERIALS AND METHODS

Animals

Six to eight-weeks-old pathogen-free Wistar female rats (Slac Laboratory Animal LLC, Shanghai, China) were housed in temperature-controlled environments and fed with standard chow *ad libitum*. All experimental protocols involving animals were conducted in accordance with the guidelines approved by the ethics committee for the use of experimental animals in Zhejiang Chinese Medical University. Blood glucose measurements were performed by collecting blood from tail veins. After blood glucose testing, the thyroid tissues were immediately collected.

Dosage Groups and Injection of Drugs

Rats were randomly assigned to one of three treatment groups after weighing: control group, HI group, or glargine group ($n = 35$ animals per group). Each treatment group was sub-divided into seven sub-groups, according to the time points; 0, 15, 30, 45, 60, 90, and 120 min ($n = 5$–10 per sub-group). Refer to Emily Jane Gallagher for a description of the grouping method (14). The HI and glargine groups were divided into five groups based in doses: control, 1, 12.5, 50, and 200 U/kg dose ($n = 5$–10). Two weeks before testing, all animals are acclimated to the feeding, injection and fasting protocol for 2 h before injection, but the water was injected in lieu of drug. Injectable drugs were prepared immediately before administration. HI (Novonordisk, Beijing, China) was diluted with saline, while glargine (Sanofi, Beijing, China) was diluted with PBS (pH = 4). Drugs were diluted in 100 μl 0.9% saline or PBS according to the following formula: weight (kg) of rat × experimental dose (1, 12.5, 50, or 200 U/kg) × 10 μl (glargine or human insulin) = mass of drug.

Protein Extraction

Thyroid tissue from each group was weighed to about 20 μg, and then treated with 200 μl working fluid (adding 1:100 protease inhibitor and phosphatase inhibitors to RIPA buffer inhibitor). The tissue was cut using ophthalmic scissors and homogenized with a tissue homogenizer on ice at 1,500 r/min. After mixing for 30 min, tissue homogenates were centrifuged at 12,000 r/min for 15 min at 4°C. The supernatant was collected.

Western Blot

The protein samples were separated by 10% sodium dodecyl sulfate polyacrylamide gel electrophoresis (SDS-PAGE), and blotted onto polyvinylidene fluoride membranes (Millipore, USA). All specific antibodies were purchased from Cell Signaling Technology. After blocking in Tris buffered saline and Tween 20 (TBST) containing 5% non-fat dried milk for 2 h, the membranes were incubated with specific antibodies in the following order: IR (1:800, CST 3025), pIGF-1R (1:800, CST, 2969), IGF-1R (1:800, CST, 3027), pErk1/2 (1:1000, CST, 4370), pAkt (1:1000, CST, 4060), Akt (1:1000, CST, 9272), β-actin antibodies (1:1000, BOSTER, BM0627). After 3 washes, the blots were incubated with horseradish-peroxidase-conjugated secondary antibodies at room temperature for 2 h, and visualized with ECL Plus chemiluminescence reagent kit (Beyotime, Shanghai, China) by being exposed to an autoradiographic film (BIO-RAD, ChemiDoc XRS System, USA). Protein expression levels were quantified using Quantity One software.

Immunoprecipitation

Samples were incubated with magnetic beads under rotation for 2 h at 4°C, after which they were washed with ice-cold

RIPA buffer. Antigens were eluted using loading buffer, and then boiled at 96°C for 5 min. The supernatant was collected after centrifugation.

Immunohistochemistry

Antigen retrieval was performed with high temperature and high pressure using citrate buffer (0.01 M, pH 6.0). Harris hematoxylin was used to stain the nuclei, and ethanol was used for dehydration. The horseradish peroxidase (HRP)-positive cells appeared yellow, with brown granules in the cytoplasm and cell membrane. Image-Pro Plus 6.0 software was used to select a region that acted as a uniform standard to evaluate the positive photos.

Statistical Analysis

Data were analyzed using one-way ANOVA, as appropriate. All statistics and data analysis were performed using SPSS21.0 software. Data are presented as the mean ± SD, and $P < 0.05$ were considered significant.

RESULTS

Glargine Displays a More Prolonged Hypoglycemic Effect Than HI

Wistar rats were fasted for 2 h before treatment. Blood sugar levels after three treatments were comparable to the levels prior to drug treatment: 5.92 ± 0.25, 5.85, and 5.97 ± 0.23 mmol/L (**Figure 1**). Subcutaneous injection of 1 U/kg of HI and glargine decreased blood glucose levels rapidly. In HI group, blood glucose levels reached a minimum of 2.90 ± 0.16 mmol/L at 45 min post-injection. Blood glucose in the glargine group reached a minimum level 45 min later than HI group, and was as low as 3.18 ± 0.17 mmol/L at 90 min post-injection. Blood glucose levels in drug treatment groups rebounded after reaching minimum, and the rebound was faster in HI-treated group compared to the glargine group. However, the area under the curve was lower in glargine group compared to the HI group, indicating that glargine produced a more prolonged hypoglycemic effect than HI. At 60 min post-injection, the blood sugar levels in both drug groups were almost similar (3.20 ± 0.21 mmol/L compared with 3.37 ± 0.09 mmol/L), therefore this time-point was used to directly compare the hypoglycemic effects of the two drugs. In comparison, blood sugar levels in the control group (injected with 0.9% normal saline at the same volume) ranged between 5.92 ± 0.25 and 5.50 ± 0.68 mmol/L. Changes in blood sugar in the experimental groups were significantly different at each time point compared with the control group ($p < 0.05$). The difference between HI and glargine group was significantly different at 15 min and 45 min time-points ($p < 0.01$). During the experiment, rats displayed normal levels of activity and no rats died after drug or saline injection.

Low Doses of Glargine Causes Lower IR Phosphorylation Level and Longer Effect Than HI in Thyroid Tissue

Wistar rats were fasted for 2 h, and then were injected with 1 U/kg of HI or glargine. Previous studies by Hansen et al. (11) and Tennagels et al. (13) indicate that this dose of insulin does not induce phosphorylation of IGF-1R in rat mammary gland or adipose tissue. Therefore, we did not immunoprecipitate IR/IGF-1R, but directly probed for pIR by western blot.

The phosphorylation level of IR in thyroid cells was slightly altered after treatment. In HI group, phosphorylation level peaked at 2.26 ± 0.57-fold change at 15 min, compared to the level of onset, and then decreased rapidly. Phosphorylation levels were close to the limit of detection at 60 min post-injection (**Figure 2**). Phosphorylation of IR after glargine treatment peaked within 15–45 min post-injection, and then decreased to 40% of the maximum 120 min after injection. The phosphorylation level of IR in thyroid cells was 1.5 times higher than that of glargine, but the peak phosphorylation level was achieved at the same time-point. Similarly, glargine produced a longer-lasting effect on IR phosphorylation compared to HI. HI and glargine had significantly different effects on IR phosphorylation at 15, 60, 90, and 120 min time-points, with glargine group displaying a 2- to 3.1-fold higher IR phosphorylation level after 60 min than HI.

Akt and ERK1/2 Phosphorylation Are Slightly Higher but Last Longer After Glargine Treatment Compared to HI

Rats were fasted for 2 h, after which they were injected with 1 U/kg of HI or glargine. The phosphorylation level of Akt was measured within 120 min. Fifteen min after injection of HI, phosphorylation of Akt reached a peak level, then fell to 19% of the maximum (**Figures 3A,B**). In glargine group, the peak phosphorylation of Akt reached at 30 min post-injection (15 min later than the HI group), then dropped to 18% of the peak value within 120 min. The results showed that glargine acted on thyroid cells, and that peak pAkt levels were 1.5 times higher after glargine treatment compared to HI treatment. At each time-point, HI and glargine groups were significantly different ($^{*}p < 0.05$, $^{**}p < 0.01$, $^{***}p < 0.001$). After 30 min, Akt phosphorylation levels were 1.2–2.3 higher in glargine group than in HI group.

The rats were fasted for 2 h, then injected with 1 U/kg of HI or glargine, and the phosphorylation levels of ERK1/2 were measured. At 15 min post-injection of HI, phosphorylation of ERK1/2 reached a maximum value of 6.39 ± 1.97-fold (which was similar to Akt), then fell and stabilized at lower levels after 30 min, and eventually dropped to 4.63 ± 0.78-folds (**Figures 3A,C**) after 120 min. The phosphorylation of ERK1/2 peaked at 30 min after glargine injection (15 min later than HI treatment). Thereafter, the levels of pERK1/2 fell slowly, and dropped to 50% of the peak value at 120 min post-injection. These results indicate that glargine acted on thyroid cells, and that the increase in ERK1/2 phosphorylation caused by glargine was 1.43 times higher than that of HI treatment. At 45, 60, and 120 min post-injection, the effects of HI and glargine treatments were significantly different ($^{*}p < 0.05$, $^{**}p < 0.01$). At 30 min post-injection, ERK1/2 phosphorylation levels

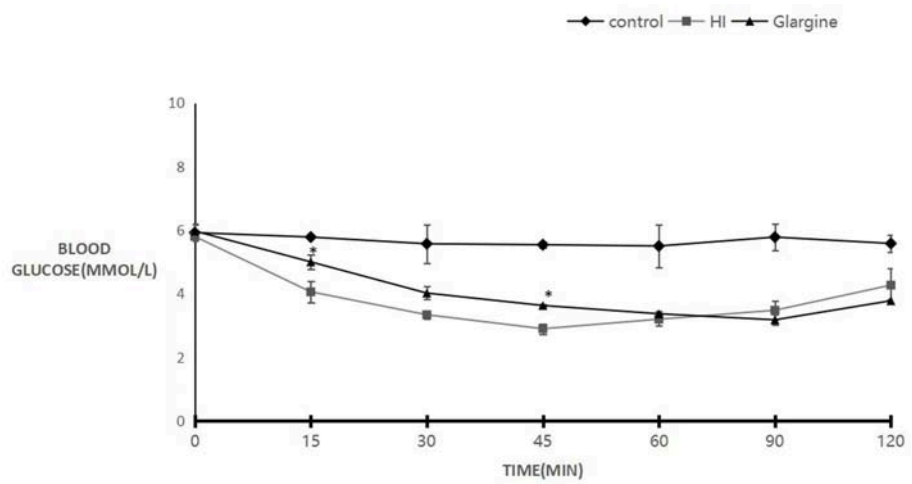

FIGURE 1 | Blood sugar levels of 8- to 10-weeks-old female Wistar rats 120 min after injection with either 0.9% saline (blank group, diamond), 1 U/kg HI (square), or 1 U/kg glargine (triangles) ($n = 10$ rats per group; compared with HI group, $^{*}P < 0.05$).

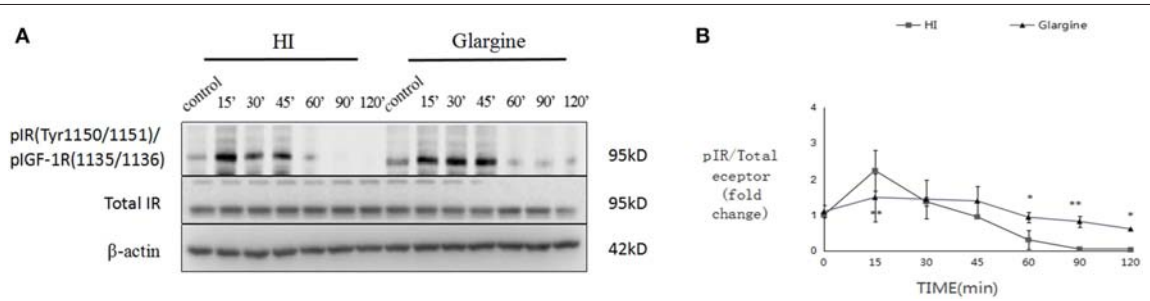

FIGURE 2 | WB images of pIR in rat thyroid cells within the first 120 min after injection of 1 U/kg HI and glargine. Plot of changes of pIR in rat thyroid cells in the first 120 min after injection with 1 U/kg HI (square) or glargine (triangle) as calculated from western blot results ($n = 5$–6; $^{*}P < 0.05$, $^{**}P < 0.01$, compared with HI group).

were about 7.6–6.2 times higher in glargine group than in HI group.

High Doses of HI Primarily Affect IR Phosphorylation, Whereas High Doses of Glargine Primarily Affect IGF-1R Phosphorylation

After 2 h of fasting, Wistar rats were injected with 1, 12.5, 50, or 200 U/kg of HI or glargine. At 60 min after injection, the average blood sugar level was 1.8 mmol/L, and there were no obvious hypoglycemic effects, with all rats surviving.

At each dose, the effects of HI or glargine treatments were significantly different from the control group ($^{***}p < 0.001$) in terms of IR and IGF-1R phosphorylation. In addition, there was a dose-dependent effect of both insulin treatments on the phosphorylation level of IGF-1Rβ/IRβ (**Figures 4A,B**). HI and glargine treatments were significantly different at the same dosage level ($p^{***} < 0.001$). At each dose, protein phosphorylation was higher in glargine group than in HI group (1.42-, 1.6-, 1.83-, and 2.28-fold higher for 1, 12.5, 50, and 200 U/kg groups, respectively). Increasing doses of insulin did not have any saturating effect on IGF-1Rβ/IRβ receptors' phosphorylation; even at the highest dose of 200 U/kg, phosphorylation was significantly higher than the other doses, especially in glargine group.

To determine pIGF-1R and pIR cross-reaction, rats were fasted and injected with drugs as described above. Thyroid tissues were collected for each dose. We then used a co-immunoprecipitation approach to calculate the change in IR and IGF-1R phosphorylation.

The IR phosphorylation levels measured at each dose are shown in **Figures 4C,D**. The phosphorylation levels of IR were significantly different in HI group compared to the control group at each dosage ($^{**}p < 0.01$, $^{***}p < 0.001$). Rats injected with high doses of glargine (50 and 200 U/kg) had a significantly higher phosphorylation compared to the control group ($^{*}p < 0.05$, $^{**}p < 0.01$). IR phosphorylation level increased with the drug dose. At the same doses, there were significant differences between HI and glargine groups ($^{\#}p < 0.05$, $^{\#\#}p < 0.01$, $^{\#\#\#}p < 0.001$). The phosphorylation level

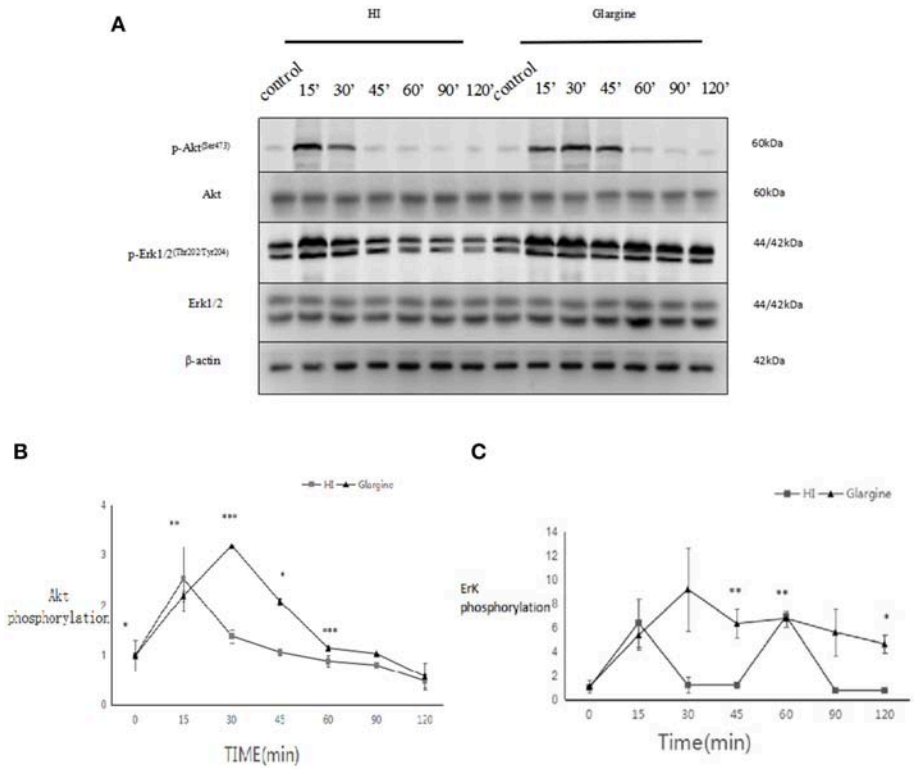

FIGURE 3 | (A) pAkt and pERK 1/2 protein levels in thyroid cells of rats injected with 1 U/kg HI or glargine up to 120 min post-injection; **(B)** Plot of changes of pAkt expression in rat thyroid cells within 120 min of injection with 1 U/kg HI (square) or glargine (triangle), as calculated from WB results ($n = 5$–6, $^{*}P < 0.05$,$^{**}P < 0.01$, $^{***}P < 0.001$ compared to the HI group); **(C)** Plot of changes in pERK1/2 in rat thyroid cells within 120 min of injection with 1 U/kg HI (square) or glargine (triangle), as calculated from WB results ($n = 5$–6).

of IR was remarkably (1.71- to 2.3-fold) higher in HI group compared to glargine group at doses above 12.5 U/kg. These findings demonstrate that HI acts on the insulin receptor in thyroid tissue.

According to WB analysis, high doses of glargine caused higher increases in IGF-1Rβ/IRβ phosphorylation than HI. No obvious dose-dependent changes in the phosphorylation level of IR were found in the precipitation analysis. Next, we measured the dose-dependent effects of the drugs on IGF-1R phosphorylation (**Figures 4E,F**). The IGF-1R phosphorylation levels were significantly different in HI and glargine groups relative to blank control at each dose ($^{*}P < 0.05$, $^{**}P < 0.01$, $^{***}P < 0.001$). The phosphorylation levels of IGF-1R increased with insulin treatment dose, with the exception of the highest HI dose, which reduced the phosphorylation level relative to lower doses. At the same dose, HI and glargine produced significantly different effects on IGF-1R phosphorylation ($^{\#\#\#}P < 0.001$). At lower doses (1 and 12.5 U/kg) HI produced a higher phosphorylation than glargine. At higher doses (50 and 200 U/kg) glargine caused higher IGF-1R phosphorylation than HI (∼1.48- and 1.92-fold higher) or blank control (7.02- to 7.12-fold higher). We conclude that high doses of glargine increase the phosphorylation of insulin receptors in thyroid tissue.

Insulin Treatment Has Dose-Dependent Effects on Akt and ERK1/2 Phosphorylation, With Glargine Having Slightly Stronger Effects Relative to HI Group

Having detected changes in the phosphorylation of IR and IGF-1R, we explored changes in phosphorylation of the downstream signaling proteins Akt and ERK1/2. As shown in **Figure 5A**, the phosphorylation of Akt and ERK1/2 was significantly different at all doses from the control group ($^{*}p < 0.05$, $^{**}p < 0.01$, $^{***}p < 0.001$), and the effects followed a dose-dependent pattern. However, it is interesting to note that Akt phosphorylation was similar after treatment with 200 U/kg dose and 50 U/kg dose of HI (2.80 ± 0.10 and 0.10 ± 0.12), indicating the saturation of Akt phosphorylation. At 12.5 and 200 U/kg doses, pAkt levels were higher after glargine treatment compared to HI treatment [1.37 times higher ($p < 0.05$) and 1.29 times higher ($^{\#\#\#}p < 0.001$), respectively]. At the highest dosage (200 U/kg), Akt phosphorylation was 3.8 times higher in glargine than in the control group.

In general, pERK increased with the dose of insulin treatment (**Figure 5**). ERK1/2 phosphorylation levels in each

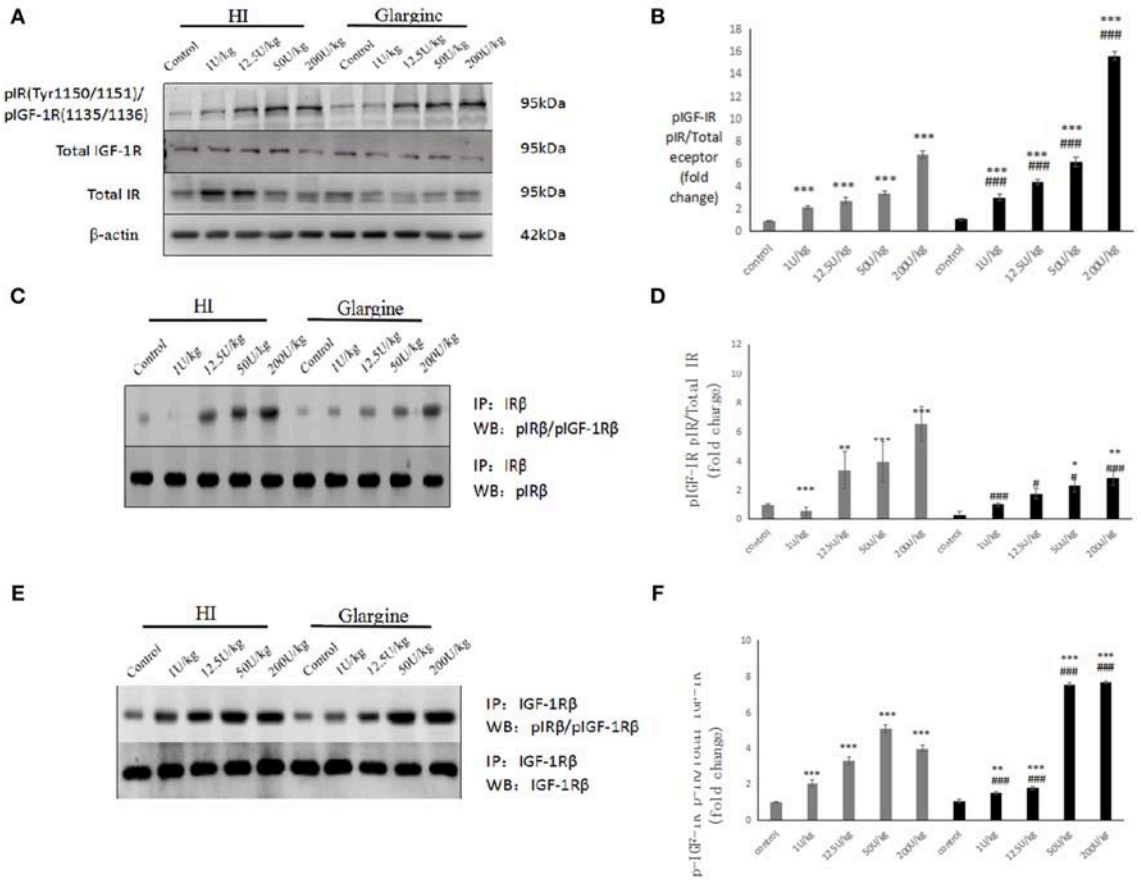

FIGURE 4 | (A,B) WB of pIGF-1R/pIR in rat thyroid tissue 60 min after injection of varying doses of HI and glargine. Histogram showing changes in IGF-1Rbeta/IR beta phosphorylation levels in thyroid cells 60 min after injection of 1–200 U/kg of HI (gray) and glargine (black), as calculated from WB results ($n = 5$–7, compared to blank group, $^{*}P < 0.05$, $^{**}P < 0.01$, $^{***}P < 0.001$; Compared to HI group, $^{\#}P < 0.05$, $^{\#\#\#}P < 0.001$); **(C,D)** Detection of pIR after immunoprecipitation of IR in rat thyroid cells 60 min after injection of different doses of HI and glargine. Histogram showing changes in IR beta phosphorylation in rat thyroid cell 60 min after injection of 1–200 U/kg HI (gray) and glargine (black) calculated from IP and WB results ($n = 5$–8, compared to blank group, $^{*}P < 0.05$, $^{**}P < 0.01$, $^{***}P < 0.001$; Compared to HI group, $^{\#}P < 0.05$, $^{\#\#\#}P < 0.001$); **(E,F)** WB of pIGF-1R following immunoprecipitation of IGF-1R from rat thyroid tissue 60 min after injection with different doses of HI and glargine. Histogram showing changes in IGF-1R beta phosphorylation in thyroid cells of rats injected with 1–200 U/kg HI (gray) and glargine (black) as calculated from IP and WB results ($n = 5$–7, compared to blank group, $^{*}P < 0.05$, $^{**}P < 0.01$, $^{***}P < 0.001$; compared to HI group, $^{\#}P < 0.05$, $^{\#\#\#}P < 0.001$).

insulin treatment group was significantly higher than in the blank group ($^{**}p < 0.05$, $^{**}p < 0.01$, $^{***}p < 0.001$). At all dosages, glargine caused significantly larger increases in pERK than HI ($^{\#\#\#}p < 0.001$). From lowest to highest dose, glargine treatment increased pERK by 1.95-, 2.39-, 1.34-, and 1.22-fold more than HI.

Changes in Cell Proliferation and Proliferation-Related Signaling Pathways in Thyroid Cells After HI or Glargine Treatment

To explore the effect of high doses of HI and glargine on thyroid cell proliferation, we divided female Wistar rats into HI and glargine treatment groups, and tested the effect of four different doses of the drugs (1, 12.5, 50 and 200 U/kg) 4 weeks after injection ($n = 10$ animals per dose). The highest dose (200 U/kg) had lethal effects; and 40% of rats in this group died. We performed an immunohistochemical examination of Ki-67, Akt, and ERK1/2 in thyroid tissue at 4 weeks after treatment. The results are shown in **Figure 6**. Round or oval follicles of varying sizes were observed in thyroid cells. Cells were considered positive for Ki-67, Akt, or ERK1/2 if the nucleus appeared brown and cells were yellow and granular. **Figure 6A** shows that HI and glargine caused a dose-dependent increase in the number of Ki-67 positive cells. The nuclei showing dark staining (positive-cells) were counted and percentage of the total cell population expressing proteins (Ki-67, p-Akt, ERK1/2) was calculated as index (mean density). We found that, in addition to the 1 U/kg dose, intermediate and high doses caused similar increases in Ki-67 as presented in **Figure 7A**, and the increases were significantly different from the blank

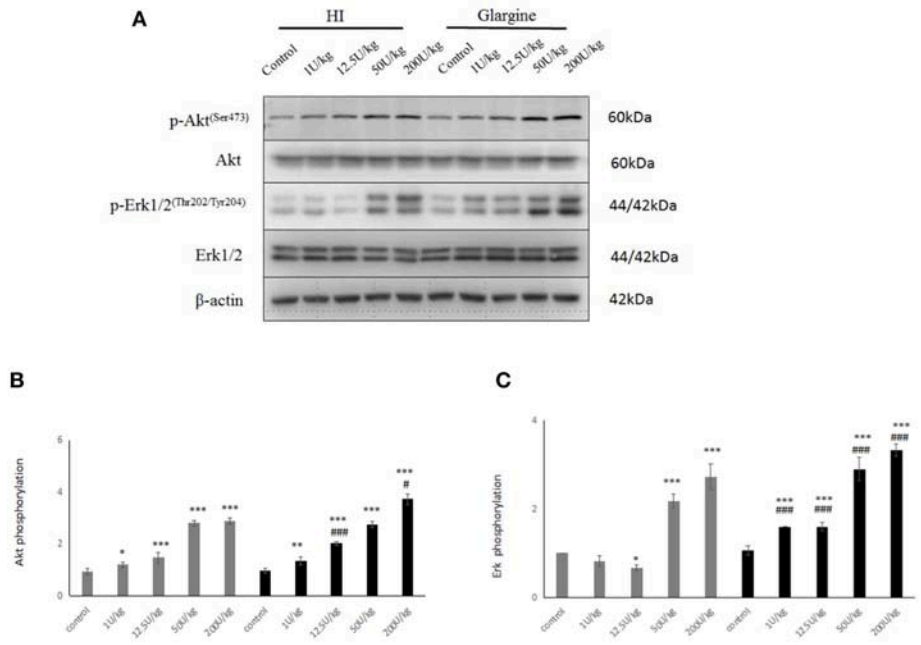

FIGURE 5 | (A) WB of pAkt, pERK1/2 in rats 60 min after injection with different doses of glargine and HI; **(B)** Histogram showing changes in Akt phosphorylation in rat thyroid cells 60 min after injection with 1–200 U/kg (gray) and the HI glargine (black), based on WB assays ($n = 5$–6; compared to blank group, $^{*}P < 0.05$, $^{**}P < 0.01$, $^{***}P < 0.001$; compared to HI group, $^{\#}P < 0.05$, $^{\#\#\#}P < 0.001$); **(C)** Histogram showing ERK1/2 phosphorylation in rat thyroid cells 60 min after injection of 1–200 U/kg HI (gray) and glargine (black), based on WB assays ($n = 5$–8; compared to blank group, $^{*}P < 0.05$, $^{**}P < 0.01$, $^{***}P < 0.001$; compared to HI group, $^{\#}P < 0.05$, $^{\#\#\#}P < 0.001$.

group. At the highest doses, HI caused higher increases in Ki-67 expression than glargine.

Akt and ERK1/2 Phosphorylation Are Slightly Higher but Last Longer After Glargine Treatment Compared to HI

The immunohistochemical labeling of pAkt showed that there were more pAkt-positive thyroid cells in insulin-treated rats compared to rats treated with blank control. The 12.5 U/kg dose of HI group displayed many cells with brown-yellow granules, whereas 1 or 200 U/kg doses of glargine also increased expression, but not in a dose-dependent manner. As shown in **Figure 7B**, there were no significant differences between any dose of HI and blank control. In contrast, glargine increased pAkt at 1 and 200 U/kg doses to about 3.8 times the level of the blank group. Glargine increased the number of pAkt positive cells more than HI at 1, 12.5, and 200 U/kg doses.

Immunohistochemical labeling of pERK revealed that the insulin treatments produced similar effects; and there were remarkably more positive cells in insulin-treated rats than in the blank group. The 150 U/kg dose of HI group displayed a high number of cells with brown-yellow granules, and there were no differences between various doses of glargine. No dose-dependent trend was observed after HI or glargine administration. As shown in **Figure 7C**, the differences between the two drug groups and the control group were statistically significant, with higher pERK in the two drug groups, but with no significant dose-dependent trend. Glargine induced higher pERK levels than HI group.

DISCUSSION

Subcutaneous injection of insulin can maintain glucose utilization at a rate of 1 mg/kg/min for 20 h, both in healthy subjects and in patients with diabetes mellitus. In contrast, glargine absorption is slower and more prolonged compared to human insulin, with no obvious peak (15–17). Several studies have confirmed that (18) when human insulin is absorbed, it primarily binds to the insulin receptor (IR), resulting in IR activation and phosphorylation. Phosphorylation of IR induces random phosphorylation of amino acid residues and activation of downstream signaling targets of IR, including the docking of IRS-1 and IRS-2, activation of signal transduction cascades, which culminates in the regulation of glucose intake and metabolism in skeletal muscle and adipose tissue. Other signaling pathways affected include phosphatidyl inositol kinase (PI3k)/Akt and MAPK. The primary signal transduction mechanism is through activation of PI3K/Akt. At high concentration, insulin can bind to IGF-1R, causing phosphorylation and activation. In general, IGF-1R is activated by IGFs under physiological conditions, and is widely expressed throughout the body. Phosphorylation of IGF-1R results in strong activation of the Ras/Raf/MAPK signal pathways. Gallagher et al. (14) investigated the effects of HI

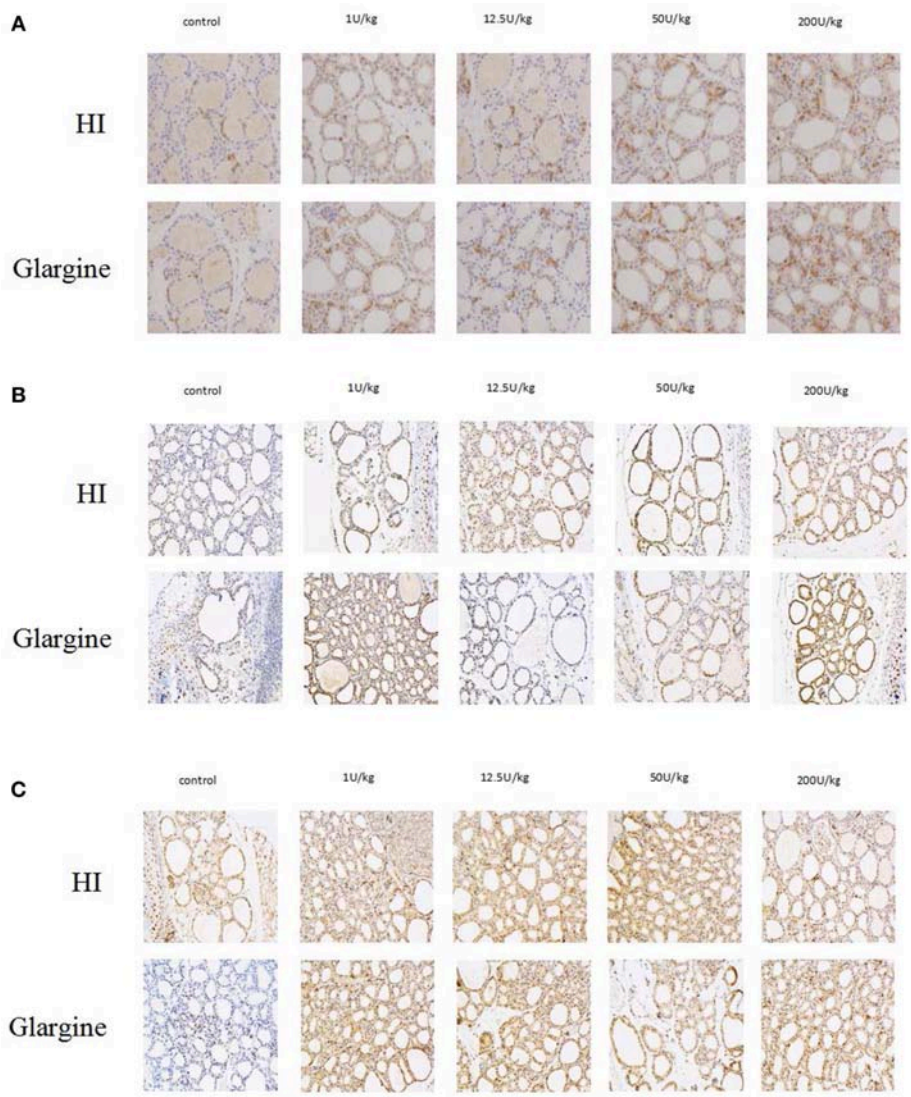

FIGURE 6 | (A) Immunolabeling of Ki-67 in thyroid gland cells of rats injected with HI and glargine for 4 weeks; **(B)** Immunolabeling of pAkt in thyroid cells of rat injected with different doses of glargine and HI for 4 weeks; **(C)** Immunolabeling of pERK1/2 in thyroid gland cells of rats injected with varying doses of HI and glargine for 4 weeks.

and glargine on transgenic mouse models of breast cancer, and found different levels of phosphorylation of IR, IGF-1R, Akt, and ERK1/2. Tennagel et al. (13) found that HI and glargine caused IR, IGF-1R, and Akt phosphorylation in skeletal muscle, fat, liver, and cardiac muscle in male Wistar rats. However, this study mentioned above did not test the effects on ERK1/2, and changes in signaling pathways compared to mammary gland epithelial cells. Our experimental results show that when HI or glargine acts on thyroid cells, it causes similar changes to those observed in mammary epithelial cells. The biological effect of insulin on target cells depends on its local concentration, the target cell properties, and IR/IGF-1R expression. The similarities observed between thyroid cells and mammary glands may be due to the small number of IR and IGF-1R in these cells, or similar local drug concentrations in these tissues. In addition, the phosphorylation of IR, IGF-1R, Akt, and ERK1/2 in thyroid cells mirrors the curves of hypoglycemic effect of HI and glargine.

In vitro experiments showed that glargine can activate IR, and that the downstream signaling pathway is similar to that of human insulin. However, amino acids in the B chain of glargine have been substituted, altering its molecular structure, which accounts for the long-lasting hypoglycemic effect of glargine and increases its affinity for IGF-1R (19, 20). Multiple *in vitro* experiments show that glargine can promote the proliferation of fat cells and breast cells by phosphorylating IGF-1R (21–23). Using immunohistochemistry and qRT-PCR, Liu et al. (24) found that IGF-1 and IGF-1R are up-regulated in thyroid tissues of patients with follicular adenoma, thyroid nodules, papillary thyroid carcinoma, and follicular thyroid

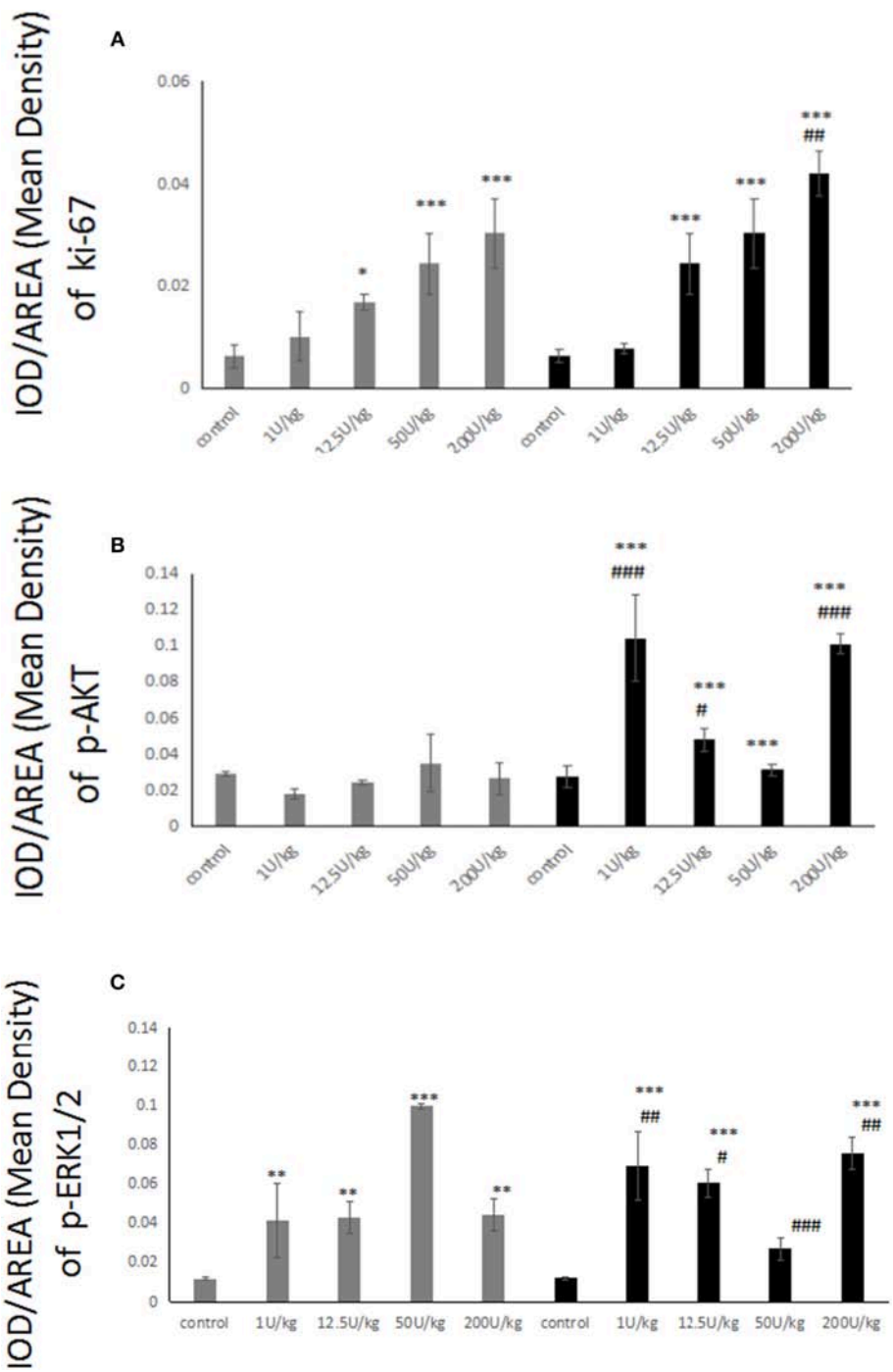

FIGURE 7 | (A) Histogram showing Ki-67-positive thyroid cells of rats injected with 1–200 U/kg HI (gray) and glargine (black) for 4 weeks ($n = 6$–10, compared to blank group, $^{*}P < 0.05$, $^{**}P < 0.01$, $^{***}P < 0.001$; compared to HI group, $^{\#}P < 0.05$, $^{\#\#}P < 0.01$, $^{\#\#\#}P < 0.001$); **(B)** Histogram showing pAkt-positive thyroid cells in rats injected with 1–200 U/kg HI (gray) and glargine (black) for 4 weeks ($n = 6$–10, compared to blank group, $^{*}P < 0.05$, $^{**}P < 0.01$, $^{***}P < 0.001$; compared to HI group, $^{\#}P < 0.05$, $^{\#\#}P < 0.01$, $^{\#\#\#}P < 0.001$); **(C)** Quantification of pERK-positive thyroid cells in rats injected with 1–200 U/kg HI (gray) and glargine (black) for 4 ($n = 6$–10, compared to blank group, $^{*}P < 0.05$, $^{**}P < 0.01$, $^{***}P < 0.001$; compared to HI group, $^{\#}P < 0.05$, $^{\#\#}P < 0.01$, $^{\#\#\#}P < 0.001$).

cancer relative to healthy controls. Compared to patients with thyroid disease, papillary thyroid carcinoma patients had the highest expression level of IGF 1 and IGF-1R protein and mRNA.

IGF-1 plays an important role in the formation and development of thyroid nodules, including thyroid cancer and thyroid adenoma. As the human insulin analog, insulin B10 aspart (AspB10) is named after its histidine substituted for

aspartic acid in the No. 10 B chain. Insulin B10 aspart has higher affinity for IR and IGF-1R than human insulin, and the duration of binding to IR is longer. In addition, insulin B10 aspart has stronger proliferation-promoting effects on mammalian cells than human insulin. In 1992, Drejer (25) tested the effects of AspB10 on female Sprague Dawley rats. Rats were injected with 12.5, 50, or 200 U/kg doses of AspB10, while controls received either saline or 200 U/kg of insulin injections. After 52 weeks, AspB10 caused dose-dependent increases in the incidence of breast cancer, while the control group had no observable increase in breast cancer. After 48 weeks, 44% of rats treated with 200 U/kg of AspB10 had benign breast tumors and 23% had malignant tumors. This study led to the withdrawal of insulin B10 aspart prescription. Although the mechanism by which insulin B10 aspart increases the risk of breast cancer is not clear, many studies (21–23) have proposed that this may be due to the high affinity of insulin B10 aspart for IGF-1R. Thus, researchers speculate that similar insulin analogs that show high affinity for IGF-1R *in vitro* may have pro-proliferative and cancer-causing effects. In this study, when female Wistar rats were treated with 12.5 U/kg glargine for 4 weeks, we observed a significantly higher number of Ki-67 positive thyroid cells compared to control rats. The proportion of Ki-67-positive cells in thyroid cancer tissues was 100%, and the proportion was 30% in benign thyroid lesions. Therefore, our results suggest that treatment with high doses of HI and glagine for 4 weeks causes thyroid cell proliferation. According to the immunoprecipitation and WB analysis, the proliferation-promoting effects of glargine may be associated with activation of IGF-1R, which is consistent with findings from previous *in vitro* experiments (21–24). In clinical practice, a low dose of 1 U/kg is used. Although this dose of HI and glargine induced higher phosphorylation of IR and IGF-1R than the control after 60 min, it did not increase thyroid cell proliferation (as measured by Ki-67-positive cell quantification) after 4 weeks of treatment. Currently, no experiments have been reported on whether extending the time of drug intervention could promote cell proliferation, or whether low doses of HI and glargine could increase the number of Ki-67-positive thyroid cells after 52 weeks of treatment. In our study, we demonstrated that both HI and insulin glargine affect the proliferation of cells in a dose-dependent manner. However, in patients treated with daily doses (0.2–0.4 IU/kg) of insulin glargine, the plasma insulin concentrations remain between 50 and 200 pmol/L or sometimes reach a slightly higher level ranging from 100 to 500 pmol/L (26, 27). The high dose of 200 IU/kg in our study that resulted in high levels of cell proliferation is rather supraphysiological. While therapeutic doses of HI and glargine do not cause thyroid cell proliferation. The published RCT ORIGIN explore effect of glargine insulin on cancer, showed that insulin glargine have a neutral association with overall and cancer-specific outcomes, including cancer-specific mortality. The results also demonstrated that exposure to glucose-lowering therapies, including metformin, and HbA1c level during the study did not alter cancer risk (28).

It is worth noting, however, that high doses of HI increase thyroid cell proliferation. *In vitro* experiments have shown that HI can promote the proliferation of thyroid follicular cells and human endometrial cells, and can increase malignant transformation of human endometrial cells (29, 30). Research into the mechanism behind this has focused on the effect of HI on IR. There are two subtypes of IR (IR-A and IR-B), and the distribution and biological effect of these subtypes are different (31). IR-A expression is increased during thyroid cancer infiltration (32). Pandini et al. (33) found that thyroid cancer tissues with low levels of differentiated cells and high numbers of undifferentiated cells have higher expression levels of IR-A. Therefore, at the start of treatment with insulin and insulin analogs, high number of IR-A are phosphorylated and activated, which may play an important role in the process of cancer development and progression. Pandini et al. (34) postulated that the combination of increased insulin and IR-A activation can increase the expression of the vascular Mrp/PRL gene and cell proliferation protein to promote cell proliferation. A study by Gallagher et al. (14) showed that HI promotes the growth of mammary gland cells and breast tumor proliferation via IR phosphorylation, rather than IGF-1R phosphorylation. In this study, we focused on thyroid cells. Analysis of Ki-67 expression by immunoprecipitation, WB, and immunohistochemistry in thyroid cells produced similar results. HI causes IR phosphorylation in thyroid cells in a dose-dependent manner, which may be due to the increase in thyroid cell proliferation at high doses of HI. There was no significant effect of IGF-1R phosphorylation on thyroid cells after high doses of HI. Therefore, it is not clear whether thyroid cell proliferation is increased through IGF-1R phosphorylation following HI treatment.

As mentioned above, HI and its analogs activate the PI3K/Akt and MAPK signaling pathways. PI3K/Akt signaling increases the number of cells by inhibiting cell apoptosis, which plays a key role in modulating the effects of insulin and IGF-1 on metabolism and mitosis (35). MAPK signaling is associated with increased DNA synthesis and cell proliferation (18). In this study, HI and glargine promoted Akt phosphorylation with increasing doses and time after administration. pAkt levels were slightly higher after HI treatment than glargine. Müller et al. (36) studied the effect of glargine and HI on rat thyroid cell lines FRTL-5 and thyroid follicular cells, and found that the two drugs enhanced the phosphorylation of PI3K/Akt. Our results are in agreement with these findings. There is also evidence that HI treatment increases cell proliferation via Akt activation in bladder cancer cells, breast cancer cells, and rat fat tissue (6). In our *in vivo* study on the effect of HI treatment for 4 weeks on thyroid tissue revealed a significant increase in pERK1/2, but no effect on pAkt level. Thus, Akt phosphorylation may not be the primary signaling pathway that mediates thyroid cell proliferation after HI administration, and pERK1/2 may play a greater role, however further studies are needed to clarify this hypothesis.

HI and glargine treatment produced a higher phosphorylation of ERK1/2 than control control, with glargine having slightly stronger effects compared to HI. According to insulin cell-signaling pathways, this could be due to the higher affinity between glargine and IGF-1R relative to IR (20), because

ERK1/2 is the primary downstream effector of IGF-1R. Previous studies also confirmed (37, 38) that ERK1/2 and MEK/ERK1/2 pathways are involved in cell survival, proliferation, differentiation, and mitosis. Kandil et al. (39) found that inhibition of MEK/ERK expression exerts cytotoxic effects on thyroid cancer cells. Our study on pERK1/2 activation after insulin administration may be pertinent to more than the role of hypoglycemic drugs, but could also shed light on mechanisms of increased thyroid cell proliferation. The further experiments are needed to characterize the effects of insulin and its analogs on thyroid cell proliferation *in vivo* and *in vitro*. It also suggests that clinicians should consider the possibility that insulin may stimulate thyroid cell proliferation during the treatment of diabetes.

CONCLUSION

Our *in vivo* experiments show that therapeutic doses of glargine have a longer-lasting hypoglycemic effect than HI, and promote the phosphorylation of IR, Akt, and ERK1/2. High doses of HI and glargine can promote thyroid cell proliferation, while therapeutic doses of HI and glargine do not cause thyroid cell proliferation. HI may be associated with IR phosphorylation, while glargine may be associated with IGF-1 phosphorylation. Both receptors can activate PI3K-Akt and MAPK signaling pathways to promote proliferation.

DATA AVAILABILITY

All datasets generated for this study are included in the manuscript and/or the supplementary files.

ETHICS STATEMENT

This study was carried out in accordance with the recommendations of Zhejiang Chinese Medical University of guidelines of committee. The protocol was approved by the Zhejiang Chinese Medical University of committee.

AUTHOR CONTRIBUTIONS

XS, KY, AS, ST, and DY substantially contributed to the conception and design of this study, drafted the work, gave final approval of the version to be published, and agreed to be accountable for all aspects of this work and ensured that issues pertaining to the accuracy or integrity of any part of this work are appropriately investigated and resolved. XZ and TC critically revised the manuscript for important intellectual content.

FUNDING

This work was supported by grants from Zhejiang Provincial Natural Science Foundation of China (LY12H07003).

REFERENCES

1. Shih SR, Chiu WY, Chang TC, Tseng CH. Diabetes and thyroid cancer risk: literature review. *Exp Diabetes Res.* (2012) 2012:578285. doi: 10.1155/2012/578285
2. Aschebrook-Kilfoy B, Sabra MM, Brenner A, Moore SC, Ron E, Schatzkin A, et al. Diabetes and thyroid cancer risk in the National Institutes of Health-AARP Diet and Health Study. *Thyroid.* (2011) 21:957–63. doi: 10.1089/thy.2010.0396
3. Junik R, Kozinski M, Debska-Kozinska K. Thyroid ultrasound in diabetic patients without overt thyroid disease. *Acta Radiol.* (2006) 47:687–91. doi: 10.1080/02841850600806308
4. Rossetti P, Porcellati F, Fanelli CG, Perriello G, Torlone E, Bolli GB. Superiority of insulin analogues versus human insulin in the treatment of diabetes mellitus. *Arch Physiol Biochem.* (2008) 114:3–10. doi: 10.1080/13813450801900777
5. Osborne CK, Bolan G, Monaco ME, Lippman ME. Hormone responsive human breast cancer in long-term tissue culture: effect of insulin. *Proc Natl Acad Sci USA*. (1976) 73:4536–40. doi: 10.1073/pnas.73.12.4536
6. Liu S, Li Y, Lin T, Fan X, Liang Y, Heemann U. High dose human insulin and insulin glargine promote T24 bladder cancer cell proliferation via PI3K-independent activation of Akt. *Diabetes Res Clin Pract.* (2011) 91:177–82. doi: 10.1016/j.diabres.2010.11.009
7. Currie CJ, Poole CD, Gale EA. The influence of glucose-lowering therapies on cancer risk in type 2 diabetes. *Diabetologia.* (2009) 52:1766–77. doi: 10.1007/s00125-009-1440-6
8. Colhoun HM, Group SE. Use of insulin glargine and cancer incidence in Scotland: a study from the Scottish Diabetes Research Network Epidemiology Group. *Diabetologia.* (2009) 52:1755–65. doi: 10.1007/s00125-009-1453-1
9. Jonasson JM, Ljung R, Talbäck M, Haglund B, Gudbjörnsdòttir S, Steineck G. Insulin glargine use and short-term incidence of malignancies-a population-based follow-up study in Sweden. *Diabetologia.* (2009) 52:1745–54. doi: 10.1007/s00125-009-1444-2
10. Hemkens LG, Grouven U, Bender R, Günster C, Gutschmidt S, Selke GW, et al. Risk of malignancies in patients with diabetes treated with human insulin or insulin analogues: a cohort study. *Diabetologia.* (2009) 52:1732–44. doi: 10.1007/s00125-009-1418-4
11. Hansen BF, Kurtzhals P, Jensen AB, Dejgaard A, Russell-Jones D. Insulin X10 revisited: a super-mitogenic insulin analogue. *Diabetologia.* (2011) 54:2226–31. doi: 10.1007/s00125-011-2203-8
12. Hansen BF, Glendorf T, Hegelund AC, Lundby A, Lützen A, Slaaby R, et al. Molecular characterisation of long-acting insulin analogues in comparison with human insulin, IGF-1 and insulin X10. *PLoS ONE.* (2012) 7:e34274. doi: 10.1371/journal.pone.0034274
13. Tennagels N, Welte S, Hofmann M, Brenk P, Schmidt R, Werner U. Differences in metabolic and mitogenic signallingof insulin glargine and AspB10 human insulin in rats. *Diabetologia.* (2013) 56:1826–34. doi: 10.1007/s00125-013-2923-z
14. Gallagher EJ, Alikhani N, Tobin-Hess A, Blank J, Buffin NJ, Zelenko Z, et al. Insulin receptor phosphorylation by endogenous insulin or the insulin analog AspB10 promotes mammary tumor growth independent of the IGF-I receptor. *Diabetes.* (2013) 62:3553–60. doi: 10.2337/db13-0249
15. Kuerzel GU, Shukla U, Scholtz HE, Pretorius SG, Wessels DH, Venter C, et al. Biotransformation of insulin glargine after subcutaneous injection in healthy subjects. *Curr Med Res Opin.* (2003) 19:34–40. doi: 10.1185/030079902125001416
16. Tennagels N, Werner U. The metabolic and mitogenic properties of basal insulin analogues. *Arch Physiol Biochem.* (2013) 119:1–14. doi: 10.3109/13813455.2012.754474
17. Hirsch IB. Insulin analogues. *N Engl J Med.* (2005) 352:174–83. doi: 10.1056/NEJMra040832
18. Mayer D, Shukla A, Enzmann H. Proliferative effects of insulin analogues on mammary epithelial cells. *Arch Physiol Biochem.* (2008) 114:38–44. doi: 10.1080/13813450801900645

19. Gammeltoft S, Hansen BF, Dideriksen L, Lindholm A, Schäffer L, Trüb T, et al. Insulin aspart: a novel rapid-acting human insulin analogue. *Expert Opin Investig Drugs.* (1999) 8:1431–42. doi: 10.1517/13543784.8.9.1431
20. Kurtzhals P, Schäffer L, Sørensen A, Kristensen C, Jonassen I, Schmid C, et al. Correlations of receptor binding and metabolic and mitogenic potencies of insulin analogs designed for clinical use. *Diabetes.* (2000) 49:999–1005. doi: 10.2337/diabetes.49.6.999
21. Bähr M, Kolter T, Seipke G, Eckel J. Growth promoting and metabolic activity of the human insulin analogue [GlyA21,ArgB31,ArgB32]insulin (HOE 901) in muscle cells. *Eur J Pharmacol.* (1997) 320:259–65. doi: 10.1016/S0014-2999(96)00903-X
22. Berti L, Kellerer M, Bossenmaier B, Seffer E, Seipke G, Häring HU. The long acting human insulin analog HOE 901: characteristics of insulin signalling in comparison to Asp(B10) and regular insulin. *Horm Metab Res.* (1998) 30:123–9. doi: 10.1055/s-2007-978849
23. Sommerfeld MR, Müller G, Tschank G, Seipke G, Habermann P, Kurrle R, et al. *In vitro* metabolic and mitogenic signaling of insulin glargine and its metabolites. *PLoS ONE.* (2010) 5:e9540. doi: 10.1371/journal.pone.0009540
24. Liu YJ, Qiang W, Shi J, Lv SQ, Ji MJ, Shi BY. Expression and significance of IGF-1 and IGF-1R in thyroid nodules. *Endocrine.* (2013) 44:158–64. doi: 10.1007/s12020-012-9864-z
25. Drejer K. The bioactivity of insulin analogues from *in vitro* receptor binding to *in vivo* glucose uptake. *Diabetes Metab Rev.* (1992) 8:259–85. doi: 10.1002/dmr.5610080305
26. Hordern SV, Wright JE, Umpleby AM, Shojaee-Moradie F, Amiss J, Russell-Jones DL. Comparison of the effects on glucose and lipid metabolism of equipotent doses of insulin detemir and NPH insulin with a 16-h euglycaemic clamp. *Diabetologia.* (2005) 48:420–6. doi: 10.1007/s00125-005-1670-1
27. Li G, Barrett EJ, Wang H, Chai W, Liu Z. Insulin at physiological concentrations selectively activates insulin but not insulin-like growth factor I (IGF-I) or insulin/IGF-I hybrid receptors in endothelial cells. *Endocrinology.* (2005) 146:4690–6. doi: 10.1210/en.2005-0505
28. Zanders MM, Yakubovich N, Dagenais GR, Rosenstock J, Probstfield J, Chang Yu P, et al. Comment on Bordeleau et al. The association of basal insulin glargine and/or n-3 fatty acids with incident cancers in patients with dysglycemia. Diabetes Care 2014;37:1360–1366. *Diabetes Care.* (2014) 37:e221–2. doi: 10.2337/dc14-1380
29. Bishop EA, Lightfoot S, Thavathiru E, Benbrook DM. Insulin exerts direct effects on carcinogenic transformation of human endometrial organotypic cultures. *Cancer Invest.* (2014) 32:63–70. doi: 10.3109/07357907.2013.877479
30. Tramontano D, Cushing GW, Moses AC, Ingbar SH. Insulin-like growth factor-I stimulates the growth of rat thyroid cells in culture and synergizes the stimulation of DNA synthesis induced by TSH and Graves'-IgG. *Endocrinology.* (1986) 119:940–2. doi: 10.1210/endo-119-2-940
31. Belfiore A, Frasca F, Pandini G, Sciacca L, Vigneri R. Insulin receptor isoforms and insulin receptor/insulin-like growth factor receptor hybrids in physiology and disease. *Endocr Rev.* (2009) 30:586–623. doi: 10.1210/er.2008-0047
32. Malaguarnera R, Frasca F, Garozzo A, Gianì F, Pandini G, Vella V, et al. Insulin receptor isoforms and insulin-like growth factor receptor in human follicular cell precursors from papillary thyroid cancer and normal thyroid. *J Clin Endocrinol Metab.* (2011) 96:766–74. doi: 10.1210/jc.2010-1255
33. Pandini G, Frasca F, Mineo R, Sciacca L, Vigneri R, Belfiore A. Insulin/insulin-like growth factor I hybrid receptors have different biological characteristics depending on the insulin receptor isoform involved. *J Biol Chem.* (2002) 277:39684–95. doi: 10.1074/jbc.M202766200
34. Pandini G, Medico E, Conte E, Sciacca L, Vigneri R, Belfiore A. Differential gene expression induced by insulin and insulin-like growth factor-II through the insulin receptor isoform A. *J Biol Chem.* (2003) 278:42178–89. doi: 10.1074/jbc.M304980200
35. Galetic I, Andjelkovic M, Meier R, Brodbeck D, Park J, Hemmings BA. Mechanism of protein kinase B activation by insulin/insulin-like growth factor-1 revealed by specific inhibitors of phosphoinositide 3-kinase–significance for diabetes and cancer. *Pharmacol Ther.* (1999) 82:409–25. doi: 10.1016/S0163-7258(98)00071-0
36. Müller K, Weidinger C, Führer D. Insulin glargine and insulin have identical effects on proliferation and phosphatidylinositol 3-kinase/AKT signalling in rat thyrocytes and human follicular thyroid cancer cells. *Diabetologia.* (2010) 53:1001–3. doi: 10.1007/s00125-010-1674-3
37. Boulton TG, Nye SH, Robbins DJ, Ip NY, Radziejewska E, Morgenbesser SD, et al. ERKs: a family of protein-serine/threonine kinases that are activated and tyrosine phosphorylated in response to insulin and NGF. *Cell.* (1991) 65:663–75. doi: 10.1016/0092-8674(91)90098-J
38. Xia Z, Dickens M, Raingeaud J, Davis RJ, Greenberg ME. Opposing effects of ERK and JNK-p38 MAP kinases on apoptosis. *Science.* (1995) 270:1326–31. doi: 10.1126/science.270.5240.1326
39. Kandil E, Tsumagari K, Ma J, Abd Elmageed ZY, Li X, Slakey D, et al. Synergistic inhibition of thyroid cancer by suppressing MAPK/PI3K/AKT pathways. *J Surg Res.* (2013) 184:898–906. doi: 10.1016/j.jss.2013.03.052

Conflict of Interest Statement: The authors declare that the research was conducted in the absence of any commercial or financial relationships that could be construed as a potential conflict of interest.

frontiers in Endocrinology

ORIGINAL RESEARCH
published: 13 September 2019
doi: 10.3389/fendo.2019.00634

In Addition to Poor Glycemic Control, a High Level of Irisin in the Plasma Portends Early Cognitive Deficits Clinically in Chinese Patients With Type 2 Diabetes Mellitus

Hongyan Lin[1,2†], *Yang Yuan*[1,2†], *Sai Tian*[1,2], *Jing Han*[1], *Rong Huang*[1,2], *Dan Guo*[1,2], *Jiaqi Wang*[1,2], *Ke An*[1,2] *and Shaohua Wang*[1*]

[1] *Department of Endocrinology, Affiliated Zhongda Hospital, Southeast University, Nanjing, China,* [2] *School of Medicine, Southeast University, Nanjing, China*

OPEN ACCESS

Edited by:
Lei Sha,
China Medical University, China

Reviewed by:
Erwin Lemche,
King's College London, United Kingdom
Ramit Ravona-Springer,
Sheba Medical Center, Israel

***Correspondence:**
Shaohua Wang
gyjwsh@126.com

[†] *These authors have contributed equally to this work as co-first authors*

Specialty section:
This article was submitted to Neuroendocrine Science, a section of the journal Frontiers in Endocrinology

Received: *17 May 2019*
Accepted: *30 August 2019*
Published: *13 September 2019*

Citation:
Lin H, Yuan Y, Tian S, Han J, Huang R, Guo D, Wang J, An K and Wang S (2019) In Addition to Poor Glycemic Control, a High Level of Irisin in the Plasma Portends Early Cognitive Deficits Clinically in Chinese Patients With Type 2 Diabetes Mellitus. Front. Endocrinol. 10:634. doi: 10.3389/fendo.2019.00634

Background and Objectives: Irisin plays an important role in the metabolism and homeostasis of energy balance, which is involved in cognitive impairment. This study aimed to investigate the role of irisin in mild cognitive impairment (MCI) among Chinese patients with type 2 diabetes mellitus (T2DM).

Methods: We recruited 133 Chinese patients with T2DM, and divided them according to the Montreal Cognitive Assessment score. Demographic data were collected and the level of irisin in the plasma was determined. In addition, the results of neuropsychological testing were examined. The concentration of irisin in the plasma was measured using an enzyme immunoassay.

Results: A total of 59 patients were diagnosed with MCI and 74 patients were included as healthy-cognition controls. The level of irisin in the plasma ($p = 0.043$) and homeostasis model of assessment for insulin resistance ($p = 0.032$) in diabetic patients with MCI were higher than those observed in the healthy controls. A higher level of irisin in the plasma was associated with impaired overall cognition, specifically executive function. Linear regression analysis suggested that irisin ($p = 0.017$) and glycosylated hemoglobin ($p = 0.036$) were independent factors of diabetic MCI.

Conclusions: The level of irisin in the plasma correlated with cognitive impairment in T2DM patients, particularly with executive function. These results further suggest that, in addition to poor glycemic control, a high level of irisin in the plasma portends early cognitive deficits clinically in Chinese patients with T2DM.

Keywords: irisin, mild cognitive impairment, executive function, diabetes mellitus, insulin resistance

INTRODUCTION

Individuals with type 2 diabetes mellitus (T2DM) exhibit a higher prevalence of mild cognitive impairment (MCI) in comparison with the general population (1). The risk of cognitive impairment in DM patients is 1.2 to 1.5-fold higher than that reported in non-DM individuals (2). Cognitive impairment is considered one of the chronic complications of DM (3). Several potential mechanisms promote the occurrence of cognitive impairment in T2DM, including hyperglycemic toxicity, insulin resistance, oxidative stress, accumulation of amyloid-beta peptide and tau hyper-phosphorylation (4–9).

Irisin, a novel glycosylated polypeptide hormone, plays an important role in the homeostasis and metabolism of energy balance (10). It had been reported to lead to brown-fat-like development by stimulating the expression of uncoupling protein-1 and altering that of several molecules (11, 12). Irisin induces the transformation of white adipose tissue into brown adipose tissue. Consequently, the increased thermogenesis may lead to weight loss and improve insulin sensitivity and glucose tolerance in mice (13, 14). The increase of circulating irisin is associated with endurance training induced reduction of abdominal visceral fat in old and middle-aged people (15). Many studies have found low level of irisin in individuals with T2DM compared to that in non-diabetic individuals (16–19). Continuous exposure to hyperglycemia and impaired insulin signaling are major causes of Alzheimer's disease (AD) and related to cognitive impairment, especially learning and memory loss (20, 21). Several studies reported that irisin may regulate insulin resistance and glucose homeostasis (12, 22, 23), potentially improving cognitive function. Furthermore, irisin may promote neurogenesis (24) and protect against neuronal damage caused by oxidative stress (25, 26). In addition, it was shown that irisin regulates the production of brain-derived neurotrophic factor (27, 28), which may enhance cognitive function and reduce synaptic dysfunction in AD (29). These findings suggest that irisin may improve cognitive function.

Therefore, the aim of this study was to investigate the association between the level of irisin in the plasma and cognition performance in patients with T2DM.

MATERIALS AND METHODS

Patients and Study Design

We recruited 133 patients (aged 45–75 years) who were admitted to the Department of Endocrinology of the Affiliated Zhongda Hospital of Southeast University (Nanjing, China) between February 2015 and June 2017. The patients were diagnosed with T2DM for ≥3 years according to the 1999 World Health Organization criteria (30). The exclusion criteria were as follows: (1) central nervous system diseases (i.e., recent stroke, head trauma, epilepsy, Parkinson's disease, depression, or other psychological illnesses) that may cause MCI; (2) drug or alcohol abuse or dependence; (3) other major illnesses, including cancer, anemia, or thyroid dysfunction; and (4) use of potential or known cognition-impairing drugs in the previous 3 months. All patients were of Chinese Han ethnic origin and provided written informed consent prior to their participation in the study. The study was approved by the Research Ethics Committee of the Affiliated Zhongda Hospital of Southeast University, Nanjing, China.

Collection of Clinical Data

We collected the demographic and clinical characteristics of the patients, including gender, age, educational level, contact details, duration of T2DM, medical history (e.g., hypertension and fatty liver), fasting blood glucose, fasting C-peptide (FCP), glycosylated hemoglobin (HbA1c), triglyceride, total cholesterol, low-density lipoprotein, and high-density lipoprotein. We obtained physical measurements (i.e., weight, height, blood pressure, and waist and hip circumference) using a standard balance beam scale. The body mass index (BMI) is defined as the body weight (kg) divided by the square of the body height (m^2).

Measurement of the Level of Irisin in the Plasma

We collected blood samples in the morning after the patients lying down for a night, and instructed the patients to avoid intense physical activity the day before. The concentration of irisin in the plasma was measured using an enzyme-linked immunosorbent assay (ELISA) kit (Cusabio, Wuhan, China) according to the instructions provided by the manufacturer. The accuracy of this kit is comparable to that of EK-067-29 produced by Phoenix Pharmaceuticals, USA (31).

Neuropsychological Testing

Neuropsychological testing, including the Montreal Cognitive Assessment (MoCA), Mini Mental State Exam (MMSE), digit span test (DST), verbal fluency test (VFT), clock drawing test, logical memory test (LMT), auditory verbal learning test, and trail making tests A and B (TMT-A and TMT-B) were performed to assess the cognitive functions (i.e., memory, attention, executive function, psychomotor speed, and visuospatial skills). Based on the MoCA scoring system, 59 patients with MoCA scores <26 and the remaining 74 patients with MoCA scores ≥26 were classified in the MCI group and normal cognition group (control group), respectively. One point was added to the MoCA score for patients with a number of education years <12 (32).

Statistical Analysis

Statistical analyses were performed using the SPSS Version 21.0 software (IBM Corp., Armonk, NY, USA). For continuous variables, analysis of variance and Student's *t*-test were used to compare differences between groups at baseline. The chi-squared (χ^2) test was employed for categorical variables. Spearman's correlation was used to examine the correlation between neuropsychological test scores and the level of irisin in the plasma. The relationship of cognitive performance with the level of irisin in the plasma, as well as demographic and clinical characteristics, was investigated using multiple linear regression analysis. A $p < 0.05$ denoted statistical significance.

RESULTS

Demographic and Clinical Characteristics

Table 1 lists the baseline characteristics and neuropsychological test scores of the patients. There were no significant differences found between the MCI and control groups in terms of age, gender, educational level, prevalence of hypertension, duration of T2DM, history of alcohol abuse or dependence, smoking history, BMI, waist-to-hip ratio, fasting blood-glucose, 2-h plasma glucose, FCP, HbA1C, total cholesterol, triglyceride, low-density lipoprotein, high-density lipoprotein, apolipoprotein A1, and apolipoprotein B ($p > 0.05$). The MCI group demonstrated a significantly higher level of irisin in the plasma and homeostasis model of assessment for insulin resistance (HOMA-IR) than the control group ($p < 0.05$). Moreover, significant differences between the two groups were also observed in the neuropsychological test scores ($p < 0.01$). The memory, attention, executive function, psychomotor speed, and visuospatial skills in the MCI group were significantly lower compared with those reported in the control group.

TABLE 1 | Demographic and clinical characteristics.

Characteristic	MCI group ($n = 59$)	Control group ($n = 74$)	p-value
Age (y)	59.76 ± 6.887	58.3 ± 8.461	0.283
Male/Female, *n* (%)	31 (52.5)/28 (47.5)	46 (62.2)/28 (37.8)	0.264
Education level (y)	9 (9–12)	11 (9–12)	0.506
Duration of diabetes(y)	11.288 ± 5.7866	9.696 ± 5.3857	0.104
Hypertension *n* (%)	37 (62.7)	43 (58.1)	0.256
Hypertension duration (y)	5 (0–13)	4 (0–10)	0.508
Fatty liver *n* (%)	30 (50.8)	30 (40.5)	0.237
Smoking *n* (%)	20 (33.9)	28 (37.8)	0.640
Drinking *n* (%)	12 (20.3)	19 (25.7)	0.471
Systolic BP (mmHg)	135.25 ± 18.502	136 ± 15.67	0.802
Diastolic BP (mmHg)	81.29 ± 11.174	80.5 ± 9.77	0.665
FBG (mmol/L)	8.3578 ± 2.71327	7.7147 ± 2.50359	0.159
2h-PG (mmol/L)	15.0769 ± 3.57025	14.3576 ± 3.8885	0.274
HbA1C (%)	9.7186 ± 2.59698	8.9243 ± 2.16414	0.057
FCP	1.2446 ± 0.75122	0.854 (0.4418-1.603)	0.141
HOMA-IR	0.4385 ± 0.23212	0.2889 (0.1557–0.5094)	0.032
BMI (kg/m^2)	25.12 ± 3.409	24.84 ± 3.045	0.903
WHR	0.9467 ± 0.06122	0.9366 ± 0.06408	0.355
TC (mmol/L)	4.7636 ± 1.08117	4.5538 ± 1.08846	0.372
TG (mmol/L)	1.8105 ± 1.14686	1.7174 ± 1.03957	0.625
LDL (mmol/L)	2.9275 ± 0.82897	2.8178 ± 0.80722	0.443
HDL (mmol/L)	1.1827 ± 0.33954	1.1749 ± 0.25705	0.88
ApoA1 (g/L)	1.0878 ± 0.26026	1.0732 ± 0.24375	0.74
ApoB (mmol/L)	0.82 ± 0.20130	0.8099 ± 0.18437	0.763
LPa (mmol/L)	258.23 ± 228.391	190.5 (108.75–310.75)	0.983
Irisin (ng/mL)	241.48 (145.208–564.815)	139.86 (82.845–500.413)	0.043
Cognition test levels			
MoCA	23 (20–24)	27 (26–28)	<0.001
VFT	14 (13–17)	16 (14–19)	<0.001
LMT	6.32 ± 4.22	10.09 ± 4.457	<0.001
DST	10.46 ± 2.054	12.03 ± 1.828	<0.001
CDT	3(2–4)	4 (3–4)	0.01
TMT-A	66 (53–85)	53 (45–58)	<0.001
TMT-B	196.44 ± 88.644	139.59 ± 48.465	<0.001
AVLT-immediate recall	15.78 ± 5.243	18.85 ± 3.788	<0.001
AVLT-delayed recall	5 (3–6)	6 (5–7)	<0.001

Continuous variables were presented as mean ± SD, while categorical variables were presented as n (%) or median (interquartile range). Student's t-test was used to compare normally distributed variables between two groups. The Mann–Whitney U-test was used for the comparison of asymmetrically distributed variables. MCI, mild cognitive impairment; FBG, fasting blood-glucose; 2h-PG, 2-h plasma glucose; HbA1c, glycosylated hemoglobin; FCP, fasting C-peptide; HOMA-IR, homeostasis model of assessment for insulin resistance; BMI, body mass index; WHR, waist-to-hip ratio; TG, triglyceride; TC, total cholesterol; LDL, low density lipoprotein; HDL, high density lipoprotein; ApoA1, apolipoprotein A1; ApoB, apolipoprotein B; LPa, lipoprotein(a); MoCA, montreal cognitive assessment; VFT, verbal fluency test; LMT, logical memory test; DST, digit span test; CDT, clock drawing test; TMT-A, trail making test-A; TMT-B, trail making test-B; AVLT, auditory verbal learning test; SD, standard deviation.

Correlation of the Level of Irisin in the Plasma With Baseline Data and Cognitive Indicators

We subsequently explored the correlation of the level of irisin in the plasma with clinical and the different neuropsychological test scores in all patients using Spearman rank correlation analysis. The level of plasma irisin was positively correlated with the BMI, FCP, HOMA-IR, and TMT-A and TMT-B scores. Of note, it was negatively correlated with the MoCA, MMSE, VFT, LMT, and DST score in total (**Table 2**). The level of irisin was positively associated with the FCP and the TMT-A score, whereas it was negatively associated with the MoCA, MMSE, and VFT score in the MCI group. In healthy-cognition controls, the level of irisin was only positively correlated with the FCP and TMT-A score. Considering the relationship between irisin and BMI, we performed a hierarchical analysis. The level of irisin in the plasma was only positively correlated with the TMT-A score in patients with normal weight. In overweight patients, it was significantly positively correlated with the BMI, FCP, duration of T2DM, and TMT-A and TMT-B scores. In contrast, it was negatively correlated with the MoCA, MMSE, VFT, LMT, DST, and auditory verbal learning test-delayed scores (**Table 2**).

Correlation of the MoCA Score With Baseline Characteristics in All Patients

The relationship between the MoCA score and baseline characteristics was assessed through Spearman rank correlation analysis. We found that the MoCA score correlated with sex,

TABLE 2 | Correlation of the level of irisin in the plasma with baseline data and cognitive indicators.

	Total ($n = 133$)	MCI group ($n = 59$)	Control group ($n = 74$)	BMI ≤ 24 ($n = 51$)	BMI > 24 ($n = 82$)
	r	*r*	*r*	*r*	*r*
BMI	0.217*	0.251	0.182	0.015	0.318**
WHR	0.023	−0.031	0.039	−0.129	0.059
FCP	0.268**	0.289*	0.237*	0.262	0.261*
HOMA-IR	0.217*	0.245	0.173	0.193	0.201
Duration of diabetes	0.165	0.104	0.167	0.055	0.224*
MoCA	−0.236**	−0.326*	−0.072	−0.169	−0.277*
MMSE	−0.234**	−0.305*	−0.001	−0.267	−0.241*
VFT	−0.248**	−0.394**	−0.092	−0.220	−0.258*
TMT-A	0.336**	0.295*	0.269*	0.323*	0.359**
TMT-B	0.237**	0.246	0.142	0.193	0.263*
LMT	−0.231**	−0.245	−0.125	−0.099	−0.346**
DST	−0.262**	−0.211	−0.204	−0.172	−0.334**
CDT	−0.072	−0.051	−0.018	−0.153	−0.015
AVLT-immediate	−0.107	−0.057	−0.046	−0.099	−0.109
AVLT-delayed	−0.149	−0.240	0.008	−0.028	−0.237*

*MCI, mild cognitive impairment; BMI, body mass index; WHR, waist-to-hip ratio; FCP, fasting C-peptide; HOMA-IR, homeostasis model of assessment for insulin resistance; MoCA, montreal cognitive assessment; MMSE, mini mental state examination; VFT, verbal fluency test; TMT-A, trail making test-A; TMT-B, trail making test-B; LMT, logical memory test; DST, digit span test; CDT, clock drawing test; AVLT, auditory verbal learning test. *$p < 0.05$ and **$p < 0.01$.*

TABLE 3 | Correlation of the MoCA score and baseline characteristics.

	Total ($n = 133$)		MCI group ($n = 59$)		Control group ($n = 74$)	
	r	*p*-value	*r*	*p*-value	*r*	*p*-value
Sex	−0.189	0.029	−0.373	0.004	−0.092	0.435
BMI	−0.013	0.883	−0.344	0.008	0.175	0.136
WC	−0.087	0.319	−0.298	0.022	0.208	0.075
Educational level	0.221	0.010	0.543	<0.001	0.162	0.167
Duration of diabetes	−0.137	0.116	−0.115	0.424	−0.154	0.168
Irisin	−0.236	0.006	−0.326	0.012	−0.072	0.540
HbA1c	−0.173	0.046	−0.146	0.271	0.177	0.131
FCP	−0.208	0.016	−0.158	0.231	−0.226	0.053
HOMA-IR	−0.239	0.006	−0.194	0.141	−0.149	0.205

MCI, mild cognitive impairment; BMI, body mass index; WC, waist circumference; HbA1c, glycosylated hemoglobin; FCP, fasting C-peptide; HOMA-IR, homeostasis model of assessment for insulin resistance.

TABLE 4 | Multivariable linear regression analysis with the MoCA score as the dependent variable.

	B	SE	Sig.	95% CI
Irisin	−0.002	0.001	0.017	−0.004–0
Educational level	0.334	0.113	0.004	0.110–0.559
HbA1c	−0.261	0.123	0.036	−0.504 to −0.018

Independent variables entered included: sex, age, irisin, educational level, duration of diabetes, HbA1C, FCP, WC, BMI, WHR, TG, TC, HDL, LDL, and HOMA-IR. MoCA, montreal cognitive assessment; HbA1c, glycosylated hemoglobin; T2DM, type 2 diabetes mellitus; FCP, fasting C-peptide; WC, waist circumference; BMI, body mass index; WHR, waist-to-hip ratio; TG, triglyceride; TC, total cholesterol; LDL, low-density lipoprotein; HDL, high-density lipoprotein; HOMA-IR, homeostasis model of assessment for insulin resistance; B, regression coefficients; SE, standard error; CI, confidence interval.

irisin, educational level, HbA1c, FCP, and HOMA-IR (**Table 3**). Subsequently, we formed a multiple linear regression model to identify independent factors associated with MCI. Age, sex, irisin, educational level, duration of T2DM, HbA1C, FCP, waist circumference, BMI, waist-to-hip ratio, triglyceride, total cholesterol, high-density lipoprotein, low-density lipoprotein, and HOMA-IR were entered as independent variables in the multiple step-wise linear regression analysis, with the MoCA score as the dependent variable. The multivariable regression analysis revealed that plasma irisin, educational level, and HbA1c were associated with MCI in T2DM patients ($p < 0.05$) (**Table 4**). These three independent variables explained 17% of the variance.

DISCUSSION

The results of the present study demonstrated that the level of irisin in the plasma of T2DM patients with MCI increased. This level was negatively associated with the MoCA, MMSE, VFT, LMT, and DST scores, whereas it was positively correlated with the TMT-A and TMT-B scores. These findings indicated worse overall cognitive, executive, and attention functions. The multivariable regression analysis indicated that a high level of plasma irisin and HbA1c may play important roles in the development of MCI in T2DM patients.

This was the first study to investigate the correlation between the level of irisin in the plasma and cognitive function in T2DM patients. Correlations were found between irisin and the MoCA, MMSE, VFT, LMT, DST, TMT-A, and TMT-B scores. Higher levels of irisin indicated poorer cognitive function in the patients. Additionally, we found that the BMI, FCP, and HOMA-IR were positively correlated with irisin, suggesting that the increased level of irisin in T2DM patients may be correlated with higher BMI, FCP, and HOMA-IR values. Previous studies suggested that the level of plasma irisin was increased in obese subjects (33–35). Furthermore, several studies showed a significant association between irisin and the HOMA-IR index (35–38), which reflects insulin resistance. All aforementioned factors have been shown to promote the development of cognitive impairment in T2DM patients (39, 40). Thus, an increased level of irisin may be a predictive factor of T2DM-associated cognitive impairment.

Based on these findings, the relationship between irisin and cognitive function is contrary to that reported by Lourenco et al. (41), which suggested that a lower level of irisin correlated with cognitive impairment. Irisin was reduced in the hippocampi and cerebrospinal fluid of AD patients compared with MCI patients or cognitively normal individuals (41). However, the level of irisin in the plasma was not significantly different in AD compared with that measured in non-demented controls. Another study suggested that irisin was positively associated with overall cognition and memory (42). Moreover, rat models showed that treatment with irisin reduced neurological deficits (25, 43) and increased hippocampal synaptic plasticity (41). The difference between our study and the others was the study population. T2DM is often accompanied by metabolic dysfunction. Similar to the increased level of insulin in insulin resistance (37, 44), the level of irisin in the plasma increased in MCI patients. In the present study, the positive association between the level of irisin in the plasma and markers of insulin resistance in T2DM patients may demonstrate an adaptive response to obesity through irisin (18). Similarly, an increased level of irisin in MCI patients may be the result of irisin resistance. This notion was supported by the negative correlation between the level of irisin and MoCA score in the MCI group rather than the control group. Considering the positive correlation between irisin and the BMI, irisin is likely to be involved in inflammatory and oxidative stress (45, 46).

In addition, in this study, the MoCA score was negatively correlated with HbA1c and positively correlated with the educational level. These findings were congruous with those reported by previous studies. Chronic exposure to hyperglycemia may damage cognitive function (47, 48). Higher education and more thinking may delay the progression of dementia (49, 50). Consequently, we encourage the elderly to participate in more intellectual activities to delay the impairment of cognitive function.

Several limitations of this study should be considered. Firstly, it was a cross-sectional study with a small sample size, which may limit the robustness of the results. Secondly, there were concerns regarding the accuracy of the irisin antibody kits (51). Further validation analyses using mass spectrometry are required to address these concerns. Thirdly, most of the hospitalized patients had uncontrolled diabetes, which lead to the selection bias in the sample. Although we have carefully considered and implemented the inclusion and exclusion criteria in order to reduce bias, it still affected the results. Moreover, we only used the MoCA for MCI diagnosis in our diabetic patients. Finally, the study did not collect data regarding the intensity of daily exercise, which may play an important role in the level of irisin and MCI.

CONCLUSION

In summary, this study showed that the MCI group had a higher level of irisin vs. the control group. Additionally, a higher level of irisin was associated with overall cognitive impairment, especially poorer executive function. Furthermore, irisin, HbA1c, and the educational level were identified as independent variables of MCI in all individuals, suggesting that low levels of irisin and HbA1c may be good predictors of MCI in T2DM patients. Further evidence, especially from longitudinal studies, is required to investigate

the value of irisin as a predictive biomarker of MCI in T2DM patients.

DATA AVAILABILITY

The datasets generated for this study are available on request to the corresponding author.

ETHICS STATEMENT

The studies involving human participants were reviewed and approved by the Research Ethics Committee of the Affiliated Zhongda Hospital of Southeast University. The patients/participants provided their written informed consent to participate in this study.

AUTHOR CONTRIBUTIONS

SW, HL, and YY contributed to the conception and design of the study. HL conducted the study and statistical analysis, and wrote the manuscript. ST participated in the data analysis and interpretation. JH, RH, DG, JW, and KA performed the data collection. All authors read and approved the submitted version of this manuscript.

FUNDING

This work was partly supported by the National Natural Science Foundation of China (No. 81570732, SW; and No. 81870568, SW), and the Jiangsu Provincial Medical Youth Talent (QNRC2016819, YY).

REFERENCES

1. Dolan C, Glynn R, Griffin S, Conroy C, Loftus C, Wiehe PC, et al. Brain complications of diabetes mellitus: a cross-sectional study of awareness among individuals with diabetes and the general population in Ireland. *Diabet Med*. (2018) 35:871–9. doi: 10.1111/dme.13639
2. Cukierman T, Gerstein HC, Williamson JD. Cognitive decline and dementia in diabetes–systematic overview of prospective observational studies. *Diabetologia*. (2005) 48:2460–9. doi: 10.1007/s00125-005-0023-4
3. Mittal K, Katare DP. Shared links between type 2 diabetes mellitus and Alzheimer's disease: a review. *Diabetes Metab Syndr*. (2016) 10(2 Suppl. 1):S144–9. doi: 10.1016/j.dsx.2016.01.021
4. Macauley SL, Stanley M, Caesar EE, Yamada SA, Raichle ME, Perez R, et al. Hyperglycemia modulates extracellular amyloid-beta concentrations and neuronal activity in vivo. *J Clin Invest*. (2015) 125:2463–7. doi: 10.1172/JCI79742
5. Gaspar JM, Baptista FI, Macedo MP, Ambrosio AF. Inside the diabetic brain: role of different players involved in cognitive decline. *ACS Chem Neurosci*. (2016) 7:131–42. doi: 10.1021/acschemneuro.5b00240
6. Kim DJ, Yu JH, Shin MS, Shin YW, Kim MS. Hyperglycemia reduces efficiency of brain networks in subjects with type 2 diabetes. *PLoS ONE*. (2016) 11:e0157268. doi: 10.1371/journal.pone.0157268
7. Lemche, E. (2018). Early life stress and epigenetics in late-onset Alzheimer's dementia: a systematic review. *Curr. Genomics*19, 522–602. doi: 10.2174/1389202919666171229145156
8. Rom S, Zuluaga-Ramirez V, Gajghate S, Seliga A, Winfield M, Heldt NA, et al. Hyperglycemia-driven neuroinflammation compromises BBB leading to memory loss in both diabetes mellitus (DM) type 1 and type 2 mouse models. *Mol Neurobiol*. (2019) 56:1883–96. doi: 10.1007/s12035-018-1195-5
9. Lee HJ, Seo HI, Cha HY, Yang YJ, Kwon SH, Yang SJ. Diabetes and Alzheimer's disease: mechanisms and nutritional aspects. *Clin Nutr Res*. (2018) 7:229–40. doi: 10.7762/cnr.2018.7.4.229
10. Grygiel-Gorniak B, Puszczewicz M. A review on irisin, a new protagonist that mediates muscle-adipose-bone-neuron connectivity. *Eur Rev Med Pharmacol Sci*. (2017) 21:4687–93.
11. Bostrom P, Wu J, Jedrychowski MP, Korde A, Ye L, Lo JC, et al. A PGC1-alpha-dependent myokine that drives brown-fat-like development of white fat and thermogenesis. *Nature*. (2012) 481:463–8. doi: 10.1038/nature10777
12. Zhang Y, Li R, Meng Y, Li S, Donelan W, Zhao Y, et al. Irisin stimulates browning of white adipocytes through mitogen-activated protein kinase p38 MAP kinase and ERK MAP kinase signaling. *Diabetes*. (2014) 63:514–25. doi: 10.2337/db13-1106
13. Lee HJ, Lee JO, Kim N, Kim JK, Kim HI, Lee YW, et al. Irisin, a novel myokine, regulates glucose uptake in skeletal muscle cells via AMPK. *Mol Endocrinol*. (2015) 29:873–81. doi: 10.1210/me.2014-1353
14. Xin C, Liu J, Zhang J, Zhu D, Wang H, Xiong L. Irisin improves fatty acid oxidation and glucose utilization in type 2 diabetes by regulating the AMPK signaling pathway. *Int J Obes*. (2016) 40, 443–451. doi: 10.1038/ijo.2015.199
15. Miyamoto-Mikami E, Sato K, Kurihara T, Hasegawa N, Fujie S, Fujita S, et al. Endurance training-induced increase in circulating irisin levels is associated with reduction of abdominal visceral fat in middle-aged and older adults. *PLoS ONE*. (2015) 10:e0120354. doi: 10.1371/journal.pone.0120354
16. Choi YK, Kim MK, Bae KH, Seo HA, Jeong JY, Lee WK, et al. Serum irisin levels in new-onset type 2 diabetes. *Diabetes Res Clin Pract*. (2013) 100:96–101. doi: 10.1016/j.diabres.2013.01.007
17. Liu JJ, Wong MD, Toy WC, Tan CS, Liu S, Ng XW, et al. Lower circulating irisin is associated with type 2 diabetes mellitus. *J Diabetes Complications*. (2013) 27:365–9. doi: 10.1016/j.jdiacomp.2013.03.002
18. Moreno-Navarrete JM, Ortega F, Serrano M, Guerra E, Pardo G, Tinahones F, et al. Irisin is expressed and produced by human muscle and adipose tissue in association with obesity and insulin resistance. *J Clin Endocrinol Metab*. (2013) 98:E769–78. doi: 10.1210/jc.2012-2749
19. Hu W, Wang R, Li J, Zhang J, Wang W. Association of irisin concentrations with the presence of diabetic nephropathy and retinopathy. *Ann Clin Biochem*. (2016) 53(Pt 1):67–74. doi: 10.1177/0004563215582072
20. Chen Z, Zhong C. Decoding Alzheimer's disease from perturbed cerebral glucose metabolism: implications for diagnostic and therapeutic strategies. *Prog Neurobiol*. (2013) 108:21–43. doi: 10.1016/j.pneurobio.2013.06.004
21. Willette AA, Bendlin BB, Starks EJ, Birdsill AC, Johnson SC, Christian BT, et al. Association of insulin resistance with cerebral glucose uptake in late middle-aged adults at risk for Alzheimer disease. *JAMA Neurol*. (2015) 72:1013–20. doi: 10.1001/jamaneurol.2015.0613
22. Yang Z, Chen X, Chen Y, Zhao Q. Decreased irisin secretion contributes to muscle insulin resistance in high-fat diet mice. *Int J Clin Exp Pathol*. (2015) 8:6490–7.
23. Al-Daghri NM, Mohammed AK, Al-Attas OS, Amer OE, Clerici M, Alenad A, et al. SNPs in FNDC5 (irisin) are associated with obesity and modulation of glucose and lipid metabolism in Saudi subjects. *Lipids Health Dis*. (2016) 15:54. doi: 10.1186/s12944-016-0224-5
24. Hashemi MS, Ghaedi K, Salamian A, Karbalaie K, Emadi-Baygi M, Tanhaei S, et al. Fndc5 knockdown significantly decreased neural differentiation rate of mouse embryonic stem cells. *Neuroscience*. (2013) 231:296–304. doi: 10.1016/j.neuroscience.2012.11.041
25. Li DJ, Li YH, Yuan HB, Qu LF, Wang P. The novel exercise-induced hormone irisin protects against neuronal injury via activation of the Akt and ERK1/2 signaling pathways and contributes to the neuroprotection of physical exercise in cerebral ischemia. *Metabolism*. (2017) 68:31–42. doi: 10.1016/j.metabol.2016.12.003
26. Peng J, Deng X, Huang W, Yu JH, Wang JX, Wang JP, et al. Irisin protects against neuronal injury induced by oxygen-glucose deprivation in part depends on the inhibition of ROS-NLRP3 inflammatory signaling pathway. *Mol Immunol*. (2017) 91:185–94. doi: 10.1016/j.molimm.2017.09.014

27. Wrann CD, White JP, Salogiannnis J, Laznik-Bogoslavski D, Wu J, Ma D, et al. Exercise induces hippocampal BDNF through a PGC-1alpha/FNDC5 pathway. *Cell Metab*. (2013) 18:649–59. doi: 10.1016/j.cmet.2013.09.008
28. Belviranli M, Okudan N, Kabak B, Erdogan M, Karanfilci M. The relationship between brain-derived neurotrophic factor, irisin and cognitive skills of endurance athletes. *Phys Sportsmed*. (2016) 44:290–6. doi: 10.1080/00913847.2016.1196125
29. Diniz BS, Teixeira AL. Brain-derived neurotrophic factor and Alzheimer's disease: physiopathology and beyond. *Neuromolecular Med*. (2011) 13:217–22. doi: 10.1007/s12017-011-8154-x
30. Alberti KG, Zimmet PZ. Definition, diagnosis and classification of diabetes mellitus and its complications. Part 1: diagnosis and classification of diabetes mellitus provisional report of a WHO consultation. *Diabet Med*. (1998) 15:539–53. doi: 10.1002/(SICI)1096-9136(199807)15:7<539::AID-DIA668>3.0.CO;2-S
31. Li M, Yang M, Zhou X, Fang X, Hu W, Zhu W, et al. Elevated circulating levels of irisin and the effect of metformin treatment in women with polycystic ovary syndrome. *J Clin Endocrinol Metab*. (2015) 100:1485–93. doi: 10.1210/jc.2014-2544
32. Nasreddine ZS, Phillips NA, Bedirian V, Charbonneau S, Whitehead V, Collin I, et al. The montreal cognitive assessment, MoCA: A brief screening tool for mild cognitive impairment. *J Am Geriatr Soc*. (2005) 53:695–9. doi: 10.1111/j.1532-5415.2005.53221.x
33. Yilmaz H, Cakmak M, Darcin T, Inan O, Sahiner E, Demir C, et al. Circulating irisin levels reflect visceral adiposity in non-diabetic patients undergoing hemodialysis. *Ren Fail*. (2016) 38:914–9. doi: 10.3109/0886022X.2016.1172918
34. Sahin-Efe A, Upadhyay J, Ko BJ, Dincer F, Park KH, Migdal A, et al. Irisin and leptin concentrations in relation to obesity, and developing type 2 diabetes: a cross sectional and a prospective case-control study nested in the Normative Aging Study. *Metabolism*. (2018) 79:24–32. doi: 10.1016/j.metabol.2017.10.011
35. Wang W, Guo Y, Zhang X, Zheng J. Abnormal irisin level in serum and endometrium is associated with metabolic dysfunction in polycystic ovary syndrome patients. *Clin Endocrinol*. (2018) 89:474–80. doi: 10.1111/cen.13805
36. Park KH, Zaichenko L, Brinkoetter M, Thakkar B, Sahin-Efe A, Joung KE, et al. Circulating irisin in relation to insulin resistance and the metabolic syndrome. *J Clin Endocrinol Metab*. (2013) 98:4899–907. doi: 10.1210/jc.2013-2373
37. Shoukry A, Shalaby SM, El-Arabi Bdeer S, Mahmoud AA, Mousa MM, Khalifa A. Circulating serum irisin levels in obesity and type 2 diabetes mellitus. *IUBMB Life*. (2016) 68:544–56. doi: 10.1002/iub.1511
38. Stratigou T, Dalamaga M, Antonakos G, Marinou I, Vogiatzakis E, Christodoulatos GS, et al. Hyperirisinemia is independently associated with subclinical hypothyroidism: correlations with cardiometabolic biomarkers and risk factors. *Endocrine*. (2018) 61:83–93. doi: 10.1007/s12020-018-1550-3
39. Umegaki H. Type 2 diabetes as a risk factor for cognitive impairment: current insights. *Clin Interv Aging*. (2014) 9:1011–9. doi: 10.2147/CIA.S48926
40. Miller AA, Spencer SJ. Obesity and neuroinflammation: a pathway to cognitive impairment. *Brain Behavior Immunity*. (2014) 42:10–21. doi: 10.1016/j.bbi.2014.04.001
41. Lourenco MV, Frozza RL, de Freitas GB, Zhang H, Kincheski GC, Ribeiro FC, et al. Exercise-linked FNDC5/irisin rescues synaptic plasticity and memory defects in Alzheimer's models. *Nat Med*. (2019) 25:165–75. doi: 10.1038/s41591-018-0275-4
42. Kuster OC, Laptinskaya D, Fissler P, Schnack C, Zugel M, Nold V, et al. Novel blood-based biomarkers of cognition, stress, and physical or cognitive training in older adults at risk of dementia: preliminary evidence for a role of BDNF, irisin, and the kynurenine pathway. *J Alzheimers Dis*. (2017) 59:1097–111. doi: 10.3233/JAD-170447
43. Asadi Y, Gorjipour F, Behrouzifar S, Vakili A. Irisin peptide protects brain against ischemic injury through reducing apoptosis and enhancing BDNF in a rodent model of stroke. *Neurochem Res*. (2018) 43:1549–60. doi: 10.1007/s11064-018-2569-9
44. Doumatey AP, Lashley KS, Huang H, Zhou J, Chen G, Amoah A, et al. Relationships among obesity, inflammation, and insulin resistance in African Americans and West Africans. *Obesity*. (2010) 18:598–603. doi: 10.1038/oby.2009.322
45. Cox AJ, West NP, Cripps AW. Obesity, inflammation, and the gut microbiota. *Lancet Diabetes Endocrinol*. (2015) 3:207–15. doi: 10.1016/S2213-8587(14)70134-2
46. Reho JJ, Rahmouni K. Oxidative and inflammatory signals in obesity-associated vascular abnormalities. *Clin Sci*. (2017) 131:1689–700. doi: 10.1042/CS20170219
47. Munshi MN. Cognitive dysfunction in older adults with diabetes: what a clinician needs to know. *Diabetes Care*. (2017) 40:461–7. doi: 10.2337/dc16-1229
48. Pruzin JJ, Nelson PT, Abner EL, Arvanitakis Z. Review: relationship of type 2 diabetes to human brain pathology. *Neuropathol Appl Neurobiol*. (2018) 44:347–62. doi: 10.1111/nan.12476
49. Ott A, Breteler MM, van Harskamp F, Claus JJ, van der Cammen TJ, Grobbee DE, et al. Prevalence of Alzheimer's disease and vascular dementia: association with education. The Rotterdam study. *BMJ*. (1995) 310:970–3. doi: 10.1136/bmj.310.6985.970
50. Baumgart M, Snyder HM, Carrillo MC, Fazio S, Kim H, Johns H. Summary of the evidence on modifiable risk factors for cognitive decline and dementia: a population-based perspective. *Alzheimers Dement*. (2015) 11:718–26. doi: 10.1016/j.jalz.2015.05.016
51. Albrecht E, Norheim F, Thiede B, Holen T, Ohashi T, Schering L, et al. Irisin - a myth rather than an exercise-inducible myokine. *Sci Rep*. (2015) 5:8889. doi: 10.1038/srep08889

Conflict of Interest Statement: The authors declare that the research was conducted in the absence of any commercial or financial relationships that could be construed as a potential conflict of interest.

frontiers in Neuroscience

CLINICAL TRIAL
published: 10 October 2019
doi: 10.3389/fnins.2019.01074

Brief Mindfulness Meditation Improves Emotion Processing

*Ran Wu[1,2†], Lin-Lin Liu[1†], Hong Zhu[2], Wen-Jun Su[1], Zhi-Yong Cao[1], Shi-Yang Zhong[1], Xing-Hua Liu[3] and Chun-Lei Jiang[1]**

[1] Laboratory of Stress Medicine, Faculty of Psychology and Mental Health, Second Military Medical University, Shanghai, China, [2] Counseling and Psychological Services Center, East China Normal University, Shanghai, China, [3] Beijing Key Laboratory of Behavior and Mental Health, School of Psychological and Cognitive Sciences, Peking University, Beijing, China

Mindfulness-based interventions have previously been shown to have positive effects on psychological well-being. However, the time commitment, teacher shortage, and high cost of classic mindfulness interventions may have hindered efforts to spread the associated benefits to individuals in developing countries. Brief mindfulness meditation (BMM) has recently received attention as a way to disseminate the benefits of mindfulness-based interventions. Most existing BMM methods are adaptations of the classic approach. Few studies have investigated the mechanisms underlying the beneficial effects of BMM. We developed a 15-min BMM named JW2016, which is based on the core concepts of mindfulness, Anapanasati (breath meditation of Buddhist Vipassana), our practical experience, and the results of scientific reports on meditation. We investigated the effects of this BMM on mood and emotion processing in an effort to create an effective, convenient, safe, and standardized BMM method that could benefit individuals with limited time or money to devote to meditation. Forty-six healthy participants (aged 18–25 years) were randomly allocated to the BMM group (n = 23) or the emotional regulation education (ERE) control group (n = 23). Forty-two of the study participants cooperated fully in all measurements and interventions (one time daily for seven consecutive days). Mood was measured with the Centre for Epidemiological Studies–Depression scale (CES-D) and the State Anxiety Inventory (SAI). Emotion processing was evaluated by assessing performance on an emotion intensity task, an emotional memory task, and an emotional dot-probe task. After intervention, the BMM group, but not the ERE group, showed a significant decreases in emotional intensity in response to positive as well as negative emotional stimuli, response time for emotional memory, and duration of attention bias toward negative emotional stimuli. Negative effects on mood state were found in the ERE group but not in the BMM group. This study demonstrated that BMM may improve aspects of emotion processing such as emotion intensity, emotional memory, and emotional attention bias. JW2016 BMM may be an effective, convenient, safe and standardized way to help practitioners remain focused and peaceful without any negative effect on emotion.

Keywords: brief mindfulness meditation, randomized controlled trial, anxiety, depression, stress, emotion intensity, emotional memory, emotional attention bias

OPEN ACCESS

Edited by:
Yu-Feng Wang,
Harbin Medical University, China

Reviewed by:
Cassandra Vieten,
Independent Researcher,
Baltimore, United States
Donghong Cui,
Shanghai Mental Health Center (SMHC), China

***Correspondence:**
Chun-Lei Jiang
cljiang@vip.163.com

†These authors share first authorship

Specialty section:
This article was submitted to Neuroendocrine Science, a section of the journal Frontiers in Neuroscience

Received: *04 July 2019*
Accepted: *24 September 2019*
Published: *10 October 2019*

Citation:
Wu R, Liu L-L, Zhu H, Su W-J, Cao Z-Y, Zhong S-Y, Liu X-H and Jiang C-L (2019) Brief Mindfulness Meditation Improves Emotion Processing. Front. Neurosci. 13:1074. doi: 10.3389/fnins.2019.01074

INTRODUCTION

Mindfulness meditation is a form of self-regulatory exercise for mind and body. The core concepts of mindfulness include paying attention to the present moment and attaining a state of consciousness in a non-judgmental/accepting manner (Bishop et al., 2004; Lutz et al., 2008). Mindfulness meditation has its roots in Vipassana (insight meditation, a Buddhist meditation technique), which purports to affect mental events by engaging a specific attentional set (Lutz et al., 2008). As a clinical intervention, mindfulness meditation has been demonstrated to produce beneficial effects on mental and physical states, especially in terms of emotional improvement and recovery from affect-related psychopathology (Kabatzinn et al., 1992; Pinniger et al., 2012; Hoge et al., 2014; Khusid and Vythilingam, 2016). Mindfulness meditation has been proven to promote well-being and emotional balance (Krygier et al., 2013; Goyal et al., 2014), to decrease stress reactivity (Pace et al., 2009; Goyal et al., 2014), and to reduce negative feelings associated with anxiety and depression (Lane et al., 2007; Hoge et al., 2014; Khusid and Vythilingam, 2016).

Instead of attempting to change emotional experiences, meditation practice trains the individual to notice and observe emotions simply as they are and to accept emotional reactions as they arise (Lutz et al., 2008). Previous studies have explored the emotional benefits of meditation from numerous perspectives. Several studies have demonstrated that meditation may help to modulate emotional responses to negative stimuli (Erisman and Roemer, 2011; Johns and Medicine, 2015). Evidence from the field of cognitive neuroscience suggests that long-term meditation practice decreases the reaction intensity of the autonomic nervous system (Vasquez-Rosati et al., 2017) and attenuates the neural responses to emotional stimuli (Sobolewski et al., 2011; Taylor et al., 2011). Meditation training may also increase cognitive flexibility (Wenksormaz, 2005; Zeidan et al., 2011) and produce positive effects on emotion-cognition interactions. One study showed that an 8-week mindfulness-based stress reduction (MBSR) course enhanced attentional orientation and improved the ability to regulate emotion (Jha et al., 2007). An 8-week mindfulness-based meditation course reduced the attentional bias for pain-related threats in patients with fibromyalgia (Vago and Nakamura, 2011). Few studies have been conducted to examine the effects of meditation on positive emotion, and studies published to date have yielded conflicting findings. The results of previous studies showed that, after meditation, positive affect in response to a positive stimulus may increase (Erisman and Roemer, 2011), decrease (Ren et al., 2012), or remain unchanged (Sobolewski et al., 2011; Taylor et al., 2011). The effects of meditation on emotion-cognition interactions remain unclear.

Although mindfulness meditation training has proven to have many positive effects, the beneficiary population is relatively small because of the associated time commitment, teacher shortage, and high cost. Recently, brief mindfulness meditation (BMM) training has attracted increasing attention. One meta-analysis reported that BMM was more effective than control programs in decreasing negative affectivity (Schumer et al., 2018). However, the minimum amount of meditation training sufficient to improve emotional reactivity remains unknown, as does the mechanism underlying the positive effects reported in the literature. Previous studies found that 5 days of meditation (20 min daily) improved coordination of the body and mind in practitioners (Tang et al., 2009). Four days of mindfulness meditation training (20 min daily) decreased negative feelings such as fatigue and anxiety and improved cognitive functions such as visuospatial processing, working memory, and executive functioning (Zeidan et al., 2010b). Three days of 20-min mindfulness meditation sessions (1 h total) was more effective than sham mindfulness or control treatment in decreasing negative mood, depression, fatigue, confusion, and heart rate (Zeidan et al., 2010c). Even a single 10-min mindfulness intervention (Erisman and Roemer, 2011) or a 15-min focused-breathing meditation (Arch and Craske, 2006) may immediately decrease the intensity and negativity of emotional responses to affectively valenced external stimuli. Individuals may therefore benefit from very small doses of meditation training. However, other studies have reported conflicting conclusions. For example, researchers found that 7 days of meditation (30 min daily) reduced anxiety-related symptoms in practitioners but did not affect depression symptoms (Chen et al., 2013). 3 days of meditation (25 min daily) reduced self-reported psychological stress reactivity but increased salivary cortisol reactivity, as assessed with the Trier Social Stress Test (Creswell et al., 2014). Additional studies will be necessary to verify the specific effects and mechanisms of BMM.

BMM is not restricted by time or place and has the advantages of convenience and low cost. These characteristics suggest that the technique could benefit individuals who do not have enough time, money, or motivation to pursue other types of meditation training. Existing BMM methods are typically adapted from a more classical approach (e.g., Zeidan et al., 2010a; Collins et al., 2017). BMM methods developed independently of classical meditation practice are not common. Additional research will be necessary to determine the optimal time and frequency for the practice of BMM. Few studies have investigated the specific mechanisms underlying the effects of BMM. In this study, we developed a 15-min BMM based on the core concepts of mindfulness and Anapanasati (breath meditation related to Buddhist Vipassana), as interpreted in the context of our practical experience and that reported in other scientific reports on meditation. We performed a randomized controlled trial to investigate the effects of this BMM on mood state (depression and anxiety) and emotion processing (emotion intensity, emotional memory, and emotional attention bias). We hypothesized that BMM may be an effective, convenient, safe, and standardized

Abbreviations: BMM, brief mindfulness meditation group; CAPS, Chinese Affective Picture System; CES-D, Centre for Epidemiological Studies–Depression Scale; DA, depressed affect; DHEAS, dehydroepiandrosterone sulfate. DSM, diagnostic and statistical manual of mental disorders; ERE, emotional regulation education group; HPA axis, hypothalamus–pituitary–adrenal axis; IAPS, International Affective Picture Set; ICD, International Classification of Diseases; IP, interpersonal problems; MBSR, mindfulness-based stress reduction; min, minute; PA positive affect; SAI, State Anxiety Inventory; SC, somatic complaints; STAI-Form Y, State-Trait Anxiety Inventory.

approach to meditation that may improve mood and emotional processing among practitioners.

MATERIALS AND METHODS

This was a randomized controlled trial that included two groups: a BMM group (treatment group) and an emotional regulation education (ERE) group (comparison group). Both programs lasted for 1 week. Outcome measures were recorded at precise time points before and after engagement in the program. The entire experiment lasted for 3 weeks and consisted of three sessions: pre-test, intervention, and post-test. The present study was approved by the Committee on Ethics of Biomedicine Research at Second Military Medical University and registered in the Chinese Clinical Trial Registry (ChiCTR1800016081).

Participation and Recruitment

The participants were recruited through campus advertisements during April and May 2017. We selected healthy people as participants to assess the efficacy and safety of meditation because there have been reports of the unwanted effects of meditation on practitioners (Cebolla et al., 2017). The following inclusion criteria were used: (1) 18–25 years of age; (2) undergraduate or graduate student; (3) in good health, with no mental illness according to established diagnostic criteria (DSM-IV-TR and ICD-10 combined); (4) ability to understand Cantonese; (5) willing to attend the BMM or ERE program.

The exclusion criteria were: (1) suffering from serious physical or mental illness or conditions expected to severely limit participation or adherence (e.g., pregnancy); (2) major life event (e.g., bereavement) or significant fluctuation in mood within the past month; (3) screening positive for major depression when evaluated with a structured diagnostic interview; (4) history of or interest in participation in a meditation program; (5) failure to participate in all scheduled sessions.

After the interview with the principal investigator, 46 students were recruited and randomly assigned to a treatment group with a list of computer-generated random numbers. Forty-two individuals completed all scheduled sessions: one dropped out because of illness; the others dropped out because they had an exam or class meeting and could not attend training. **Table 1** shows the baseline demographic characteristics, for each intervention group and for the overall study population. Informed consent was obtained from all study participants.

Measurements

Measurements included the participants' demographic information (age, sex, and education status), mood state (depression, anxiety) and emotion processing (emotion intensity, emotional memory, and emotional attention bias). Mood state and emotion processing were assessed before and after the program. Emotion processing was assessed using before and after testing, using different visual information each time.

TABLE 1 | Baseline demographic characteristics by intervention group and total sample.

Variable	Total Sample (*n* = 43)	BMM (*n* = 22)	ERE (*n* = 20)
Age, mean (SD)	21.64 (2.14)	21.64 (2.34)	21.65 (1.95)
Gender (Female), No. (%)	32 (76.2)	18 (81.8)	14 (70)
Education (undergraduate), No. (%)	22 (52.4)	11 (50)	11 (55)

Mood State

Depression

Depression was assessed using the CES-D, which investigated how often the participants had experienced specific depressive symptoms during the last week. Radloff (1977) originally proposed that the 20 items were categorized into four symptom groups: depressed affect (DA), somatic complaints (SC), interpersonal problems (IP), and positive affect (PA). Items were rated on a scale ranging from 1 (rarely or none of the time) to 4 (most or all of the time) (Radloff, 1977). The CES-D has been validated to be fit for Chinese adolescents and young adults (Radloff, 1991; Yen et al., 2000; Li and Hicks, 2010). However, in previous studies, Chinese students tended to have higher CES-D scores than members of the general population (Li and Hicks, 2010).

State anxiety

State anxiety (feelings of anxiety at a given moment) were assessed with a 20-item subscale of the State-Trait Anxiety Inventory (STAI-Form Y; Spielberger, 1983). Each item evaluated by the SAI is scored on a scale ranging from 1 (absent) to 4 (intense). The Chinese version of this test has been validated as a good psychometric index (Yan et al., 2014).

Emotion Processing

Emotion intensity

An emotion intensity task was used to assess emotional intensity when participants were exposed to emotional stimuli (Ochsner and Gross, 2005; Taylor et al., 2011). The emotion-eliciting stimuli were selected from the International Affective Picture Set (IAPS; Center for the Study of Emotion and Attention [CSEA-NIMH], 1999). Pictures were selected to produce three distinct picture sets: positive, neutral, and negative. Each set included 66 pictures (6 for practice, 60 for evaluation). All pictures were randomly assigned to use in the pre- or post-test evaluation. For each of the three sets of pictures, there was no significant difference in pre- vs. post-test valence or arousal (**Table 2**). Each trial included four steps. First, a point for fixation appeared on the computer screen for 0.5 s. Second, a randomly selected image appeared on the computer screen. Participants were instructed to observe the image for 4 s and to try to remember it. Next, the image disappeared, and a Likert scale appeared. Participants were instructed to rate the strength of their emotional response on a scale of 1–5 (weak to strong). After the participants had rated their emotion intensity, the word "RELAX" appeared on the screen for 4 s, after which the next image appeared (**Figure 1A**).

Emotional memory

After completing the emotion intensity task, participants were immediately asked to finish the emotional memory task (Groch et al., 2011). Recognition memory was assessed by asking participants to assign the term "familiar" or "novel" to each

TABLE 2 | Valence and arousal of the pictures in the pre-test and post-test in the emotion intensity task [Mean (SD)].

		Pre-test	Post-test	*t*-test (*t*)
Positive	Valence	7.04 (0.46)	7.06 (0.59)	−0.13
	Arousal	5.74 (0.36)	5.78 (0.67)	−0.25
Neutral	Valence	5.11 (0.44)	5.13 (0.70)	−0.10
	Arousal	4.57 (0.54)	4.59 (0.66)	−0.11
Negative	Valence	2.73 (0.64)	2.71 (0.73)	0.08
	Arousal	5.42 (0.76)	5.41 (0.65)	0.05

of 66 previously presented targets and 66 matched distractors (6 for practice, 60 for evaluation). The "novel" pictures were selected from the IAPS, which includes equal numbers of positive, neutral, and negative pictures. For all three sets of pictures, there was no significant difference in valence or arousal between pre- vs. post-test values, or between target vs. distractor pictures (**Table 3**). The picture remained on the screen until the participant had recorded his or her response (**Figure 1B**). Participants were asked to respond as correctly and as rapidly as possible. Accuracy and response time (correct responses only) were computed and analyzed.

Emotional attention bias

The attentional dot-probe task was used to assess emotional attention bias (Tsotsos et al., 1995). Three types of emotional faces taken from the Chinese Affective Picture System (CAPS) (Gong et al., 2011) were used for this task: 60 faces displaying negative emotion and 60 faces displaying positive emotion. Each face displaying a negative or positive emotion was paired with a matched neutral face. Another 60 neutral-neutral face pairs were used as filler. There were thus three types of face pairs: sad–neutral, happy–neutral, and neutral–neutral (60 pictures each). For each trial, a pair of faces (emotional–neutral) was presented on the screen, with one face on the left and the other face on the right. The emotional faces appeared in the right or left position with equal frequency. After fixation had been achieved, a given face pair was presented for 0.8 s, followed immediately by presentation of a probe in one of the two locations previously occupied by faces (**Figure 1C**). Participants were required to indicate the orientation of the dot by pressing a labeled key on the keyboard. The dot remained on the screen until the participant had recorded a response. For the "congruent" condition, the probe and the emotional face appeared in the same position. For the "incongruent" condition, the probe and the emotional face appeared in opposite positions. Attentional bias reaction time scores were calculated for each participant by subtracting the mean reaction time for congruent conditions from the mean reaction time for incongruent conditions (correct responses only).

Intervention and Control

The interventions were single-blind in design; participants did not know the purpose of the experiment. A psychological counselor who has 10 years of mindfulness training and emotion education experience and knew the purpose of the experiment delivered the formalized program curriculum to participants in the two conditions. In order to reduce the potential bias, the leader conducted the intervention via audio instructions only, rather than providing one-on-one guidance.

Intervention: BMM

The BMM program used in this study was designed by a facilitator with more than 10 years of experience and training in meditation. This 15-min BMM (JW2016*)* was developed based on the core concepts of mindfulness and Anapanasati (Buddhist Vipassana breath meditation) (Chavan, 2007), in combination with knowledge gained from our practical experience and from scientific reports on meditation. We considered the validity and operability and tried to find a balance among practice time, frequency, and desired outcomes. Over 7 consecutive days, 22 participants attended training, in the same room and at the same time every day. On the first day of the meditation program, before meditation training, participants attended a 30-min lecture on mindfulness meditation theory. After that, participants sat on their cattail hassocks and followed audio instructions on how to practice the skills that would be tested. The audio instructions comprised 1 min of guided preparation and 15 min of mindfulness meditation training. Participants were instructed to close their eyes, relax, and focus on the flow of their breath. They were told to passively notice and acknowledge the thoughts arising randomly and to simply let "them" go, by bringing the attention back to the breath. As a manipulation check after each meditation session, each participant was asked "Did you feel that you were truly meditating?" Participants were allowed to ask questions about the meditation training. They were not asked to complete meditation homework or to practice outside of the intervention setting.

Control: ERE

The 20 participants in the ERE group received emotional education over the course of 1 week. On the first day, participants attended a 30-min lecture on emotion education and the emotion regulation theory proposed by Gross (1998). Participants were taught to recognize and regulate their own emotions. Participants then spent 15 min per day for 7 consecutive days promoting emotional awareness and regulation. No homework was given.

Statistical Analysis

All statistical analyses were conducted with SPSS 21.0. Mood state and emotion processing scores were analyzed with an independent-sample *t*-test to test for between-group effects of intervention training and with a dependent-sample *t*-test to test for within-group effects (pre- vs. post-test). A significance level of 0.05 was used for all statistical tests.

RESULTS

Mood State

The CES-D and SAI scores obtained are presented in **Table 4**. There was no significant effect of BMM training on mood state. Analysis of the post-test data revealed CES-D subscale and total

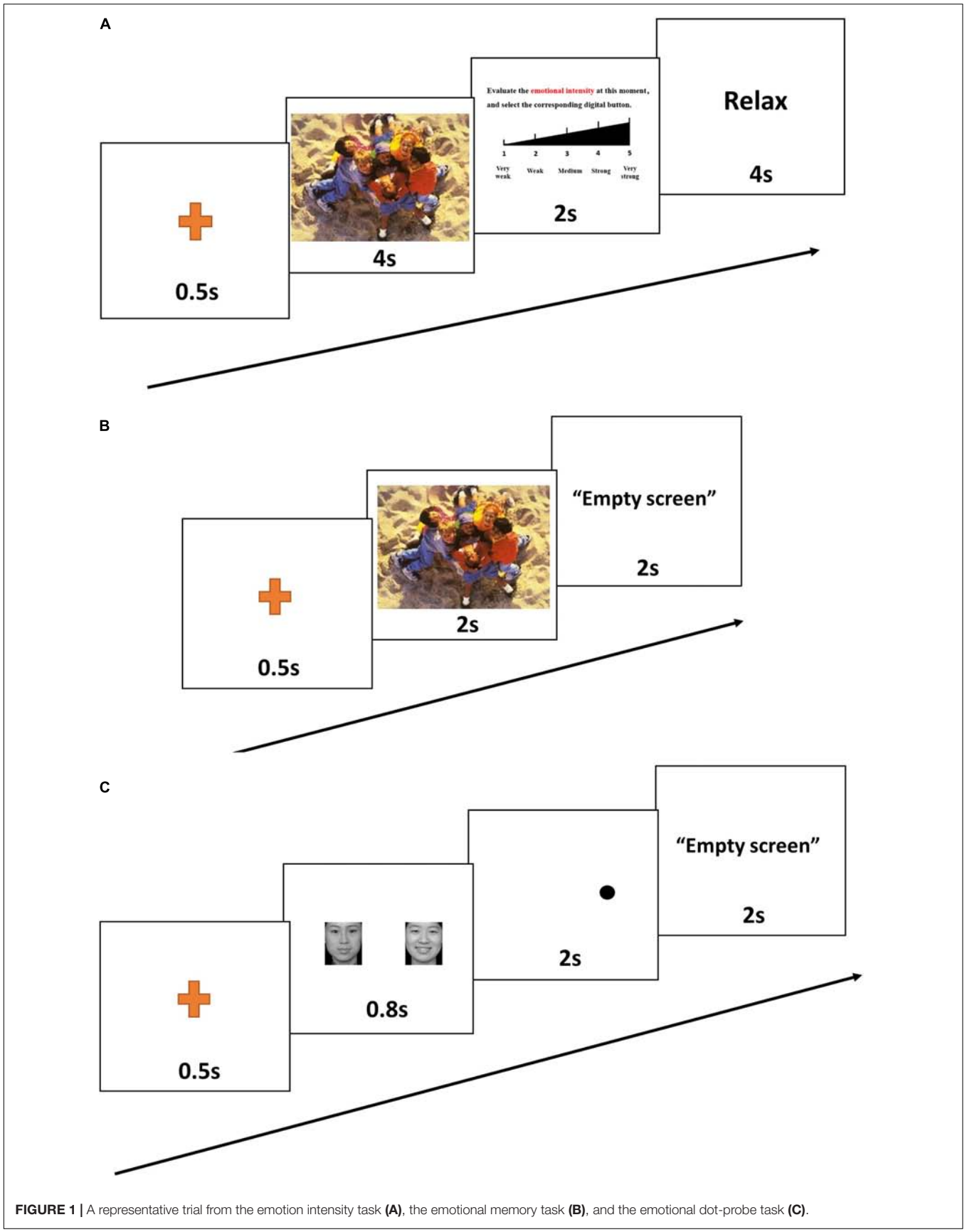

FIGURE 1 | A representative trial from the emotion intensity task **(A)**, the emotional memory task **(B)**, and the emotional dot-probe task **(C)**.

TABLE 3 | Valenceand arousal of the pictures in the pre-test and post-test in the emotional memory task [Mean (SD)].

		Pre-test target	Post-test target	Pre-test distractor	Post-test distractor	ANOVA (pre-post), *F*	ANOVA (tar-dis), *F*
Positive	Valence	7.04 (0.46)	7.02 (0.42)	6.98 (0.47)	7.06 (0.59)	0.00	0.16
	Arousal	5.74 (0.36)	7.06 (0.59)	7.02 (0.42)	6.98 (0.47)	0.03	0.22
Neutral	Valence	5.11 (0.44)	5.78 (0.67)	5.75 (0.54)	5.66 (0.60)	0.01	0.05
	Arousal	4.57 (0.54)	5.13 (0.70)	5.11 (0.44)	5.07 (0.61)	0.33	1.30
Negative	Valence	2.73 (0.64)	4.59 (0.66)	4.67 (0.57)	4.81 (0.75)	0.06	0.03
	Arousal	5.42 (0.76)	2.71 (0.73)	2.77 (0.61)	2.74 (0.68)	0.62	0.03

Column "ANOVA (pre-post)" for main effect of pre/post test; Column "ANOVA (tar-dis)" for main effect of target/distractor pictures.

TABLE 4 | Results of pre-and post-test outcomes of mood state in two groups using *t*-test.

			Mean (SD)		Mean change from pre-test (SD)		*t*-test within group *t*, *d*		Between-group *t*-test	Between-group *t*-test for mean change
			BMM	ERE	BMM	ERE	BMM	ERE	*t*, *d*	*t*, *d*
CES-D	DA	pre	6.77 (5.34)	5.70 (3.99)					0.81, 0.25	
		post	5.77 (5.25)	13.40 (4.47)	−1.00 (4.19)	7.76 (2.14)	1.12, 0.19	−15.80***, −1.78	−5.16***, −1.59	−8.58***, −2.65
	PE	pre	7.32 (2.92)	7.95 (1.96)					−0.96, −0.30	
		post	8.05 (2.89)	10.10 (3.08)	0.73 (2.37)	2.24 (2.49)	−1.44, −0.25	−3.82**, −0.79	−2.45*, −0.76	−2.04*, −0.63
	SC	pre	6.27 (3.60)	4.60 (2.04)					1.91, 0.59	
		post	5.41 (3.53)	10.15 (3.13)	−0.86 (3.17)	5.62 (2.13)	1.28, 0.24	−11.47***, −1.90	−4.74***, −1.46	−7.84***, −2.42
	IP	pre	1.36 (1.65)	0.75 (0.97)					1.57, 0.49	
		post	1.18 (1.37)	2.95 (1.32)	−0.18 (1.44)	2.19 (0.93)	0.59, 0.12	−10.34***, −1.81	−4.23***, −1.31	−6.40***, −1.98
	Total	pre	21.73 (8.10)	19.00 (4.90)					1.36, 0.42	
		post	20.41 (7.84)	36.60 (7.40)	−1.32 (6.47)	17.81 (4.49)	0.96, 0.17	−17.49***, −2.43	−7.09***, −2.19	−11.21***, −3.46
SAI	SAI	pre	46.05 (3.75)	47.20 (4.91)					−0.84, −0.26	
		post	47.82 (5.43)	44.55 (11.43)	1.77 (5.59)	−2.57 (11.73)	−1.49, −0.38	0.99, 0.30	1.22, 0.38	1.56, 0.48

*$0.01 < p < 0.05$, **$0.001 < p < 0.01$, ***$p < 0.001$.

scores that were significantly higher in the ERE group than in the BMM group. These differences reflected an increase in post-test CES-D scores in the ERE group (all $p < 0.05$) rather than a decrease in post-test CES-D scores in the BMM group (all $p > 0.05$). There was no significant difference in pre- vs. post-test scores within groups and no significant difference in SAI scores between groups. The results of a between-group *t*-test for mean changes between pre- vs. post-test scores showed that mean change in CES-D scores (four subscales and total scores) differed significantly between the ERE group and the BMM group. However, mean change in SAI was similar between groups.

Emotion Processing

The *t*-test was used to analyze the effects of BMM on emotion processing (**Table 5**). The results show that BMM training was effective in reducing emotional reaction intensity, in improving performance on tasks related to emotional memory, and in reducing attentional bias toward negative stimuli.

Emotion Intensity

The study groups did not differ at baseline in terms of emotion intensity (all $p > 0.05$). Positive and negative emotion intensity recognized by participants decreased significantly after intervention in the BMM group (positive: $t = 2.70$, $p = 0.013$, $d = 0.44$; negative: $t = 3.36$, $p = 0.003$, $d = 0.47$). Negative emotion intensity recognized by participants increased significantly after intervention in the ERE group ($t = -4.39$, $p < 0.001$, $d = -0.51$). After intervention, negative emotion intensity recognized by participants was significantly higher in the ERE group than in the BMM group ($t = -2.21$, $p = 0.033$, $d = -0.68$). Significant group differences in mean pre- vs. post-test change were observed for negative emotion intensity ($t = -5.50$, $p < 0.001$, $d = -1.70$).

Emotional Memory

Groups did not differ at baseline in terms of emotional memory or accuracy or emotional memory response time (all $p > 0.05$). There was no significant difference between pre- vs. post-test values or between groups in terms of the accuracy of emotional memory. However, response time was significantly affected by participation in the BMM program. In the BMM group, emotional memory response time was significantly faster in post-test, compared with pre-test (positive: $t = 4.58$, $p < 0.001$, $d = 0.86$; neutral: $t = 3.17$, $p = 0.005$, $d = 0.57$; negative: $t = 4.22$, $p < 0.001$, $d = 0.82$). In the ERE group, post-test values of negative emotional memory response time were significantly decreased, compared with pre-test values ($t = 3.33$, $p = 0.004$, $d = 0.73$). The between-group *t*-test revealed no significant change.

Emotional Attention Bias

In the attentional dot-probe task, no between-group difference in attentional bias was found for either pre-test or post-test

TABLE 5 | Results of pre-and post-test outcomes of emotion processing in two groups using *t*-test.

			Mean (SD)		Mean change from pre-test (SD)		*t*-test within group *t*, *d*		Between-group *t*-test	Between-group for *t*-test mean change
			BMM	ERE	BMM	ERE	BMM	ERE	*t*, *d*	*t*, *d*
Emotion intensity	Positive	pre	3.08 (0.80)	2.85 (0.72)					1.01, 0.31	
		post	2.75 (0.61)	2.76 (0.81)	−0.33 (0.57)	−0.08 (0.44)	2.70*, 0.44	0.84, 0.11	−0.04, −0.01	−1.55, −0.48
	Neural	pre	2.32 (0.66)	2.17 (0.51)					0.91, 0.28	
		post	2.10 (0.50)	2.15 (0.48)	−0.22 (0.64)	−0.01 (0.35)	1.62, 0.37	0.17, 0.03	−0.35, −0.11	−1.30, −0.40
	Negative	pre	3.88 (0.45)	3.72 (0.57)					1.08, 0.33	
		post	3.67 (0.44)	4.02 (0.57)	−0.21 (0.29)	0.29 (0.30)	3.36**, 0.47	−4.39***, −0.51	−2.21*, −0.68	−5.50***, −1.70
Emotional memory	Positive(R)	pre	0.93 (0.05)	0.86 (0.19)					1.73, 0.53	
		post	0.91 (0.05)	0.87 (0.20)	−0.02 (0.05)	0 (0.26)	1.90, 0.49	−0.08, −0.02	−0.19, −0.06	−0.47, −0.15
	Positive(T)	pre	0.85 (0.08)	0.86 (0.11)					1.22, 0.38	
		post	0.78 (0.09)	0.83 (0.12)	−0.07 (0.07)	−0.03 (0.11)	4.58***, 0.86	1.05, 0.22	−0.23, −0.07	−1.64, −0.51
	Neural(R)	pre	0.89 (0.08)	0.84 (0.18)					1.54, 0.48	
		post	0.89 (0.06)	0.83 (0.17)	0 (0.08)	−0.01 (0.23)	−0.28, −0.07	0.17, 0.05	−1.13, −0.35	0.25, 0.08
	Neutral(T)	pre	0.86 (0.08)	0.86 (0.12)					1.04, 0.32	
		post	0.80 (0.10)	0.82 (0.10)	−0.05 (0.07)	−0.04 (0.12)	3.17**, 0.57	1.53, 0.37	−1.62, −0.50	−0.31, −0.10
	Negative(R)	pre	0.93 (0.05)	0.86 (0.19)					1.64, 0.51	
		post	0.92 (0.04)	0.86 (0.20)	−0.01 (0.04)	−0.01 (0.26)	1.17, 0.22	0.09, 0.03	−0.54, −0.17	−0.08, −0.02
	Negative(T)	pre	0.88 (0.08)	0.91 (0.12)					1.38, 0.43	
		post	0.81 (0.09)	0.83 (0.09)	−0.07 (0.08)	−0.08 (0.10)	4.22***, 0.82	3.33**, 0.73	−0.97, −0.30	0.28, −0.09
Emotional attention bias	Positive	pre	−0.010 (0.016)	0 (0.018)					−2.01, −0.62	
		post	−0.004 (0.016)	−0.012 (0.025)	0.006 (0.024)	−0.011 (0.025)	−1.34, −0.39	2.07, 0.58	1.00, 0.31	2.41*, 0.74
	Negative	pre	0.010 (0.016)	0.003 (0.025)					1.17, 0.36	
		post	−0.010 (0.014)	0.003 (0.024)	−0.020 (0.024)	−0.006 (0.025)	3.93***, 1.32	1.15, 0.27	−1.34, −0.41	−1.89, −0.58

*$0.01 < p < 0.05$, **$0.001 < p < 0.01$, ***$p < 0.001$.

values (all $p > 0.05$). Significant treatment effects on attentional bias toward negative emotion were observed in the BMM group ($t = 3.93$, $p < 0.001$, $d = 1.32$). Before intervention, participants in the BMM group showed attentional bias, characterized by longer first-fixation duration when viewing negative facial expressions. However, in the post-test evaluation, participants in the BMM group did not show attentional bias toward negative emotion. The between-group *t*-test for mean change revealed significant differences between groups in attentional bias toward positive emotion ($t = 2.41$, $p = 0.021$, $d = 0.74$). After intervention, attentional bias toward positive emotion increased in the BMM group but decreased in the ERE group. Neither group showed attentional bias toward positive emotion.

DISCUSSION

This was a randomized controlled trial that aimed to compare BMM with ERE in terms of the effects on mood state and emotion processing. BMM significantly affected the intensity of positive and negative emotions, emotional memory, and negative emotional attention bias. Negative impact on mood state was found in the ERE group, but not the BMM group. The present study demonstrated that JW2016 BMM (15 min a day for 7 consecutive days) is effective in improving emotion processing.

Emotional intensity, emotional memory, and emotional attention bias improved in the participants in the BMM group. After intervention, emotional intensity toward negative stimuli decreased in the BMM group compared with the ERE group, which was consistent with the results of previous studies (Arch and Craske, 2006; Erisman and Roemer, 2011; Johns and Medicine, 2015). Emotional intensity toward positive stimuli also decreased after BMM, compared with ERE training; however, this trend was not significant. These results are consistent with those reported by Ren, who found that meditation training could create a peaceful state of mind, but inconsistent with those reported by most previous studies on the topic. Most previous studies on the topic have indicated that meditation practice has no effect on positive emotional responses (Sobolewski et al., 2011; Taylor et al., 2011). In the BMM group, emotional memory response time significantly decreased under all emotion conditions. These findings may indicate that memory improved after BMM. However, in the ERE group, only negative emotional memory response time decreased significantly. This results suggests that ERE training strengthened memories of negative information. In the attentional dot-probe task, a substantial change in negative emotional attention bias was observed in the BMM group. This finding is consistent with the results of previous studies (Garland and Howard, 2013) and may indicate that participants reduced attention to negative information after the intervention.

No significant change in symptoms related to depression and state anxiety was observed in the BMM group after intervention. There are several possible explanations for these findings. Firstly, BMM may have a limited capacity to improve mood. BMM does not utilize effective aspects of psychotherapy, such as the therapeutic alliance, which are known to contribute to the therapeutic effect (Leuchter et al., 2014). The therapeutic alliance could be incorporated into BMM practice. Secondly, the duration of intervention may not have been long enough. In previous studies, emotional symptoms were alleviated after meditation training 25–30 min per day over 3–5 days (Chen et al., 2013; Creswell et al., 2014). If the daily practice time were to be shortened, the number of days required for practice would increase considerably (Berghoff et al., 2017). For example, stress declined after 2 weeks' participation in a 10-min daily meditation training session, whereas the increase in self-compassion in this group was significantly less than the increase observed in the group that practiced meditation for 20 min daily (Berghoff et al., 2017). Thirdly, the participants in this study were healthy students without obvious symptoms of depression or anxiety. Meditation training was more effective in improving mood state in patients with affective disorders such as major depression and anxiety (Goyal et al., 2014; Fan et al., 2015; Jain et al., 2015). Ceiling effects may partly explain the limited improvement in mood state among healthy people. More research is needed to verify the hypothesis presented above.

In addition, we found that BMM training had no negative effect on participants' emotional processing or mood. BMM may not only contribute to a peaceful state of mind but also improve cognitive functions such as emotional memory and attention. However, in the ERE group, depression and emotional intensity in response to negative stimuli increased after intervention. These results imply that ERE training could exacerbate the negative emotional experiences of participants. Training may increase emotional awareness and reflection. It may have been difficult for participants to learn to adjust their emotions over such a short period of time without one-on-one coaching. Educators should therefore pay more attention to the mood status of participants during ERE training and provide more emotional guidance during the early stages of ERE.

The mechanism by which BMM improves emotional processing may be complicated. From the neuroendocrine perspective, one of the paths linking brief meditation to emotional improvement may be the hypothalamus–pituitary–adrenal (HPA) axis. Numerous studies have found that meditation [a 4-day mindfulness meditation (Turakitwanakan et al., 2013) or 48 hr of Integrated Amrita Meditation (Vandana et al., 2011)] may decrease the stress response and levels of cortisol (the end-product of the HPA axis). Emotional regulation may predict the symptomatic stress response and the recovery of salivary cortisol (Krkovic et al., 2018). In healthy individuals, the adaptive emotion regulation strategy was associated with greater cortisol recovery after exposure to a stressor (Lewis et al., 2017). This finding suggests that adaptive emotional regulation predicts improved HPA regulation. Our unpublished research also verified that BMM may lower salivary cortisol levels in college students with high suicide risk. In terms of the neuroendocrine mechanism, meditation may improve emotion processing by improving regulation of the HPA axis. In addition, Carlson et al. (2004) found that 8-week MBSR could increase plasma dehydroepian-drosterone sulfate (DHEAS), which is the major secretary product of the human adrenal and acts as a buffer against stress-related hormones. From a neurobiological perspective, the findings presented above suggest that meditation may influence the function and structure of the brain. For example, participation in an 8-week MBSR course may reduce the response of the right amygdala to emotional stimuli (Desbordes et al., 2012) and increase the density of regional gray matter in the brain (Holzel et al., 2011). Some neurochemical studies have shown that long-term meditation may regulate the neurotransmitters closely related to emotion processing, such as dopamine (Jung et al., 2010) and serotonin (Solberg et al., 2004). However, there is currently no evidence that briefer meditation sessions have the same effects. More studies are needed to verify whether brief meditation sessions achieve the same effect.

The present study has some limitations. Firstly, we failed to include a blank control manipulation, such as a waiting list group. Current evidence suggests that emotion processing is a relatively stable condition that is unlikely to be improved naturalistically, while mood state is more susceptible to interference (Etkin et al., 2011; Rock et al., 2016). Secondly, the interventions were single-blind in design; the same counselor delivered the curriculum to participants in each of the two conditions, and knew the purpose of the experiment. Though the leader conducted the intervention via audio instructions without one-on-one guidance, it may still be difficult to avoid unintentionally more enthusiastic or thoughtful intervention in the BMM group. Thirdly, the 1-week duration of the meditation program used for this study may not have been sufficient to achieve the maximum improvement possible. Future studies could prolong the training time and test the effects of meditation at different time points. Fourthly, small sample size was another drawback of this study. A *post hoc* power analysis was conducted with G*Power 3.1. All statistical decisions were made using an alpha level of 0.05. Based on the sample size of this study, the power to demonstrate significant differences in post-intervention emotion processing ranged from 0.74 to 0.99 in both groups. Except for the powers of three indicators (positive emotion intensity after BMM, 0.74; negative emotion intensity after BMM, 0.87; neutral emotion memory, 0.89), the powers of other indicators were >0.95. Fifthly, there were too few males in the sample, which limited the power of the sex difference and made the results more applicable to females. Last but not the least, although this study discussed the mechanism of the effect of BMM through inference, physiological indicators such as hormones were not measured, which limited our exploration of the mechanism underlying the effects of intervention.

CONCLUSION

This study demonstrated that JW2016 BMM (15 min a day for 7 consecutive days) was able to improve emotion processing including emotion intensity, emotional memory, and emotional attention bias, without any negative effect on the

emotions of healthy practitioners. This BMM method may be applied to the emotional self-care of healthy people and/or the emotional rehabilitation of patients with affective disorders. It could be an effective, convenient, safe, and standardized way to improve emotion processing and to remain focused and peaceful. If JW2016 BMM could help healthy people to improve their emotion processing, it may also benefit a broader population. More empirical studies will be needed to verify the effects of BMM. We will also work on popularizing BMM to benefit more people.

DATA AVAILABILITY STATEMENT

The data used to support the findings of this study are available from the corresponding author upon request.

ETHICS STATEMENT

The studies involving human participants were reviewed and approved by Committee on Ethics of Biomedicine Research, The Second Military Medical University. The patients/participants provided their written informed consent to participate in this study.

AUTHOR CONTRIBUTIONS

RW and C-LJ were responsible for the development of this particular study. RW wrote the first draft. RW and L-LL participated in the study design and performed the data analyses. C-LJ, RW, and X-HL designed the meditation method. RW, L-LL, and HZ were the principal researchers for the tests and interventions. W-JS, Z-YC, and S-YZ were responsible for conception of the project, questionnaire design, and manuscript review. All authors read and approved the final manuscript.

FUNDING

This work was supported by the Military Medical Research Project (BWS17J027 and AHJ16J001) and the Shanghai Philosophy and Social Science Project (Youth Project in Education) (B1901).

ACKNOWLEDGMENTS

We thank Meng-Yang Wu, M.A., for refining the language in the manuscript.

REFERENCES

Arch, J. J., and Craske, M. G. (2006). Mechanisms of mindfulness: emotion regulation following a focused breathing induction. *Behav. Res. Ther.* 44, 1849–1858. doi: 10.1016/j.brat.2005.12.007

Berghoff, C. R., Wheeless, L. E., Ritzert, T. R., Wooley, C. M., and Forsyth, J. P. (2017). Mindfulness meditation adherence in a college sample: comparison of a 10-min versus 20-min 2-week daily practice. *Mindfulness* 8, 1513–1521. doi: 10.1007/s12671-017-0717-y

Bishop, S. R., Lau, M., Shapiro, S., Carlson, L., Anderson, N. D., Carmody, J., et al. (2004). Mindfulness: a proposed operational definition. *Clin. Psychol. Sci. Pract.* 11, 230–241. doi: 10.1093/clipsy/bph077

Carlson, L. E., Speca, M., Patel, K. D., and Goodey, E. (2004). Mindfulness-based stress reduction in relation to quality of life, mood, symptoms of stress and levels of cortisol, dehydroepiandrosterone sulfate (DHEAS) and melatonin in breast and prostate cancer outpatients. *Psychoneuroendocrinology* 29, 448–474. doi: 10.1016/s0306-4530(03)00054-4

Cebolla, A., Demarzo, M., Martins, P., Soler, J., and Garcia-Campayo, J. (2017). Unwanted effects: is there a negative side of meditation? A multicentre survey. *PLoS One* 12: e0183137. doi: 10.1371/journal.pone.0183137

Center for the Study of Emotion and Attention [CSEA-NIMH], (1999). *The International Affective Picture System Digitized Photographs*. Gainesville, FL: Center for the Study of Emotion and Attention.

Chavan, D. V. (2007). Vipassana: the Buddha's tool to probe mind and body. *Prog. Brain Res.* 168, 247–253. doi: 10.1016/S0079-6123(07)68019-4

Chen, Y., Yang, X., Wang, L., and Zhang, X. (2013). A randomized controlled trial of the effects of brief mindfulness meditation on anxiety symptoms and systolic blood pressure in Chinese nursing students. *Nurse Educ. Today* 33, 1166–1172. doi: 10.1016/j.nedt.2012.11.014

Collins, K. R. L., Stebbing, C., Stritzke, W. G. K., and Page, A. C. (2017). A brief mindfulness intervention attenuates desire to escape following experimental induction of the interpersonal adversity implicated in suicide risk. *Mindfulness* 8, 1096–1105. doi: 10.1007/s12671-017-0686-1

Creswell, J. D., Pacilio, L. E., Lindsay, E. K., and Warren, K. (2014). Brief mindfulness meditation training alters psychological and neuroendocrine responses to social evaluative stress. *Psychoneuroendocrinology* 44, 1–12. doi: 10.1016/j.psyneuen.2014.02.007

Desbordes, G., Negi, L. T., Thaddeus, W. W., Pace, B., Wallace, A., Raison, C. L., et al. (2012). Effects of mindful-attention and compassion meditation training on amygdala response to emotional stimuli in an ordinary non meditative state. *Front. Hum. Neur.* 6:292. doi: 10.3389/fnhum.2012.00292

Erisman, S. M., and Roemer, L. (2011). A preliminary investigation of the effects of experimentally- induced mindfulness on emotional responding to film clips. *Emotion* 10, 72–82. doi: 10.1037/a0017162.A

Etkin, A., Egner, T., and Kalisch, A. R. (2011). Emotional processing in anterior cingulate and medial prefrontal cortex. *Trends Cogn. Sci.* 15, 85–93. doi: 10.1016/j.tics.2010.11.004

Fan, L., Wang, X., and Jiang, T. (2015). The effect of body-mind relaxation meditation induction on major depressive disorder : a resting-state FMRI study. *J. Affect. Disord.* 183, 75–82. doi: 10.1016/j.jad.2015.04.030

Garland, E. L., and Howard, M. O. (2013). Mindfulness-oriented recovery enhancement reduces pain attentional bias in chronic pain patients. *Psychother. Psychosom.* 82, 311–318. doi: 10.1159/000348868

Gong, X., Huang, Y. X., Wang, Y., and Luo, Y. J. (2011). Revision of the Chinese facial affective picture system. *Chin. Ment. Health J.* 25, 40–46.

Goyal, M., Singh, S., Sibinga, E., Gould, N., Rowland-Seymour, A., Sharma, R., et al. (2014). Meditation programs for psychological stress and well-being : a systematic review and meta-analysis. *JAMA Intern. Med.* 174, 357–368. doi: 10.1001/jamainternmed.2013.13018

Groch, S., Wilhelm, I., Diekelmann, S., Sayk, F., Gais, S., and Born, J. (2011). Contribution of norepinephrine to emotional memory consolidation during sleep. *Psychoneuroendocrinology* 36, 1342–1350. doi: 10.1016/j.psyneuen.2011.03.006

Gross, J. J. (1998). Gross, J. J. The emerging field of emotion regulation: an integrative review. *Rev. Gen. Psychol.* 2, 271–299. doi: 10.1037//1089-2680.2.3.271

Hoge, E. A., Bui, E., Marques, L., Metcalf, C. A., Morris, L. K., Robinaugh, D. J., et al. (2014). Randomized controlled trial of mindfulness meditation for generalized anxiety disorder: effects on anxiety and stress reactivity. *J. Clin. Psychiatry* 74, 786–792. doi: 10.4088/JCP.12m08083

Holzel, B. K., Carmody, J., Vangel, M., Congleton, C., Yerramsetti, S. M., Gard, T., et al. (2011). Mindfulness practice leads to increases in regional brain gray matter density. *Psychiatry. Res.* 191, 36–43. doi: 10.1016/j.pscychresns.2010.08.006

Jain, F. A., Walsh, R. N., Eisendrath, S. J., Christensen, S., and Rael Cahn, B. (2015). Critical analysis of the efficacy of meditation therapies for acute and subacute phase treatment of depressive disorders: a systematic review. *Psychosomatics* 56, 140–152. doi: 10.1016/j.psym.2014.10.007

Jha, A. P., Jason, K., and Baime, M. J. (2007). Mindfulness training modifies subsystems of attention. *Cogn. Affect. Behav. Neurosci.* 7, 109–119. doi: 10.3758/cabn.7.2.109

Johns, M., and Medicine, H. (2015). Intensive meditation training influences emotional responses to suffering. *Emotion* 15, 775–793. doi: 10.1037/emo0000080

Jung, Y. H., Kang, D. H., Jang, J. H., Park, H. Y., Byun, M. S., Kwon, S. J., et al. (2010). The effects of mind body training on stress reduction, positive affect, and plasma catecholamines. *Neurosci. Lett.* 479, 138–142. doi: 10.1016/j.neulet.2010.05.048

Kabatzinn, J., Massion, A. O., Kristeller, J., Peterson, L. G., Fletcher, K. E., Pbert, L., et al. (1992). Effectiveness of a meditation-based stress reduction program in the treatment of anxiety disorders. *Am. J. Psychiatry* 149, 936–943. doi: 10.1176/ajp.149.7.936

Khusid, M. A., and Vythilingam, M. (2016). The emerging role of mindfulness meditation as effective self-management strategy, part 1: clinical implications for depression, post-traumatic stress disorder, and anxiety. *Mil. Med.* 181, 961–968. doi: 10.7205/MILMED-D-14-00677

Krkovic, K., Clamor, A., and Lincoln, T. M. (2018). Emotion regulation as a predictor of the endocrine, autonomic, affective, and symptomatic stress response and recovery. *Psychoneuroendocrinology* 94, 112–120. doi: 10.1016/j.psyneuen.2018.04.028

Krygier, J. R., Heathers, J. A., Shahrestani, S., Abbott, M., Gross, J. J., and Kemp, A. H. (2013). Mindfulness meditation, well-being, and heart rate variability: a preliminary investigation into the impact of intensive Vipassana meditation. *Int. J. Psychophysiol.* 89, 305–313. doi: 10.1016/j.ijpsycho.2013.06.017

Lane, J. D., Seskevich, J. E., and Pieper, C. F. (2007). Brief meditation training can improve perceived stress and negative mood. *Altern. Ther.* 13, 38–44. doi: 10.1378/chest.10-1160

Leuchter, A. F., Hunter, A. M., Tartter, M., and Cook, I. A. (2014). Role of pill-taking, expectation and therapeutic alliance in the placebo response in clinical trials for major depression. *Br. J. Psychiatry J. Ment. Sci.* 205, 443–449. doi: 10.1192/bjp.bp.113.140343

Lewis, E. J., Yoon, K. L., and Joormann, J. (2017). Emotion regulation and biological stress responding: associations with worry, rumination, and reappraisal. *Cogn. Emot.* 11, 1–12. doi: 10.1080/02699931.2017.1310088

Li, Z., and Hicks, M. H. (2010). The CES-D in Chinese American women: construct validity, diagnostic validity for major depression, and cultural response bias. *Psychiatry Res.* 175, 227–232. doi: 10.1016/j.psychres.2009.03.007

Lutz, A., Slagter, H. A., Dunne, J. D., and Davidson, R. J. (2008). Attention regulation and monitoring in meditation. *Trends Cogn. Sci.* 12, 163–169. doi: 10.1016/j.tics.2008.01.005

Ochsner, K. N., and Gross, J. J. (2005). The cognitive control of emotion. *Trends Cogn. Sci.* 9, 242–249. doi: 10.1016/j.tics.2005.03.010

Pace, T. W. W., Negi, L. T., Adame, D. D., Cole, S. P., Sivilli, T. I., Brown, T. D., et al. (2009). Effect of compassion meditation on neuroendocrine, innate immune and behavioral responses to psychosocial stress. *Psychoneuroendocrinology* 34, 87–98. doi: 10.1016/j.psyneuen.2008.08.011

Pinniger, R., Brown, R. F., Thorsteinsson, E. B., and Mckinley, P. (2012). Argentine tango dance compared to mindfulness meditation and a waiting-list control: a randomised trial for treating depression. *Complement. Ther. Med.* 20, 377–384. doi: 10.1016/j.ctim.2012.07.003

Radloff, L. S. (1977). The CES-D scale: a self-report depression scale for research in the general population. *Appl. Psychol. Meas.* 1, 385–401. doi: 10.1177/014662167700100306

Radloff, L. S. (1991). The use of the Center for Epidemiologic Studies Depression Scale in adolescents and young adults. *J. Youth Adolesc.* 20, 149–166. doi: 10.1007/BF01537606

Ren, J., Huang, L., and Zhang, Z. X. (2012). Meditation makes a peaceful state of mind: people's positive and negative emotional response can be reduced by meditation training. *Acta Psychol. Sin.* 30, 627–646.

Rock, P., Goodwin, G., Wulff, K., McTavish, S., and Harmer, C. (2016). Effects of short-term quetiapine treatment on emotional processing, sleep and circadian rhythms. *J. Psychopharmacol.* 30, 273–282. doi: 10.1177/0269881115626336

Schumer, M. C., Lindsay, E. K., and David Creswell, J. (2018). Brief mindfulness training for negative affectivity: a systematic review and meta-analysis. *J. Consult. Clin. Psychol.* 86, 569–583. doi: 10.1037/ccp0000324

Sobolewski, A., Holt, E., Kublik, E., and Wróbel, A. (2011). Impact of meditation on emotional processing-A visual ERP study. *Neurosci. Res.* 71, 44–48. doi: 10.1016/j.neures.2011.06.002

Solberg, E. E., Holen, A., Ekeberg, Ø., Østerud, B., Halvorsen, R., and Sandvik, L. (2004). The effects of long meditation on plasma melatonin and blood serotonin. *Med. Sci. Monit.* 10, 96–101.

Spielberger, C. D. (1983). *State-Trait Anxiety Inventory (Form Y)*. Palo Alto, CA: Mind Garden, 19.

Tang, Y., Ma, Y., Fan, Y., Feng, H., Wang, J., Feng, S., et al. (2009). Central and autonomic nervous system interaction is altered by short-term meditation. *Proc. Natl. Acad. Sci. U.S.A.* 106, 8865–8870. doi: 10.1073/pnas.0904031106

Taylor, V. A., Grant, J., Daneault, V., Scavone, G., Breton, E., Roffe-vidal, S., et al. (2011). NeuroImage Impact of mindfulness on the neural responses to emotional pictures in experienced and beginner meditators. *Neuroimage* 57, 1524–1533. doi: 10.1016/j.neuroimage.2011.06.001

Tsotsos, J. K., Culhane, S. M., Kei Wai, W. Y., Lai, Y., Davis, N., and Nuflo, F. (1995). Modeling visual attention via selective tuning. *Artif. Intell.* 78, 507–545. doi: 10.1016/0004-3702(95)00025-9

Turakitwanakan, W., Mekseepralard, C., and Busarakumtragul, P. (2013). Effects of mindfulness meditation on serum cortisol of medical students. *J. Med. Assoc. Thai.* 96(Suppl.), 90–95.

Vago, D. R., and Nakamura, Y. (2011). Selective attentional bias towards pain-related threat in fibromyalgia: preliminary evidence for effects of mindfulness meditation training. *Cogn. Ther. Res.* 35, 581–594. doi: 10.1007/s10608-011-9391-x

Vandana, B., Vaidyanathan, K., Saraswathy, L. A., Sundaram, K. R., and Kumar, H. (2011). Impact of integrated amrita meditation technique on adrenaline and cortisol levels in healthy volunteers. *Evid. Based Complement. Alternat. Med.* 2011, 1–6. doi: 10.1155/2011/379645

Vasquez-Rosati, A., Brunetti, E. P., Cordero, C., and Maldonado, P. E. (2017). Pupillary response to negative emotional stimuli is differentially affected in meditation practitioners. *Front. Hum. Neurosci.* 11:209. doi: 10.3389/fnhum.2017.00209

Wenksormaz, H. (2005). Meditation can reduce habitual responding. *Altern. Ther. Heal. Med.* 11, 42–58.

Yan, Y., Lin, R., Tang, X., He, F., Cai, W., and Su, Y. (2014). The relationship between worry tendency and sleep quality in Chinese adolescents and young adults: the mediating role of state-trait anxiety. *J. Health Psychol.* 19, 778–788. doi: 10.1177/1359105313479628

Yen, S., Robins, C. J., and Lin, N. (2000). A cross-cultural comparison of depressive symptom manifestation: China and the United States. *J. Consult. Clin. Psychol.* 68, 993–999. doi: 10.1037//0022-006X.68.6.993

Zeidan, F., Gordon, N. S., Merchant, J., and Goolkasian, P. (2010a). The effects of brief mindfulness meditation training on experimentally induced pain. *J. Pain* 11, 199–209. doi: 10.1016/j.jpain.2009.07.015

Zeidan, F., Johnson, S. K., Diamond, B. J., David, Z., and Goolkasian, P. (2010b). Mindfulness meditation improves cognition: evidence of brief mental training. *Conscious. Cogn.* 19, 597–605. doi: 10.1016/j.concog.2010.03.014

Zeidan, F., Johnson, S. K., Gordon, N. S., and Goolkasian, P. (2010c). Effects of brief and sham mindfulness meditation on mood and cardiovascular variables. *J. Altern. Complement. Med.* 16, 867–873. doi: 10.1089/acm.2009.0321

Zeidan, F., Martucci, K. T., Kraft, R. A., Gordon, N. S., Mchaffie, J. G., and Coghill, R. C. (2011). Brain mechanisms supporting modulation of pain by mindfulness meditation. *J. Neurosci. Off. J. Soc. Neurosci.* 31, 5540–5548. doi: 10.1523/jneurosci.5791-10.2011

Conflict of Interest: The authors declare that the research was conducted in the absence of any commercial or financial relationships that could be construed as a potential conflict of interest.

frontiers in Neuroscience

ORIGINAL RESEARCH
published: 22 October 2019
doi: 10.3389/fnins.2019.01134

Alterations in Cortical Thickness in Young Male Patients With Childhood-Onset Adult Growth Hormone Deficiency: A Morphometric MRI Study

Hongbo Yang[1†], Kang Li[1†], Xinyu Liang[2], Bin Gu[2], Linjie Wang[1], Gaolang Gong[2], Feng Feng[3], Hui You[3], Bo Hou[3], Fengying Gong[1], Huijuan Zhu[1] and Hui Pan[1]**

[1] Department of Endocrinology, Key Laboratory of Endocrinology of National Health Commission, The Translational Medicine Center of PUMCH, Peking Union Medical College Hospital, Chinese Academy of Medical Sciences & Peking Union Medical College, Beijing, China, [2] State Key Laboratory of Cognitive Neuroscience and Learning & IDG/McGovern Institute for Brain Research, Beijing Normal University, Beijing, China, [3] Department of Radiology, Peking Union Medical College Hospital, Chinese Academy of Medical Sciences & Peking Union Medical College, Beijing, China

Background: The growth hormone (GH)/insulin-like growth factor-1 (IGF-1) axis plays an important role in brain structure and maintenance of brain function. There is a close correlation between serum GH and IGF1 levels and age-related cognitive function. The effects of childhood-onset growth hormone deficiency (GHD)on brain morphology are underestimated so far.

Methods: In this cross-sectional study, T1-weighted magnetic resonance imaging was assessed in 17 adult males with childhood-onset GHD and 17 age and gender-matched healthy controls. The cortical thickness was analyzed and compared between the two groups of subjects. Effects of disease status and hormone levels on cortical thickness were also evaluated.

Results: Although there was no difference in whole brain volume or gray matter volume between the two groups, there was decreased cortical thickness in the parahippocampal gyrus, posterior cingulate gyrus and occipital visual syncortex in the adult growth hormone deficiency (AGHD) group, and increased cortical thickness in a partial area of the frontal lobe, parietal lobe and occipital visual syncortex in AGHD group. Cortical thickness of the posterior cingulum gyrus was prominently associated with FT3 serum levels only in control group after adjusting of IGF-1 levels.

Conclusion: These results suggest that young adult male patients with childhood-onset GHD have alterations in cortical thickness in different brain lobes/regions.

Keywords: childhood-onset adult growth hormone deficiency, cortical thickness, structure MRI, growth hormone, insulin-like growth factor 1

OPEN ACCESS

Edited by:
Keith Maurice Kendrick, University of Electronic Science and Technology of China, China

Reviewed by:
Shu Zhang, Stony Brook University, United States
Rong Zhang, Peking University, China

***Correspondence:**
Huijuan Zhu
shengxin2004@163.com
Hui Pan
panhui2011111@163.com

[†]These authors have contributed equally to this work

Specialty section:
This article was submitted to Neuroendocrine Science, a section of the journal Frontiers in Neuroscience

Received: *08 May 2019*
Accepted: *08 October 2019*
Published: *22 October 2019*

Citation:
Yang H, Li K, Liang X, Gu B, Wang L, Gong G, Feng F, You H, Hou B, Gong F, Zhu H and Pan H (2019) Alterations in Cortical Thickness in Young Male Patients With Childhood-Onset Adult Growth Hormone Deficiency: A Morphometric MRI Study. Front. Neurosci. 13:1134. doi: 10.3389/fnins.2019.01134

INTRODUCTION

Adult growth hormone deficiency (AGHD) is a debilitating condition that occurs due to insufficient secretion of GH from the pituitary gland. AGHD is caused by hereditary defects of GH synthesis and secretion or resulted from tumor, head injury, and head radiation or pituitary surgery. Besides metabolic disorders, osteoporosis, sarcopenia and decreased quality of life, impaired cognitive function is one of the important characteristics of AGHD (Molitch et al., 2011; Uzunova et al., 2015). AGHD can be divided into childhood-onset and adulthood-onset, according to the age of onset. Most cases of isolated growth hormone deficiency (GHD) in childhood are idiopathic and transient, while in patients with multiple pituitary hormone deficiency (MPHD), GHD generally persists into adulthood (Berberoğlu et al., 2008; Yang et al., 2017).

Brain morphology and function could be influenced during early stages of development in the uterus and can dynamically change during adulthood (Buchanan et al., 1992). GH is a peptide synthesized by the anterior pituitary that stimulates insulin-like growth factor-1 (IGF-1) secretion from the liver. GH receptor and IGF1 receptor have been localized in brain regions important in cognitive functioning, including the hippocampus, amygdala and parahippocampal areas (Adem et al., 1989). The GH/IGF1-axis plays an essential role during early brain development and persists in several brain regions with continuous renewal and remodeling during adulthood (Wrigley et al., 2017). In neural stem cells, IGF-1 is a controlling switch for long-term proliferation (Supeno et al., 2013). A higher serum IGF-1 level is associated with better working memory and mental processing speed in healthy subjects (Aleman et al., 1999). Morphologically, higher serum IGF-1 levels are associated with significantly increased cerebral blood flow in the left dorsolateral prefrontal cortex and left premotor cortex (Arwert et al., 2005).

Despite the role of the GH/IGF-1 axis in normal brain development and function, the effects of GHD on brain structure are not fully understood thus far. It was reported that reduced thalamic and globus pallidum volumes were related to deficits in cognitive function and motor performance in children with isolated GHD (Webb et al., 2012). In patients with MPHD, GHD is usually permanent and recombinant human GH (rhGH) replacement is usually stopped after completion of linear growth. Higher incidence of mental disorders and increased prevalence of cognitive dysfunction were reported in hypopituitary women with GH deficiency (Bülow et al., 2002). There were also several studies to evaluate the effects of GH replacement therapy in cognitive function improvement in AGHD patients. But interpretation of data is complicated by participants selection as well as neuropsychological tests used in these studies (van Dam, 2005). Morphological variations in the brains of patients with childhood-onset AGHD after cessation of rhGH treatment have received little research attention to date.

Recently, voxel-based statistical analysis based on an ^{18}F-FDG PET study found that adult patients with GHD due to traumatic brain injury had decreased cerebral glucose metabolism in cortical areas involved in intellectual function, executive function and working memory (Park et al., 2016). No direct assessment of cortical thickness of AGHD patients has been reported so far. Cortical thickness provides direct and reliable information about the density, size and arrangement of cortical cells, thus yielding insights into the regional integrity of the cerebral cortex. One of the main challenges in evaluation of brain structure variations in patients with AGHD is the lack of homogeneity in etiology, course of disease and variation of hormone replacement therapy. In this cross-sectional study, cortical thickness of adult males with childhood-onset AGHD due to pituitary hypoplasia or pituitary stalk interruption was compared to age- and gender-matched healthy controls. The effects of disease status and hormone levels on cortical thickness were also evaluated.

SUBJECTS AND METHODS

Participants

In this cross-sectional study, a total of 17 consecutive male patients with childhood-onset AGHD were enrolled from January 2011 to March 2013 in Peking Union Medical College Hospital (Wilson, 1993). Inclusion criteria included: (1) all patients fulfilled the diagnosis criteria of AGHD according to the clinical guideline of the American Endocrine Society (Molitch et al., 2011). Twelve patients underwent insulin tolerance test and peak value of GH was lower than 3 ng/ml. The diagnosis was confirmed in the other five patients with IGF-1 levels below the age-adjusted normal range and deficiencies in three or more pituitary axes at the same time., (2) linear growth was finished and bone age $\geq$18 years, (3) rhGH had been stopped at least one year after final height, (4) prednisone, L-thyroxine and testosterone replacement therapy were sustained as needed at least one year before enrollment, and (5) right handedness and with no contraindication to MRI. A total of 17 healthy age-matched male subjects were enrolled as controls. All controls were right-handed and education-matched. Medical history of major neurological or psychiatric disorders was documented in neither the AGHD group nor the control group. The study protocol was approved by the Ethics Committees of Peking Union Medical College Hospital. Written informed consent was obtained from all subjects and all data were de-identified before analysis.

Clinical Assessment

Main demographic data were obtained from medical charts. Weight and height were measured in the early morning. Body mass index (BMI) was calculated as weight (kg) divided by height (m) squared. Questionnaires about education levels were assessed. Blood samples were also obtained in early morning. Serum levels of IGF1, free thyroxine (FT4) free triiodothyronine (FT3), thyrotropin (TSH), total testosterone and fasting blood glucose were tested in the department of the clinical laboratory using standard protocols (Zhu et al., 2017).

MRI Image Acquisition

Imaging was performed on a 3 T MR scanner (General Electric Medical Systems, GE sign VH/I Excite I 3.0 T). Lying in supine position, participants fixed their heads using

foam padding to avoid head movement. A scout for anterior commissure-posterior alignment was done first, then sagittal three-dimensional (3D) volumetric T1-weighted magnetization-prepared rapid acquisition gradient echo (MPRAGE) images were obtained (128 sagittal slices, repetition time (TR) = 2530 ms, echo time (TE) = 3.39 ms, inversion time (TI) = 1100 ms, slice thickness = 1.33 mm, field of view (FOV) = 256 × 256 mm^2, voxel size = 1.33 × 1.00 × 1.00 mm^3).

Image Processing

Cortical thickness was extracted from the structural MR T1 images by using a routine pipeline of the CIVET software (version 1.1.9; Montreal Neurological Institute at McGill University, Canada). A flowchart for cortical thickness assessment was described previously (Liu et al., 2014). In brief, the original images were linear registered to stereotaxic space using the average NMI-ICBM152 model, for obtaining better segmentation following (Collins et al., 1994). Then the non-uniformity artifacts of images were corrected by the Non-parametric Non-uniform intensity Normalization (N3) algorithm (Sled et al., 1998), which was shown to be accurate and robust (Sled et al., 1998). By using an advanced neural classifier, the registered and corrected images were then segmented into white matter (WM), grey matter (GM), cerebrospinal fluid (CSF) and background (Zijdenbos et al., 2002; Jussi et al., 2004). The inner and outer GM surfaces were extracted from each hemisphere by using the constrained Laplacian-based automated segmentation with proximities (CLASP) algorithm (MacDonald et al., 2000; Kim et al., 2005). Specifically, the inner surface was reconstructed by deforming a spherical polygon model to the WM/GM boundary with a total of 81,924 vertices (40,962 of each hemisphere). The outer surface was then initiated from the inner surface and was expanded to the GM/CSF fluid boundary along the Laplacian field generated from a skeletonized CSF fraction image (Cherng-Min and Shu-Yen, 2001; Cherng-Min et al., 2002). Cortical thickness was defined as the Euclidean distance between linked vertices on the inner and outer surfaces (Lerch and Evans, 2005). For each subject, we visually evaluated the results of segmentation and reconstruction using the recommended method, and ensured that no error and failure was appeared. Finally, a 20-mm 2-D smoothing was applied on cortical thickness map for less noise and better sensitivity in statistics analysis.

Statistical Analysis

Numerical data are expressed as the mean ± standard deviation, and *t*-tests were used to compare data between two groups. A general linear model (GLM) was used for thickness modeling at each surface vertex as a linear combination of effects related to variables of interests and effects of potential confounds (years of education, age and BMI). The main effect of groups and the interaction between groups and hormone levels were tested. As described previously, a random field theory (RFT)-based method was used at the cluster level for all cortical analysis in order to correct for multiple comparisons. Cortical clusters with an FWE-corrected $p < 0.05$ were considered significant. After the interaction analyses, we performed the *post hoc* tests for the significant clusters. We used the Pearson's correlations (r) to quantify the relationship between hormone levels and averaged cortical thickness of clusters within each group. All statistical analyses were carried out using the SurfStat toolbox[1] in MATLAB (Yaojing et al., 2015).

RESULTS

Demographic, Clinical and Biochemical Characteristics

Demographic and clinical characteristics are listed in **Table 1**. Nine of AGHD patients (9/17) were born with breech or foot presentation. MRI revealed pituitary hypoplasia or pituitary stalk interruption in all these patients. All patients had MPHD. All patients had MPHD and sustained glucocorticoid and levothyroxine replacement since childhood. Testosterone replacement was started at 18 years old and after completion of linear growth in all patients. AGHD group had received 32.5 ± 3.5 months of replacement therapy with rhGH and stopped after completion of linear growth.

There was no difference in chronological age (25.0 ± 3.6 vs. 24.0 ± 3.9 years, $p = 0.87$) or school-education years between AGHD group and the control group. The AGHD group had a 9.5 cm lag in final height (163.5 ± 6.7 vs. 173.0 ± 5.1 cm, $p < 0.001$) and lower body weight (62.1 ± 10.3 vs. 71.5 ± 8.2 kg, $p = 0.006$) compared with the control group. BMI was similar between the two groups. AGHD group presented with a significant decrease in IGF1 levels at the time of the study (49.1 ± 26.1 vs. 234.0 ± 88.1 ng/ml, $p < 0.001$). With monthly intramuscular injections of testosterone undecanoate, serum levels of the AGHD group were similar to that of the control group ($p = 0.75$). With daily replacement with levothyroxine, serum levels of FT4 and FT3 in the AGHD group were in the lower quartile of the normal range, but were significantly lower than controls ($p < 0.001$).

[1]http://www.math.mcgill.ca/keith/surfstat/

TABLE 1 | General baseline data and distribution of all subjects.

	AGHD group (*n* = 17)	Controls (*n* = 17)	*p*
Age (years)	25.0 ± 4.6	24.0 ± 3.9	0.87
Height (cm)	163.5 ± 6.7	173.0 ± 5.1	< 0.001
Weight (kg)	62.1 ± 10.3	71.5 ± 8.2	0.006
BMI (kg/m^2)	23.2 ± 3.3	23.9 ± 2.8	0.47
Education duration (years)	11.4 ± 3.2	12.1 ± 3.0	0.55
Fasting blood glucose (mmol/L)	5.0 ± 0.5	5.1 ± 0.4	0.65
IGF-1 (ng/ml)	49.1 ± 26.1	234.0 ± 88.1	< 0.001
IGF-1 SDS	−5.04 ± 1.60	−0.35 ± 1.17	< 0.001
FT3 (pg/ml)	2.8 ± 0.7	3.7 ± 0.3	< 0.001
FT4 (ng/dl)	0.9 ± 0.4	1.0 ± 0.2	< 0.001
TSH (μIU/ml)	1.4 ± 1.2	1.9 ± 0.8	0.18
Testosterone (ng/dl)	462.9 ± 161.3	478.0 ± 121.4	0.75

TABLE 2 | Comparison of whole brain volume and gray matter between study groups.

	AGHD group (n = 17)	Control group (n = 17)	p
Whole brain volume (mm^3)	1526.54 ± 134.38	1464.61 ± 141.50	0.20
Gray matter volume (mm^3)	697.69 ± 59.09	661.08 ± 59.09	0.08

Alterations of Brain Volumes

As shown in **Table 2**, there was no difference in whole brain volume (p = 0.20) or gray matter volume (p = 0.08) between the AGHD and control groups.

Alteration of Cortical Thickness in Different Lobes and Regions

Compared with the control group, the AGHD group showed decreased cortical thickness in the parahippocampal gyrus (Brodmann's area 27), posterior cingulate gyrus (Brodmann's area 29, 30) and occipital visual syncortex Brodmann's area 17, 18, 19)(**Figure 1A** and **Table 3**). While in the partial area of the frontal lobe (Brodmann's area 9, 10, 11, 47), parietal lobe (Brodmann's area 7,39) and occipital visual syncortex (Brodmann's area 17, 18, 19), the AGHD group showed increased cortical thickness (**Figure 1B** and **Table 3**). The significant clusters are different and exclusive, although some of them belong to same Brodmann's region like Brodmann's area 17, 18, 19. There was no overlap between these parts.

Interaction Analysis

The associations between cortical thickness and serum IGF-1 levels were not significantly different between the two groups after adjusting for serum levels of FT3. Meanwhile associations between groups and serum FT3 levels and the effects on cortical thickness was found in our data (F = 16.55, df = 1, 29, $p < 0.001$). Cortical thickness of the posterior cingulum gyrus was prominently only associated with serum levels of FT3 in control group after adjusting for IGF-1 levels (AGHD group, $r = -0.28$, p = 0.27; control group, $r = -0.66$, p = 0.004; **Figure 2**).

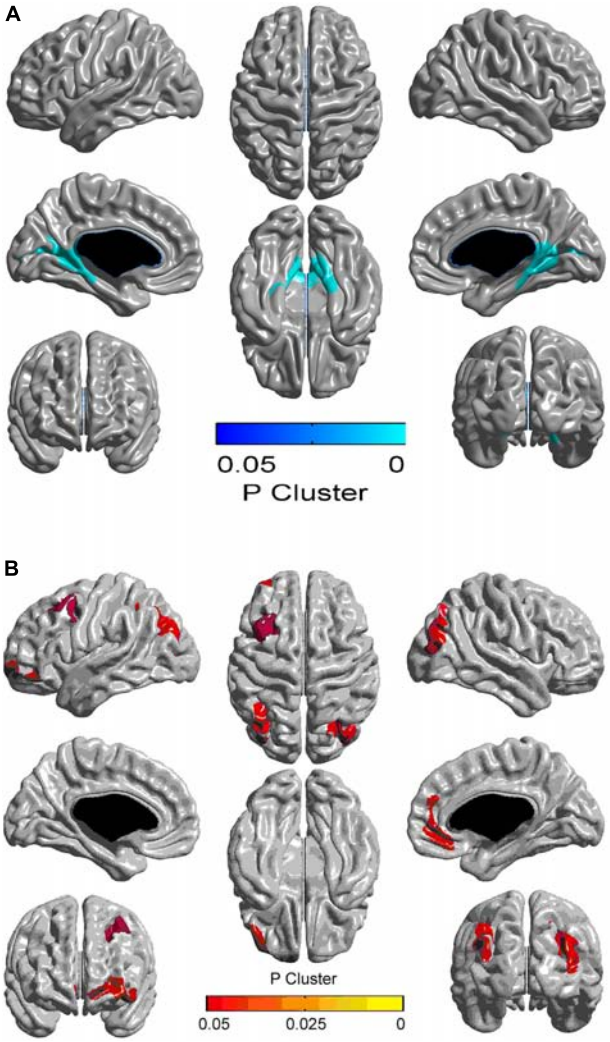

FIGURE 1 | Alterations in cortical thickness in young male patients with childhood-onset adult growth hormone deficiency. Clusters with FWE-corrected $p < 0.05$ are shown, and the color corresponds to the p-value. Areas in blue represent decreased cortical thickness in AGHD compared to controls, and yellow area represent increased thickness. **(A)** Clusters of significantly reduced cortical thickness in the AGHD group compared to controls. **(B)** Clusters of significantly increased cortical thickness in the AGHD group compared to controls.

DISCUSSION

This cross-sectional study focused on cortical thickness alterations of young male patients with childhood-onset AGHD after cessation of rhGH replacement therapy. Our results showed that: (1) Compared to age-, gender- and education-matched controls, the AGHD group had significantly decreased IGF1 levels. With routine replacement of levothyroxine, serum FT4 and FT3 levels in the AGHD group were in the lower quartile of the normal range, but were significantly lower than for the controls. (2) Although there was no difference in whole brain volume or gray matter volume between the two groups, there was a decreased cortical thickness in the parahippocampal gyrus, posterior cingulate gyrus and occipital visual syncortex in the AGHD group, as well as an increased cortical thickness in the partial area of the frontal lobe, parietal lobe and occipital visual syncortex. (3) Cortical thickness of the posterior cingulum gyrus was prominently associated with serum levels of FT3 in the control group after adjusting of IGF-1 levels, and the relationship was not observed in AGHD group.

The GH/IGF-1 axis plays an important role in brain development and maintenance of cognitive function (Annenkov, 2009). The GH receptor is prominently expressed in the hypothalamus, hippocampus, putamen and choroid plexus (Lai et al., 1993). Meanwhile, IGF-1 receptors are expressed in cerebellum, prefrontal cortex, caudate nucleus, amygdala, hippocampal and parahippocampal area (Bondy and Lee, 1993). During adolescence, gene expression in hippocampal area was reported to be regulated by IGF1 (Yan et al., 2011). In mice,

TABLE 3 | Regional variation of cerebral cortex thickness in AGHD patients compared with normal control.

Cortex thickness: AGHD vs. control	Brodmann's areas	Cluster size	Peak *x*	Peak *y*	Peak *z*	Peak *T*-value
AGHD > control	7, 10, 11, 19, 39	1225	−37	−57	44	4.63
	17, 18, 19	731	45	−79	−18	5.13
	9	191	−27	14	49	3.8
	47	157	−46	44	−16	4.59
AGHD < control	17, 18, 19, 27, 29, 30	2720	21	−55	1	7.23
	23	115	−21	−69	5	4.89

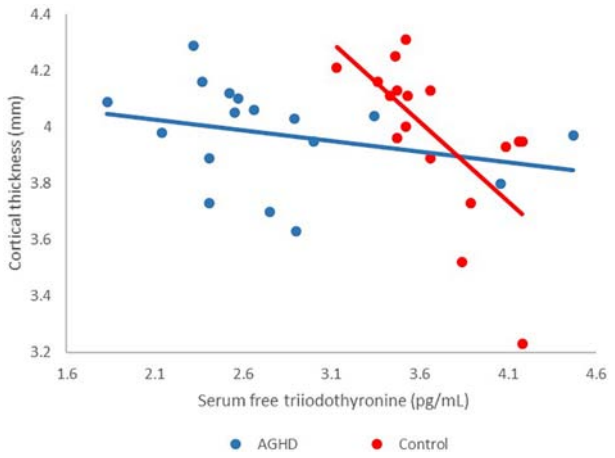

FIGURE 2 | Effects of interaction between groups and serum FT3 levels on cortical thickness. Red points, controls; blue points, AGHD patients.

the GH/IGF-1 axis plays a specific role in corticospinal tract development, and corticospinal axon growth will be impaired as the result of an interruption to IGF-1 signaling (Ozdinler and Macklis, 2006). However, how the disease process impacts the structural integrity of the brain in humans still needs further investigation. In children with isolated GHD, it was reported that there were decreased volumes in the right hippocampus, right pallidum and left thalamus, compared to controls (Webb et al., 2012). However, no previous studies have evaluated the structural characteristics in patients with MPHD after cessation of rhGH replacement therapy so far. In our study, all subjects had childhood-onset MPDH and stopped rhGH replacement therapy after completion of linear growth. Cortical thickness in the parahippocampal gyrus, posterior cingulate gyrus and occipital visual syncortex decreased, while cortical thickness in partial area of the frontal lobe, parietal lobe, occipital visual syncortex and angular gyrus increased in our AGHD subjects. The variations of cortical thickness in the cingulate cortex and frontal lobe are consistent with previous reports from young patients with GH receptor deficiency (Nashiro et al., 2017), since IGF-1 signaling is supposed to play an important role in brain regeneration in these areas. However, variations of cortical thickness in the occipital visual syncortex, angular gyrus and parahippocampal gyrus have not been described in AGHD patients before, and functional implications need to be further investigated.

Patients with AGHD were reported to have impaired cognitive function (memory and attention) in several neuropsychological studies, and there are several reports evaluating GH replacement therapy in cognitive function improvement in AGHD patients (Falleti et al., 2006). Several structures are known to play important roles in cognitive function, including memory and learning, and distribution of IGF-1 receptors reportedly interact with the hippocampal cholinergic system and are involved in cognitive development (Araujo et al., 1989; Bondy and Lee, 1993). In the elderly, higher concentrations of serum IGF-1 levels were associated with better performance on cognitive function tests, which suggested that the GH/IGF-1 axis may affect cognitive function throughout life (Al-Delaimy et al., 2009). In our AGHD subjects, decreased cortical thickness was found in parahippocampal gyrus, posterior cingulate gyrus and occipital visual syncortex. The parahippocampal gyrus surrounds the hippocampus and is part of the limbic system and plays an important role in memory encoding and retrieval. It was reported that parahippocampal cortical thickness was reduced in people at ultra-high risk of psychosis (Tognin et al., 2014). The posterior cingulate cortex is made up of an area around the midline of the brain, communicates with various brain networks simultaneously and is involved in diverse functions (Leech et al., 2012). Reduced cortical thickness of the posterior cingulate was reported in patients with improved migraines, and thus, it was hypothesized to be related with chronic pain development (Amaral et al., 2018). The occipital visual syncortex is located in the occipital lobe and is involved in visual information processing. Childhood onset of blindness significantly affects the cortical thickness of the primary visual cortex (Li et al., 2017). Cortical thickness changes of the above three areas have not been evaluated in GHD thus far. There are also some regions with increased cortical thickness, some of which play different roles in cognition, semantic processing and sensory afferents. The significance of these alterations, and whether rhGH replacement has any effect on them, needs further assessments.

At the same time, the associations between cortical thickness and serum IGF-1 levels were not significantly different between two groups after adjusting for serum levels of FT3. Meanwhile an association between groups and serum FT3 levels and the effects on cortical thickness was found in our data. Cortical thickness of posterior cingulum gyrus was prominently associated with serum levels of FT3 only in the control group after adjusting for IGF-1 levels. These results may suggest that the effects of the thyroid hormone on cortical thickness in AGHD patients have been lessened in the presence of GHD. The thyroid hormone plays an

essential role in early stages of brain development (Cuevas et al., 2005), and structures including the hippocampus, striatum and cortex are reported to be abnormal in rats (Rami et al., 1986), mice (Gil-Ibañez et al., 2013) and children (Clairman et al., 2015) with hypothyroidism. Children with congenital hypothyroidism showed cortical thinning or thickening in a few areas (Clairman et al., 2015), which are different from all the changed areas found in our study. The interaction between the GH and thyroid hormone and its effects on the maintenance of cortical thickness in different regions of the brain is not clear to date, and animal models may provide further information for this interplay.

There are several limitations in this study. The first and most important one is the limited number of subjects, however, there was relatively good homogeneity in the etiology, age of onset, duration of rhGH treatment and time course since cessation of rhGH treatment, which provided a general uniform background for morphology evaluation. Stable rules in interaction analysis will be warranted with more samples in further investigation. Another limitation is the cross-sectional nature of this study, which does not provide a cause-effect rationale for GHD and changes in cortical thickness. The third limitation is cognitive tests had not been assessed in AGHD patients since alterations of cortical thickness may be related to changed cognitive function. Further prospective studies are needed to shed new lights on the effects of GH replacement therapy on brain structure changes and cognitive function improvement in AGHD patients.

In summary, our findings indicate that young male patients with childhood-onset AGHD who are no longer receiving GH replacement have alterations in cortical thickness in different brain lobes/regions. It will be important to expand on these results in a larger sample size, ideally incorporating not only structural, but also functional brain measures.

DATA AVAILABILITY STATEMENT

The raw data supporting the conclusions of this manuscript will be made available by the authors, without undue reservation, to any qualified researcher.

ETHICS STATEMENT

The study protocol was approved by the Ethics Committees of Peking Union Medical College Hospital. Written informed consent was obtained from all subjects and all data were de-identified before analysis.

AUTHOR CONTRIBUTIONS

HY and KL collected the clinical information, image data, and drafted the manuscript. XL, BG, and GG analyzed the MRI image data. LW and FG helped with clinical and biochemical data analysis. FF, HY, and BH were responsible for the MRI image acquisition. HZ and HP designed the study protocol and revised the manuscript.

FUNDING

This work was supported by the National Natural Science Foundation of China (Nos. 81400774 and 81970678), the CAMS Innovation Fund for Medical Science (CAMS-2016-I2M-1-002 and 2016-I2M-1-008), the PUMCH Youth Fund (No. 3332016128), and the Non-profit Central Research Institute Fund of Chinese Academy of Medical Sciences (Nos. 2017PT32020 and 2018PT32001).

REFERENCES

Adem, A., Jossan, S. S., d'Argy, R., Gillberg, P. G., Nordberg, A., Winblad, B., et al. (1989). Insulin-like growth factor 1 (IGF-1) receptors in the human brain: quantitative autoradiographic localization. *Brain Res.* 503, 299–303. doi: 10.1016/0006-8993(89)91678-8

Al-Delaimy, W. K., von Muhlen, D., and Barrett-Connor, E. (2009). Insulinlike growth factor-1, insulinlike growth factor binding protein-1, and cognitive function in older men and women. *J. Am. Geriatr. Soc.* 57, 1441–1446. doi: 10.1111/j.1532-5415.2009.02343.x

Aleman, A., Verhaar, H. J., De Haan, E. H., De Vries, W. R., Samson, M. M., Drent, M. L., et al. (1999). Insulin-like growth factor-I and cognitive function in healthy older men. *J. Clin. Endocrinol. Metab.* 84, 471–475. doi: 10.1210/jc.84.2.471

Amaral, V. C. G., Tukamoto, G., Kubo, T., Luiz, R. R., Gasparetto, E., and Vincent, M. B. (2018). Migraine improvement correlates with posterior cingulate cortical thickness reduction. *Arq. Neuropsiquiatr.* 76, 1501–1557. doi: 10.1590/0004-282x20180004

Annenkov, A. (2009). The Insulin-Like Growth Factor (IGF) Receptor Type 1 (IGF1R) as an Essential Component of the Signalling Network Regulating Neurogenesis. *Mol. Neurobiol.* 40, 195–215. doi: 10.1007/s12035-009-8081-0

Araujo, D. M., Lapchak, P. A., Collier, B., Chabot, J. G., and Quirion, R. (1989). Insulin-like growth factor-1 (somatomedin-C) receptors in the rat brain: distribution and interaction with the hippocampal cholinergic system. *Brain Res.* 484, 130–138. doi: 10.1016/0006-8993(89)90355-7

Arwert, L. I., Veltman, D. J., Deijen, J. B., Lammertsma, A. A., Jonker, C., and Drent, M. L. (2005). Memory performance and the growth hormone/insulin-like growth factor axis in elderly: a positron emission tomography study. *Neuroendocrinology* 81, 31–40. doi: 10.1159/000084872

Berberoğlu, M., Sı klar, Z., Darendeliler, F., Poyrazoğlu, S., Darcan, S., Işgüven, P., et al. (2008). Evaluation of permanent growth hormone deficiency (GHD) in young adults with childhood onset GHD: a multicenter study. *J. Clin. Res. Pediatr. Endocrinol.* 1, 30–37. doi: 10.4008/jcrpe.v1i1.7

Bondy, C. A., and Lee, W. H. (1993). Patterns of insulin-like growth factor and igf receptor gene expression in the brain: functional implications. *Ann. N. Y. Acad. Sci.* 692, 33–43. doi: 10.1111/j.1749-6632.1993.tb26203.x

Buchanan, C. M., Eccles, J. S., and Becker, J. B. (1992). Are adolescents the victims of raging hormones: evidence for activational effects of hormones on moods and behavior at adolescence. *Psychol. Bull.* 111, 62–107. doi: 10.1037//0033-2909.111.1.62

Bülow, B., Hagmar, L., Ørbaek, P., Osterberg, K., and Erfurth, E. M. (2002). High incidence of mental disorders, reduced mental well-being and cognitive function in hypopituitary women with GH deficiency treated for pituitary disease. *Clin. Endocrinol.* 56, 183–193. doi: 10.1046/j.0300-0664.2001.01461.x

Cherng-Min, M., and Shu-Yen, W. (2001). A medial-surface oriented 3-d two-subfield thinning algorithm. *Pattern Recognit. Lett.* 22, 1439–1446. doi: 10.1016/s0167-8655(01)00083-6

Cherng-Min, M., Shu-Yen, W., and Jiann-Der, L. (2002). Three-dimensional topology preserving reduction on the 4-subfields. *IEEE Trans. Pattern* 24, 1594–1605. doi: 10.1109/tpami.2002.1114851

Clairman, H., Skocic, J., Lischinsky, J. E., and Rovet, J. (2015). Do children with congenital hypothyroidism exhibit abnormal cortical morphology. *Pediatr. Res.* 78, 286–297. doi: 10.1038/pr.2015.93

Collins, D. L., Neelin, P., Peters, T. M., and Evans, A. C. (1994). Automatic 3D intersubject registration of MR volumetric data in standardized talairach space. *J. Comput. Assist. Tomogr.* 18, 192–205. doi: 10.1097/00004728-199403000-00005

Cuevas, E., Ausó, E., Telefont, M., Morreale de Escobar, G., Sotelo, C., and Berbel, P. (2005). Transient maternal hypothyroxinemia at onset of corticogenesis alters tangential migration of medial ganglionic eminence-derived neurons. *Eur. J. Neurosci.* 22, 541–551. doi: 10.1111/j.1460-9568.2005.04243.x

Falleti, M. G., Maruff, P., Burman, P., and Harris, A. (2006). The effects of growth hormone (GH) deficiency and GH replacement on cognitive performance in adults: a meta-analysis of the current literature. *Psychoneuroendocrinology* 31, 681–691. doi: 10.1016/j.psyneuen.2006.01.005

Gil-Ibañez, P., Morte, B., and Bernal, J. (2013). Role of Thyroid hormone receptor subtypes α and β on gene expression in the cerebral cortex and striatum of postnatal mice. *Endocrinology* 154, 1940–1947. doi: 10.1210/en.2012-2189

Jussi, T., Alex, Z., and Alan, E. (2004). Fast and robust parameter estimation for statistical partial volume models in brain MRI. *Neuroimage* 23, 84–97. doi: 10.1016/j.neuroimage.2004.05.007

Kim, J. S., Singh, V., Lee, J. K., Lerch, J., Ad-Dab'bagh, Y., and MacDonald, D. (2005). Automated 3-D extraction and evaluation of the inner and outer cortical surfaces using a Lapcalcian map and partial volume effect classification. *Neuroimage* 27, 210–221. doi: 10.1016/j.neuroimage.2005.03.036

Lai, Z., Roos, P., Zhai, O., Olsson, Y., Fhölenhag, K., and Larsson, C. (1993). Age-related reduction of human growth hormone-binding sites in the human brain. *Brain Res.* 621, 260–266. doi: 10.1016/0006-8993(93)90114-3

Leech, R., Braga, R., and Sharp, D. J. (2012). Echoes of the brain within the posterior cingulate cortex. *J. Neurosci.* 32, 215–222. doi: 10.1523/JNEUROSCI.3689-11.2012

Lerch, J. P., and Evans, A. C. (2005). Cortical thickness analysis examined through power analysis and a population simulation. *Neuroimage* 24, 163–173. doi: 10.1016/j.neuroimage.2004.07.045

Li, Q., Song, M., Xu, J., Qin, W., Yu, C., and Jiang, T. (2017). Cortical thickness development of human primary visual cortex related tothe age of blindness onset. *Brain Imaging Behav.* 11, 1029–1036. doi: 10.1007/s11682-016-9576-8

Liu, Y., Xie, T., He, Y., Duan, Y., Huang, J., and Ren, Z. (2014). Cortical Thinning Correlates with Cognitive Change in Multiple Sclerosis but not in Neuromyelitis Optica. *Eur. Radiol.* 24, 2334–2343. doi: 10.1007/s00330-014-3239-1

MacDonald, D., Kabani, N., Avis, D., and Evans, A. C. (2000). Automated 3-D extraction of inner and outer surfaces of cerevral cortex from MRI. *Neuroimage* 12, 340–356. doi: 10.1006/nimg.1999.0534

Molitch, M. E., Clemmons, D. R., Malozowski, S., Merriam, G. R., Shalet, S. M., Vance, M. L., et al. (2011). Evaluation and treatment of adult growth hormone deficiency: an Endocrine Society clinical practice guideline. *J. Clin. Endocrinol. Metab.* 96, 1587–1609. doi: 10.1210/jc.2011-0179

Nashiro, K., Guevara-Aguirre, J., Braskie, M. N., Hafzalla, G. W., Velasco, R., and Balasubramanian, P. (2017). Brain structure and function associated with younger adults in growth hormone receptor-deficient humans. *J. Neurosci.* 37, 1696–1707. doi: 10.1523/JNEUROSCI.1929-16.2016

Ozdinler, P. H., and Macklis, J. D. (2006). IGF-I specifically enhances axon outgrowth of corticospinal motor neurons. *Nat. Neurosci.* 9, 1371–1381. doi: 10.1038/nn1789

Park, K. D., Lim, O. K., Yoo, C. J., Kim, Y. W., Lee, S., Park, Y., et al. (2016). Voxel-based statistical analysis of brain metabolism in patients with growth hormone deficiency after traumatic brain injury. *Brain Inj.* 30, 407–413. doi: 10.3109/02699052.2015.1127997

Rami, A., Patel, A. J., and Rabié, A. (1986). Thyroid hormone and development of the rat hippocampus: morphological alterations in granule and pyramidal cells. *Neuroscience* 19, 1217–1226. doi: 10.1016/0306-4522(86)90135-1

Sled, J. G., Zijdenbos, A. P., and Evans, A. C. (1998). A nonparametric method for automatic correction of intensity nonuniformity in MRI data. *IEEE Trans. Med. Imaging* 17, 87–97. doi: 10.1109/42.668698

Supeno, N. E., Pati, S., Hadi, R. A., Ghani, A. R., Mustafa, Z., Abdullah, J. M., et al. (2013). IGF-1 acts as controlling switch for long-term proliferation and maintenance of EGF/FGF-responsive striatal neural stem cells. *Int. J. Med. Sci.* 10, 522–531. doi: 10.7150/ijms.5325

Tognin, S., Riecher-Rössler, A., Meisenzahl, E. M., Wood, S. J., Hutton, C., and Borgwardt, S. J. (2014). Reduced parahippocampal cortical thickness in subjects at ultra-high risk for psychosis. *Psychol. Med.* 44, 489–498. doi: 10.1017/S0033291713000998

Uzunova, I., Kirilov, G., Zacharieva, S., Shinkov, A., Borissova, A. M., and Kalinov, K. (2015). Individual risk factors of the metabolic syndrome in adult patients with growth hormone deficiency – a cross-sectional case-control study. *Exp. Clin. Endocrinol. Diabetes* 123, 39–43. doi: 10.1055/s-0034-1390460

van Dam, P. S. (2005). Neurocognitive function in adults with growth hormone deficiency. *Horm. Res.* 64(Suppl. 3), 109–114. doi: 10.1159/000089326

Webb, E. A., O'Reilly, M. A., Clayden, J. D., Seunarine, K. K., Chong, W. K., and Dale, N. (2012). Effect of growth hormone deficiency on brain structure, motor function and cognition. *Brain* 135, 216–227. doi: 10.1093/brain/awr305

Wilson, J. D. (1993). Peking Union Medical College Hospital, a palace of endocrine treasures. *J. Clin. Endocrinol. Metab.* 76, 815–816. doi: 10.1210/jcem.76.4.8473387

Wrigley, S., Arafa, D., and Tropea, D. (2017). Insulin-like growth factor 1: at the crossroads of brain development and aging. *Front. Cell Neurosci.* 11:14. doi: 10.3389/fncel.2017.00014

Yan, H., Mitschelen, M., Bixler, G. V., Brucklacher, R. M., Farley, J. A., and Han, S. (2011). Circulating IGF1 regulates hippocampal IGF1 levels and brain gene expression during adolescence. *J. Endocrinol.* 211, 27–37. doi: 10.1530/JOE-11-0200

Yang, H., Zhu, H., Yan, K., and Pan, H. (2017). Childhood-onset adult growth hormone deficiency: clinical, hormonal, and radiological assessment in a single center in China. *Horm. Res. Paediatr.* 88, 155–159. doi: 10.1159/000478527

Yaojing, C., Peng, L., Bin, G., Zhen, L., Xin, L., and Alan, C. (2015). The effects of an APOE promoter polymorphism on human cortical morphology during nondemented aging. *J. Neurosci.* 35, 1423–1431. doi: 10.1523/JNEUROSCI.1946-14.2015

Zhu, H., Xu, Y., Gong, F., Shan, G., Yang, H., and Xu, K. (2017). Reference ranges for serum insulin-like growth factor 1 (IGF-1) in healthy Chinese adults. *PLoS One* 12:e0185561. doi: 10.1371/journal.pone.0185561

Zijdenbos, A. P., Forghani, R., and Evans, A. C. (2002). Automatic "pipeline" analysis of 3-D MRI data for clinical trials: application to multiple sclerosis. *IEEE Trans. Med. Imaging* 21, 1280–1290.

Conflict of Interest: The authors declare that the research was conducted in the absence of any commercial or financial relationships that could be construed as a potential conflict of interest.

frontiers in Neuroscience

ORIGINAL RESEARCH
published: 13 December 2019
doi: 10.3389/fnins.2019.01317

Oxytocin Inhibition of Metastatic Colorectal Cancer by Suppressing the Expression of Fibroblast Activation Protein-α

Mingxing Ma[1], Li Li[2], He Chen[2] and Yong Feng[3]**

[1] Department of Colorectal Surgery, Shengjing Hospital, China Medical University, Shenyang, China, [2] Department of Forensic Medicine, Harbin Medical University, Harbin, China, [3] Department of General Surgery, Affiliated Shengjing Hospital, China Medical University, Shenyang, China

Oxytocin (OXT) and its receptor (OXTR) are present in the gastrointestinal system and are involved in gastrointestinal tumorigenesis. However, the effect of OXTR signaling on the development of colorectal cancer (CRC) and its underlying mechanisms remain unexplored. To address these issues, we first examined the expressions of OXT, OXTR, and several cancer-associated proteins using colon "tissue chips" from a spectrum of malignant progression of the colon, which included normal colon tissue, chronic colitis, colorectal adenoma, and colorectal adenocarcinoma (CAC). The results showed that the expressions of OXT and OXTR decreased gradually with the malignant progression of the disease. Stimulation of CAC tissues with OXT increased OXTR expression while down-regulated FAPα and CCL-2 protein expressions in a concentration- and time-dependent manner. Moreover, cell invasion experiment showed that OXT treatment reduced the invasion ability of colon cancer cells and blocking OXTR with atosiban blocked OXT-reduced invasion ability of human colon cancer cell lines Ls174T and SW480. The results indicate that OXT has the potential to inhibit CRC development via down-regulating the immunosuppressive proteins FAPα and CCL-2. When the OXTR signaling is weakened, colon tissues may transform to CRC. These findings also highlight the possibility of applying OXT to inhibit CRC development directly.

Keywords: colorectal cancer, fibroblast activation protein-α, oxytocin, oxytocin receptor, metastasis

OPEN ACCESS

Edited by:
Xue Qun Chen,
Zhejiang University, China

Reviewed by:
Ben Nephew,
Worcester Polytechnic Institute, United States
Hao Zhang,
Dalian Medical University, China

****Correspondence:***
He Chen
chenhe_2008@aliyun.com
Yong Feng
fengy@sj-hospital.org

Specialty section:
This article was submitted to Neuroendocrine Science, a section of the journal Frontiers in Neuroscience

Received: *06 March 2019*
Accepted: *25 November 2019*
Published: *13 December 2019*

Citation:
Ma M, Li L, Chen H and Feng Y (2019) Oxytocin Inhibition of Metastatic Colorectal Cancer by Suppressing the Expression of Fibroblast Activation Protein-α. Front. Neurosci. 13:1317. doi: 10.3389/fnins.2019.01317

INTRODUCTION

Colorectal cancer (CRC), a cancer that affects the colon, rectum, or appendix, is the third most common malignant disease in the world and the second most common cancer type in the United States (El-Shami et al., 2015), Europe, and Poland (Witold et al., 2018) in addition to being a leading cause of cancer-related mortality. With the exception of the United States, the incidence of CRC in most regions of the world is expected to increase continuously in the coming decades, due to population growth and changes in the demographic structure (Tsoi et al., 2017). Importantly, the trend toward a higher incidence of CRC primarily occurs among young adults (Austin et al., 2014),

which may have a large impact on the working population and thus have a negative impact on the development of human society.

The pathogenesis of CRC involves the activation of oncogenesis and the mutation of mismatch repair genes or the inactivation of tumor suppressor genes, which further activate the oncogenic signal transduction pathways to promote proliferation, migration, invasion, and apoptosis of cancer cells (Andres et al., 2018), such as p53 (Tiwari et al., 2018). In the CRC metastases, the fibroblast activation protein-alpha (FAPα) plays a critical role. It has been reported that in all CRC samples examined, FAPα was expressed in cancer-associated fibroblasts, but not in normal colon, hyperplastic polyps, or adenoma samples. CRC cells, but not adenoma cells, can activate fibroblasts by inducing FAPα expression in order to increase their migration and invasion by releasing the transforming growth factor (TGF; Hawinkels et al., 2014). Furthermore, in mouse CRC model, cancer-associated fibroblasts with high FAPα expression induce resistance to immune checkpoint blockade by up-regulating C–C motif chemokine ligand 2 (CCL-2) secretion, recruiting myeloid cells, and decreasing T-cell activity (Chen et al., 2017). Therefore, clarifying the regulation of FAPα expression in cancer-associated fibroblasts and its associated cytokines probably provide an optional target for suppressing CRC migration.

Oxytocin (OXT) is a neuropeptide produced in both the central nervous system and peripheral tissues. OXT has been implicated in preventing the emergence of certain tumors by identifying, destroying, and eliminating mutant cells in a timely manner, such as breast cancer, prostate cancer, trophoblast-endothelial-derived tumor cells, and endometrial cancer cells (Imanieh et al., 2014; Shin et al., 2016). In the gastrointestinal (GI) tract, a lesser number of small bowel and pancreatic neuroendocrine tumors (NETs) express OXT receptor (OXTR) gene, which is significantly different from the adjacent normal tissue (Carr et al., 2013). However, the absolute expression of OXTR in the NETs varies greatly according to the types of primary tumors and is close to the somatostatin receptor type 2 in the small bowel NETs but not in the pancreatic NETs (Sherman et al., 2013). Moreover, OXT can both stimulate and inhibit the growth of certain tumors, such as osteosarcoma cells at different stages of cell differentiation (Petersson, 2008). Thus, it remains a question about the expression of OXT and OXTR in CRCs and the functions of OXTR signaling in CRC development.

To address these issues, expressions of OXT and OXTR were first identified in normal colon tissue, chronic colitis, tubular adenoma, and colonic adenocarcinoma (CAC) of tissue chips. Then, freshly excised normal colon and CAC tissues were stimulated with OXT and expression of OXTR, FAPα, TGF-β, and CCL-2 proteins were analyzed. Additionally, using Transwell migration assay, we observed effects of OXT with and without OXTR antagonist on the migration of colon cancer cells. The results highlight for the first time that OXT may inhibit CAC migration by inhibiting the expression of immune suppression-associated proteins, FAPα and CCL-2.

MATERIALS AND METHODS

In the present study, human CRC tissue chips, CRC surgical specimens, and colon cancer cell lines were used to study the effect of OXTR signaling on CRC development. The study protocols following the principles of the Declaration of Helsinki were respectively approved by the Ethics Committees of the China Medical University and the Harbin Medical University. Written informed consent was obtained from all patients.

Tissue Collection

Tumor tissues and normal tissues adjacent to a tumor (or precancerous tissues) were collected from CRC patients. The patients were referred to either Shengjing Hospital of China Medical University or Harbin Medical University Cancer Hospital, who received conventional laparotomy between May 2016 and May 2017. The grading and staging of the CRC tumor were performed by a pathologist based on the WHO diagnostic criteria. None of the patients' tissues received any chemotherapy or other kinds of therapies. The CRC tissues from six patients aged between 49 and 65 years (2 males and 4 females) were pathologically identified as well-differentiated CAC and were used to assess the association of OXTR signaling with CRC development. All specimens were collected and made anonymous according to ethical and legal standards.

Detection of Cancer-Associated Proteins in the Spectrum of Human CAC Tissue Chip

The human CAC tissue chips were purchased from Alenabio (Xi'an, China), containing normal colon tissue, chronic colitis, colonic tubular adenoma, and well-differentiated CAC. The tissue chip was dewaxed using conventional methods and then incubated with hydrogen peroxide for 15 min. The first antibodies, including FAPα (1:300, Abcam), OXTR (1:300, Abcam), OXT (1:200, Abcam), and CCL-2 (1:200, Bioss) were added to the incubation overnight at 4°C. The corresponding secondary antibodies (50 μl, 1:1000) were added to the reaction that was incubated for 30 min at room temperature (21–23°C). After coloration, the photographs of the images were taken with an imaging system (Life Science), and the positive immunohistochemical staining was represented with brown stains visible under a light microscope.

OXT Treatment and Fluorescent Immunohistochemistry of CRC-Related Proteins in CAC Tissues

Freshly dissected CAC tissue and normal colon tissue (control) were separately placed in a 5-ml centrifuge tube containing 4°C of Tyrode's solution and allowed to acclimate for 30 min at room temperature. The tissue was cut into 1-mm square tissue pieces in a glass dish, and the same number of tissue blocks was placed in 12-well plates. In 2 ml of pre-heated 37°C Tyrode's solution containing 0.1 nM OXT, the tissue blocks were incubated for 0, 10, 30, and 120 min, respectively. In another set of study, the tissue blocks were incubated for 30 min in the reaction containing

OXT in 1 pM, 0.1 nM, and 10 nM in 2 ml of Tyrode's solution, and then placed in liquid nitrogen for later preparation of frozen tissue sections. In the sectioning, tissues were embedded in OCT at -20°C and cut into 2-μm-thick sections.

Fluorescent immunohistochemistry was performed as previously described (You et al., 2011; Delorme and Garabedian, 2018). In brief, the cryosections of the control and CAC tissues were incubated with the following primary antibodies: FAPα, OXTR, CCL-2, and TGF-β (1:100), for 1 h after conventional permeation and blocking non-specific binding. Then, the sections were further processed with the corresponding secondary antibodies. Sections were examined with a fluorescence microscope (Nikon Eclipse FN1) through a CCD camera (Nikon DS-Ri2). To avoid false-positive or -negative immunostaining results, serial dilutions of the primary antibody, pre-absorbed primary antibody staining, and no primary and no secondary antibody controls were applied.

Invasion Ability of Human Colon Cancer Cells

To study cell invasiveness, Transwell chambers (6.5 mm diameter, 8 μm pore size, Millipore) coated with Matrigel (BD Biosciences, Bedford, MA, United States) were used. Human colon cancer cell lines (Ls174T, ATCC, United States; SW480, Cell Bank, Chinese Academy of Sciences) of 5×10^5/ml in 170 μl of serum-free medium were added to the upper chamber. The vehicle and OXT (0.1 nM) with or without atosiban (0.1 μM) were added to the upper chamber at 30 μl, respectively. Then, a medium (PRMI 1640) containing 10% fetal bovine serum was added to the lower chamber. Next, the cells could invade the Matrigel for 48 h. The non-invading cells on the upper surface of the membrane were removed with a cotton swab and the invading cells were counted in microscopic fields for each membrane under 40 × magnification.

Data Analysis

All data are expressed as mean ± standard error of the mean. Multiple comparisons were statistically analyzed using the Mann–Whitney *U*-test or one-way analysis of variance, followed by a Student–Newman–Keuls *post hoc* test. All statistical analyses were performed using GraphPad Prism software version 5.0 and $P < 0.05$ was considered statistically significant.

RESULTS

Expressions of OXT, OXTR, FAPα, and CCL-2 in the CAC Chips

To reveal the regulation of OXTR signaling in the development of CRC, expressions of OXT, OXTR, FAPα, and CCL-2 were first examined in CAC chips. The results showed that the expressions of OXT and OXTR were relatively high in normal tissue, and the expressions in chronic colitis, tubular adenoma, and well-differentiated CAC decreased gradually (**Figure 1**).

In contrast, the expressions of the cancer-associated proteins FAPα and CCL-2 in the CACs were more pronounced than the normal colon tissue. In the tissue with chronic colitis, CCL-2 but not FAPα was also significantly high compared to the control (**Figure 2**). These findings are consistent with other reports in cancerous tissues (Henriksson et al., 2011; Chen et al., 2017).

Time- and Dose-Associated Effects of OXT on the Expression of Different CRC Molecules

Similar to the findings on the chips, OXT and OXTR were also observed in patients' colon tissues. In normal tissues adjacent to the CAC, both the OXT and OXTR were observed in the myenteric neural plexus and submucosal tissues. In the

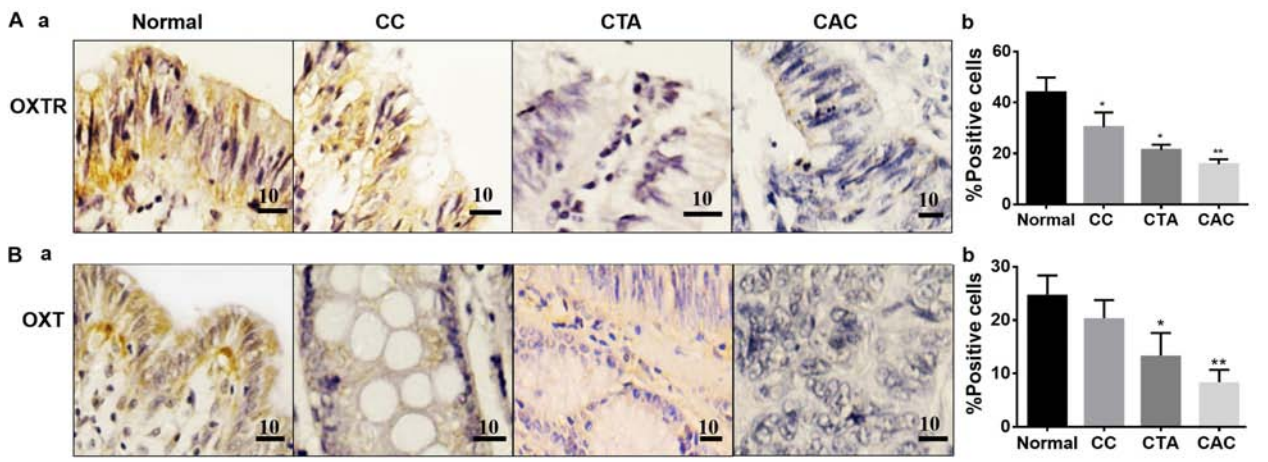

FIGURE 1 | Expressions of oxytocin (OXT) receptor (OXTR) and OXT in different colon tissues. **(A)** Exemplary staining of OXTR (Aa) in normal colon tissue (Normal), chronic colitis (CC), colonic tubular adenoma (CTA), and well-differentiated adenocarcinoma of the colon (CAC) (a, from left to right) and their summaries in bar graph (b), respectively. **(B)** Exemplary staining of OXT (a) in the tissues stated in Aa and the summary (b), respectively. Positive immunohistochemical staining is indicated by brown spots. The unit of scale bars is μm. Comparisons between groups linked to the horizontal line(s) were performed by means of a one-way analysis of variance, followed by a Student–Newman–Keuls test. $^*P < 0.05$, $^{**}P < 0.01$, and $n = 20$–30.

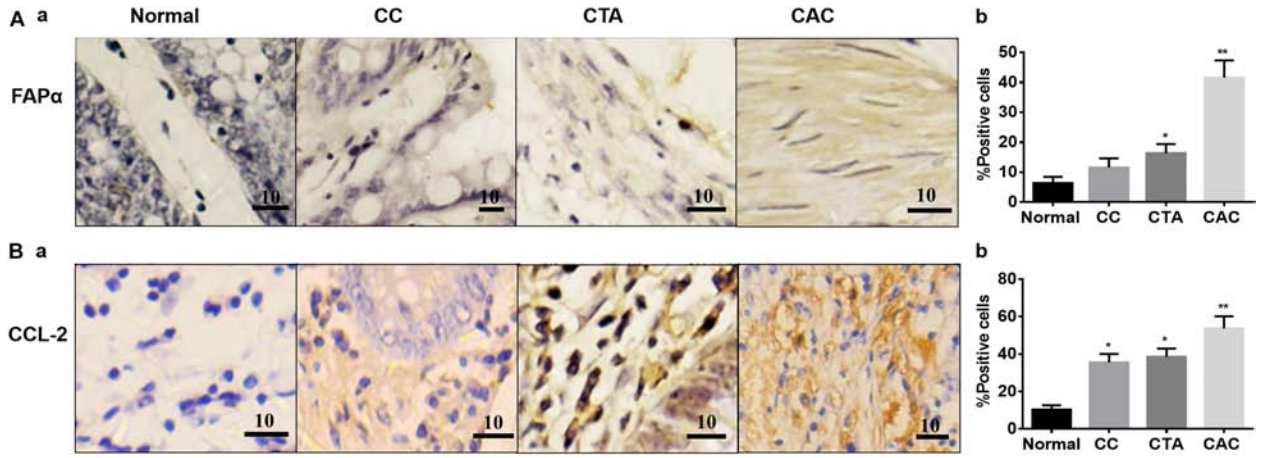

FIGURE 2 | Expressions of fibroblast activation protein-α (FAPα) and C–C motif chemokine ligand 2 (CCL-2) proteins in different colon tissues. **(A)** Exemplary staining of FAPα in Normal, CC, CTA, and CAC and their summaries, respectively. **(B)** Exemplary staining of CCL-2 (a) in the tissues stated in Aa and the summary (b), respectively. Kindly refer to **Figure 1** for other annotations.

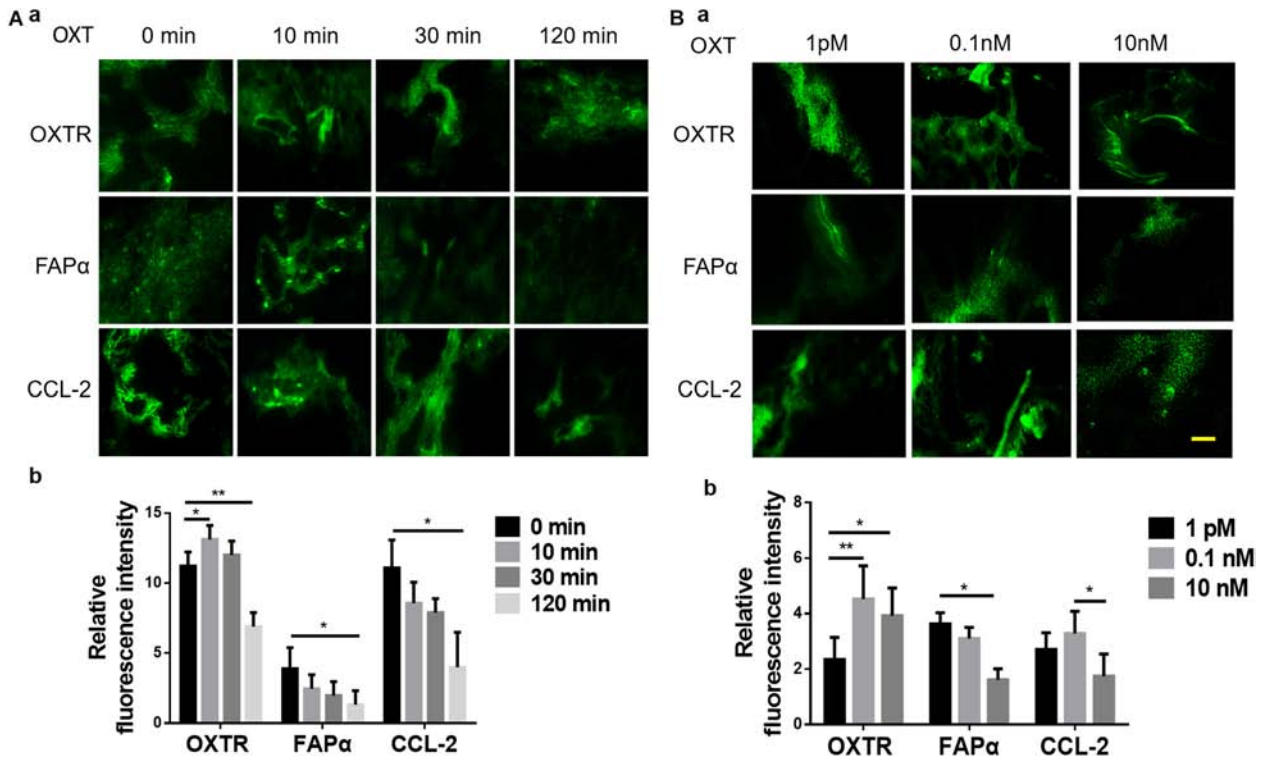

FIGURE 3 | Time- and dose-associated effects of OXT on the expression of OXTR, FAPα, and CCL-2 in fresh human colon tissues of patients with colorectal cancer (CRC). **(A,B)** Time-associated effect and the dose-associated effect in exemplary fluorescent images (a) and the summaries in bar graphs (b) for FAPα **(A)** and CCL-2 **(B)**, respectively. The scale bars are equal to 10 μm. Kindly refer to **Figure 1** for other annotations.

CAC, OXT was mostly absent while the OXTR was weak (**Supplementary Figure 1**).

The negative association between OXT/OXTR and FAPα suggests the presence of a causal relationship between a decrease in OXTR signaling and the development of CRC. Since the biological effect of OXT possesses significant features of time and dose dependence, as shown in OXT neurons (Wang and Hatton, 2006; Wang et al., 2006), we first examined the temporal effect of OXT on the expression of OXTR, FAPα, and CCL-2. The results showed that in normal tissues, OXT increased the expression of OXTR at 10 and 30 min; this effect decreased significantly after 120 min; FAPα and CCL-2 proteins decreased significantly

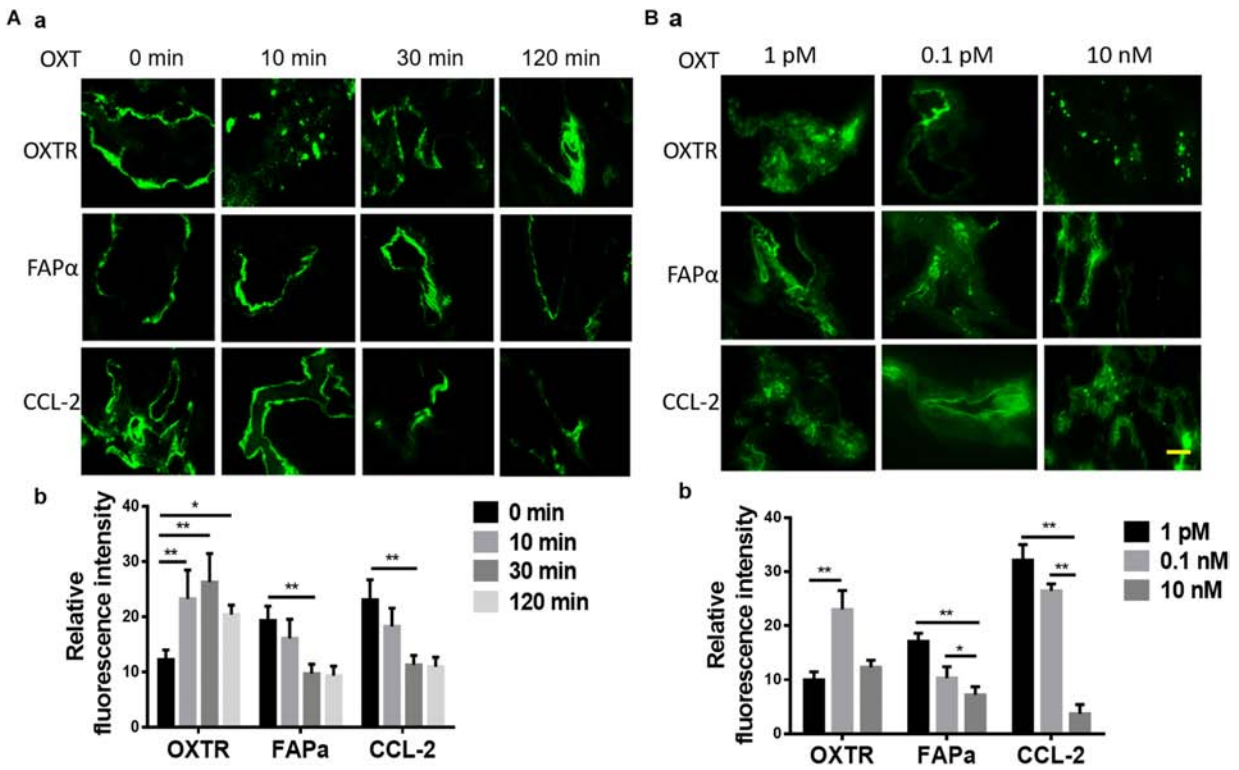

FIGURE 4 | Time- and dose-associated effects of OXT on the expression of OXTR, FAPα, and CCL-2 in CAC tissues of patients with CRC. **(A,B)** Time-associated effect and the dose-associated effect in exemplary fluorescent images (a) and the summaries in bar graphs (b) for FAPα **(A)** and CCL-2 **(B)**, respectively. The scale bars are equal to 10 μm. Kindly refer to **Figure 1** for other annotations.

after 10 min (**Figure 3A**). Furthermore, in response to increased concentrations of OXT (1 pM, 0.1 nM, 10 nM), OXTR levels increased significantly, but FAPα levels decreased significantly. CCL-2 increased significantly with 0.1 nM OXT, but decreased significantly with 10 nM (**Figure 3B**). This finding supports presence of a physiological action of OXT in colon tissues.

In CAC, treatment with OXT for 10 min or 30 min significantly increased the expression of OXTR but decreased FAPα and CCL-2; OXT-increased expression of OXTR became insignificant at 120 min when FAPα and CCL-2 did not show further decrease (**Figure 4A**). This finding is consistent with the general regulation of receptor internalization and decomposition after prolonged hormonal stimulation.

Further analysis of the response of CAC-associated tissues to different doses (1 pM, 0.1 nM, or 10 nM) of OXT stimulation for 10 min revealed that OXT dose-dependently altered the expression of OXTR, FAPα, and CCL-2 in CACs. As shown in **Figure 4B**, compared to 1 pM OXT, 0.1 nM OXT markedly reduced the expression of FAPα and CCL-2 while increasing OXTR expression. A higher dose of OXT (10 nM) further reduced FAPα and CCL-2, but its effect on OXTR expression did not significantly differ from the effect of 1 pM OXT. These time- and dose-dependent OXT effects are in agreement with OXT effects in neural tissues (Wang and Hatton, 2006; Wang et al., 2006).

Noticeably, OXT did not significantly affect the expression of TGF-β at different times and doses (**Supplementary Figure 2**).

Effects of OXT on the Invasion Ability of Human Colon Cancer Cells

To establish a causal relationship between OXTR signaling and CRC cell metastases, the study evaluated the role of OXTR signaling in the invasion ability of human colon cancer cells using the Matrigel invasion/Transwell migration assay, with six duplicates in each group. As shown in **Figure 5**, OXT (0.1 nM) significantly reduced the Transwell number of colon cancer cell line, Ls174t (**Figure 5A**) and SW480 cells (**Figure 5B**). By contrast, pretreatment with OXTR antagonist atosiban (0.1 μM) did not have a significant effect on Transwell activity by itself; however, it did block the inhibitory effects of OXT on this Transwell activity. This finding is in line with the inhibitory effect of OXT on the expressions of FAPα and CCL-2.

DISCUSSION

The present study found that OXT and OXTR not only are present in colon tissues but also correlate with CAC migration. Clearly, the expressions of OXT and OXTR in CAC tissues were low, whereas activation of OXTR signaling reduced the expression of FAPα and CCL-2. Importantly, blocking OXTR activation inhibited OXT-induced reduction of colon cancer cell migration in both types of colon cancer cell lines. These

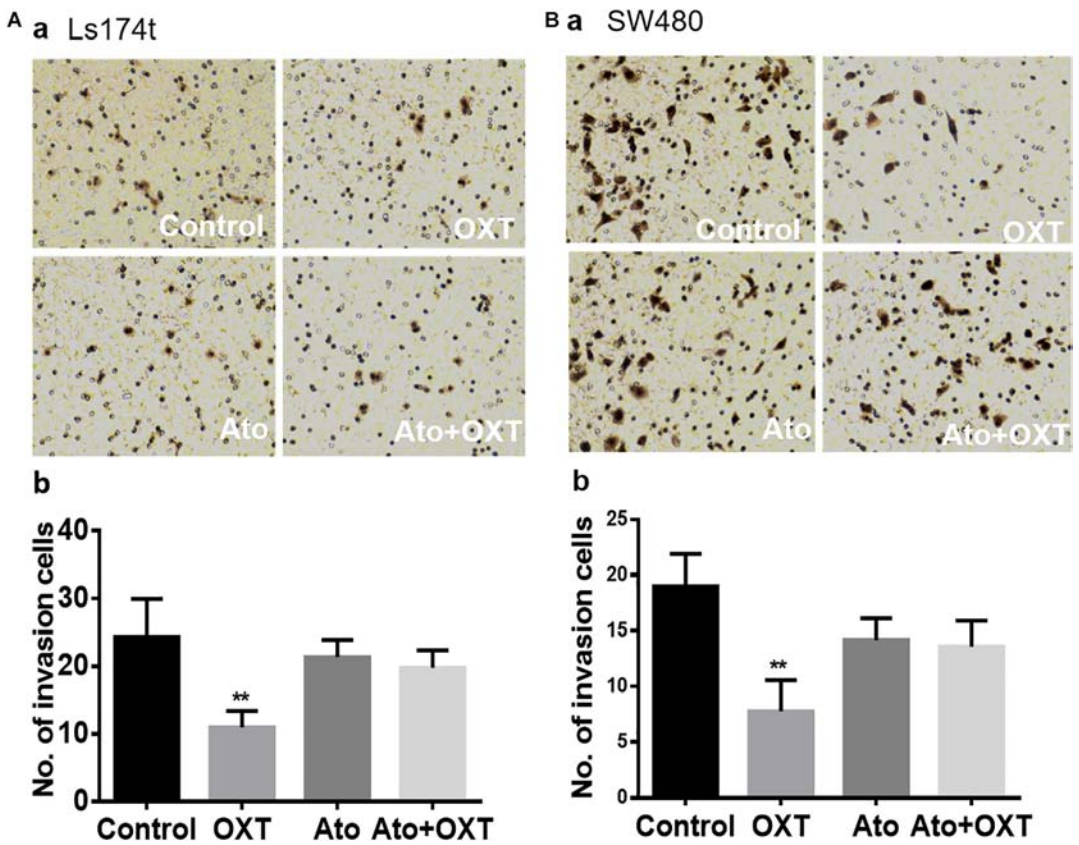

FIGURE 5 | Effects of OXT on the Transwell ability of CAC cells. **(A,B)** Representative images of Transwell membranes for the Ls174T (**A**a) and SW480 (**B**a) colon cancer cell lines and their summaries (**A**b,**B**b), respectively. The four panels as marked in white represent the effects of the vehicle, OXT, atosiban, and atosiban plus OXT, respectively. $^{**}P < 0.01$ compared to vehicles.

findings highlight the possibility of suppressing CRC metastases by applying OXT directly.

General Anticancer Effect of OXT and Its Approaches

Oxytocin is a neuropeptide composed of nine amino acids, which is widely distributed throughout the body and plays an important role in various bodily functions (Yang et al., 2013). In addition to promoting breastfeeding and childbirth (Hatton and Wang, 2008), OXT can directly or indirectly inhibit tumorigenesis. For example, chronic exposure to social stress is common in humans, especially in nursing mothers (Murgatroyd et al., 2015) and can increase the risk of inflammation-related CRC (Peters et al., 2012; Antoni and Dhabhar, 2019). Intranasal application of OXT reduces maternal depression to relieve social stress and pulsatile pattern of OXT actions can directly suppress precancerous lesions of the mammary glands. The later effect is associated with suppression of oxidative stress-induced expressions of phosphorylated extracellular signal-regulated protein kinase 1/2 and cyclooxygenase-2, as shown in rats (Liu et al., 2016).

This anticancer effect is also associated with the immune regulatory functions of OXT. Intranasal OXT application to F1 rat dams was reported to increase serum interferon-γ level in F2 juvenile female offspring (Murgatroyd et al., 2016), which is associated with apoptosis of small-cell lung cancer (Zhou et al., 2006). It was also reported that peripheral use of OXT reduced stress-induced visceral hypersensitivity and activation of enteric glial reactivity (Xu et al., 2018), thereby increasing the defense of GI tract to inflammatory challenges. In the present study, we also found that OXT can reduce the expression of CCL-2, which helps to restore immune checkpoint blockade and increase T-cell activity to inhibit the development of CRCs (Chen et al., 2017). Nevertheless, there is still a need to collect direct evidence of the suppression effect of OXT from CRC *in vivo*; OXT can suppress carcinogenesis at multiple levels including the colon tissue as discussed below.

Protective Effects of OXT and OXTR Signaling in Colon Tissue

In association with the body's immune functions, OXT has been recognized to maintain immune surveillance, defense, and homeostasis through many approaches (Li et al., 2017). The insufficient OXT and dysfunctions of OXTR signaling are likely associated with varieties of immune lesions, including carcinogenesis (Hou et al., 2016; Adamo et al., 2018). Our present findings further support this view by presenting the reduced

expressions of OXT and OXTR in CAC tissues and by the suppressive effects of exogenous OXT on the expression of CRC metastasis-associated proteins, FAPα and CCL-2.

Colon OXT-secreting cells can influence CRC development through autocrine and paracrine functions. OXT and OXTR are widely expressed in human GI tract (Monstein et al., 2004; Ohlsson et al., 2006). They are mainly present in the nerve cell bodies and in the nerve fibers of the myenteric and submucosal ganglia (Ohlsson et al., 2006) in the jejunum, ileum, proximal colon, and distal colon (Yu et al., 2011). In addition to enteric neurons, the proximal colonic muscle strips (Wang et al., 2016) and crypt-villus enterocytes (Klein et al., 2013; Welch et al., 2014) also express OXTRs.

Unlike the inhibitory effect of the brain OXT on the feeding and mobility of the GI tract (Sabatier et al., 2013), direct effect of OXT on the GI tract is to increase its motility by causing smooth muscle contraction, as shown in the stomach (Qin et al., 2009) and the duodenum (Li et al., 2007). Thus, reduced OXT and OXTR signaling in the colon tissues likely reduce the movement of colon, which creates a favorable microenvironment for the accumulation of inflammatory agents and carcinogens, thereby facilitating CRC development.

Consistently, OXT can reduce necrotizing enterocolitis, a GI inflammatory disease of unknown etiology (Gross Margolis et al., 2017). In OXTR knockout mice, the intestinal villi and crypts were shorter, intestinal permeability to macromolecules was greater, and experimental colitis was more severe than wild-type mice (Welch et al., 2014). In the present study, we further identified that OXT-induced reduction of CCL-2 is also a manifestation of the anti-inflammatory effect of OXT in the GI system. Thus, the disruption of OXTR signaling in the GI tract can impair the immune defense function of OXT to carcinogenesis under the influence of oncogenic genetic and environmental factors.

Inhibitory Effects of OXT on CRC Migration

Oxytocin is involved in the inhibition of metastasis of many types of cancers. For example, OXT inhibits metastatic ovarian cancer by suppressing the matrix metallopeptidase-2 expression and vascular endothelial growth factor (Ji et al., 2018). OXT down-regulates the invasion of head and neck squamous cell carcinoma cells by up-regulation of early growth response-1 and the subsequent increase in p53, and phosphatase and tensin, and p21 expression (Kim et al., 2017). The present Matrigel invasion study also confirms that OXT significantly inhibits the migration of colon cancer cells, which is mediated by OXTR. They together strongly support the inhibitory role of OXTR signaling in metastatic cancers, including CAC.

Migration involves many signaling pathways, such as integrin αvβ6 (Peng et al., 2018), TGF-β (Tiwari et al., 2018), and guanylate cyclase C (Rappaport and Waldman, 2018) as well as FAPα and CCL-2. In the present study, we specifically investigated the participation of FAPα and its associated proteins. Clearly, FAPα is a target for OXT suppression of CAC cell migration, since OXT treatment significantly reduced

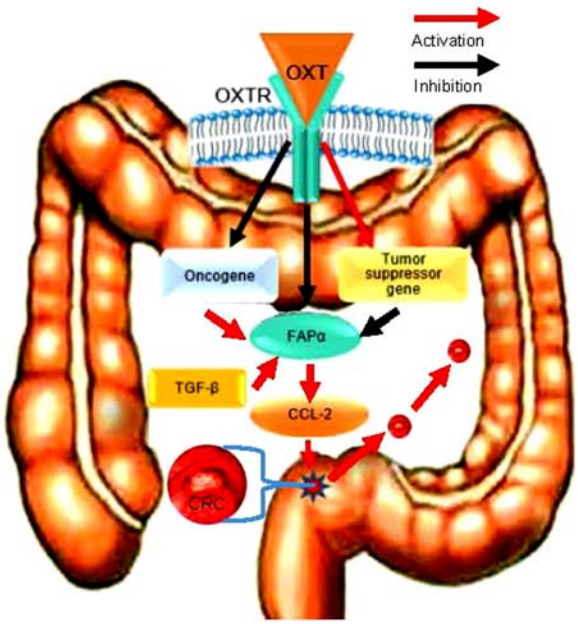

FIGURE 6 | Schematic diagram of the pathway for OXT inhibition of CRC metastasis. FAPα activity is under the facilitatory influence of TGF-β and the inhibitory influence of OXT; increased OXTR signaling can antagonize the effect of TGF-β and cause the inhibition of CCL-2 action, thereby suppressing FAPα-associated CRC cell migration/metastasis.

the expression of FAPα. Clearly, both CCL-2 and TGF-β are the downstream signals of FAPα (Henriksson et al., 2011; Meulendijks et al., 2016; Chen et al., 2017; Mohr et al., 2017), and OXT decreased CCL-2 expression but not TGF-β. Thus, the major downstream signal of OXTR-FAPα signaling is CCL-2 but not TGF-β. However, TGF-β could function as an upstream signal of the FAPα to influence CRC development independently. Noticeably, OXT suppression of CRC migration through the FAPα-CCL-2 signaling is dominant over the migration-promoting effect of TGF-β signaling as proved by our migration study. This finding is consistent with the anti-inflammatory effect of OXT and its possible function in curbing the migration of CAC cells, as previously studied (Wang, 2016). Thus, our study highlights the therapeutic value of suppression of CRC migration, at least for CAC.

CONCLUSION

Colorectal cancer development is associated with the reduction of OXTR signaling since OXT can suppress FAPα and CCL-2 expressions and their associated CAC migration via OXTR (**Figure 6**). Since OXT is a safe agent in clinical application and that the CRC is readily accessible than other GI cancers, it is possible to suppress CRC metastasis by direct application of OXT.

It is worth noting that our observations are limited to a well-differentiated CAC, and we cannot rule out the possibility of different expression patterns of OXT and OXTRs, as well as their role in other types of human CRC. In addition, prior to

conducting clinical trials of OXT treatment for CRCs, further observation of the anti-metastatic effects of OXT is required, particularly by *in vivo* approaches.

DATA AVAILABILITY STATEMENT

All datasets generated for this study are included in the article/**Supplementary Material**.

ETHICS STATEMENT

The study was approved by Shengjing Hospital of China Medical University. Ethical Approval Letter of Scientific Research (Chinese Original Translation). Ethical Document No. 2016PS255K. Research Project: Studies on the expressions of oxytocin and its receptor in colorectal cancer. Department of application: Department of Colorectal Surgery. Principal Investigator: Mingxing Ma. Contents Reviewed (1) Designation: Patient Consent Form and (2) Eligibility of the Researcher: Approaches of Sampling and others. Conclusion of Review: This project meets the requirements of ethical principles and performing this project is granted. Granter: Ethical Committee of China Medical University (Official Seal). Date of Approval: May 31, 2016. Valid for 4 years from the approval date.

AUTHOR CONTRIBUTIONS

MM and LL collected and analyzed the data. MM and HC wrote the first draft of the manuscript. HC and YF conceived the project.

FUNDING

This work was supported by the Natural Science Foundation of Liaoning Province, China (2019-ZD-0747) and Shengjing Hospital of China Medical University.

ACKNOWLEDGMENTS

We thank Yeping Ling, Yanwen Yao, Zenghui Xiong, and Jiahuan Tan (Department of Forensic Medicine, Harbin Medical University, Harbin, China) for technique assistance in the study.

SUPPLEMENTARY MATERIAL

The Supplementary Material for this article can be found online at: https://www.frontiersin.org/articles/10.3389/fnins.2019.01317/full#supplementary-material

REFERENCES

Adamo, S., Pigna, E., Lugara, R., Moresi, V., Coletti, D., and Bouche, M. (2018). Skeletal muscle: a significant novel neurohypophyseal hormone-secreting organ. *Front. Physiol.* 9:1885. doi: 10.3389/fphys.2018.01885

Andres, S. F., Williams, K. N., and Rustgi, A. K. (2018). The molecular basis of metastatic colorectal cancer. *Curr. Colorectal. Cancer Rep.* 14, 69–79. doi: 10.1007/s11888-018-0403-z

Antoni, M. H., and Dhabhar, F. S. (2019). The impact of psychosocial stress and stress management on immune responses in patients with cancer. *Cancer* 125, 1417–1431. doi: 10.1002/cncr.31943

Austin, H., Henley, S. J., King, J., Richardson, L. C., and Eheman, C. (2014). Changes in colorectal cancer incidence rates in young and older adults in the United States: what does it tell us about screening. *Cancer Causes Control* 25, 191–201. doi: 10.1007/s10552-013-0321-y

Carr, J. C., Sherman, S. K., Wang, D., Dahdaleh, F. S., Bellizzi, A. M., O'Dorisio, M. S., et al. (2013). Overexpression of membrane proteins in primary and metastatic gastrointestinal neuroendocrine tumors. *Ann. Surg. Oncol.* 20(Suppl. 3), S739–S746. doi: 10.1245/s10434-013-3318-6

Chen, L., Qiu, X., Wang, X., and He, J. (2017). FAP positive fibroblasts induce immune checkpoint blockade resistance in colorectal cancer via promoting immunosuppression. *Biochem. Biophys. Res. Commun.* 487, 8–14. doi: 10.1016/j.bbrc.2017.03.039

Delorme, P., and Garabedian, C. (2018). [Modalities of birth in case of uncomplicated preterm premature rupture of membranes: CNGOF Preterm Premature Rupture of Membranes Guidelines]. *Gynecol. Obstet. Fertil. Senol.* 46, 1068–1075. doi: 10.1016/j.gofs.2018.10.021

El-Shami, K., Oeffinger, K. C., Erb, N. L., Willis, A., Bretsch, J. K., Pratt-Chapman, M. L., et al. (2015). American cancer society colorectal cancer survivorship care guidelines. CA Cancer. *J. Clin.* 65, 428–455. doi: 10.3322/caac.21286

Gross Margolis, K., Vittorio, J., Talavera, M., Gluck, K., Li, Z., Iuga, A., et al. (2017). Enteric serotonin and oxytocin: endogenous regulation of severity in a murine model of necrotizing enterocolitis. *Am. J. Physiol. Gastrointest Liver Physiol.* 313, G386–G398. doi: 10.1152/ajpgi.00215.2017

Hatton, G. I., and Wang, Y. F. (2008). Neural mechanisms underlying the milk ejection burst and reflex. *Prog. Brain Res.* 170, 155–166. doi: 10.1016/S0079-6123(08)00414-7

Hawinkels, L. J., Paauwe, M., Verspaget, H. W., Wiercinska, E., van der Zon, J. M., van der Ploeg, K., et al. (2014). Interaction with colon cancer cells hyperactivates TGF-β signaling in cancer-associated fibroblasts. *Oncogene* 33, 97–107. doi: 10.1038/onc.2012.536

Henriksson, M. L., Edin, S., Dahlin, A. M., Oldenborg, P. A., Oberg, A., Van Guelpen, B., et al. (2011). Colorectal cancer cells activate adjacent fibroblasts resulting in FGF1/FGFR3 signaling and increased invasion. *Am. J. Pathol.* 178, 1387–1394. doi: 10.1016/j.ajpath.2010.12.008

Hou, D., Jin, F., Li, J., Lian, J., Liu, M., Liu, X., et al. (2016). Model Roles of the hypothalamo-Neurohypophysial System in Neuroscience Study. *Biochem. Pharmacol.* 5:211. doi: 10.4172/2167-0501.1000211

Imanieh, M. H., Bagheri, F., Alizadeh, A. M., and Ashkani-Esfahani, S. (2014). Oxytocin has therapeutic effects on cancer, a hypothesis. *Eur. J. Pharmacol.* 741, 112–123. doi: 10.1016/j.ejphar.2014.07.053

Ji, H., Liu, N., Yin, Y., Wang, X., Chen, X., Li, J., et al. (2018). Oxytocin inhibits ovarian cancer metastasis by repressing the expression of MMP-2 and VEGF. *J. Cancer* 9, 1379–1384. doi: 10.7150/jca.23769

Kim, J., Kang, S. M., Lee, H. J., Choi, S. Y., and Hong, S. H. (2017). Oxytocin inhibits head and neck squamous cell carcinoma cell migration by early growth response-1 upregulation. *Anticancer Drugs* 28, 613–622. doi: 10.1097/CAD.0000000000000501

Klein, B. Y., Tamir, H., Hirschberg, D. L., Glickstein, S. B., and Welch, M. G. (2013). Oxytocin modulates mTORC1 pathway in the gut. *Biochem. Biophys. Res. Commun.* 432, 466–471. doi: 10.1016/j.bbrc.2013.01.121

Li, L., Kong, X., Liu, H., and Liu, C. (2007). Systemic oxytocin and vasopressin excite gastrointestinal motility through oxytocin receptor in rabbits. *Neurogastroenterol. Motil.* 19, 839–844. doi: 10.1111/j.1365-2982.2007.00953.x

Li, T., Wang, P., Wang, S. C., and Wang, Y. F. (2017). Approaches mediating oxytocin regulation of the immune system. *Front. Immunol.* 7:693. doi: 10.3389/fimmu.2016.00693

Liu, X., Jia, S., Zhang, Y., and Wang, Y.-F. (2016). Pulsatile but not tonic secretion of oxytocin plays the role of anti-precancerous lesions of the mammary glands in rat dams separated from the pups during lactation. *Math. J. Neuro* 1:002.

Meulendijks, D., Lassen, U. N., Siu, L. L., Huitema, A. D., Karanikas, V., Mau-Sorensen, M., et al. (2016). Exposure and tumor Fn14 expression as determinants of pharmacodynamics of the anti-TWEAK monoclonal antibody RG7212 in Patients with Fn14-positive solid tumors. *Clin. Cancer Res.* 22, 858–867. doi: 10.1158/1078-0432.CCR-15-1506

Mohr, A. M., Gould, J. J., Kubik, J. L., Talmon, G. A., Casey, C. A., Thomas, P., et al. (2017). Enhanced colorectal cancer metastases in the alcohol-injured liver. *Clin. Exp. Metastasis.* 34, 171–184. doi: 10.1007/s10585-017-9838-x

Monstein, H. J., Grahn, N., Truedsson, M., and Ohlsson, B. (2004). Oxytocin and oxytocin-receptor mRNA expression in the human gastrointestinal tract: a polymerase chain reaction study. *Regul. Pept.* 119, 39–44. doi: 10.1016/j.regpep.2003.12.017

Murgatroyd, C. A., Hicks-Nelson, A., Fink, A., Beamer, G., Gurel, K., Elnady, F., et al. (2016). Effects of chronic social stress and maternal intranasal oxytocin and vasopressin on offspring interferon-gamma and behavior. *Front. Endocrinol.* 7:155. doi: 10.3389/fendo.2016.00155

Murgatroyd, C. A., Pena, C. J., Podda, G., Nestler, E. J., and Nephew, B. C. (2015). Early life social stress induced changes in depression and anxiety associated neural pathways which are correlated with impaired maternal care. *Neuropeptides* 52, 103–111. doi: 10.1016/j.npep.2015.05.002

Ohlsson, B., Truedsson, M., Djerf, P., and Sundler, F. (2006). Oxytocin is expressed throughout the human gastrointestinal tract. *Regul. Pept.* 135, 7–11. doi: 10.1016/j.regpep.2006.03.008

Peng, C., Zou, X., Xia, W., Gao, H., Li, Z., Liu, N., et al. (2018). Integrin alphavbeta6 plays an Bi-directional regulation role between colon cancer cells and cancer-associated fibroblasts. *Biosci. Rep.* 38:BSR20180243. doi: 10.1042/BSR20180243

Peters, S., Grunwald, N., Rummele, P., Endlicher, E., Lechner, A., Neumann, I. D., et al. (2012). Chronic psychosocial stress increases the risk for inflammation-related colon carcinogenesis in male mice. *Stress* 15, 403–415. doi: 10.3109/10253890.2011.631232

Petersson, M. (2008). Opposite effects of oxytocin on proliferation of osteosarcoma cell lines. *Regul. Pept.* 150, 50–54. doi: 10.1016/j.regpep.2008.02.007

Qin, J., Feng, M., Wang, C., Ye, Y., Wang, P. S., and Liu, C. (2009). Oxytocin receptor expressed on the smooth muscle mediates the excitatory effect of oxytocin on gastric motility in rats. *Neurogastroenterol. Motil.* 21, 430–438. doi: 10.1111/j.1365-2982.2009.01282.x

Rappaport, J. A., and Waldman, S. A. (2018). The guanylate cyclase C-cGMP signaling axis opposes intestinal epithelial injury and neoplasia. *Front. Oncol.* 8:299. doi: 10.3389/fonc.2018.00299

Sabatier, N., Leng, G., and Menzies, J. (2013). Oxytocin, feeding, and satiety. *Front. Endocrinol.* 4:35. doi: 10.3389/fendo.2013.00035

Sherman, S. K., Carr, J. C., Wang, D., O'Dorisio, M. S., O'Dorisio, T. M., and Howe, J. R. (2013). Gastric inhibitory polypeptide receptor (GIPR) is a promising target for imaging and therapy in neuroendocrine tumors. *Surgery* 154, 1206–1213. doi: 10.1016/j.surg.2013.04.052

Shin, K. J., Lee, Y. J., Yang, Y. R., Park, S., Suh, P. G., Follo, M. Y., et al. (2016). Molecular mechanisms underlying psychological stress and cancer. *Curr. Pharm. Des.* 22, 2389–2402. doi: 10.2174/1381612822666160226144025

Tiwari, A., Saraf, S., Verma, A., Panda, P. K., and Jain, S. K. (2018). Novel targeting approaches and signaling pathways of colorectal cancer: An insight. *World J. Gastroenterol.* 24, 4428–4435. doi: 10.3748/wjg.v24.i39.4428

Tsoi, K. K. F., Hirai, H. W., Chan, F. C. H., Griffiths, S., and Sung, J. J. Y. (2017). Predicted increases in incidence of colorectal cancer in developed and developing regions, in association with ageing populations. *Clin. Gastroenterol. Hepatol.* 15:892-900.e4. doi: 10.1016/j.cgh.2016.09.155

Wang, R., Guo, L. Y., Suo, M. Y., Sun, Y., Wu, J. Y., Zhang, X. Y., et al. (2016). Role of the nitrergic pathway in motor effects of oxytocin in rat proximal colon. *Neurogastroenterol. Motil.* 28, 1815–1823. doi: 10.1111/nmo.12883

Wang, Y.-F. (2016). Center role of the oxytocin-secreting system in neuroendocrine-immune network revisited. *J. Clin. Exp. Neuroimmunol.* 1:102. doi: 10.4172/jceni.1000102

Wang, Y. F., and Hatton, G. I. (2006). Mechanisms underlying oxytocin-induced excitation of supraoptic neurons: prostaglandin mediation of actin polymerization. *J. Neurophysiol.* 95, 3933–3947. doi: 10.1152/jn.01267.2005

Wang, Y. F., Ponzio, T. A., and Hatton, G. I. (2006). Autofeedback effects of progressively rising oxytocin concentrations on supraoptic oxytocin neuronal activity in slices from lactating rats. *Am. J. Physiol. Regul. Integr. Comp. Physiol.* 290, R1191–R1198.

Welch, M. G., Margolis, K. G., Li, Z., and Gershon, M. D. (2014). Oxytocin regulates gastrointestinal motility, inflammation, macromolecular permeability, and mucosal maintenance in mice. *Am. J. Physiol. Gastrointest. Liver Physiol.* 307, G848–G862. doi: 10.1152/ajpgi.00176.2014

Witold, K., Anna, K., Maciej, T., and Jakub, J. (2018). Adenomas - Genetic factors in colorectal cancer prevention. *Rep. Pract. Oncol. Radiother.* 23, 75–83. doi: 10.1016/j.rpor.2017.12.003

Xu, S., Qin, B., Shi, A., Zhao, J., Guo, X., and Dong, L. (2018). Oxytocin inhibited stress induced visceral hypersensitivity, enteric glial cells activation, and release of proinflammatory cytokines in maternal separated rats. *Eur. J. Pharmacol.* 818, 578–584. doi: 10.1016/j.ejphar.2017.11.018

Yang, H. P., Wang, L., Han, L., and Wang, S. C. (2013). Nonsocial functions of hypothalamic oxytocin. *ISRN Neurosci.* 2013:179272. doi: 10.1155/2013/179272

You, Q., Wang, X. S., Fu, S. B., and Jin, X. M. (2011). Downregulated expression of inhibitor of growth 4 (ING4) in advanced colorectal cancers: a non-randomized experimental study. *Pathol. Oncol. Res.* 17, 473–477. doi: 10.1007/s12253-010-9301-7

Yu, Q., Ji, R., Gao, X., Fu, J., Guo, W., Song, X., et al. (2011). Oxytocin is expressed by both intrinsic sensory and secretomotor neurons in the enteric nervous system of guinea pig. *Cell Tissue Res.* 344, 227–237. doi: 10.1007/s00441-011-1155-0

Zhou, J., Chen, J., Zhong, R., Mokotoff, M., Shultz, L. D., and Ball, E. D. (2006). Targeting gastrin-releasing peptide receptors on small cell lung cancer cells with a bispecific molecule that activates polyclonal T lymphocytes. *Clin. Cancer Res.* 12(7 Pt 1), 2224–2231. doi: 10.1158/1078-0432.ccr-05-1524

Conflict of Interest: The authors declare that the research was conducted in the absence of any commercial or financial relationships that could be construed as a potential conflict of interest.

frontiers in Neuroscience

ORIGINAL RESEARCH
published: 17 December 2019
doi: 10.3389/fnins.2019.01351

Activation of the G Protein-Coupled Estrogen Receptor Elicits Store Calcium Release and Phosphorylation of the Mu-Opioid Receptors in the Human Neuroblastoma SH-SY5Y Cells

Xiaowei Ding[1,2], Ting Gao[2], Po Gao[2], Youqiang Meng[3], Yi Zheng[1], Li Dong[2], Ping Luo[2], Guohua Zhang[2], Xueyin Shi[1] and Weifang Rong[1,2]**

[1] Department of Anesthesiology, Xin Hua Hospital, School of Medicine, Shanghai Jiao Tong University, Shanghai, China, [2] Department of Anatomy and Physiology, Faculty of Basic Medical Sciences, School of Medicine, Shanghai Jiao Tong University, Shanghai, China, [3] Department of Neurosurgery, Xin Hua Hospital Chongming Branch, School of Medicine, Shanghai Jiao Tong University, Shanghai, China

OPEN ACCESS

Edited by:
Xue Qun Chen,
Zhejiang University, China

Reviewed by:
Liu Chuanyong,
Shandong University, China
Xiao Yu,
Shandong University, China

***Correspondence:**
Xueyin Shi
shixueyin1128@163.com
Weifang Rong
weifangrong@shsmu.edu.cn;
weifangrong@hotmail.com

Specialty section:
This article was submitted to Neuroendocrine Science, a section of the journal Frontiers in Neuroscience

Received: 09 May 2019
Accepted: 02 December 2019
Published: 17 December 2019

Citation:
Ding X, Gao T, Gao P, Meng Y, Zheng Y, Dong L, Luo P, Zhang G, Shi X and Rong W (2019) Activation of the G Protein-Coupled Estrogen Receptor Elicits Store Calcium Release and Phosphorylation of the Mu-Opioid Receptors in the Human Neuroblastoma SH-SY5Y Cells. Front. Neurosci. 13:1351. doi: 10.3389/fnins.2019.01351

Estrogens exert extensive influences on the nervous system besides their well-known roles in regulation of reproduction and metabolism. Estrogens act via the nuclear receptor ERα and ERβ to regulate gene transcription (classical genomic effects). In addition, estrogens are also known to cause rapid non-genomic effects on neuronal functions including inducing fast changes in cytosolic calcium level and rapidly desensitizing the μ type opioid receptor (MOR). The receptors responsible for the rapid actions of estrogens remain uncertain, but recent evidence points to the G protein-coupled estrogen receptor (GPER), which has been shown to be expressed widely in the nervous system. In the current study, we test the hypothesis that activation of GPER may mediate rapid calcium signaling, which may promote phosphorylation of MOR through the calcium-dependent protein kinases in neuronal cells. By qPCR and immunocytochemistry, we found that the human neuroblastoma SH-SY5Y cells endogenously express GPER and MOR. Activation of GPER by 17β-estradiol (E2) and G-1 (GPER selective agonist) evoked a rapid calcium rise in a concentration-dependent manner, which was due to store release rather than calcium entry. The GPER antagonist G15, the PLC inhibitor U73122 and the IP3 receptor inhibitor 2-APB each virtually abolished the calcium responses to E2 or G-1. Activation of GPER stimulated translocation of PKC isoforms (α and ε) to the plasma membrane, which led to MOR phosphorylation. Additionally, E2 and G-1 stimulated c-Fos expression in SH-SY5Y cells in a PLC/IP3-dependent manner. In conclusion, the present study has revealed a novel GPER-mediated estrogenic signaling in neuroblastoma cells in which activation of GPER

is followed by rapid calcium mobilization, PKC activation and MOR phosphorylation. GPER-mediated rapid calcium signal may also be transmitted to the nucleus to impact on gene transcription. Such signaling cascade may play important roles in the regulation of opioid signaling in the brain.

Keywords: estrogens, G protein-coupled estrogen receptor, calcium mobilization, μ opioid receptor, protein kinase C, protein phosphorylation

INTRODUCTION

Estrogens exert an extraordinarily wide spectrum of actions in the human body. Besides the well-known roles in regulation of reproduction and metabolism, estrogens also exert multifaceted influences on neuronal development and neuronal functions (Jensen and Desombre, 1973). Traditionally, estrogens are known to act by interacting with two nuclear receptors, ERα and ERβ, which function as ligand-activated transcription factors to regulate gene transcription (Jensen and Desombre, 1973; Kuiper et al., 1996; Mosselman et al., 1996; Paech et al., 1997). In addition to this slow genomic mode of actions which typically develop with latencies ranging from an hour to several days, estrogens also directly alter neuronal electrical activity in various brain regions within seconds to minutes, which may underlie the fast effects of estrogens on brain functions such as female reproductive behavior, memory and cognition, neuroprotection and pain (Woolley, 1999; Kelly and Ronnekleiv, 2009; Ogawa et al., 2018).

Although the existence of the non-genomic estrogenic actions is now widely accepted, the mechanisms (the receptors and the signaling cascades) that mediate such effects remain uncertain and much debated. A number of candidate receptors have been proposed, including the classical ERα that may alternatively be bound to the plasma membrane, several ERα variants (ERα-52, ERα-46, and ERα-36), membrane-associated ER-X, the $G\alpha_q$-coupled mERs and more recently the G protein-coupled estrogen receptor (GPER, also known as GPR30) (Rainville et al., 2015).

G protein-coupled estrogen receptor reportedly is enriched in discrete regions of the nervous system, including the hypothalamus, the hippocampus, the cerebral cortex, the dorsal horn of spinal cord and the primary afferent neurons, therefore is ideally positioned to mediate the rapid non-genomic estrogenic actions on reproductive behavior, memory and cognition and pain (Shughrue et al., 1997, 2000; Brailoiu et al., 2007; Kuhn et al., 2008; Dun et al., 2009; Hazell et al., 2009; Takanami et al., 2010; Lu et al., 2013). Indeed, numerous recent studies underscore the role of GPER in mediating the rapid estrogenic effects in the nervous system. For examples, intracerebroventricular infusion of the GPER agonist G-1 rapidly facilitates the female sexual behavior in estradiol-primed rats (Long et al., 2014, 2017). Activation of GPER in the dorsal hippocampus enhances social and object recognition and memory in the rat within 40 min (Paletta et al., 2018). In spinal cord slice *in vitro*, G-1 directly depolarizes superficial dorsal horn neurons; *in vivo*, intrathecal application of G-1 results in pain-related behaviors characterized by caudally directed scratching, biting and licking (Deliu et al., 2012).

Concerning the signaling cascades of the non-genomic effects, it occurs that estrogens may mediate rapid calcium signaling in neuronal and non-neuronal cells by modulating Ca^{2+} influx or inducing store Ca^{2+} release (Picotto et al., 1999; Rubio-Gayosso et al., 2000; Huang and Jan, 2001; Chen et al., 2002; Kuo et al., 2010; Petrovic et al., 2011). Thus, 17β−estradiol (E2) induces rapid Ca^{2+} influx in hippocampal neurons through activation of L-type Ca^{2+} channels, which probably mediates estrogen-induced neuroprotection (Wu et al., 2005, 2011; Zhao et al., 2005). E2 was also found to induce rapid Ca^{2+} release from intracellular Ca^{2+} stores in hypothalamic astrocytes and in embryonic midbrain dopaminergic neurons (Beyer and Raab, 1998; Kuo et al., 2010). In most cases, the receptor(s) responsible for the rapid Ca^{2+} rise was not clear, but recent evidence indicate that GPER may mediate estrogen-induced Ca^{2+} signaling. Revankar et al. (2005) expressed GPER as a fusion protein with green fluorescent protein (GFP) in COS7 cell (monkey kidney fibroblast) and found that activation of GPER resulted in intracellular Ca^{2+} mobilization and synthesis of phosphatidylinositol 3,4,5-trisphosphate in the nucleus. Incidentally, GPER is enriched in the hypothalamic-pituitary axis and the hippocampal formation (Paletta et al., 2018), where E2 has been reported to elicit cytosolic Ca^{2+} changes. Nevertheless, whether GPER mediates rapid Ca^{2+} signaling in neuronal cells is still uncertain.

Intracellular Ca^{2+} as a second messenger may activate protein kinases such as PKC and PKA to phosphorylate downstream effector proteins, which plays fundamental roles in neuronal signaling. Interestingly, E2 was found to rapidly attenuate the ability of mu-opioids to hyperpolarize hypothalamic neurons by uncoupling the μ-opioid receptors (MOR) from activating G protein-regulated inward rectifying potassium (GIRK) channels (Lagrange et al., 1997). Similarly, E2 uncouples other Gi/o-GPCRs, sepcifically $GABA_B$ and opioid receptor-like (ORL)-1, from activating GIRK channels and the effect was dependent upon activation of PLC, PKA, and PKC (Conde et al., 2016). Therefore, estrogens appear to mediate a Ca^{2+}-dependent phosphorylation and desensitization of Gi/o-coupled GPCRs through activating PKC and PKA. Whether GPER can initiate such non-genomic estrogenic signaling cascades remains to be determined.

The current study aims to test the hypothesis that GPER may mediate rapid Ca^{2+} signaling and subsequent Ca^{2+}-dependent phosphorylation of MOR through activation of PKC in the human neuroblastoma SH-SY5Y cell line. Indeed, we found that SH-SY5Y cells endogenously express GPER and

MOR and activation of GPER rapidly stimulates PLC/IP3-dependent store Ca^{2+} release with subsequent PKC activation and MOR phosphorylation.

MATERIALS AND METHODS

Chemicals

G protein-coupled estrogen receptor agonist G-1 and GPER antagonist G-15 were purchased from Cayman Chemical Company (Ann Arbor, MI, United States). The pan-PKC inhibitor Ro 31-8820 was bought from ApexBio Technology Company (Houston, TX, United States). 17β-estradiol (E2) and other reagents were purchased from Sigma-Aldrich (St. Louis, MO, United States) unless otherwise mentioned.

Cell Culture

The human neuroblastoma cell line, SH-SY5Y, was purchased from the Cell Repository of Chinese Academy of Sciences (Shanghai, China). The murine neuroblastoma Neuro-2a (N2A) cells (a wild type line and N2A cells stably expressing human influenza virus HA, YPYDVPDYA, epitope-tagged MOR) were provided by Dr. Yu Qiu (Shanghai Jiao Tong University School of Medicine). Cells were cultured in Dulbecco Modified Eagle Medium (DMEM), supplemented with 10% (v/v) fetal bovine serum (FBS), 100 units/ml penicillin, 100 μg/ml streptomycin, 0.11 g/L sodium pyruvate and 2 mM glutamine. 250 μg/ml G418 was added into the medium for Neuro-2a cell line stably expressing human MOR (N2AMT). Cells were incubated at 37℃ in a humidified atmosphere containing 5% CO_2.

Western Blot Analysis

Cells cultured to 80% confluence were collected and placed in RIPA buffer containing protease inhibitors and phosphatase inhibitors to extract total proteins. Protein concentration was determined by BCA assay (Pierce, Rackford, IL, United States). We used the Biotin-Avidin-System to extract plasma membrane proteins. Briefly, SH-SY5Y cells were washed in phosphate-buffered saline (PBS) and subsequently incubated with Sulfo-NHS-LC-biotin (250 μg/ml in PBS) for 30 min and then with 10 mM glycine counteracted superfluous biotin for 20 min at 4℃. After extraction of total protein, NeutrAvidin Agarose Beads (Thermo Scientific, CN, United States) were added to the whole-cell lysates and incubated on rotating mixer for 3 h at 4℃. The mixture was centrifuged at 10,000 *g* for 30 min at 4°C. Subsequently, the beads were washed for five times and the plasma membrane proteins were eluted and denatured by 2 × SDS-PAGE sample loading buffer at 100℃ for 5 min. 25 μg of total proteins or 30 μl sample loading buffer containing plasma membrane proteins were electrophoresed on 4–8% Tris-glycine ready gels (Bio-rad, Hercules, CA, United States). The separated proteins were transferred from the gel to the surface of nitrocellulose membranes (Bio-rad). The membranes were blocked with 5% fat-free dry milk or 5% BSA (for detection of phosphorylated MOR, PKCα, Na^+-K^+-ATPase) in Tris-buffered saline (TBS) containing 0.1% Tween-20 for 2 h. Subsequently, the membranes were incubated with primary antibodies for 18 h at 4°C: rabbit GPER (1:1000, Abcam, Cat# ab39742, RRID:AB_1141090), rabbit anti-pMOR (1:1000, Cell Signaling Technology, Cat# 3451, RRID:AB_331619), rabbit anti-MOR (1:500, Novus, Cat# NBP1-31180, RRID:AB_2251717), rabbit anti-PKCα (1:1000, Cell Signaling Technology, Cat# 2056, RRID:AB_2284227), mouse anti-PKCε (1:1000, BD Biosciences, Cat# 610085, RRID:AB_397492), rabbit anti-Na^+-K^+-ATPase (1:3000, Abcam, Cat# ab76020, RRID:AB_1310695) and mouse anti-β-actin (1:2000, Bioworld Technology, BS6007M). Bound primary antibodies were detected with HRP-conjugated anti-rabbit (1:3000, Bio-Rad, Cat# 170-6515, RRID:AB_11125142) or anti-mouse (1:3000, Bio-Rad, Cat# 170-6516, RRID:AB_11125547) secondary antibody. Immunoreactive bands were visualized using enhanced chemiluminescence (Thermo, Indianapolis, IN, United States), and digital imaging was captured with an Image Quant LAS 4000 mini (GE Healthcare, Life Science). The density of specific bands was analyzed using NIH ImageJ software and was normalized against the loading controls (β-actin, GAPDH or Na^+-K^+-ATPase).

Immunofluorescence Staining

SH-SY5Y cells were seeded on glass coverslips and cultured for 24 h and fixed with 4% paraformaldehyde for 15 min. After washing with PBS, the cells were first incubated with 50 mM PBS containing 10% normal goat serum and 0.5% TritonX-100 at room temperature for 2 h to block non-specific binding and this was followed by incubation with rabbit anti-GPER (1:500, Abcam, Cat# ab39742, RRID:AB_1141090) or rabbit anti-MOR (1:500, Novus, Cat# NBP1-31180, RRID:AB_2251717) at 4°C overnight. The cells were rinsed with PBS for four times and were then incubated with goat anti-rabbit Alexa fluor 568 (1:1000; Molecular Probes-Invitrogen, Cat# A-11077, RRID:AB_141874) or 488 (1:1000; Molecular Probes-Invitrogen, Cat# R37116, RRID:AB_2556544) secondary antibody at room temperature for 1.5 h. GPER or MOR were counter-stained with a nuclear marker DAPI (1: 1000, Thermo Fisher Scientific, Cat# PA5-62248, RRID:AB_2645277) at room temperature for 10 min. The coverslips were mounted on glass slides and the cells were viewed under the fluorescent microscope (Leica DM2500, Leica Microsystems Limited).

Real-Time Reverse Transcription-Polymerase Chain Reaction (RT-PCR)

Total RNA of SH-SY5Y and Neuro-2a cells was extracted with Trizol (Invitrogen, Shanghai, China) according to the manufacturer's instructions and reversely transcribed into cDNA using oligo-dT primers. Real-time quantitative PCR was then performed using SYBR Green (Qiagen, Shanghai, China) as the reporter dye. All cDNA samples were analyzed in duplicate. The relative level of target mRNA was calculated by the method of $2^{-\Delta\Delta Ct}$ with GAPDH as the loading control. The primer sets for real-time PCR are as follows:

GPER (human): Forward 5′-TCACGGGCCACATTG TCAACCTC-3′ and Reverse 5′-GCTGAACCTCACATC CGACTGCTC-3′;

GAPDH (human): Forward 5′-GGAGCGAGATCCC TCCAAAAT-3′ and Reverse 5′-GGCTGTTGTCATACTTC TCATGG-3′;

GPER (mouse): Forward 5′-CCTCTGCTACTCCCT CATCG-3′ and Reverse 5′-ACTATGTGGCCTGTC AAGGG-3′;

GAPDH (mouse): Forward 5′-TGTCTTCACCACCAT GGAGA-3′ and Reverse 5′-CGGCCATCACGCCAC AGCTT-3′.

Calcium Imaging

Cells were incubated with 1 μM Fluo-4-AM (Molecular Probes-Invitrogen) and 0.01% pluronic (Sigma-Aldrich) in the extracellular solution (NaCl 136 mM, KCl 5.4 mM, $MgCl_2$ 1 mM, $CaCl_2$ 1.8 mM, HEPES 10 mM, Glucose 10 mM, and NaH_2PO_4 0.33 mM, pH7.4, osmotic pressure 300 mOsm/L, $MgCl_2$ replaced $CaCl_2$ for calcium free solution) at 25℃ for 1 h. The cells were continuously superfused with the extracellular solution and imaged using an inverted microscope (Leca DMI4000B). Drugs (or vehicle control) were applied through a micro-perfusion tube positioned to the vicinity of the cells in the field of view. Fluorescent signal was excited at 510 nm and acquired at 580 nm, and taken every 3 s through a CCD camera. The signal was monitored online and analyzed offline, using Leica AF6000 software (Leica). The fluorescent traces were calculated as:

$$\%\ \text{change in fluorescence} = \frac{\text{F-F0}}{\text{F0}} \times 100$$

(F0: the baseline fluorescence of cells before treatments, F: the fluorescence of cells with drugs treatments).

Statistical Analysis

Data are expressed as mean ± SEM. Statistical analysis was performed using GraphPad Prism 6 (GraphPad Software Inc., United States). Differences between two groups were analyzed by unpaired or paired *t*-test (two-tailed). Multiple comparisons were made by one-way analysis of variance (ANOVA) with Tukey's *post hoc* testing. Differences were considered statistically significant when a *P* value was less than 0.05.

RESULTS

SH-SY5Y Cells Endogenously Express GPER and MOR

G protein-coupled estrogen receptor mRNA expression in SH-SY5Y, wild type N2A and N2A cell line stably expressing human MOR (N2AMT) was analyzed through RT-PCR. GPER mRNA appeared to be more abundant in SH-SY5Y cells than in N2A and N2AMT cells (**Figure 1A**). Immunofluorescent staining confirmed SH-SY5Y cells endogenously express GPER and MOR (**Figure 1B**). GPER immunostaining was located at peri-nuclear sites. Western blot analysis detected GPER in total but not in cytoplasmic membrane protein samples (**Figure 1C**). Therefore, the endogenously expressed GPER in SH-SY5Y cells was located on certain peri-nuclear organelles, but not on the cytoplasmic membrane.

GPER Mediates Rapid Intracellular Calcium Rise in SH-SY5Y Cells

To test the hypothesis that activation of GPER mediates rapid Ca^{2+} signaling, SH-SY5Y and the Neuro-2a cells were exposed to either 17β-estradiol (E2) or G-1, the latter being a GPER selective agonist that does not bind ERα or ERβ (Bologa et al., 2006). Brief exposure (30 s) of SH-SY5Y cells to increasing concentration of E2 or G-1 (0.01–10 μM) both produced fast and concentration-dependent increases in cytosolic Ca^{2+} levels (**Figures 1D–F**). Acetylcholine (ACh) was a positive control. Consistent with the intracellular localization of GPER in this cell line, the cell impermeable BSA-conjugated E2 (E2-BSA, 1 μM) was not effective (**Figure 1J**). In addition, the GPER selective antagonist G15 (Dennis et al., 2009) (3 μM) almost completely blocked the Ca^{2+} responses to E2 and G-1 (G15 + E2: 24.43 ± 3.10% vs. E2: 207.0 ± 20.70%, $P < 0.001$, $n = 78$ cells; G15 + G-1: 18.59 ± 2.79% vs. G-1: 201.0 ± 19.74%, $P < 0.001$, $n = 56$ cells, **Figures 1G–I**). In contrast to the SH-SY5Y cells, Neuro-2a cells did not respond to E2 or G-1 (1 μM) with a Ca^{2+} rise, consistent with the low GPER mRNA expression in this cell line (**Figure 1K**). It was noticed that Neuro-2a cells responded to ATP (100 μM) with a rapid Ca^{2+} rise but not to ACh. These results support the hypothesis that activation of GPER by E2 may mediate rapid Ca^{2+} signaling in neuroblastoma cells.

GPER-Mediated Calcium Rise in SH-SY5Y Cells Is Due to Store Calcium Release

We next investigated whether GPER-mediated Ca^{2+} rise is due to Ca^{2+} influx or store Ca^{2+} release. In the Ca^{2+}-free extracellular solution, E2 (1 μM) and G-1(1 μM) both still elicited rapid increases in cytosolic Ca^{2+} with similar magnitudes as seen in the regular Ca^{2+}-containing solution (**Figures 2A–C**) (E2 Ca^{2+}-free: 154.1 ± 11.77%, $n = 55$ cells vs. E2 Ca^{2+}-containing: 174.5 ± 20.09%, $n = 60$ cells, $P > 0.05$; G-1 Ca^{2+}-free: 149.8 ± 8.40%, $n = 55$ cells vs. G-1 Ca^{2+}-containing: 176.5 ± 14.34%, $n = 62$ cells, $P > 0.05$, **Figure 2G**), suggesting that the GPER agonists evoked store Ca^{2+} release rather than Ca^{2+} influx. In support, the broad-spectrum voltage-dependent Ca^{2+} channel blocker $CdCl_2$ (200 μM) failed to block the increase in $[Ca^{2+}]_i$ elicited by E2 or G-1 (**Figures 2D,E**) (E2 + $CdCl_2$: 56.24 ± 9.51% vs. E2: 53.38 ± 10.40%, $n = 41$ cells, $P > 0.05$; G-1 + $CdCl_2$: 114.25 ± 14.50% vs. G-1: 93.66 ± 16.06%, $n = 28$ cells, $P > 0.05$, **Figure 2H**), whereas depletion of store Ca^{2+} with thapsigargin (1 μM, 5 min) virtually prevented E2 or G-1 from inducing a Ca^{2+} rise (**Figure 2F**). Furthermore, treatment of SH-SY5Y cells with the PLC inhibitor U73122 (3 μM) completely blocked the rapid Ca^{2+} rise in response to E2 or G-1 (**Figures 2A,B**, **3A–C**). Analogously, E2 or G-1-induced Ca^{2+} rise was abolished in the presence of 2-APB (3 μM), an

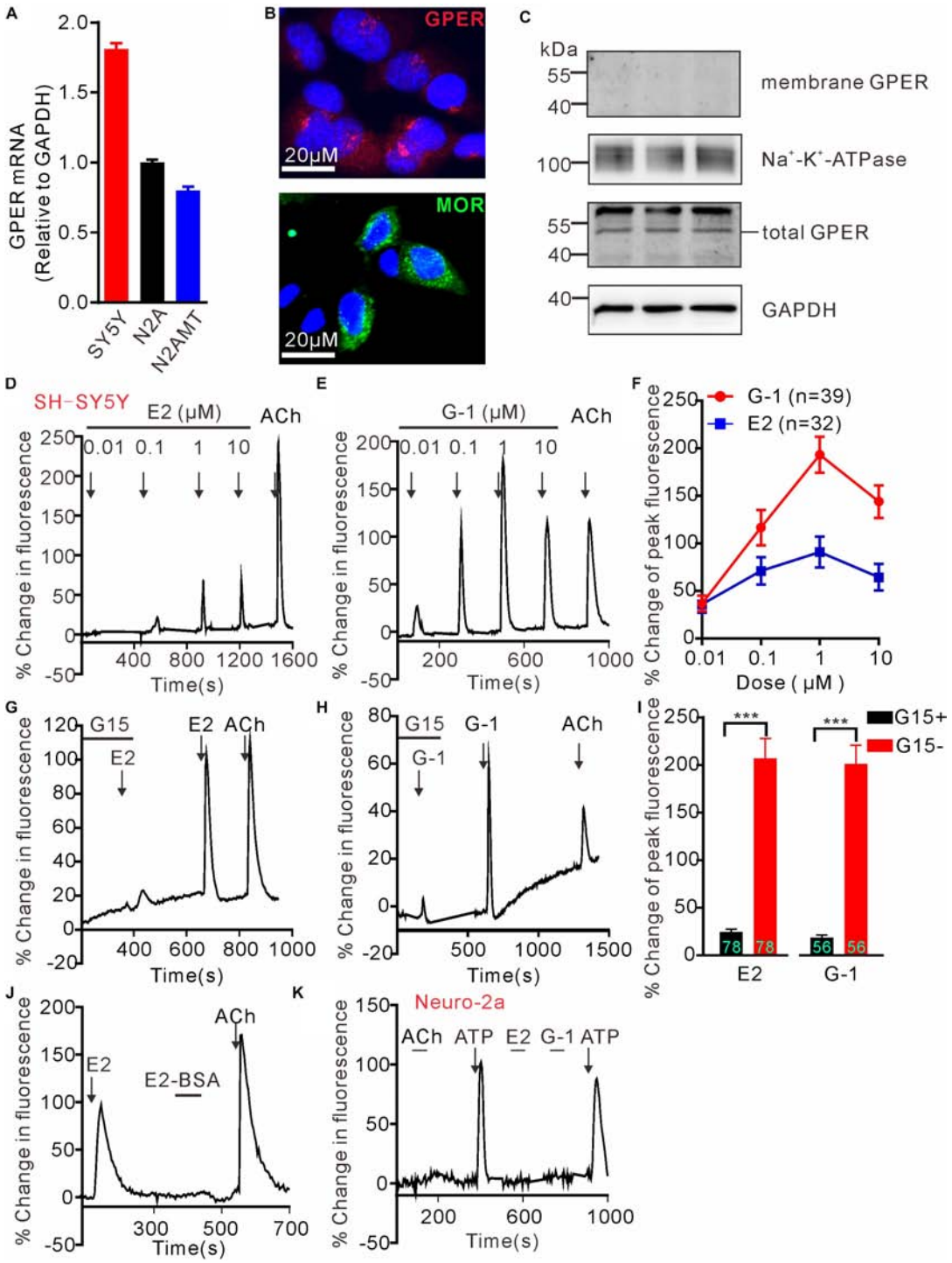

FIGURE 1 | G protein-coupled estrogen receptor mediates calcium rise in SH-SY5Y cells. **(A)** RT-PCR analysis shows relatively higher expression of GPER mRNA in SH-SY5Y cells than in Neuro-2a (N2A) cells. N2AMT is a line of Neuro-2a stably expressing human μ type opioid receptor (hMOR). **(B)** Immunofluorescent staining for GPER and MOR in SH-SY5Y cells. GPER immunofluorescence is located at certain perinuclear organelle. **(C)** Western blot detection of GPER in cytoplasmic membrane fraction vs. total protein. Whereas GPER immunoreactivity is abundant in the total protein samples, it could not be detected within the cytoplasmic membrane protein sample. **(D–J)** Fluo-4-based imaging of cytosolic [Ca^{2+}] transients in response to GPER agonists 17-β estradiol (E2) and G-1. Note E2 and G-1 both caused concentration-dependent rapid Ca^{2+} rise, which was prevented by GPER antagonist G15. The membrane impermeable BSA-conjugated E2 was unable to evoke a rapid Ca^{2+} rise. **(K)** Neither E2 nor G-1 was able to cause a Ca^{2+} rise in N2A cells. The example traces **(D**,**E**,**G**,**H**,**J**,**K)** are the average percentage change in fluorescence of 7–26 cells in one visual field. Values in bar graphs **(F**,**I)** are averaged peak percentage changes of 32∼78 cells from three to four independent tests. Note that the responses to the lowest concentration (0.01 μM) of E2 or G-1 in separate experiments were quite variable (e.g., **D,E**), but on average the peak response to E2 or G-1 (0.01 μM) were similar **(F)**. ***$P < 0.001$, paired *t*-test.

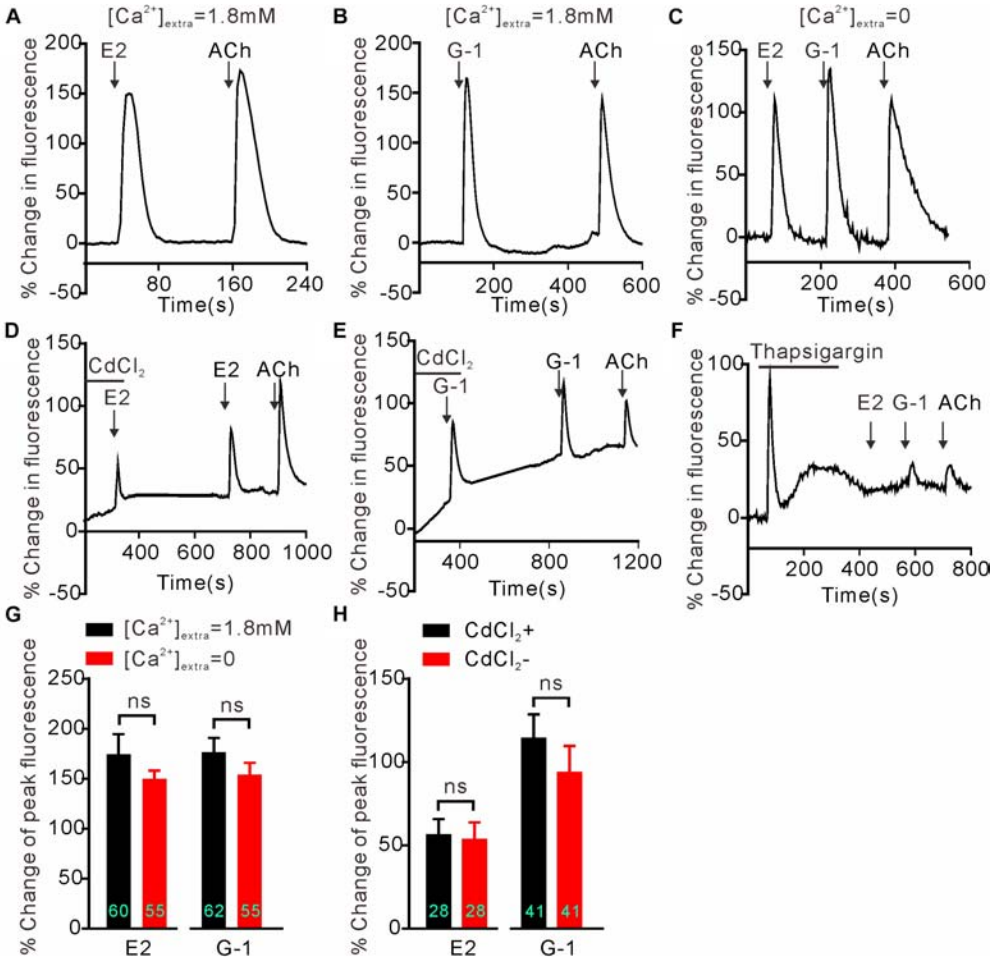

FIGURE 2 | Intracellular calcium rise elicited by E2 or G-1 was independent of calcium influx in SH-SY5Y cells. **(A–C,G)** E2 and G-1 both caused rapid Ca^{2+} rise with or without extracellular Ca^{2+}. **(D,E,H)** The non-selective voltage-gated calcium channel blocker $CdCl_2$ had no effect on the Ca^{2+} rise induced by E2 or G-1. **(F)** Depletion of store Ca^{2+} using thapsigargin prevented E2 or G-1 or ACh from evoking a rapid Ca^{2+} rise. The example traces **(A–F)** are the average percentage change in fluorescence of 10–29 cells in one visual field. **(G,H)** Averaged peak percentage changes in fluorescence in different conditions. ns, not significant, unpaired **(G)** or paired **(H)** *t*-test, $n = 28{\sim}62$ cells from three to four independent tests.

IP3R inhibitor (**Figures 3D,E**) (E2 + 2-APB: 7.12 ± 1.30% vs. E2: 231.5 ± 16.41%, $n = 48$ cells, $P < 0.001$; G-1 + 2-APB: 22.01 ± 2.73% vs. G-1: 148.9 ± 7.82%, $n = 48$ cells, $P < 0.001$, **Figure 3F**). Therefore, activation of GPER may elicit PLC/IP3-mediated store Ca^{2+} release.

GPER Activation Stimulates PKC Isoforms

Intracellular Ca^{2+} as an important second messenger may activate the Ca^{2+}-dependent protein kinases (PKCs) characterized by translocation of cytosolic PKCs to the plasma membrane. Previous reports have implicated PKCα and PKCε in regulation of pain and μ-opioid signaling (Bailey et al., 2009; Zheng et al., 2011; Illing et al., 2014). Hence we focused on these two PKC isoforms to test whether GPER-mediated Ca^{2+} signaling may stimulate PKCs. We took advantage of the biotin-avidin method to extract plasma membrane proteins and to detect the possible translocation/activation of PKCα and PKCε following GPER activation in SH-SY5Y cells. As a positive control, cells treated with the PKC agonist PMA (1 μM) for 5 min manifested pronounced translocation of PKCα and PKCε to the plasma membrane (**Figures 4A,B,G,H**). In a similar manner, a 5 min treatment of the cells with E2 or G-1 (1 μM) significantly increased membrane translocation of PKCα and PKCε (**Figures 4C–F,I–L**).

GPER Activation Facilitates MOR Phosphorylation in PKC-Dependent Manner

In the hypothalamus, estrogens may rapidly desensitize MOR probably by activating PLC, PKA, and PKCs and uncouple MOR from activating GIRK channels (Kelly et al., 1999). We therefore investigated whether activation of GPER may promote MOR phosphorylation in SH-SY5Y cells. As a positive control, cells

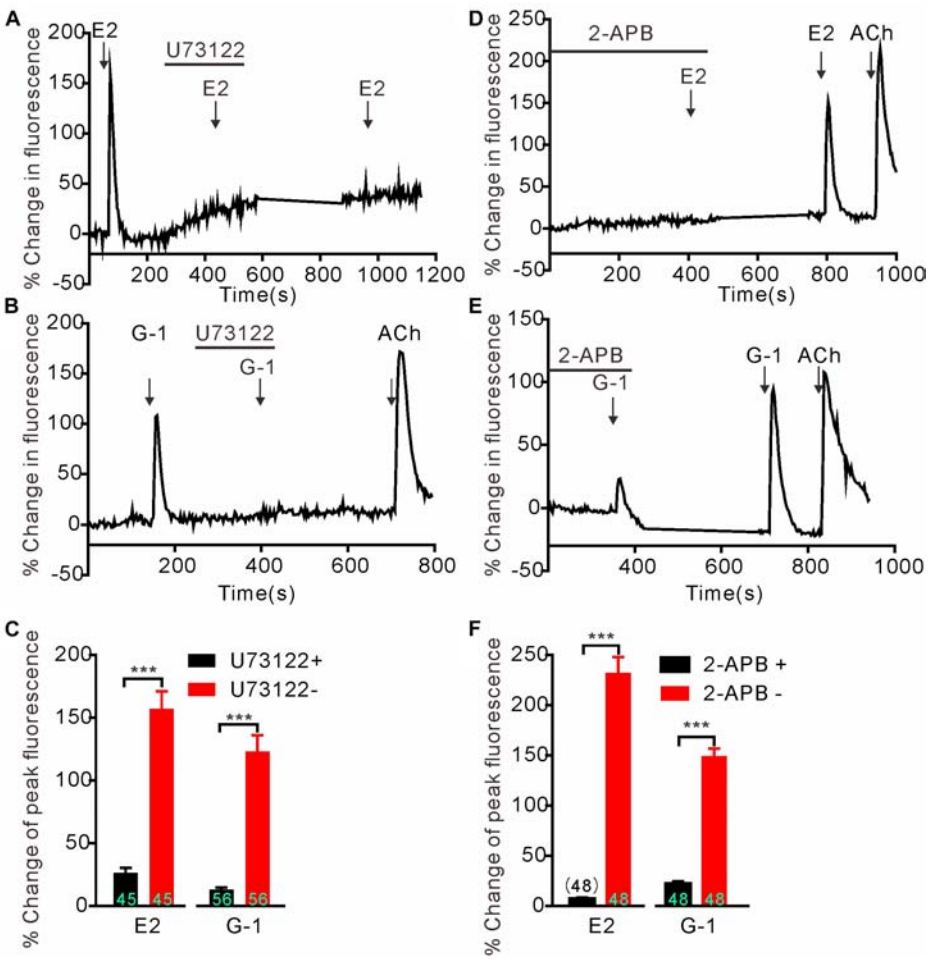

FIGURE 3 | G protein-coupled estrogen receptor-mediated rapid calcium rise in SH-SY5Y cells is via the PLC/IP3 pathway. **(A–C)** The PLC inhibitor U73122 (3 μM) completely blocked the calcium response to E2 (1 μM) and G-1 (1 μM). **(D–F)** The store calcium release channel (IP3R) blocker, 2-APB, virtually abolished G-1 or E2-evoked calcium responses. The example traces **(A,B,D,E)** are the average percentage change in fluorescence of 16–25 cells in one visual field. **(C,F)** The averaged peak percentage changes in fluorescence in different conditions. ***$P < 0.001$, paired *t*-test. $n = 45$∼56 cells from three to four independent tests.

were treated with the PKC agonist PMA (1 μM) for 30 min, which resulted in an increase of phosphorylated MOR (pMOR) level compared with the vehicle group (**Figure 5**). Similarly, cells exposed to E2 or G-1 (1 μM) also had significantly higher levels of pMOR, which was prevented by co-administration of pan-PKC inhibitor Ro 31-8820 (3 μM, which inhibits PKCα, PKCβI, PKCβII, PKCγ, and PKCε) (**Figure 5**). Therefore, activation of GPER may promote MOR phosphorylation in a PKC-dependent manner.

GPER-Mediated Rapid Calcium Signaling Elicits Indirect Genomic Effects

Previous studies indicate that the rapid non-genomic estrogenic signaling via second messengers (such as cAMP or Ca^{2+}) is also transmitted to the nucleus to affect gene transcription and protein synthesis, leading to an indirect (not via the classic nuclear receptor ER α/β) genomic effect (Guo et al., 2002). To investigate whether GPER-mediated rapid Ca^{2+} signaling may elicit such indirect genomic effects, we exposed SH-SY5Y cells with E2 or G-1 and detected c-Fos, which is an immediate early gene that responds to extracellular signals. Cells were treated with E2 (1 μM) or G-1 (1 μM) for 15, 30, and 60 min, respectively. Whole lysate western blot showed that both E2 and G-1 caused time-dependent increases in c-Fos protein expression (**Figures 6A–C**). Moreover, the E2 or G-1-induced c-Fos expression was almost completely negated in the presence of the GPER antagonists G15, the IP3R inhibitor 2-APB, or the PLC inhibitor U73122 (**Figures 6D–F**). These results indicate that GPER-mediated rapid PLC/IP3-dependent Ca^{2+} signaling may be transmitted to the nucleus to regulate gene transcription and protein synthesis.

DISCUSSION

Estrogens, primarily 17β-estradiol (E2), are known to exert major influences on the nervous system with slow genomic and rapid

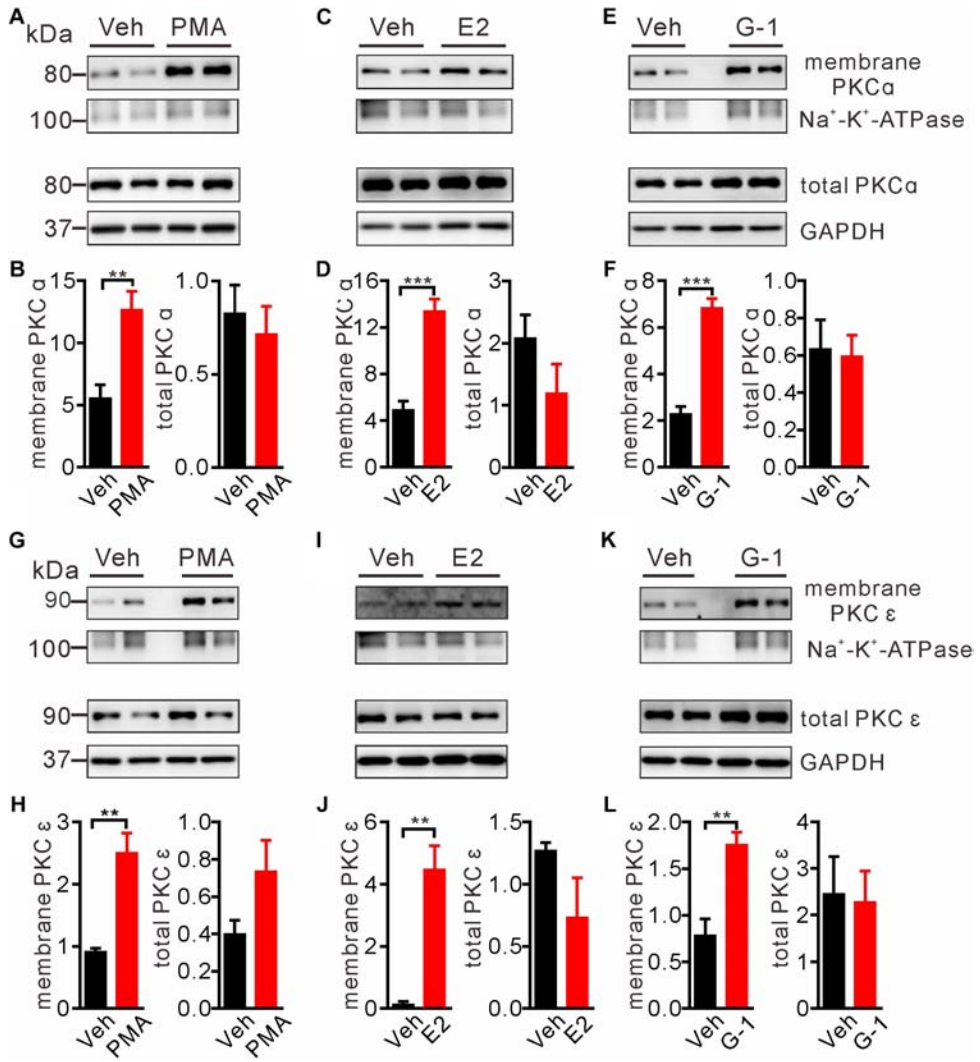

FIGURE 4 | E2 and G-1 promoted translocation of PKC isoforms to the plasma membrane. **(A,B,G,H)** Cells treated with the pan-PKC agonist PMA (1 μM) for 5 min had significantly higher PKCα and PKCε in the plasma membrane protein samples, compared with vehicle-treated cells. **(C,D,I,J)** Cells treated with E2 (1 μM) for 5 min had increased PKCα and PKCε in the plasma membrane protein samples as compared with cells treated with vehicle. **(E,F,K,L)** Cells treated with G-1 (1 μM) for 5 min had increased PKCα and PKCε in the plasma membrane protein samples as compared with cells treated with vehicle. After detected PKCα bands **(C,E)**, the nitrocellulose membrane was stripped and re-blocked by 5% fat-free dry milk in TBST, followed by incubation with PKCε primary antibody, then PKCε bands was detected **(I,K)**. So the loading controls are the same. Membrane PKCα or PKCε is a relative value with Na^+-K^+-ATPase as the internal reference for plasma membrane protein; total PKCα or PKCε is the relative value with GAPDH as the internal reference for total protein. $^{**}P < 0.01$, $^{***}P < 0.001$, unpaired *t*-test, averaged data from three to four independent experiments.

non-genomic effects. Whilst it is clear that two nuclear receptors, ERα and ERβ, mediate the slow genomic effects, the receptor(s) responsible for the rapid non-genomic effects in the nervous system remain uncertain. The current study demonstrates that the human neuroblastoma SH-SY5Y cells endogenously express G protein-coupled estrogen receptor (GPER) and activation of GPER may induce a rapid increase in cytosolic Ca^{2+}, which is due to PLC/IP3-dependent store Ca^{2+} release and is followed by PKC activation and MOR phosphorylation. Furthermore, GPER-mediated Ca^{2+} signaling may also be transmitted to the nucleus to induce c-Fos expression. To the best of our knowledge, this is for the first time that GPER is shown to mediate calcium release and PKC-dependent phosphorylation of MOR in neuroblastoma cells. Our findings strongly support GPER as a mediator of the rapid non-genomic estrogenic effects in the nervous system.

Ca^{2+} as a ubiquitous intracellular messenger regulates diverse neuronal functions. Ca^{2+} may bind to synaptotagmin to trigger synaptic vesicle release (Emptage et al., 2001). Ca^{2+} also binds to calmodulin (CaM) to form CaM-Ca^{2+} complex, activating Ca^{2+}/CaM-dependent protein kinases (CAMKs) or the Ca^{2+}/CaM-dependent serine/threonine phosphatase calcineurin, which plays an important role in the regulation of synaptic plasticity (Yakel, 1997; Wayman et al., 2008; Kim et al., 2016; Sugawara et al., 2017). Ca^{2+} activates the

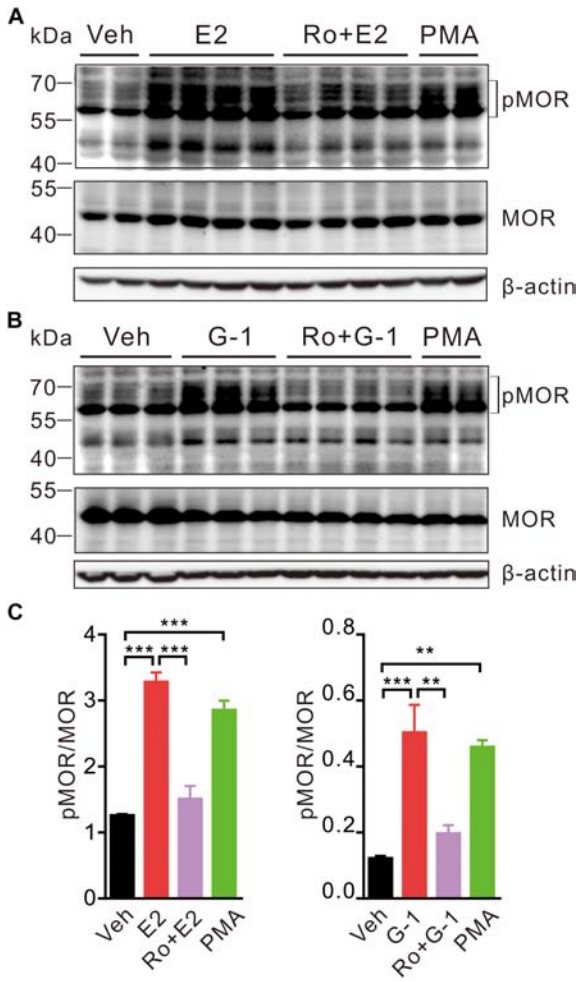

FIGURE 5 | E2 and G-1 stimulate phosphorylation of MOR in a PKC-dependent manner. **(A,B)** SH-SY5Y cells treated with PMA (1 μM), E2 (1 μM), or G-1 (1 μM) for 30 min showed increased level of phosphorylated MOR (pMOR) as compared with the vehicle group. In the presence of the pan-PKC inhibitor (Ro 31-8820, Ro, 3 μM), E2 and G-1 failed to increase pMOR expression. **(C)** The averaged pMOR level (relative to β-actin) in cells with different treatments. After detection of pMOR **(A,B)**, the nitrocellulose membrane was stripped and re-blocked by 5% fat-free dry milk in TBST, followed by incubation with MOR primary antibody, then MOR band was detected. $^{**}P < 0.01$, $^{***}P < 0.001$, one-way ANOVA with Tukey's *post hoc* test, averaged data from three to four independent experiments.

Ca^{2+}-dependent protein kinase (PKC) system to promote phosphorylation of various GPCRs and ion channels, thereby regulating neuronal excitability, synaptic transmission and plasticity (Ritter et al., 2012; Fukuchi et al., 2015b; Li et al., 2017; Rajagopal et al., 2017; Summers et al., 2019).

Previous studies indicate that estrogens may induce rapid changes in cytosolic Ca^{2+} in hippocampal neurons, hypothalamic astrocytes and embryonic midbrain dopaminergic neurons (Brailoiu et al., 2007; Noel et al., 2009; Kuo et al., 2010). Furthermore, E2 was found to rapidly desensitize μ-opioid receptor (MOR) in hypothalamic neurons in PLC, PKA, and PKC-dependent manners, suggesting that Ca^{2+} signaling probably underlies estrogenic suppression of MOR function (Lagrange et al., 1997; Conde et al., 2016). MOR is best known for the regulation of pain and analgesia, but also plays important roles in regulation of reproductive behaviors, neuroprotection and cognition (Long et al., 2014; Jacobson et al., 2018; Liu et al., 2018; Vaidya et al., 2018). Therefore, it is of great interest to understand the identity of the receptor(s) which may mediate estrogenic suppression of MOR signaling.

The primary goal of this study is to test whether GPER can initiate rapid Ca^{2+} signaling and PKC-dependent phosphorylation of MOR in neuronal cells. To this end, we set to search for a neuronal cell line co-expressing GPER and MOR. qPCR showed that GPER mRNA appears to be relatively more abundant in the human neuroblastoma SH-SY5Y cells than in the murine Neuro-2a cells. Our immunofluorescent staining shows presence of GPER immunoreactivity at peri-nuclear sites and western blot assay could detect GPER immunoreactivity in whole-cell protein extract but not in membrane protein extract. Therefore, GPER is located intracellularly, in line with other reports indicating GPER being localized to the endoplasmic reticulum or the Golgi apparatus (Filardo and Thomas, 2005; Cheng et al., 2011). We found that GPER agonists E2/G-1 induced a rapid increase in intracellular calcium in SH-SY5Y cells but not in Neuro-2a cells. Currently, the reason for the lack of calcium response in Neuro-2a cells can only be speculated. One possibility is that GPER protein expression may be low in Neuro-2a cells, as suggested by the relative lower GPER mRNA than in SH-SY5Y cells. The other possibility is that GPER might be coupled to a different signaling cascade in this cell line. Due to the uncertain specificity of commercial GPER antibodies (in our hands, most GPER antibodies do not work very well with mouse samples), we have not been able to determine GPER protein expression in the murine-derived Neuro-2a cells. In this respect, it would be useful to test whether Neuro-2a cells transfected with GPER gene may respond to E2/G-1 with a calcium rise.

SH-SY5Y cells probably express ERα, ERβ, $G\alpha_q$-mER as well GPER (Barbati et al., 2012; Mateos et al., 2012; Nakaso et al., 2014; Gray et al., 2016; Shen et al., 2016; Cheng et al., 2017). However, the following lines of evidence from this study indicate that activation of GPER but not the classical ERs or ER variants may initiate rapid Ca^{2+} signaling: (1) SH-SY5Y but not Neuro-2a cells responded to E2 and the GPER selective agonist G-1 with rapid rises in cytosolic Ca^{2+} in concentration-dependent manners, consistent with the relative abundance of GPER mRNA in this cell line; (2) Either E2 or G-1-induced Ca^{2+} rise was blocked by the GPER antagonist G15; (3) The membrane impermeable E2-BSA failed to cause a significant Ca^{2+} response, consistent with the intracellular localization of GPER in SH-SY5Y cells.

E2 has been shown to induce rapid Ca^{2+} influx through activation of L-type calcium channels (Wu et al., 2005, 2011; Zhao et al., 2005) or rapid store Ca^{2+} release in some neuronal cells (Beyer and Raab, 1998; Kuo et al., 2010). We found that GPER-mediated Ca^{2+} rise in SH-SY5Y cells was due to store release rather than Ca^{2+} entry since either E2 or G-1 still induced rapid increases in cytosolic Ca^{2+} in the extracellular Ca^{2+}-free condition and in the presence of cadmium, a broad-spectrum voltage-dependent Ca^{2+} channel blocker. Depletion of the Ca^{2+}

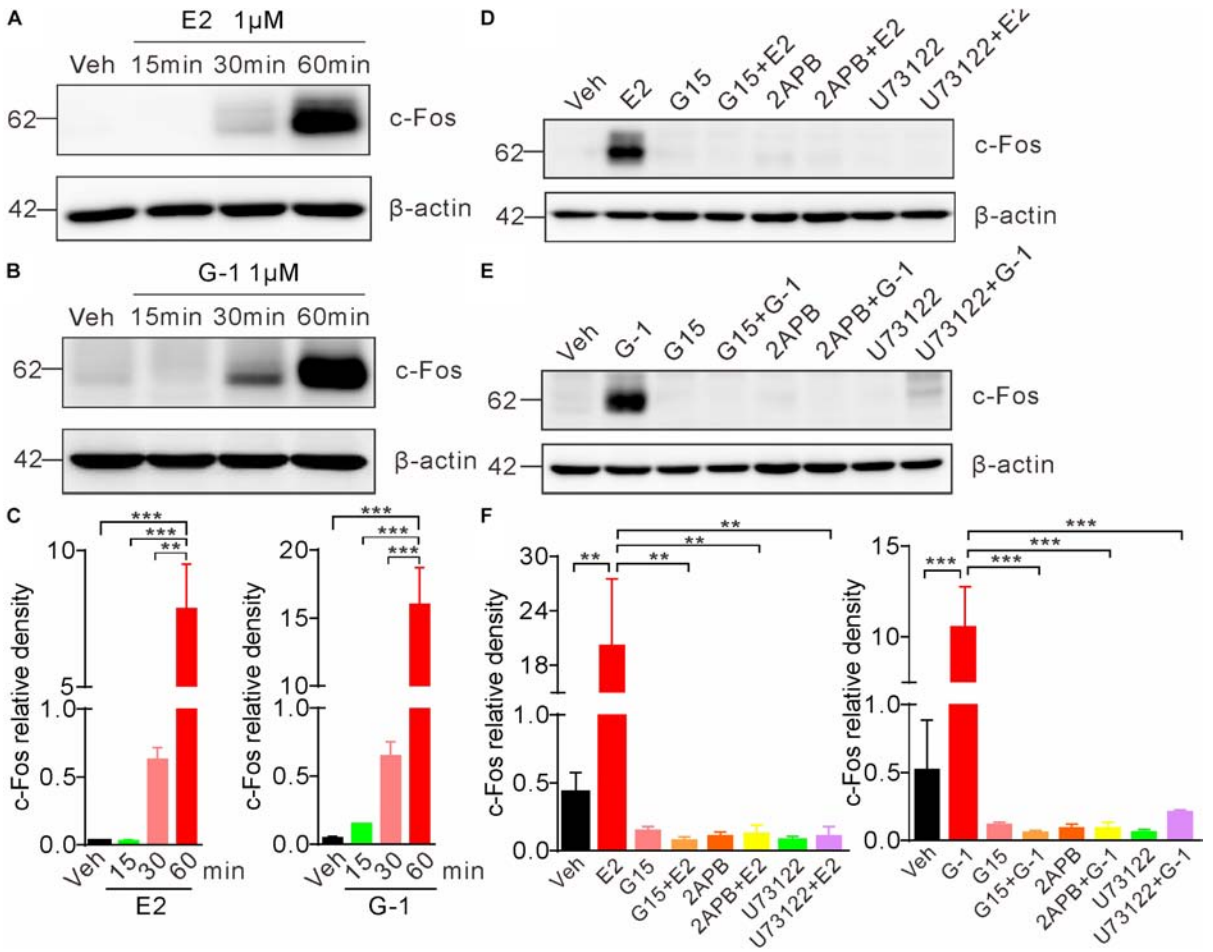

FIGURE 6 | Activation of GPER induces c-Fos expression in SH-SY5Y cells. **(A–C)** Cells treated with E2 (1 μM) or G-1(1 μM) showed time-dependent increases in c-Fos expression. **(D–F)** E2 and G-1-induced c-Fos expression was prevented by the GPER antagonist G15 (1 μM), PLC inhibitor U73122 (1 μM), and IP3R inhibitor 2-APB (1 μM). c-Fos density was relative to β-actin. $^{**}P < 0.05$, $^{***}P < 0.01$, one-way ANOVA with Tukey's *post hoc* test, averaged data from three independent experiments.

store with thapsigargin prevented E2 or G-1 from inducing a change in intracellular Ca^{2+} level. Furthermore, the IP3 receptor inhibitor 2-APB and the PLC inhibitor U73122 virtually abolished either E2 or G-1-induced Ca^{2+} response, confirming activation of GPER induces store Ca^{2+} release through PLC and IP3 pathway.

Previously, Grassi et al. (2015) reported that estrogen receptor modulator raloxifene may down-regulate vasopressin mRNA in SH-SY5Y cells. By using G-1, G-15 and a PKC inhibitor, authors concluded that the raloxifene effect was mediated by GPER and PKC. In the present study, we were able to confirm that GPER-initiated Ca^{2+} signaling may activate PKCs and consequently promote phosphorylation of MOR. PKCα, PKCε, and PKCγ promote the phosphorylation of Serine 363, Threonine 370, and Serine 375 at C-terminal of MOR, which has been implicated in the development of pain and morphine tolerance (Zeitz et al., 2001; Hua et al., 2002; Bjornstrom and Sjoberg, 2005; Newton et al., 2007; Smith et al., 2007; Doll et al., 2011; Bowman et al., 2015). We found that activation of GPER in SH-SY5Y cells promoted membrane translocation of PKCα and PKCε and elevated the expression of phosphorylated-MOR (pMOR), which was negated by the PKC inhibitor Ro 31-8820. These data reveal a novel estrogenic signaling cascade mediated by GPER which ultimately leads to phosphorylation and desensitization of MOR. This signaling mechanism may be relevant to the well-documented gender dymorphisms of pain, morphine analgesia, neuroprotection and cognition as well as the regulation of reproductive behaviors.

Previous studies indicate that the rapid non-genomic estrogenic signaling may also alter gene transcription (Guo et al., 2002; Bjornstrom and Sjoberg, 2005). In a prostate cancer cell (PC-3) line, G-1 may inhibit prostate cancer cell (PC-3) growth, which was mediated through GPER, followed by activation of c-jun/c-fos (Chan et al., 2010). On the other hand, an increase in cytosolic Ca^{2+} may stimulate c-Fos expression, accounting for the neuronal activity-dependent immediate early gene expression and long lasting changes of neural functions

(Fukuchi et al., 2015a). Hence we tested whether GPER-mediated Ca^{2+} rise may stimulate c-Fos expression. Indeed either E2 or G-1 stimulated c-Fos expression within 30 min, which was prevented in the presence of the GPER antagonist G15, the IP3R blocker 2APB or the PLC inhibitor U73122. Therefore, GPER-mediated rapid Ca^{2+} signaling may also be transmitted to the nucleus leading to the indirect (i.e., not via the nuclear recetpor, ERα or ERβ) genomic effects.

In the present work, we did not attempt to identify the G protein subtype coupled to GPER. Nevertheless, the profile of the E2/G-1-induced calcium and PKC responses was reminiscent of the Gq-mER-mediated effects previously reported by Qiu et al. (2003) in hypothalamic proopiomelanocortin (POMC) neurons. They showed that E2 rapidly attenuated the potency of $GABA_B$ agonist to activate the GIRK current in POMC neurons and the signaling cascade involved $G\alpha_q$-mediated PLC activation upstream of PKCδ, PKA and changes in gene transcription. The effects were mimicked by BSA-conjugated E2 and a non-steroidal compound STX that does not bind ERα or ERβ, leading to the proposal of a Gq-coupled membrane-associated estrogen (STX) receptor (Gq-mER). Although intracellular calcium was not measured in that study, it is conceivable that activation of Gq-mER may also signal through IP3-mediated store calcium release and activation of calcium-dependent PKC isoforms, similarly to the GPER-mediated signaling shown in the current study. The molecular identity of Gq-mER is still unknown. It would be interesting to examine whether Gq-mER and GPER are related or separate mechanisms for rapid estrogenic signaling.

CONCLUSION

The present study revealed a novel GPER-mediated estrogenic signaling cascade in neuroblastoma cells. Estrogens may activate the intracellularly located GPER to trigger rapid PLC/IP3-dependent store Ca^{2+} release, which in turn activates PKC isoforms to phosphorylate the μ opioid receptor. The rapid Ca^{2+} signaling may also be transmitted to the nucleus to impact on gene transcription. Such signaling cascade may play important roles in the regulation of opioid signaling in the brain.

DATA AVAILABILITY STATEMENT

All datasets generated for this study are included in the article/supplementary material.

AUTHOR CONTRIBUTIONS

All authors participated in the development of this research and drafting of the manuscript. WR, XS, and GZ made substantial contributions to the conception or design of the work, critically revised the manuscript, supervised the experiments and data analysis, acquired funding, designed the experiments, and analyzed the data. XD, TG, and PG performed the experiments and participated in the analysis of results. YM and LD participated in the immunofluorescence staining experiments. YZ and PL participated in the calcium imaging experiments.

FUNDING

This work was funded by the National Natural Science Foundation of China (Grants #81570493 and #81873728), the Science and Technology Commission of Shanghai Municipality (Grant #18JC1420302), and Xin Hua Hospital (Grant #JZPI201705).

ACKNOWLEDGMENTS

The authors wish to thank Dr. Yu Qiu for the gift of Neuro-2a cell lines.

REFERENCES

Bailey, C. P., Oldfield, S., Llorente, J., Caunt, C. J., Teschemacher, A. G., Roberts, L., et al. (2009). Involvement of PKC alpha and G-protein-coupled receptor kinase 2 in agonist-selective desensitization of mu-opioid receptors in mature brain neurons. *Br. J. Pharmacol.* 158, 157–164. doi: 10.1111/j.1476-5381.2009.00140.x

Barbati, C., Pierdominici, M., Gambardella, L., Malchiodi Albedi, F., Karas, R. H., Rosano, G., et al. (2012). Cell surface estrogen receptor alpha is upregulated during subchronic metabolic stress and inhibits neuronal cell degeneration. *PLoS One* 7:e42339. doi: 10.1371/journal.pone.0042339

Beyer, C., and Raab, H. (1998). Nongenomic effects of oestrogen: embryonic mouse midbrain neurones respond with a rapid release of calcium from intracellular stores. *Eur. J. Neurosci.* 10, 255–262. doi: 10.1046/j.1460-9568.1998.00045.x

Bjornstrom, L., and Sjoberg, M. (2005). Mechanisms of estrogen receptor signaling: convergence of genomic and nongenomic actions on target genes. *Mol. Endocrinol.* 19, 833–842. doi: 10.1210/me.2004-0486

Bologa, C. G., Revankar, C. M., Young, S. M., Edwards, B. S., Arterburn, J. B., Kiselyov, A. S., et al. (2006). Virtual and biomolecular screening converge on a selective agonist for GPR30. *Nat Chem Biol.* 2, 207–212. doi: 10.1038/nchembio775

Bowman, S. L., Soohoo, A. L., Shiwarski, D. J., Schulz, S., Pradhan, A. A., and Puthenveedu, M. A. (2015). Cell-autonomous regulation of Mu-opioid receptor recycling by substance P. *Cell Rep.* 10, 1925–1936. doi: 10.1016/j.celrep.2015.02.045

Brailoiu, E., Dun, S. L., Brailoiu, G. C., Mizuo, K., Sklar, L. A., Oprea, T. I., et al. (2007). Distribution and characterization of estrogen receptor G protein-coupled receptor 30 in the rat central nervous system. *J. Endocrinol.* 193, 311–321. doi: 10.1677/JOE-07-0017

Chan, Q. K., Lam, H. M., Ng, C. F., Lee, A. Y., Chan, E. S., Ng, H. K., et al. (2010). Activation of GPR30 inhibits the growth of prostate cancer cells through sustained activation of Erk1/2, c-jun/c-fos-dependent upregulation of p21, and induction of G(2) cell-cycle arrest. *Cell Death Differ.* 17, 1511–1523. doi: 10.1038/cdd.2010.20

Chen, W. C., Cheng, J. S., Chou, K. J., Tang, K. Y., Huang, J. K., Tseng, L. L., et al. (2002). Effect of 17β-estradiol on intracellular Ca(2)+ levels in renal tubular cells. *Pharmacology* 64, 84–90. doi: 10.1159/000056155

Cheng, S. B., Quinn, J. A., Graeber, C. T., and Filardo, E. J. (2011). Down-modulation of the G-protein-coupled estrogen receptor, GPER, from the cell surface occurs via a trans-Golgi-proteasome pathway. *J. Biol. Chem.* 286, 22441–22455. doi: 10.1074/jbc.M111.224071

Cheng, Y. F., Zhu, G., Wu, Q. W., Xie, Y. S., Jiang, Y., Guo, L., et al. (2017). GPR30 activation contributes to the puerarin-mediated neuroprotection in

MPP(+)-Induced SH-SY5Y cell death. *J. Mol. Neurosci.* 61, 227–234. doi: 10.1007/s12031-016-0856-y

Conde, K., Meza, C., Kelly, M. J., Sinchak, K., and Wagner, E. J. (2016). Estradiol rapidly attenuates ORL-1 receptor-mediated inhibition of proopiomelanocortin neurons via Gq-Coupled, membrane-initiated signaling. *Neuroendocrinology* 103, 787–805. doi: 10.1159/000443765

Deliu, E., Brailoiu, G. C., Arterburn, J. B., Oprea, T. I., Benamar, K., Dun, N. J., et al. (2012). Mechanisms of G protein-coupled estrogen receptor-mediated spinal nociception. *J. Pain.* 13, 742–754. doi: 10.1016/j.jpain.2012.05.011

Dennis, M. K., Burai, R., Ramesh, C., Petrie, W. K., Alcon, S. N., Nayak, T. K., et al. (2009). In vivo effects of a GPR30 antagonist. *Nat. Chem. Biol.* 5, 421–427. doi: 10.1038/nchembio.168

Doll, C., Konietzko, J., Pöll, F., Koch, T., Höllt, V., and Schulz, S. (2011). Agonist-selective patterns of mu-opioid receptor phosphorylation revealed by phosphosite-specific antibodies. *Br. J. Pharmacol.* 164, 298–307. doi: 10.1111/j.1476-5381.2011.01382.x

Dun, S. L., Brailoiu, G. C., Gao, X., Brailoiu, E., Arterburn, J. B., Prossnitz, E. R., et al. (2009). Expression of estrogen receptor GPR30 in the rat spinal cord and in autonomic and sensory ganglia. *J. Neurosci. Res.* 87, 1610–1619. doi: 10.1002/jnr.21980

Emptage, N. J., Reid, C. A., and Fine, A. (2001). Calcium stores in hippocampal synaptic boutons mediate short-term plasticity, store-operated Ca2+ entry, and spontaneous transmitter release. *Neuron* 29, 197–208. doi: 10.1016/S0896-6273(01)00190-8

Filardo, E. J., and Thomas, P. (2005). GPR30: a seven-transmembrane-spanning estrogen receptor that triggers EGF release. *Trends Endocrinol. Metab.* 16, 362–367. doi: 10.1016/j.tem.2005.08.005

Fukuchi, M., Kanesaki, K., Takasaki, I., Tabuchi, A., and Tsuda, M. (2015a). Convergent effects of Ca(2+) and cAMP signals on the expression of immediate early genes in neurons. *Biochem. Biophys. Res. Commun.* 466, 572–577. doi: 10.1016/j.bbrc.2015.09.084

Fukuchi, M., Tabuchi, A., Kuwana, Y., Watanabe, S., Inoue, M., Takasaki, I., et al. (2015b). Neuromodulatory effect of galphas- or galphaq-coupled G-protein-coupled receptor on NMDA receptor selectively activates the NMDA receptor/Ca2+/calcineurin/cAMP response element-binding protein-regulated transcriptional coactivator 1 pathway to effectively induce brain-derived neurotrophic factor expression in neurons. *J. Neurosci.* 35, 5606–5624. doi: 10.1523/JNEUROSCI.3650-14.2015

Grassi, D., Ghorbanpoor, S., Acaz-Fonseca, E., Ruiz-Palmero, I., and Garcia-Segura, L. M. (2015). The selective estrogen receptor modulator raloxifene regulates arginine-vasopressin gene expression in human female neuroblastoma cells through G protein-coupled estrogen receptor and ERK signaling. *Endocrinology* 156, 3706–3716. doi: 10.1210/en.2014-2010

Gray, N. E., Zweig, J. A., Kawamoto, C., Quinn, J. F., and Copenhaver, P. F. (2016). STX, a novel membrane estrogen receptor ligand, protects against Amyloid-beta toxicity. *J. Alzheimers Dis.* 51, 391–403. doi: 10.3233/JAD-150756

Guo, Z., Krucken, J., Benten, W. P., and Wunderlich, F. (2002). Estradiol-induced nongenomic calcium signaling regulates genotropic signaling in macrophages. *J. Biol. Chem.* 277, 7044–7050. doi: 10.1074/jbc.M109808200

Hazell, G. G., Yao, S. T., Roper, J. A., Prossnitz, E. R., O'Carroll, A. M., and Lolait, S. J. (2009). Localisation of GPR30, a novel G protein-coupled oestrogen receptor, suggests multiple functions in rodent brain and peripheral tissues. *J. Endocrinol.* 202, 223–236. doi: 10.1677/JOE-09-0066

Hua, X. Y., Moore, A., Malkmus, S., Murray, S. F., Dean, N., Yaksh, T. L., et al. (2002). Inhibition of spinal protein kinase C alpha expression by an antisense oligonucleotide attenuates morphine infusion-induced tolerance. *Neuroscience* 113, 99–107. doi: 10.1016/S0306-4522(02)00157-4

Huang, J. K., and Jan, C. R. (2001). Mechanism of estrogens-induced increases in intracellular Ca(2)+ in PC3 human prostate cancer cells. *Prostate* 47, 141–148. doi: 10.1002/pros.1057

Illing, S., Mann, A., and Schulz, S. (2014). Heterologous regulation of agonist-independent mu-opioid receptor phosphorylation by protein kinase C. *Br. J. Pharmacol.* 171, 1330–1340. doi: 10.1111/bph.12546

Jacobson, M. L., Wulf, H. A., Browne, C. A., and Lucki, I. (2018). Opioid modulation of cognitive impairment in depression. *Prog. Brain Res.* 239, 1–48. doi: 10.1016/bs.pbr.2018.07.007

Jensen, E. V., and Desombre, E. R. (1973). Estrogen-receptor interaction. *Science* 182, 126–134. doi: 10.1126/science.182.4108.126

Kelly, M. J., Lagrange, A. H., Wagner, E. J., and Rønnekleiv, O. K. (1999). Rapid effects of estrogen to modulate G protein-coupled receptors via activation of protein kinase A and protein kinase C pathways. *Steroids* 64, 64–75. doi: 10.1016/S0039-128X(98)00095-6

Kelly, M. J., and Ronnekleiv, O. K. (2009). Control of CNS neuronal excitability by estrogens via membrane-initiated signaling. *Mol. Cell. Endocrinol.* 308, 17–25. doi: 10.1016/j.mce.2009.03.008

Kim, K., Saneyoshi, T., Hosokawa, T., Okamoto, K., and Hayashi, Y. (2016). Interplay of enzymatic and structural functions of CaMKII in long-term potentiation. *J. Neurochem.* 139, 959–972. doi: 10.1111/jnc.13672

Kuhn, J., Dina, O. A., Goswami, C., Suckow, V., Levine, J. D., and Hucho, T. (2008). GPR30 estrogen receptor agonists induce mechanical hyperalgesia in the rat. *Eur. J. Neurosci.* 27, 1700–1709. doi: 10.1111/j.1460-9568.2008.06131.x

Kuiper, G. G., Enmark, E., Pelto-Huikko, M., Nilsson, S., and Gustafsson, J. A. (1996). Cloning of a novel receptor expressed in rat prostate and ovary. *Proc. Natl. Acad. Sci. U.S.A.* 93, 5925–5930. doi: 10.1073/pnas.93.12.5925

Kuo, J., Hamid, N., Bondar, G., Prossnitz, E. R., and Micevych, P. (2010). Membrane estrogen receptors stimulate intracellular calcium release and progesterone synthesis in hypothalamic astrocytes. *J. Neurosci.* 30, 12950–12957. doi: 10.1523/JNEUROSCI.1158-10.2010

Lagrange, A. H., Rønnekleiv, O. K., and Kelly, M. J. (1997). Modulation of G protein-coupled receptors by an estrogen receptor that activates protein kinase A. *Mol. Pharmacol.* 51, 605–612. doi: 10.1124/mol.51.4.605

Li, S., Zeng, J., Wan, X., Yao, Y., Zhao, N., Yu, Y., et al. (2017). Enhancement of spinal dorsal horn neuron NMDA receptor phosphorylation as the mechanism of remifentanil induced hyperalgesia: roles of PKC and CaMKII. *Mol. Pain* 13:1744806917723789. doi: 10.1177/1744806917723789

Liu, A., Zhang, H., Qin, F., Wang, Q., Sun, Q., Xie, S., et al. (2018). Sex Associated Differential Expressions of the Alternatively Spliced Variants mRNA of OPRM1 in Brain Regions of C57BL/6 Mouse. *Cell. Physiol. Biochem.* 50, 1441–1459. doi: 10.1159/000494644

Long, N., Long, B., Mana, A., Le, D., Nguyen, L., Chokr, S., et al. (2017). Tamoxifen and ICI 182,780 activate hypothalamic G protein-coupled estrogen receptor 1 to rapidly facilitate lordosis in female rats. *Horm. Behav.* 89, 98–103. doi: 10.1016/j.yhbeh.2016.12.013

Long, N., Serey, C., and Sinchak, K. (2014). 17beta-estradiol rapidly facilitates lordosis through G protein-coupled estrogen receptor 1 (GPER) via deactivation of medial preoptic nucleus mu-opioid receptors in estradiol primed female rats. *Horm. Behav.* 66, 663–666. doi: 10.1016/j.yhbeh.2014.09.008

Lu, Y., Jiang, Q., Yu, L., Lu, Z. Y., Meng, S. P., Su, D., et al. (2013). 17beta-estradiol rapidly attenuates P2X3 receptor-mediated peripheral pain signal transduction via ERalpha and GPR30. *Endocrinology* 154, 2421–2433. doi: 10.1210/en.2012-2119

Mateos, L., Persson, T., Katoozi, S., Gil-Bea, F. J., and Cedazo-Minguez, A. (2012). Estrogen protects against amyloid-beta toxicity by estrogen receptor alpha-mediated inhibition of Daxx translocation. *Neurosci. Lett.* 506, 245–250. doi: 10.1016/j.neulet.2011.11.016

Mosselman, S., Polman, J., and Dijkema, R. (1996). ERβ: identification and characterization of a novel human estrogen receptor. *FEBS. Lett.* 392, 49–53. doi: 10.1016/0014-5793(96)00782-X

Nakaso, K., Tajima, N., Horikoshi, Y., Nakasone, M., Hanaki, T., Kamizaki, K., et al. (2014). The estrogen receptor beta-PI3K/Akt pathway mediates the cytoprotective effects of tocotrienol in a cellular Parkinson's disease model. *Biochim. Biophys. Acta* 1842, 1303–1312. doi: 10.1016/j.bbadis.2014.04.008

Newton, P. M., Kim, J. A., McGeehan, A. J., Paredes, J. P., Chu, K., Wallace, M. J., et al. (2007). Increased response to morphine in mice lacking protein kinase C epsilon. *Genes Brain Behav.* 6, 329–338. doi: 10.1111/j.1601-183X.2006.00261.x

Noel, S. D., Keen, K. L., Baumann, D. I., Filardo, E. J., and Terasawa, E. (2009). Involvement of G protein-coupled receptor 30 (GPR30) in rapid action of estrogen in primate LHRH neurons. *Mol. Endocrinol.* 23, 349–359. doi: 10.1210/me.2008-0299

Ogawa, S., Tsukahara, S., Choleris, E., and Vasudevan, N. (2018). Estrogenic regulation of social behavior and sexually dimorphic brain formation. *Neurosci. Biobehav. Rev.* doi: 10.1016/j.neubiorev.2018.10.012 [Epub ahead of print].

Paech, K., Webb, P., Kuiper, G. G., Nilsson, S., Gustafsson, J., Kushner, P. J., et al. (1997). Differential ligand activation of estrogen receptors ERα and ERβ at AP1 sites. *Science* 277, 1508–1510. doi: 10.1126/science.277.5331.1508

Paletta, P., Sheppard, P. A. S., Matta, R., Ervin, K. S. J., and Choleris, E. (2018). Rapid effects of estrogens on short-term memory: possible mechanisms. *Horm. Behav.* 104, 88–99. doi: 10.1016/j.yhbeh.2018.05.019

Petrovic, S., Velickovic, N., Stanojevic, I., Milosevic, M., Drakulic, D., Stanojlovic, M., et al. (2011). Inhibition of mitochondrial Na+-dependent Ca(2)+ efflux by 17beta-estradiol in the rat hippocampus. *Neuroscience* 192, 195–204. doi: 10.1016/j.neuroscience.2011.06.030

Picotto, G., Vazquez, G., and Boland, R. (1999). 17β-oestradiol increases intracellular Ca(2)+ concentration in rat enterocytes. Potential role of phospholipase C-dependent store-operated Ca(2)+ influx. *Biochem. J.* 339, 71–77. doi: 10.1042/bj3390071

Qiu, J., Bosch, M. A., Tobias, S. C., Grandy, D. K., Scanlan, T. S., Ronnekleiv, O. K., et al. (2003). Rapid signaling of estrogen in hypothalamic neurons involves a novel G-protein-coupled estrogen receptor that activates protein kinase C. *J. Neurosci.* 23, 9529–9540. doi: 10.1523/JNEUROSCI.23-29-09529.2003

Rainville, J., Pollard, K., and Vasudevan, N. (2015). Membrane-initiated non-genomic signaling by estrogens in the hypothalamus: cross-talk with glucocorticoids with implications for behavior. *Front. Endocrinol.* 6:18. doi: 10.3389/fendo.2015.00018

Rajagopal, S., Burton, B. K., Fields, B. L., El, I. O., and Kamatchi, G. L. (2017). Stimulatory and inhibitory effects of PKC isozymes are mediated by serine/threonine PKC sites of the Cav2.3alpha1 subunits. *Arch. Biochem. Biophys.* 621, 24–30. doi: 10.1016/j.abb.2017.04.002

Revankar, C. M., Cimino, D. F., Sklar, L. A., Arterburn, J. B., and Prossnitz, E. R. (2005). A transmembrane intracellular estrogen receptor mediates rapid cell signaling. *Science* 307, 1625–1630. doi: 10.1126/science.1106943

Ritter, D. M., Ho, C., O'Leary, M. E., and Covarrubias, M. (2012). Modulation of Kv3.4 channel N-type inactivation by protein kinase C shapes the action potential in dorsal root ganglion neurons. *J. Physiol.* 590, 145–161. doi: 10.1113/jphysiol.2011.218560

Rubio-Gayosso, I., Sierra-Ramirez, A., García-Vazquez, A., Martinez-Martinez, A., Muñoz-García, O., Morato, T., et al. (2000). 17β-estradiol increases intracellular calcium concentration through a short-term and nongenomic mechanism in rat vascular endothelium in culture. *J. Cardiovasc. Pharmacol.* 36, 196–202. doi: 10.1097/00005344-200008000-00009

Shen, B., Wang, Y., Wang, X., Du, Y., Guo, S., and Cong, L. (2016). Estrogen induced the expression of ADAM9 through estrogen receptor alpha but not estrogen receptor beta in cultured human neuronal cells. *Gene* 576, 823–827. doi: 10.1016/j.gene.2015.11.014

Shughrue, P. J., Lane, M. V., and Merchenthaler, I. (1997). Comparative distribution of estrogen receptor-α and -β mRNA in the rat central nervous system. *J. Comp. Neurol.* 388, 507–525. doi: 10.1002/(SICI)1096-9861(19971201)388:4<507::AID-CNE1>3.0.CO;2-6

Shughrue, P. J., Scrimo, P. J., and Merchenthaler, I. (2000). Estrogen binding and estrogen receptor characterization (ERα and ERβ) in the cholinergic neurons of the rat basal forebrain. *Neuroscience* 96, 41–49. doi: 10.1016/S0306-4522(99)00520-5

Smith, F. L., Gabra, B. H., Smith, P. A., Redwood, M. C., and Dewey, W. L. (2007). Determination of the role of conventional, novel and atypical PKC isoforms in the expression of morphine tolerance in mice. *Pain* 127, 129–139. doi: 10.1016/j.pain.2006.08.009

Sugawara, T., Hisatsune, C., Miyamoto, H., Ogawa, N., and Mikoshiba, K. (2017). Regulation of spinogenesis in mature Purkinje cells via mGluR/PKC-mediated phosphorylation of CaMKIIbeta. *Proc. Natl. Acad. Sci. U.S.A.* 114, E5256–E5265. doi: 10.1073/pnas.1617270114

Summers, K. C., Bogard, A. S., and Tavalin, S. J. (2019). Preferential generation of Ca(2+)-permeable AMPA receptors by AKAP79-anchored protein kinase C proceeds via GluA1 subunit phosphorylation at Ser-831. *J. Biol. Chem.* 294, 5521–5535. doi: 10.1074/jbc.RA118.004340

Takanami, K., Sakamoto, H., Matsuda, K., Hosokawa, K., Nishi, M., Prossnitz, E. R., et al. (2010). Expression of G protein-coupled receptor 30 in the spinal somatosensory system. *Brain Res.* 1310, 17–28. doi: 10.1016/j.brainres.2009.11.004

Vaidya, B., Sifat, A. E., Karamyan, V. T., and Abbruscato, T. J. (2018). The neuroprotective role of the brain opioid system in stroke injury. *Drug Discov. Today* 23, 1385–1395. doi: 10.1016/j.drudis.2018.02.011

Wayman, G. A., Lee, Y. S., Tokumitsu, H., Silva, A. J., and Soderling, T. R. (2008). Calmodulin-kinases: modulators of neuronal development and plasticity. *Neuron* 59, 914–931. doi: 10.1016/j.neuron.2008.08.021

Woolley, C. S. (1999). *Effects of Estrogen in the CNS. Curr. Opin. Neurobiol.* 9, 349–354. doi: 10.1016/S0959-4388(99)80051-8

Wu, T. W., Chen, S., and Brinton, R. D. (2011). Membrane estrogen receptors mediate calcium signaling and MAP kinase activation in individual hippocampal neurons. *Brain Res.* 1379, 34–43. doi: 10.1016/j.brainres.2011.01.034

Wu, T. W., Wang, J. M., Chen, S., and Brinton, R. D. (2005). 17Beta-estradiol induced Ca2+ influx via L-type calcium channels activates the Src/ERK/cyclic-AMP response element binding protein signal pathway and BCL-2 expression in rat hippocampal neurons: a potential initiation mechanism for estrogen-induced neuroprotection. *Neuroscience* 135, 59–72. doi: 10.1016/j.neuroscience.2004.12.027

Yakel, J. L. (1997). Calcineurin regulation of synaptic function: from ion channels to transmitter release and gene transcription. *Trends. Pharmacol. Sci.* 18, 124–134. doi: 10.1016/S0165-6147(97)01046-8

Zeitz, K. P., Malmberg, A. B., Gilbert, H., and Basbaum, A. I. (2001). Reduced development of tolerance to the analgesic effects of morphine and clonidine in PKC? mutant mice. *Pain* 102, 245–253. doi: 10.1016/S0304-3959(01)00353-0

Zhao, L., Chen, S., Wang, J. M., and Briton, R. D. (2005). 17β-estradiol induces Ca(2)+ influx, dendritic and nuclear Ca(2)+ rise and subsequent cyclic AMP response element-binding protein activation in hippocampal neurons: a potential initiation mechanism for estrogen neurotrophism. *Neuroscience* 132, 299–311. doi: 10.1016/j.neuroscience.2004.11.054

Zheng, H., Chu, J., Zhang, Y., Loh, H. H., and Law, P. Y. (2011). Modulating micro-opioid receptor phosphorylation switches agonist-dependent signaling as reflected in PKCepsilon activation and dendritic spine stability. *J. Biol. Chem.* 286, 12724–12733. doi: 10.1074/jbc.M110.177089

Conflict of Interest: The authors declare that the research was conducted in the absence of any commercial or financial relationships that could be construed as a potential conflict of interest.

Advantages of publishing in Frontiers

OPEN ACCESS
Articles are free to read for greatest visibility and readership

FAST PUBLICATION
Around 90 days from submission to decision

HIGH QUALITY PEER-REVIEW
Rigorous, collaborative, and constructive peer-review

TRANSPARENT PEER-REVIEW
Editors and reviewers acknowledged by name on published articles

Frontiers
Avenue du Tribunal-Fédéral 34
1005 Lausanne | Switzerland

Visit us: www.frontiersin.org
Contact us: info@frontiersin.org | +41 21 510 17 00

REPRODUCIBILITY OF RESEARCH
Support open data and methods to enhance research reproducibility

DIGITAL PUBLISHING
Articles designed for optimal readership across devices

FOLLOW US
@frontiersin

IMPACT METRICS
Advanced article metrics track visibility across digital media

EXTENSIVE PROMOTION
Marketing and promotion of impactful research

LOOP RESEARCH NETWORK
Our network increases your article's readership